THE UNIVERSITY
of LIVERPOOL

PREDICTION OF TWO AND THREE DIMENSIONAL TURBULENT FLOWS

Thesis submitted in accordance with the requirements of
The University of Liverpool for the degree of
Doctor in Philosophy

by

Othman A. Karim
BSCE, MSc(Eng)

SEPTEMBER 1996

ABSTRACT

During the past decade, a number of numerical methods have been proposed for the solution of turbulent flow. Advancement in computer technology has resulted in dramatic increase in the use of Computational Fluid Dynamics (CFD) codes by the engineering community. The advent of many new numerical schemes has enabled researchers to solve a wider variety of problems. Currently there are numerous general commercial programs for solving fluid mechanics problems on the international market. Among these is FLUENT/PreBFC package, which has been developed by FLUENT Inc, USA. This package has been installed in the Sun-workstation at the University of Liverpool by the Computer Services Department.

In the present study, extensive testing procedures have been implemented to investigate the suitability of the package in simulating various turbulent flows in the field of hydraulic engineering, both in two and three-dimensions. These include turbulent wall jets under shallow and deep submergence, submerged offset jets, flow around piers and spur-dykes and finally jet-forced water circulation in water-supply reservoirs. The results are compared with experimental results of previous researches mainly of the Department of Civil Engineering, University of Liverpool, as well as other research establishment.

The FLUENT CFD model was, capable, in most cases, of producing predictions giving a good fit to the experimental results. When an accurate fit was not attained, the main features of the measured flow were still reproduced qualitatively; and the lack of correspondence was attributed to either inaccurate input data, numerical errors and of equal significance, experimental errors.

ACKNOWLEDGEMENTS

The author wishes to express his deep gratitude and sincere thanks to his supervisor, Dr. K.H.M. Ali, Senior Lecturer, and his co-supervisor, Dr. B. A. O'Connor, Professor of Maritime Civil Engineering, Department of Civil Engineering, for their patient guidance and their invaluable assistance throughout this study.

The author is very grateful for the financial support of the Malaysian Government and Universiti Kebangsaan Malaysia, without which this research would have been impossible.

The author also wishes to acknowledge the assistance of Dr. Ren Liu of Fluent Europe and Mr. Dave Tyson of Computer Services Department, University of Liverpool for assistance and useful comments regarding the CFD package used in the present study.

Thanks are also due to my fellow colleague, for the pleasure sharing with them the 2nd floor Research Room, and all my friends. The assistance of all the other who have in one way or another contributed in the completion of this thesis is also acknowledged.

Finally, I thank my family, my wife Bushro Ali, and my children, Anas, Hanan, Ammar Faiz and Aliya Fatin, for their unstinting encouragement, interest, support and patience during this research.

TABLE OF CONTENTS

CHAPTER 3 PREDICTION OF FLOW PATTERNS IN LOCAL SCOUR HOLES CAUSED BY TURBULENT WATER JETS

LIST OF TABLES

LIST OF FIGURES

CHAPTER

1

CHAPTER 1

INTRODUCTION

1.1 GENERAL

Turbulence is so much part of our daily life that we are often not aware of its 'presence', or even benefit from it without realising. Few examples of turbulent flows include: the flow in the earth's atmosphere, *e.g.* around buildings and driving cars; and the flow in the pipes of the water supply system. Numerous examples of turbulent flows can also be given for industrial environments, like the airplane and petrochemical industry.

Besides the practical importance of turbulent flows, turbulence is also challenging because it is one of the most important phenomena in nature which are still not completely understood. Several tools, like experiments and, more recently, numerical simulations, are available to obtain information on turbulent flows in order to increase our understanding of turbulence.

In hydraulics, the flows of practical relevance are almost always turbulent; this means that the flow exhibits an irregular behaviour both in space and time. Due to these complexities, the turbulent motion and the heat mass-transfer phenomena associated with it are extremely difficult to describe and thus predict theoretically. Yet, the basic task of hydraulic engineering is that of predicting water-flow phenomena, and, because "predictions" by way of experiments are usually very expensive, calculation methods are in great practical demand. Empirical methods simply correlate experimental results and can therefore be

used with confidence only for direct interpolation of these results; the Chezy equation is a typical example.

With the aid of dimensional analysis, experimental data are often condensed into many useful empirical formulae. However these can describe only the simplest phenomena of interest and are not suitable for complex geometries. Whenever there are more than just a few parameters determining the problem in question, generally valid empirical correlations are difficult if not impossible to attain.

During the past decade, a number of numerical methods has been proposed for the solution of turbulence flow, however the implementation of the numerical codes cannot be considered as fully completed because of limited information with regards to physical modelling and also validation (*i.e.* lack of numerical solutions and experimental results for comparison). Some of the suggested models have not been tested properly (or not at all) and are therefore difficult to access; others are used no longer because they have been found to perform poorly.

The use of Computational Fluid Dynamics (CFD) codes by the engineering community has increased dramatically in the last few years. This rise in interest and use has resulted from improvements in the predictive capabilities of codes, reductions in the cost of computer technology, and increase in the cost of complicated instrumentations and expertise necessary to perform experiments as well as to maintain the experimental facilities. The advent of many new numerical schemes has enabled researchers to solve a wider variety of problems.

Currently there are numerous general commercial programs for solving fluid mechanics problem on the international market. Among these is FLUENT/PreBFC package, which has been developed by FLUENT Inc, USA. The package has been reported to predict well many hydrodynamics applications especially in the field of mechanical and aeronautical but very few in the field of hydraulics.

Consequently, the aim of present study is to investigate the suitability of the package for application to a wide variety of hydraulics problem. Experimental results obtained by previous researchers at the Department of Civil Engineering, University of Liverpool and other research establishment were used as benchmarks.

1.2 BRIEF REMARKS ON FLUENT

FLUENT is a multi-purpose computer software for modelling fluid flow, heat transfer and chemical reaction which enable a rapid analysis of complex flows. FLUENT applies computer simulation methods to analyse and solve practical design problems based on fundamental principles of computational fluid dynamic (CFD) such as the conservation of mass, momentum and energy.

The software has been installed at the University of Liverpool. It runs from a SparcCentre 2000 based machine which has the capacity of 1,840Mhz cpus and 576 Megabytes Memory. It has 62.1 Gb disks for local filestore and swap space. The User and applications filestore is provided on 7 separate fileservers. The FLUENT license at The University of Liverpool enables 10 (ten) users to run the program simultaneously. Since the beginning of the present study the software has been updated twice. The original version was 3.0 dated March 1990. It was later updated to version 4.2 on June 1993 with the inclusion of closure model based on ReNormalisation Group technique. Currently the version available is Version 4.3 which is more user-friendly with the addition of Graphical User Interface (GUI) facility.

FLUENT is a two part program consisting of a preprocessor, PreBFC V4, and a main module, FLUENT as depicted in Figure 1.1. PreBFC V4 was used to define the geometry and a structured grid of the problem to be modeled. The grid information was then imported from PREBFC to FLUENT. The physical models,

fluid/material properties, and boundary conditions that describe the problem to be modeled were next added to the grid information and stored in Case-File that is a record of all the inputs for problem definition. The results of the calculation were stored in Data-File.

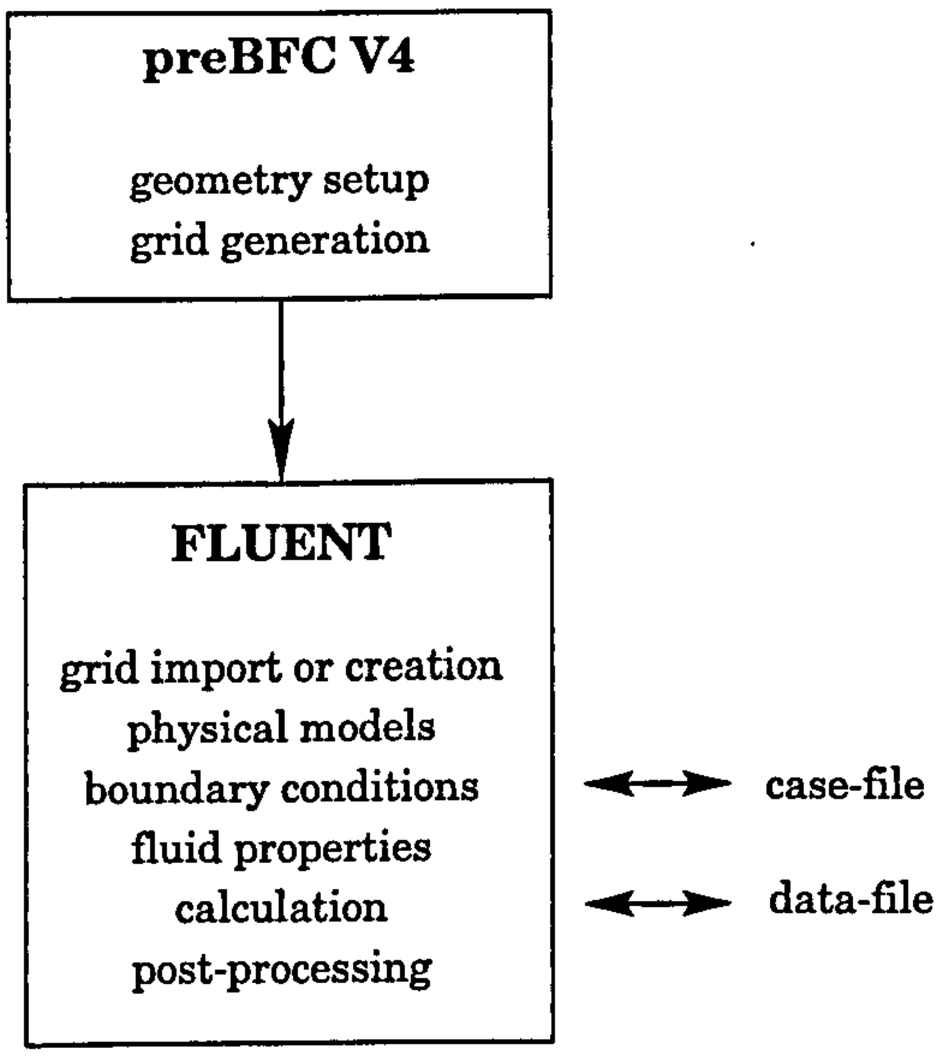

Figure 1.1 Basic Program Structure (after FLUENT Inc)

1.3 OUTLINE OF THIS THESIS

First, a brief review of the governing equations of turbulence flow is presented in Chapter 2. Its representation and the three closure models included in the FLUENT package, namely k-ε model, Reynolds averaging Stress Model (RSM) and ReNormalisation Group k-ε (RNG) are highlighted. The mathematics of the modified k-ε method based on Renormalization-Group (RNG) theory is discussed in greater details.

Secondly, the performance of the code and the closure models incorporated in FLUENT is evaluated in Chapter 3 by means of simulations of flow patterns in local scour holes caused by two and three-dimensional turbulent water jets. The results from the calculations are compared with experimental data.

Another class of turbulent water jets i.e. submerged offset jets in the vicinity of a solid boundary is simulated in Chapter 4. The flow was simulated for highly-curved offset jets impinging on rigid flat surface and scoured bed.

In Chapter 5 and Chapter 6 the numerical models were used to investigate the 3-dimensional flow pattern in the vicinity of bridge pier and spur-dyke respectively. Experimental investigations on flow around two offshore piles arrangement carried out at Hydraulics Laboratory of The University of Liverpool are also presented in Chapter 5.

Chapter 7 simulate the jet-forced water circulation in water-supply reservoirs. Various shapes of reservoirs ranging from a simple circular shape to a more complex shape (Prescot No. 3 and No. 4 reservoirs, City of Liverpool, UK) are investigated.

Finally, the general comments and conclusions are summarised in Chapter 8.

CHAPTER

CHAPTER 2

THE GOVERNING EQUATIONS AND TURBULENCE MODELS

2.1 INTRODUCTION

The equations that describe the spatial and temporal evolution of fluid flow have been known for a long time. In this chapter, several elementary aspects of turbulent flows are briefly reviewed alongside with their representation in FLUENT. Only the most relevant aspects related to the present study are considered. For a thorough introduction to turbulence theory, one is referred to a textbook on turbulence, like Batchelor (1957) or Hinze (1975). Detailed descriptions of turbulence theory incorporated in the FLUENT package can be found in FLUENT User's Guide.

Laminar and turbulent flows alike are governed by the law of mass, momentum and energy conservation. The basic equations describing laminar flow are described first, and their extension to turbulent flow, is evaluated later.

2.2. BASIC CONSERVATION EQUATIONS FOR LAMINAR FLOWS

The conservation of mass, or continuity equation is:

$$\frac{\partial \rho}{\partial t} + \frac{\partial}{\partial x_i}(\rho u_i) = S_m \qquad (2.1)$$

Equation (2.1) is the general form of the mass conservation equation and is valid for incompressible as well as compressible flows. The source S_m is the mass added to the continuous phase from the dispersed second phase (*e.g.* due to vaporisation of liquid droplets). For a Newtonian single-phase model with constant density and viscosity, the above equation reduced to a simpler relationship given by:

$$\frac{\partial}{\partial x_i}(u_i) = 0 \qquad (2.2)$$

Conservation of momentum in the ith direction in an inertial (non-accelerating) reference frame, is described by (Navier-Stokes Equation) :

$$\frac{\partial}{\partial t}(\rho u_i) + \frac{\partial}{\partial x_j}(\rho u_i u_j) = -\frac{\partial p}{\partial x_i} + \frac{\partial \tau_{ij}}{\partial x_j} + \rho g_i + F_i \qquad (2.3)$$

where p is the static pressure, τ_{ij} is the stress tensor and, g_i and F_i are gravitational acceleration and external body forces in the i direction respectively.

The stress τ_{ij} is given by:

$$\tau_{ij} = \left[\mu\left(\frac{\partial u_i}{\partial x_j} + \frac{\partial u_j}{\partial x_i}\right)\right] - \frac{2}{3}\mu\frac{\partial u_l}{\partial x_l}\delta_{ij} \qquad (2.4)$$

where μ is the molecular viscosity and the second term on the right hand side is the effect of volume dilation. δ_{ij} is the Kronecker delta in which $\delta_{ij} = 1$ for $i = j$, and, $\delta_{ij} = 0$ for $i \neq j$.

In the present study, only isothermal flows will be considered, hence the energy (or temperature) equations will not be used. However, the conservation of energy in terms of conservation of the static enthalpy, h, is included here for completeness, and is defined as:

$$h = \sum_{i'} m_{i'} h_{i'} \tag{2.5}$$

where

$$h = \int_{T_{ref}}^{T} c_{p,i'}\, dT \tag{2.6}$$

where T_{ref} is a reference temperature and $c_{p,i'}$ is the specific heat at constant pressure of species i'.

2.3 BASIC CONSERVATION EQUATIONS FOR TURBULENT FLOWS

For laminar flow with small Reynolds number, the equations of motion can be discretised and solved directly from a computational point of view. For turbulent flows, the situation is different and more complicated. In the remainder of this chapter, the principles of the numerical simulation equations for turbulent flows are described.

Modelling of turbulent flows requires appropriate modelling procedures to describe the effects of turbulent fluctuations of velocity and scalar quantities on the basic conservation equations presented earlier. Many of the important processes in turbulent flow take place on a very small scale (*i.e.* 0.1 mm). The equations can be solved only by means of numerical techniques which calculate the dependent

variables at discrete points in the flow. The solution of one cubic centimetre domain, for example, would require 10^6 grid points of 0.1 mm mesh size in all three directions. Therefore, it would require extensive and expensive sources of computing effort, and it is impossible to solve the continuity and momentum equations for realistic turbulent flows. Fortunately, however, the design engineer is not interested in every detail of the turbulent motion, but mainly in the time-averaged velocity and pressure. The next section will present standard equations governing these quantities and their representation in FLUENT.

2.3.1 Reynolds Averaging of the Conservation Equations

The conservation equations are obtained from those for laminar flows using a time averaging procedure commonly known as Reynolds averaging.

The Reynolds averaging procedure (Hinze, 1975) for scalar equations can be illustrated using a generic transport equation for a conserved scalar quantity ϕ:

$$\underbrace{\frac{\partial}{\partial t}(\rho\phi)}_{\textit{Accumulation}} + \underbrace{\frac{\partial}{\partial x_i}(\rho u_i \phi)}_{\textit{Convection}} = \underbrace{D_\phi}_{\textit{Diffusion}} + \underbrace{S_\phi}_{\textit{Source}} \tag{2.7}$$

The value of ϕ in turbulent flow is assumed to be comprised of a mean value and a fluctuating part:

$$\phi = \overline{\phi} + \phi' \tag{2.8}$$

where $\overline{\phi}$ is the time averaged value of ϕ defined as:

$$\overline{\phi} = \frac{1}{\Delta t}\int_0^{\Delta t} \phi \; dt \tag{2.9}$$

and Δt is a time scale much larger than the largest time scale of turbulent fluctuations. Turbulent fluctuations ϕ' are assumed to be random such that:

$$\overline{\phi'} = 0 \tag{2.10}$$

Substitution of Equation 2.8 in the general conservation equation (Eq.2.7) and time integration over a sufficiently large time interval yields:

$$\frac{\partial}{\partial t}(\overline{\rho}\,\overline{\phi}) + \frac{\partial}{\partial x_i}(\overline{\rho}\,\overline{u_i}\,\overline{\phi}) = -\frac{\partial}{\partial x_i}\,(\overline{\rho u_i'\phi'}) + D_\phi + S_\phi \tag{2.11}$$

This result assumes that density fluctuations are negligible. In all the following equations, the overbar will be dropped from the averaged quantities ($\overline{\rho}$, $\overline{\phi}$, and $\overline{u}$) for the sake of convenience.

The terms in Equation 2.11 are similar to those in its laminar flow counterpart, (*e.g.* Eq. 2.1) except that each quantity now is represented by its time averaged value and a new term containing the correlation $u_i'\phi'$ appears on the right-hand side. Physically, this correlation multiplied by the density represents the transport or "diffusion" of ϕ due to turbulent fluctuations.

2.3.2 Reynolds Averaging of the Momentum Equations

In the Reynolds averaging of the momentum equations, the velocity at a point is considered as a sum of the mean (time averaged) and fluctuating components:

$$u_i = \overline{u_i} + u'_i \tag{2.12}$$

Substituting expressions of this form into the basic momentum balance (and dropping the overbar on the mean velocity) yields the ensemble-averaged momentum equations for predicting turbulent flows (Hinze, 1975):

$$\frac{\partial}{\partial t}(\rho u_i) + \frac{\partial}{\partial x_j}(\rho u_i u_j) = \frac{\partial}{\partial x_j}\left(\mu\left[\frac{\partial u_i}{\partial x_j} + \frac{\partial u_j}{\partial x_i}\right] - \left(\frac{2}{3}\mu\frac{\partial u_l}{\partial x_l}\right)\right)$$

$$- \frac{\partial p}{\partial x_i} + \rho g_i + F_i + \frac{\partial}{\partial x_j}(\rho\overline{u'_i u'_j}) \qquad (2.13)$$

Equation 2.13 has the same form as fundamental momentum balance (Equation 2.8) with velocities now representing time averaged (or mean-flow) values and the effect of turbulence incorporated through the "Reynolds stresses", $\overline{\rho u'_i u'_j}$. Note that $\overline{u'_i u'_j}$ is an asymmetric second order tensor since:

$$\overline{u_i' u_j'} = \overline{u_j' u_i'} \qquad (2.14)$$

and hence has six unique terms. The stress represents the transfer of momentum by the turbulent motion. Because of its presence, Equations 2.11 and 2.13 do not constitute a closed set.

In order to close the system, some of the correlations are usually approximated in terms of quantities that can be calculated. "Model" assumptions about turbulence are thereby introduced which may not always be realistic. Instead of the real turbulent fluid we thus consider an idealised "model" fluid which is governed by the laws prescribed as "turbulence model". By a "model of turbulence" Launder and Spalding (1972) mean: " *a set of equations which when solved with the mean flow equations, allow calculation of the relevant correlations and so simulate the behaviour of real fluids in important respects*".

2.4 MODELS FOR TURBULENT FLOWS

The main task of a turbulence model is to provide expressions or closure models that allow the evaluation of the correlations of the unique terms mentioned earlier in term of mean flow quantities. The number of turbulence models suggested in the literature over the last decades is rather large. The developments of the turbulent models classified as One-Equation Models, Two Equation Models and Multi-equations Models can be found in many turbulence textbooks, among others Launder and Spalding (1972). In this section, the standard turbulence closure models incorporated in FLUENT are discussed. The models are:

i) the standard k-ε model

ii) the Differential Reynolds Stress Model (RSM), and

iii) the ReNormalization Group (RNG) k-ε model.

2.4.1 The Standard k-ε Turbulence Model

The standard k-ε model has been the workhorse of engineering turbulence models for more than two decades and has the desirable properties of robustness, economy, and a fairly wide domain of applicability. The model is an eddy-viscosity model in which the Reynolds stresses are assumed to be proportional to the mean velocity gradients, with the constant of proportionality being the turbulent eddy viscosity, μ_t. This assumption, known as the Boussinesq hypothesis, provides the following expression for the Reynolds stresses (Hinze, 1975):

$$\rho \overline{u_i' u_j'} = \rho \frac{2}{3} k \delta_{ij} - \mu_t \left(\frac{\partial u_i}{\partial x_j} + \frac{\partial u_j}{\partial x_i} \right) + \frac{2}{3} \mu_t \frac{\partial u_l}{\partial x_l} \delta_{ij} \qquad (2.15)$$

Here k is the turbulent kinetic energy :

$$k = \frac{1}{2}\sum_i \overline{u_i'^2} \tag{2.16}$$

FLUENT ignores the term $\frac{2}{3}\mu_t \frac{\partial u_l}{\partial x_l}$ under the assumption that the divergence of velocity has a negligible effect on the turbulence stress sensor.

Equation 2.15 for the Reynolds stresses is analogous to that describing the shear stresses arising in laminar flow (Equation 2.4) with the turbulent viscosity μ_t playing the same role as the molecular viscosity μ. Therefore the form of Reynolds averaged momentum equations remains identical to the form of the laminar momentum (Equation 2.3) except that μ is replaced by an effective viscosity μ_{eff}:

$$\mu_{eff} = \mu + \mu_t \tag{2.17}$$

The turbulent or eddy viscosity μ_t is obtained by assuming that it is proportional to the product of a turbulent velocity scale and length scale. In the k-ε model, these velocity and length scales are obtained from two parameters: k, the turbulent kinetic energy and ε, the dissipation rate of k. The velocity scale is taken to be $\sqrt{k}$ and the length scale is taken to be $\sqrt{k^3}/\varepsilon$. Hence μ_t is given by:

$$\mu_t = \rho\, C_\mu \frac{k^2}{\varepsilon} \tag{2.18}$$

where C_μ is an empirically derived constant of proportionality (set to a default value 0.09 in FLUENT).

The values of k and ε are obtained by solution of the conservation equations (Launder and Spalding, 1972):

$$\frac{\partial}{\partial t}(\rho k) + \frac{\partial}{\partial x_i}(\rho u_i k) = \frac{\partial}{\partial x_i}\left(\frac{\mu_t}{\sigma_k} \frac{\partial k}{\partial x_i} \right) + G_k + G_b - \rho\varepsilon \tag{2.19}$$

$$\frac{\partial}{\partial t}(\rho\varepsilon) + \frac{\partial}{\partial x_i}(\rho u_i \varepsilon) = \frac{\partial}{\partial x_i}\left(\frac{\mu_t}{\sigma_\varepsilon} \frac{\partial \varepsilon}{\partial x_i} \right) +$$

$$C_{1\varepsilon}\frac{\varepsilon}{k}(G_k + (1 - C_{3\varepsilon})G_b) - C_{2\varepsilon}\rho\frac{\varepsilon^2}{k} \tag{2.20}$$

where $C_{1\varepsilon}$, $C_{2\varepsilon}$ and $C_{3\varepsilon}$ are empirical constants, σ_k and σ_ε are "Prandtl" numbers governing the turbulent diffusion of k and ε, G_k is the rate of production of turbulent kinetic energy:

$$G_k = \mu_t \left(\frac{\partial u_j}{\partial x_i} + \frac{\partial u_i}{\partial x_j} \right) \frac{\partial u_i}{\partial x_i} \tag{2.21}$$

and G_b is generation of turbulence due to buoyancy:

$$G_b = -g_i \frac{\mu_t}{\rho\sigma_h} \frac{\partial \rho}{\partial x_i} \tag{2.22}$$

The coefficients are empirical constants which have the following empirically derived values (Launder and Spalding, 1972) :

$$C_{1\varepsilon} = 1.44,\ C_{2\varepsilon} = 1.92,\ C_{3\varepsilon} = 0.09,\ \sigma_k = 1.0,\ \sigma_\varepsilon = 1.3$$

2.4.1.1 Boundary Conditions for k and ε at the Walls

FLUENT uses an equilibrium assumption to derive the boundary conditions for k and ε. Under this assumption, the production and dissipation of turbulence are assumed to be equal in the boundary layer, implying the following boundary condition for the dissipation rate in the near-wall cells (Launder and Spalding, 1972) :

$$\varepsilon_p = \frac{C_\mu^{\frac{3}{4}} k_p^{\frac{3}{2}}}{\kappa y_p} \tag{2.23}$$

The near-wall value for k is computed by solving the complete transport equation for k in the near-wall control volume, with the wall shear stress included in the production term and zero normal gradient assumed for k at the wall.

FLUENT applies wall functions for the calculation of shear stress in the turbulent boundary layer at wall boundaries.

One major limitation of the k-ε model is that μ_t is isotropic. This implies that the velocity and length scales are the same in all directions. In complex flows, such as highly swirling flows, the velocity and length scales can vary significantly with direction. For such flows the k-ε model is inadequate and can produce physically incorrect results. The RSM, which computes the individual Reynolds stresses, provides a better alternative in such cases, and is discussed next.

2.4.2 The Reynolds Stress Model (RSM)

The RSM model involves solving the transport equations for the individual stresses $\overline{u_i' u_j'}$. These transport equations can be derived from the momentum equation. The resulting equation for component i is multiplied by the fluctuating velocity u_j, and the equation for the component j is multiplied by u_i. Summation of the two equations, and subsequent time-averaging yields the desired equation for the individual stresses $\overline{u_i' u_j'}$ (detailed derivation can be found in Hinze, 1959). The equation contains triple order velocity correlations and pressure velocity correlations that must be modeled to obtain closure. The RSM used in FLUENT uses the following equations (Launder *et al*, 1975):

$$\frac{\partial \overline{u_i' u_j'}}{\partial t} + u_k \frac{\partial \overline{u_i' u_j'}}{\partial x_k} = \frac{\partial}{\partial x_k}\left(\frac{\nu_t}{\sigma_k}\frac{\partial \overline{u_i' u_j'}}{\partial x_k}\right) + P_{ij} + \Phi_{ij} - \varepsilon_{ij} + R_{ij} \qquad (2.24)$$

Where P_{ij} is the stress production rate, Φ_{ij} is a source/sink due to the pressure/strain correlation, ε_{ij} is the viscous dissipation and R_{ij} is the rational term.

The production term is computed without modelling assumptions as:

$$P_{ij} = -\left(\overline{u_i' u_k'}\frac{\partial u_j}{\partial x_k} + \overline{u_j' u_k'}\frac{\partial u_i}{\partial x_k}\right) \qquad (2.25)$$

The pressure-strain term redistributes the energy among its components (when $i = j$) and reduces shear stresses (when $i \neq j$). this term therefore tends to make turbulence more isotropic and is modeled as:

$$\Phi_{ij} = -C_3\frac{\varepsilon}{k}\left(\overline{u_i' u_j'} - \frac{2}{3}\delta_{ij}k\right) - C_4\left(P_{ij} - \frac{2}{3}\delta_{ij}P\right) \qquad (2.26)$$

where $P = \frac{1}{2} P_{ii}$, and C_3 and C_4 are empirical constants whose values are $C_3 = 1.8$ and $C_4 = 0.60$.

The dissipation term is approximated by the isotropic dissipation rate ε:

$$\varepsilon_{ij} = \frac{2}{3}\delta_{ij}\varepsilon \qquad (2.27)$$

This assumption is reasonable for high Reynolds number flows where the small-scale motions responsible for the dissipation of turbulence are isotropic. ε is derived by solution of Equation (2.20)

FLUENT uses the standard equilibrium wall function to compute shear stresses at wall boundaries when the RSM model is used. Wall functions are also used to compute the near-wall boundary condition for the individual Reynolds stresses as given below.

2.4.2.1 Boundary Conditions for the Reynolds Stresses

At flow inlets FLUENT requires values for each Reynolds stress, $\overline{u_i' u_j'}$, and for the turbulent dissipation rate, ε. These quantities can be input directly or derived from the turbulence intensity and characteristic length. At walls, FLUENT computes the near-wall values of the Reynolds stresses and ε from wall functions in the orthogonal coordinate system uniquely defined by the wall normal vector (η) and

the streamwise tangent vector (τ) *i.e.* $\lambda = \tau \times \eta$. To determine the isotropic turbulence production term P, it is assumed that the production and dissipation of turbulence near the wall is equal. This assumption, together with the "law of the wall", determines the turbulence production uniquely. The production tensor P_{ij} determined in the η, τ, λ coordinate system is then transformed to the Cartesian (or cylindrical) coordinate system as required. These transformed tensor components are subsequently used in the Reynolds stress transport equations in the near-wall region.

2.4.3 Renormalization Group Theory-Based Model (RNG)

FLUENT also incorporates a modified k-ε model based on Renormalization-Group (RNG) theory. Since the appearance of this algebraic turbulence model, its practical applications to turbulence problem have been significant. Its first application to engineering calculation was proposed by Martinelli *et al.* (1988). This powerful RNG-based k-ε turbulence model provides both accuracy and efficiency in the modelling of turbulent flows. This model follows the two equation turbulence modelling framework and has been derived from the original governing equations for fluid flow using mathematical techniques called Renormalization Group (RNG) methods.

The RNG k-ε model differs from the standard k-ε two-equation turbulence model and its variant in several important ways:

(i) Constants and functions in the RNG model are evaluated by the theory and not by empiricism. The model, therefore, is widely applicable without modification.

(ii) Low-Reynolds-number effects are included in the RNG theory, permitting laminar-like behaviour to be predicted.

(iii) New terms appear in the dissipation rate transport equation including a rate-of-strain term, which is important for the treatment of nonequilibrium effects and flows in the rapid distortion limit (e.g. separated flows and stagnation flows).

(iv) The turbulence transport equations are extended to permit predictions of swirling flows.

One important shortcoming of the standard k-ε model is that spuriously high generation rates of turbulence energy are predicted around impingement points or other regions of high strain rate or streamline curvature (Launder and Spalding, 1973). This excess of turbulence energy, according to them, creates high levels of turbulent viscosity. As the spurious turbulence energy is convected downstream, the high turbulent viscosity tends to overpredict mixing and to suppress separation and/or fluctuations which result in vortex shedding. The RNG k-ε model, on the other hand, accounts for these normal stresses and high rates of strain and yields much better accuracy.

2.4.3.1 Mathematical Description of the RNG k-ε Model.

Renormalization group (RNG) methods are a general framework for "model building" in which the complex dynamics of physical problems are described in terms of so-called "coarse-grained" equations of motion governing the large-scale, long-time behaviour of the physical system.

The mathematics of RNG theory allows similar coarse-graining of physical phenomena and has been applied to a range of physical processes including critical

phenomena, high-energy particle physics, and, in the context of fluid dynamics, turbulence, combustion and heat transfer. The key idea is that the RNG method is applicable to scale-invariant problem phenomena lacking externally imposed characteristic length and time scales. For turbulence, this means that the method can describe the small scale (small eddies) that should be statistically independent of the external initial conditions and dynamical forces that create them through various kinds of instability phenomena. In other words, the RNG method gives a theory of the Kolmogorov equilibrium range of turbulence, comprising the so-called inertial range of small-scale eddies whose energy spectrum follows the famous Kolmogorov law $E(k) \alpha k^{-5/3}$. The importance of the RNG approach is that once the inertial range eddies can be accounted for in a quantitatively correct way, we may then obtain coarse-grained equations of motion for the other relevant variables of the turbulence, including the mean velocity, rms velocities, etc.

Turbulent flows have eddies that range in size from so-called "energy-containing eddies" of size L, the integral scale, down to eddies of size $L/Re^{3/4}$, where $Re = v_{rms}L/\nu$ is the Reynolds number. Still smaller eddies exist, but they have exceedingly low energy due to viscous dissipation. Thus accurate solution of the three-dimensional Navier Stokes equations for a turbulent flow requires storage of order $O(Re^{9/4})$ and computational work of order $O(Re^3)$. If Re is large, these computational requirements are enormous. RNG methods reduce this computational requirement by eliminating the inertial-range eddies from the equations of motion, yielding equations for averaged flow quantities at the integral scale of the turbulence.

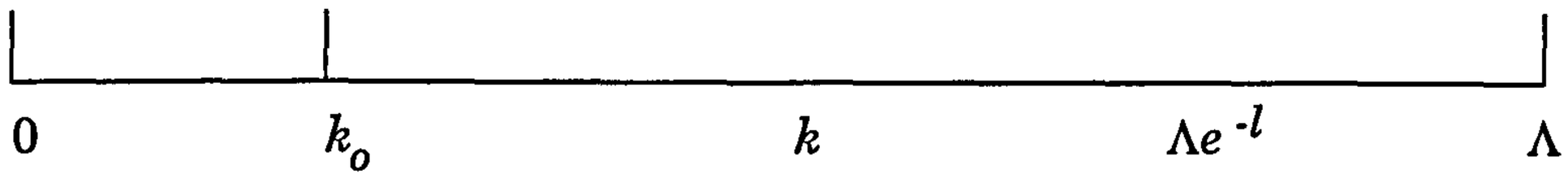

Figure 2-1 : Scales of Effective Excitation in Turbulence (after FLUENT Inc)

Figure 2.1 shows the scales of effective excitation in turbulence, ranging from the low wavenumber $k_o = 2\pi/L$ (large-scale eddies) to the high wavenumber viscous cutoff Λ (smallest-energy-containing eddies). The idea of the RNG method is to remove narrow band of modes near Λ by representing these modes in terms of lower modes in the interval $k_o < k < \Lambda e^{-\ell}$ ($\ell << 1$). When this narrow band of modes is removed, the resulting equations of motion for the remaining modes constitute a modified system of Navier-Stokes equations in which there is a modified (effective) viscosity, modified force, and modified nonlinear coupling. Once the first band of modes is removed from the dynamics, the process of removal of degrees of freedom is repeated iteratively, so that more and more modes are removed from the dynamics as illustrated schematically in Figure 2.2. In this way, the RNG method gives an effective calculus for the removal of modes from the Navier-Stokes equations, thereby rendering them computable on relatively coarser grids at high Reynolds number.

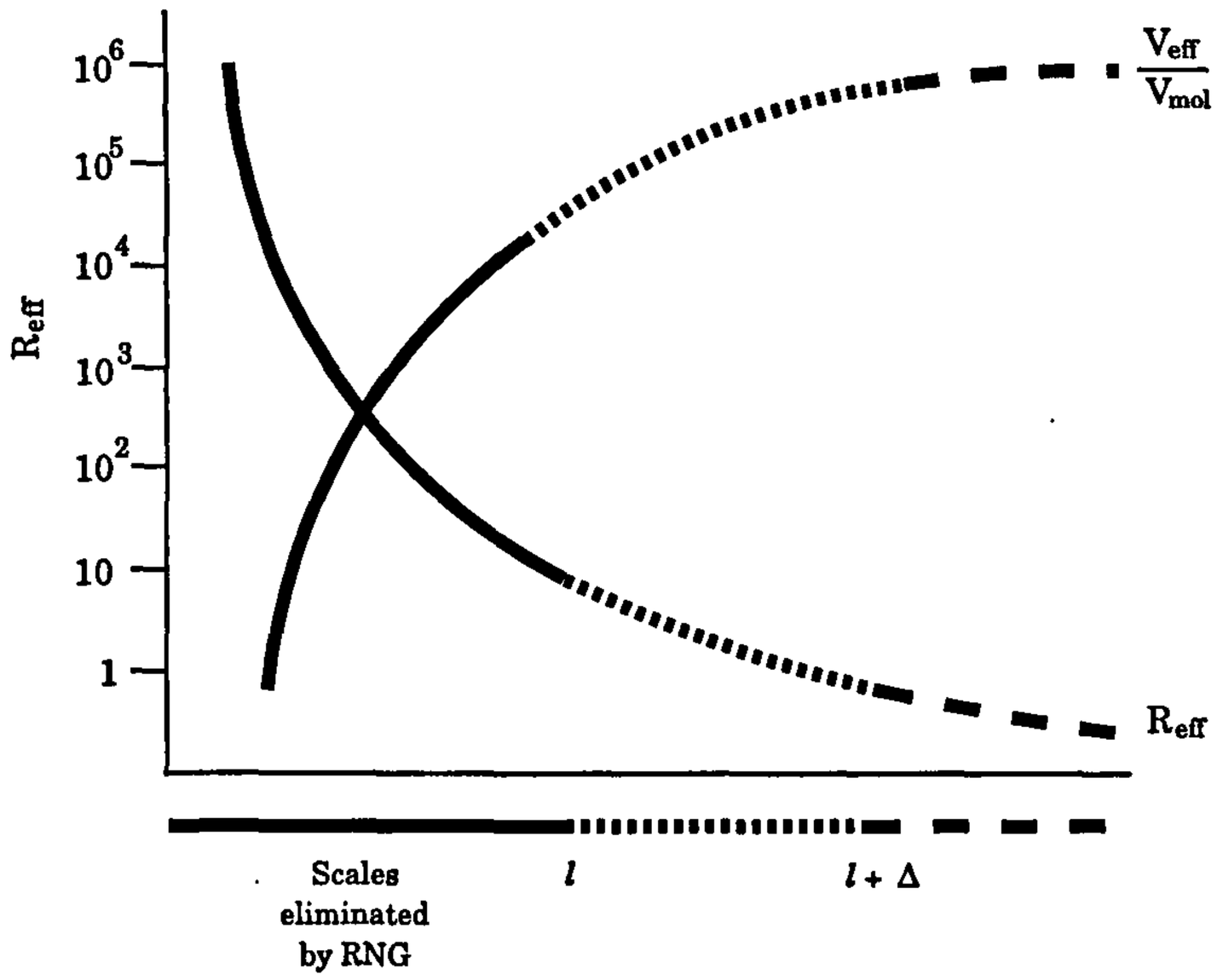

Figure 2.2: Modification of the Effective Reynolds Number and Viscosity by the Scale Elimination Procedure (after FLUENT Inc)

2.4.3.2 Evaluation of the Effective Viscosity in the RNG k-ε Model

Through the elimination procedure outlined above, RNG theory develops an equation for the variation of effective viscosity with Reynolds number, which is of the form:

$$\frac{d\nu}{d\ell} = \frac{A\varepsilon\ell^3}{[\ \nu(\ell)\ ]^2} \tag{2.28}$$

where A is constant derived by the RNG theory.

Integration of the equation over the eddy length scale, noting that $\nu = \nu_{mol}$ when $\ell = \ell_d$ (where ℓ_d is the Kolmogorov dissipation scale $L/Re^{3/4}$), gives:

$$\nu(\ell) = \nu_{mol}\left[1 + \frac{3A\varepsilon}{4\nu_{mol}^3}(\ell^4 - \ell_d^4)\right]^{\frac{1}{3}} \qquad (\ell \geq \ell_d) \qquad (2.29)$$

The above equation gives an interpolation formula for $\nu(\ell)$ between the molecular viscosity ν_{mol} valid at dissipation scales and the high Reynolds-number limit of L >> ℓ_d, thus:

$$\nu \approx \nu_t = \left[0.094L\right]^2 \, |\nabla \overline{u}| \qquad (2.30)$$

where ν_t is the turbulent viscosity (ν_{eff} - ν_{mol}). This result is remarkably close to Prandtl's classical mixing length theory (which was derived originally as a semi-empirical fit to experimental data). Noting that the total kinetic energy contained in the inertial range eddies of scale less than L is $k = 0.71\varepsilon^{2/3}L^{2/3}$, therefore ν_t becomes:

$$\nu_t = C_\mu \frac{k^2}{\varepsilon} \qquad (2.31)$$

with C_μ = 0.0845. This result of the RNG theory is very close to the standard k-ε model expression for effective viscosity in which C_μ is empirically determined to be 0.09. FLUENT's RNG k-ε model, however, extends the prediction of effective viscosity beyond this high Reynolds number limit, computing ν_{eff} using Equation 2.29, recast in terms of k and ε. The result is a differential relationship between ν_{eff} and $k/\sqrt{\varepsilon}$; a simplified algebraic form of the relationship is given as:

$$\nu_{eff} = \nu_{mol}\left[1 + \sqrt{\frac{C_\mu}{\nu_{mol}}}\frac{k}{\sqrt{\varepsilon}}\right]^2 \tag{2.32}$$

FLUENT's RNG k-ε model employs this equation in its calculation of effective viscosity, yielding an accurate description of how the effective turbulent transport varies with the effective Reynolds number (or eddy scale), allowing accurate extension of the model to low-Reynolds number and near-wall flows.

The transport equations for k and ε in the RNG model are (Yakhot *et al*, 1986):

$$\frac{\partial k}{\partial t} + u_i\frac{\partial k}{\partial x_i} = \nu_t S^2 - \varepsilon + \frac{\partial}{\partial x_i}\alpha\nu_t\frac{\partial k}{\partial x_i} \tag{2.33}$$

and

$$\frac{\partial \varepsilon}{\partial t} + u_i\frac{\partial \varepsilon}{\partial x_i} = C_{1\varepsilon}\frac{\varepsilon}{k}\nu_{tS}^2 - C_{2\varepsilon}\frac{\varepsilon^2}{k} - R + \frac{\partial}{\partial x_i}\alpha\nu_t\frac{\partial \varepsilon}{\partial x_i} \tag{2.34}$$

where α is the inverse Prandtl number for turbulent transport. The rate-of-strain term R is given by:

$$R = 2\nu_{mol}S_{ij}\overline{\frac{\partial u_l}{\partial x_i}\frac{\partial u_l}{\partial x_j}} \tag{2.35}$$

This term is expressed in the RNG k-ε model equations as:

$$R = \frac{C_\mu\eta^3(1 - \eta/\eta_o)}{1+\beta\eta^3}\frac{\varepsilon^2}{k} \tag{2.36}$$

where $\eta = Sk/\varepsilon$, $\eta_o \approx 4.38$, and $S^2 = 2S_{ij}S_{ij}$ is the modulus of rate-of-strain tensor. The RNG theory gives values of the constants $C_{1\varepsilon} = 1.42$ and $C_{2\varepsilon} = 1.68$ and $\alpha = 1.39$ in comparison with the "standard" values $C_{1\varepsilon} \approx 1.4$ and $C_{2\varepsilon} \approx 1.9$, and $\alpha = 1$. The reduced value of $C_{2\varepsilon}$ decreases both k and ε, leading to smaller values of ν_{eff}. In regions of small strain rate, the term R tends to increase ν_{eff} slightly but still typically smaller than its value in the standard theory. However, in regions of large strain rate, the sign of R is changed and ν_{eff} is decreased even more. This feature partially accounts for the strong anisotrophy in regions of large shear and is responsible for some of the marked improvement of the RNG model in the treatment of massive flow separation and anisotropic large-scale eddies.

2.5 SHEAR STRESS CALCULATIONS AT WALLS

Solution of the momentum equation (2.3), in the near wall region requires a description of the near-wall pressure gradient and shear-stress. The pressure gradient is assumed to be zero at wall. In laminar flows, the shear stress at the wall is calculated as:

$$\tau_w = \mu \frac{\partial u}{\partial n}\Big|_{wall} \approx \mu \frac{\Delta u}{\Delta n} \tag{2.37}$$

where u is the velocity component parallel to the wall and n is the coordinate normal to the wall. Δu and Δn are determined using values stored in the computational cell adjacent to the wall.

Wall functions are empirical functions used at the near wall grid point to estimate the effect of the wall on turbulent flow. These functions are used in lieu of

resolving the entire turbulent boundary layer. This eliminates the need to fully resolve all regions of a turbulent boundary layer and allows the near wall grid point to be placed relatively far from the wall (in the log region of the turbulent boundary layer). This approach thus reduces the computer effort required for turbulent flows simulation.

In turbulent flows FLUENT employs Launder and Spalding's (1972) log-law of the wall to compute the wall shear stress:

$$\frac{uC_\mu^{\frac{1}{4}}k^{\frac{1}{2}}}{\frac{\tau_w}{\rho}} = \frac{1}{\kappa}\ln(Ey^*) \tag{2.38}$$

which under equilibrium conditions reverts to the standard log-law:

$$\frac{u}{u_*} = \frac{1}{\kappa}\ln(Ey^*) \tag{2.39}$$

where $u_* = \sqrt{\tau_w/\rho}$, u is the fluid velocity at a point in the log-law layer, κ is von-Karman's constant, E is an empirical constant by default equal to 9.8 (smooth wall), and y^+ is the dimensionless distance from the wall:

$$y^* = \frac{C_\mu^{\frac{1}{4}}\rho k_p^{\frac{1}{2}}y}{\mu} \tag{2.40}$$

By assuming local equilibrium conditions and constant shear stress in the turbulent boundary layer, Equation 2.40 becomes:

$$y^* = \frac{\rho u_* y}{\mu} \tag{2.41}$$

FLUENT applies Equation 2.38 in turbulent flows when $y^+ > 11.225$. When y^+ falls below this value, the near wall-cell centre lies in the viscous sublayer of the turbulent boundary layer. FLUENT then reverts to Equation 2.37 for calculation of the wall shear stress since the wall function is not valid in the sublayer.

In addition to the standard wall function described above, a two-layer based nonequilibrium wall function is also provided in FLUENT for turbulent flows. This wall function uses the same linear-logarithmic laws for velocity as the standard wall function, but it relaxes the local equilibrium assumption i.e. production = dissipation) which is adopted by the standard wall function in computing the budget of the turbulent kinetic energy at wall-neighbouring cells. Thus, the two-layer wall function, in effect, partly accounts for nonequilibrium effects neglected in the standard wall function. Detailed derivation of the method is given in FLUENT's User Guide.

2.6 BED ROUGHNESS PARAMETERS

FLUENT enables users to include the effect of bed roughness through determination of the wall parameters termed as CAPPA and ELOG. CAPPA is von Karman's constant, κ, and is equal to 0.42. ELOG is the wall roughness parameter. The default value for ELOG is 9.8 which describes a smooth wall. Determination of ELOG for non-smooth walls is described below.

If the average roughness height K_s is such that $K_s^+ = \rho K_s u_* / \mu$ is of the order of 10 - 12, the roughness entirely obscures the viscous sublayer and the near wall flow is independent of viscosity. The logarithmic law of the wall (Equation 2.39) then becomes:

$$\frac{u}{u_*} = \frac{1}{\kappa}\ln(Ey^+) \quad - \quad \Delta B\ (K_s^+) \tag{2.42}$$

where ΔB is the amount by which the rough wall velocity profile shifts downward. It depends on the dimensionless roughness K_s^+ and can be approximated as:

$$\Delta B = \frac{1}{\kappa}\ln K_s^+ - 3.0 \approx \frac{1}{\kappa}\ln(0.3K_s^+) \tag{2.43}$$

Substituting the above equation in (2.42) and equating to (2.39) yields the modified value of the parameter ELOG (E'):

$$E' = \frac{E}{(1 + 0.3K_s^+)} \tag{2.44}$$

where E is the empirical constant taken as 9.8. K_s^+ can be estimated from the following relationship:

$$K_s^+ = \frac{K_s}{d}\, Re_d \sqrt{\frac{\lambda}{8}} \tag{2.45}$$

where λ is the friction factor obtained from the roughness height K_s and Reynolds number based on the hydraulic diameter d.

2.7 COMPUTATIONAL TECHNIQUES IN FLUENT

FLUENT uses a control volume based technique to solve the conservation equations for mass, momentum, energy and turbulence quantities described in the preceding sections. This control volume based technique consists of (Patankar, 1980):

1. Division of the domain into discrete control volumes, using a general curvilinear grid (see Figure 2.3)

2. Integration of the governing equations on the individual control volumes to construct the algebraic equations for discrete unknowns (velocities and scalars).

3. Solution of the discretised equations.

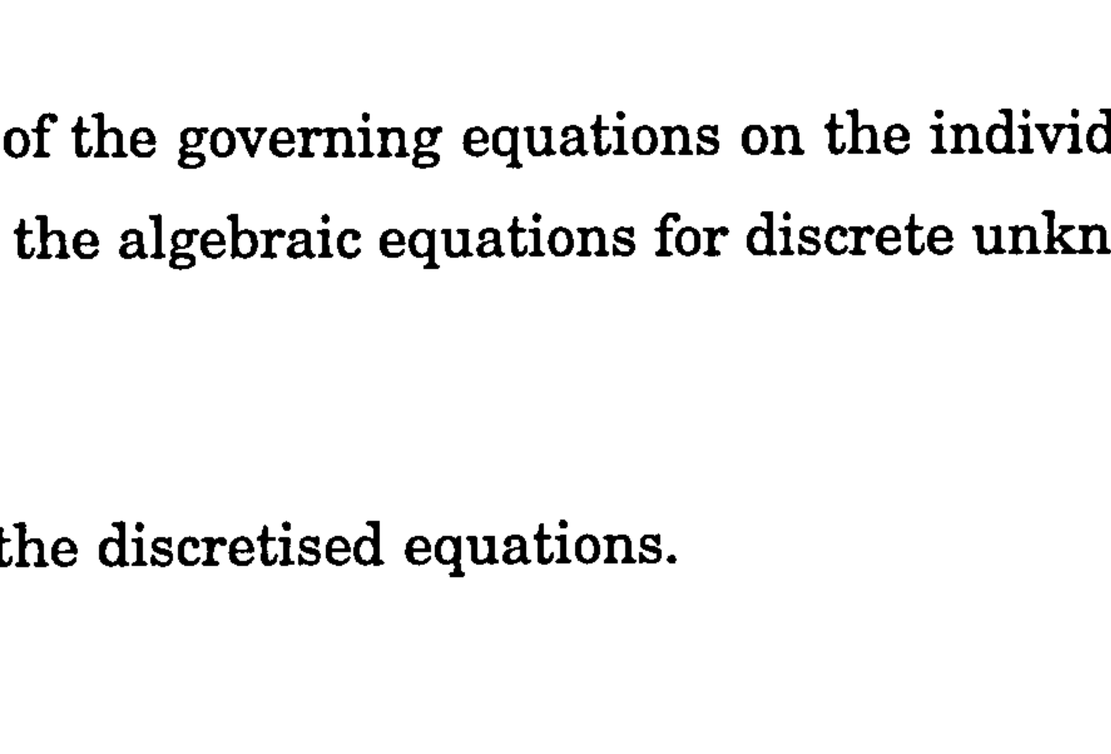

Figure 2.3 : Non-Staggered Control Volume Storage Scheme

The interpolation is accomplished either using the Power Law, Blended Second Order Upwind/Central Difference, or QUICK interpolation schemes. The procedures of the abovementioned techniques, as well as the velocity-pressure coupling termed as SIMPLE and SIMPLEC, are summarised in the following sections. Detailed descriptions of the techniques are given in the FLUENT User's Guide.

2.7.1 The Power Law Scheme

The power law interpolation scheme interpolates the face value of a variable, ϕ, using the exact solution to a one-dimensional convection-diffusion equation. This one dimensional equation describes the flux of ϕ as:

$$\frac{\partial}{\partial x}(\rho u \phi) = \frac{\partial}{\partial x}\Gamma\frac{\partial \phi}{\partial x} \tag{2.46}$$

where Γ and ρu are constant across the interval ∂x. This equation can be integrated to yield the following solution describing how ϕ varies with x:

$$\frac{\phi(x) - \phi_0}{\phi_L - \phi_0} = \frac{\exp(Pe\,\frac{x}{L}) - 1}{\exp(Pe) - 1} \tag{2.47}$$

where:

$$\phi_0 = \phi|_{x=0}$$
$$\phi_L = \phi|_{x=L}$$

and Pe is the Peclet number given as:

$$Pe = \frac{\rho u L}{\Gamma} \tag{2.48}$$

FLUENT uses Equation (2.47) in an equivalent "power-law" format (Patankar, 80) as its default interpolation scheme.

The variation of $\phi(x)$ between $x = 0$ and $x = L$ is depicted in Figure 2.4 for a range of values of the Peclet number. It can be seen that for large Pe, the value of ϕ at $x = L/2$ is approximately equal to the upstream value. This implies that when the flow is dominated by convection, interpolation can be accomplished by simply letting the face value of a variable be set equal to its "upwind" or upstream value. When the $Pe = 0$ (no flow, or pure diffusion), Figure 2.4 shows that ϕ may be interpolated via a simple linear average between the values at $x = 0$ and $x = L$.

When the Peclet number has an intermediate value, the interpolated value for ϕ at $x = L/2$ must be derived by applying the "power law" equivalent of Equation 2.47.

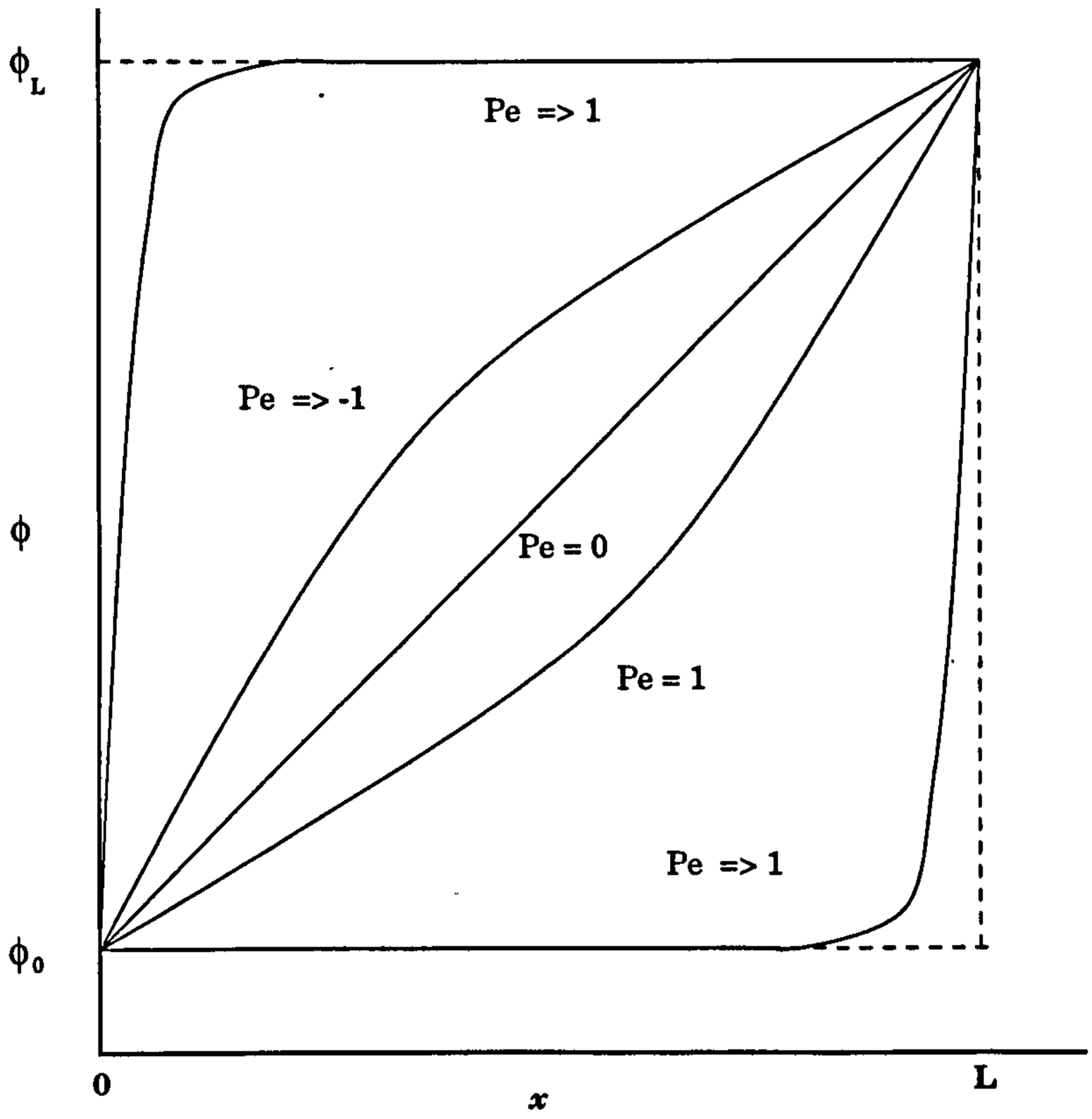

Figure 2.4 : Variation of a Variable ϕ Between x=0 and x=L (Eq. 2.46)

(after FLUENT Inc.)

2.7.2 Higher order Interpolation Schemes

As an alternative to the Power-Law Differencing Scheme, FLUENT provides two higher order schemes : QUICK (Leonard, 1979) and a blended Second Order Upwind/Central Difference scheme. These schemes compute the face value of an

unknown (*e.g.* ϕ_f) based on the values stored at the two adjacent cell centers (ϕ_P and ϕ_E) and on a third cell center at an additional upstream point (*e.g.* ϕ_W). Using the nomenclature depicted in Figure 2.5, the face value can be written in terms of these neighbour values as:

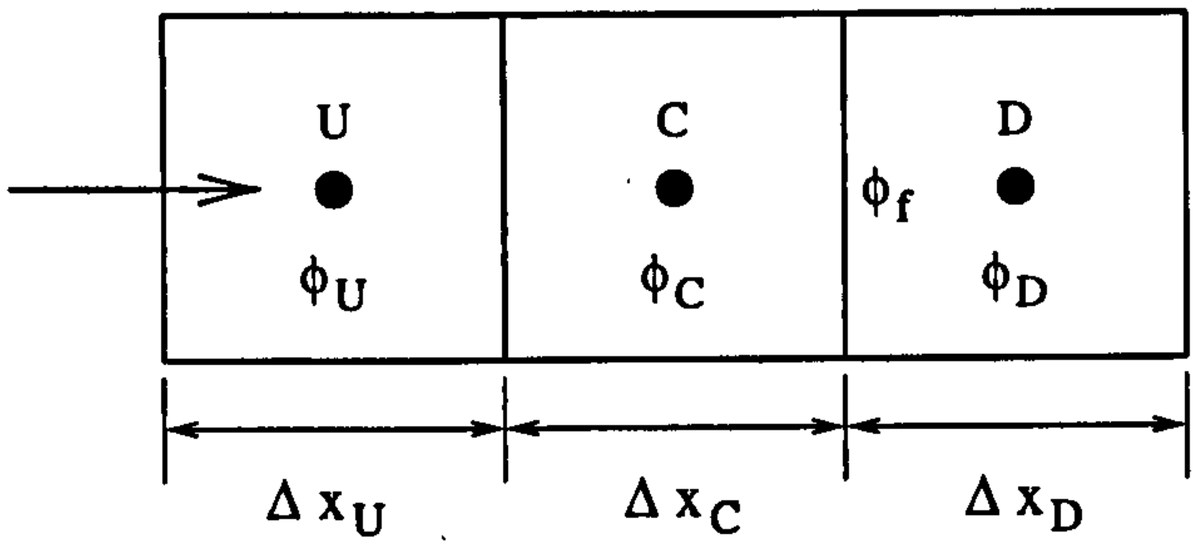

Figure 2.5 : Central, Downwind, and Upwind Cell Nomenclature Employed in the Higher Order Interpolation Scheme (after FLUENT Inc.)

$$\phi_f = \theta \left[\frac{\Delta x_D}{\Delta x_C + \Delta x_D} \phi_C + \frac{\Delta x_C}{\Delta x_C + \Delta x_D} \phi_D \right] + (1 - \theta) \left[\frac{\Delta x_U + 2\Delta x_C}{\Delta x_U + \Delta x_C} \phi_C - \frac{\Delta x_C}{\Delta x_U + \Delta x_C} \phi_U \right] \quad (2.49)$$

where ϕ_f is the face value, ϕ_D is the downstream value, ϕ_C is the cell center value and ϕ_U is the upstream value. Equation 2.49 computes the face value with second or third order accuracy, depending upon the choice of θ, as shown in Table 2.1

TABLE 2.1 : Values of θ in Common Discretisation Schemes

Discretisation Scheme	θ
Second-Order Central Difference	1
Second-Order Upwind	0
QUICK	3/4
Third-Order Upwind	2/3

2.7.3 The Pressure-Velocity Coupling Algorithms

The continuity and momentum equations, in three dimensions, provide four equation for solution of four unknowns: u_1, u_2, u_3 and p. Simultaneous solution of this (linearised) equation set would provide a solution in which all four unknowns satisfy each of the (linearised) mass and momentum equations. Because a simultaneous solution is computationally intensive, the equations are solved sequentially. In the sequential solution process, an equation describing the update of pressure is required, and is not explicitly available via the mass or momentum balances. The SIMPLE (Semi-Implicit Method for Pressure-Linked Equations) family of algorithms (Patankar, 1980) is based on using a relationship between velocity and pressure corrections in order to recast the continuity equation in terms of a pressure correction calculation.

The discretised one-dimensional momentum equation can be written in a shortened notation as:

$$A_P u_P = \sum_{NB} A_{NB} u_{NB} + (p_w - p_e)A + S \qquad (2.50)$$

where A_P and A_{NB} are coefficients containing the convection and diffusion contributions in the momentum equation, Equation 2.50, and the subscript *NB* refers to neighbour points (*e.g. E, W* in 1D or *E, W, N, S* in 2D).

2.7.3.1 The SIMPLE Algorithm

The SIMPLE (Semi-Implicit Method for Pressure-Linked Equations) algorithm starts with substitution of a guessed pressure field, p^*, into the momentum equations which can be solved to obtain a "guessed" velocity field, u^*:

$$A_P u_P^* = \sum_{NB} A_{NB} u_{NB}^* + (p_w^* - p_e^*)A + S \qquad (2.51)$$

Equation 2.51 is solved for the "guessed" velocity field (*e.g.* u^*_P). The actual velocity and pressure fields are related to the "guessed" values, u^*_P and p^*, and:

$$u_P = u_P^* + u_P' \qquad (2.52)$$

$$p_e = p_e^* + p_e' \qquad (2.53)$$

where u'_P and p'_e are the velocity correction and pressure correction, respectively. Substitution of Equations 2.52 and 2.53 into Equation 2.50, followed by substraction of 2.51, yields a "momentum balance" in terms of the velocity and pressure corrections:

$$A_P u_P' = \sum_{NB} A_{NB} u_{NB}^* + (p_w' - p_e')A + S \qquad (2.54)$$

Equation 2.54 is used to relate the pressure and velocity corrections as:

$$u_P' = \frac{1}{A_P}(p_w' - p_e') \qquad (2.55)$$

where the term containing the neighbour influences ($\Sigma_{NB}A_{NB}u'_{NB}$) is simply dropped for convenience (and will be zero at convergence since it involves only velocity corrections at the neighbour points).

Equations similar to Equation 2.55 are used to cast the continuity equation in terms of an equation for the pressure correction. The basic mass balance:

$$(\rho uA)_e - (\rho uA)_w = 0 \tag{2.56}$$

is first written in terms of the velocity $u^* + u'$:

$$(\rho A)_e(u^* + u')_e - (\rho A)_w(u^* + u')_w = 0 \tag{2.57}$$

Using equations like Equation 2.55, the continuity equation can be recast as an equation for the pressure correction:

$$\begin{aligned}(\rho Au^*)_e - (\rho Au^*)_w + (\rho A)_e\frac{1}{(A_P)_e}(p_P' - p_E') \\ -(\rho A)_w\frac{1}{(A_P)}(p_W' - p_P') = 0\end{aligned} \tag{2.58}$$

Equation 2.58 can now be solved for a correction to the pressure-field which is then used to compute the velocity correction via Equation 2.55. Finally, the velocity and pressure are updated via Equations 2.52 and 2.53.

2.7.3.2 The SIMPLEC Algorithm

The SIMPLEC algorithm is a variant on the standard SIMPLE algorithm desribed above. The term C in SIMPLEC stands for consistent, because the inventors of this algorithm felt that it was more consistent than the SIMPLE algorithm. The derivation of SIMPLEC is the same as that for SIMPLE from Equations 2.50-2.54. From that point on, the SIMPLEC derivation proceeds as follows.

Equation 2.54 is used to relate the velocity and pressure corrections, after substraction of a new term, ($\sum_{NB} A_{NB} u'_P$) from both the left and right hand sides.

$$\left(A_P - \sum_{NB} A_{NB}\right) u_P' = \sum_{NB} A_{NB}(u_{NB}' - u_P') + (p_w' - p_e')A \qquad (2.59)$$

Next, the term involving the difference (u'_{NB} - u'_P) is dropped, under the arguement that this term is small and will vanish at convergence when the corrections are zero. The resulting relationship between pressure and velocity correction becomes:

$$u_P' = \frac{1}{A_P - \sum_{NB} A_{NB}}(p_w' - p_e')A \qquad (2.60)$$

Equation 2.60 can be contrasted to the correction relationship used in SIMPLE (Equation 2.55) by noting that here the neighbour term which is dropped involves a difference term ($\sum_{NB} A_{NB}(u'_{NB} - u'_P)$) which is small compared to the neighbour term ($\sum_{NB} A_{NB} u'_{NB}$) dropped in SIMPLE.

Equations similar to Equation 2.60 are used to cast the continuity equation in terms of an equation for the pressure correction. The mass balance equation (in 1D Cartesian form) is first written in terms of the velocity $u^* + u'$:

$$(\rho A)_e (u^* + u')_e - (\rho A)_w (u^* + u')_w = 0 \qquad (2.61)$$

Using equations similar to Equation 2.60, this continuity equation can be recast in terms of pressure correction as:

$$(\rho A u^*)_e - (\rho A u^*)_w + (\rho A)_e \frac{1}{(A_P - \sum_{NB} A_{NB})_e}(p_P' - p_E') - (\rho A)_w \frac{1}{(A_P - \sum_{NB} A_{NB})_w}(p_W' - p_P') = 0 \qquad (2.62)$$

Equation 2.62 can now be solved for a correction to the pressure field which is then used to compute the velocity correction via Equation 2.60. Finally, using Equations 2.52 and 2.53 , the velocity and pressure corrections thus obtained are used to update the current velocity and pressure fields.

Since both methods are only corrections of the variables, both methods will give the same solution when converged. The question of which method to use only influences the convergence speed.

2.7.4 The Iterative Solution Procedure

The SIMPLE and SIMPLEC algorithms described above relate the velocity and pressure fields which satisfy the linearised momentum and continuity equations at a point. Because FLUENT does not solve the equations at all points simultaneously, and because the equations are coupled and non-linear, an iterative solution procedure is required with iterations continuing until all equations are satisfied at all points. Each iteration consists of the steps which are illustrated in Figure 2.6

2.7.4.1 Line by Line Solution of The Equations

The algebraic equation to be solved by FLUENT for any variable ϕ at point P may be written as:

$$A_P\phi_P = \sum_{NB} A_{NB}\phi_{NB} + S_\phi \qquad (2.63)$$

where the subscript NB denotes neighbour values, the coefficients A_P adn A_{NB} contain convection and diffusion coefficients, and S_ϕ is the source of ϕ in the control volume surrounding point P. For each unknown, ϕ, an equation of this form must be solved at all points within the domain.

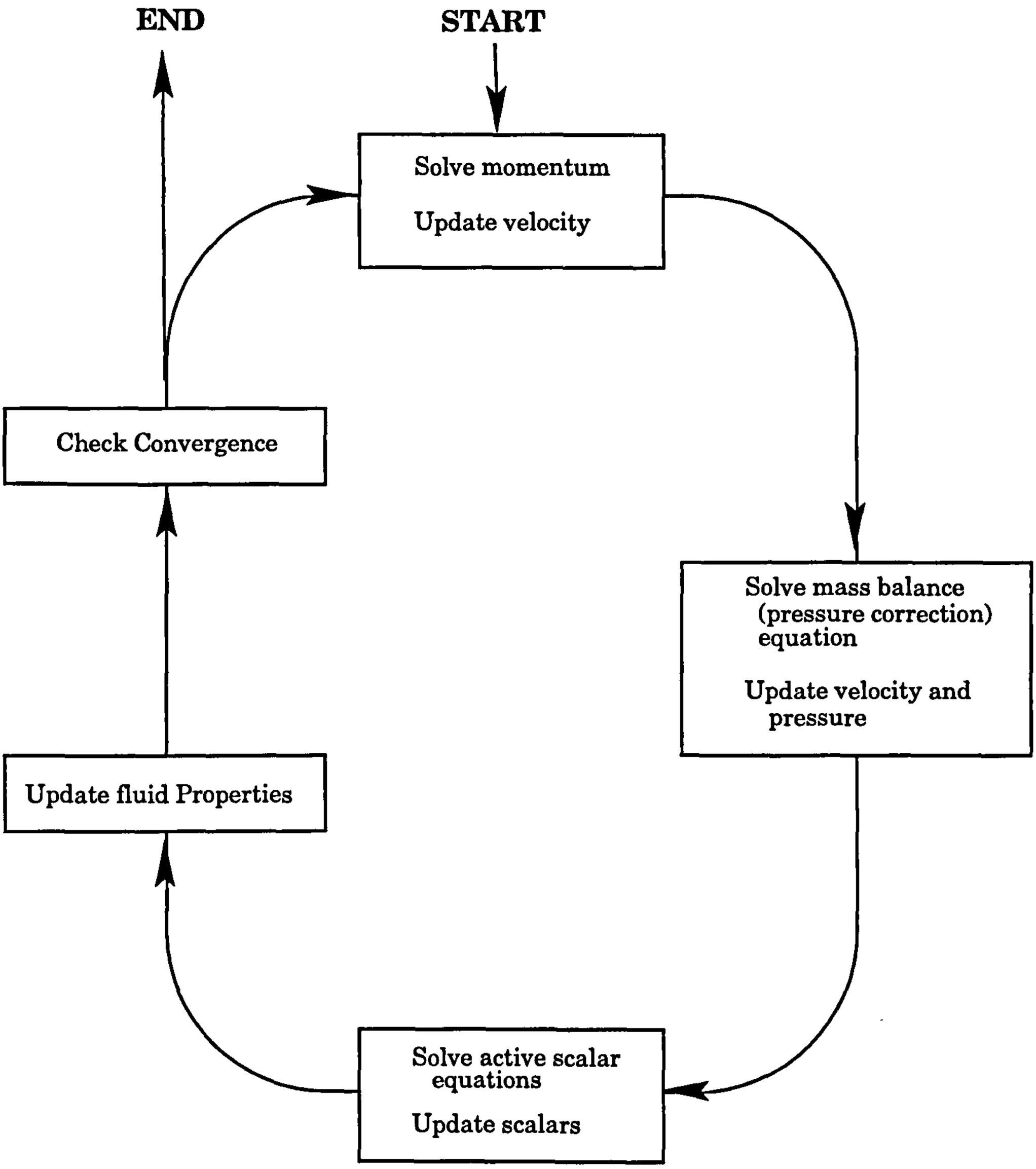

Figure 2.6 : Overview of The solution Process in FLUENT (After FLUENT Inc)

This solution process may be accomplished via a "line-by-line" solver, in which the equations along a single "line" of cells (*e.g.* a line of I = constant) are solved simultaneously. The line-by-line solver give rise to a tri-diagonal matrix which is solved via Gaussian elemination to update the values of ϕ along the line

considered. This procedure, also referred to as Line Gauss Seidel (LGS), is repeated for all lines in the domain so that ϕ is updated at all points P. FLUENT provides flexibility in its line-by-line solution procedure, giving the user control over the direction(s) of the lines to be considered and over the number of times each line is visited in order to update a given variable within each global iteration loop. While the LGS solver is good at reducing local errors, it is relatively poor at reducing errors which require collective change of many cell values (long wavelength errors). Therefore the speed of solution of the LGS solver deteriorates with increasing grid size. FLUENT provides two devices to speed up the LGS procedure:

a) One-Dimensional block correction

b) Multigrid (MG) acceleration

Both methods accelerate the convergence of the equations by deriving global corrections that drive the solution toward global conservation. Each of the methods is described in the later sections.

Sometimes a problem shows extremely slow convergence, with the residuals for one or more equations remaining nearly constant over a large number of iterations. In addition to modifications in the underrelaxation parameters, two other types modifications in the solver parameters are available :

a) The sweep direction, which controls the way in which cells are grouped together to be solved.

b) The number of sweeps on each equation, which controls the extent to which the solution of any single equation is refined during each iteration.

If an exact solution were performed on a computational domain with N cells, an $N \times N$ matrix would need to be solved. Rather than solve a problem via this "direct method", FLUENT uses an iterative solution technique, solving the

equations simultaneously for small groups of cells, one group at a time. The groups contain either a complete row or a complete columns of cells, starting at one boundary and ending at other. The solver sweep direction is the direction in which these group of cells are formed, *i.e.* columns represent one direction while rows represent another.

Figure 2.7 illustrates a solver sweep in direction 2. *Sweep direction 2* means that the equations are solved simultaneously for a single column of cells (or a sweep of cells in the J-th direction). The solver than marches foward in the positive I-direction to solve the next column of cells.

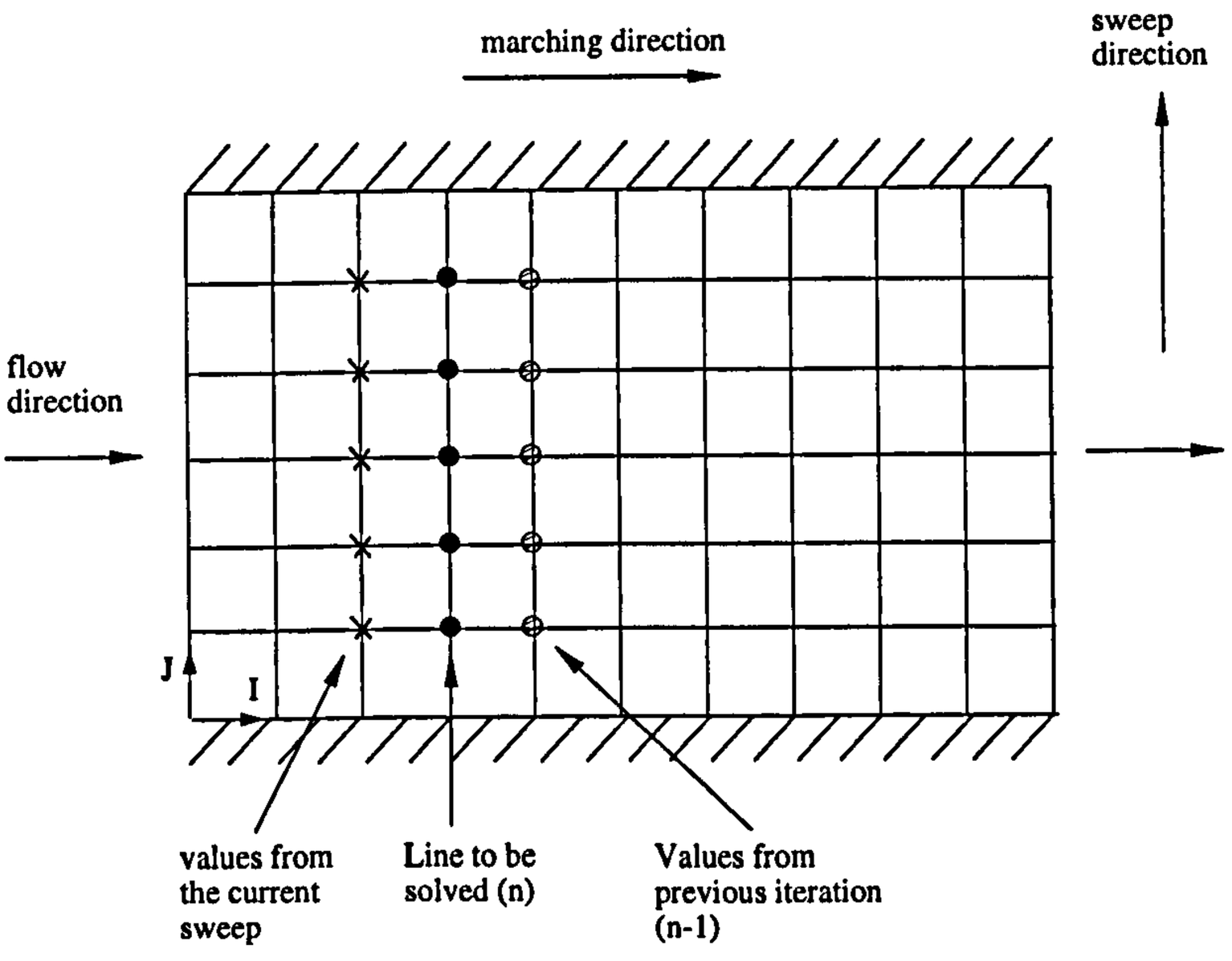

Figure 2.7 : Illustration of Sweep Direction 2

FLUENT uses an alternating sweep direction, by default, sweeping lines in the I direction and then sweeping lines in the J direction. This technique is particularly useful for problems in which there is no single dominant flow direction, *e.g.*, flows with jet or particles injected into a crossflow. In 3D, the solver operates such that the marching direction is always the same, and the sweep direction alternates.

In addition to choosing the solver sweep direction, one can also control the accuracy with which each equation is solved during each iteration. This is accomplished by increasing the number of sweeps of an equation, and it is particularly useful for equations that have difficulty converging. Figure 2.8 illustrates the process in which 5 sweeps are performed for the the pressure.

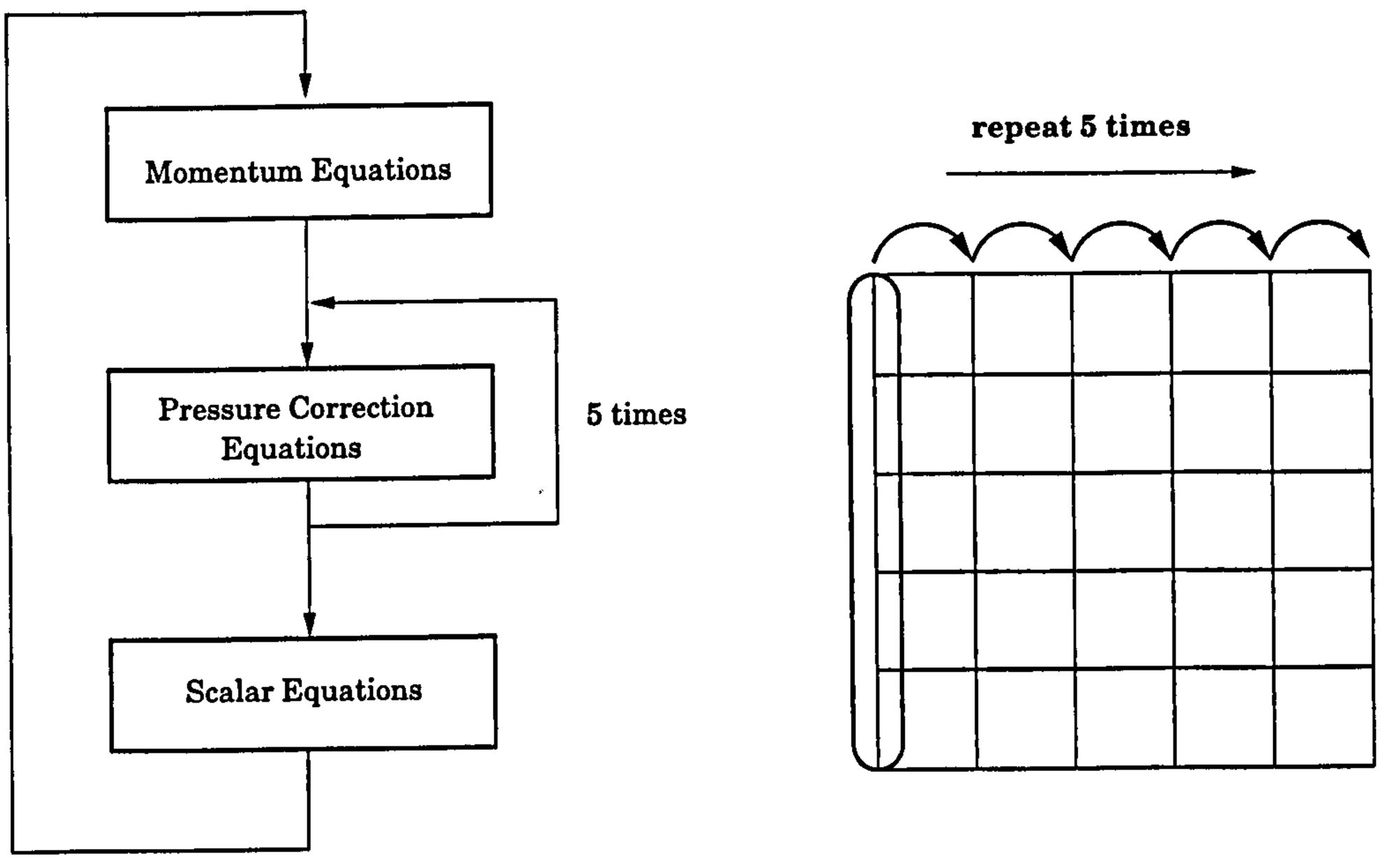

Figure 2.8 : Multiple Sweeps of the Pressure Equations (after FLUENT Inc)

2.7.4.2 1D Block Correction

FLUENT provides an optional block correction procedure for solving of the governing equations. In the block correction procedure, the transport equations for a variable ϕ are assumed in each plane of constant I, J, K, and the resulting set of "one-dimensional" equations are solved for a correction to ϕ on each plane. Consider the discretised equation for ϕ_{ijk} at point P in 3D:

$$\begin{aligned} A^{P}_{ijk}\phi_{ijk} &+ A^{E}_{ijk}\phi_{i+1jk} + A^{W}_{ijk}\phi_{i-1jk} \\ &+ A^{N}_{ijk}\phi_{ij+1k} + A^{S}_{ijk}\phi_{ij-1k} \\ &+ A^{U}_{ijk}\phi_{ijk+1} + A^{D}_{ijk}\phi_{ijk+1} \end{aligned} \tag{2.64}$$

where the superscripts E, W, N, S, U and D represent the east, west, north, south, up and down neighbours of the point P. For the case of 3D to 1D block correction in the I direction, the equations are summed in each I plane:

$$\begin{aligned} \sum_j \sum_k (A^{P}_{ijk}\phi_{ijk} &+ A^{N}_{ijk}\phi_{ij+1k} + A^{S}_{ijk}\phi_{ij-1k} \\ &+ A^{U}_{ijk}\phi_{ijk-1} + A^{D}_{ijk}\phi_{ijk-1} + \sum_j \sum_k A^{E}_{ijk}\phi_{i+1jk} \\ &+ \sum_j \sum_k A^{W}_{ijk}\phi_{i-1jk} = \sum_j \sum_k b_{ijk} \end{aligned} \tag{2.65}$$

If $\tilde{\phi}_{ijk}$ is the current best estimate of the solution, the improved solution will be given $\phi_{ijk} = \tilde{\phi}_{ijk} + \delta_I$. Here δ_I is the correction over the plane. Substituting this into the above equation yields:

$$\begin{aligned} \sum_j \sum_k (A^{P}_{ijk} &+ A^{N}_{ijk} + A^{S}_{ijk} + A^{U}_{ijk} + A^{D}_{ijk})\delta_I \\ &+ \sum_j \sum_k A^{E}_{ijk}\delta_{I+1} + \sum_j \sum_k A^{W}_{ijk}\delta_{I-1} = b_I \end{aligned} \tag{2.66}$$

where:

$$\overline{b} \equiv \sum_j \sum_k (b_{ijk} - A^P{}_{ijk}\phi_{ijk} - A^E{}_{ijk}\phi_{i+1jk} - A^W{}_{ijk}\phi_{i-1jk} - A^N{}_{ijk}\phi_{ij+1k} - A^S{}_{ijk}\phi_{ij-1k} - A^U{}_{ijk}\phi_{ijk+1} - A^D{}_{ijk}\phi_{ijk-1}) \quad (2.67)$$

Defining a set of coefficient for these 1D equations, the correction equation can be written as:

$$\overline{A}^P{}_I \delta_I + \overline{A}^E{}_I \delta_{I+1} \overline{A}^W{}_I \delta_{I-1} = \overline{b}_I \quad (2.68)$$

where

$$\overline{A}^P{}_I = \sum_j \sum_k (A^P{}_{ijk} + A^N{}_{ijk} f^N + A^S{}_{ijk} f^S + A^U{}_{ijk} f^U + A^D{}_{ijk} f^D) \quad (2.69)$$

$$\overline{A}^E{}_I = \sum_j \sum_k A^E{}_{ijk} \quad (2.70)$$

$$\overline{A}^W{}_I = \sum_j \sum_k A^W{}_{ijk} \quad (2.71)$$

The factors f^N, f^S, and f^D are used to remove the influence neighbours in the J or K directions in the I-direction block correction equation. This is accomplished by setting $f^N = 1$ if N is a computational cell and 0 otherwise, with similar treatments for f^S, f^U, and f^D.

The correction equations, (Equation 2.68) for the correction δ_I at each plane I are solved using the tri-diagonal matrix algorithm, and the unknowns are corrected using $\phi_{ijk} = \tilde{\phi}_{ijk} + \delta_I$. Similar equations are derived and solved for the corrections in the J and K directions.

2.7.4.3 The Additive Correction Multigrid Scheme

Additive Correction (Hutchinson *et al.*, 1986) is a technique which seeks to apply a correction, ϕ', to the current solution field, ϕ^*, such that the resulting corrected solution $\phi^* + \phi'$, obeys a global conservation of ϕ within some subregion considered. In FLUENT, the subregions considered are constructed via grouping together of neighbouring control volumes. The equations to be solved on each multigrid level are constructed via summation of the equations on the original fine grid level. This summation, over the fine grid cells used to construct the coarse grid element, can be written as:

$$\sum_i \sum_j \sum_k [A^P_{ijk}\phi_{ijk} = A^E_{ijk}\phi_{i+1jk} + A^W_{ijk}\phi_{i-1jk} + A^N_{ijk}\phi_{ij+1k} + A^S_{ijk}\phi_{ij-1k} + A^U_{ijk}\phi_{ijk+1} + A^D_{ijk}\phi_{ijk-1} + b_{ijk}] \quad (2.72)$$

where the coefficients A^E, A^W, A^N, A^S, A^U, and A^D are the neighbour coefficients (A_{NB}) of the point P at cell ijk of the fine grid. Next, the unknowns, ϕ_{ijk}, are assumed to consist of the current solution value in each cell, ϕ^*_{ijk}, and a correction, ϕ'_{ijk}, on the IJK-th block of the coarse grid level:

$$\phi_{ijk} = \phi^*_{ijk} + \phi'_{IJK} \quad (2.73)$$

Substitution of Equation 2.73 into 2.72 yields an equation to be solved for correction field, ϕ'_{IJK}, on the coarse grid level. This correction equation relates the correction in the neighbour blocks on the coarse grid to the corrections in the neighbours block on the coarse grid. The set of equations derived via similar summations on each coarse grid block are then solved iteratively, using an alternating direction Line-Gauss-Seidel solution method. The set of corrections thus obtained are then added to the current fine grid solution as in equation 2.73. The resulting corrected solution then satisfies global balances on the coarse grid level. Satisfaction of local conservation on the fine grid level then proceeds as usual using the line solver to update ϕ^*_{ijk}.

2.7.5 Residuals

The process of obtaining a converged solution is a great importance in numerical simulations. At each iteration of its solution algorithm, FLUENT reports a residual for each equation that has been solved. These residuals provide a measure of the degree to which each equation is satisfied throughout the flow field. The residuals are computed for each conservation equation by summing the imbalance in the equation for all cells in the domain.

After discretisation, the conservation equation in two-dimensions for a general variable, ϕ_P, can be written as:

$$A_P \phi_P = A_E \phi_E + A_W \phi_W + A_N \phi_N + A_S \phi_S + S_C \qquad (2.74)$$

where

$$A_P = A_E + A_W + A_N + A_S - S_P \qquad (2.75)$$

The nomenclature for these equations is displayed in Figure 2.9. The quantity ϕ might be any dependent variable (u velocity, turbulence energy, enthalphy, *etc.*). The coefficients A_E, A_W, A_N and A_S are the finite difference coefficients which combine convection and diffusion through the control volume surrounding P. The quantities S_C and S_P are the components of the linearised source term which incorporate any terms in the equation which do not fall into the convection/diffusion form.

The normalised residual, R, computed by FLUENT, is the imbalance in Equations 2.74 , summed over all the computational points P divide by summed over the computational nodes:

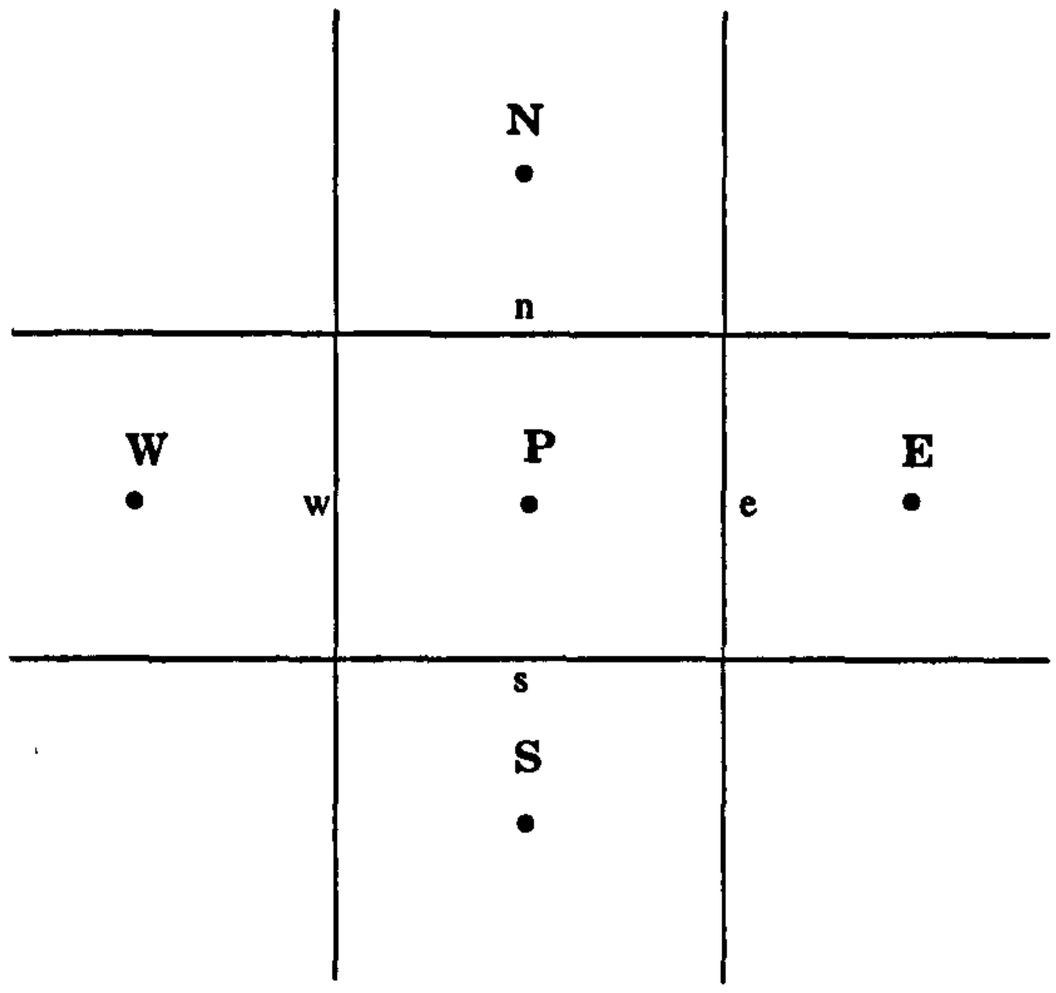

Figure 2.9 : Typical Computational Cell surrounding Node P

$$R = \frac{\sum_{nodes\ P} | [A_E \phi_E + A_W \phi_W + A_N \phi_N + A_S \phi_S + S_C - A_P \phi_P] |}{\sum_{nodes\ P} | (A_P \phi_P)|} \tag{2.76}$$

The residual for pressure, however, is the imbalance in the continuity (pressure correction) equation:

$$R = \sum_{nodes\ P} |(C_W - C_E + C_S - C_N)| \tag{2.77}$$

where C_W, C_E, C_S, C_N are the convection of mass (kg/s) through each face of the control volume surrounding point P. Normalisation of the pressure residual is accomplished by dividing by the residual (or continuity imbalance) at the second iteration:

$$R = \frac{R_{iteration\ N}}{R_{iteration\ 2}} \tag{2.78}$$

Generally, a solution is well converged when the normalised residuals are on the order of 1×10^{-3}. An important exception is the enthalpy residual which should be about 1×10^{-6}. If the residuals have decreased to this level, are monotonically decreasing, and the flow field looks unchanged from the solution 50 iterations earlier, then the solution can be called "converged".

2.7.6 Underrelaxation

Because of the nonlinearity of the equation set being solved by FLUENT, it is not generally possible to obtain a solution by fully substituting the "improved" values for each variable which have been generated by the approximate solution of the finite-difference equation. Convergence can be achieved, however, by underrelaxation which reduces the change in each variable produced during each iteration. In a simple form, the new value of the variable ϕ_P at node P depends upon the old value $\phi_{P,old}$, the computed change in ϕ_P, $\Delta\phi_P$, and the underrelaxation factor, α, as follows (Patankar, 1980):

$$\phi_P = \phi_{P,old} + \alpha\Delta\phi_P \tag{2.79}$$

In FLUENT, the default underrelaxation parameters for all variables except the velocities are set to low values in order to ensure convergence in the largest possible number of cases. Unfortunately, this may not give rise to the fastest rate of convergence, and an improvement can often be obtained by judicious increase in one or more parameters.

Underrelaxation factors for the transport equation are set in the range of 0 to 1. The smaller the factor, the heavier is the degree of underrelaxation and the greater is the degree of control exercised over the change permitted from one iteration to the next. While small underrelaxation factors damp out nonlinearities, they also serve to inhibit the rate of convergence for more straightfoward problems.

2.8 CONCLUSIONS

All the relevant governing equations in turbulence flow and the method of closure in FLUENT have now been described. The three turbulence closure models incorporated in FLUENT are; the standard k-ε Model, the Reynolds Stress Model the and ReNormalizationGroup Theory-based Model. The package was designed to be widely applicable to various engineering problems. In what follows, we examine how well the closure models work, in particular, in dealing with hydraulic problems.

In the following chapters, an evaluation of the three turbulence closure models, based on a critical comparison of prediction against the experimental results of previous researchers at Department of Civil Engineering, University of Liverpool and other research establishments is presented.

NOTATIONS

Notation is explained in the text of the thesis as it is used. The following list is intended for reference and covers only the notation which is used repeatedly.

C_μ	Empirically derived constant of proportionality (= 0.09)
$C_{1\varepsilon}$, $C_{2\varepsilon}$, $C_{3\varepsilon}$	Empirical constants
C_3, C_4	Empirical constants
E	Empirical constant by default equal to 9.8 (smooth wall)
$E(k)$	Kolmogorov equilibrium range of turbulence = $k^{-5/3}$
ELOG	Wall roughness parameter.
F_i	External body forces in the i direction
g_i	Gravitational acceleration in the i direction
G_k	Rate of production of turbulent kinetic energy
G_b	Generation of turbulence due to buoyancy
k	Turbulent kinetic energy
k_o	Low wavenumber
K_s	Average roughness height
K_s^+	Dimensionless roughness
ℓ_d	Kolmogorov dissipation scale
n	The coordinate normal to the wall
p_i	Static pressure
P_{ij}	Stress production rate
Re	Reynolds number
R_{ij}	Rational term
S_m	Mass added to the continuous phase from the dispersed second phase
y^+	Dimensionless distance from the wall
α	Inverse Prandtl number for turbulent transport
Δt	Time scale
ε	Dissipation rate of k
ε_{ij}	Viscous dissipation

κ	von-Karman's constant (CAPPA)
Λ	High wavenumber viscous cutoff
ν	Kinematic viscosity
$\sigma_k, \sigma_\varepsilon$	"Prandtl" numbers governing the turbulent diffusion of k and ε
δ_{ij}	Kronecker delta ($\delta_{ij} = 1$ for $i = j$, and, $\delta_{ij} = 0$ for $i \neq j$)
μ	Molecular viscosity
μ_t	Turbulent eddy viscosity
μ_{eff}	Effective viscosity
τ_{ij}	Stress tensor
ϕ	Conserved scalar quantity
$\overline{\phi}$	Time averaged value of ϕ
ϕ'	Turbulent fluctuations
Φ_{ij}	Source/sink due to the pressure/strain correlation

REFERENCES

Batchelor, G.K. (1967), "An Introduction to Fluid Dynamics", Cambridge Univ, Press, Cambridge, England.

FLUENT User's Guide, (1993), Fluent Incorporated, Lebanon, New Hampshire. U.S.A.

Hinze, J.O., (1975), "Turbulence", McGraw-Hill Publishing Co., New York.

Hutchinson, B.R. and Raithby, G.D., "A Multigrid Method Based on Additive Correction Strategy," *Numer Heat Transfer*, V.9, pp. 511-537, 1986.

Launder, B.E., Reece, G.J., and Rodi, W., (1975), "Progress in the Development of a Reynolds-Stress Turbulence Closure," *J. Fluid Mech.*, V68(part3), pp. 537-566.

Launder, B.E. and Spalding, D.B., (1972) "Lectures in Mathematical Models of Turbulence", Academic Press.

Leonard, B.P., " A Stable and Accurate Convective Modelling Procedure Based on Quadratic Upstream Interpolation," *Comput Methods Appl. Mech. Eng.*, V. 19, pp. 59-98, 1979.

Martinelli, L., and Jameson, A., (1988), "Validation of a Multigrid Method for the Reynolds Averaged Equations", AIAA-88-0414, 1988.

Patankar, S.V., (1980) "Numerical Heat Transfer and Fluid Flow", Hemisphere Publishing Corp, Washington, DC, 1980.

So, R.M.C (ed.) , Speziale, C.G. (ed.) , Launder, B.E. (ed.), (1993), "Near-wall Turbulent Flows" Proceedings of the Conference held 15-17 March 1993.

Yakhot, Victor and Orszag, Steve A., (1986), "Renormalisation Group Analysis of Turbulence," Basic Theory, *J. of Sci Comput*, V.1, No. 1, pp. 1-51.

CHAPTER

CHAPTER 3

PREDICTION OF FLOW PATTERNS IN LOCAL SCOUR HOLES CAUSED BY TURBULENT WATER JETS

3.1 INTRODUCTION

Prediction of local scour holes that develop downstream of hydraulic structures plays an important role in their design. Excessive local scour can progressively undermine the foundation of the structure. Because complete protection against scour is too expensive, generally, the maximum scour depth and the upstream slope of the scour hole have to be predicted to minimise the risk of failure.

The localised scour phenomenon has been the subject of extensive investigations by many researchers and numerous literature exists for scour caused by 2- and 3-dimensional turbulent jets. Most of the studies conducted on scour have been empirical because of the complexity of the physical processes.

The pioneering investigation on scour due to a jet was done by Rouse (1939). Scour due to a horizontal wall jet was studied by Laursen (1952). Scour by circular impinging jets was studied by Doddiah *et al.* (1953), Poreh and Hefez (1967), Sarma and Sivasankar (1967), Westrich and Kobus (1973), and Rajaratnam dan Beltaos (1977). Iwagki *et al.* (1958) undertook an analytical study of scour caused by a three-dimensional jet. Carstens (1966) developed an empirical formula for sediment transport rate by analysing the experimental data of Laursen (1952). Scour caused by impinging plane jets was studied by Altinbilek and Okyay (1973) and by Francis and Ghosh (1974). Scour by circular and

rectangular turbulent wall jets was studied by Rajaratnam and Berry (1977) and Rajaratnam and Humpries (1984) respectively. The scour due to plane wall jets in shallow tailwater was examined by Rajaratnam and MacDoughall (1983). Hassan and Narayanan (1985) investigated local scour downstream of rigid aprons. Local scour caused by a submerged wall jet was studied by Ali and Lim (1986). Uyumaz (1988) investigated scour patterns downstream of vertical gates. Mason (1988) studied plunge pool scour. A study of the scour pattern in shallow tailwater was done by Johnston (1990).

The studies of the aforementioned investigators have made important contributions to the knowledge of the phenomena of local scour downstream of hydraulic structures in the relevant flow situations.

As mentioned in the previous chapter, "prediction" by way of experiments are usually very expensive. In practise, nearly all jets of importance are turbulent in nature, this would, normally, require expensive and sophisticated instrumentations in order to be able to measure the quantities desired. Since the computer capability has drastically increased numerical simulation seemed a promising means as an alternative. Furthermore, the flexibility in defining the geometry in the numerical analysis enables various design options to be considered at a relatively faster time and lower cost. The wealth of experimental data available in the literatures makes it possible to validate the numerical simulation before it can be used more confidently. The purpose of the present study is therefore aimed at verifying the effectiveness of the numerical routine incorporated in the FLUENT package as described in Chapter 2. In this chapter the validation begins with the simulation of flows in rigid and scoured beds caused by turbulent water jets. Two categories of submergence of water jet were selected:

a) The deeply submerged jet where the tailwater depth, H, is many times the height of the jet opening ($H >> y_o$), and

b) The jet with minimum submergence - in this case, H is approximately equal to the height of the jet opening. ($H \approx y_o$)

In the following section, a brief review of the mechanism of the scour by water jets is presented.

3.2 LOCAL SCOUR CAUSED BY TURBULENT WATER JETS

3.2.1 Introduction

The entrainment, transportation and deposition of sediment depends as much on the properties of the sediment as upon the hydraulic characteristics of the flow. Generally speaking, the scouring mechanism involves a combination of two relative motions: that of the flow field relative to the boundary, and that of the bed material relative to the overlying flowing fluid.

In general, localised scour can occur in two ways (1) clear-water scour; and (2) live-bed scour. Clear-water scour refers to the situation where no sediment is supplied from upstream into the scour zone. Live-bed scour, on the other hand, occurs when there is general bed load transport by the stream. Sediment is continuously being supplied to the areas subjected to scour. The present analysis deals mainly with the clear-water scour.

3.2.2 The Classical Wall Jet (CWJ)

Since the turbulent wall jet is the scouring agent investigated in the present study, it is useful to introduce the general characteristics of the CWJ first. The wall jet is defined as a jet of fluid, impinging tangentially (or at angle) on a boundary surrounded by stationary (or moving fluid). The case of the classical wall jet, i.e. the plane turbulent wall jet issuing into the same stationary fluid of semi-finite extent on a smooth boundary, is shown in the sketch (Sketch 1) below.

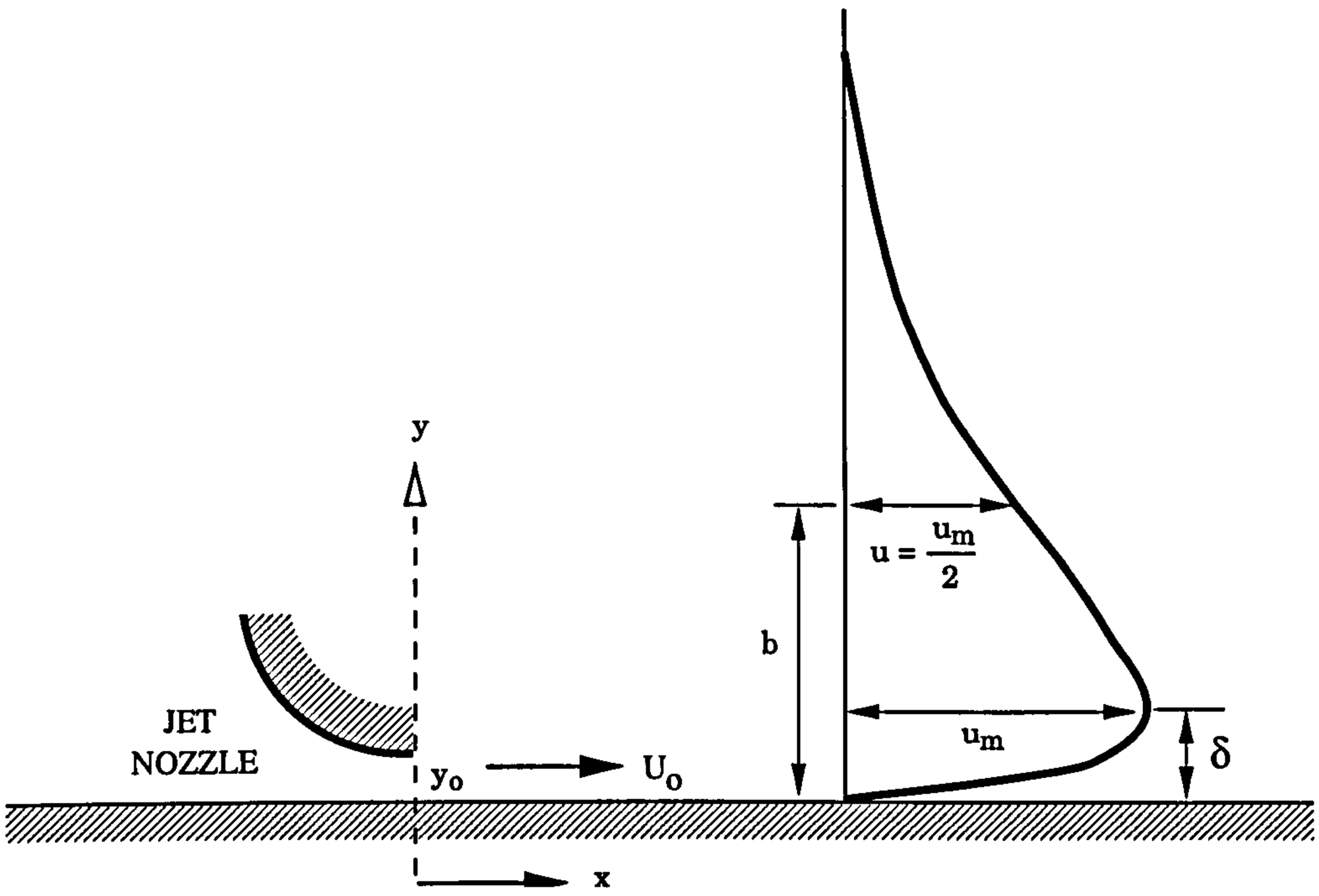

SKETCH 1 : DEFINITION SKETCH OF THE CLASSICAL WALL JET

Experimental investigations on the plane turbulent wall jet under zero pressure gradient have been studied extensively, and a comprehensive bibliography on wall jets can be found in the book by Rajaratnam (1976). It was found that for sections located at a longitudinal distance x greater than 15 times the thickness of the jet opening, y_o, the transverse velocity plotted in dimensionless co-ordinates is similar for all sections. For these similar velocity distributions, the non-dimensionalised

velocity, known as the velocity scale, is the velocity divided by the maximum velocity at that section, u_m. The corresponding length scale is the normal distance, b, from the boundary to the horizontal plane at which $u=u_m/2$ and the velocity gradient, du/dy is negative.

3.2.3 Description of the mechanism of scour by water jet

Consider a turbulent jet issuing from a 2-D or 3-D nozzle. As the diffused jet starts to flow over the initially flat erodible bed, the scouring potential of the jet, created by the high incoming velocity, is usually so strong that the sand grains are immediately dislodged from the surface and transported downstream at a rapid rate. For a small time period, the vertical dimensions of the scour hole increase at a faster rate than the horizontal dimensions and the bed material is transported mainly as bed loads.

As the scour hole gradually enlarges with time, the depth of flow also increases. From the principle of continuity, the expanding cross sectional area would require a reduction in the mean flow velocity. Accordingly, the local velocity near the scoured bed decreases as the depth of the hole increases. Hence, the rate of erosion decreases as time progresses. For larger time periods, the bed velocity eventually reduces to a certain "critical" value whence the flow (near the bed) becomes incapable of removing further bed material from the scour area. At this point, we could say that the scour geometry has reached its "equilibrium" or "asymptotic" condition. Implicitly, this suggests that the local bed velocity is directly related to the concept of a threshold of a particulate movement.

Conventionally, it has been accepted that the boundary shear stress is a logical choice of a key variable to characterise the incipient motion of particles. The bed shear stress is a function of the local bed velocity and the friction factor, which is

often assumed to be constant, therefore, measurements of the bed velocity and distributions in a scour hole will enable the scouring process to be examined.

3.2.4 Description of the flow patterns in local scour hole

Interesting observations were made by Rajaratnam and Berry (1977) regarding the velocity distributions (using an air jet) along scour hole at the asymptotic state. They noted that the jet behaves like a free jet up to the section of maximum erosion and from this section up to the ridge section, it behaves like an obliquely impinging jet, developing wall-like velocity profiles in the vicinity of the ridge. Figure 3.1 shows a typical plot of Rajaratnam and Berry's velocity distributions. The velocity results showed that up to approximately the section of maximum erosion, the variation of u_m / U_o was well described by the simple circular jet equation:

$$\frac{u_m}{U_o} = 6.67 \left(\frac{x}{y_o} \right) \tag{3.1}$$

in which u_m is the maximum velocity of the velocity profile at any x distance from the nozzle, y_o is the jet thickness, and U_o is the average jet velocity. The velocity profiles for this region in the vertical and horizontal planes (through the maximum velocity points) were found to be similar (see definition sketch - Sketch 2) and the data were described well by the exponential equation:

$$\frac{u}{u_m} = e^{-0.693(y/b)^2} \tag{3.2}$$

and

$$b = 0.097x \tag{3.3}$$

where y = vertical distance from the axis of jet at any x direction, and b = vertical distance from the axis to the point where $u = u_m/2$.

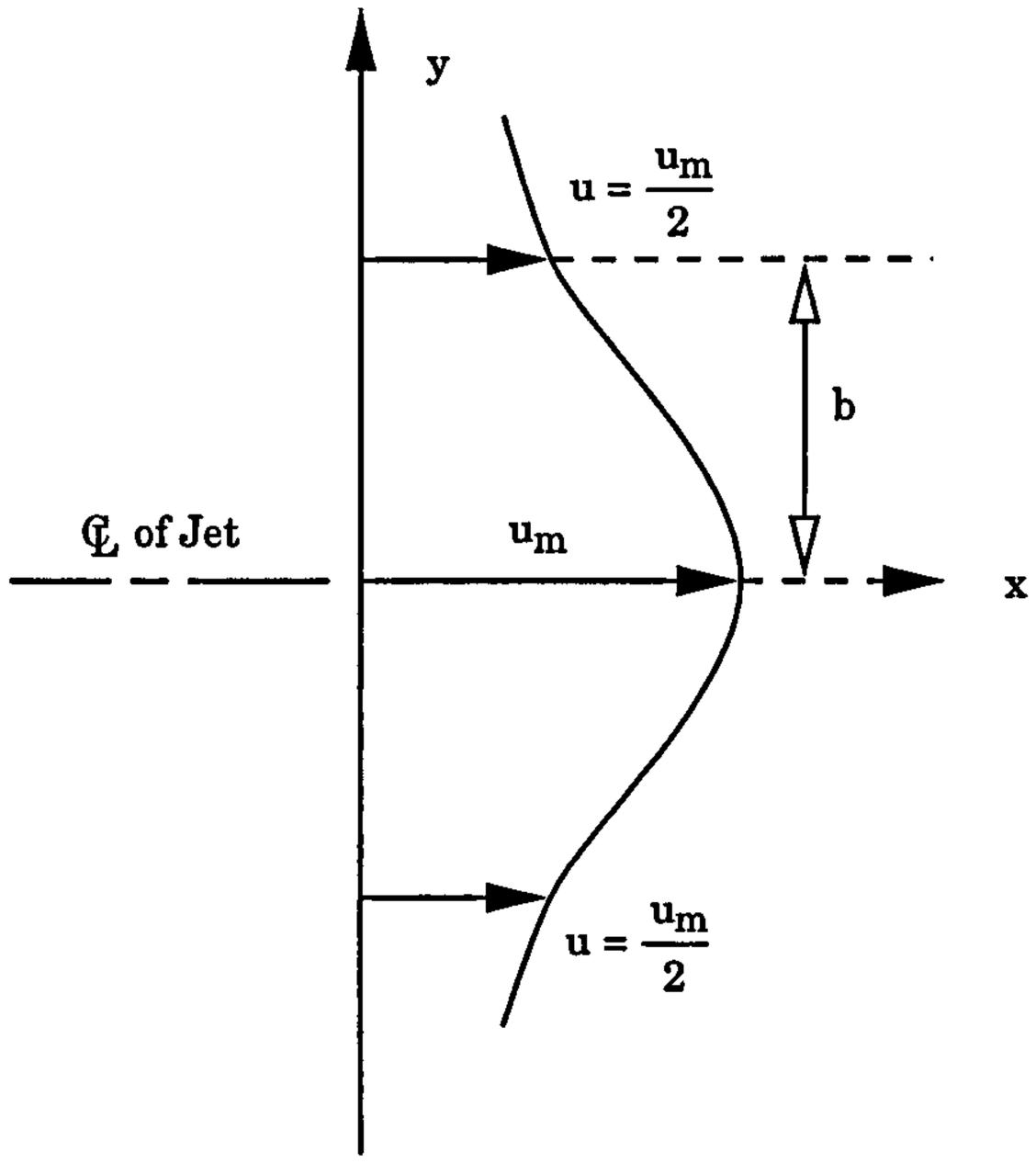

SKETCH 2 : DEFINITION SKETCH OF A TYPICAL VELOCITY PROFILE

The flow pattern in the scour hole was also studied by Breusers (1967). Velocity measurements were made with a propeller current meter. Figure 3.2 shows an example of the velocity distributions . The distributions of the turbulence intensity (r.m.s. deviation) was also determined. Figure 3.3 shows the variation of maximum scour depth and bed velocity (measured at 15 mm from the bottom) as a function of time as observed by Breusers. It can be seen that the mean velocity near the bed decreases rapidly as the depth of scour increases, whereas turbulence intensity, u', remains almost uniform for the whole test period.

Theoretical computation of velocity profiles in the scour hole was attempted by Breusers (1975), based on the method of Rosiinski (1961). This method was also used by Ali and Lim(1986) to predict the velocity distribution in a scour hole caused by 2-D turbulent wall jets. Ali and Lim (1986) performed an extensive investigation into the hydrodynamic behaviour of 2-D and 3-D turbulent wall jets with minimum tailwater depth ($H \approx y_o$).

3.3 MODELS VALIDATION

3.3.1 Introduction

As mentioned earlier, the aim of this chapter is to verify the effectiveness of the numerical procedure available in FLUENT in predicting the flow characteristics of turbulent wall jets. For that purpose velocity measurements carried out by Wu and Rajaratnam (1995) and Ali and Lim (1986) were used as benchmarks. The analysis were divided into three sections:

a) Flat bed - deep submergence (Wu and Rajaratnam)
b) Flat bed - shallow submergence (Ali and Lim, T=0)
c) Scoured bed - shallow submergence (Ali and Lim, T = 15, 90 and 400 mins.)

The experimental setup and procedures are briefly described in the following section in order to appreciate the domain to be modelled.

3.3.2 Wu and Rajaratnam's Experiments (1995)

The experiments were conducted in the T. Blench Hydraulics Laboratory of the University of Alberta. The submerged jets were produced in a flume, 7.60 m long,

0.466 m wide and 0.60 m deep. The horizontal bottom was made of aluminum and the side walls were made of glass. The tailwater depth was controlled by a vertical gate located at the downstream end of the flume. Water entered the flume under a sluice gate with a streamlined lip. The time-averaged velocity field was measured with either a pitch probe or a Prandtl probe.

Four experiments were done and are summarised in the following table:

TABLE 3.1 Summary of Wu and Rajaratnam's Experiments

Run	y_o(m)	H(m)	U_o(m/s)	F_o
1	0.010	0.44	1.72	5.48
2	0.015	0.53	2.86	7.46
3	0.015	0.46	2.86	7.46
4	0.015	0.39	2.86	7.46

where: y_o = thickness of jet

H = tailwater depth

U_o = uniform velocity

F_o = Froude number = $u_o / \sqrt{(g y_o)}$

In these experiments, the gate and hence the depth of the supercritical stream leaving the gate was equal to 10 and 15 mm. To ensure that the flow was two dimensional, they measured the velocity field in the central vertical plane (CVP) and another vertical plane located at a transverse distance of 0.1 times the width of the flume from the CVP. Their comparison of the longitudinal velocity profiles showed that at least in the central part of the flume, the flow was two dimensional.

3.3.3 Ali and Lim's Experiments (1986)

The experimental set-up for the sluice-gate experiments is shown diagrammatically in Figure 3.4. The long channel had the dimensions of 5.0m long, 0.61 m wide and 0.5 m deep. The sluice gate was constructed from two pieces of 1.9 cm thick plywood cut to the width of the channel. One piece was screwed to the channel wall and had a height of 30 cm from the channel bottom. The second piece formed the sluice gate and was also fixed to the channel wall with a slot opening of 5.08 cm. To ensure uniform and two-dimensional flow, two pieces of half-rounded perspex pipes were used to form well-designated sluice entrance, one on each side of the slot opening.The working section was 2 m from the downstream end of the channel. Sand was filled to a height of 30 cm in the working section. At the end of the channel, a sluicing arrangement allowed the tailwater depth to be regulated.

The bed material used was uniform sand with the following characteristics: d_{50} = 0.82 mm, σ_g = 1.126, specific gravity of 2.66, angle of repose $\Phi = 33°$, and, porosity of 0.403.

At the end of the experiment, measurements of the scour hole were made using a depth gauge. Figure 3.6 shows the time evolution of centreline bed-profiles obtained with tailwater depth, H = 6.7 cm. For present model verification analysis a period of t = 0 (initial bed), 15, 60 and 400 (asymptotic) were simulated.

The time development of scour represents a very complicated flow phenomenon involving the movement of sediment-water mixture along the bed of the scour hole. Because of the continuously changing flow boundary as scour progresses with time, the velocity distribution pattern in the scour hole would likewise be different at different stages of the erosion process. In order to investigate these transient non-uniform flow patterns, a steady-state flow model was necessary.

Lim converted the loose sand scour hole into a fixed-bed model so that the flow characteristics in the hole at the instant of time could be studied in detail. He obtained this by covering and moulding the scour-hole in-situ with tin foil. The tin foil was coated with the sand grains used in the experiment, to simulate the original roughness of the bed.

The velocities were measured using a miniature streamflow current meter. The measuring head of the current meter was 16mm in diameter. The "floor velocity" was measured at y=0.8 cm (equal to half of the diameter of the streamflow meter) above the bed of scoured hole. Since the probe only records positive velocity, reversed flow was judged by observing the direction in which the rotor turned. Based on the measured "floor" velocity, they calculated the boundary shear stress using method developed by Melville and Raudkivi (1977):

$$\tau_b = \frac{\rho f u_b^2}{8} \tag{3.4}$$

where f is the friction factor obtained using the Colebrook-White equation:

$$\frac{1}{f^{1/2}} = -2 \log_{10}\left(\frac{k_s}{14.83 H_T} + \frac{2.52}{f^{1/2} R_H}\right) \tag{3.5}$$

k_s is the height of the sand roughness and $R_H = u_b H_T / \nu$. Typical velocity profiles and corresponding boundary shear stress at various stages of the scour process are shown in Figure 3.6 and Figure 3.7 respectively.

3.4 SIMULATIONS USING FLUENT

The experiments mentioned in the above section were simulated using the FLUENT package. Descriptions of the package and the governing equations were given in Chapter 2. As mentioned in Chapter 1 (Section 1.2), FLUENT V4 is a two part program consisting of a preprocessor, PreBFC V4, and a main module (see Figure 1.1). PreBFC V4 was used to define the geometry and a structured grid of the problem to be modeled. The grid information was then imported from PREBFC to FLUENT. The physical models, fluid/material properties, and boundary conditions that describe the problem to be modeled were next added to the grid information and stored in Case-File that is a record of all the inputs for problem definition. The modelling steps are summarised as follows:

1. Import the preBFC Grid File;
2. Choose the basic equations;
3. Set the physical constants;
4. Set the boundary conditions;
5. Calculate the solution;
6. Examine the results; and
7. Save the results.

In this section the modelling process (*i.e* setting up the grid and the appropriate boundary conditions for the water flow calculation) is described.

3.4.1 Geometry Setup and Grid system

FLUENT employs a grid-based geometry, in which the geometry of the model is determined by control volumes defined by the grid. There are two options available (Sketch 3):

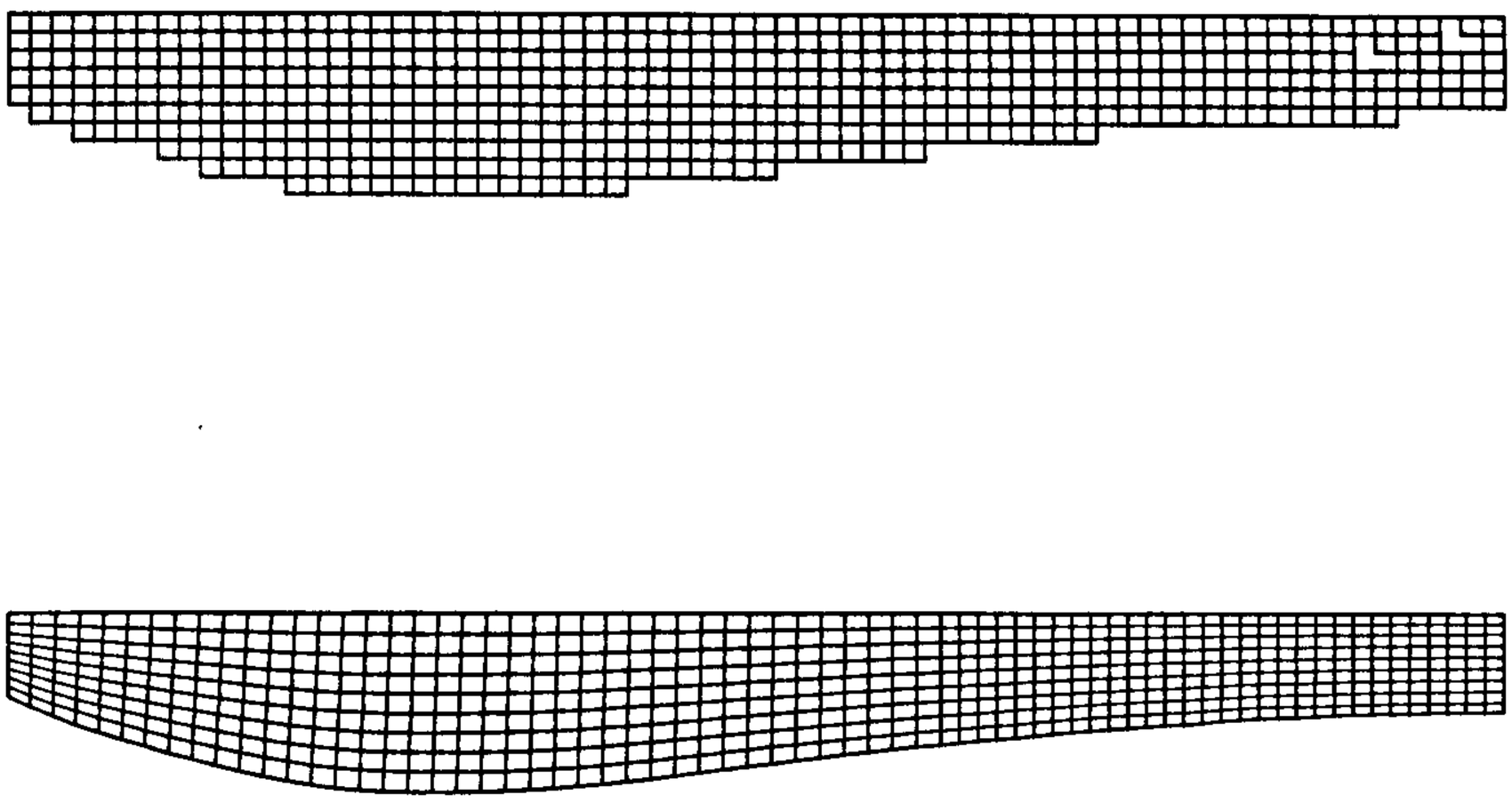

SKETCH 3 : Cartesian grid vs. Curvilinear BFC grid

(i) Cartesian or cylindrical co-ordinates in which the grid lines are aligned with the Cartesian (x,y,z) or cylindrical (z,r,θ) co-ordinates and may not conform to oblique or curved profile of the physical geometry. The boundary is represented by series of staggered lines (steps).

(ii) Curvilinear body-fitted co-ordinates (BFC) in which grid lines are determined by a co-ordinates system that conforms to the geometric boundary of the model.

Since the velocity and the shear stress distribution close to the bed are the main important properties to be investigated in the present analysis, the curvilinear grid will be used as the more simple cartesian coordinate system will not give an accurate description of the flow at the physical boundaries of the scoured bed.

The hydrodynamic geometries of the problems were discretised using PreBFC. Here the word "geometry" is used for the part of the hydraulic system that is

being investigated. Typical computational grid and grid assignment of Ali and Lim's experiment are shown in Figure 3.8 and 3.9 respectively.

3.4.2 Selecting Physical Models

Prior to setting the boundary conditions and physical properties of the fluid, the basic equations (or Model) is selected. The turbulence models available (as detailed in Chapter 2) are: k-ε Model, RNG Model and RSM Model. In this chapter the simulation was carried out for all the three models and the comparisons are described in 3.5.

3.4.3 Setting Physical Constants

Next, the physical constants of the fluid are set. The density and dynamic viscosity of the water were respectively set to 1000 kg/m^3 and 0.001 kg/m-s.

3.4.4 Boundary Conditions

Before the calculation can be made for the flow in the scour hole, it was necessary to specify the boundary conditions. Typical boundary conditions assignment are shown in Figure 3.8. FLUENT's treatment of the unknown variables at these boundaries is briefly described in this section.

Inlet Boundaries (I)

An Inlet boundary is a boundary at which flow enters (or exits) at a known velocity, composition and temperature. In turbulent flows, the k and ε values at the inlet boundary are also defined. It should be pointed out that diffusion of all scalars at the inlet boundary is assumed to be zero. At boundaries which are denoted as pressure boundaries, the fluid pressure is defined instead of velocity. FLUENT will

then solve a loss-free momentum balance (*e.g.* Bernoulli's equation) to obtain the inlet velocity.

Outlet Boundaries (O)

An outlet boundary condition is one at which values of all variables are extrapolated from the interior cells adjacent to the outlet. Additionally in subsonic flows, the normal velocities at the outlet are adjusted to satisfy an overall mass balance for the computational domain. The outlet condition corresponds to fully-developed flow condition.

Wall Boundaries (W)

At wall boundaries, the normal velocity component is constrained to zero. Walls may be treated to follow the slip (frictionless) or no-slip (with friction). The wall roughness parameters (ELOG) are computed following the procedures outlined in Chapter 2. Frictionless walls are used in the approximate modelling of a free-surface. In practical terms this meant that the x velocity component of the velocities are set to the values in the layer below. Different wall type may be assigned to different wall zone *i.e* W1,W2, *etc.*

3.4.5 Solving The Problems

3.4.5.1 Solution Parameters

The following solution-parameters were used for all runs:

Underrelaxation:	*0.2 (velocity, turbulence k.e. and eddy dissipation)*
	0.5 (pressure)
Sweeps :	*Alternating Direction with 2 (u,v)*

Convergence Criteria : *1 x 10^{-3} residual sum*

Algorithm : *SIMPLE*

Solver : *Power Law Differencing Scheme*

The process of obtaining a converged solution is of a great importance in numerical simulations procedure. The residuals or normalised residuals are a measure of the degree to which each equation is satisfied throughout the flow field. Generally, a solution is well converged when the normalised residuals are on the order of 1 x 10^{-3}. If the residuals have decreased to this level, are monotonically decreasing, and the flow field looks unchanged from the solution 50 iterations earlier, then the solution can be considered "converged". Sometimes one may not need to generate a completely converged solution, if the basic features of the flow field can be picked-up right away. However, for sound quantitative results, complete convergence of the solution is essential.

3.4.5.2 Choosing the Discretisation Scheme

The choice of a particular scheme is not a clear-cut issue. Some judicious experimentation of the relative stability characteristics of both schemes for a given number of iterations may be required before picking one of the schemes. The default solver or discretization scheme used was Power-Law Differencing Scheme. Sketch 4 shows the plot of the normalised residuals (for Lim's case - T = 400 mins) during the iteration. It can be seen that the solution converged steadily. Alternatively, a higher order scheme termed as blended Second Order Upwind/Central Difference scheme was also applied in order to investigate the significance of the scheme. While the higher order scheme was supposed to provide improved accuracy, it was found that numerical instability occurred during the iterations (see Sketch 5). For that reason, the Power-Law scheme was chosen for the present analysis.

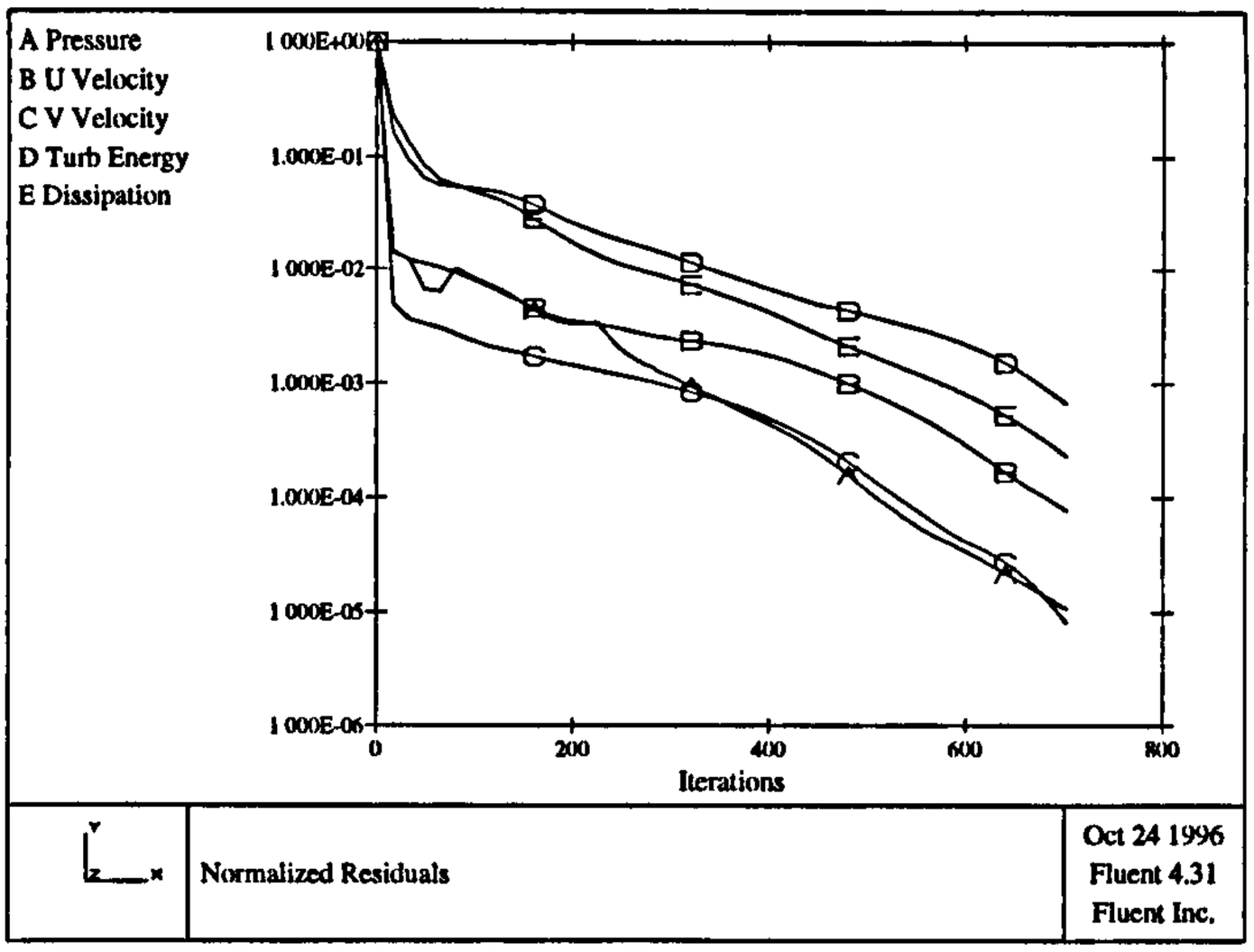

Sketch 4 : Residuals Plot for Power-Law Scheme (Lim's Exp. - T = 400 mins)

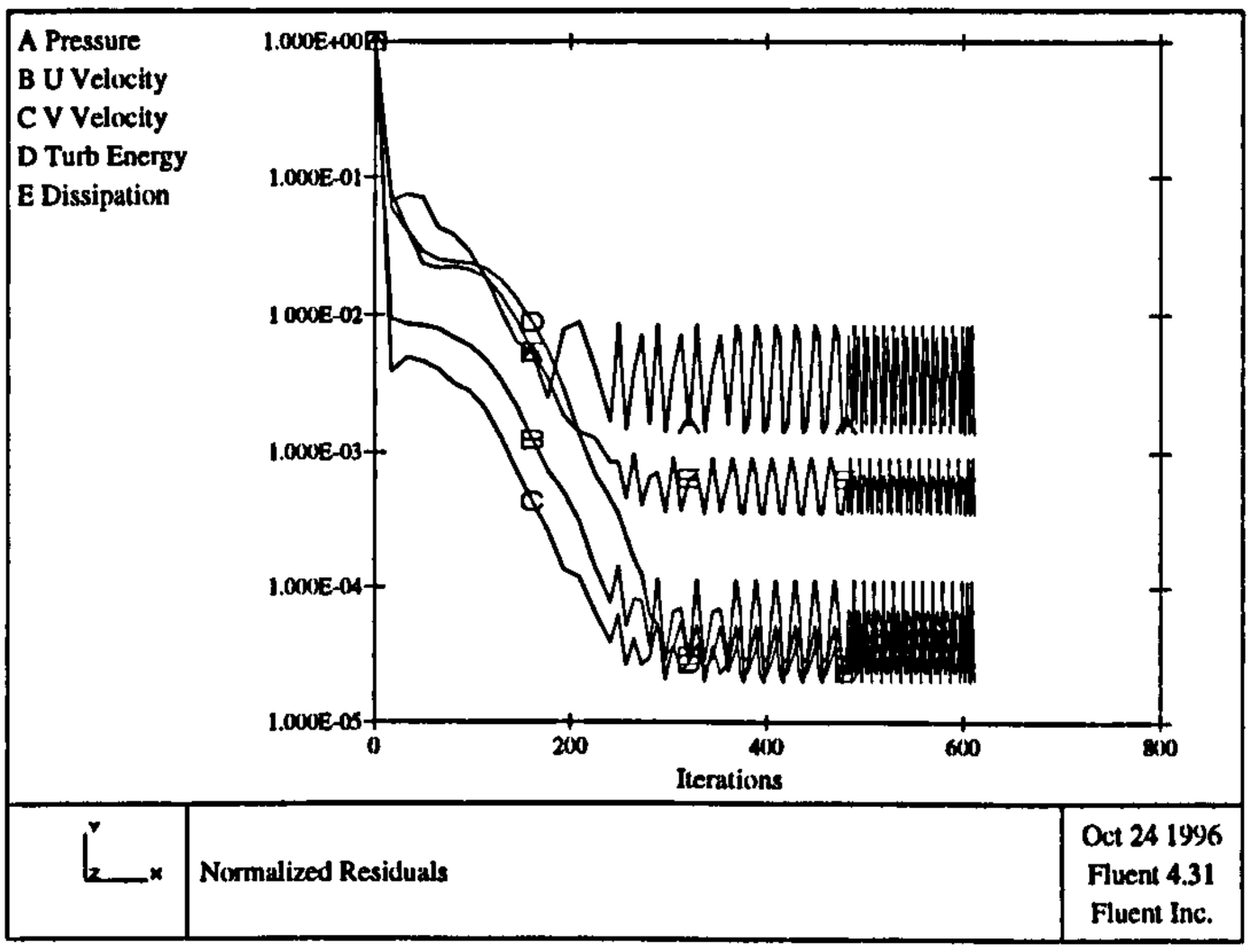

Sketch 5 : Residuals plot for Higher-Order Scheme (Lim's Exp. - T = 400mins)

If the normalised residuals were converging stably but at a slower rate, the underrelaxation factor can be increased for the velocity, turbulence kinetic energy and eddy dissipation, to speed up the convergence. However, this has to be done carefully as an increase in the underrelaxation factors may also lead to a sudden divergence. An increase in the underrelaxation factors will only has an effect on

the speed of convergence and not on the final converged solutions of the flow fields. Similarly, as mentioned in Chapter 2, the use of the pressure-velocity coupling algorithms, either SIMPLE or SIMPLEC, will give the same solution when converged as both methods are only corrections of the variables. The question of which method to use only influences the convergence speed. In the present simulation the default algorithm *i.e.* SIMPLE was used. A trial run using SIMPLEC does not exhibits any significance increase in the convergence speed.

3.5 RESULTS AND DISCUSSIONS

3.5.1 General

This section reports the results obtained from the numerical simulation. The FLUENT's results are compared with the selected benchmarks experimental results.

The three closure models available in FLUENT were tested using scoured bed profile (T=400 mins) obtained by Ali and Lim. Comparisons of the results are presented in Figure 3.10. There are no significant variations in the computed values between Standard k-ε model and the RNG k-ε model. However, as shown in Table 3.2, the RNG model converges twice as fast as the other models, thereby increasing the computational efficiency. The RSM model yield good agreement except at sections beyond that of maximum scour.

TABLE 3.2 Comparison of converging time between different Closure Model in FLUENT (T= 400mins)

CLOSURE MODEL	Number of iterations to converge
Standard k-ε	1225
RNG k-ε	705
RSM	763

Study was also made to see the effect of different grid sizes. The grid sizes used are given in the following table.

TABLE 3.3 Grid Sizes used in the study (T= 400mins)

Run	Grid Nodes
1	71 x 11
2	140 x 11
3	71 x 20
4	140 x 20

In the finite difference solution, the absolute size of cells within the grid is an important issue, since if the cells are too large, the solution obtained can be dependent on the cell size rather than purely on the physical constraints of the solution domain and the input conditions. It is therefore desirable to keep cell sizes small in order to avoid a grid-dependent solution. However, for a model domain of fixed size, reduction of the grid cell size results in a large number of nodes, which in turn leads to a greater requirement for computational resources. It is therefore equally desirable for efficiency that all sizes are no smaller than is absolutely necessary to achieve a grid-independent solution.

Another issue in the sizing of grid cells is the detail with which, and the locations at which, output is required. It is helpful if the cell centres can be located close to experimental measuring sections. As mentioned earlier, the floor velocities used by Ali and Lim to calculate the bed shear stress were measured at 0.8 cm from the bed. Therefore, the grid assignment in Run 1 is such that the location of the first node (J=2) was located 0.8 cm above the bed. In run 2, the number of grids is doubled in the I direction, whereas in Run 3, number of grids is doubled in J direction. Grid size in run 4 is doubled in both I and J directions. The results for different grid sizes used are shown in Figure 3.11. It can be seen that the predicted bed shear stress is lower near the sluice gate and higher further downstream for finer vertical grid (J direction). Grid arrangements in Run 1 and Run 2 gave better comparison with the calculated values of bed shear but due to the less number of grid nodes involved in Run 1, the number of iterations required to converge is less than Run 2. For this reason, grid arrangement in Run 1 was adopted for the rest of the analysis.

3.5.2 Flat-bed shallow submergence

Figure 3.12 shows the velocity contours at the initial flat bed condition for shallow submergence case ($H \approx d_o$). The figure shows that the flow is very symmetrical about the centreline of the jet. The floor velocity calculated by FLUENT at 0.8 cm above the bed was 32 cm/s. This compared well with measured value obtained by Ali and Lim, which was 35 cm/s.

Figure 3.13 shows the comparison between the bed shear stress obtained using FLUENT (Equation 2.38) and Ali and Lim (using Equation 3.1). Again the agreement is reasonably good with an average value of about 0.45 N/m^2.

3.5.3 Scoured-bed shallow submergence

Figures 3.14 - 3.16 show the velocity contours for three different scour conditions caused by 5.08 cm by 60.71 cm jet obtained from FLUENT. Note that the scale of these plots is distorted in the vertical direction. Figures 3.17 and 3.18 show the velocity profile and the velocity vectors for T = 400 mins respectively. Reversed flow can be seen in these figures. These confirm the observation made by Ali and Lim (1986), Rosiinski(1961), Breusers(1967), and other researchers in their experiments. It can be seen in Figure 3.18, that the negative velocities (roller) ends in the section of maximum scour forming a boundary line between reversed and forward velocities in the bottom zone.

Figures 3.19 show the computed bed shear stress distribution for T=15, 90 and 400 mins. The values, represent the x-components of the shear force at each wall-fluid interface divided by the area of that interface. These values are compared to the qualitative values computed by Ali and Lim (based on u_b at y=0.8 cm from bed) and are shown in Figures 3.20 - 3.22. It can be seen that a good agreement was obtained between the values calculated from the experimentally measured "floor" velocities and those obtained from FLUENT.

3.5.4 Flat-bed deep submergence

Figures 3.23 show typical mean velocity fields of Run1 and Run 2 obtained by Wu and Rajaratnam, whereas Figures 3.24 - 3.27 display the result of the analysis using FLUENT for Run 1 - 4 (Table 3.1). The figures show that the flow is essentially horizontal for a distance up to about 100 y_o and the vertical velocity component becomes significant only after this section. The velocity profiles show clearly the wall jet structure near the bed and the recirculating flow near the water surface.

Wu and Rajaratnam plotted the longitudinal velocity profiles in a non-dimensional form for each experiment, using u_m and b as the velocity and length scales respectively (Figure 3.28). They observed that except for the sections very close to the nozzle (within the potential core region) and far away from the nozzle (near the end of the jump), the velocity profiles at all sections, in the forward flow region, are similar. This is in agreement with the description of the classical wall jet given in section 3.2.2. FLUENT's results indicate the same observation and are shown in Figure 3.29.

3.6 THREE-DIMENSIONAL WALL JET

If the width of the wall jet is less than the width of the downstream channel, then it can be treated as a restricted form of 3-D rectangular wall jet. The main difference between this jet and the classical wall jet (CWJ) is in the fact that the jet issuing from the nozzle does not initially occupy the full width of the channel. As a result, the jet undergoes diffusion in the horizontal direction in addition to the diffusion in the vertical direction. Schematic representation of three-dimensional wall-jets is shown in Figure 3.30.

In their study of this type of jet, Rajaratnam and Subramanya (1967) found that the flow had to be considered in two parts: a boundary layer region and free mixing region. This study of diffusion characteristics along the centreline of this jet, led the authors to the following conclusions:

(a) the velocity distribution in the boundary layer region followed the power law; the exponent being between 1/10 and 1/12;

(b) the velocity distribution in the free-mixing region, the zone of established flow was similar for all b/B ratios (i.e. width of nozzle, b/width of channel, B) and is the same as the CWJ curve;

(c) the velocity and length scales were affected by the b/B ratio and can only

be satisfactory compared with the CWJ for $b/B > 0.75$. For $b/B < 0.75$ the growth of the boundary layer plays a significant part but no satisfactory method of correlation was found by the authors.

Lim (1985) conducted a fairly extensive study of the turbulent wall jet originating from 5.08 cm x 5.08 cm, 5.08 cm x 10.16 cm and, 5.08 cm x 20.32 cm nozzles, for both deep and shallow submergence. He studied the effect of the various jets on local scouring developments. For the present study, the shallow submergence three-dimensional jet originating from 5.08 cm x 5.08 cm was simulated using FLUENT. Two cases, namely; flat bed and scoured bed at asymptotic stage (t= 360 mins) were considered. Comparisons were made between FLUENT's output and Lim's experimental results and are reported in the following section.

3.6.1 Simulation of the Flow in Local Scour with Minimum Jet Submergence

Figures 3.31 and 3.32 show respectively the measured and predicted velocity contours for 5.08 cm X 5.08 cm JET measured along the centreline of the scour profiles. FLUENT predicted reasonably well the flow pattern produced by the square nozzle. This is further justified by the maximum velocity decay plot as shown in Figure 3.33. Velocities predicted by FLUENT are slightly smaller than the measured values.

Figure 3.34 show the bed contours as observed by Lim, at the asymptotic stage (t = 360 mins). Figure 3.35 depicted the simulated bed profile created using PreBFC. The predicted velocity vectors near the bed and near the surface are shown in Figure 3.36. The measured and predicted velocity contours in the centre plane of the scour hole are shown in Figure 3.37. Fairly good agreement can be observed between the two as illustrated in Figure 3.38. It can be seen that the mean flow velocity for any section decreases continuously in the flow direction, unlike the

2-D flow situation, where the mean velocity increases as the flow boundary converges. It can also be seen that there is no reversed flow in the 3-D jet near the bottom zone of the hole for scour at the asymptotic state. Velocity measurements conducted by Rajaratnam and Berry (1977) with 3-D circular air jet (see Figure 3.1) also found no reversed flow at the asymptotic state.

Figures 3.39 and 3.40 show the measured and the predicted plot of floor velocity isovels for t = 360 mins., respectively. The flow distribution resembles that of a diverging-converging flow situation, that is, once a scour hole is formed, the jet immediately diffuses and expands into the hole creating a region of intense mixing and shearing. The diffusion causes a general decrease in the mean flow velocity and an increase in the pressure gradient. For sections beyond that of maximum erosion, the velocity profiles generally become more uniform and the converging bed causes the mean flow velocity to increase.

As mentioned earlier Ali and Lim calculated the boundary shear stress using floor velocity data (as presented in Figure 3.39) using Equation 3.4 and 3.5. The calculated shear stress distribution is shown in Figure 3.41. Figure 3.42 shows the shear stress predicted by FLUENT. In general, it can be seen in both figures that (like 2-D) the bed shear stress is lowest around the region of maximum erosion and is highest near the crest region.

3.7 CONCLUSIONS

1. The numerical prediction scheme provided by FLUENT was used to predict the 2-D flow velocity distribution and the bed shear stress for both flat bed and scoured bed. The computed values were then compared to the experimental values obtained by other researchers.

2. The FLUENT features allowed the basic turbulence equations and associated closure models to be solved with relative ease. The PreBFC and grid-generation facility in FLUENT enabled the use of variable finite-different grid sizes so as to minimise demand for computer resources whilst still achieving useful simulation results. The use of Body-Fitted Co-ordinates gave better representation of the scoured-bed than the Cartesian Co-ordinates, resulting in more reliable bed shear stresses.

3. Overall, the results showed a close agreement with the various selected experimental results. In the case of bed shear stress, FLUENT results are consistent with the calculated results of Ali and Lim. The k-ε and the RNG k-ε models describe the flow at the boundary better than the RSM model. No significant difference in the results was observed between the k-ε and the RNG k-ε, except that RNG k-ε model converged twice as fast as the standard k-ε model.

In the following chapters FLUENT will be employed to investigate the flow characteristics in different classes of turbulent flows namely - offset jets, flow around bridge piers and spur-dykes and flow circulation in water supply reservoirs.

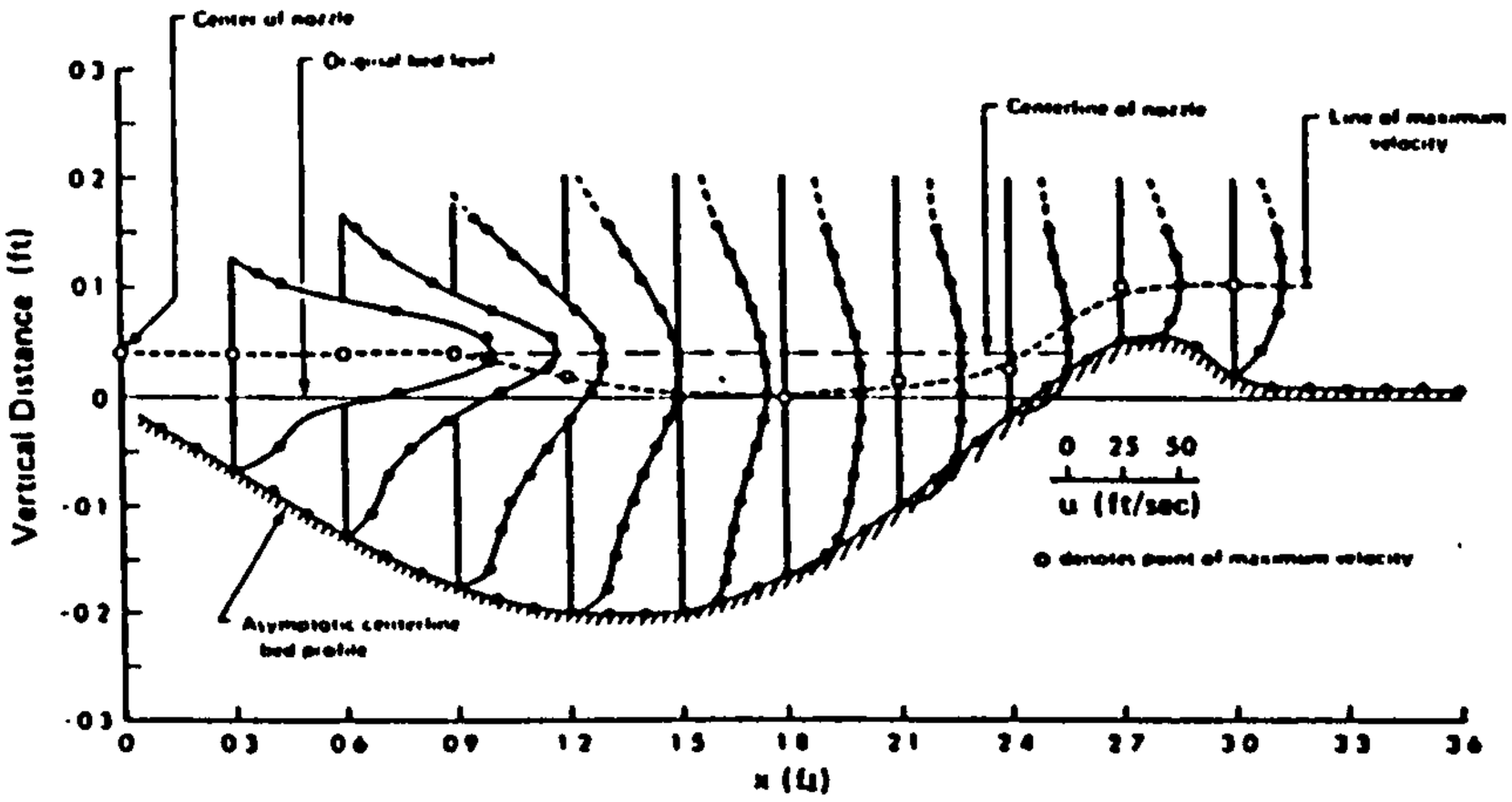

Figure 3.1 : Velocity distribution of 3-D air jet in the asymptotic state (yo = 0.925 in, U_o = 113 ft/sec, d_{50} = 1.4 mm, S = 1.041)
(After Rajaratnam & Berry, 1977)

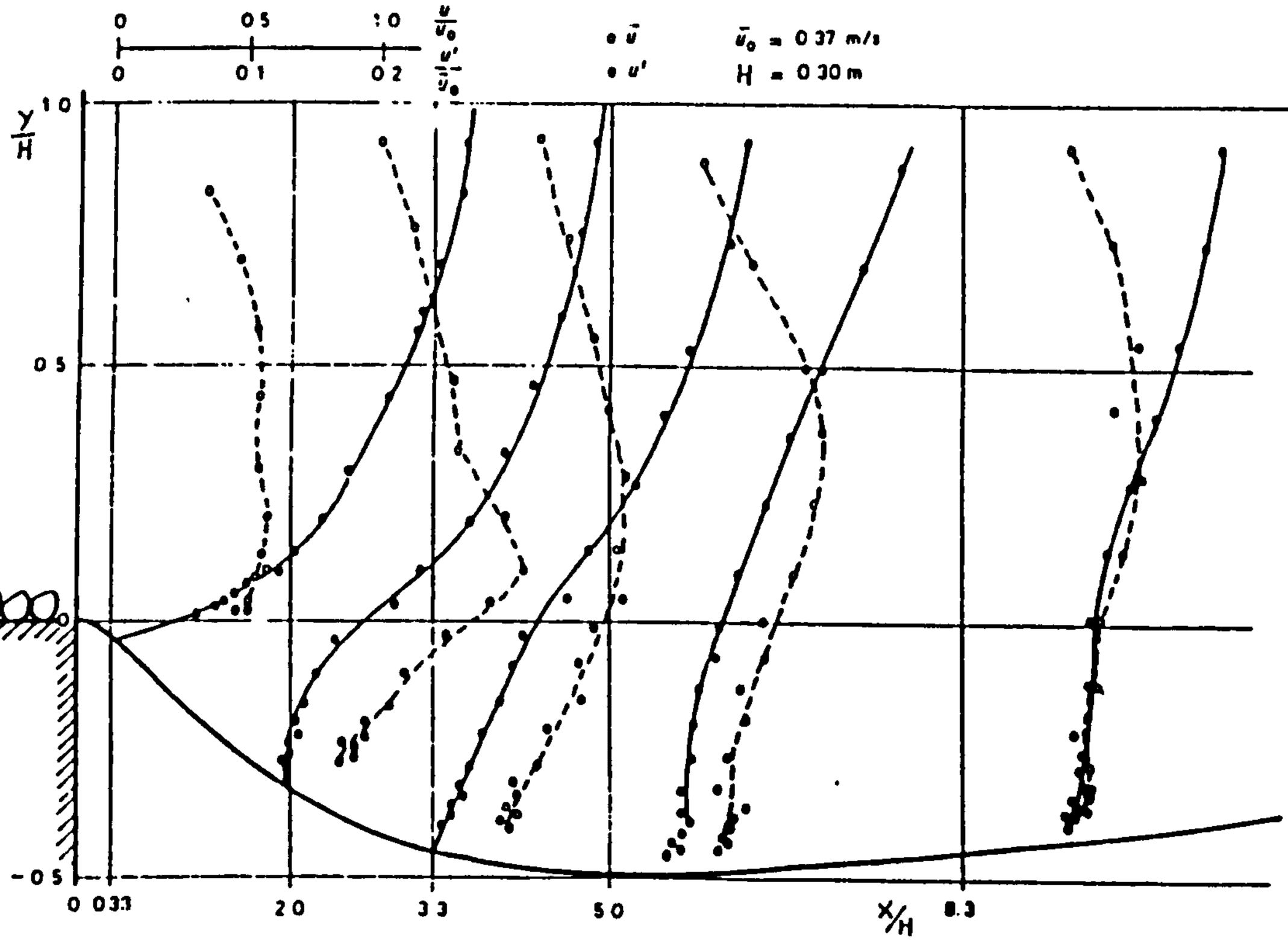

Figure 3.2 : Velocity and turbulence-intensity in the scouring hole
(After Breusers, 1967)

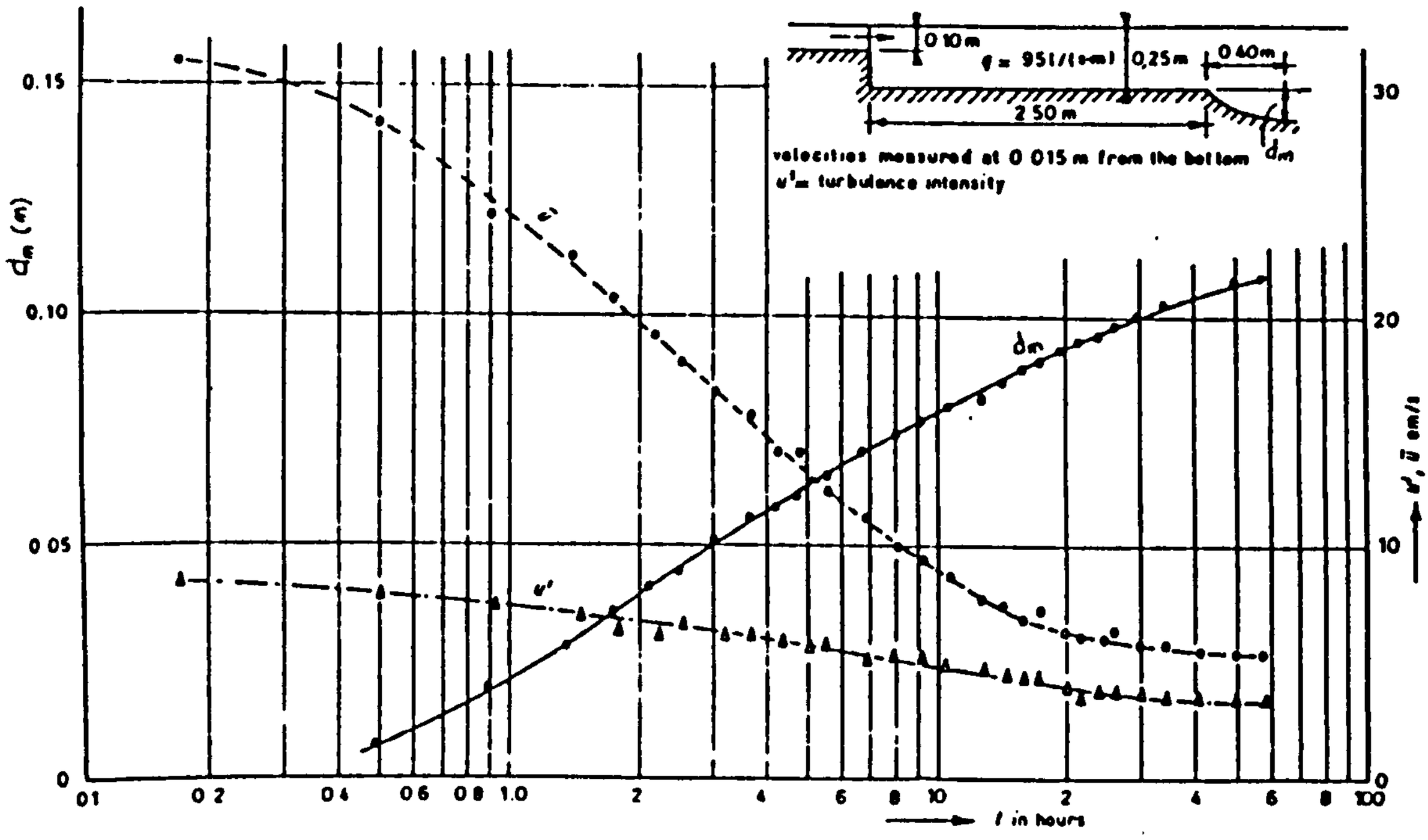

Figure 3.3 : Scour Depth and Floor Velocity as a function of time (After Breusers. 1967)

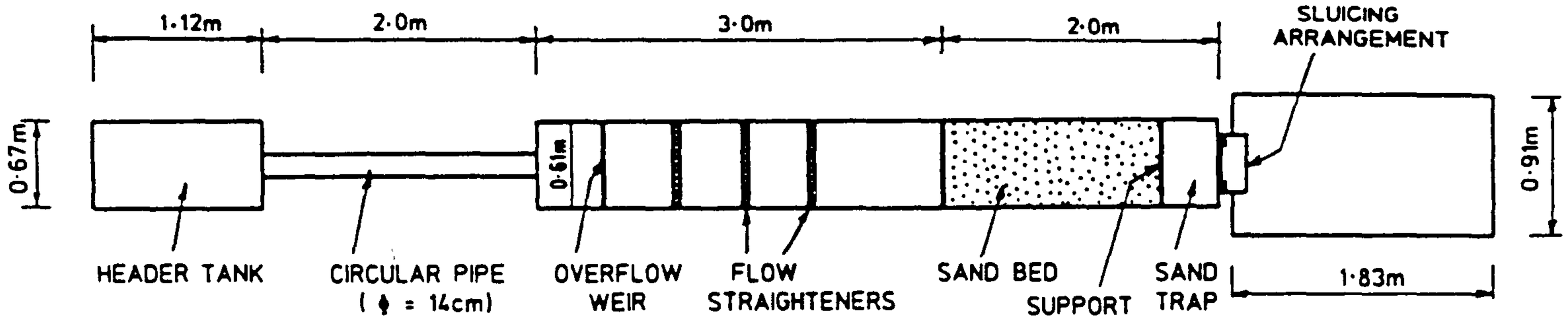

Figure 3.4 : Laboratory Layout For The Sluice Gate Experiment (After Lim, 1985)

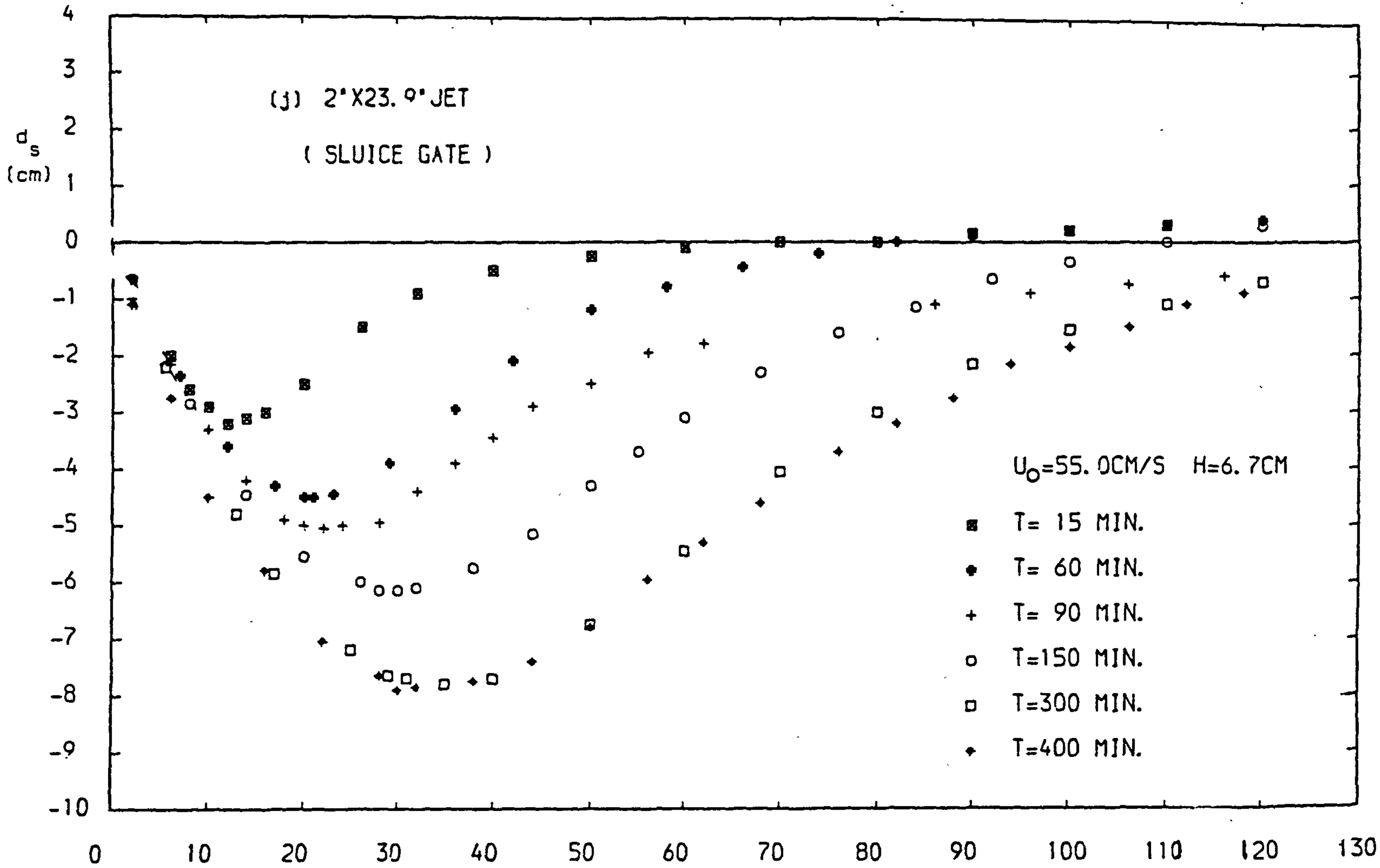

FIGURE 3.5 : Time Evolution of Centerline Bed Profiles with H = 6.7 cm (After Lim, 1985)

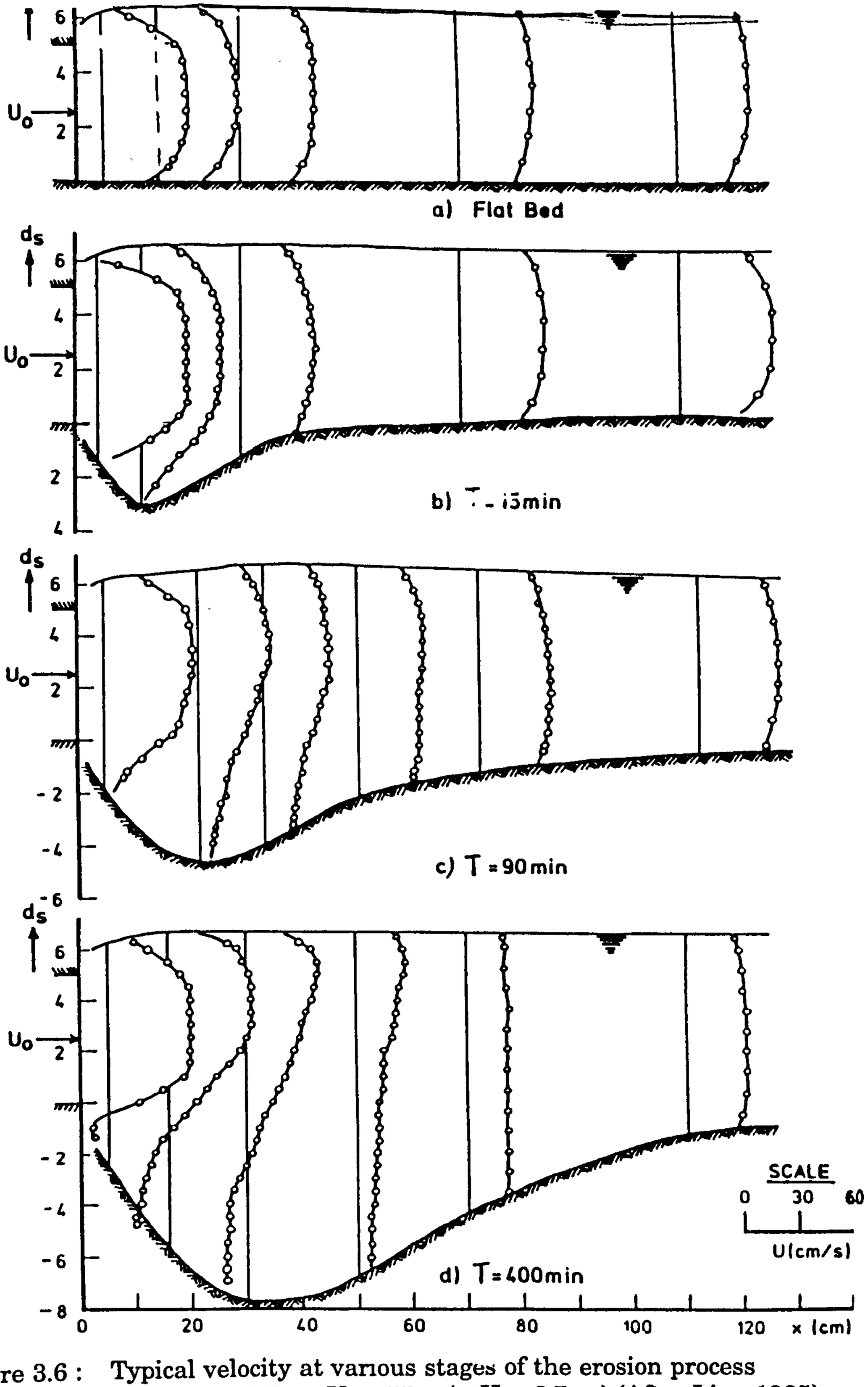

Figure 3.6 : Typical velocity at various stages of the erosion process (5.08cm x 60.7cm, U_o = 55cm/s, H = 6.7cm) (After Lim, 1985)

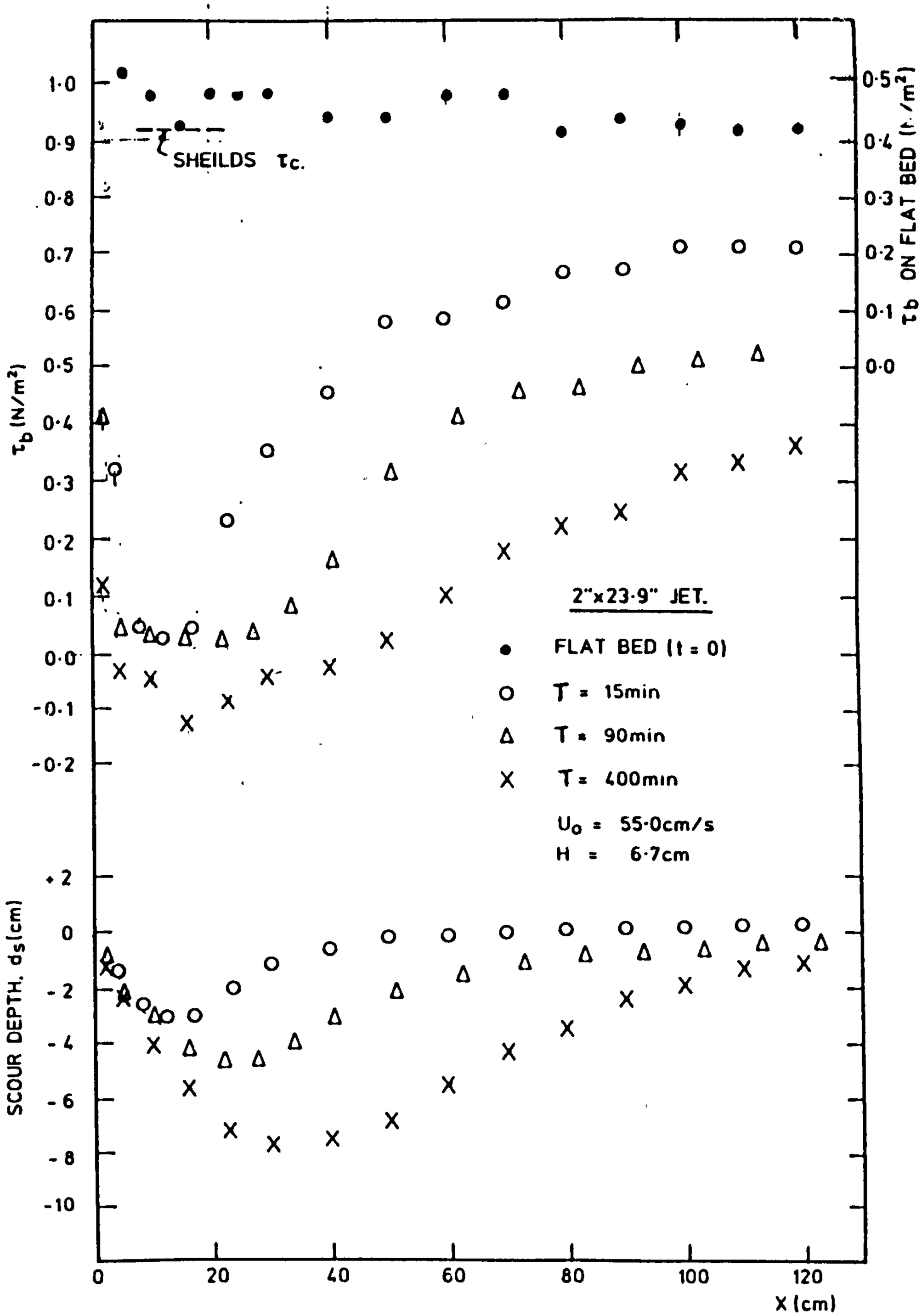

Figure 3.7 : 5.08cm x 60.7cm Jet - Boundary shear stress distribution along the centreline bed profile. (After Lim, 1985)

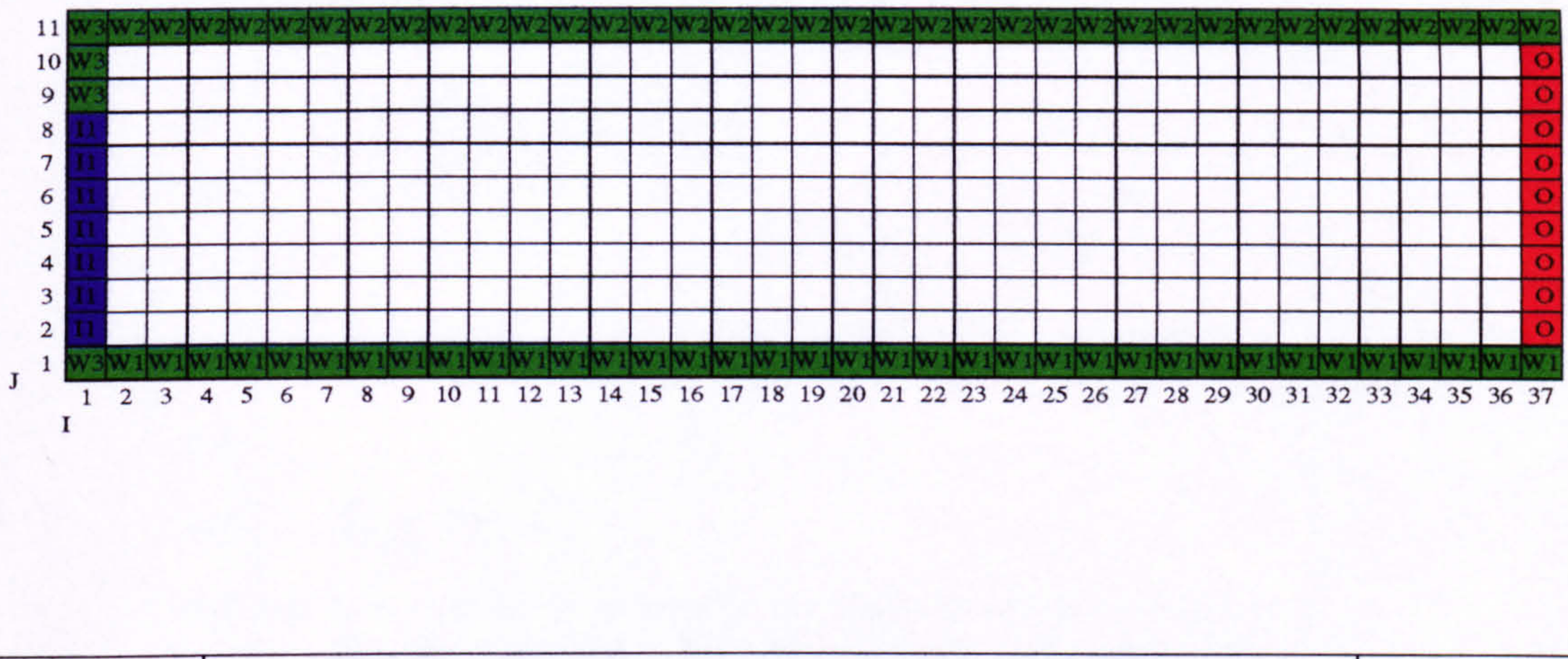

Figure 3.8 : Computational Grid
LOCAL SCOURING (T = 400 mins)

Fluent 4.31
Fluent Inc.

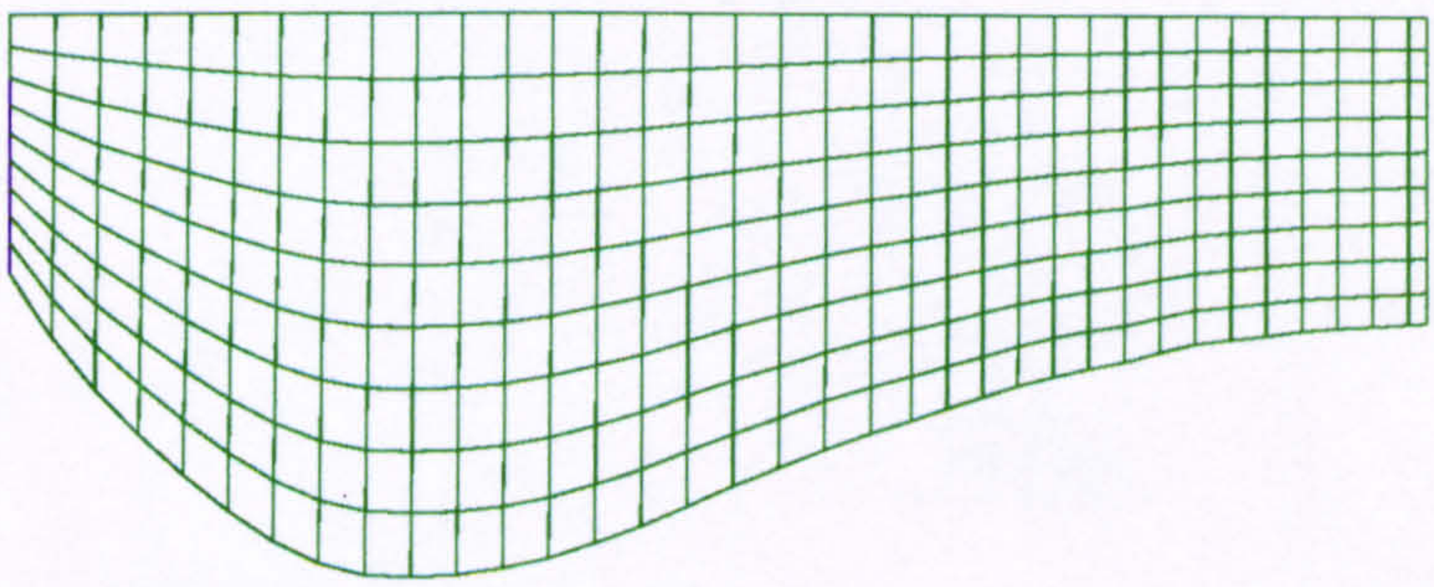

Figure 3.9 : Physical Grid
LOCAL SCOURING (T = 400 mins)

Fluent 4.31
Fluent Inc.

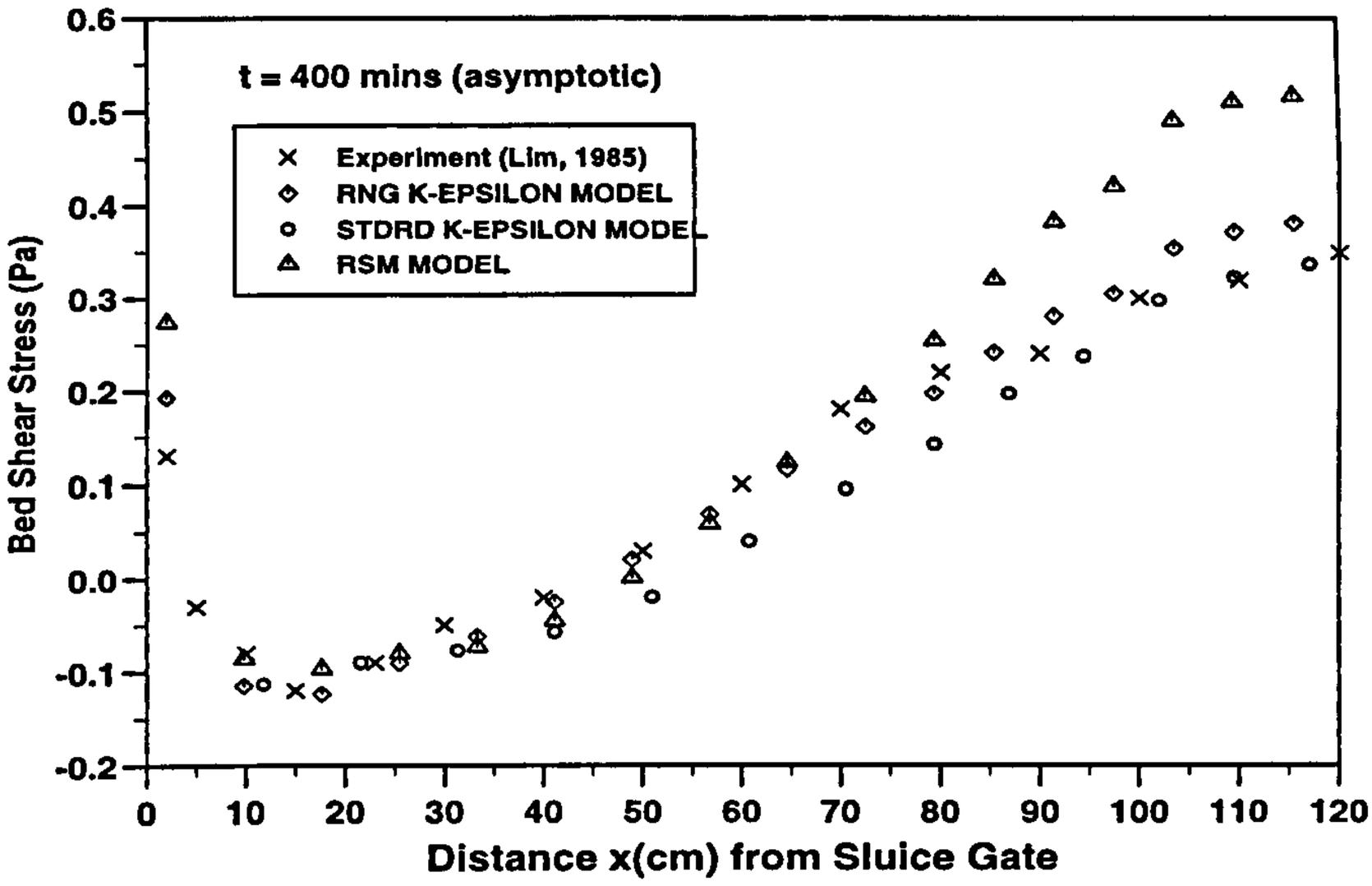

Figure 3.10 : Comparison between three closure models available in FLUENT (T = 400 mins)

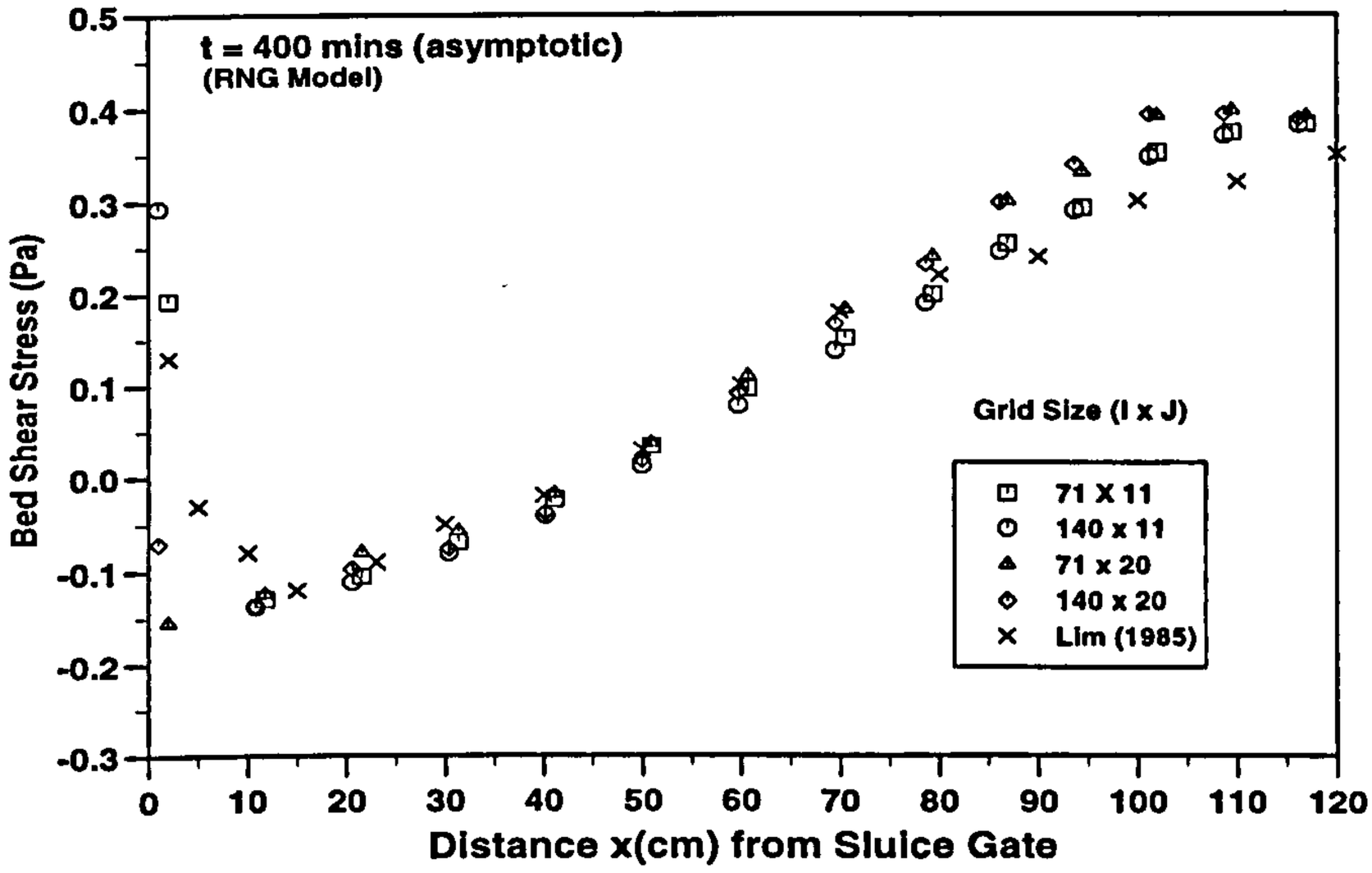

Figure 3.11 : Effect of Different Grid Sizes (T = 400 mins)

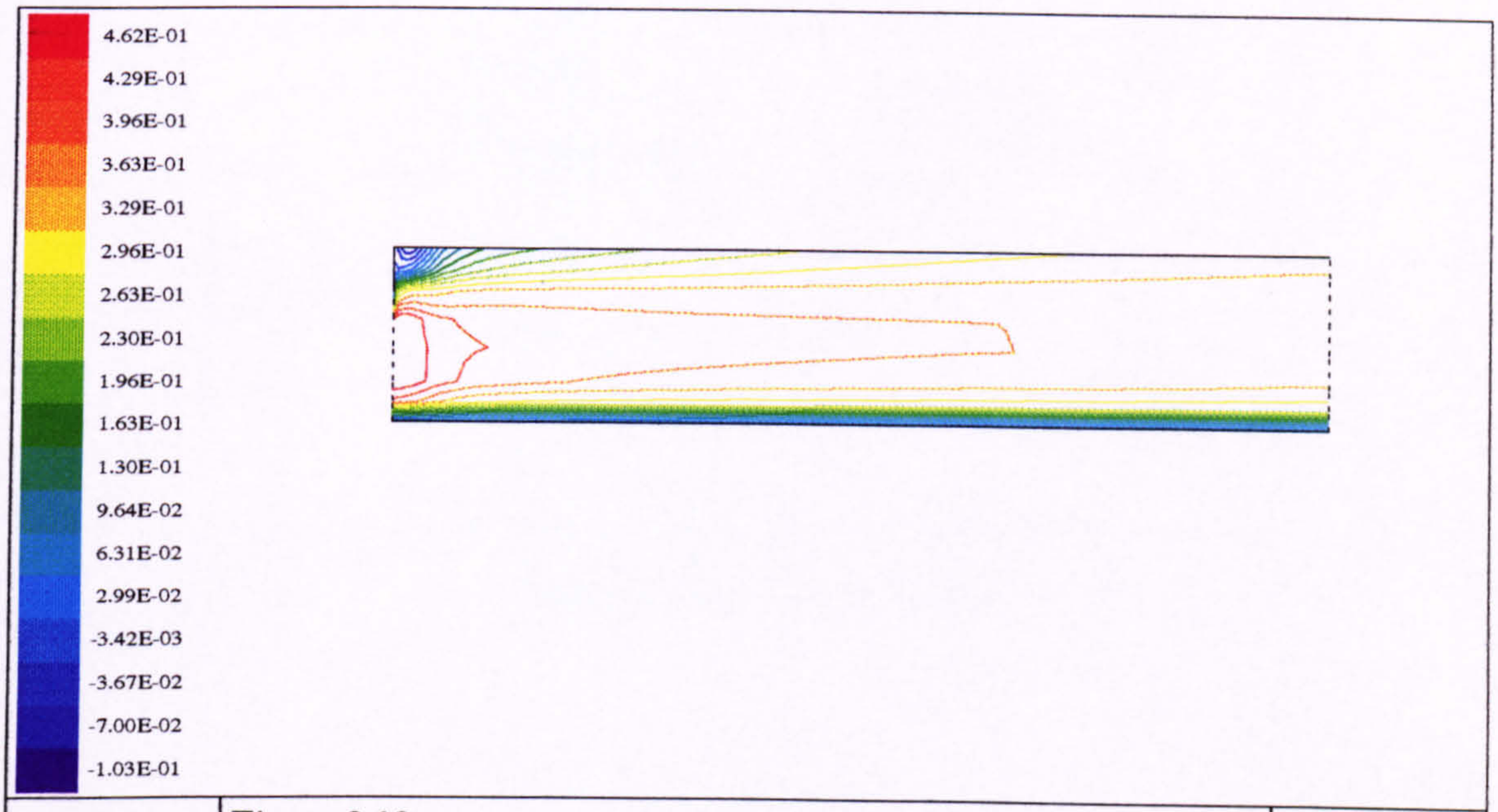

Figure 3.12
INITIAL BED CONDITION (T = 0)
U Velocity Profile (m/s)

Fluent 4.31
Fluent Inc.

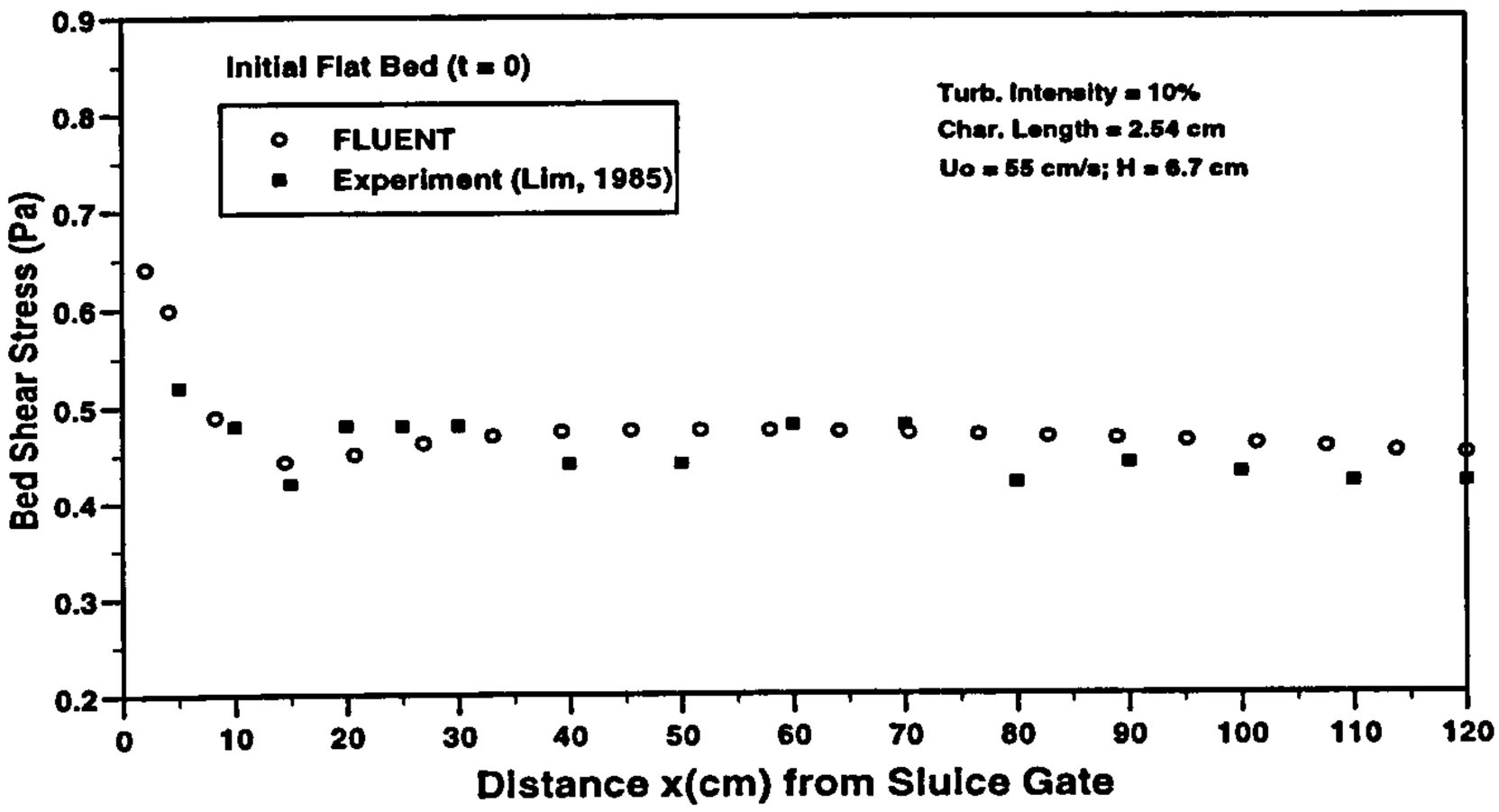

Figure 3.13 : Bed shear stress distribution (Initial flat bed condition)

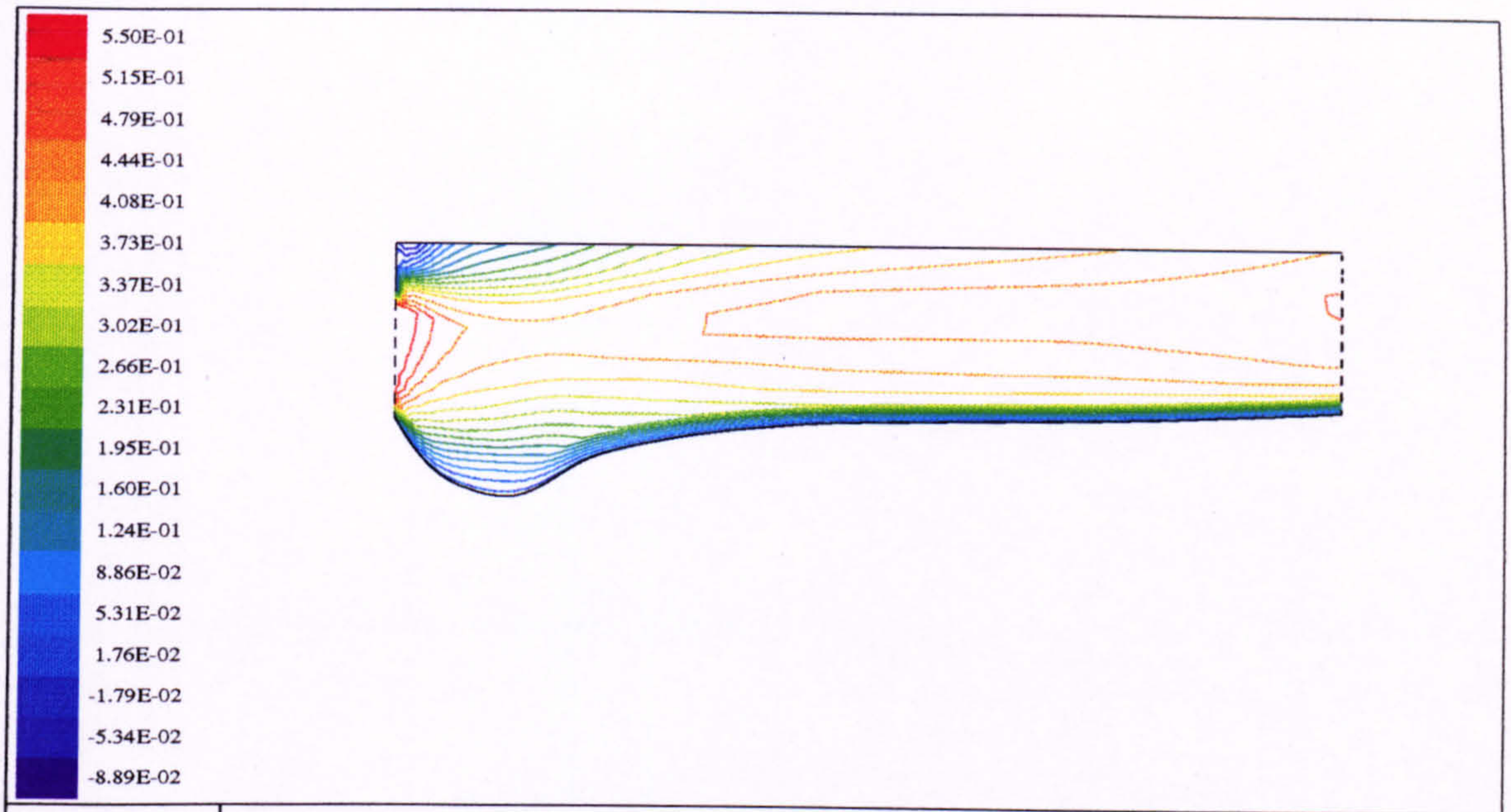

Figure 3.14
LOCAL SCOURING (T = 15 mins)
U Velocity Profile (m/s)

Fluent 4.31
Fluent Inc.

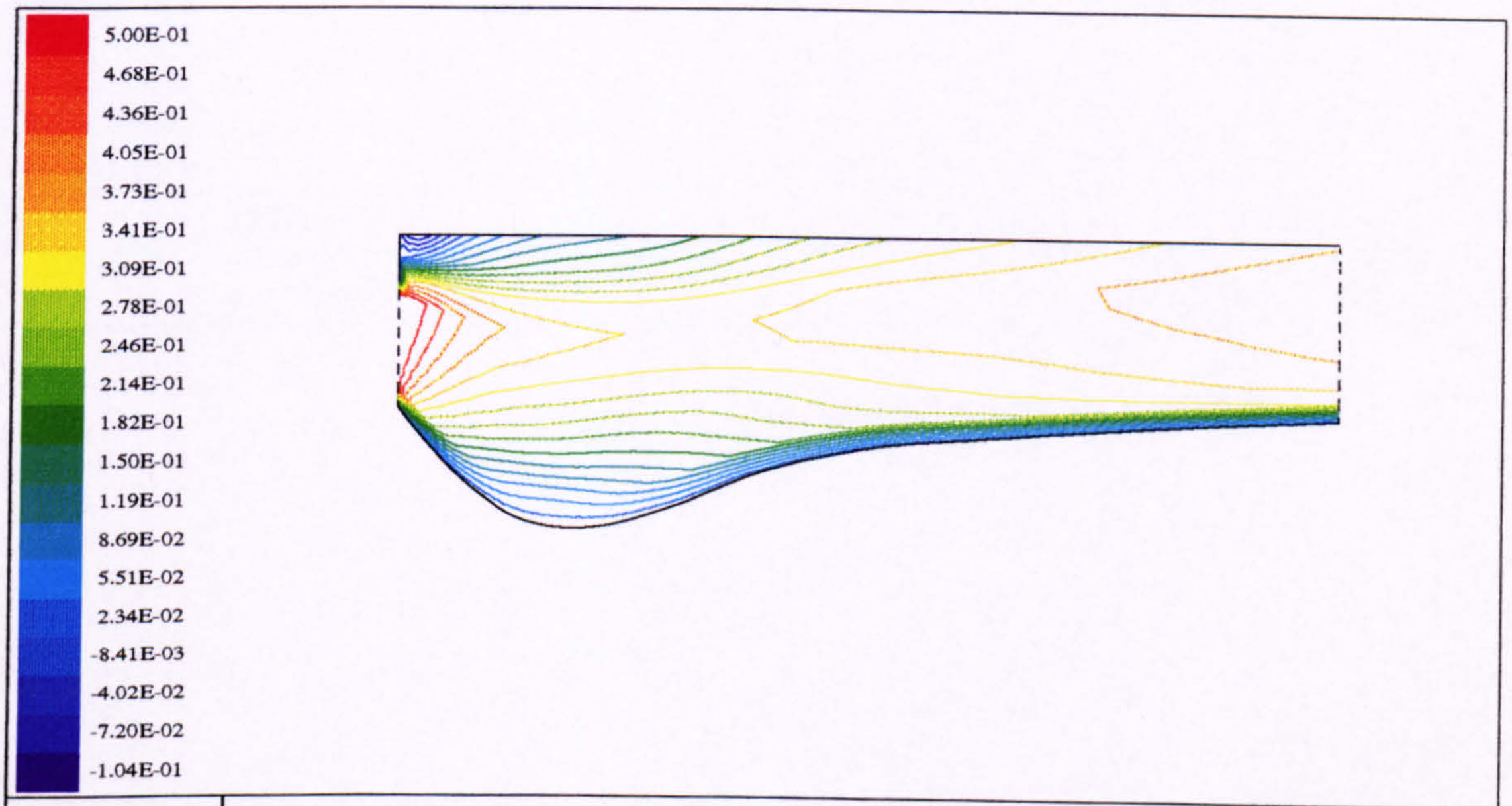

Figure 3.15
LOCAL SCOURING (T = 90 mins)
U Velocity Contour (m/s)

Fluent 4.31
Fluent Inc.

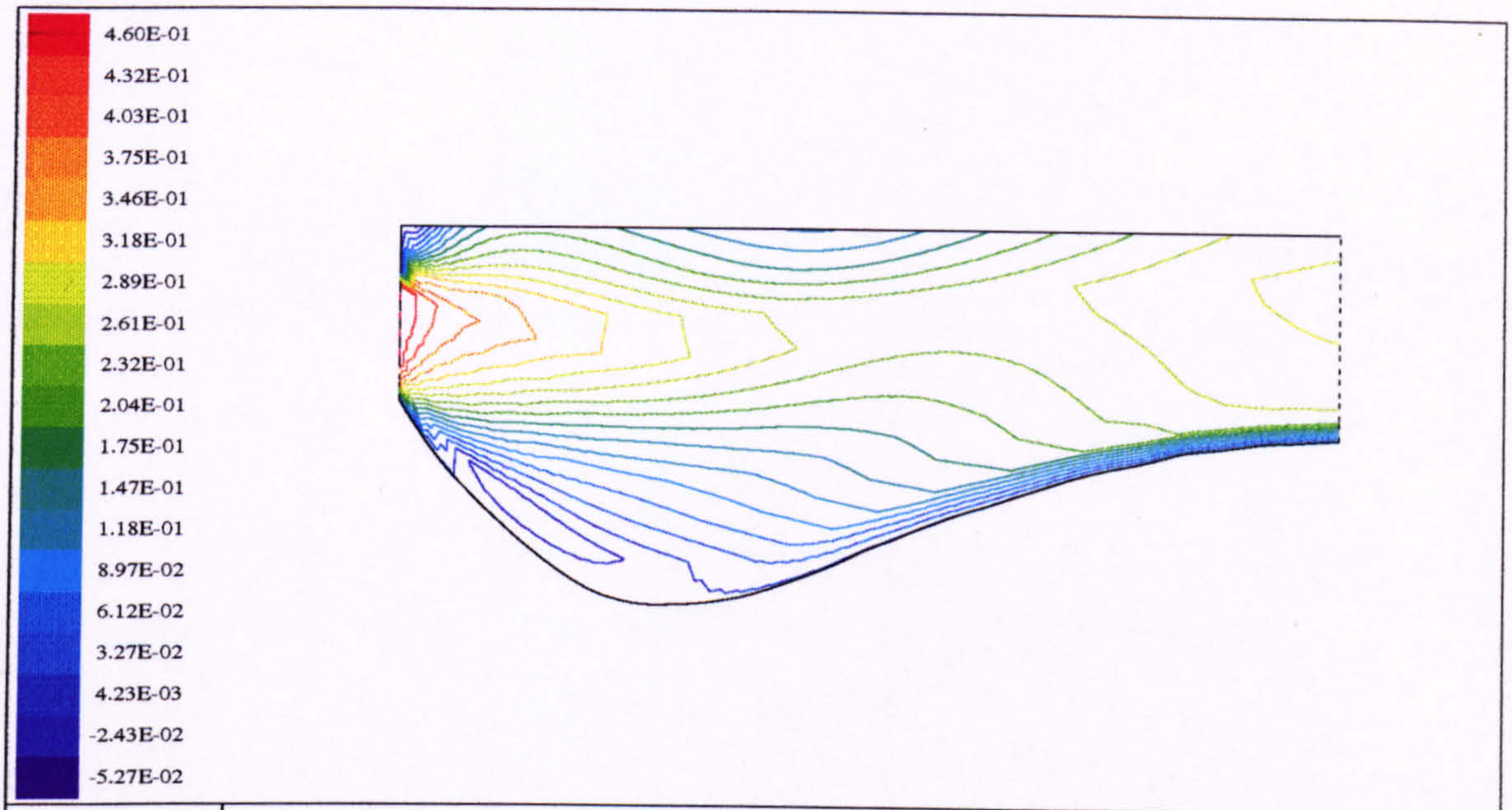

Figure 3.16
Local Scouring (T = 400 mins)
U Velocity Contour

Fluent 4.31
Fluent Inc.

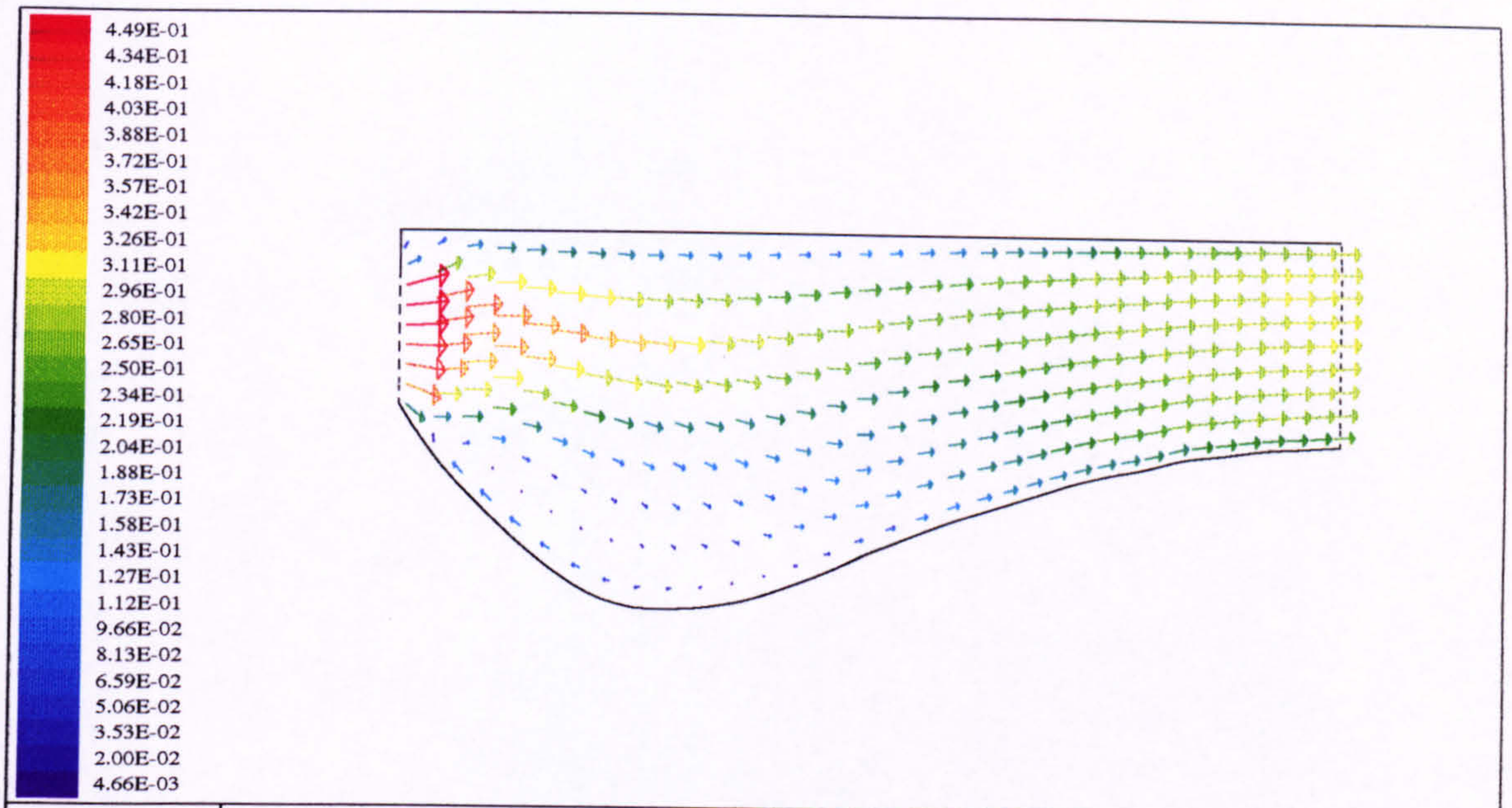

Figure 3.17
Local Scouring (T = 400 mins)
U Velocity Vector

Fluent 4.31
Fluent Inc.

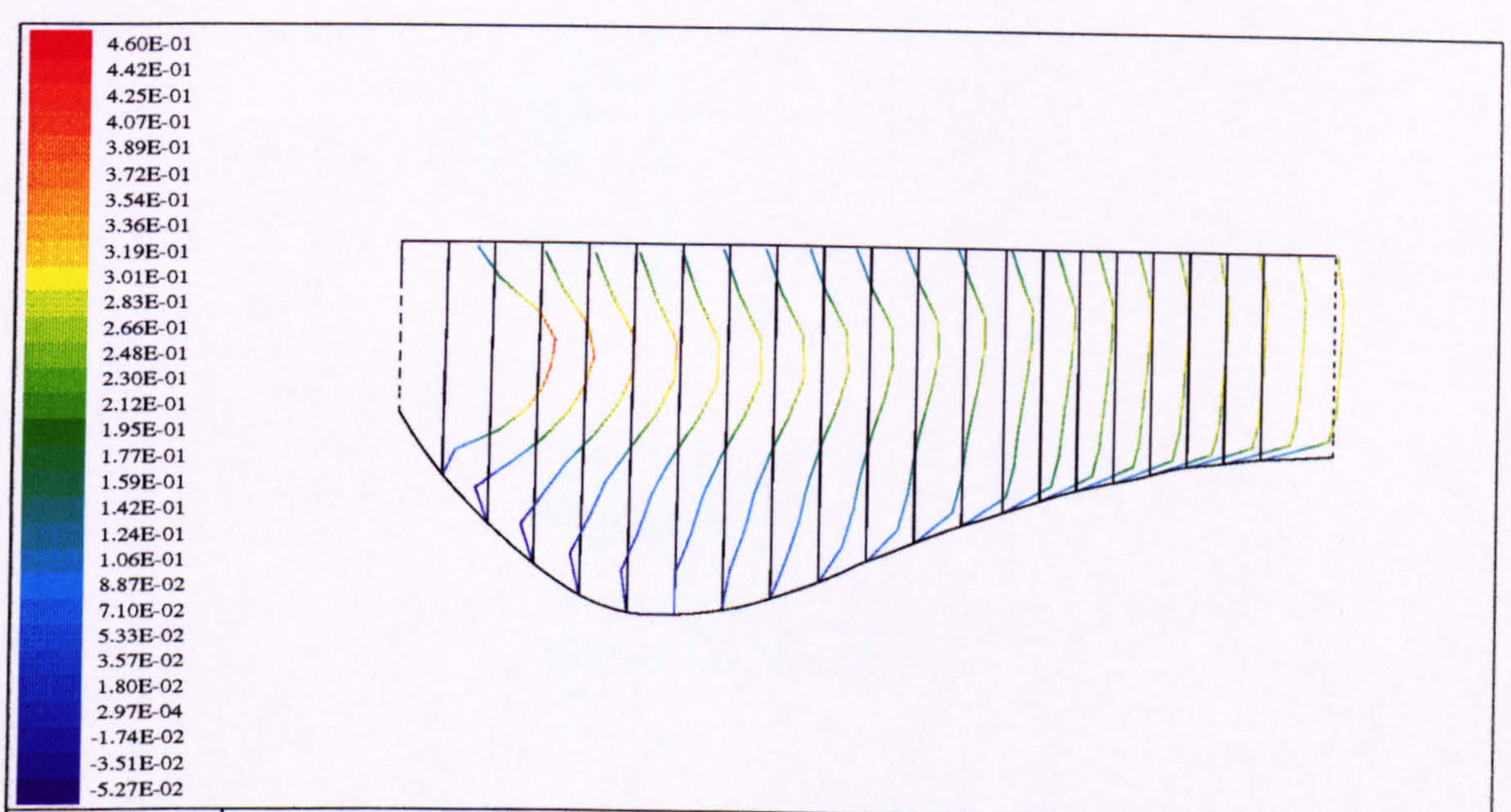

Figure 3.18
Local Scouring (T = 400 mins)
U Velocity Profile

Fluent 4.31
Fluent Inc.

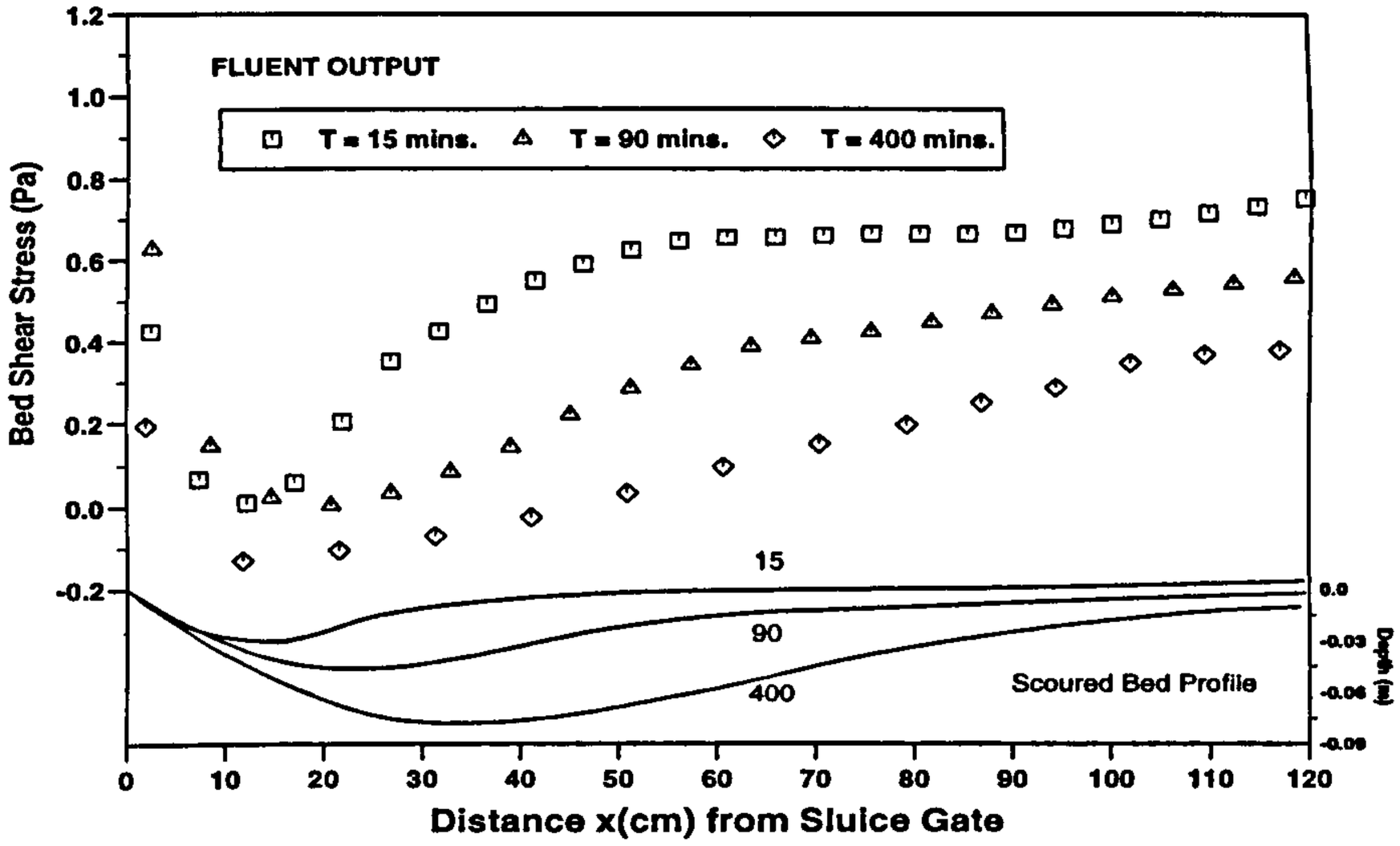

Figure 3.19 :Bed shear stress distribution (T=15, 90 and 400 mins)

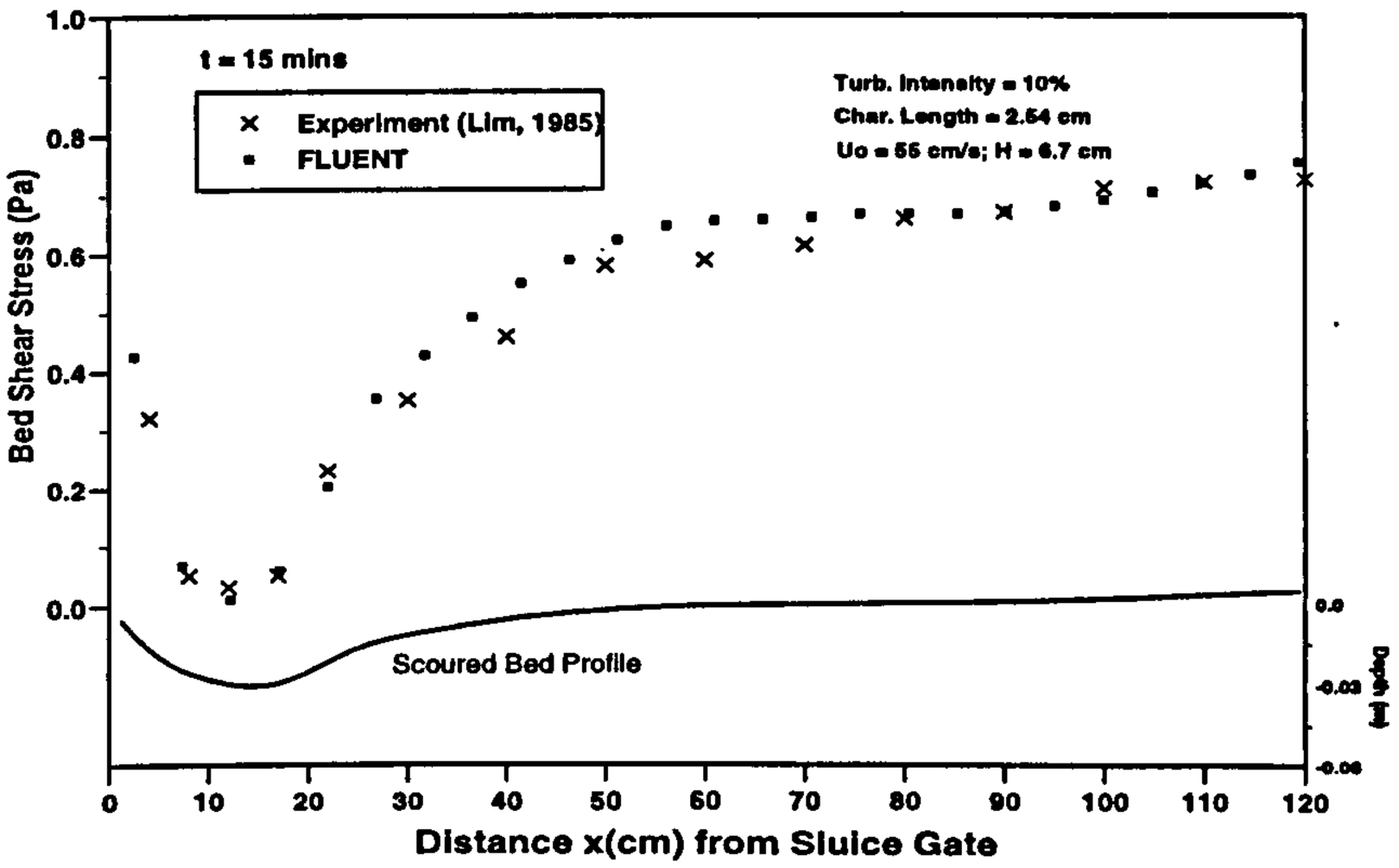

Figure 3.20 :Bed shear stress distribution (T=15 mins)

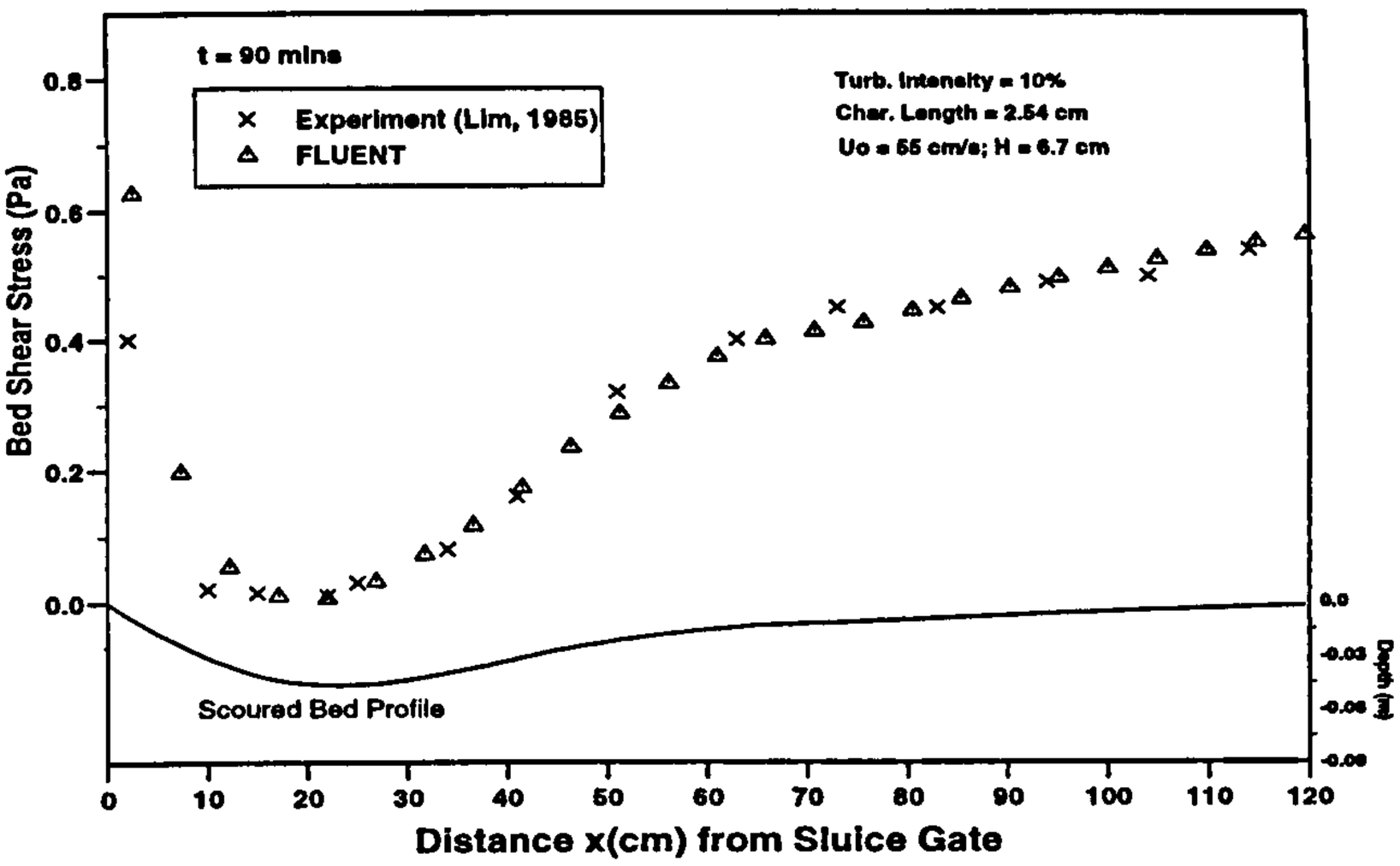

Figure 3.21 :Bed shear stress distribution (T=90 mins)

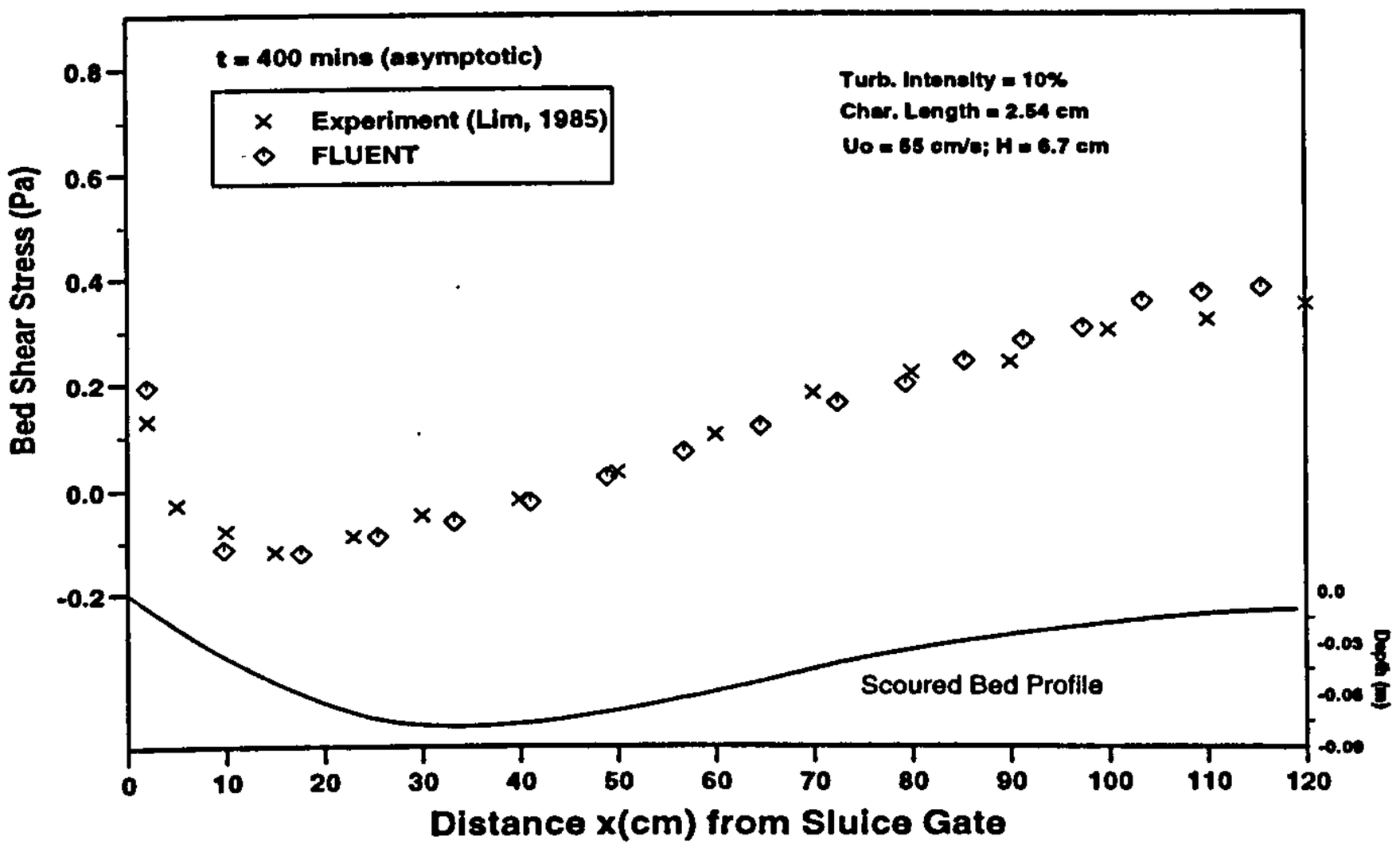

Figure 3.22 :Bed shear stress distribution (T = 400 mins)

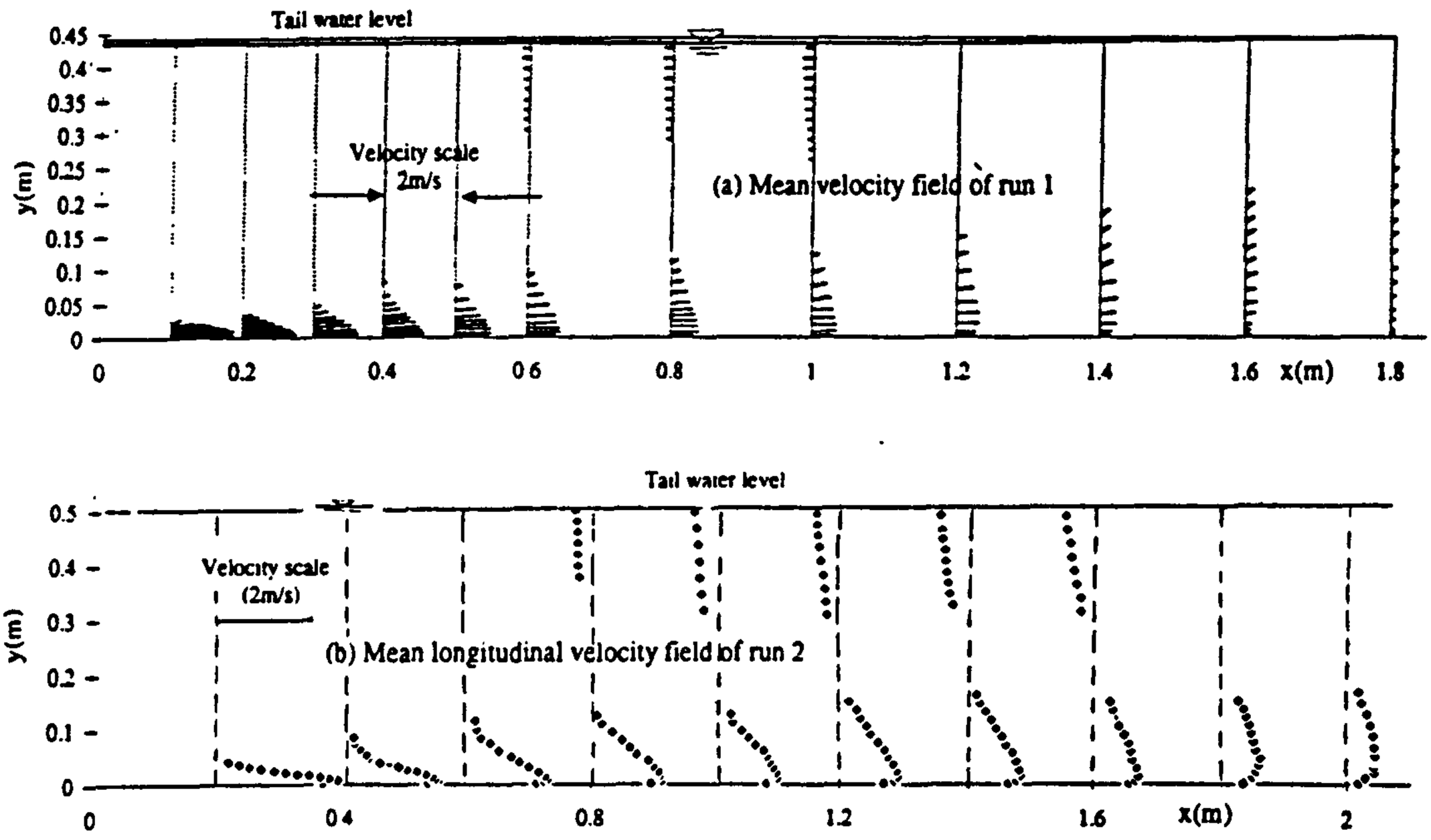

Figure 3.23 : Typical velocity fields of submerged wall-jets

(After Wu and Rajaratnam, 1995)

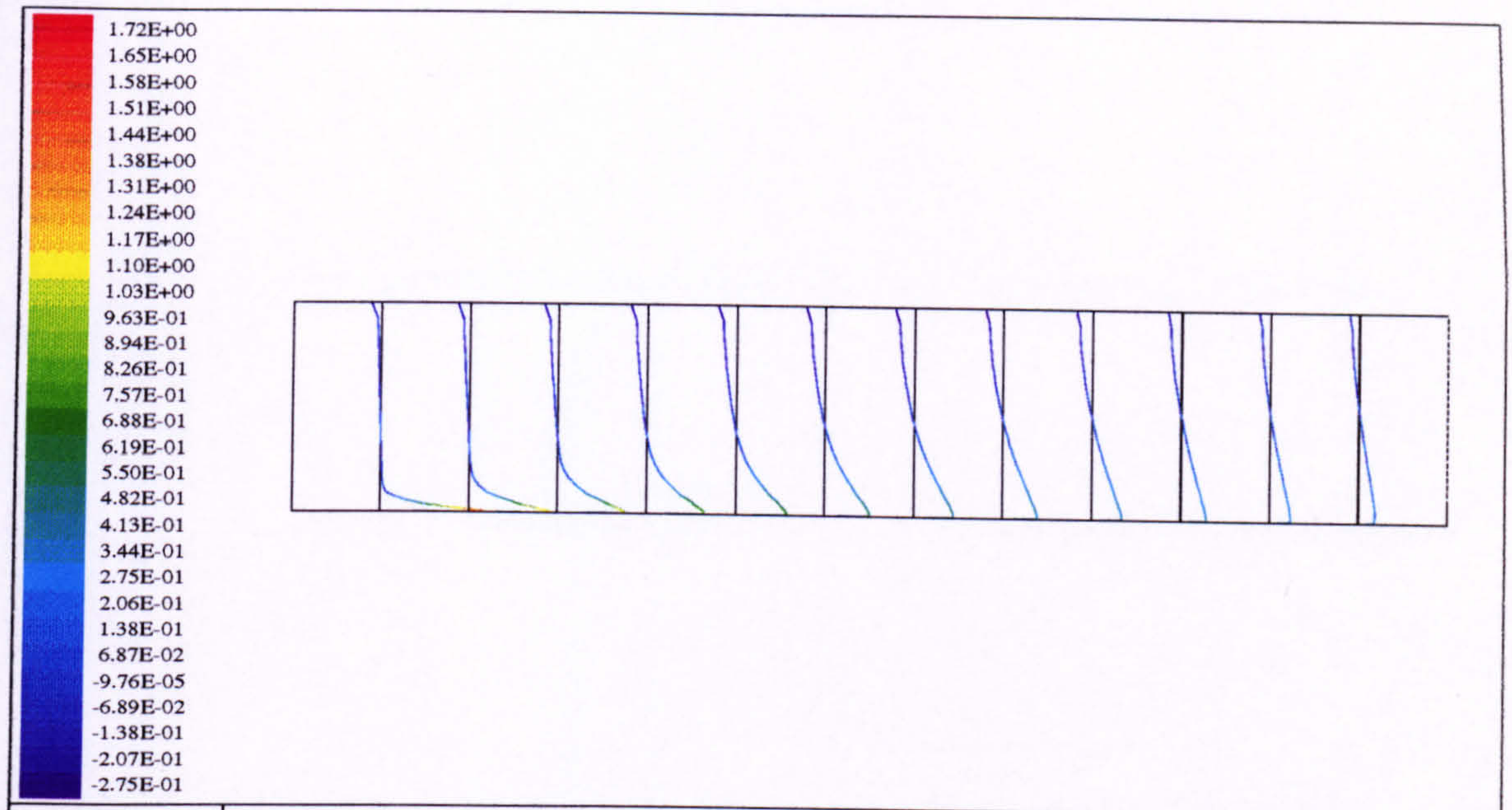

Figure 3.24 (a) : Fo = 5.48, H = 0.44m, yo = 0.010m
U-Velocity (M/S)
Max = 1.720E+00 Min = -2.753E-01

Fluent 4.31
Fluent Inc.

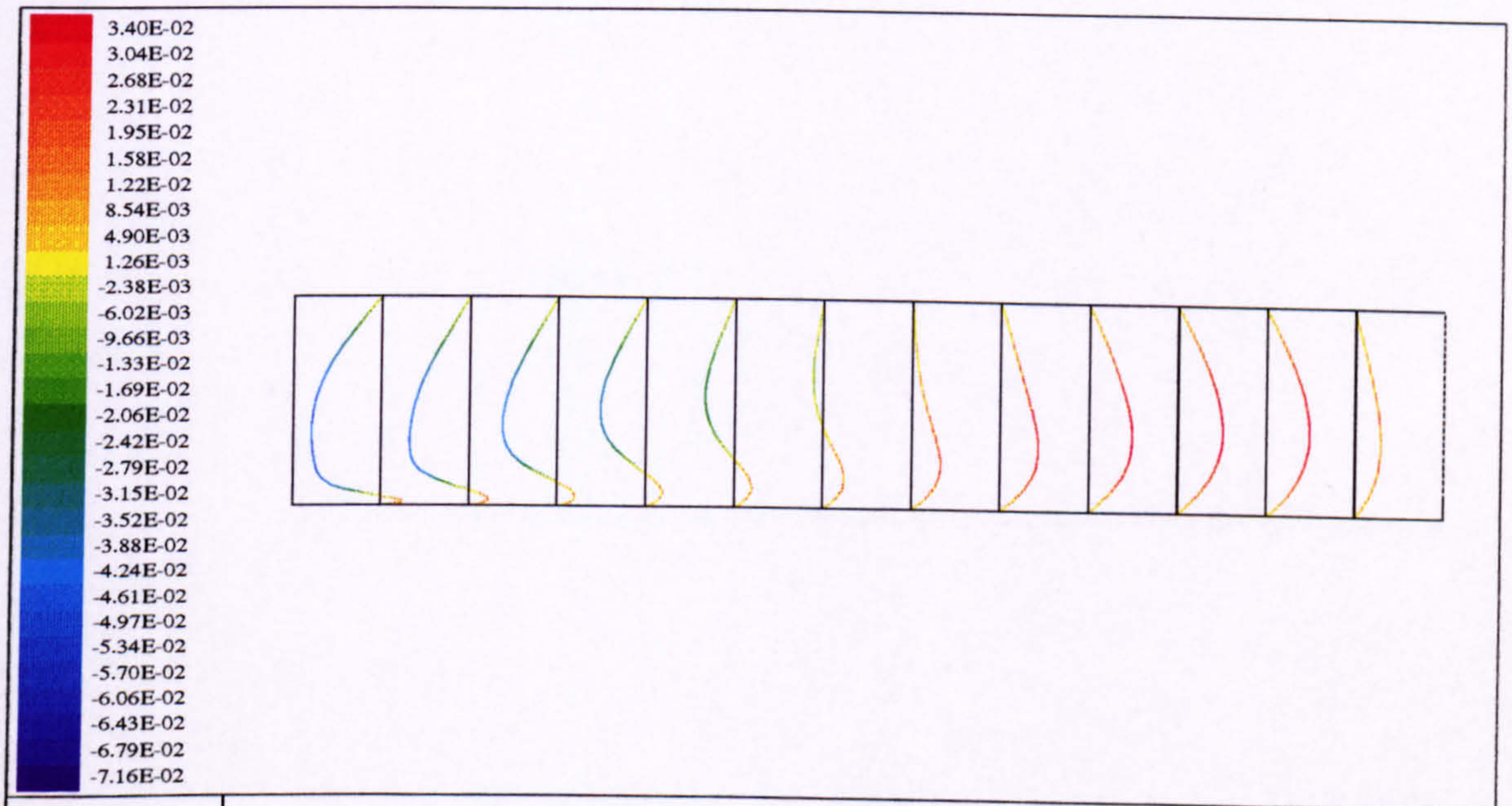

Figure 3.24 (b) : Fo = 5.48, H = 0.44m, yo = 0.010m
V-Velocity (M/S)
Max = 3.404E-02 Min = -7.157E-02

Fluent 4.31
Fluent Inc.

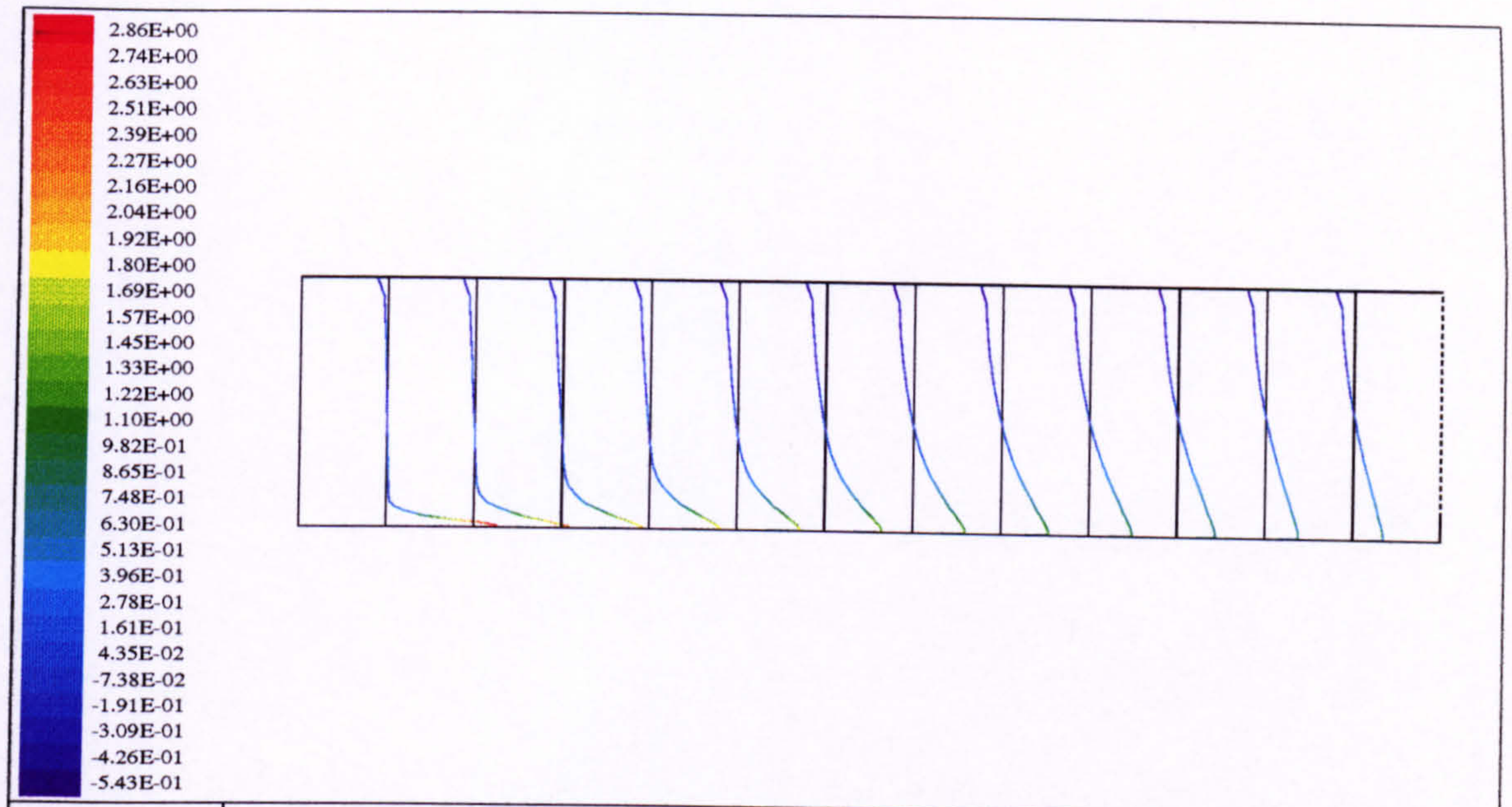

Figure 3.25 (a) : Fo = 7.46, H = 0.53m, yo = 0.015m
U-Velocity (M/S)
Max = 2.860E+00 Min = -5.433E-01

Fluent 4.31
Fluent Inc.

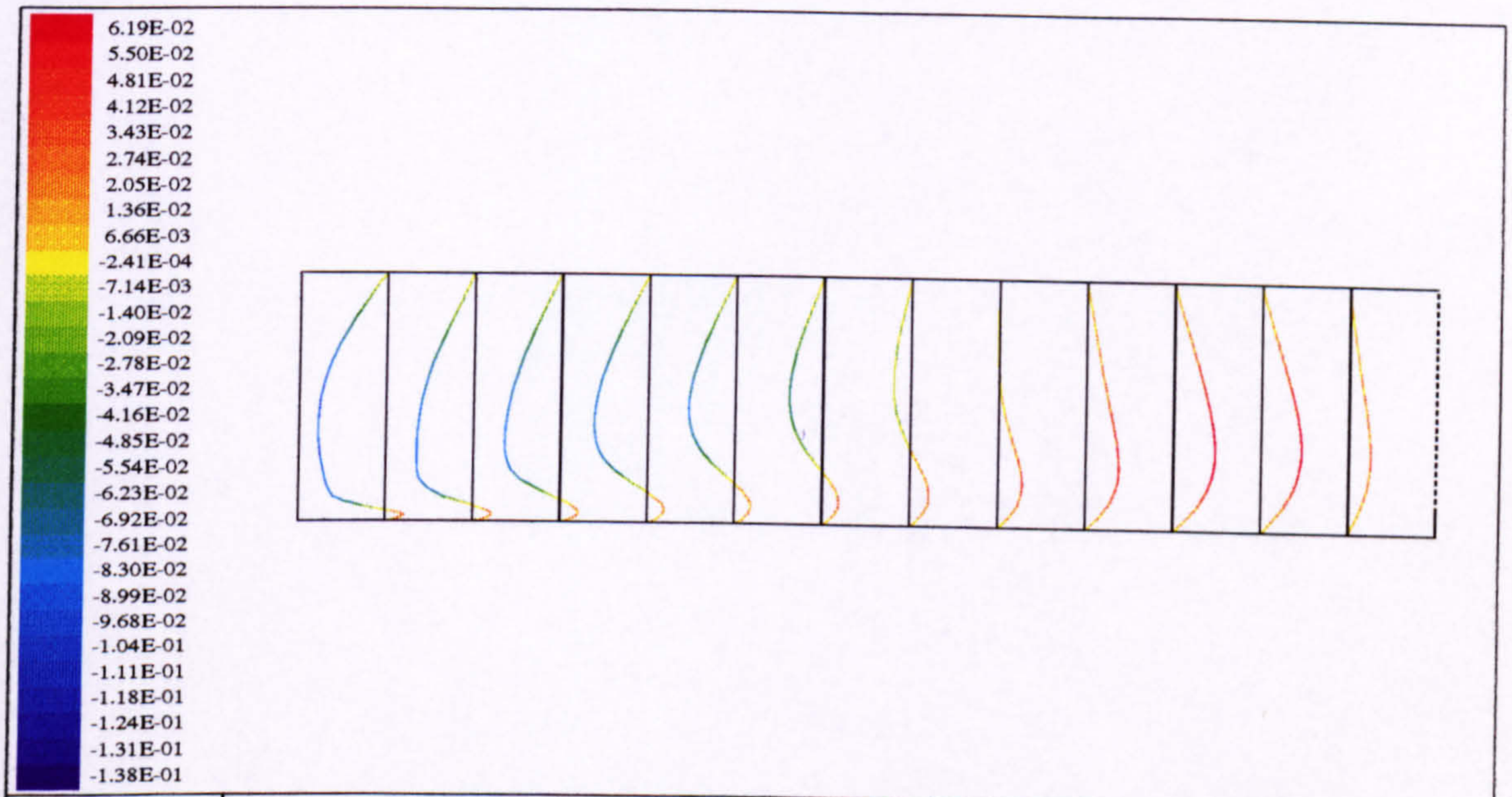

Figure 3.25 (b) : Fo = 7.46, H = 0.53m, yo = 0.015m
V-Velocity (M/S)
Max = 6.186E-02 Min = -1.382E-01

Fluent 4.31
Fluent Inc.

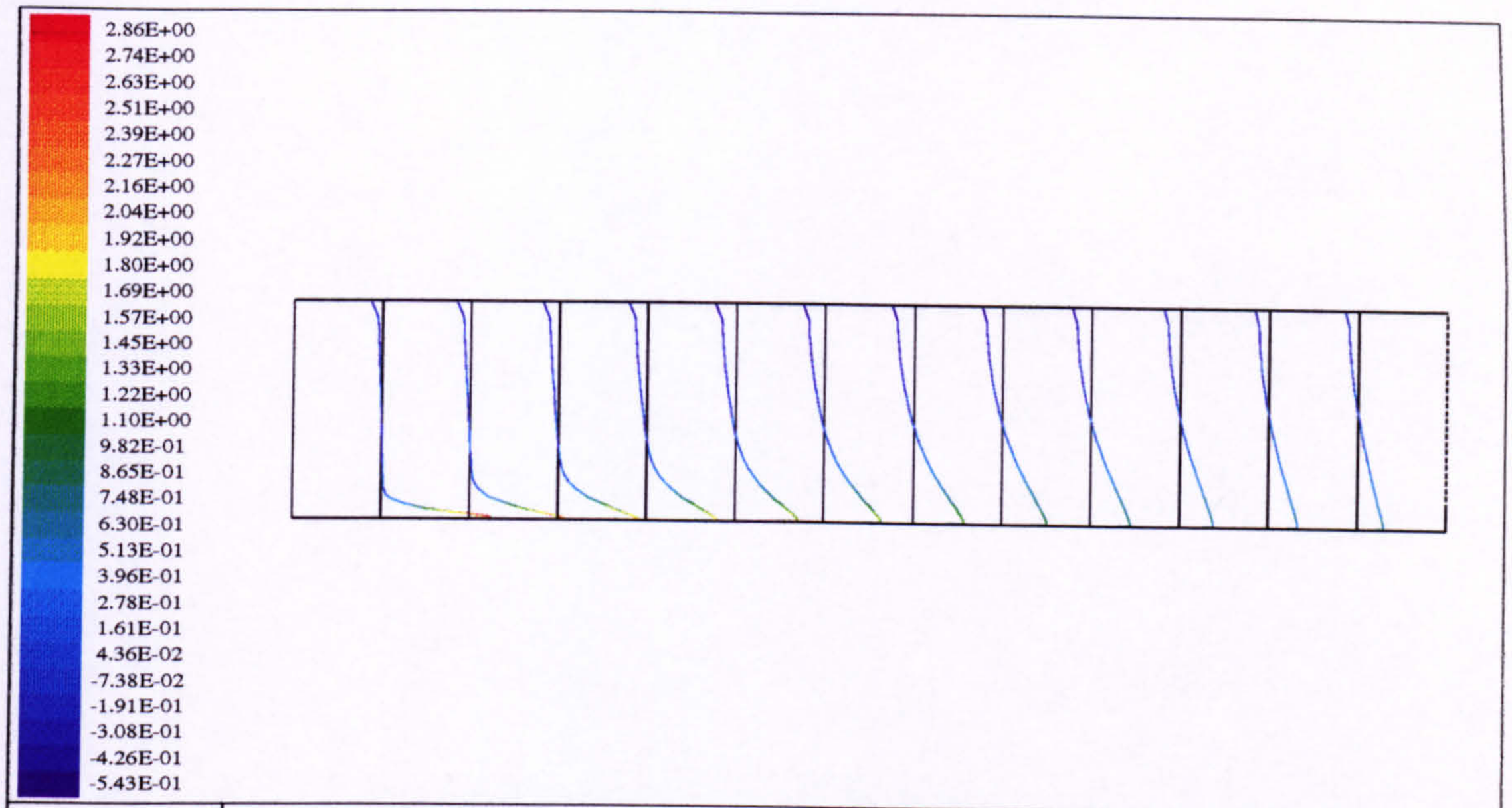

Figure 3.26 (a) : Fo = 7.46, H = 0.46m, yo = 0.015m
U-Velocity (M/S)
Max = 2.860E+00 Min = -5.432E-01

Fluent 4.31
Fluent Inc.

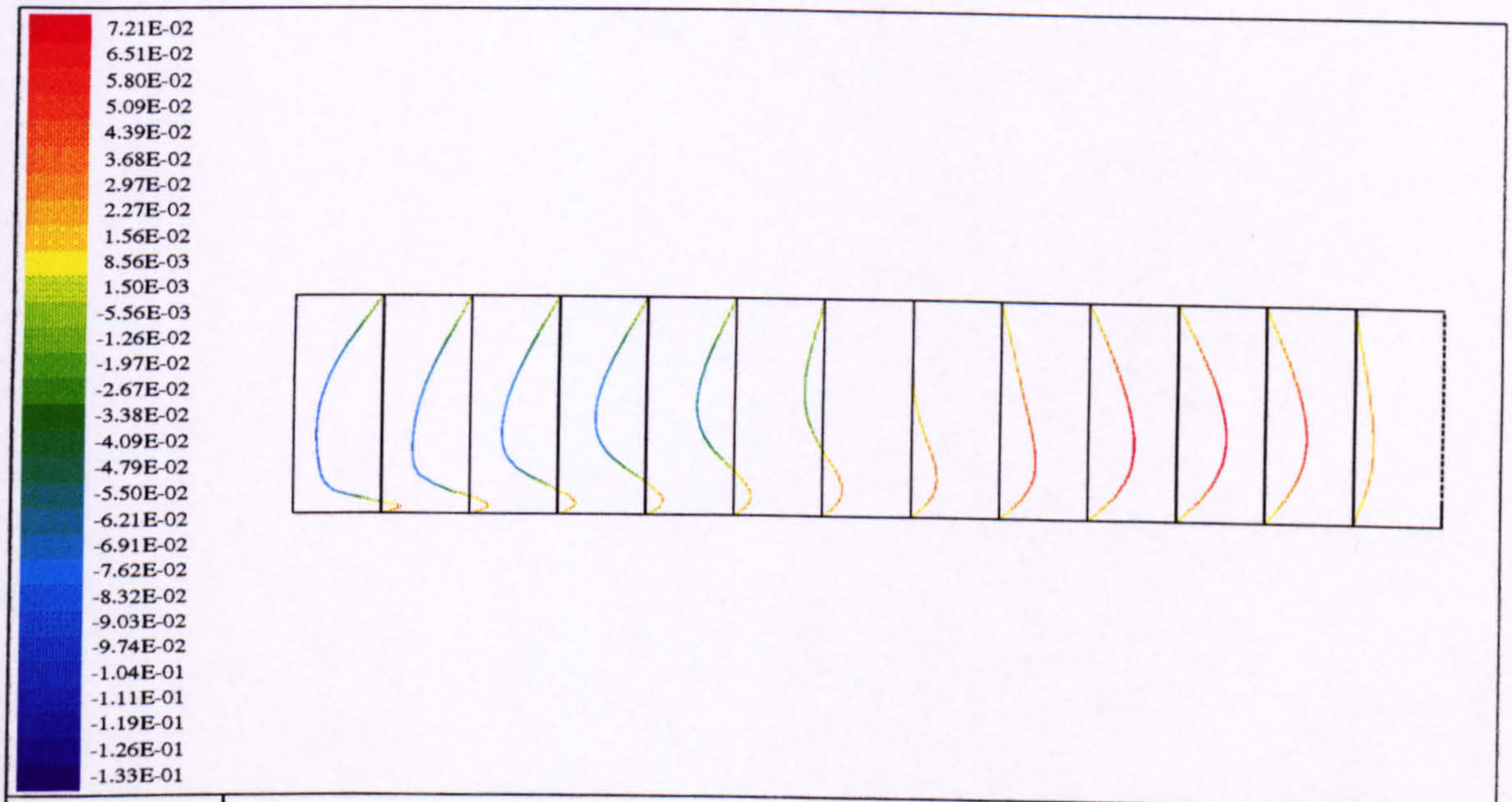

Figure 3.26 (b) : Fo = 7.46, H = 0.46m, yo = 0.015m
V-Velocity (M/S)
Max = 7.212E-02 Min = -1.327E-01

Fluent 4.31
Fluent Inc.

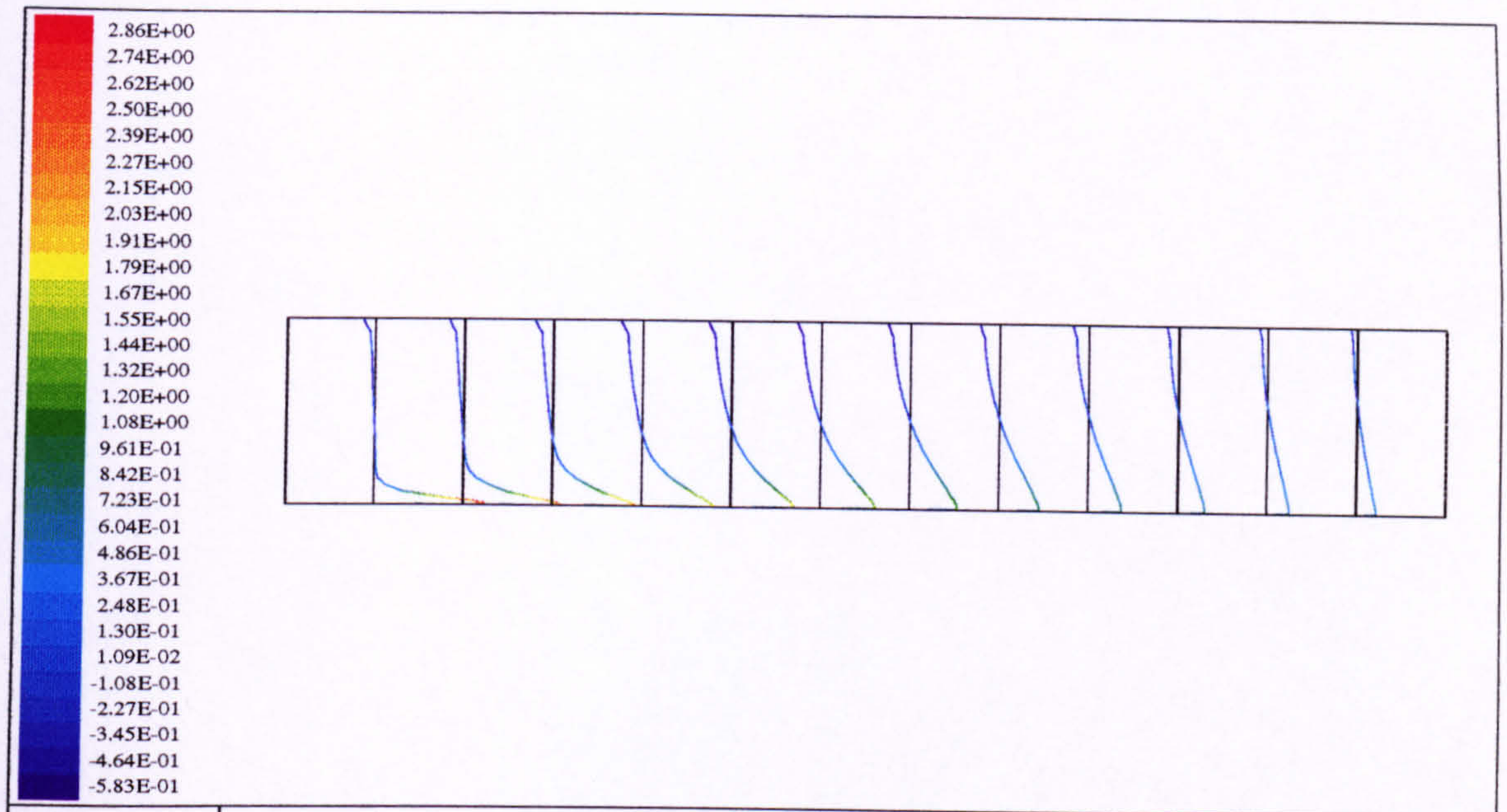

Figure 3.27 (a) : Fo = 7.46, H = 0.39m, yo = 0.015m
U-Velocity (M/S)
Max = 2.860E+00 Min = -5.827E-01

Fluent 4.31
Fluent Inc.

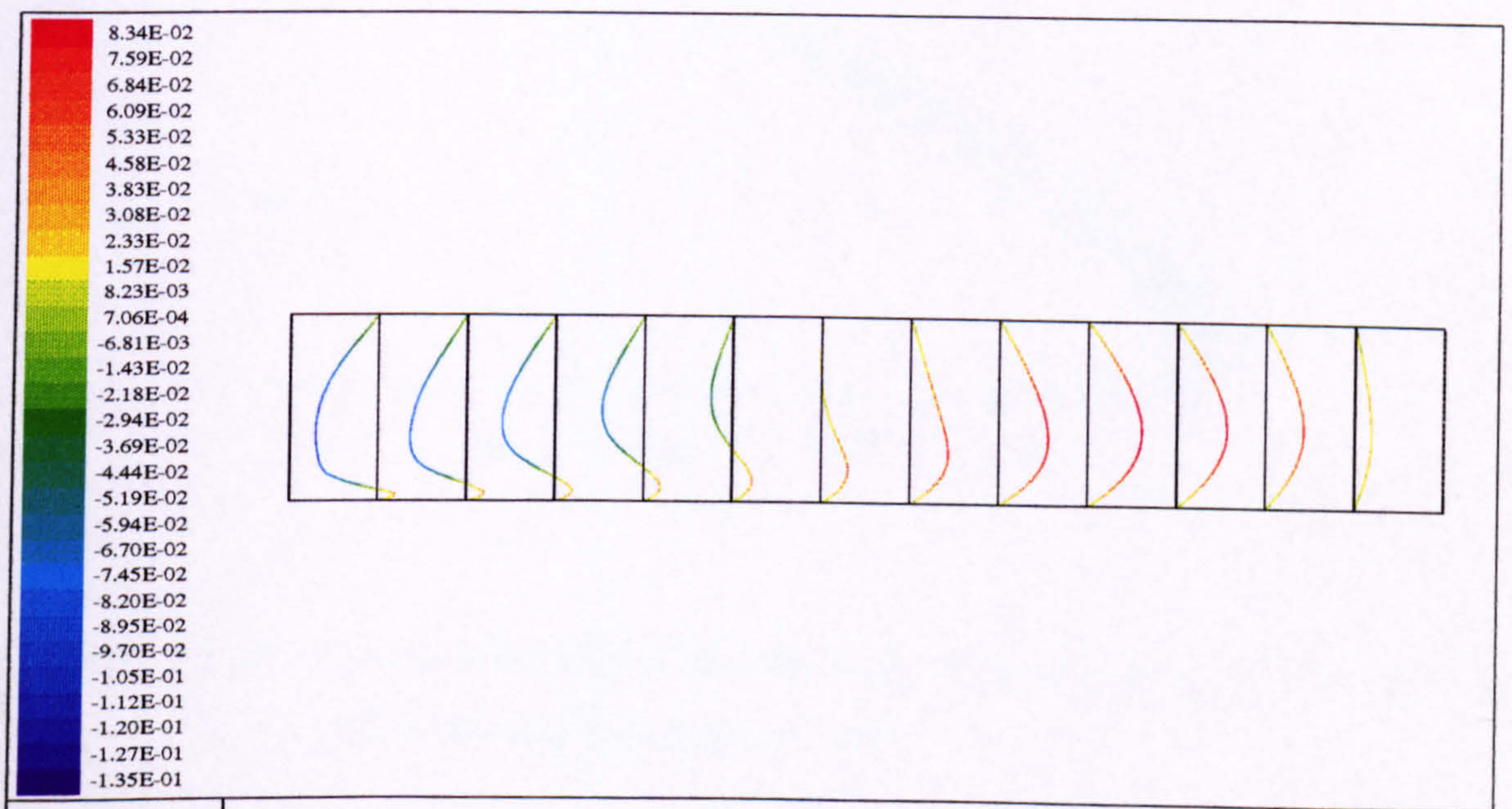

Figure 3.27 (b) : Fo = 7.46, H = 0.39m, yo = 0.015m
V-Velocity (M/S)
Max = 8.341E-02 Min = -1.346E-01

Fluent 4.31
Fluent Inc.

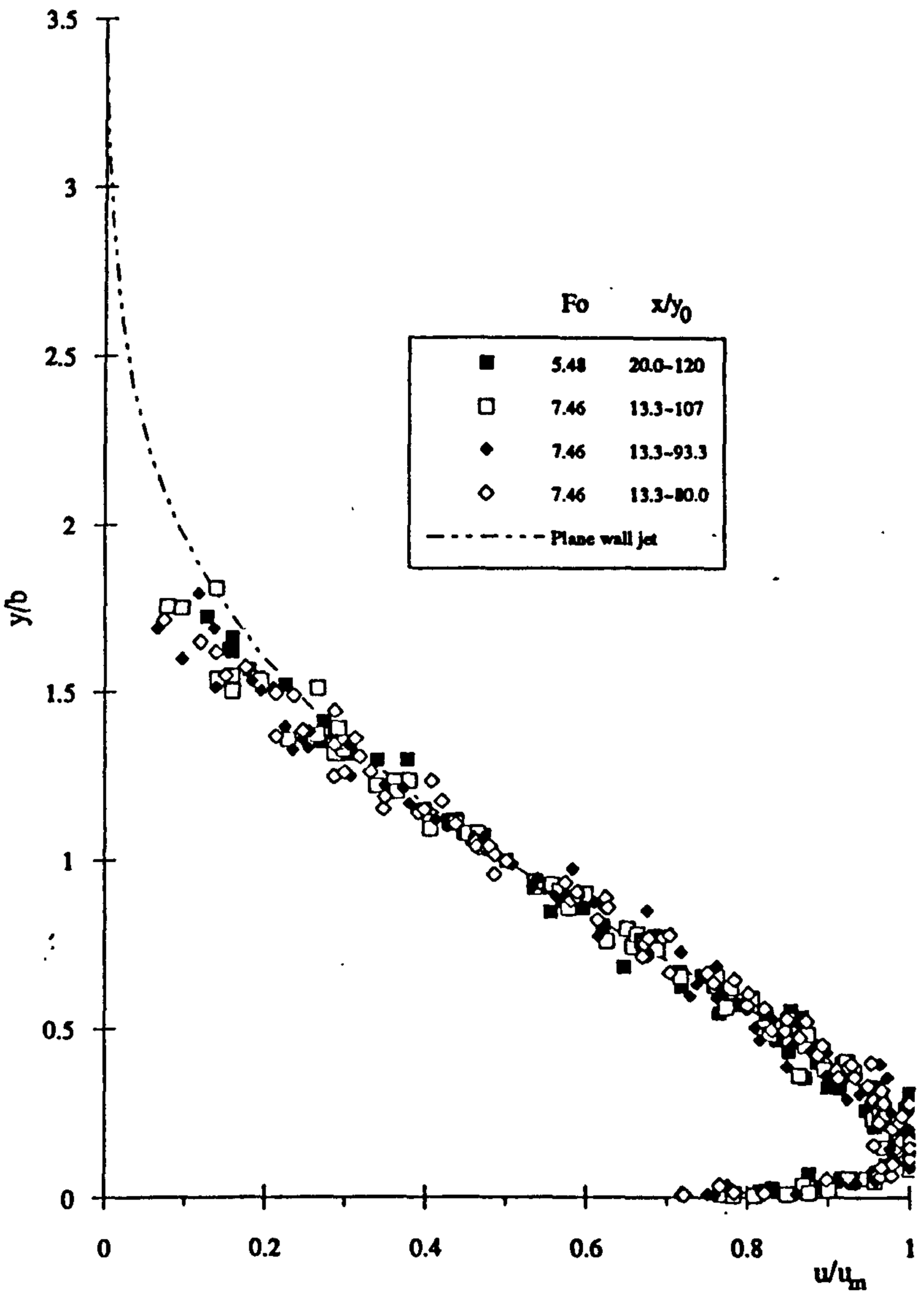

Figure 3.28 : Consolidated plot of non-dimensional longitudinal velocity profile (After Wu and Rajaratnam, 1995)

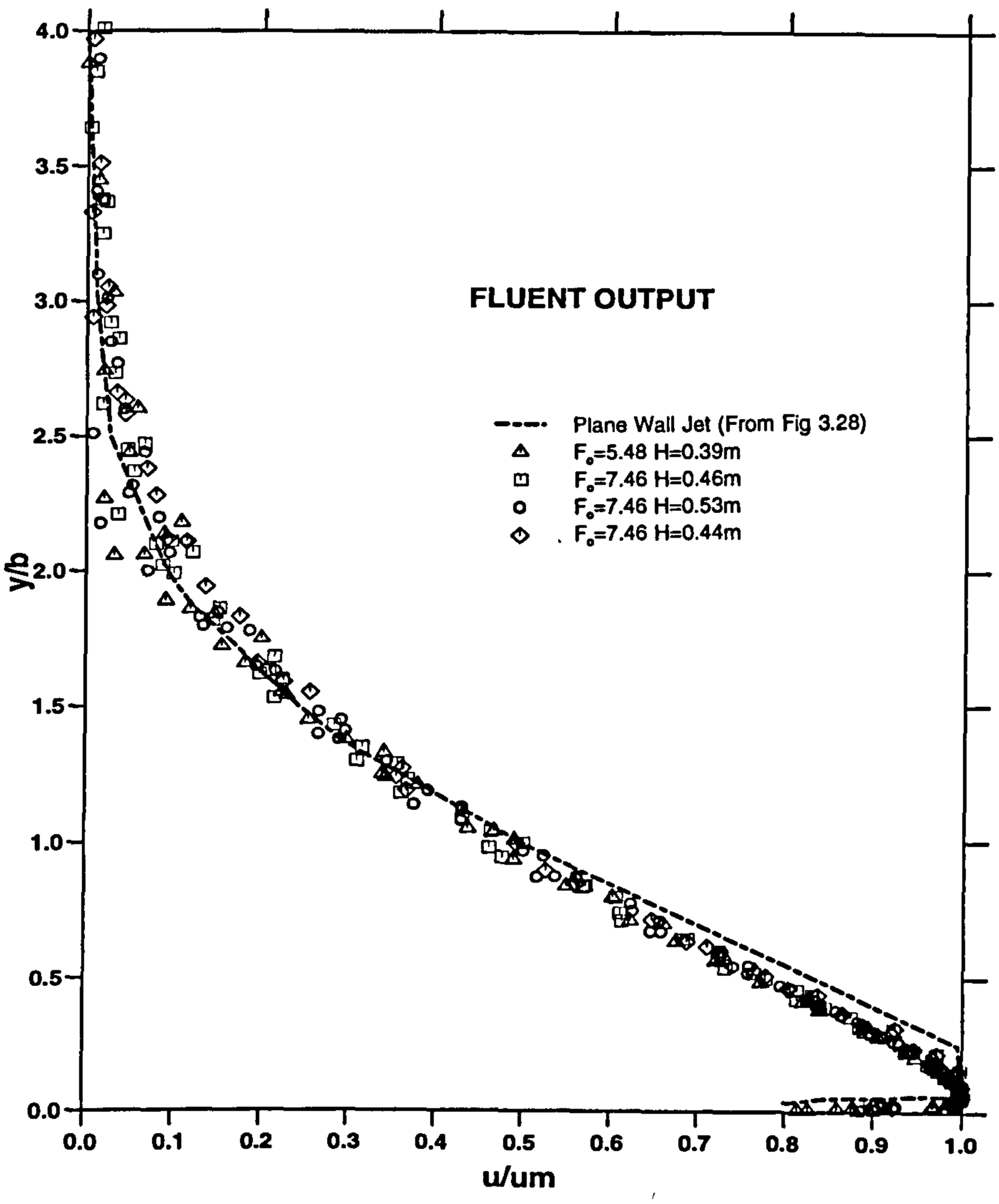

Figure 3.29 : Consolidated plot of non-dimensional longitudinal velocity profile (FLUENT output)

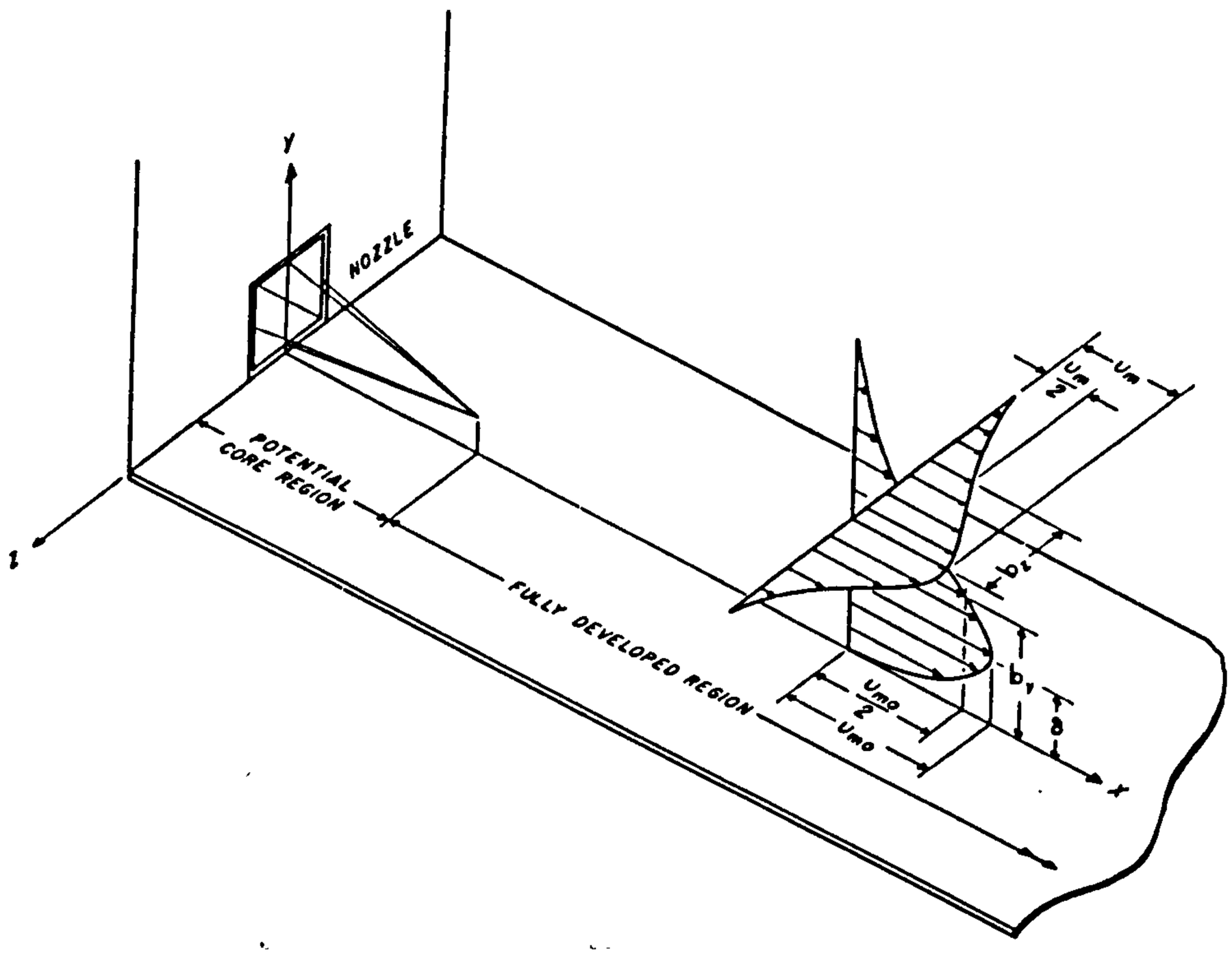

Figure 3.30 : Schematic Representation of Three-Dimensional Wall Jets (After Rajaratnam, 1976)

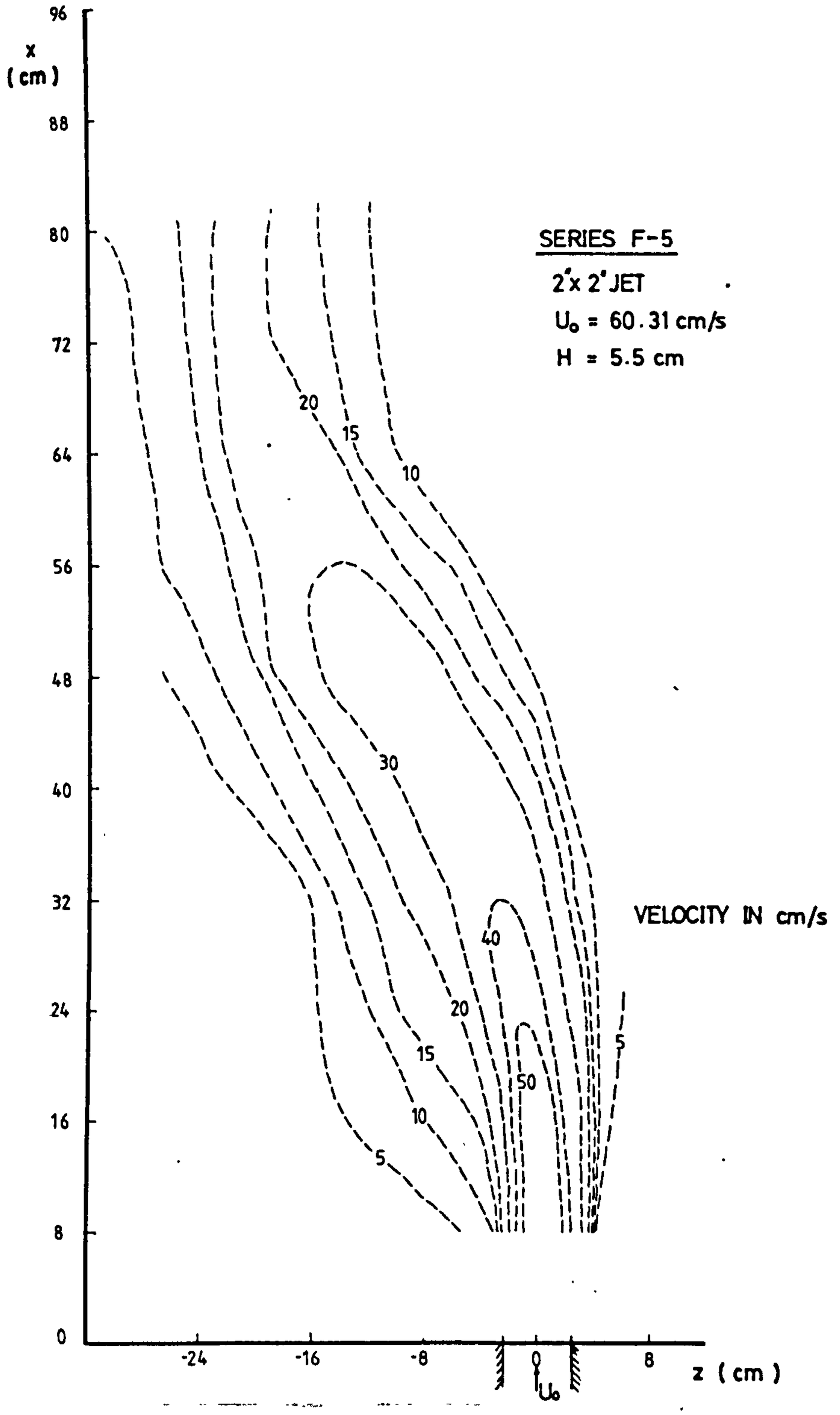

Figure 3.31 : Measured Floor Velocity (Flat Bed)
(After Lim, 1985)

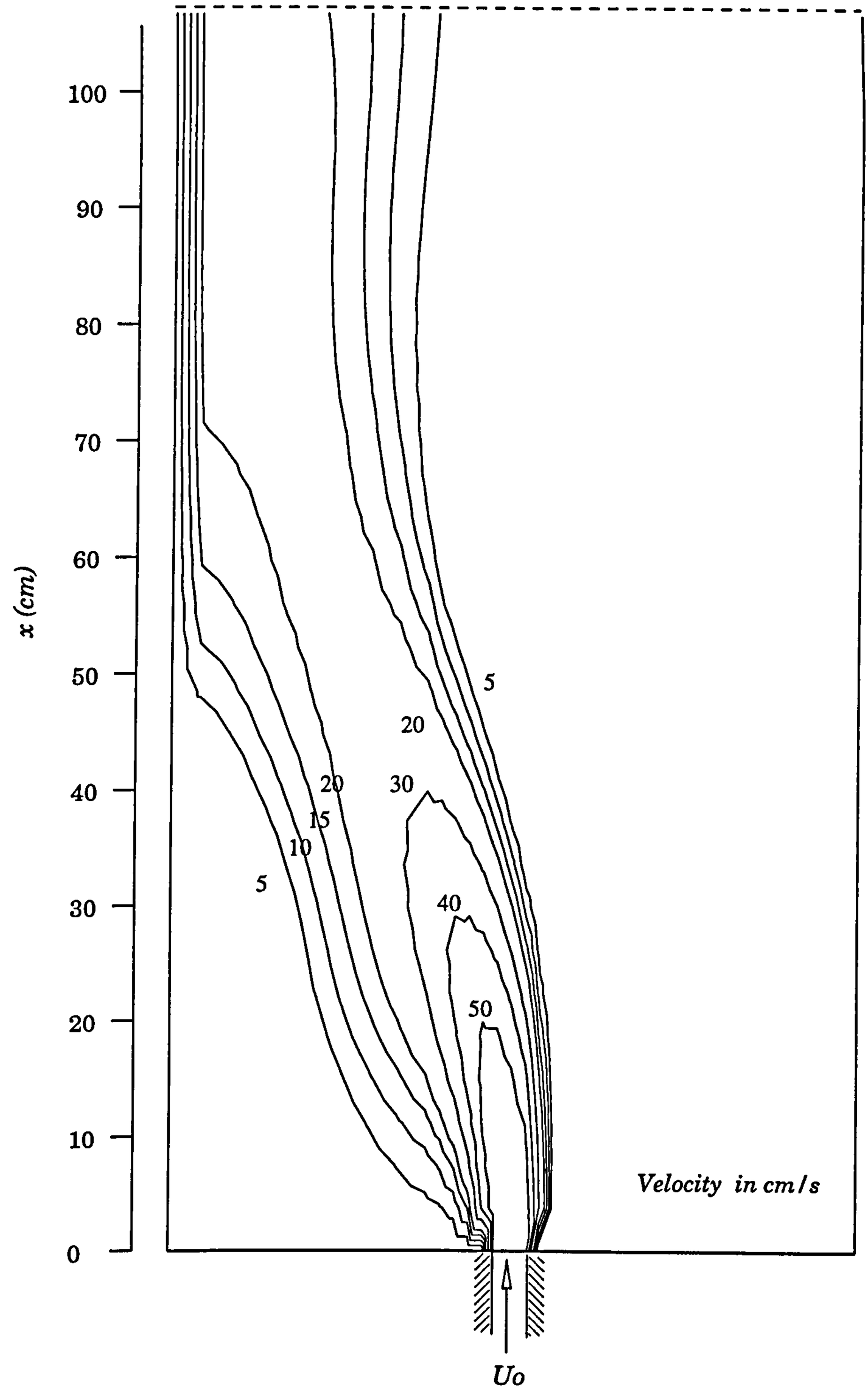

Figure 3.32 : Predicted Floor Velocity Contours (Flat bed).
(5.08cm x 5.08cm JET, Uo = 60.31 cm/s, H = 5.5cm)

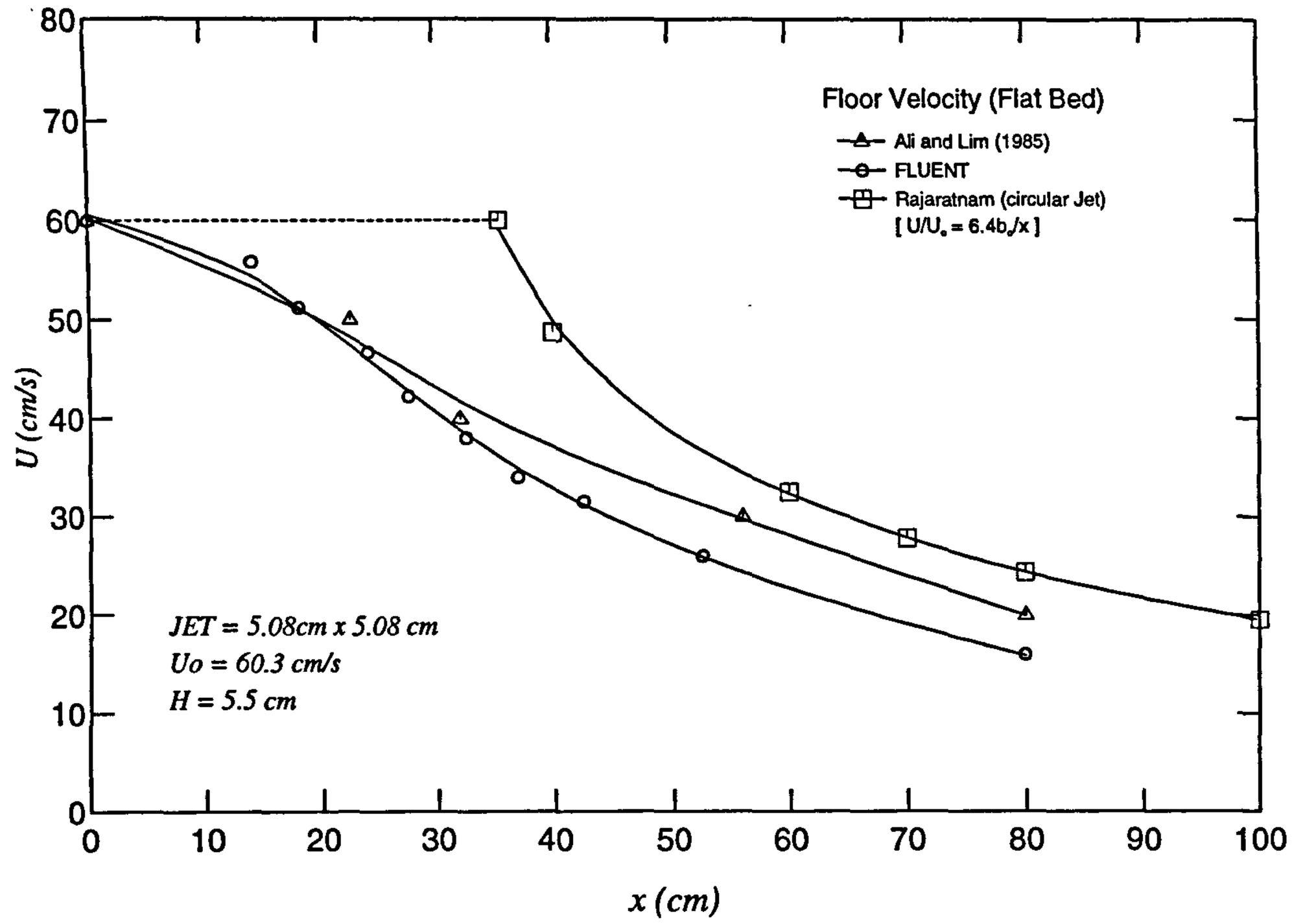

Figure 3.33 : Maximum Velocity Decay Plot (Flat-bed)

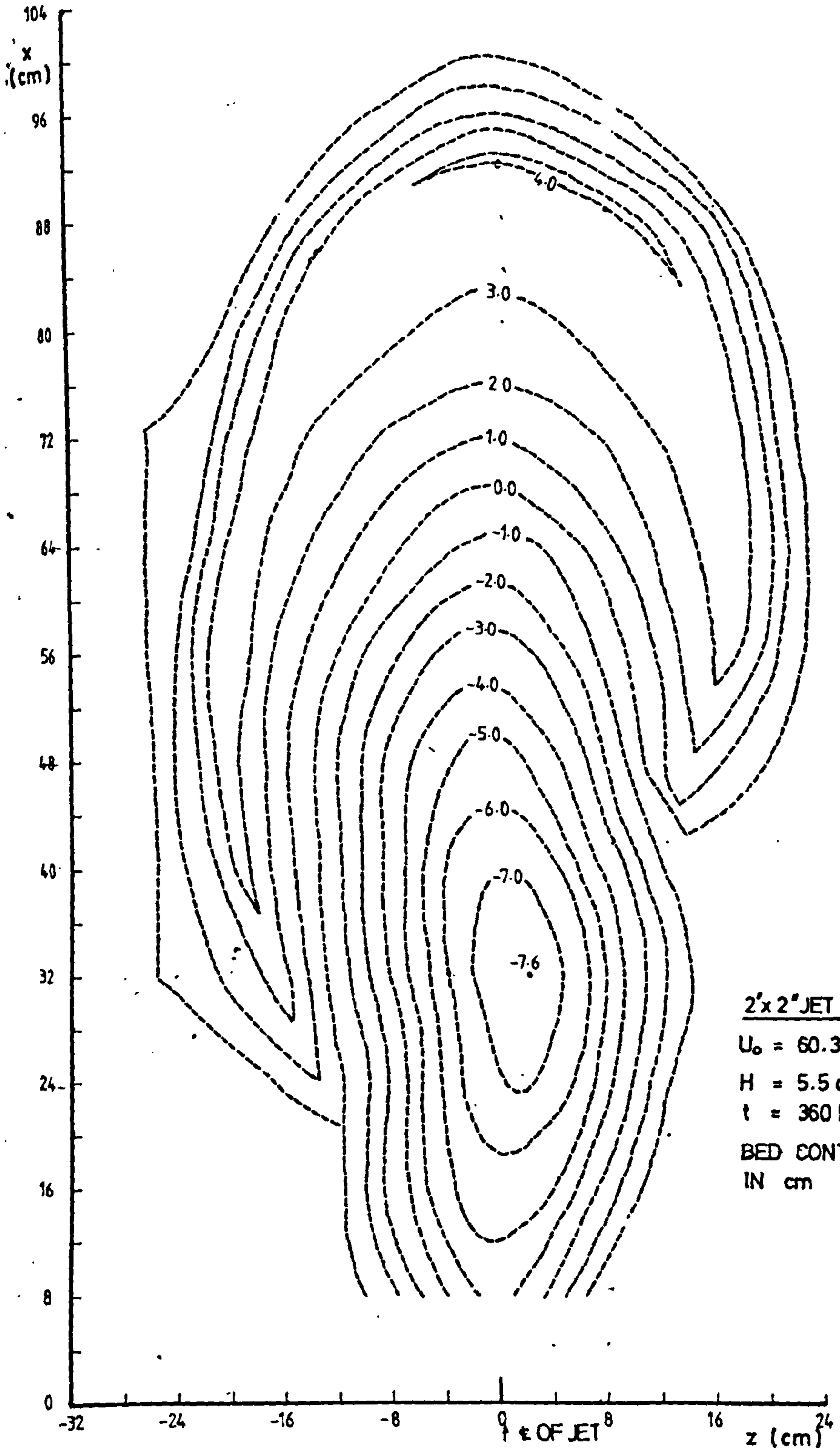

Figure 3.34 : Bed Contours at t = 360 mins (After Lim, 1985)

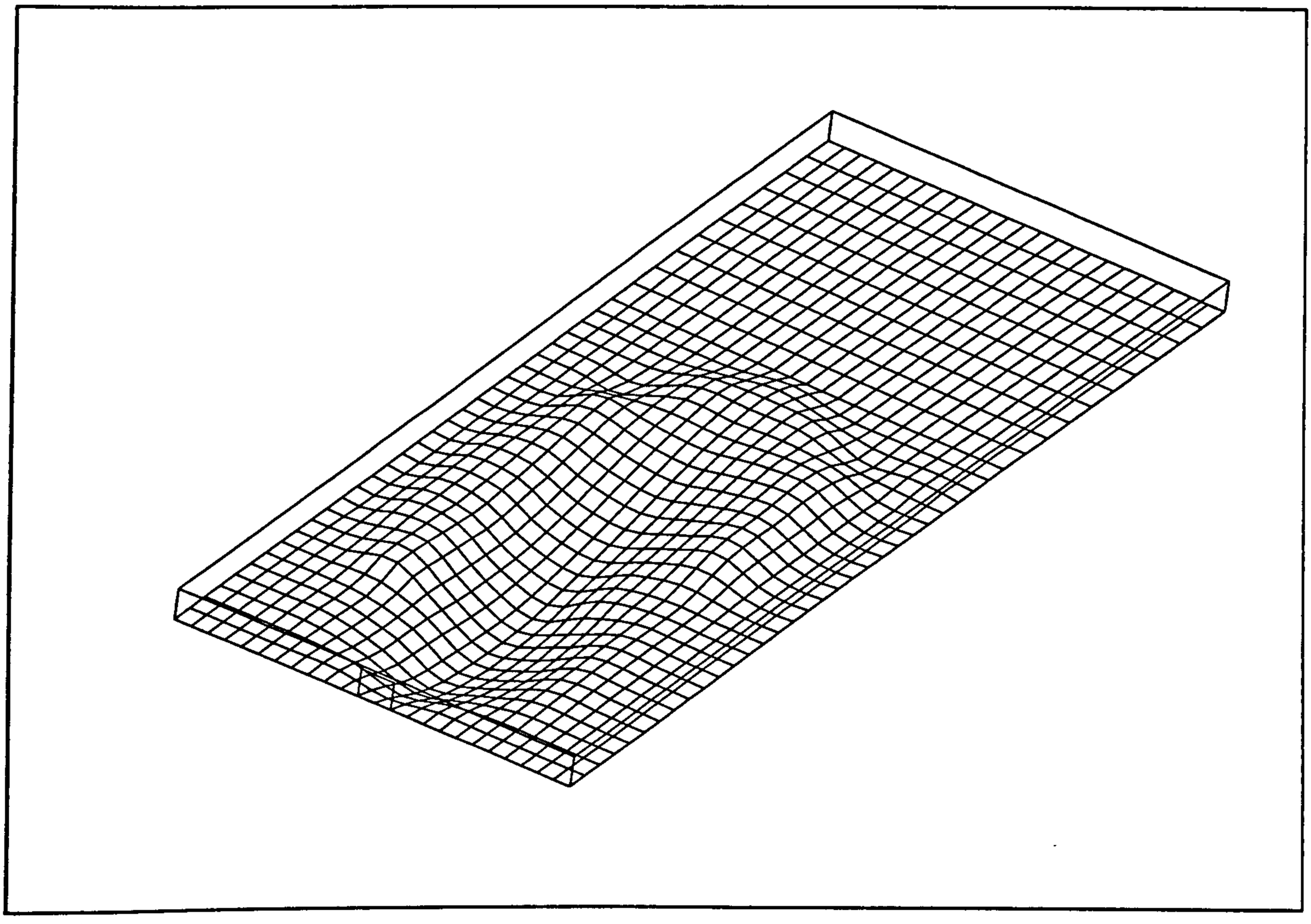

Figure 3. 35 : Simulated bed profile used in FLUENT

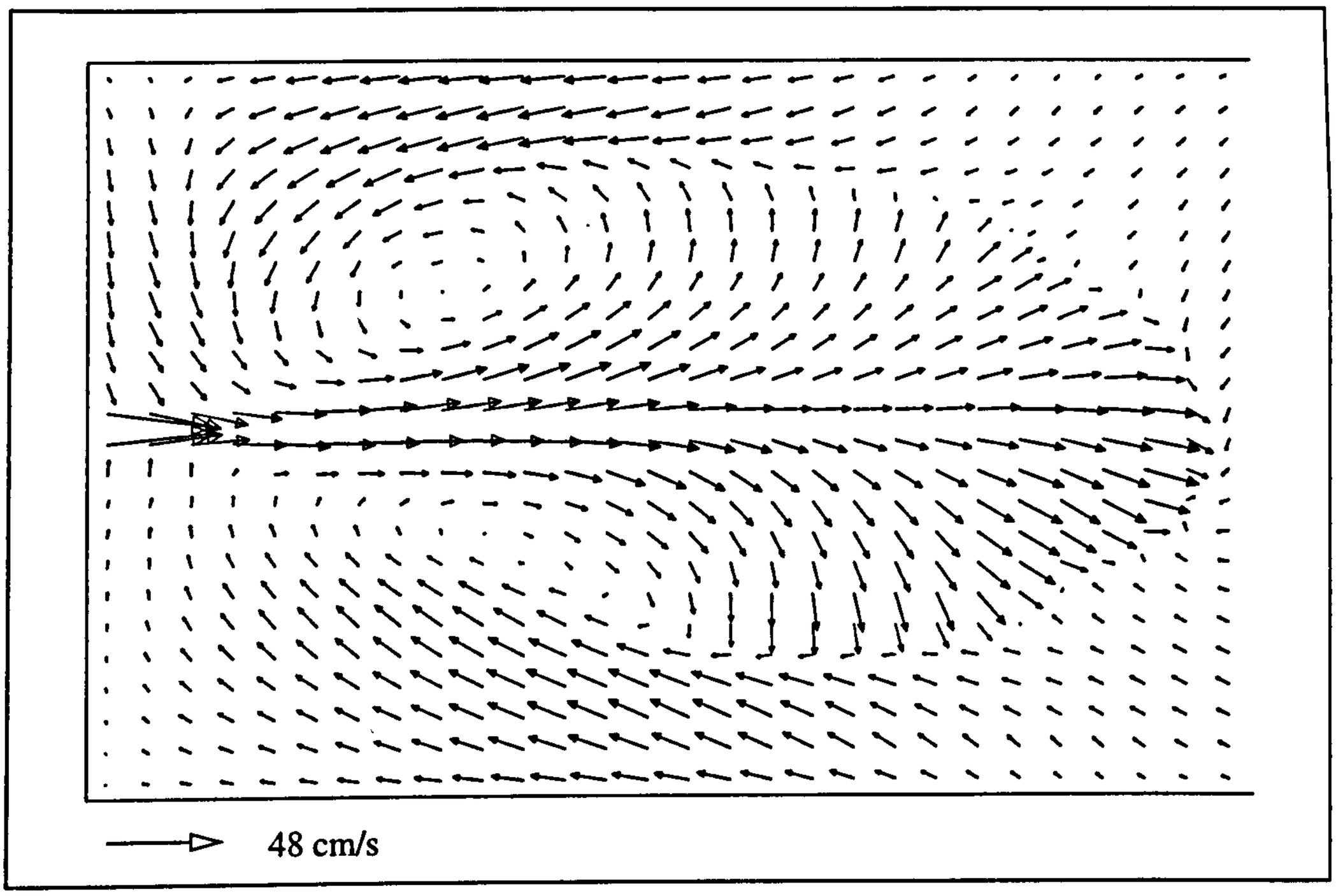

Figure 3.36 (a) : Predicted Velocity Vectors near Bed (t = 360 mins)

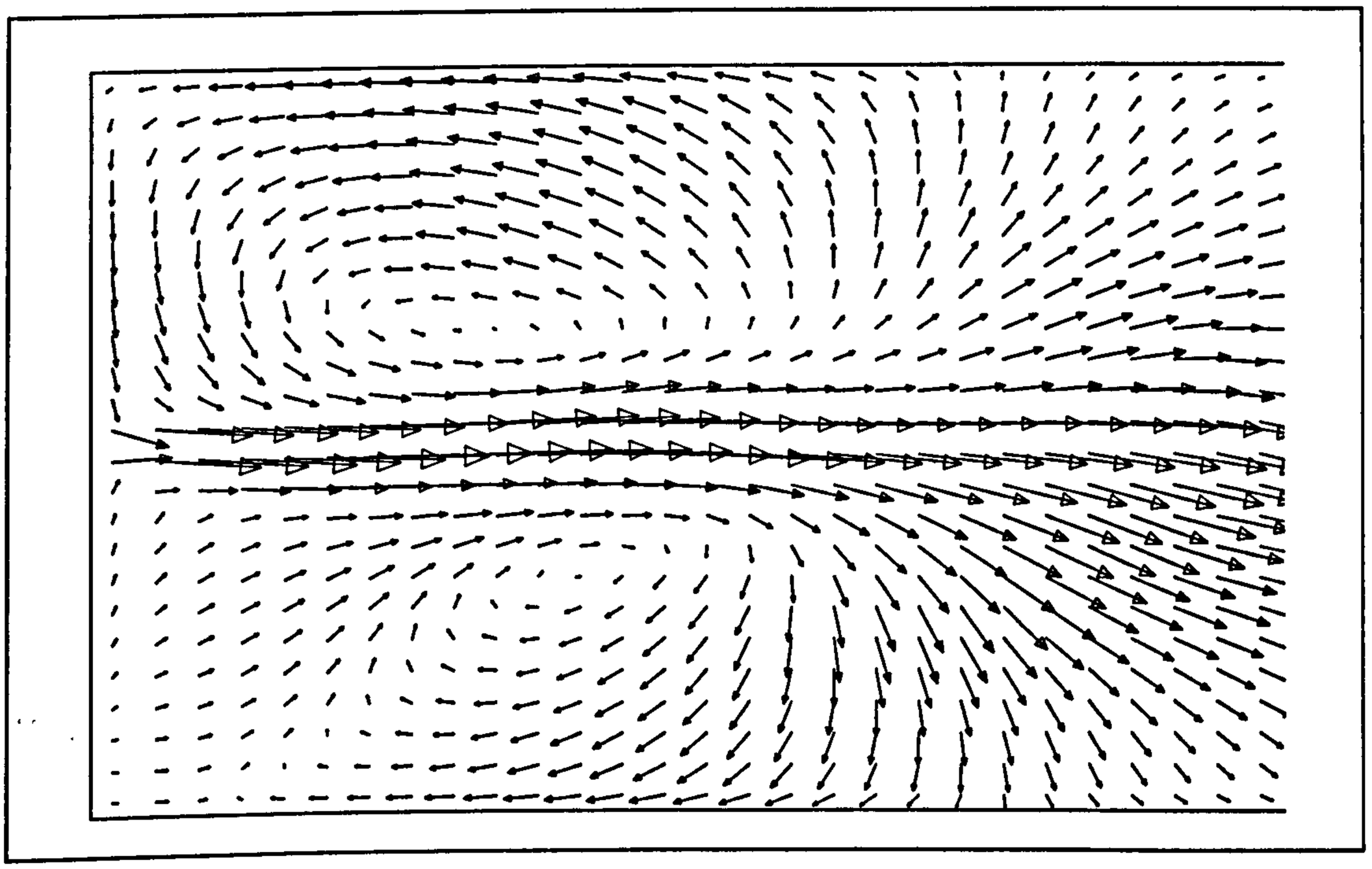

Figure 3.36 (b) : Predicted Velocity Vectors near Surface (t = 360 mins)

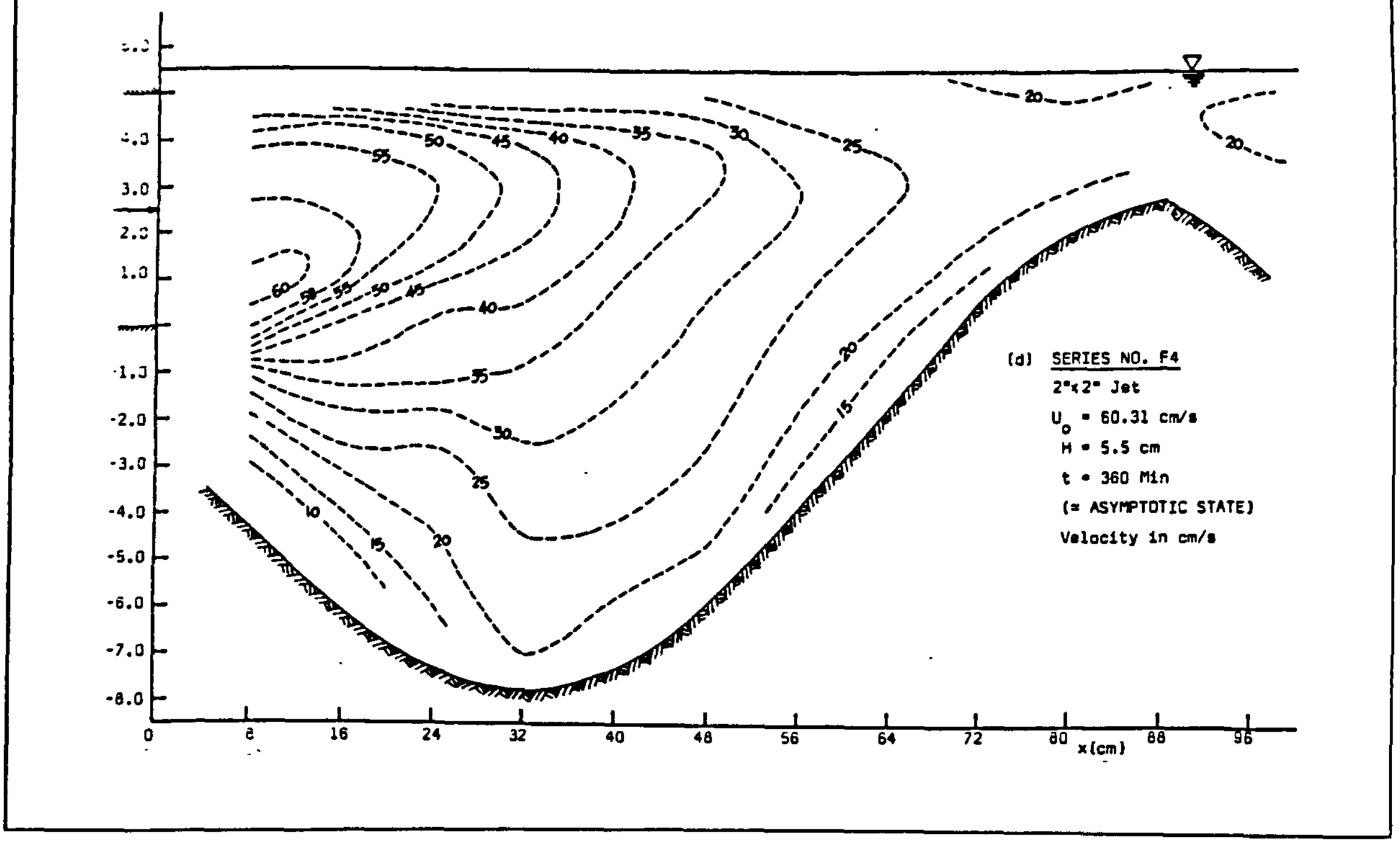

Figure 3.37(a) : Measured Velocity Contours in the Centre Plane of Scour Hole (t = 360 mins)

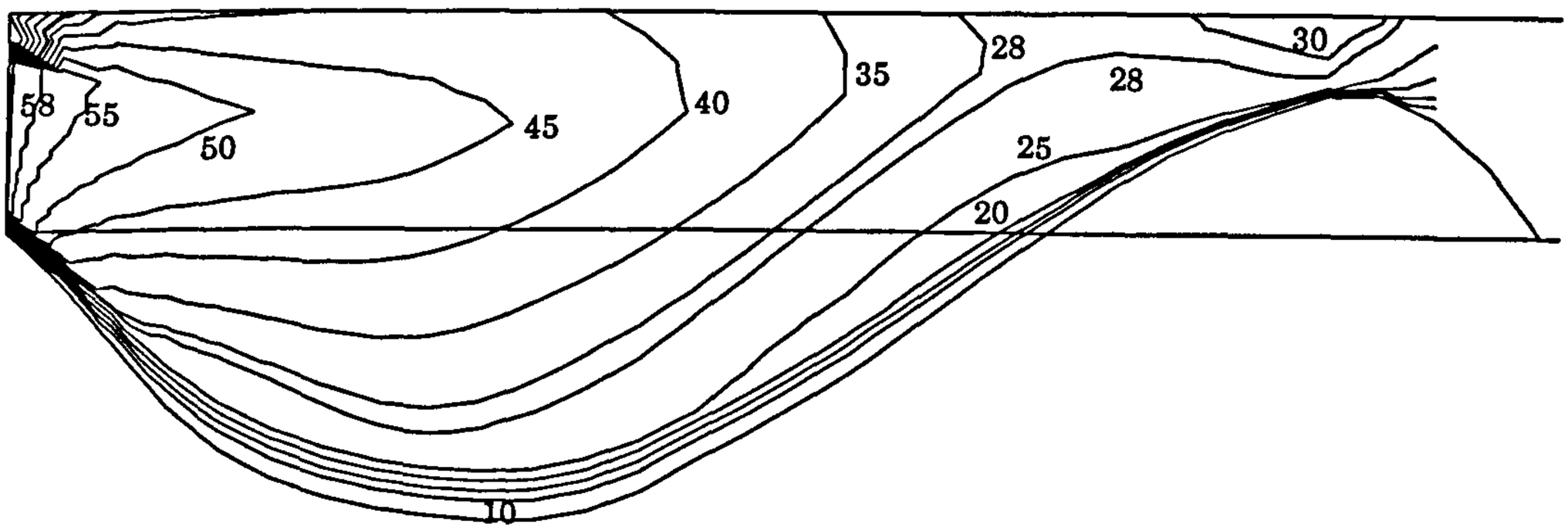

Velocity (cm/s)
(Note : Scale distorted in vertical direction : 3x)

Figure 3.37(b) : Predicted Velocity Contours in the Centre Plane of Scour Hole (t = 360 mins)

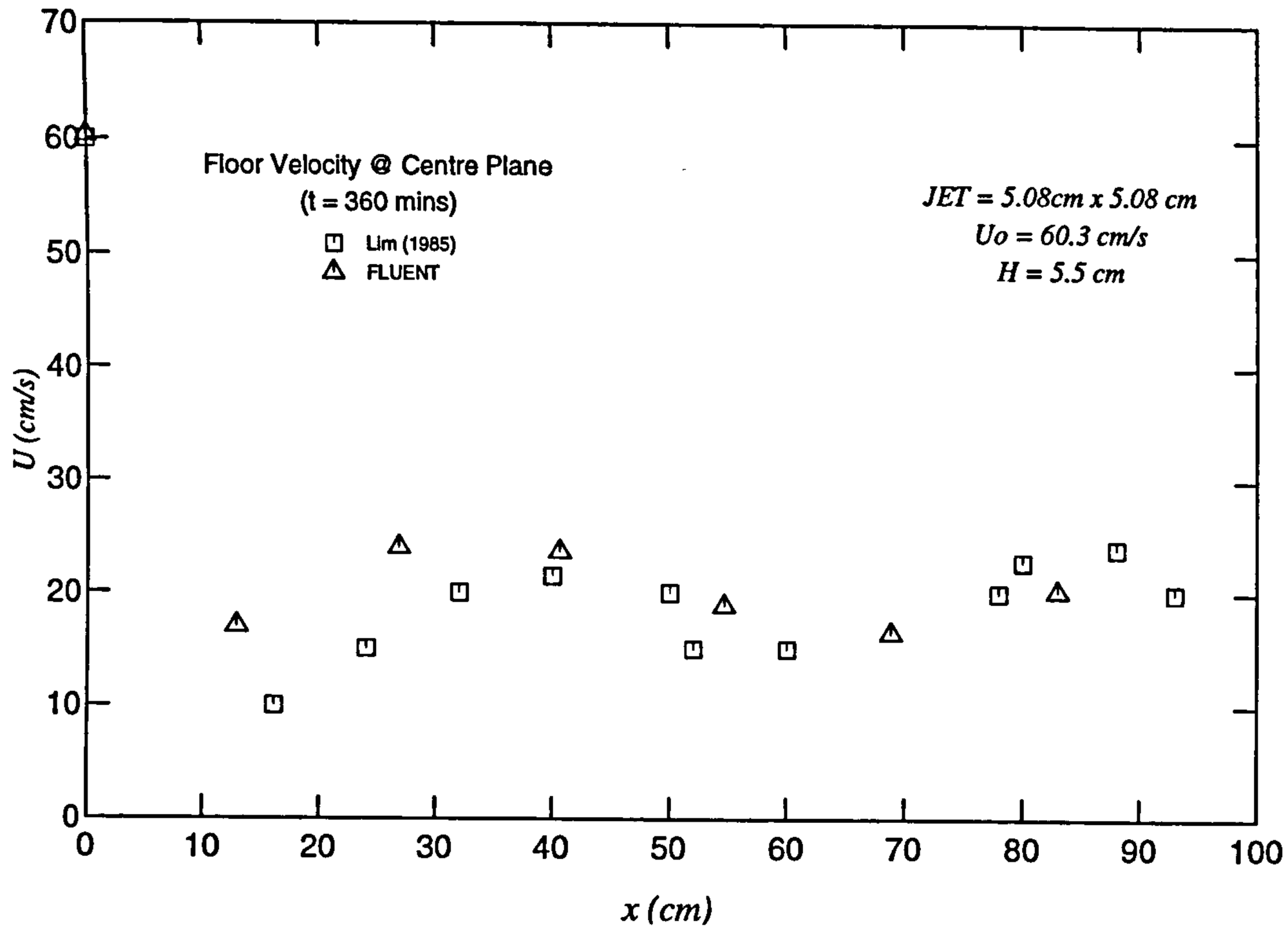

Figure 3.38 : Maximum Velocity Decay Plot (t = 360 mins)

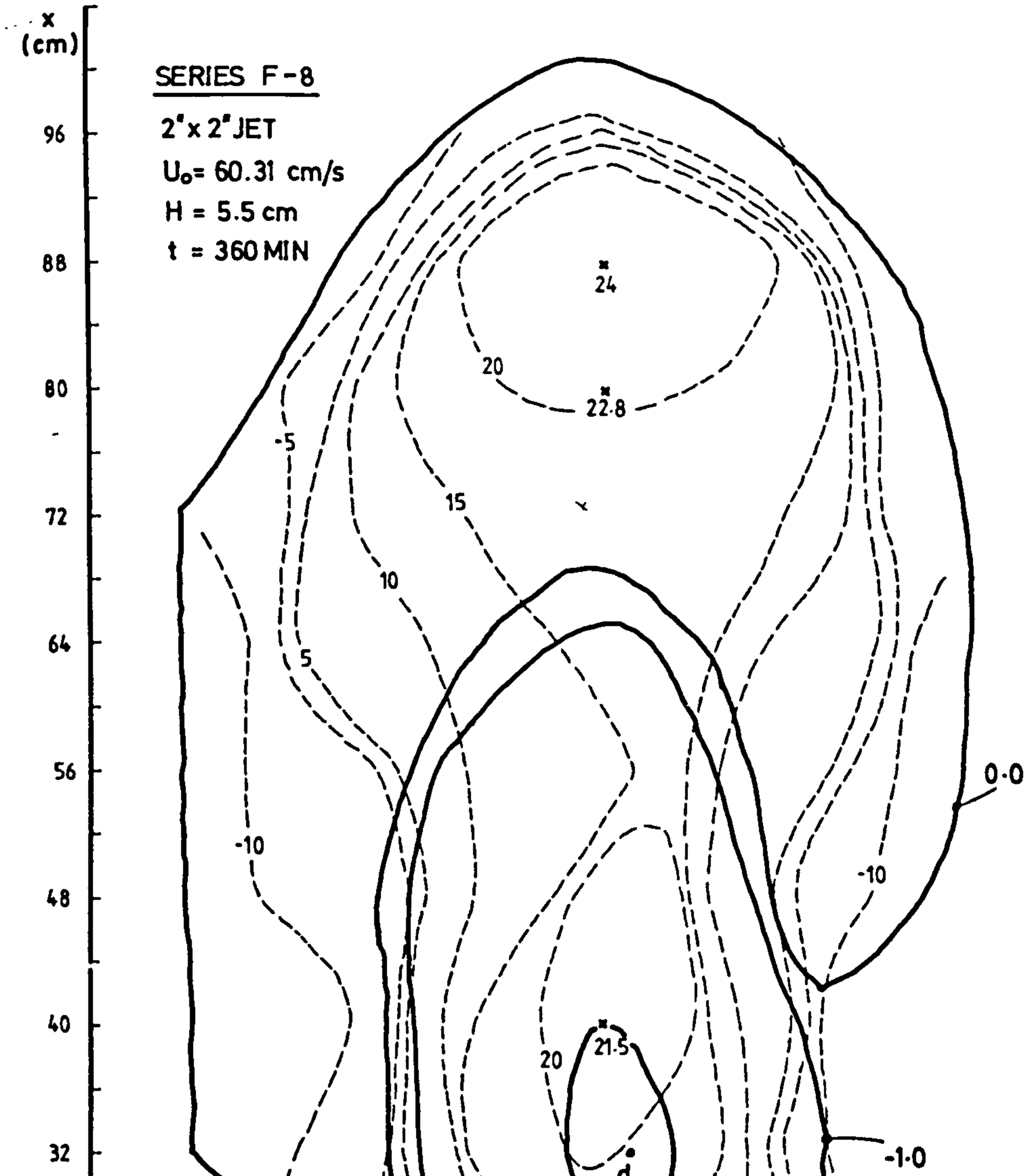

Figure 3.39 : Measured Floor Velocity (t = 360 mins)
(After Lim, 1985)

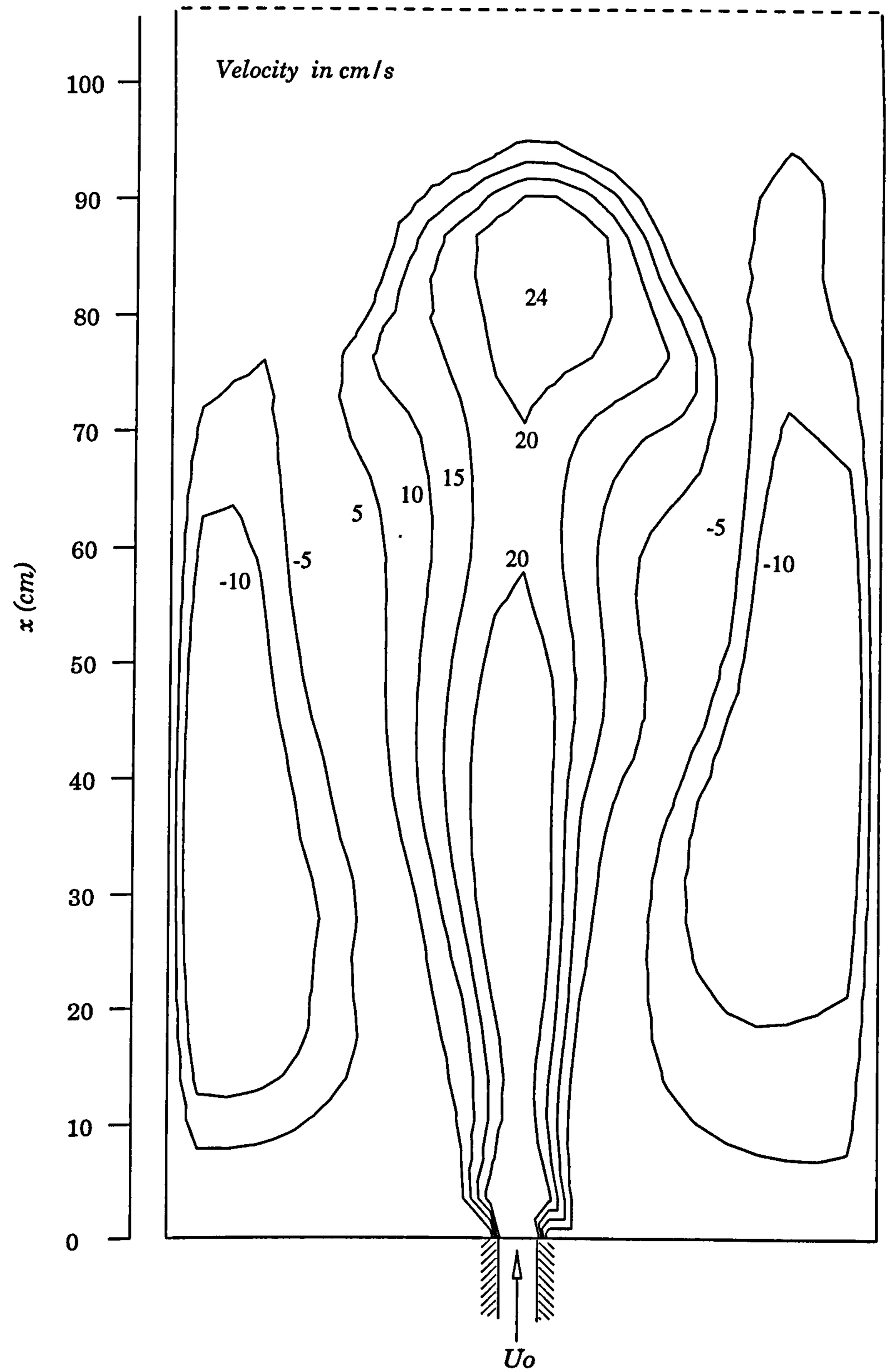

Figure 3.40 : Predicted Floor Velocity Contours at t= 360 min.
(5.08cm x 5.08cm JET, Uo = 60.31 cm/s, H = 5.5cm)

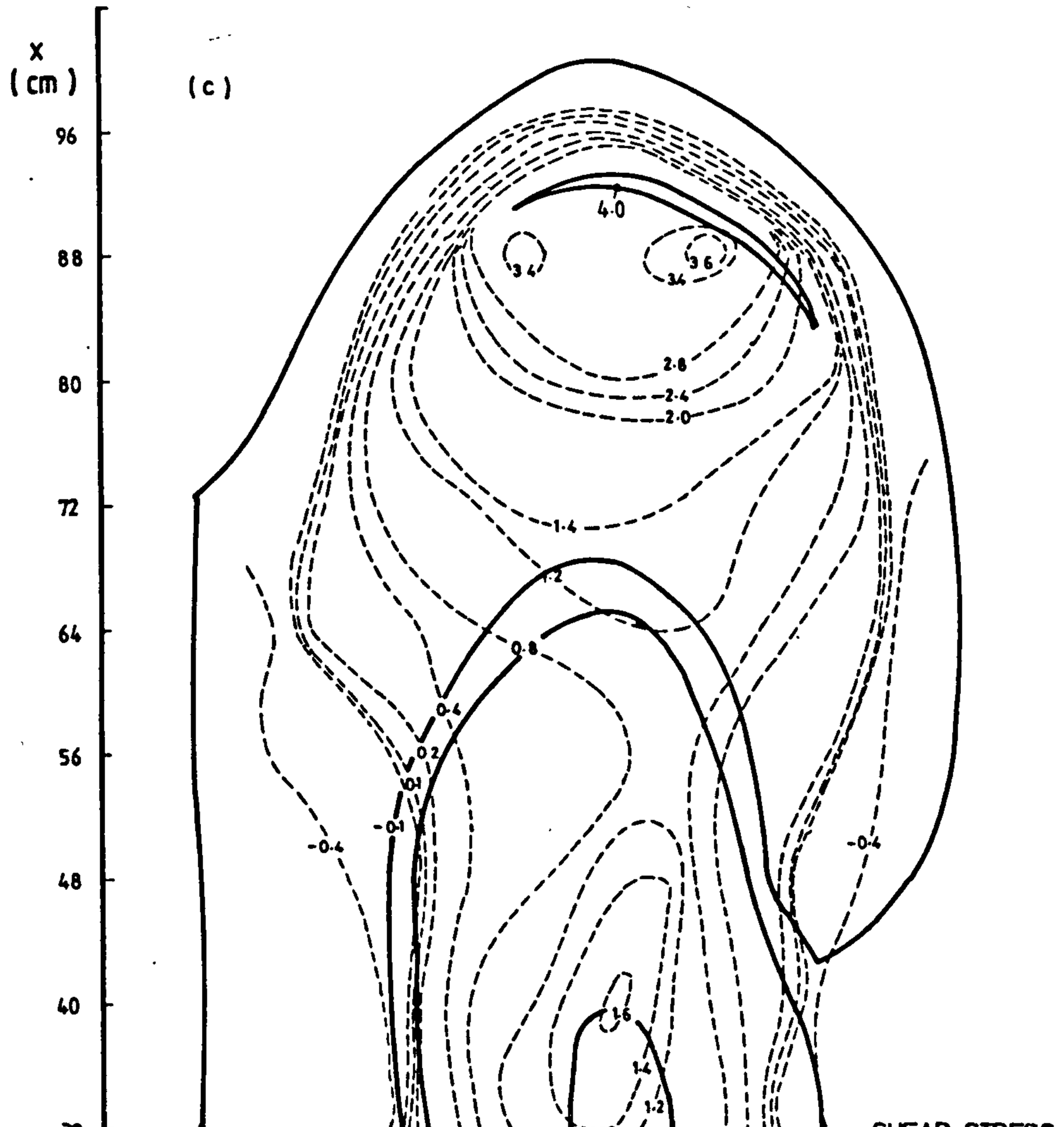

Figure 3.41 : Calculated Bed Shear Stress at t = 360 mins (After Lim, 1985)
(5.08 cm x 5.08 cm JET, Uo = 60.31 cm/s, H = 5.5 cm)

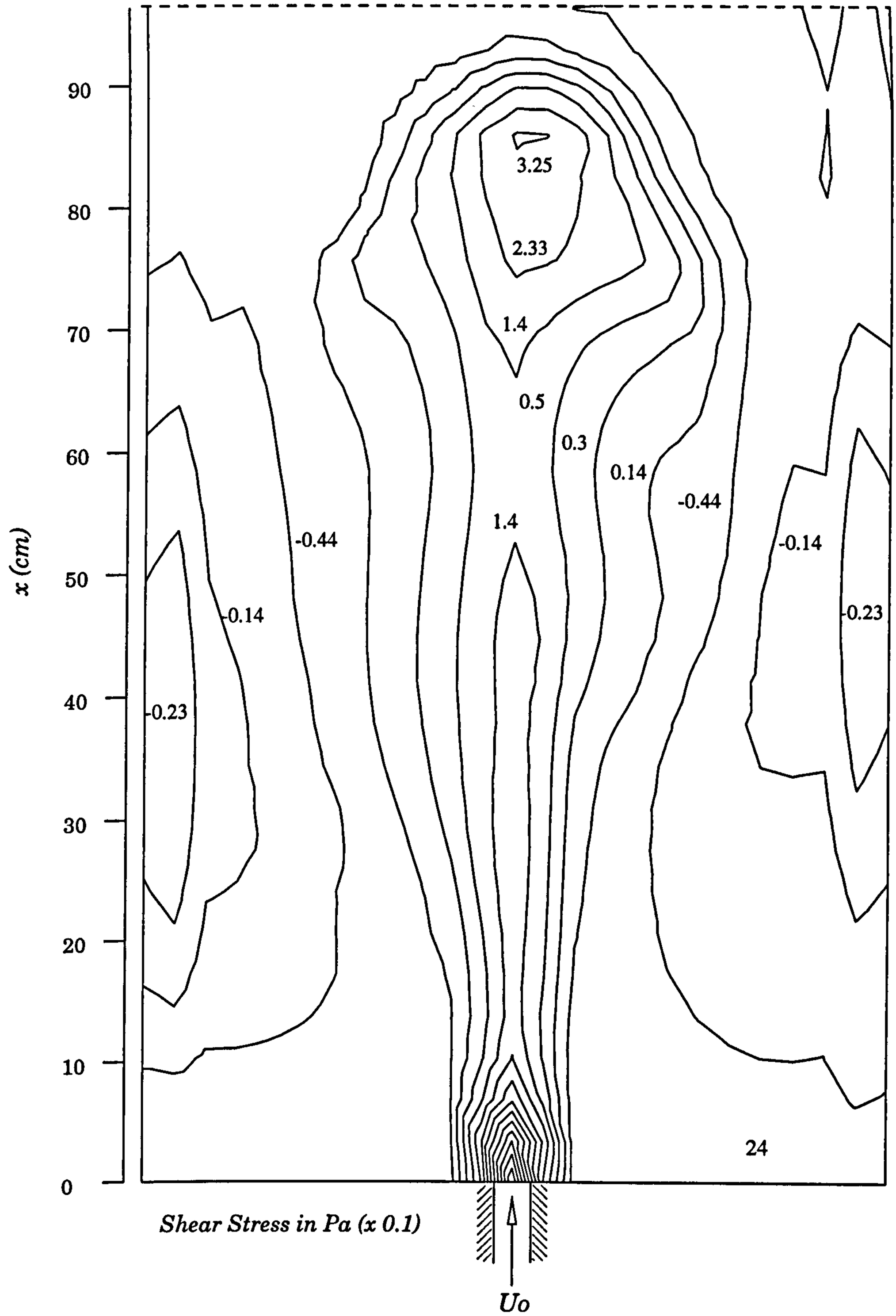

Figure 3.42 : Predicted Bed Shear Stress at t= 360 min.
(5.08cm x 5.08cm JET, Uo = 60.31 cm/s, H = 5.5cm)

NOTATIONS

b	Vertical distance from the axis to the point where $u = u_m/2$
f	Friction factor
F_o	Froude number = $U_o/\sqrt{(gy_o)}$
g	Acceleration due to gravity
H	Tailwater depth
k_s	Height of rough sand
S	Submergence factor
u_m	Maximum velocity of the velocity profile at any x distance from the nozzle
U_o	Average jet velocity
y_o	Jet thickness
y	Vertical distance from the axis of jet at any x direction
τ_b	Bed shear stress

REFERENCES

Ali, K.H.M., and Lim, S.Y. (1986). "Local scour caused by submerged wall-jets." *Proc. Institution of Civil Engineers*, London, England, 81(2), pp 607-645

Altinbilek, H.D., and Oykay, S. (1973). "Localized scour in a horizontal sand bed under vertical jets." *Proc. IAHR Congress*, International Association for Hydraulic Research, 1, pp 99-106

Blaisdell, F.W., and Anderson, C.L. (1991). "Pipe plunge pool dissipator." *J.Hydr. Engrg.*, ASCE, 117(3), pp 303-323

Breusers, H.N.C.,(1967)."Time scale of two-dimensional local scour." *Proc. 12th Congress.*, IAHR, Fort Collins, Vol 3. pp C321-8

Breusers, H.N.C.,(1975)."Computation of velocity profiles in scour holes." *Proc. 16th Congress.*, IAHR, Sao Paulo, Vol 2. pp C300-306

Carsten, .M. R. (1966). "Similarity laws for local scour." *J. Hydr. Div.*, ASCE, 92(3) pp 13-36

Doddiah, D., Albertson, M.L., and Thomas, R. (1953). "Scour from jets." *Proc. IAHR Congress*, International Association for Hydraulic Research, pp 161-169

Francis, J.R.D., and Ghosh, S.N. (1974). "A new look at local erosions in alluvial rivers." *Proc. 5th Australasian Conf on Hydr. and Fluid Mech.*, University of Canterbury, Canterbury, New Zealand, pp 71-77

Hassan, N.M.K., and Narayanan, R. (1985)."Local scour downstream of an apron." *J. Hydr. Engrg.*, ASCE, 111(11), pp 1371-1385

Iwagaki, Y., Smith, G.L., and Albertson, M.L. (1958). "Analytical study of mechanics of scour for three dimensional jet." *Hydr. Conf.*, ASCE, New York, N.Y.

Johnston, A.J. (1990). "Scourhole developments in shallow tailwater." *J. Hydr Res.*, IAHR, 28(3), pp 341-354

Lim, S.Y., (1985) "Scour and particle diffusion caused by water jets" PhD Thesis, University of Liverpool.U.K.

Mason, P.J. (1988). "Effects of air-entrainment on plunge pool scour." *J. Hydr. Engrg.*, ASCE, 115(3), pp 385-399

Melville, B.W. and Raudkivi, A.J. (1977). "Flow Characteristics in local scour at bridge piers". *J. Hydr. Res.* Vol 15, No. 4, pp. 373-380

Poreh, M., and Hefez, E. (1967). "Initial scour and sediment motion due to an impinging jet." *Proc. IAHR Congress*, International Association for Hydraulic Research, 3, 8

Rajaratnam, N., (1976), "Turbulent Jets", Elsevier Scientific Publishing Co., Amsterdam, The Netherlands, 1976.

Rajaratnam, N., and Beltaos, S., (1977). "Erosion by impinging circular turbulent jets." *J. Hydr. Div.*, ASCE, 103(10), pp 1191-1205

Rajaratnam, N., and Berry, B. (1977). "Erosion by circular turbulent wall-jets." *J. Hydr. Res.*, 15(3), pp 277-289

Rajaratnam, N., and Humpries, J.A.,(1933)."Diffusion of Bluff Wall Jets in Finite Depth Tailwater", *J. of Hydr. Engineering,* ASCE, Vol 109, No. 11, pp 1471 - 1486

Rajaratnam, N., and MacDoughall, R.K. (1983). "Erosion by plane wall jets with minimum tailwater." *J. Hydr. Div.*, ASCE, 109(7), pp 1061-1064

Rosiinski, K.I., (1961). "Hydraulic of Scouring Pits" *Chapter 2 from "Problems of River Runoff Control", Acad Sci. USSR,*. Section for Scientific Study of Water Enginering Problems.

Rouse , H., (1939). "Criteria for Similarity in The Transportation of Sediment", *Proc. Hyd. Conf. Studies Engineering Bull.*, Univ. of Iowa, pp. 33-49

Sarma, K.V.M., and Sivasankar, R. (1967), "Scour under vertical circular jets." J. *Inst. of Engrs,*. Calcutta, India, 48(3), pp 568-579

Sedimentation Transportation Mechanics: Erosion of Sediment. (1962) by the Task Committee on Preparation of Sedimentation Manual of the Committee on Sedimentation, *J. of Hydr Div.*, ASCE, Vol 88, No HY4, July, pp. 109-127

Uyumaz, A., (1988). "Scour downstream of vertical gate." *J. Hydr. Engrg.*, ASCE, 114(7), pp 811-816

Westrich, B., and Kobus, H., (1973). "Erosion of a uniform sand bed by continuous and pulsating jets." *Proc. IAHR Congress*, International Association for Hydraulic Research, 1, pp 91-98.

Wu, S., and Rajaratnam, N., (1995). "Free jumps, submerged jumps and wall jets", *J. of Hydr Res.*, ASCE, Vol. 33, No. 2. pp 197-212.

CHAPTER

4

CHAPTER 4

PREDICTION OF TURBULENT OFFSET JET

4.1 INTRODUCTION

Hydraulic structures such as sluices and sluice gates sometimes work under submerged conditions. The fluid streams issuing from such submerged outlets can be analysed as turbulent jets. If the confining boundaries are sufficiently far from the opening, the jet can be analysed as free turbulent jet, about which extensive information is readily available.

If, on the other hand, the opening is like a sluice gate occupying the full width of the channel, and the jet issues tangentially to the bed, the flow can be analysed as a wall jet (Chapter 3). However, submerged plane openings situated at considerable heights above the bed (for example, a sluice gate situated over an abrupt drop) create complex flow patterns. Such jet, are called offset jets and are studied herein.

The case of an offset jet in the vicinity of a solid boundary is of special interest because of its practical application, e.g. in thermal discharges from power plants, or in two and three-dimensional jets whose invert is higher than the level of the downstream bed. It is therefore essential that the erosive power of an offset-jet is understood in order to enable adequate safety factors to be included in the design of any structure where scour is expected.

4.2 BASIC FEATURES OF THE OFFSET-JET

The typical flow geometry of a two-dimensional offset-jet impinging on a rigid bed or a scoured bed are shown in Figures 4.1 and 4.2 respectively. A plane, incompressible, turbulent water jet is discharged into quiescent ambient surroundings in the vicinity of a plate offset from and parallel to the axis of the jet. When the jet enters the tailwater, its action is similar to that of a turbulent free jet, in that it entrains fluid from the surrounding tailwater. However, when the jet efflux is close to a solid boundary there is only a finite volume of fluid which is available to be entrained between the jet and the bed boundary. Therefore, the surrounding fluid being entrained must be replenished by a back flow near the plate. This will set up vortices in the surrounding fluid. Because of the back flow and the vortices set up in the region, the pressure below the jet will be considerably lower than that above the jet, and consequently the jet deflects toward the boundary and eventually attaches to it.

By attaching to the boundary, the jet encloses a region of eddying motion known as the recirculation region (Figure 4.1). The jet region extending from the nozzle's exit to the point of attachment is commonly referred to as the pre-attachment region. A dividing streamline is defined as that which extends from the lower nozzle's exit to a location on the wall which separates the forward and reversed jet flow. Across this streamline there is no mass flow. The portion above the dividing streamline is accelerated along the boundary because of the jet's positive pressure and the fluid below this streamline is assumed to be part of the recirculating region, on average, contains a fixed amount of fluid. Thus, any fluid entrained on the lower side of the jet is returned to the recirculation region in the impingement zone.

In the pre-attachment region, pressures are generally lower than hydrostatic. As the jet approaches the boundary, the pressures inside the jet increases, reaching a maximum as the jet attaches to the boundary.

In the second, or impingement region the pressure decreases, eventually reaching a hydrostatic value, and the acceleration ceases. The jet then undergoes turbulent diffusion analogous to that of a plane turbulent wall jet in what is known as the wall jet region. This forward flow beyond the impingement region is also designated as "reattached wall jet". A typical velocity profile before and after reattachment is shown in Figure 4.1.

The important parameters associated with this flow geometry are as follows: the length of the offset plate, the ratio of the jet offset to the nozzle thickness (h/b_o), the jet Reynolds number, $U_j b_o/\nu$, the initial turbulence intensity of the jet, and the uniformity of the initial jet velocity profile. A relatively wide range of these flow parameters has been considered by previous investigators.

4.3 OFFSET-JET LITERATURE REVIEW

The problem of an offset jet interacting with an adjacent parallel boundary has been previously described along with the important flow parameters which must be considered. The first reported study on this particular problem is that of Bourque and Newman (1960). Since that time several investigators have attempted to study various aspects of the problem. The following brief review aims to cover significant results obtained by these investigators. The review is divided into two sections; experimental and theoretical.

4.3.1 Review of Experimental Investigations

In this section each parameter studied in the previous experiments is considered separately.

(a) <u>Attachment Point</u>

The primary objective of most of the offset jet attachment studies was to determine the length of the pre-attachment region, X_A, that is to find the point of flow attachment. Experimentally, many different techniques have been used to find the location of the attachment point. Bourque and Newman (1960) and Parameswaran and Alpay (1975) used tufts on the offset plate, Rajaratnam and Subramanya (1968) used coloured dye injection technique. Parameswaran and Alpay (1975) also used suspension of Titanium oxide in penetrating oil on the side walls and the offset plate. Kumada *et al* (1973) and Sawyer (1960) defined the attachment point as the point of maximum wall static pressure. Salehi (1988) obtained the location of the attachment point by considering detailed mean velocity measurements in the horizontal direction.

Using dimensional analysis, Bourque and Newman (1960) showed that the attachment length became independent of Reynolds number, offset ratio, and plate length as each became sufficiently large. They also found that the attachment flow characteristics were not influenced by the length of the offset plate as long as it was approximately 3.7 times the attachment length. They also found that the flow characteristics became independent of Reynolds number when it was sufficiently large, approximately 2500 at an offset ratio of fifty. All the subsequent studies were performed at Reynolds number well above these values and well within the turbulent range. Attached flow at high Reynolds number and long offset plate values thus became dependent only upon the offset ratio.

Bourque and Newman (1960), Parameswaran and Alpay (1975), and Rajaratnam *et al* (1968) found that the attachment length became almost a constant for large values of the offset ratio. Bourque and Newman found the limiting value of the offset ratio to be 35. Salehi (1988) conducted experiments for offset ratio less than 3.5 and found that the division between the forward and reversed flow occur in the vicinity of x/b_o = 40. Nozaki *et al* (1981) studied the effects of turbulence intensity on attachment and found that the flow was independent of turbulence intensity for initial turbulence level larger than 0.06.

(b) Pressure Distribution

The variation of the static pressure along the offset wall was measured by most of the previous investigators who observed the same general trends (Figure 4.3). The wall static pressure, at the beginning of the pre-attachment region was negative and reached a minimum value at a point which corresponded closely to the centre position of the vortex. The centre position of the vortex was measured by Parameswaran and Alpay (1975) who found it to be located approximately two-third of the distance to the attachment point. From the minimum pressure point, the wall static pressure then increased rapidly becoming positive and reaching a maximum value very near to the attachment point. In fact, Kumada *et al* (1973) and Sawyer (1960) defined the attachment point as the point of maximum wall static pressure.

After attachment, the wall static pressure decreased monotonically in the downstream direction and tended toward zero. As the offset ratio was increased, the magnitudes of the maximum and minimum wall static pressure decreased. The distance from the nozzle's exit at which these extremes occurred, however, increased with increasing offset-ratio. At larger offset ratios, the pressure profiles tended to merge into one, corresponding to a limiting value of attachment distance.

Kumada *et al* (1973) suggested that a distinct change in the wall static pressure profile occurred at an offset ratio of approximately six, suggesting a change in the character of the recirculation region at that point. They stated that the values of the maximum and minimum wall static pressures remained essentially constant for offset ratios between two and six, although the locations of these points moved as the ratio changes. The suggestion of a change in recirculation region's character at an offset ratio of six has not been brought forward by any of the above investigators.

(c) Velocity Distributions

Sawyer (1960), Rajaratnam and Subramanya (1968) and Ayukawa and Sakouchi (1976) measured velocity profiles normal to the curved jet and found them to be similar to those of a free jet, as given by Gortler (1942). Sawyer (1960) found that the velocity profiles of the jet as it curved towards the boundary exhibited no obvious asymmetry (Figure 4.4). This observation was in apparent disagreement with the argument put forward by Prandtl (1929). The later indicated that there should be enhanced entrainment in the outer portion of a curved jet, and reduced mixing in the inner portion, due to the influence of centrifugal forces on particles of fluid which transfer momentum from layer to layer.

In a later paper, Sawyer (1963) resolved this discrepancy by postulating that there must be a flow of fluid across the jet's centreline for the observed symmetry of the velocity profiles to be compatible with different entrainment rates on the two sides of the jet. A first-order mixing length theory was used to show that the effects of different entrainment rates on the two sides of the jet did not substantially alter the velocity profiles from their jet shapes. He therefore, concluded that the total entrainment to the jet would remain unchanged.

Pelfrey (1984) in his experimental work on an air offset-jet made detailed mean velocity measurements using a directionally sensitive LDA system. By using the velocity profiles (see Figure 4.5) he determined the jet entrainment and found it to be significantly different from that of either a free jet or a wall jet. Pelfrey also showed that the entrainment parameter in the pre-attachment region was influenced by the recirculation region's pressure. Pelfrey also obtained turbulence characteristics, including: distribution of higher order moments, energy spectra, autocorrelation functions, and integral scales.

In the impingement and wall jet regions, the flow is assumed to be essentially parallel to the wall and to behave like a wall jet. Parameswaran and Alpay (1975) divided the velocity profile downstream of attachment into an inner region, below the point of maximum velocity, and outer region, above the point of maximum velocity. They found that the inner region was fairly well represented by a power law profile, the exponent of which depended upon the offset ratios from one to seven. A one eleventh power law profile seemed to best fit their data. The flow in the outer region was found to be similar to one-half of the Gortler profile.

Hoch and Jiji (1981) also divided the flow downstream of attachment into an inner region and outer region. They said that in the inner region, except for the excess pressure, the jet behaviour was similar to a one-seventh power law profile. The outer region was well represented by one-half of a Gaussian distribution.

Rajaratnam and Subramanya (1968) stated that the decay of the maximum velocity of the attached wall jet could be separated into two regions (Figure 4.6):

1. a characteristic decay region, where the rate of maximum velocity decay was dependent upon the value of the offset ratio; and

2. the classical wall jet decay region, where the decay rate was the same as that of the classical wall jet.

As the jet left the nozzle and flowed toward the plate, the maximum velocity decayed quickly up to the attachment point. After attachment, the rate of decay recovered somewhat and approached that of the classical wall jet at further distance downstream of the nozzle (Figure 4.6). Kumada *et al* (1973) stated that in the attached wall jet region, the gradient of the velocity decay equalled that of the wall jet regardless of the offset ratio. Parameswaran and Alpay (1975) stated that the decay of maximum velocity for various offset ratios behaved in the same manner as that of a plane wall jet in stagnant surroundings. Hoch and Jiji (1981) gave measurements of maximum velocity decay which seemed to agree with those of Rajaratnam and Subramanya (1968).

Parameswaran and Alpay (1975) found that the rate of growth of the outer layer of the attached wall jet, beyond the attachment point, was similar to that of a plane wall jet. The angle of inclination of the line joining points at which the velocity was equal to one-half the maximum velocity and passing through the virtual origin of the attached wall jet for offset ratios greater than three was found to be 3.8 degree and appeared to be independent of the jet's exit velocity. The growth of the inner layer beyond attachment, however, did not exhibit any kind of similarity.

(d) Shear Stress

The shear stress along the wall, downstream of the attachment point, was measured by Parameswaran and Alpay (1975) and Rajaratnam and Subramanya (1968). Rajaratnam and Subramanya found that the time-averaged wall shear stress was zero at the attachment point, then increased rapidly to a maximum, and finally decreased monotonically in the downstream direction (Figure 4.7). The

shear stress distribution did exhibit some similarity in shape beyond the attachment point. Rajaratnam and Subramanya (1968) suggested dimensionless parameters which reduced the shear stress profiles to a single curve which was independent of the offset ratio (Figure 4.8). No measurements of shear stresses in the pre-attachment region were reported.

4.3.2 Review of Theoretical Investigations

Bourque and Newman (1960) were among the first to investigate the velocity and pressure distributions of a two-dimensional jet in the vicinity of a solid boundary. The problem was greatly simplified by assuming that the presence of the boundary had little effect on the velocity distribution of the jet. Thus, the velocity field was taken from the solution of the two-dimensional free turbulent jet. This assumption implied a zero pressure gradient along the jet trajectory. This was accomplished by assuming that the radius of curvature of the jet centreline and the pressure inside the recirculation region were constant.

With the velocity known, the introduction of an additional equation, or closure assumption, was necessary to determine the only remaining unknown: the radius of curvature. This was achieved by applying the horizontal component of momentum locally at the point of re-attachment while neglecting local pressure variation.

Bourque and Newman (1960) applied this solution using the Gortler (1942) velocity distribution for a two-dimensional free turbulent jet. This velocity distribution was in terms of a constant jet spread parameter, σ. Some adjustment of this parameter was necessary to obtain satisfactory agreement with the experimental results. The value of the jet spread parameter differed from its free jet value because of reduced entrainment on the lower side of the jet.

Though reasonable results for the position of the reattachment point were obtained, the assumption of constant radius of curvature and base pressure were not borne out by the experimental results. For example, measurements by Bourque and Newman (1960) and Rajaratnam and Subramanya (1968) have shown that the pressure distribution within the recirculation region is not uniform (Figure 4.3). The wide variation of the wall static pressure in the pre-attachment region would indicate that a uniform recirculation pressure is not possible. This model also failed to account for the rise in pressure and deceleration pressure of the jet as it approached the point of reattachment.

A similar analysis was developed, independently, by Sawyer (1960) at Cambridge. Sawyer in his paper (1963) modified his earlier analysis to account for the different entrainment rates along the inner and outer edges of the jet and to account for the initial mixing region of the jet. He also included pressure forces for the momentum balance near the reattachment point. In a later paper, Bourque (1967) also made some improvement to his predictions, by assuming the path of dividing streamline to be a sine curve. Bourque (1967) pointed out that this assumption compensated for the unrealistic model of constant pressure in the recirculation region. He still, however, failed to obtain a detailed pressure distribution and relate it to the velocity field.

Boucher (1968), instead of the Gortler profile, used a power law distribution for the jet velocity as proposed by Brown and Simpson (1964). Boucher obtained good agreement with experiments for jets attaching to an inclined as well as a parallel offset surface. He also concluded that the entrainment rate was not much affected by curvature.

Perry (1967) by modifying the model of Bourque and Newman (1960), and using a spread parameter, (σ), of 10, obtained a good prediction for low offset ratio attaching jets and inclined plates.

To solve the flow field of a jet towards a surface, Stoy *et al* (1973), applied an integral method for the solution of governing equations and used the entrainment assumption as the closure. Also, they assumed an empirical relationship for the pressure on the centreline of the jet.

Hoch and Jiji (1981) used a fifth degree polynomial to approximate the jet trajectory and left the recirculation region pressure as a parameter to be obtained in the solution. They assumed a Gaussian-shaped velocity profile for the curved jet. They also took into account the zone of flow establishment.

Ali and Salehi (1991) developed a general integral method which combined the strip integral method, in a curvilinear coordinate system, with the k-ε or the algebraic stress turbulence models (ASM) to predict the velocity fields of different flow situations, including those of offset jets impinging on rigid and scoured bed. They found that the algebraic stress model gave better agreement for curved and wall affected flows. However, the position of the attachment point of maximum scour section, was overpredicted.

4.3.3 Concluding Remarks Regarding the Literature Review

Most of the investigations of two-dimensional jet-boundary interaction were primarily concerned with the pre-attachment region, focusing on the determination of the point of reattachment. To achieve this, simplifications such as the assumptions of constant pressure in the recirculation region and constant jet-axis radius of curvature were introduced. These assumptions facilitated the use of the free jet velocity distribution, thus bypassing the need to solve for the velocity. Although these models gave reasonable results for the position of the point of reattachment as a function of the offset height, the assumption regarding velocity, pressure and radius of curvature were unrealistic.

It is apparent that there is a need for a more substantive model, based on sounder physical reasoning which could be extended to give the velocity, and pressure distributions in all regions of the jet. Also, detailed velocity measurements, especially in the recirculating zone are necessary for a better understanding of this type of flow.

4.4 APPLICATION OF FLUENT TO OFFSET JETS

4.4.1 Introduction

This section describes applications of the FLUENT package to offset jet flow phenomena. Three experiments carried out by previous investigators , Rajaratnam and Subramanya(1968) , Ali and Salehi (1991) and Ali and Whalley (1992) were selected as benchmarks for the turbulence modelling capabilities in FLUENT.

The experimental setup and procedures of each experiments are briefly described in the following section.

4.4.2 Rajaratnam and Subramanya's Experiments (1968)

The experiments were conducted at the Hydraulic laboratory of the University of Alberta, Canada. A recirculating flume 18 in. wide, 36 in. deep, and 16 ft. long, with aluminum bottom and plexiglass sides was used. An inlet hood attached to an aluminum gate provided the nozzle. The step below the nozzle was provided by raising the level of the bed upstream of the gate by means of aluminum box-like units. The discharge was measured by means of a commercial orifice meter located in the supply line. The experiments were conducted under conditions of

deep-submergence i.e., the water surface was essentially deep and level for a considerable distance downstream of the nozzle. A summary of selected experiments used in this study is given in Table 4.1.

TABLE 4.1 : Summary of Rajaratnam and Subramanya's experiments

Test No.	q ft^3/s/ft	b_o (in.)	h (in.)	X_A (in.)	Y_t (in.)	U_o (in.)
A-2	0.683	1.000	3.312	9.75	25.5	8.23
B-2	0.480	0.550	3.312	7.50	19.3	10.9
C-1	0.604	0.750	1.344	4.50	20.2	9.85
D-2	0.875	1.340	1.344	5.00	27.1	8.00

The velocity field was measured using Prandtl-type pitot static tube of 3 mm external diameter. It should be noted that no corrections were made for the angle of attack, the effects of turbulence and pitot displacement. A typical velocity distribution at different sections observed in Run A-2 is shown in Figure 4.9.

The shear stress on the bed, τ_o, was measured using a Preston tube of external diameter 3 mm; the ratio of the internal to external diameter is 0.60. A typical bed shear stress plots is shown in Figure 4.7.

4.4.3 Ali and Salehi's Experiments (1991)

The experiments were carried out at the Hydraulic Laboratory, The University of Liverpool, using a 5.0 m long, 0.6 m wide and 1.0 m deep channel. A vertical sluice gate, constructed from a 1 in. thick perspex cut to the width of the channel,

was supported by a metal frame and could be lifted by means of a gear box. The sluice gate opening was measured by using two dial gauges located on top of the gate, which had an accuracy of 0.01mm. A bottom vertical weir was fixed to the channel wall and had a height of 30.3 cm. To ensure uniform and two-dimensional flow, they used two pieces of half-rounded perspex pipes to form a well-designed sluice entrance.

For the two-dimensional offset jet impinging on a rigid bed, a single jet height of 30 cm, and nozzle thickness of 1.145 cm was used. Two different initial jet velocity were used; U_j = 90 (RIGID1) and U_j = 150 cm/s (RIGID2).

For the clear-water scour experiments, the working section of the channel was 1.7m from the downstream end of the channel. This section was filled with sand to the desired height. At the end of the channel a vertical sharp-crested weir of adjustable height was used to regulate the water level in the channel.

The bed material used was non-cohesive sand of median size of 0.82 mm and geometric standard deviation of 1.126. The specific gravity, S, angle of repose, φ, and the porosity of the bed material were, 2.66, 33°, and 0.403 respectively. The average fall velocity, w, of the bed material was 11.0 cm/s.

During the course of the experiments, measurements of the scour hole were made using photographic records of the gauges located along the centreline of the channel. Figure 4.10 shows the time evolution of centreline bed-profiles obtained for test case S205 (jet height, h = 20.15cm; jet velocity, U_j = 69 cm/s)

Velocity measurements were made only during the "asymptotic" stage (t = 4770 mins.) in which the bed was hardly changing with time. For this reason, they decided that there was no need to freeze the scour hole in the same way that most

of the previous investigators did. All velocities were measured using a streamflow miniature current meter manufactured by Nixon Instrumentation Ltd. The measuring head of the meter was 16 mm in diameter. The velocity measurements were taken over a grid of location in both horizontal and vertical planes by mean of two types of probe; a straight probe to measure the horizontal velocities, and a bent probe to measure the vertical velocities. Typical resultant velocity vectors for the flow are shown in Figure 4.11.

4.4.4 Ali and Whalley's (1992) Experiments

The experiments were an extension to the scour experiments carried out by Ali and Salehi (1991), except that in here two different jet heights were used: 10 cm (RUN 1) and 20 cm (RUN 2). Here the jet height was defined as vertical distance from the initial bed level to the lower part of the sluice opening. The test procedures and instrumentations used are essentially the same as those used by Ali and Salehi. The initial uniform inlet velocity, U_j, was 64 cm/s. The resultant velocity vectors for the flows as observed in the experiments are shown in Figure 4.12.

4.5 SIMULATIONS USING FLUENT

The experiments mentioned in the previous section were simulated using the FLUENT CFD package. Descriptions of the package and the governing equations were given in Chapter 2.

4.5.1 Geometry Setup and Grid System

As mentioned in a previous chapter, FLUENT provides two choices of grid coordinates system; (i) Cartesian, and, (ii) Curvilinear or Body Fitted Coordinates (BFC). The scoured bed geometry in the present study was defined using the 2-dimensional BFC system. The BFC system allows the geometry to be defined such that the mesh of computational cells being fitted or mapped onto the boundaries of the geometry. This is necessary in modelling the curved topology of the scoured bed, especially when the velocity and shear stress distribution near the bed are the important parameters to be determined. The simplicity of the Cartesian system, which modelled the bed as series of steps can cause inaccuracies in the calculation of these variables, which, in turn, may cause inaccuracies in the numerical solution of the entire domain.

In general, it is desirable to increase the grid resolution in regions where the flow variables exhibit large gradients. In the present analysis, more refined grids are provided at an area between the bed and the jet, and between the sluice gate upto the where the reattchment point is expected to occur. Several trial runs were made with various grid arrangements to ensure that the final grid was sufficiently refined, *i.e.* when further refinement did not perceptibly change the computed results. Typical grid arrangements for the rigid and the scoured bed are shown in Figure 4.13.

Since the FLUENT CFD package cannot simulate a free surface directly, the water surface in the experiments was modelled by means of a "rigid-lid" or horizontal fixed boundary. The surface is defined as a frictionless wall or slip wall, that is, links to all velocity components were cut. By doing so the value at the boundary will be set equal to the value of the preceding cell.

4.5.2 Solution Parameterss

The following solution-parameters were used for all cases, unless otherwise specified:

Underrelaxation:	*0.2 (velocity, turbulence k.e. and eddy dissipation)*
	0.5 (pressure)
Sweeps :	*Alternating Direction with 2 (u,v)*
Convergence Criteria :	*1 x 10^{-3} residual sum*
Algorithm :	*SIMPLE*
Solver :	*Power Law Differencing Scheme (Default)*

Three different turbulence models available in FLUENT were applied to the above cases. The default solver or discretization scheme used was Power-Law Differencing Scheme. Alternatively, a higher order scheme termed as blended Second Order Upwind/Central Difference scheme was also applied in order to investigate the significance of the scheme. While the higher order scheme was supposed to provide improved accuracy, it was found that in some events, numerical instability occurred during the iterations. Detailed descriptions of the solution method based on various schemes mentioned above can be found in the FLUENT User's Guide.

4.6 RESULTS AND DISCUSSIONS

4.6.1 General

Figures 4.14 (a) - (c) show the predicted jet profiles for different degrees of submergence. The jet opening and initial inlet velocity used are similar to Test A-2 of Rajaratnam and Subramanya(1968). A jet entering a reservoir will immediately entrain the fluid that was originally at rest. Due to the high shearing forces at the edges of the jet, mixing and entrainment increase as the jet progresses further from the efflux section. This outward spreading and deceleration is symmetrical about the centreline for a free jet. This is shown in Figure 4.14 (a). However, if a free surface is relatively close to the efflux section (Figure 4.14(b)) , then only the bottom half of the jet has an almost infinite supply of water available for entrainment, whereas the supply of water available for entrainment in upper half is restricted by the free surface. Hence, the ambient fluid entrained into the jet from upper half must be replenished by a backflow of water near the free surface. A vortex will be established in this region enclosed by the upper surface of the jet, the wall containing the slot and the free-surface. The pressure in this region will be lower than the pressure below the jet and results in a pressure difference that produce a net lift effect that deflects the jet towards the free surface. If the solid bed is the boundary that limits the entrainment of fluid, then jet deflection is somewhat like that of the free-surface mentioned above. This time, however, the jet deflects towards the bed. Qualitatively, this pattern is correctly predicted by FLUENT as can be seen in Figures 4.14(a)-(c).

4.6.2 Offset Jet Impinging on Rigid Bed

Figure 4.14(c) shows the predicted velocity contours and the velocity profiles for test A-2 (Table 4.1) of Rajaratnam and Subramanya(1968). The velocity profiles at various sections along the streamwise direction are shown in Figure 4.15. Comparing Figure 4.15 and 4.9, it can be seen that although the general pattern of the flow is in good agreement, FLUENT underpredicted the value of the maximum velocity U_m. The same observation can be seen from comparing Figure 4.16 and Figure 4.7. The predicted bed shear stress values are in the order of 25 - 30% smaller than the measured values. It should be noted here that the measurement techniques used by Rajaratnam and Subramanya (1968) during the test are very crude and as mentioned in Section 4.4.2, no corrections were made to the measured values for the effects of turbulence and pitot displacement. Possible errors which may occur in the measurements are: (1) The error caused by the presence of a Pitot tube near the bottom which results in the shifting of the streamlines and hence the reading of a higher impact pressure than the true one; (2) the error due to turbulence. Therefore, in order to verify the differences between the measured and the computed values, it is also of equal important to assess possible errors occured in the laboratory study.

The maximum velocity, U_m, in general decreases with the increase in distance away from the wall containing the jet, x, due to turbulent diffusion. Figure 4.17 shows the decay of the non-dimensional maximum velocity U_m/U_j in the downstream direction, x. Rajaratnam and Subramanya (1968) stated that the decay of the maximum velocity of the attached wall jet could be separated in two regions; characteristic decay region and classsical wall jet decay region. Similarly, FLUENT exhibits the existence of the two regions. As the jet left the nozzle and flowed toward the plate, the maximum velocity decayed quickly up to attachment point. After the attachment the rate of decay approached that of the classical wall

jet. Again, it can be seen from this figure that the experimental value of U_m / U_j are higher than those predicted by FLUENT.

Figures 4.18 show the simulated velocity contours for test RIGID1 and RIGID2 (Table 4.2) of Ali & Salehi (1991). The location of the intersection of the dividing streamlines with the offset jet channel, i.e. the reattachment point, X_A, is taken at the location where the wall static pressure is maximum.(Kumada. et al (1973)). Table 4.3 shows a comparison between the predicted and measured reattachment length ratio for the case of an offset jet impinging on rigid bed. In most cases, it can be seen that FLUENT 's results are smaller than the measured values by 2 - 21%. RNG and standard k-ε models gave better estimation compared to RSM and Higher Order Discretization scheme. It is interesting to note that the attachment lengths for both cases, RIGID1 and RIGID 2 are the same, although different inlet velocity were used. The same trend was observed by Ali and Salehi (1992). This also confirms the observation made by Bourque and Newman (1960) where the attachment flow characteristics became independent of Reynolds number when it was sufficiently large, approximately 2500. The Reynolds number for both tests based on the jet opening are respectively 10 323 and 17 175. Attached flow thus became dependent only upon the offset ratio. Figures 4.19 show the predicted flow field for different jet height. It can be seen from these figures that the attachment lengths increase with the increase in jet height. This is also true in the case of Rajaratnam and Subramanya's results, as can be seen in Table 4.2.

Examination of Figures 4.15, 4.18 and 4.19 confirms the observation made by Ali and Salehi (1992) that after impingement of the jet, the flow behaves like a wall jet. As the wall pressure gradient in the area between the point of attachment and point of minimum pressure is negative, the maximum velocity of the backflow increases. However, from the point of minimum wall pressure towards the vertical wall, the pressure gradient is positive, therefore the maximum velocity of the backflow decreases in this direction.

Table 4.2 Comparisons between measured and predicted attachment lengths ratio

Experiments	Offset Ratio h/b_o	Measured X_A/b_o	Predicted X_A/b_o	% Difference
Rajaratnam :				
A-2	3.81	9.50	8.40 (RNG) 8.40 (k-ε) 7.75 (RSM) 7.50 (HO)	11.58 (-) 11.58 (-) 18.42 (-) 21.05 (-)
B-2	6.52	13.64	13.09 (RNG) 13.06 (k-ε) 13.30 (HO)	4.03 (-) 4.25 (-) 2.50 (-)
C-1	2.29	6.00	6.40 (RNG)	6.66 (+)
D-2	1.50	3.73	3.58 (RNG)	4.02 (-)
Ali & Salehi:				
RIGID1 (U_j = 90 cm/s)	26.16	40.3	38.0 (RNG) 38.0 (k-ε) 35.5 (HO)	5.71 (-) 5.71 (-) 12.0 (-)
RIGID2 (U_j = 150 cm/s)	26.16	40.3	38.0 (RNG) 38.0 (k-ε)	5.71 (-) 5.71 (-)

Notes: RNG - Turbulence model based on Renormalization Group

RSM - Reynolds Stress Model

k- ε - standard k-ε Turbulence Model

HO - Higher Order discretization scheme

(-) - underestimated (+) - overestimated

To define a trajectory for the offset jet is very useful in theoretical work. The locus of the position of the maximum velocity was chosen as the reference streamline (represented by dotted line in Figure 4.1). Figure 4.20(a) shows the line of trajectory of the maximum velocity locations . A least square fit was performed to smooth out the data for the locus of maximum velocity predicted by FLUENT. A fourth order polynomial with coefficients:

C_0 = 0.99702 C_1 = -0.19492 C_2 = 0.32689

C_3 = -1.00959 C_4 = 0.48066

was found to best fit the FLUENT result for all cases considered, based on minimum residuals. The expression for Ym/h is therefore given by:

$$\frac{Y_m}{h} = C_0 + C_1\left(\frac{X}{X_A}\right) + C_2\left(\frac{X}{X_A}\right)^2 + C_3\left(\frac{X}{X_A}\right)^3 + C_4\left(\frac{X}{X_A}\right)^4 \quad (4.1)$$

where Y_m is the vertical distance between the point of maximum velocity and the bed. Figure 4.20(b) shows the best-fit curve of locus of maximum velocity for results obtained by other researchers.

4.6.3 Offset Jet Impinging on Scoured Bed

While scour is taking place, the behaviour and movement of the sediment-water mixture along the bed of the scour represents a very complex, unsteady and non-uniform shear flow problem. A thorough analytical study of the flow patterns would be very difficult, even for the two-dimensional case because the scoured bed profiles and hence, the velocity distributions are continuously changing as the scour progresses with time.

Experimental results pertaining to location of maximum scour obtained by Ali and Salehi (1991), and, Ali and Whalley(1992) are summarised in the following table (definition of parameters is given in Figure 4.2).

Table 4.3 Summary of Offset-Jet Experimental Results

	h (cm)	b_o (cm)	U_j (cm/s)	x_m (cm)	d_m (cm)	Asymptot Time (mins)
Ali & Salehi (Test S205)	20.2	1.18	69	42	9.2	4770
Ali & Whalley (RUN 1)	10.58	1.16	64	25	3.0	480
Ali & Whalley (RUN 2)	20.58	1.16	64	45	4.0	1230

It is obvious that under supposedly similar test conditions (Test S205 and RUN 2), the results vary significantly. Ali and Salehi judged that the asymptotic state was achieved after 4770 mins, whereas in later experiments Ali and Whalley observed that the aymptotic state was reached after only 1230 mins. Consequently, the maximum scour depth d_m, for Test S205 was found to be twice as deep as in RUN2.

There are many factors that influence the experimental results, which were not reported by the investigators, such as the temperature, smoothness of sluice gate, exact form of the velocity profile at the sluice gate, the outflow conditions and the Reynolds number. These factors may in one way or the other, affect the simulated results as will be discussed later in this section.

Figures 4.21 and 4.22 show the simulated velocity vectors of Ali and Salehi for different grids arrangement. These two figures illustrate the sensitivity of the grids sizes adopted in numerical simulation calculation. Figure 4.21 shows the converged solution using coarser grids. The jet, on leaving the sluice, immediately dips to the bed and runs along the bed. With finer grids (see Figure 4.13), the jet travels some distances downstream before it attaches to the bed (figure 4.21). A similar pattern was observed in the experiments. As further refinement of the grids did not change the computed results, the grid arrangement as shown in Figure 4.13 was therefore used for the rest of the analysis. Figures 4.23 and 4.24 show the simulated velocity vectors of Ali and Whalley's experiments, for offset jet height 10 cm and 20 cm respectively. Figures 4.25-4.27 show the floor velocity plots along the scour holes. The experimental results showed that the jet attached to the bed at a location of maximum scour depth. However, figures 4.23 to 4.27 show that in all cases FLUENT overestimated the attachment length. Figures 4.26 and 4.27 clearly indicate the high variation in experimental velocity reading. It should be reiterated here that in their experiments, unlike many other reasearches, the bed was not "frozen" and the velocity measurements were taken directly above the bed at the asymptotic state. It can therefore, be argued that one of the reason for such high variation is due to the local disturbance caused by the velocity propeller meter placed very near to the bed.

Ali and Salehi as well as Ali and Whalley reported the existence of humping at side wall and hollowing at the middle of the scoured bed. It is clear that the

attached flow to the bed will be different in the case of two-dimensional or nearly two-dimensional compared to three-dimensional flow. If spanwise flow from the edge of the jet is permitted, the vortex will not be strong as entrainment will bring fluid from the sides. Hence, a pressure difference large enough to cause the jet to deflect. As the numerical model simulated the flow in two-dimensional, it is therefore very important to ensure that the flow conditions studied in the experiments are two-dimensional or nearly two dimensions, or otherwise differences in measured and calculated results should be expected.

4.7 CONCLUSIONS

FLUENT results for simulated offset jet flow fields have been compared with results from various experimental data. Two cases have been considered; offset jet impinging on rigid bed, and, offset jet impinging on scoured bed.

In general the FLUENT results exhibit good qualitative agreement throughout the flow field. In rigid bed cases the predicted attachment length were reasonably accurate to within 10% when RNG and k-ε models are used. However large errors were found using the RSM model. Numerical instability occurred using the Higher Order scheme. For the scoured bed analysis, FLUENT overpredicted the attachment length.

Extensive testing procedures have been implemented to ensure that the equations and solution algorithms used by FLUENT would provide an accurate simulation of the flow. However, inaccuracies may arise on specific engineering problems regarding the spacing of the computational grid, suitability of the physical model utilised, or the choice of boundary conditions. It was shown that the grid spacing would be of great importance to the modelling accuracy. Clearly demonstrated in

this exercise is that the results from FLUENT ought to be subjected to critical interpretation, as errors in input data (i.e. bed profiles, inlet velocity, etc.) could introduce serious errors as those caused by the numerical approximations. In short, in order to verify the differences between the measured and the computed values, it is also of equal important to access possible errors occured in the laboratory studies.

It is therefore very difficult to report simulation results which do not predict the experimental data within acceptable level of accuracy, especially after making every effort to provide the best solution possible and still falling short. However, the author believes that such an exercise provides credibility to this growing CFD industry and will ultimately serve the interest of the engineering and scientific community.

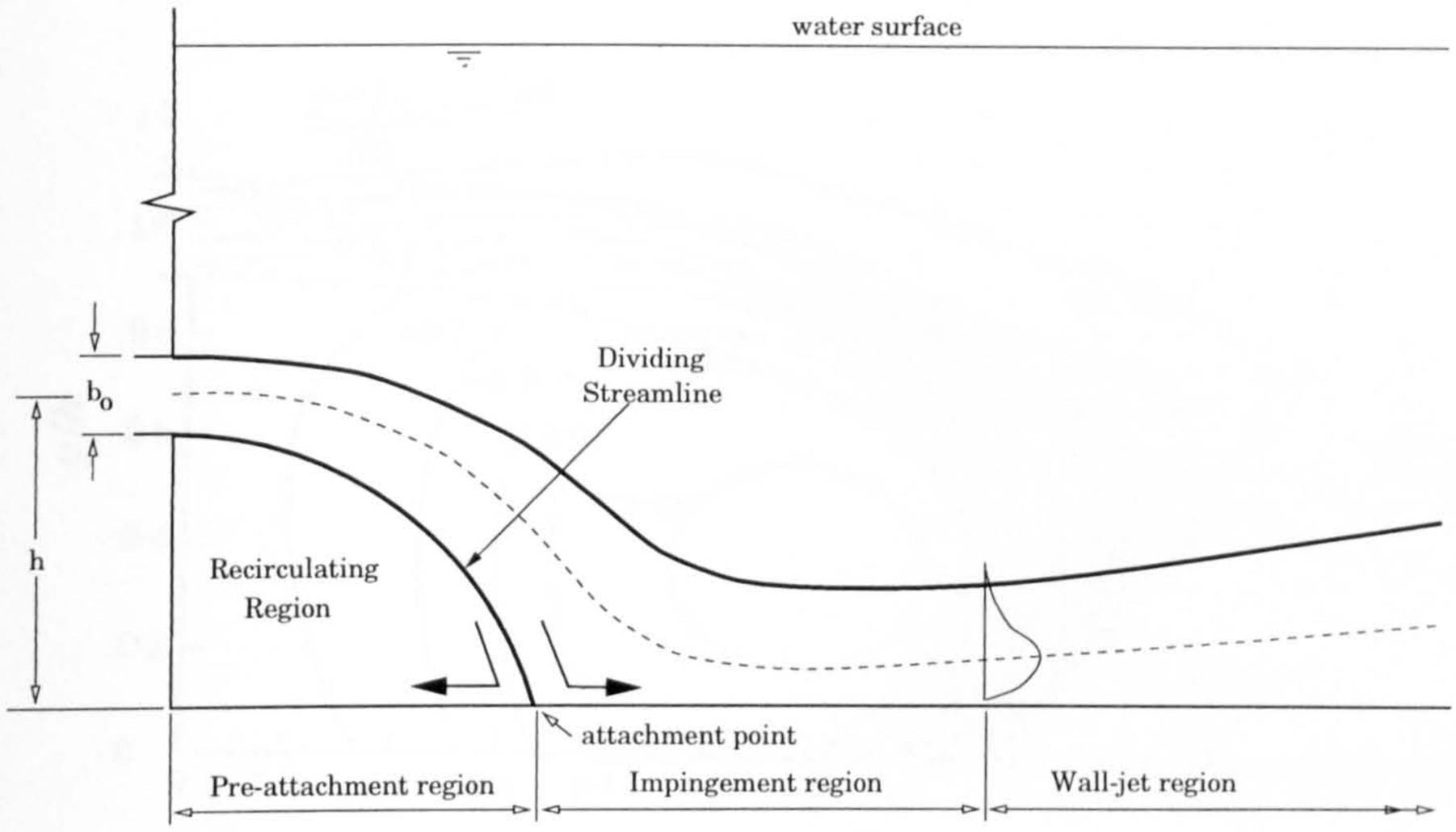

Figure 4.1 : Typical flow geometry of offset-jet

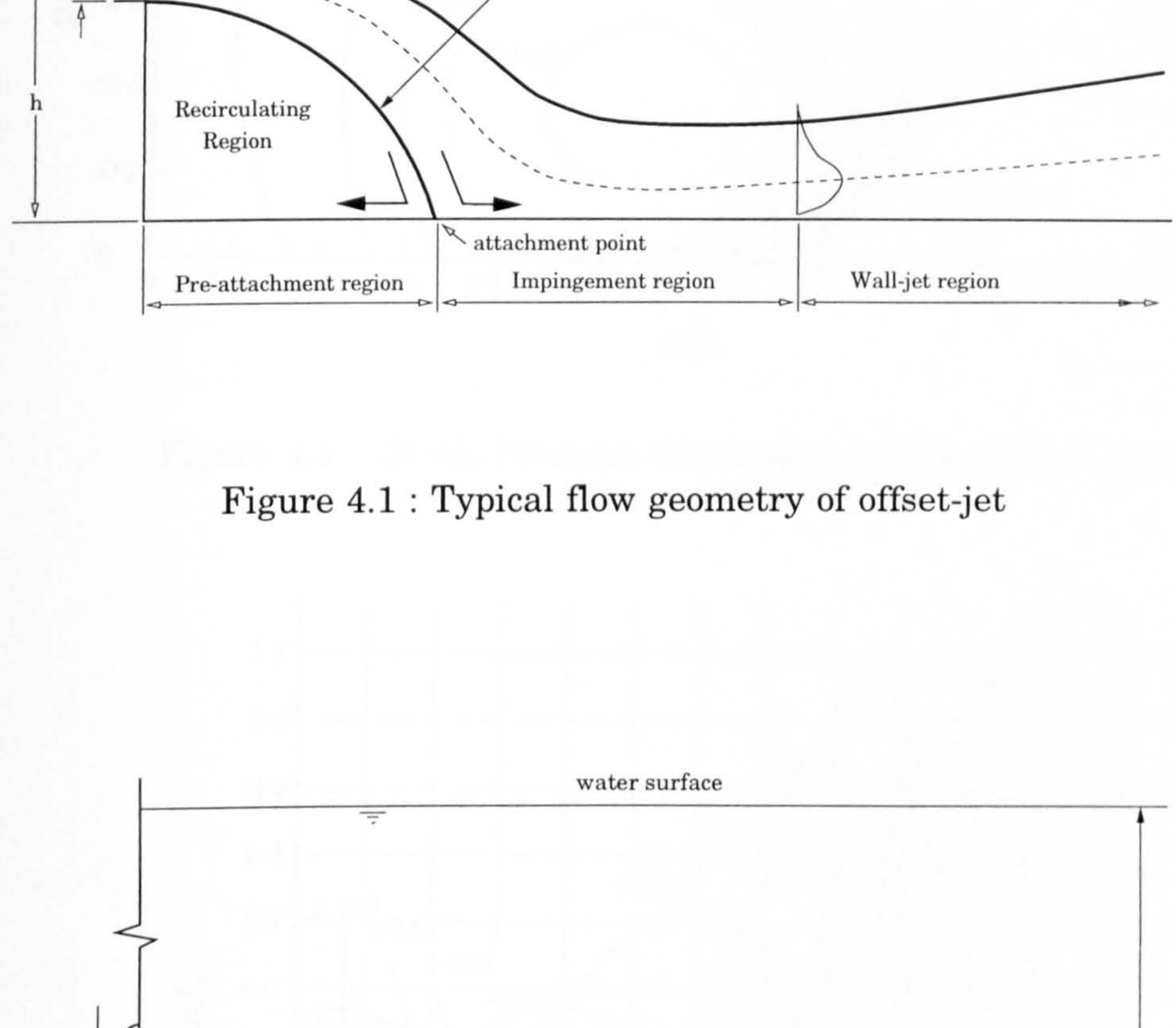

Figure 4.2 : Definition sketch for a scour hole

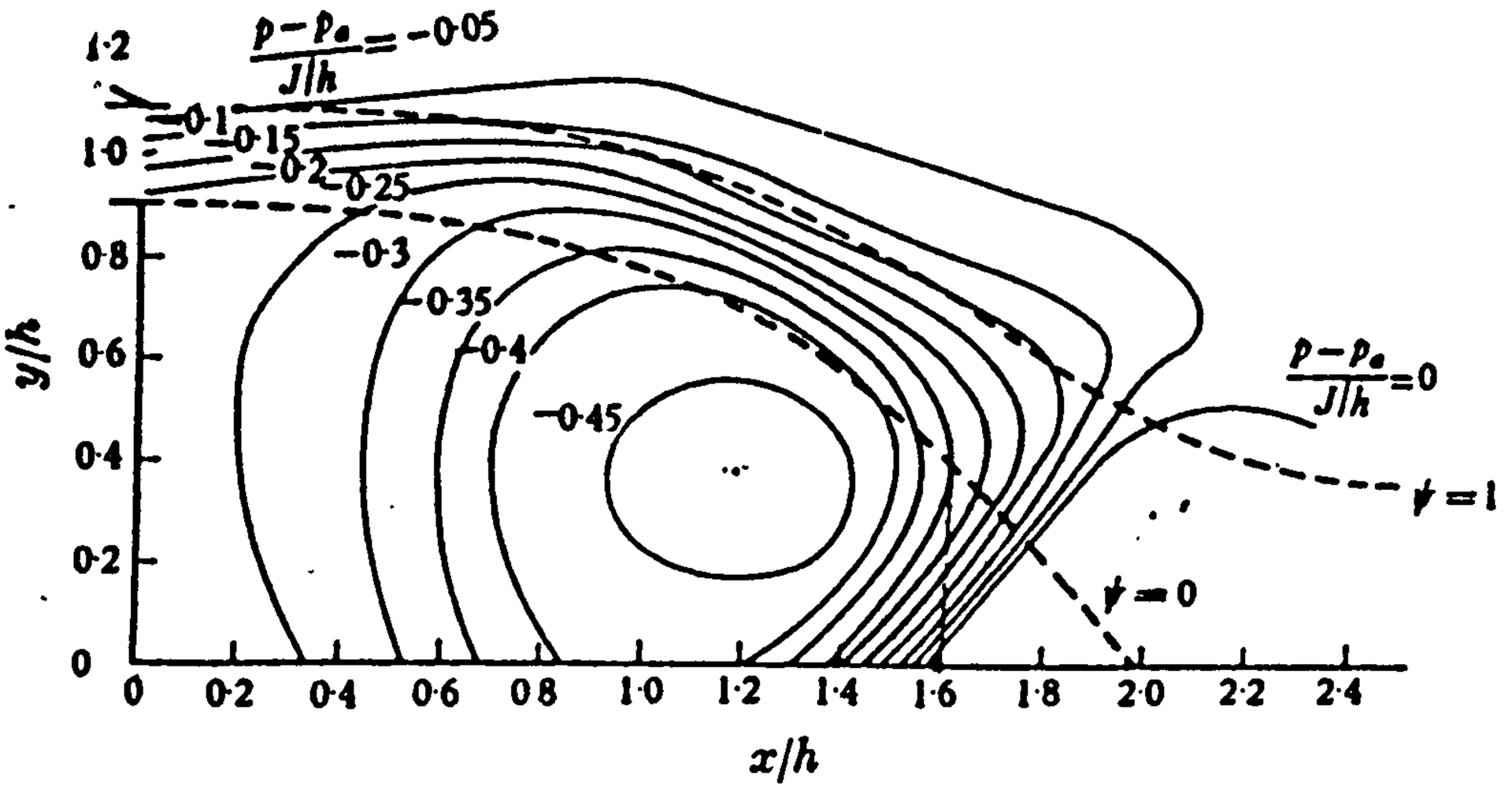

Figure 4.3 : Static Pressure Contours for Cases $h/b_o = 5.62$
(after Sawyer (1960))

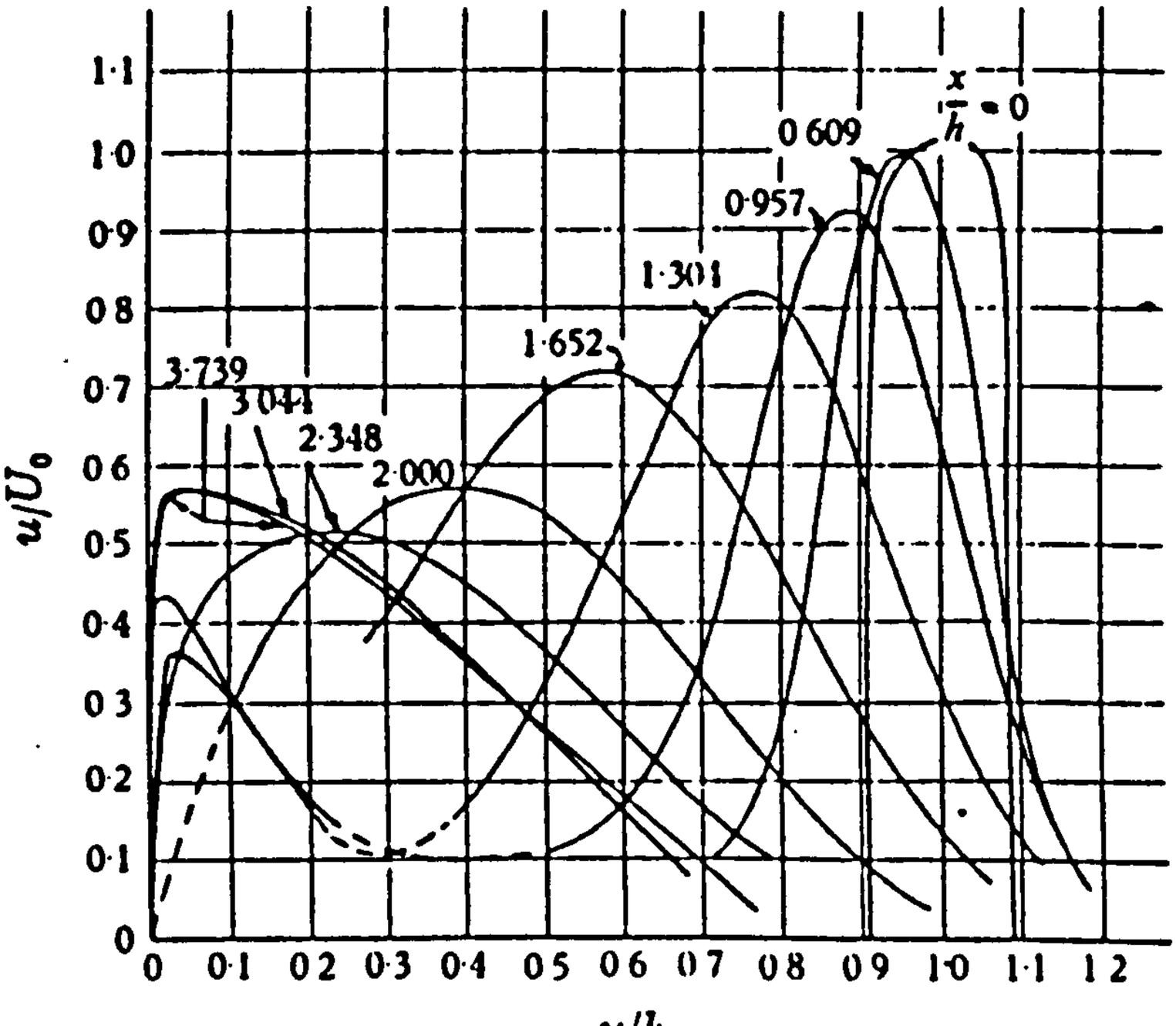

Figure 4.4 : Velocity Profiles for Case $h/b_o = 5.62$
(After Sawyer (1960))

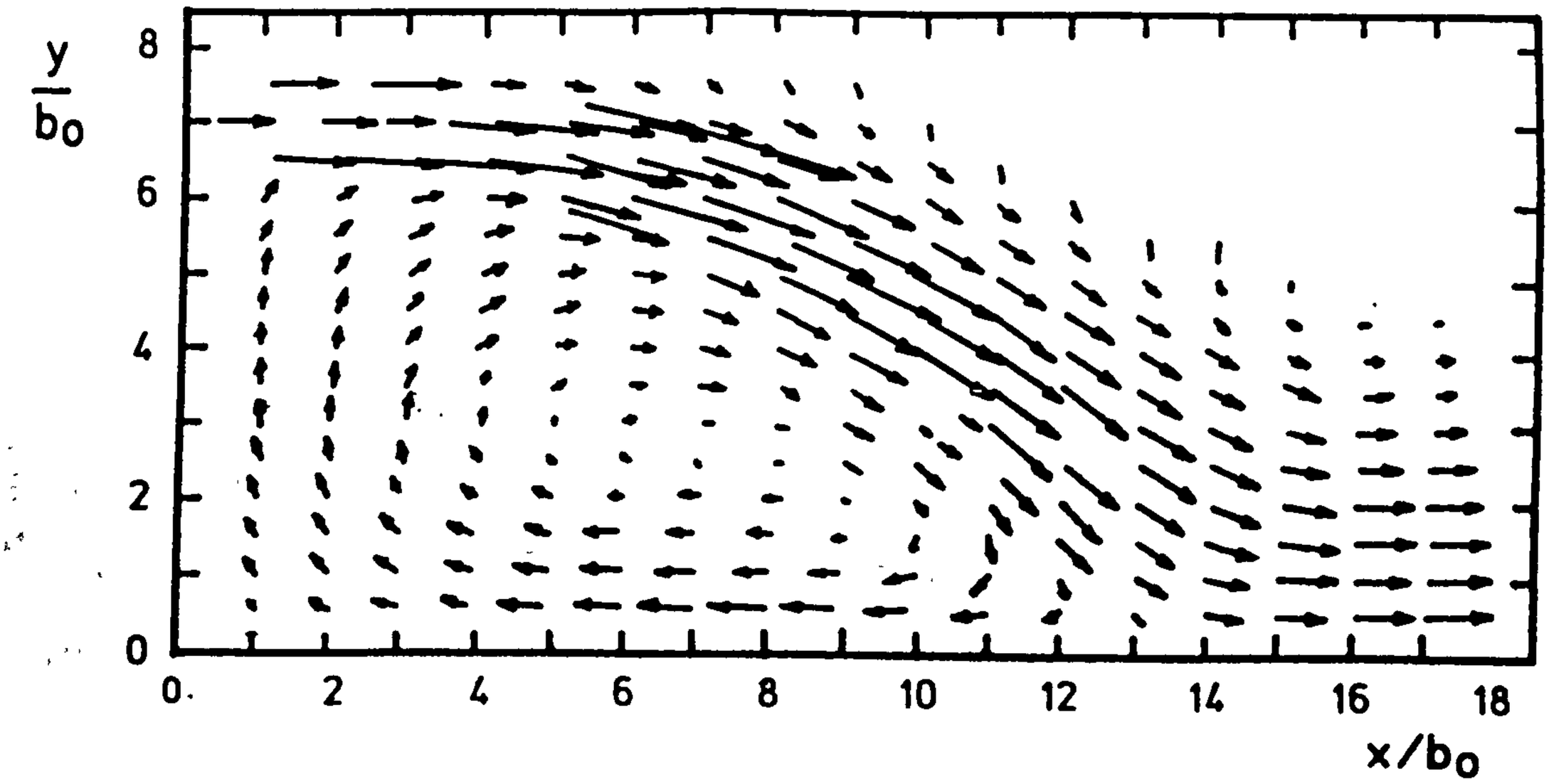

Figure 4.5 Velocity Vectors of an Offset Jet (After Pelfrey (1984))

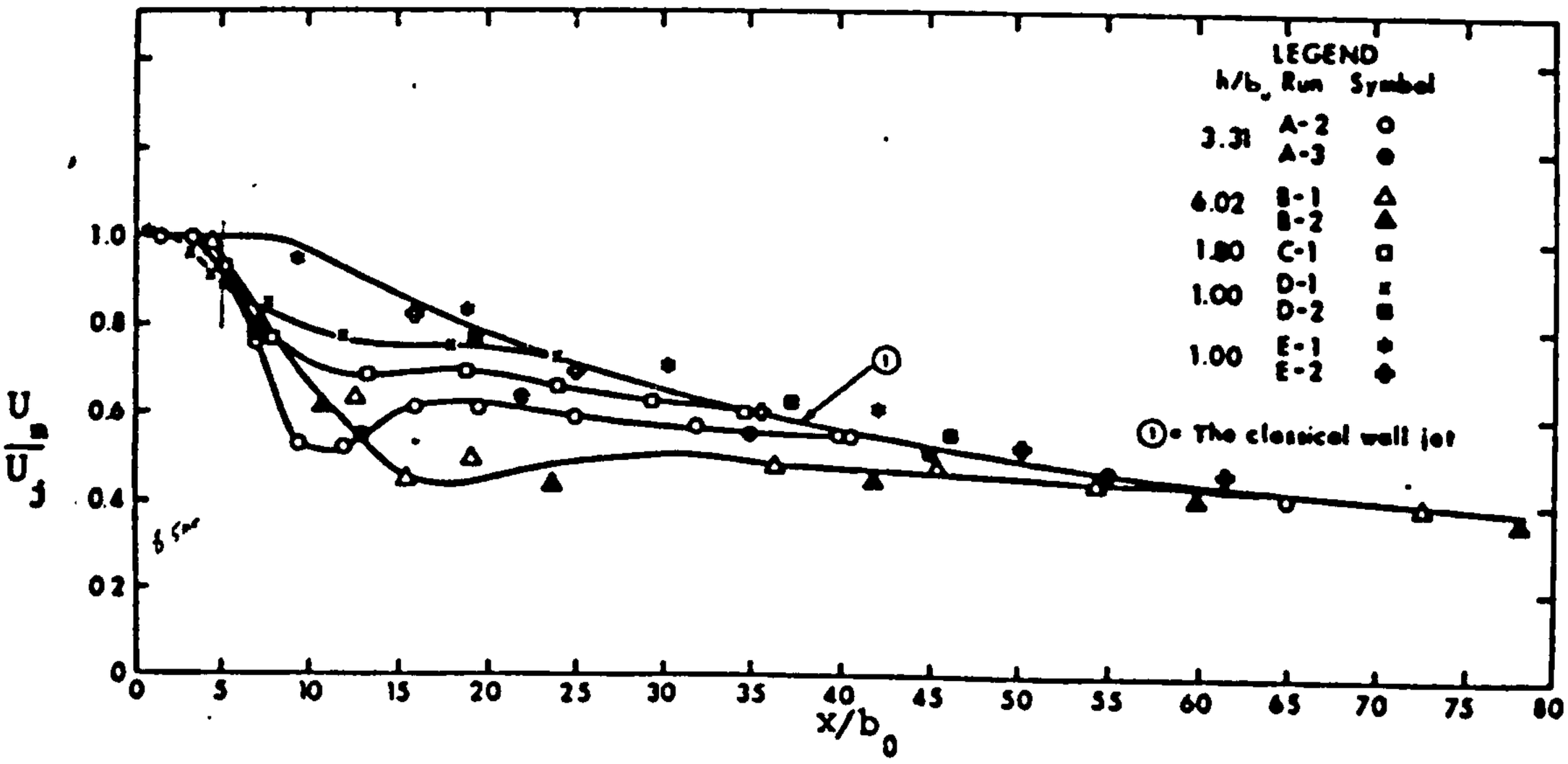

Figure 4.6 Decay of Max. Velocity for Offset Jets
(After Rajaratnam (1968))

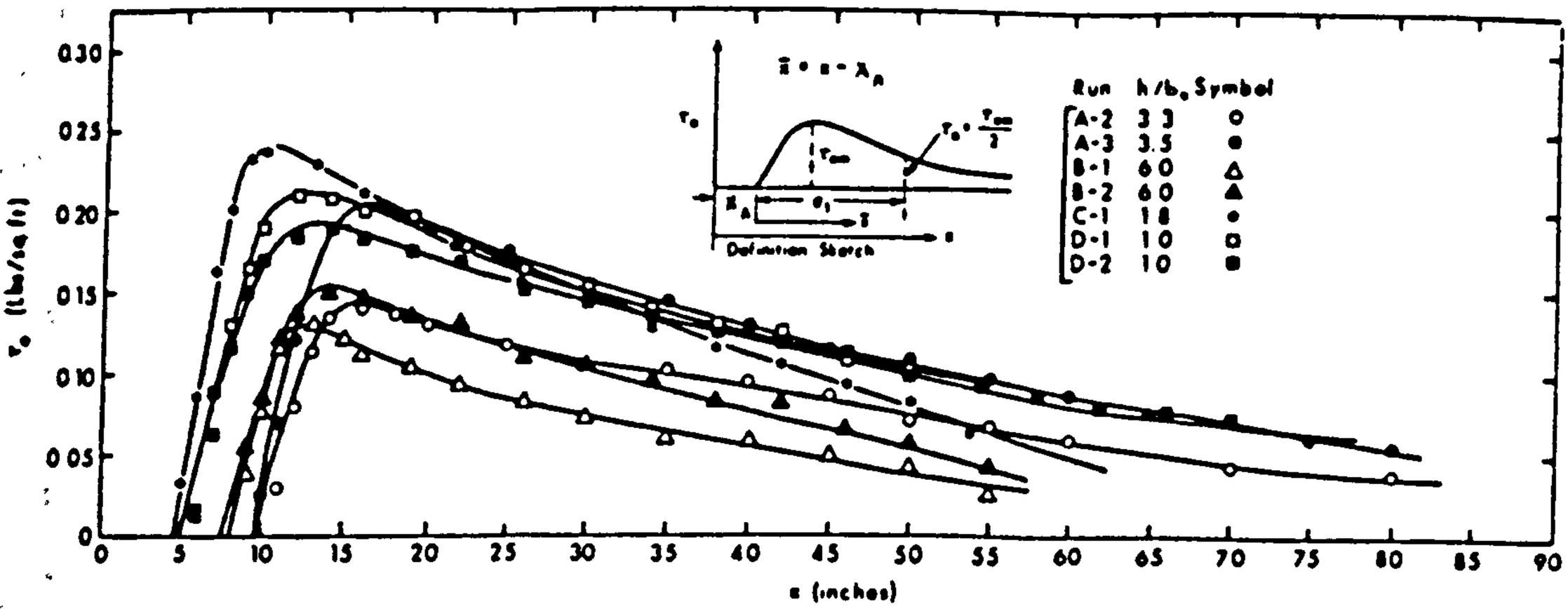

Figure 4.7 Bed Shear Stress Plots (After Rajaratnam (1968))

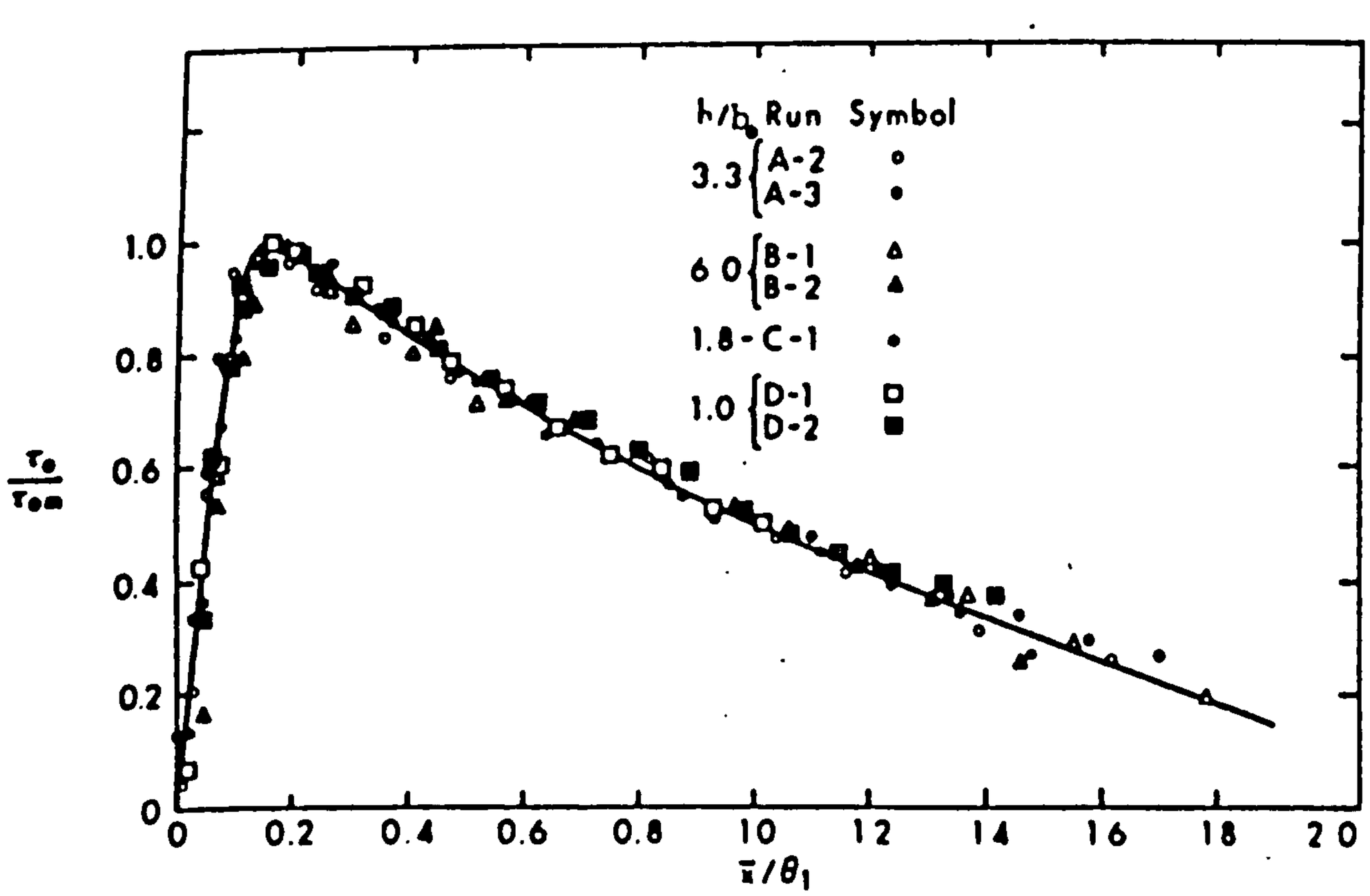

Figure 4.8 Distribution of the Bed Shear Stress (After Rajaratnam (1968))

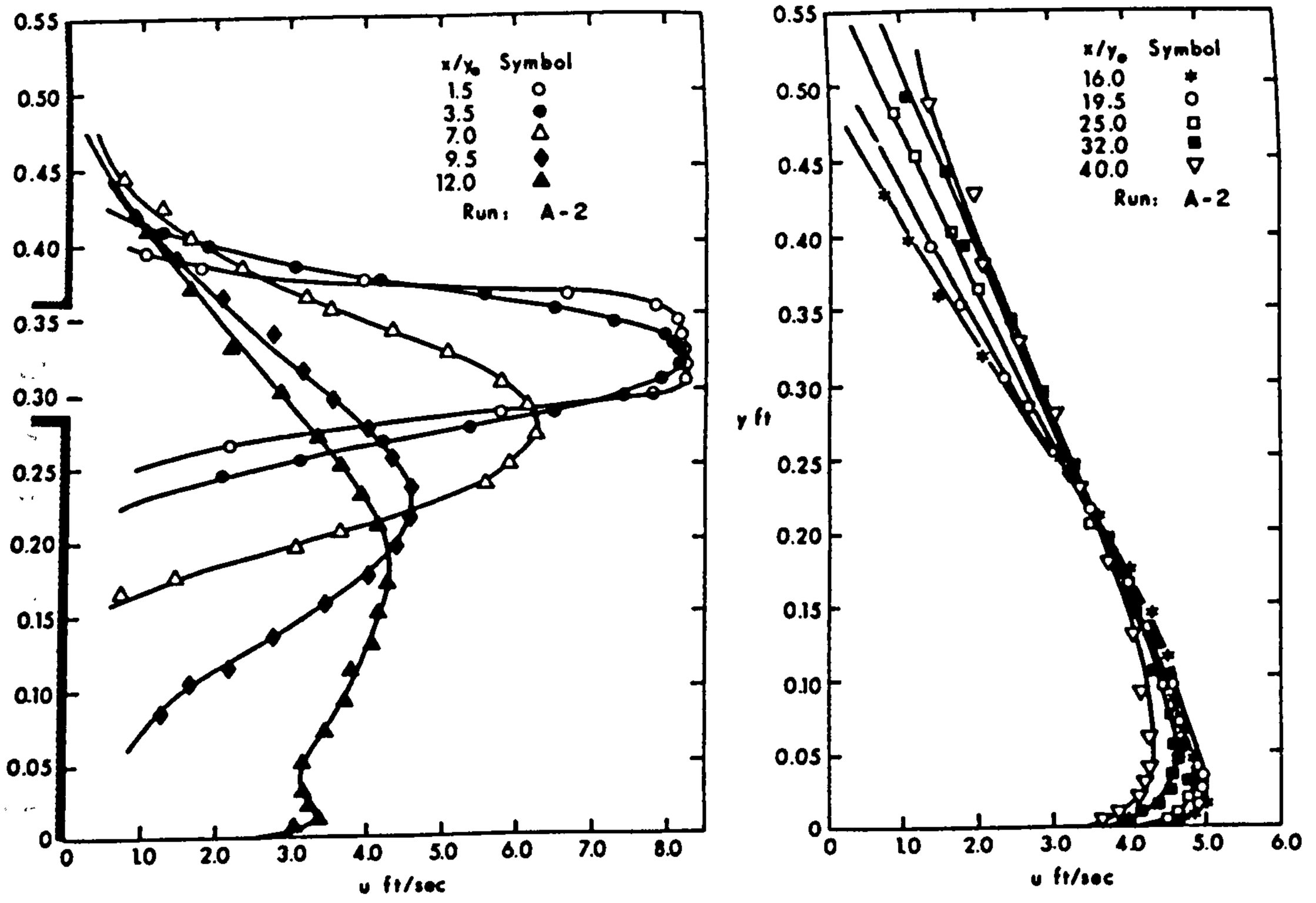

Figure 4.9 : Typical Velocity Distribution Plot (After Rajaratnam(1968))

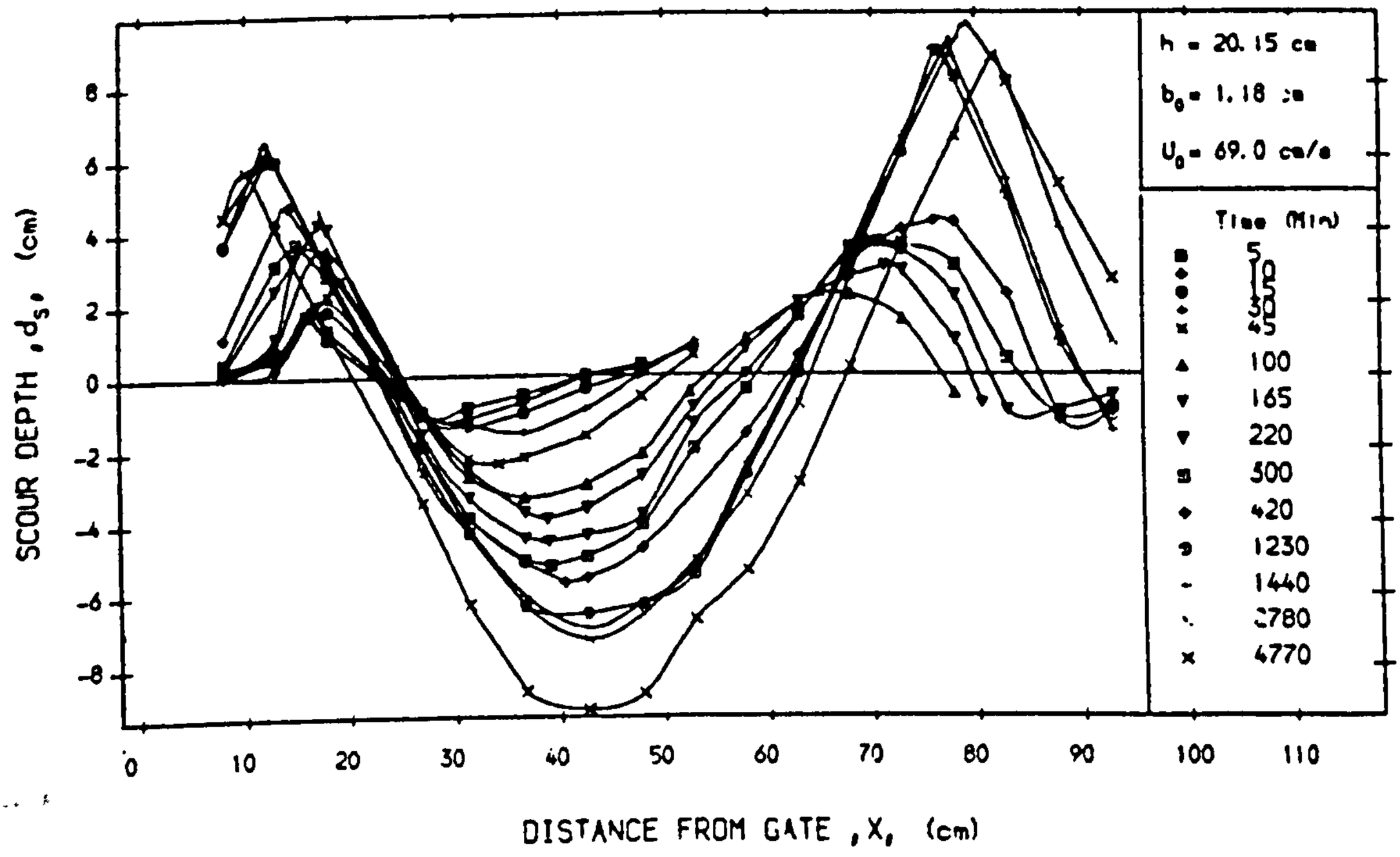

Figure 4.10 : Progress of Scour Hole Profile With Time (Test No. S205) (After Ali and Salehi (1991))

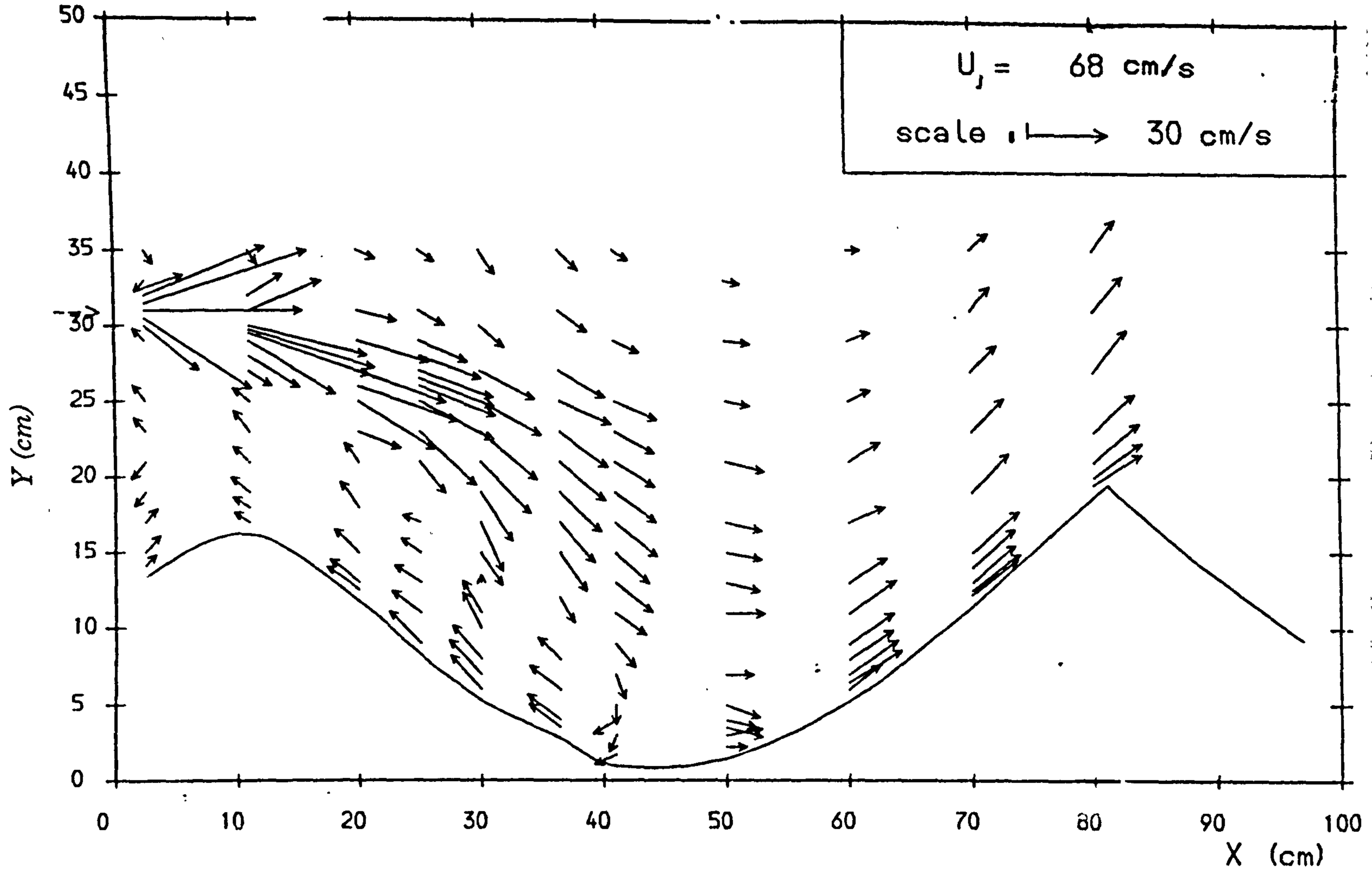

Figure 4.11 Velocity Vectors in The Scour Hole (After Ali and Salehi (1991))

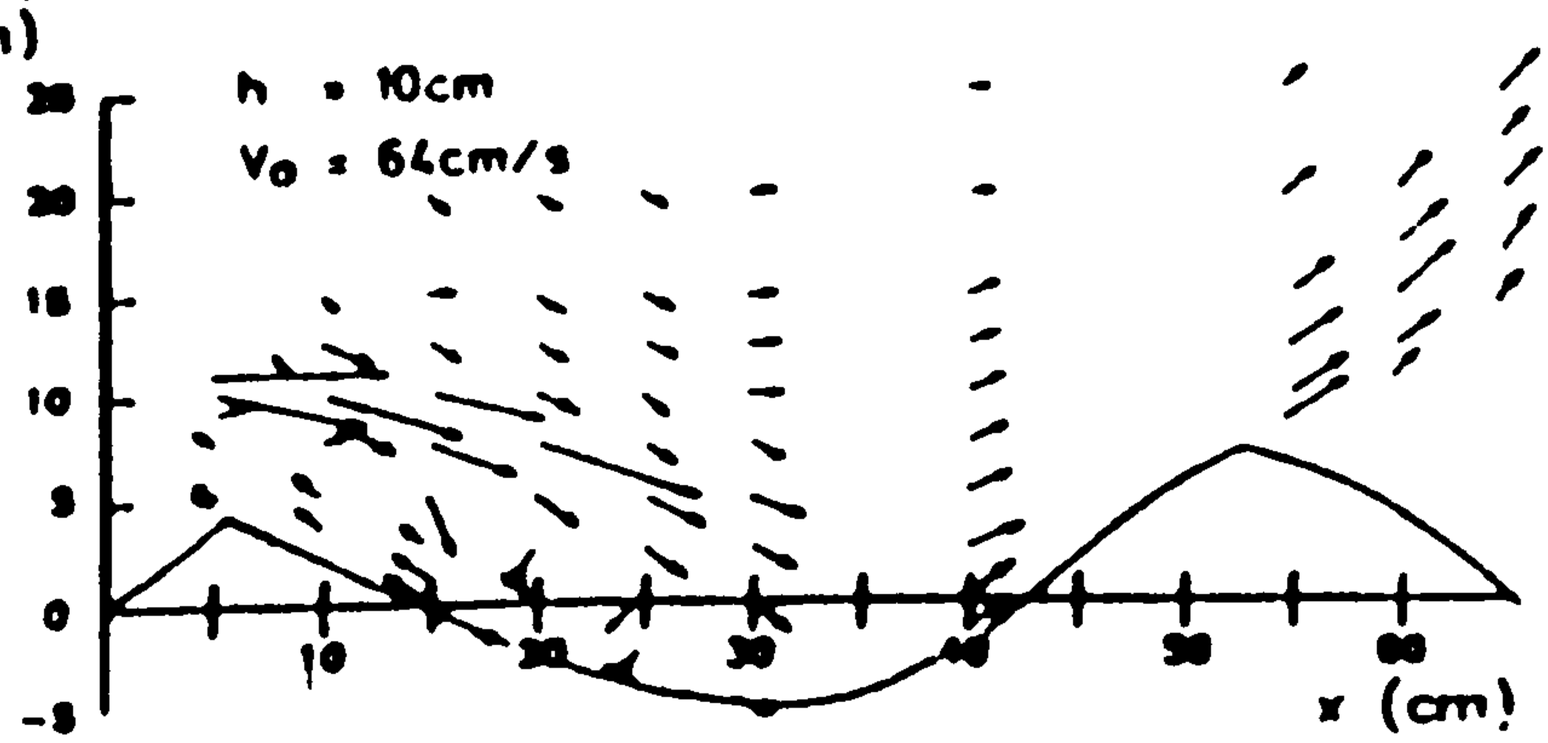

Figure 4.12 : Velocity Vectors for offset-jet height (a) h= 10cm; (b) h=20cm (after Ali and Whalley (1992))

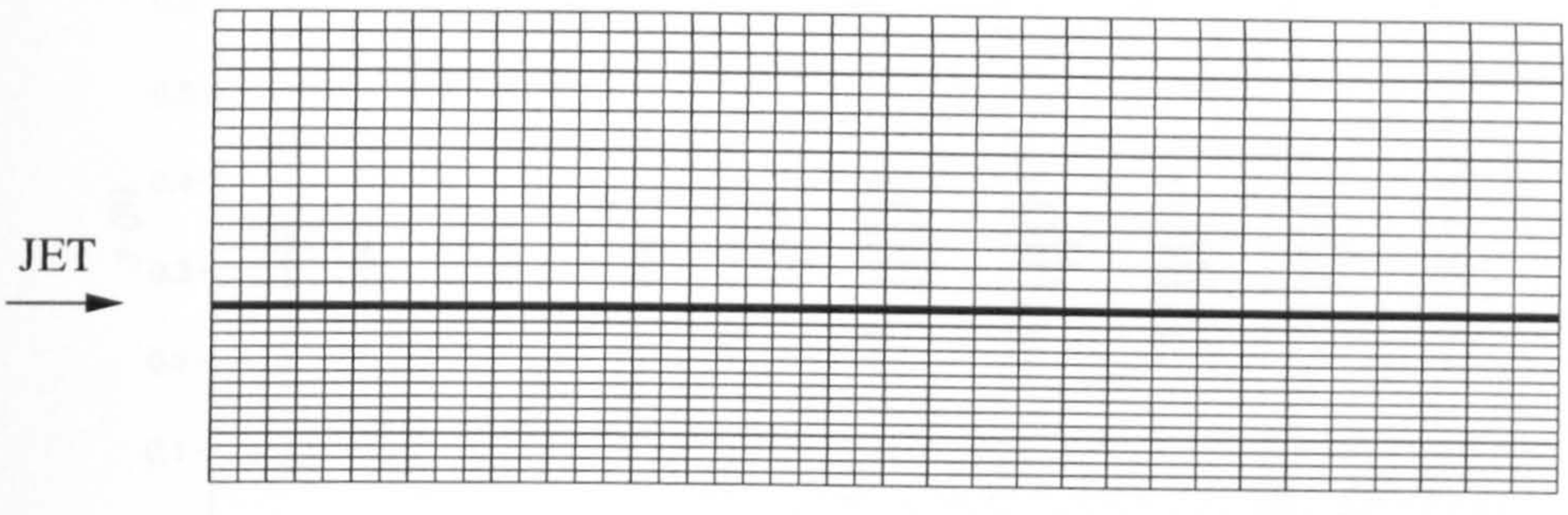

Y Z X	Grid (40 X 35)	OFFSET JET Fluent 4.31 Fluent Inc.

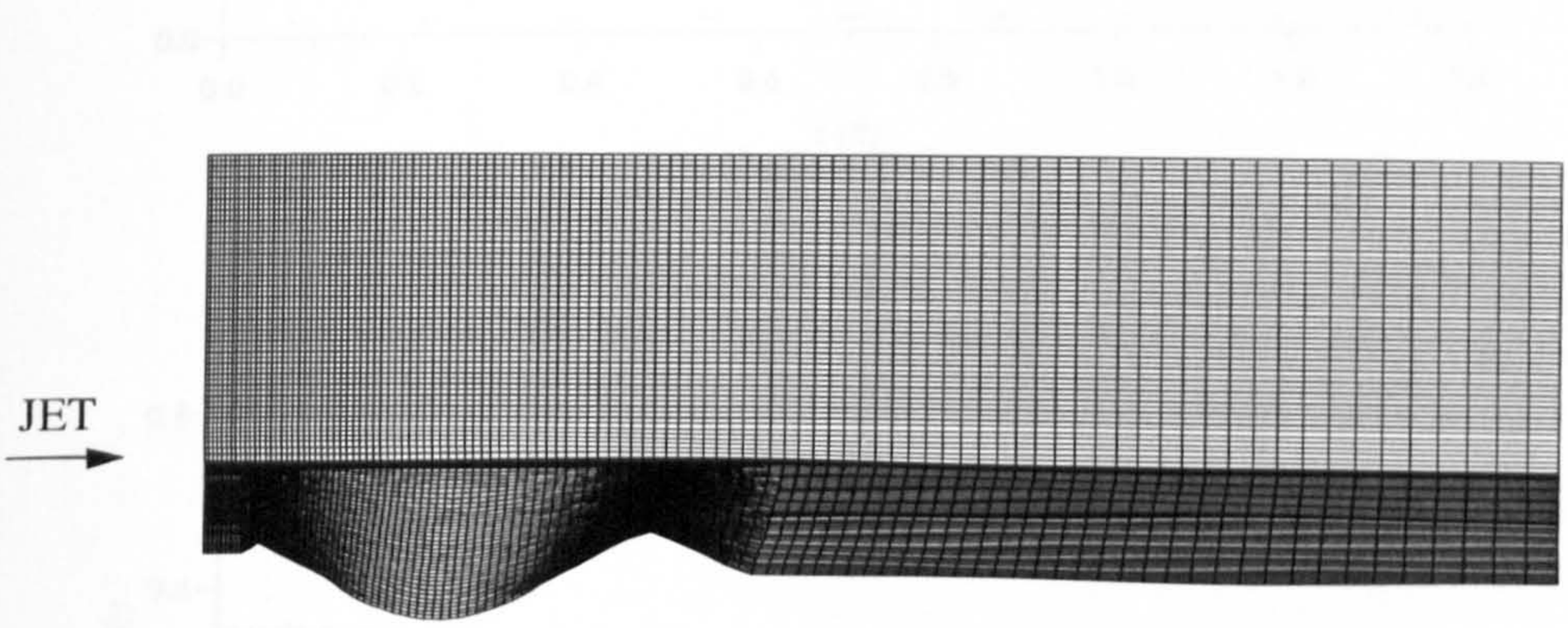

Y Z X	OFFSET JET (ASYMPTOTIC) Grid (109 X 99)	OFFSET JET Fluent 4.31 Fluent Inc.

Figure 4.13 : Typical Grid Arrangements of Rigid and Scoured bed for FLUENT Analysis

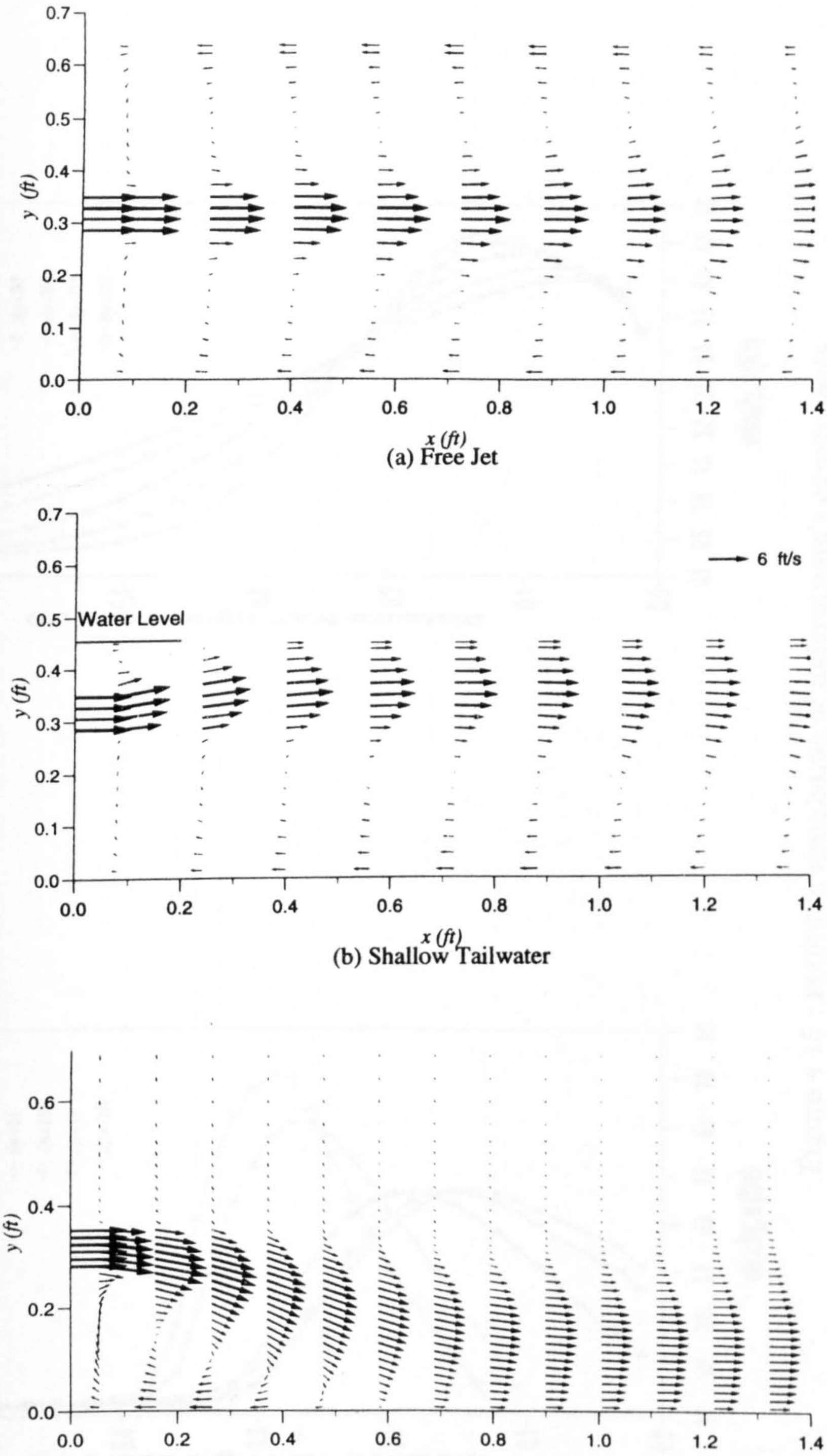

(a) Free Jet

(b) Shallow Tailwater

(c) Deep Tailwater

Figure 4.14 : FLUENT's prediction of jet behaviour for various degree of submergence

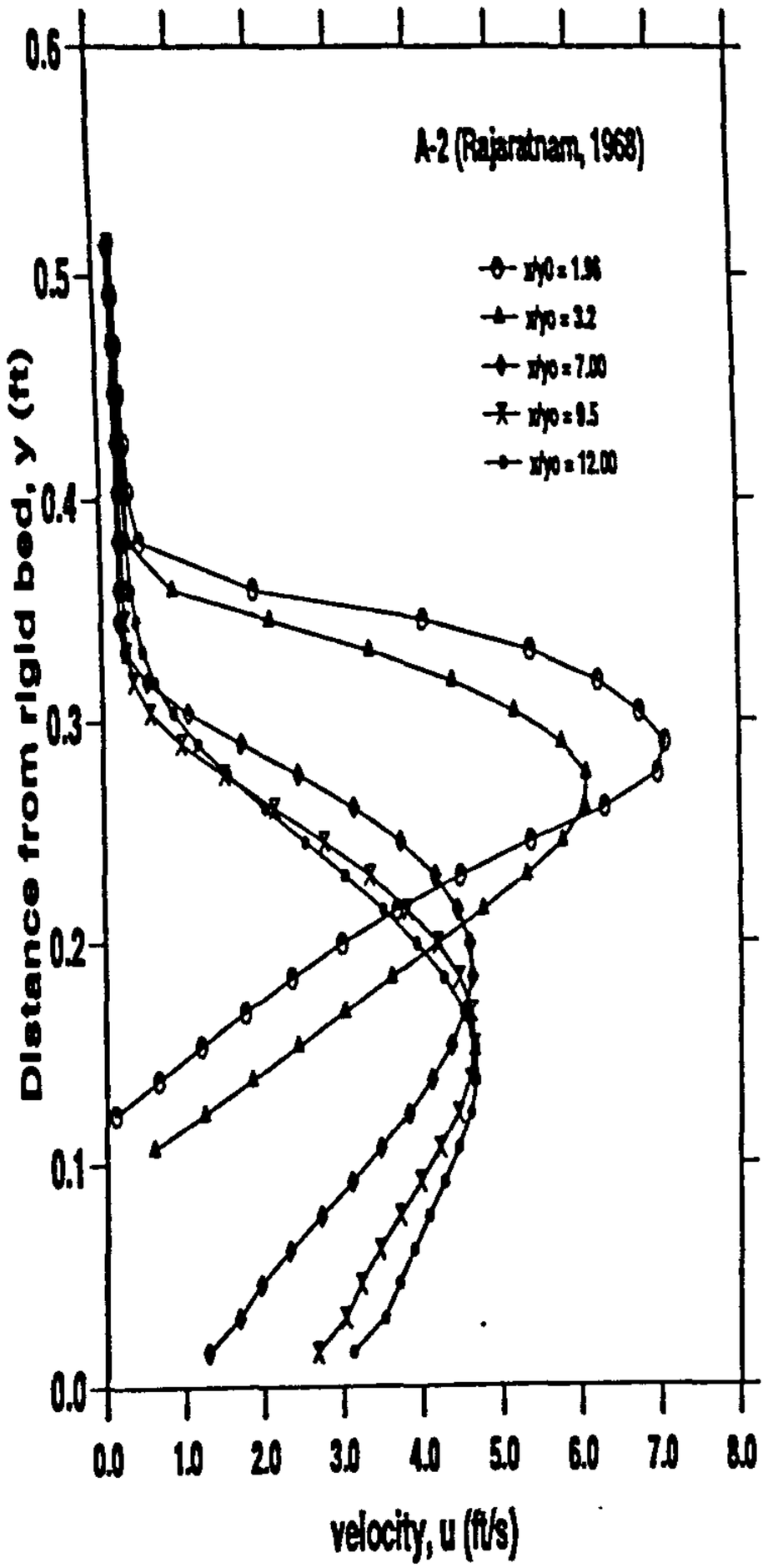

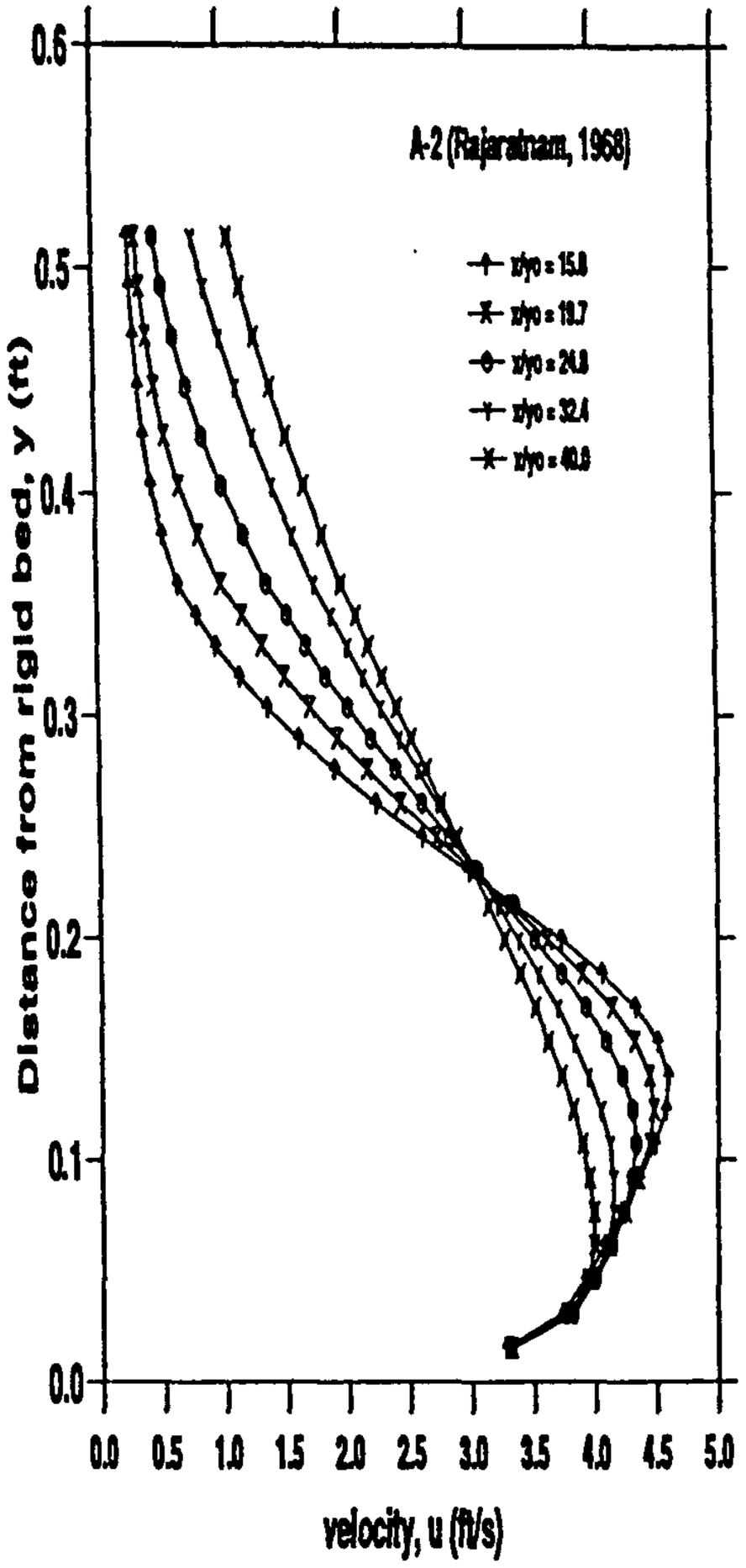

Figure 4.15 : FLUENT's simulation of Rajaratnam's experiments

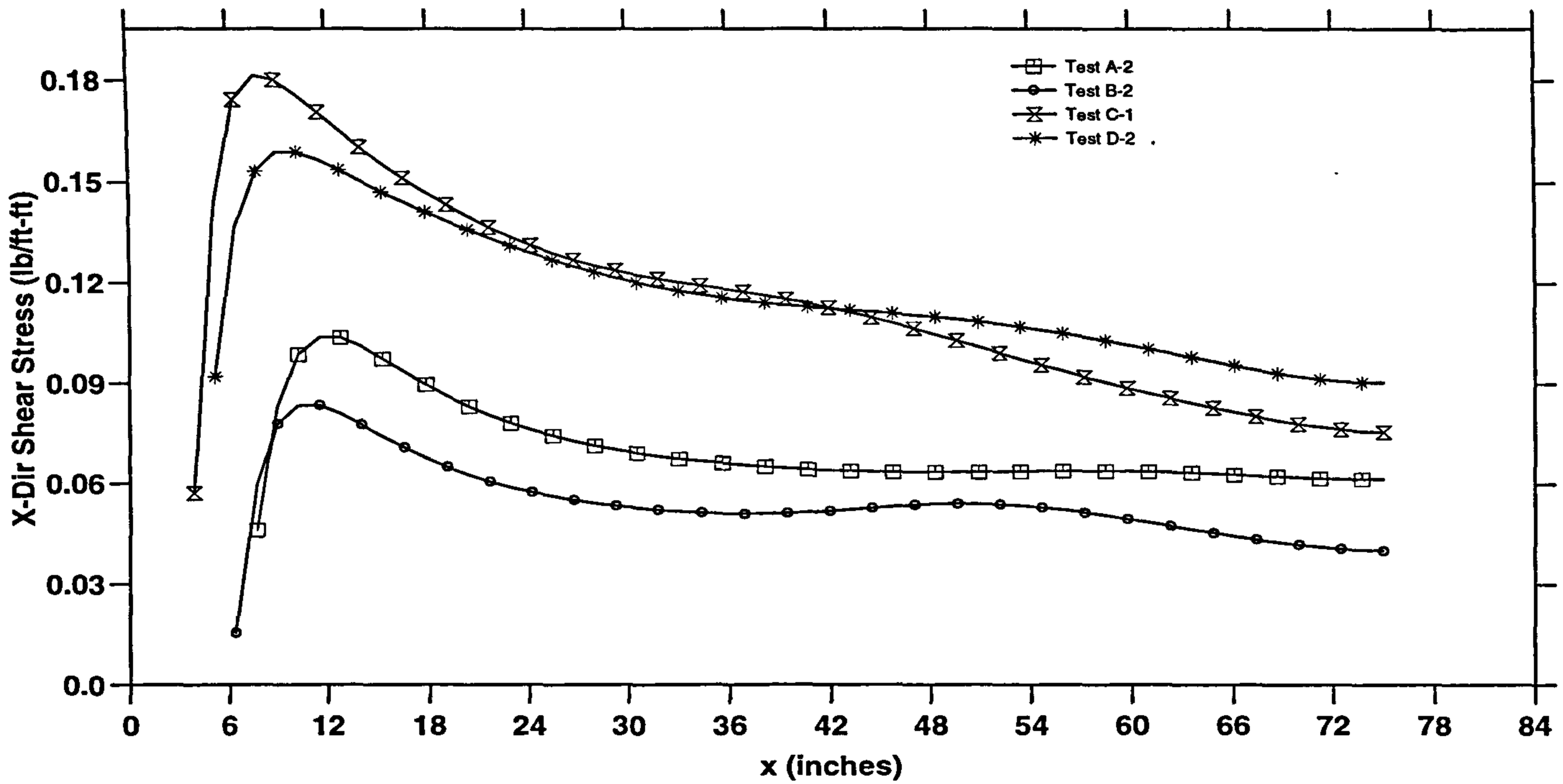

Figure 4.16 : Bed Shear Stress predicted by FLUENT (for Rajaratnam's Experiments)

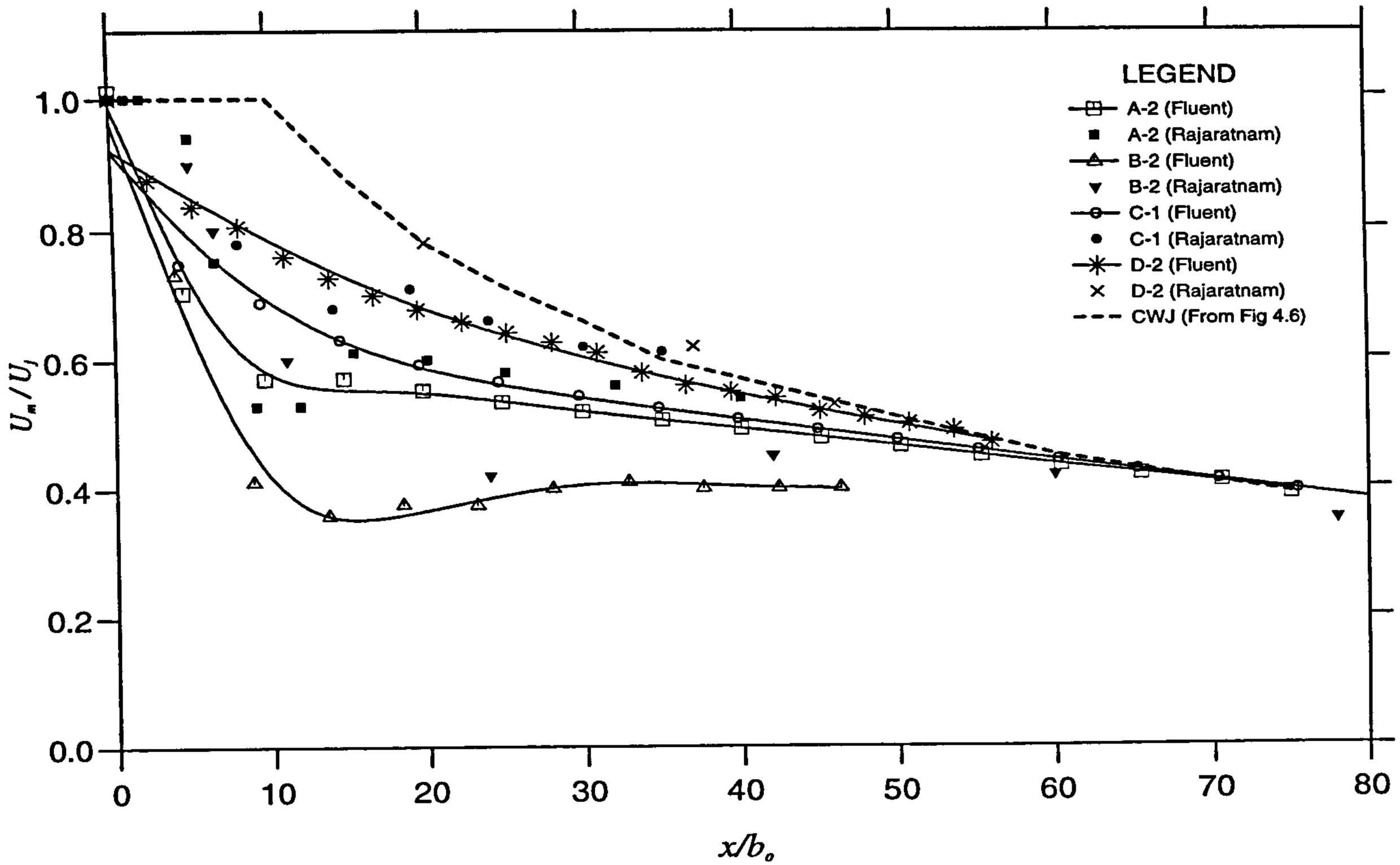

Figure 4.17 : Decay of the Maximum Velocity for Offset Jets

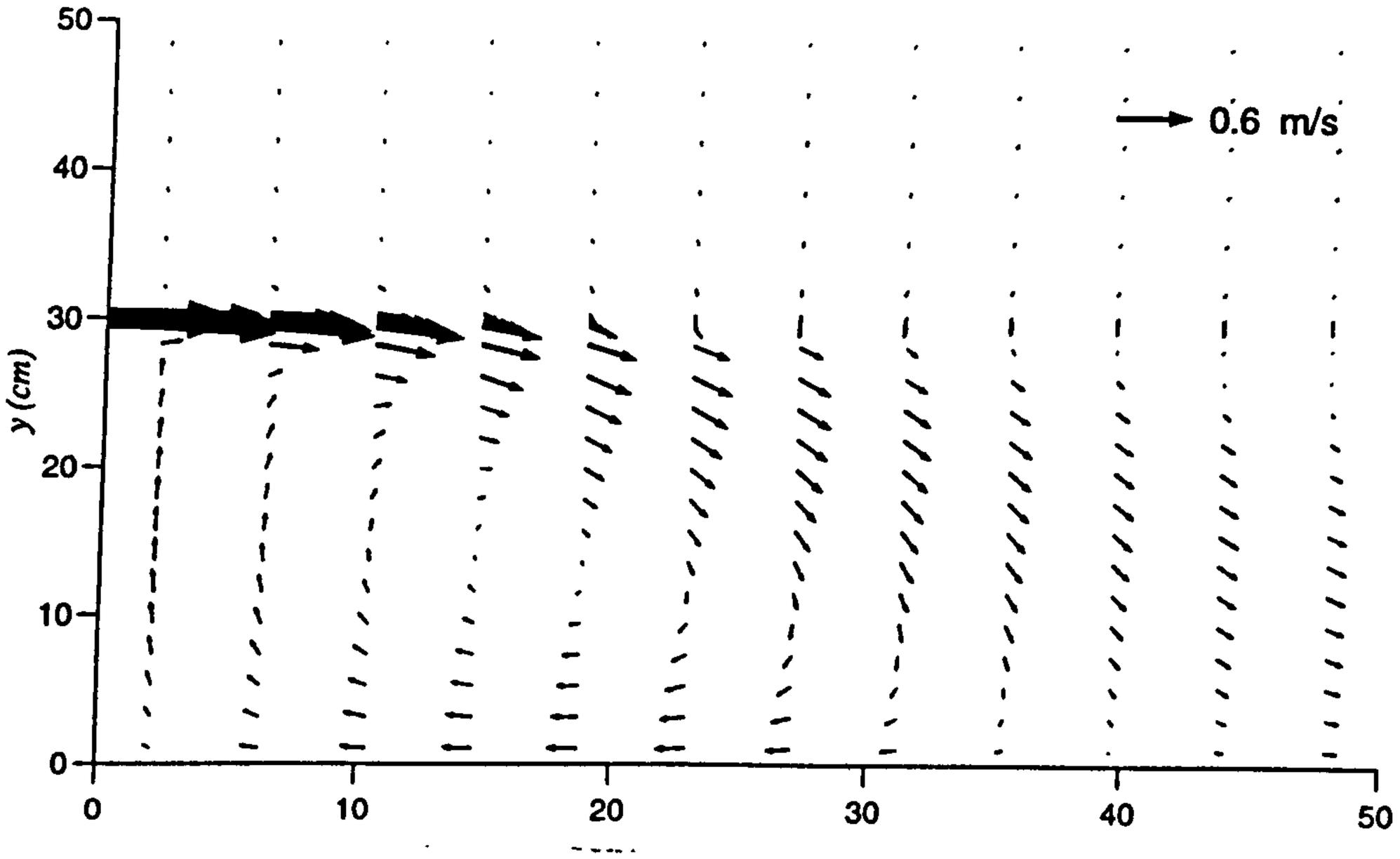

Figure 4.18(a) : Simulation of RIGID1 (Ali & Salehi, U_j = 0.90 m/s)

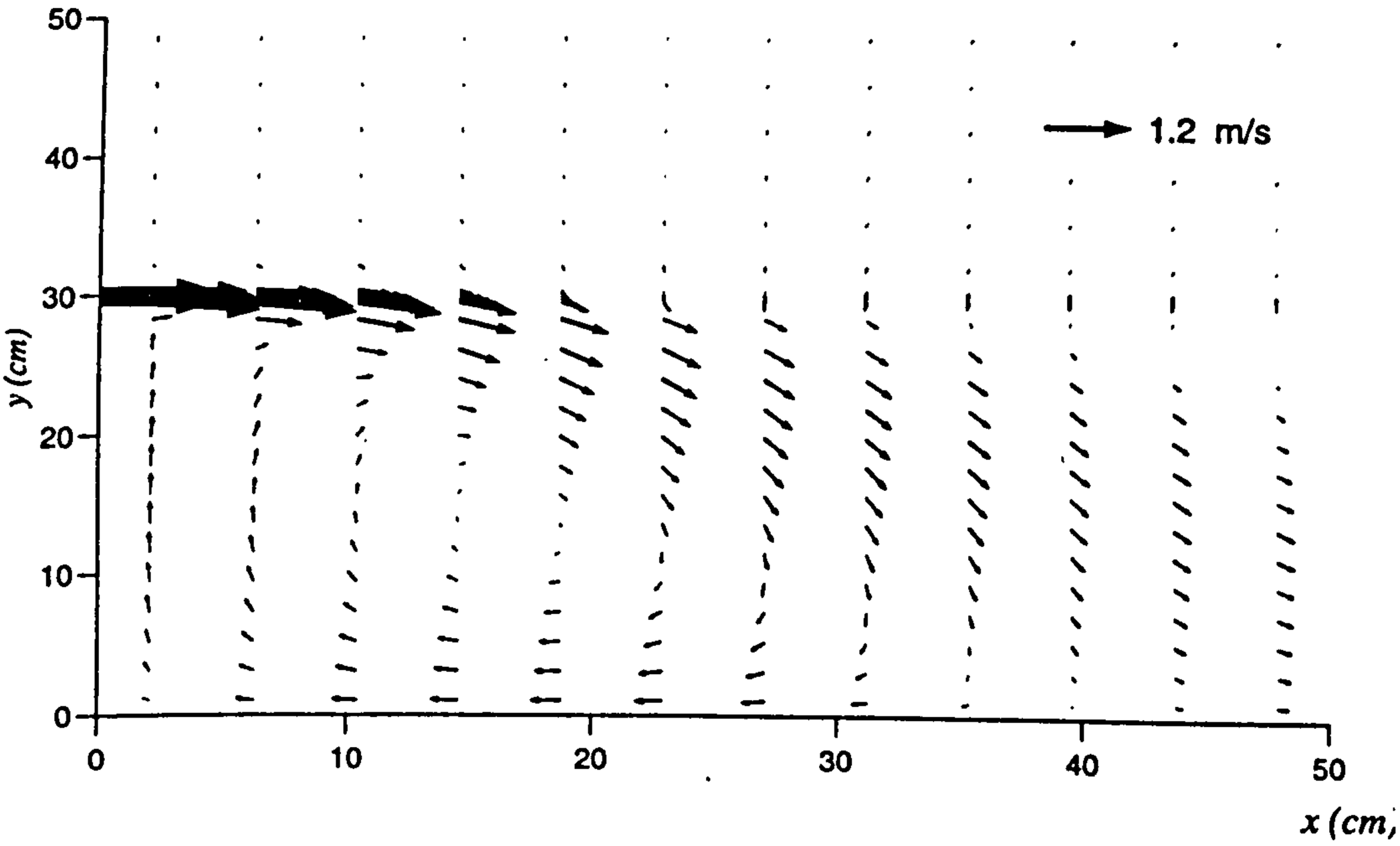

Figure 4.18(b) : Simulation of RIGID2 (Ali & Salehi, U_j = 1.50 m/s)

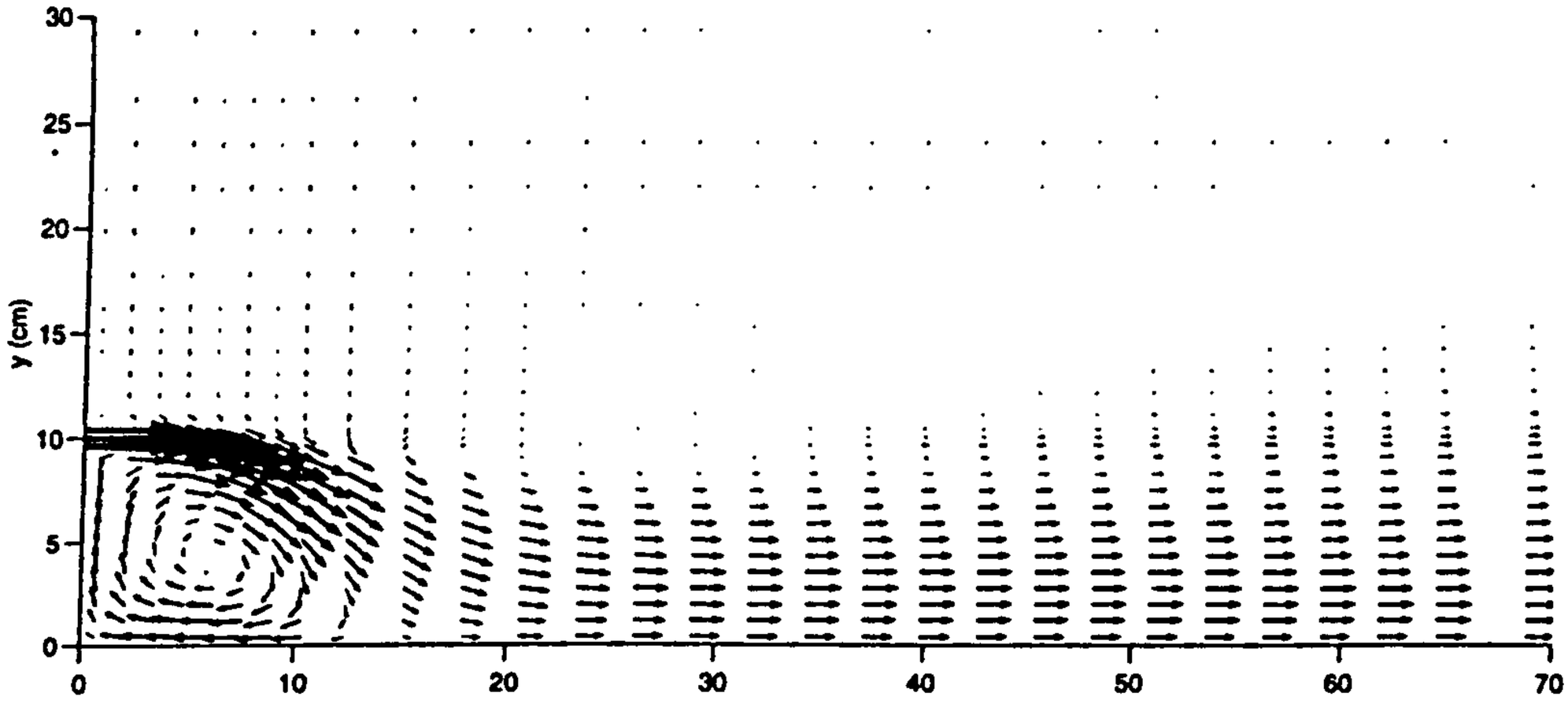

Figure 4.19(a) : Simulation of RUN 1 (h=10 cm) of Ali and Whalley

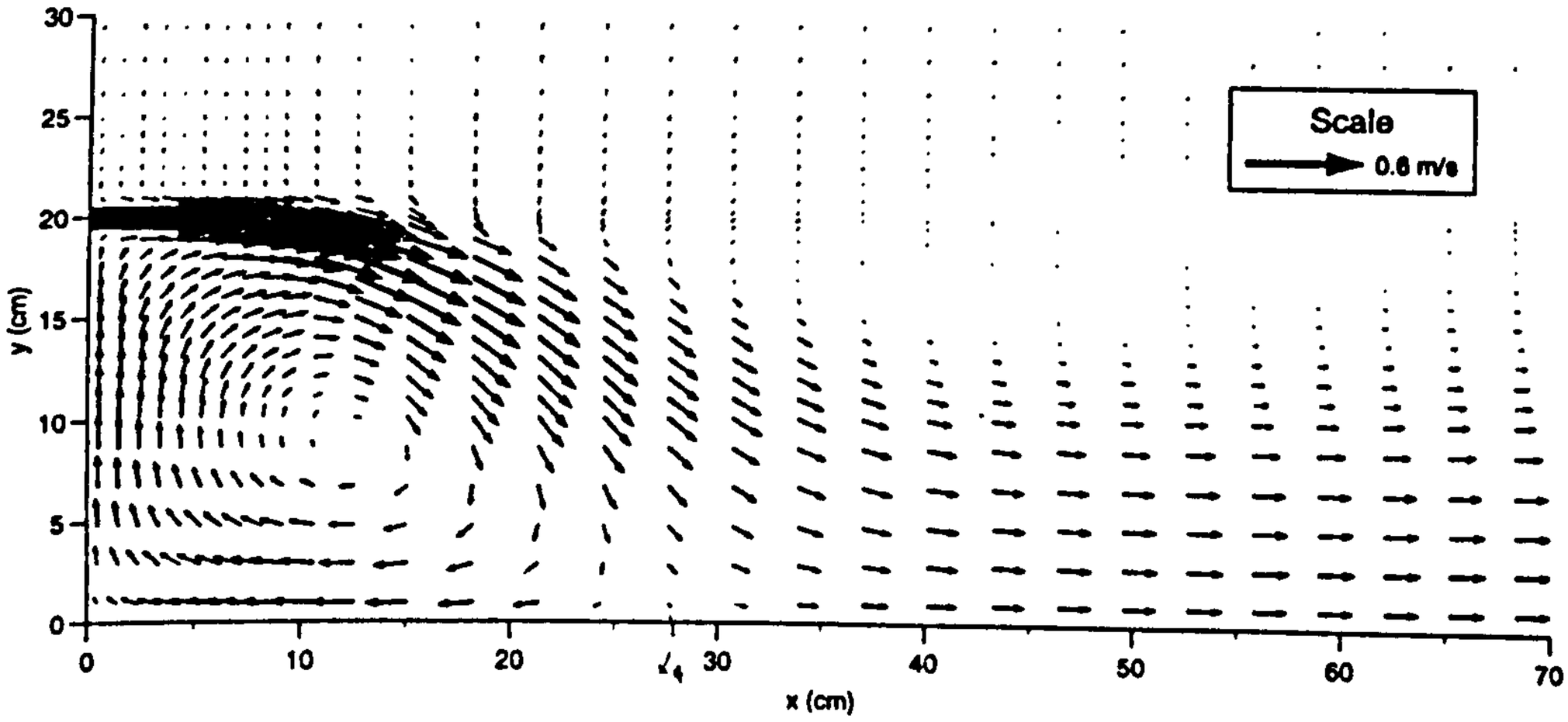

Figure 4.19(b) : Simulation of RUN 2 (h = 20 cm) of Ali and Whalley

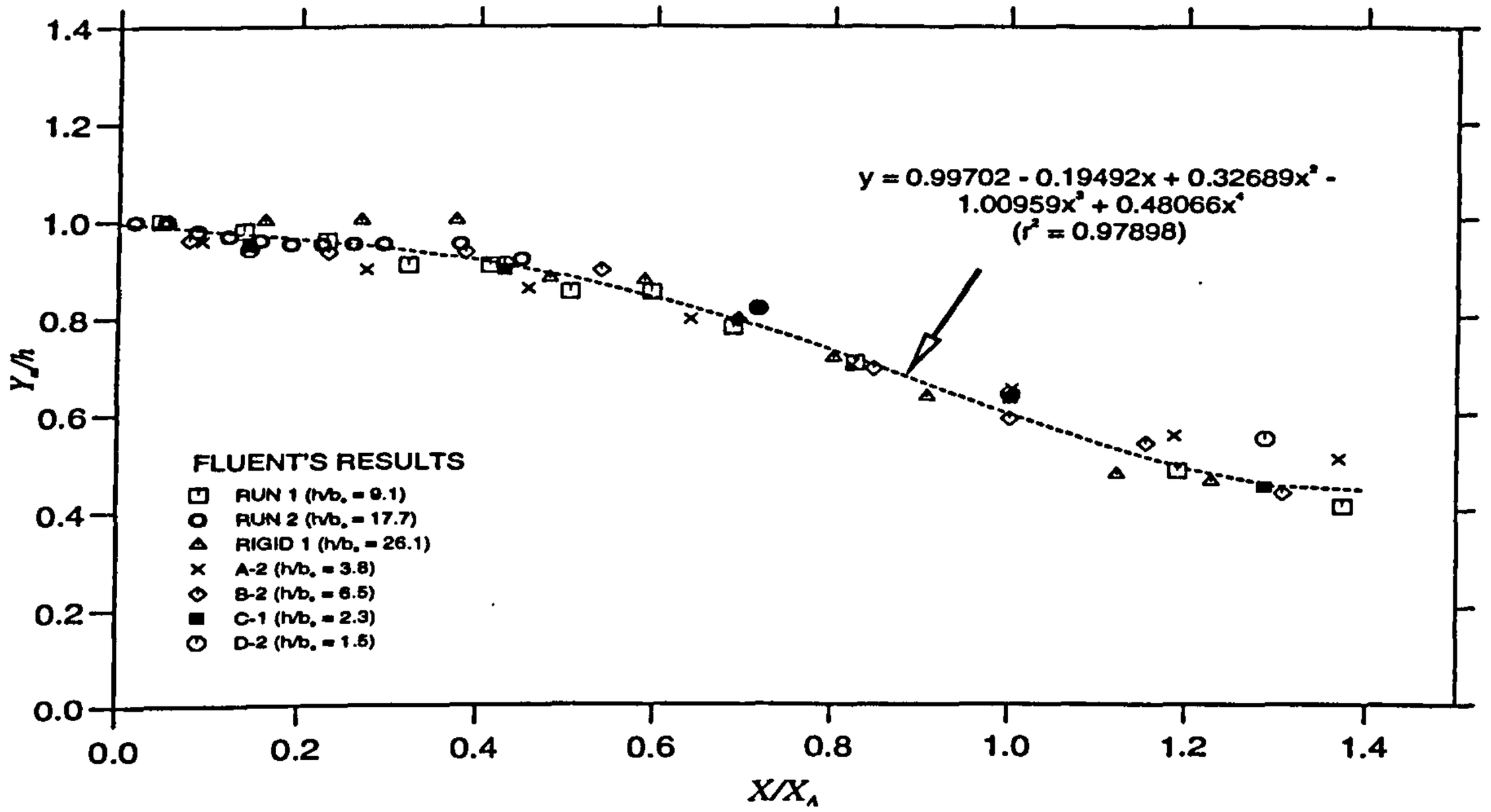

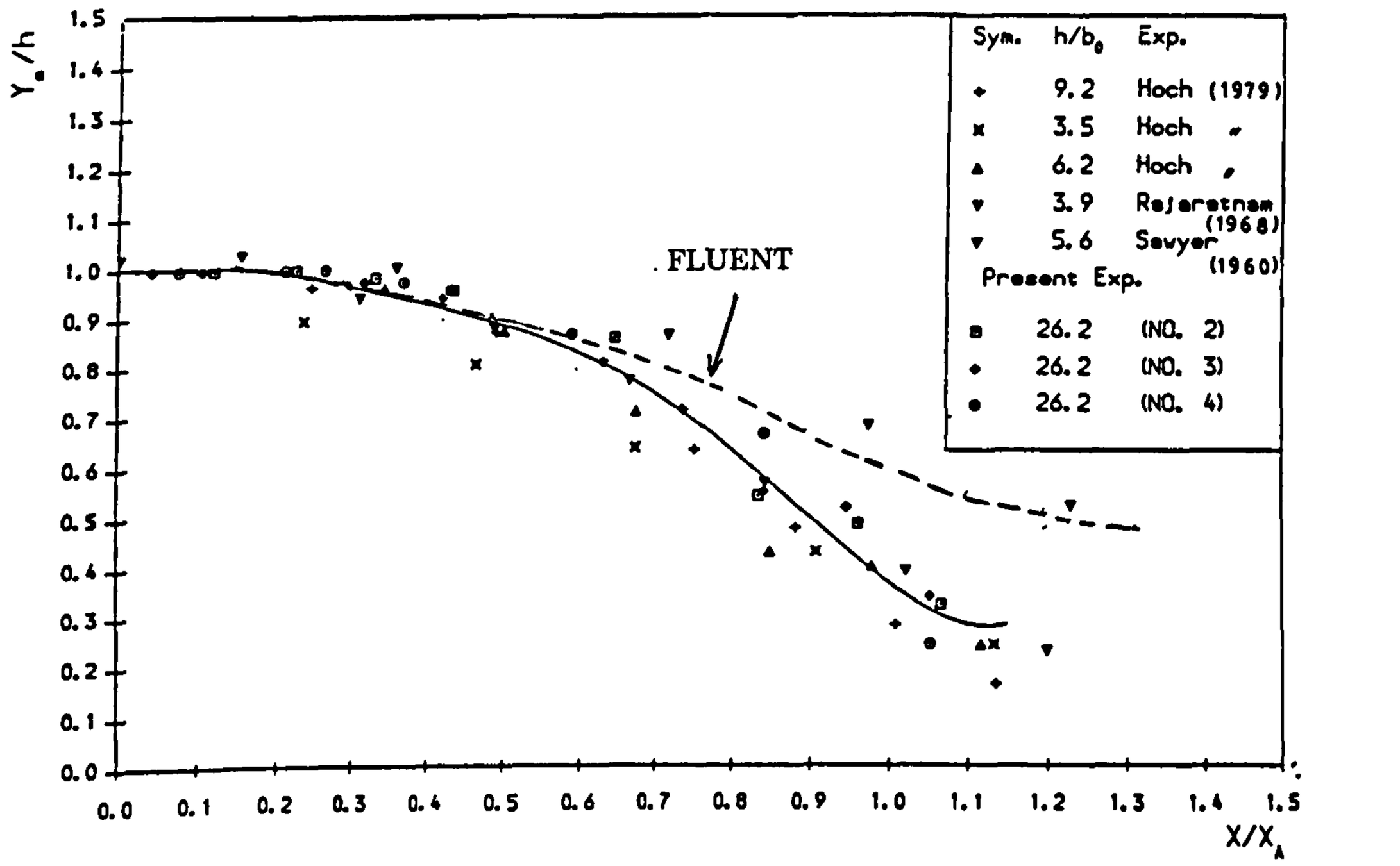

Figure 4.20 : Locus of Maximum Velocity

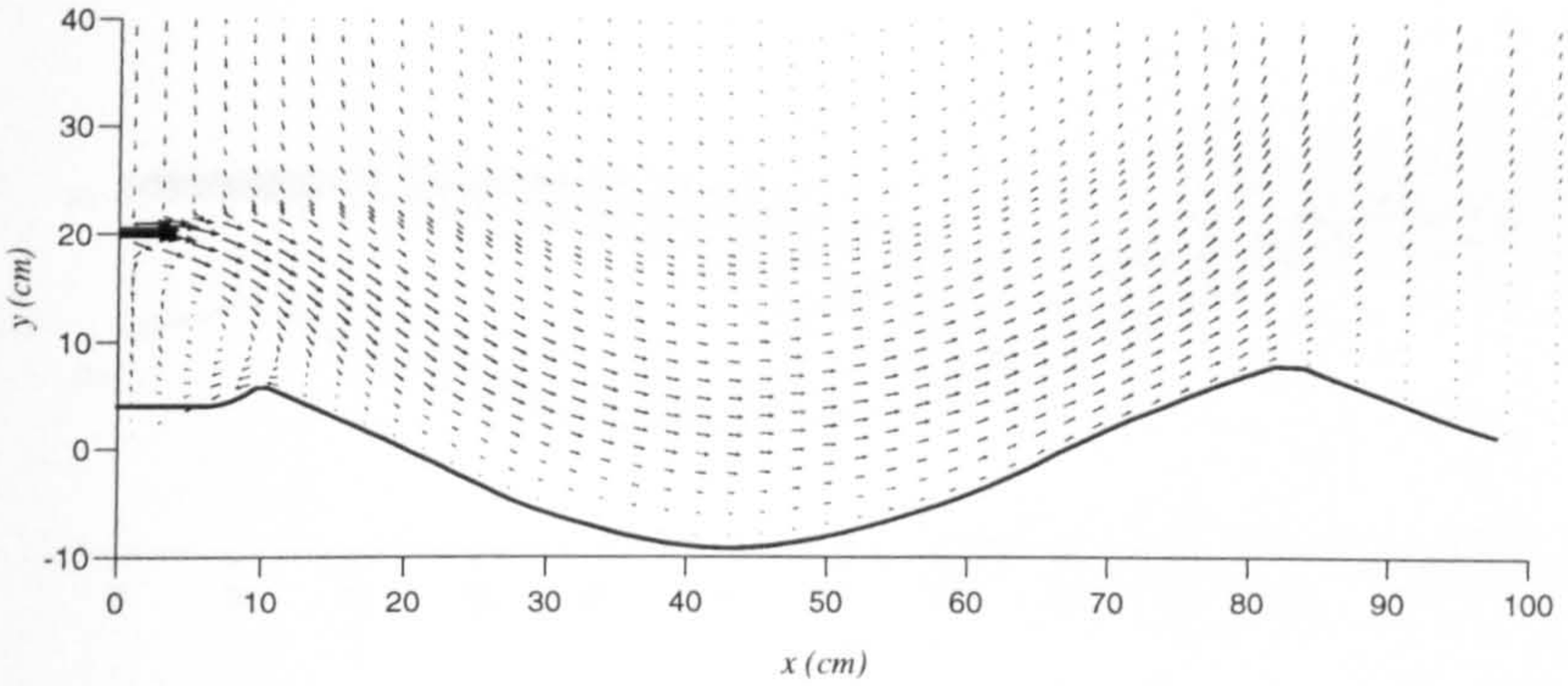

Figure 4.21 : Simulated Velocity Vectors (h=20cm) of Ali and Salehi (Coarse grids)

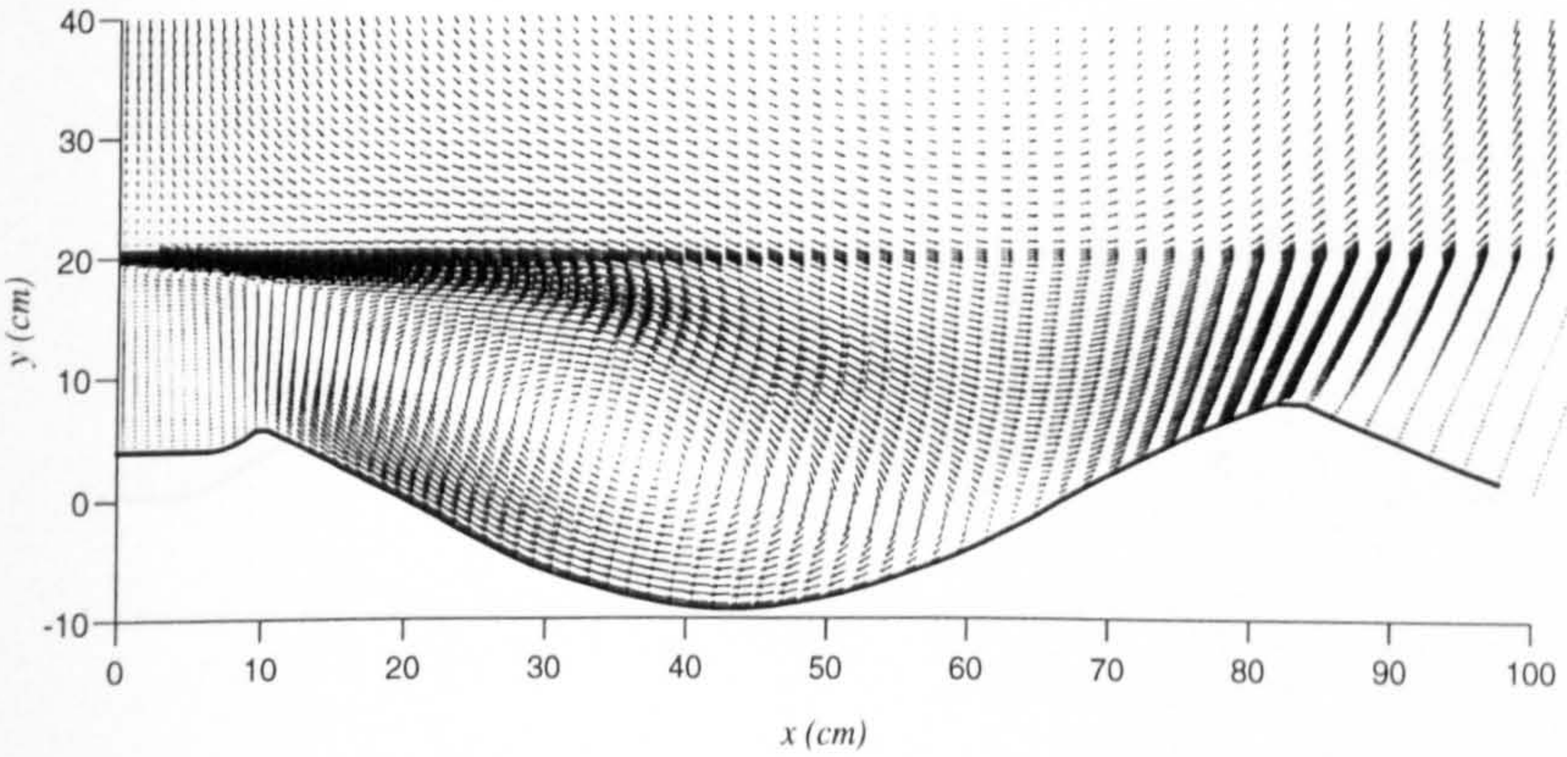

Figure 4.22 : Simulated Velocity Vectors (h=20cm) of Ali and Salehi (Finer grids)

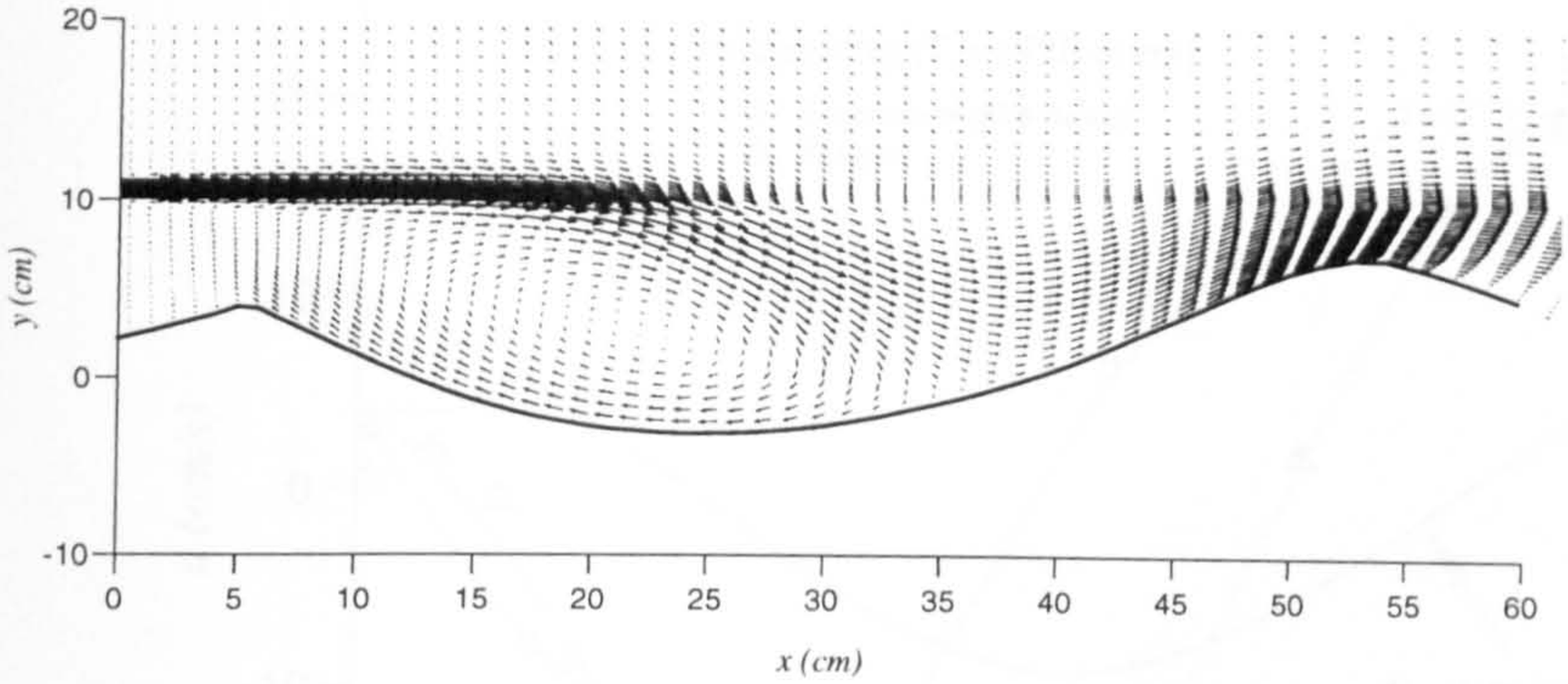

Figure 4.23 : Simulated Velocity Vectors (h = 10 cm) of Ali and Whalley

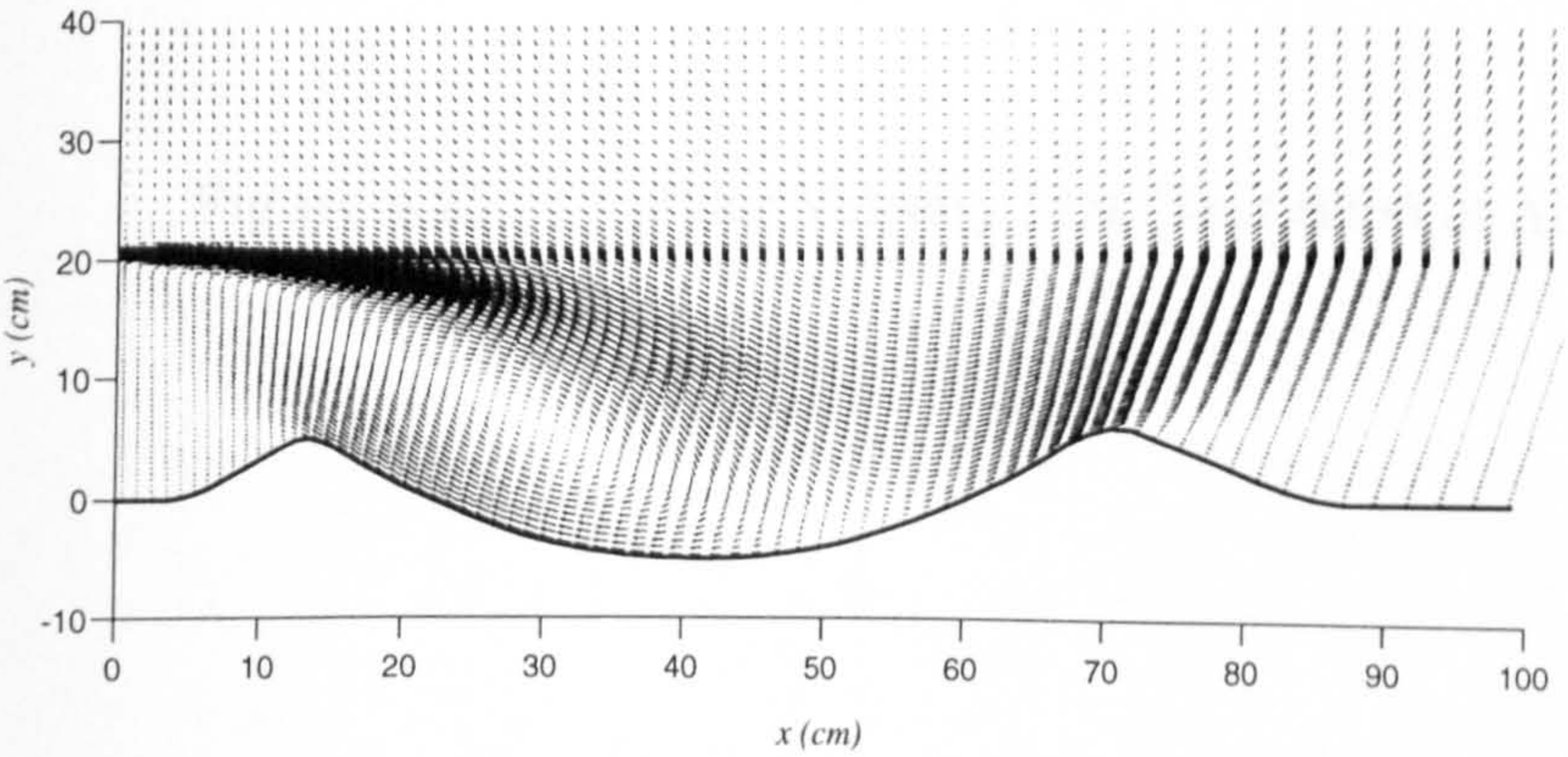

Figure 4.24 : Simulated Velocity Vectors (h = 20cm) of Ali and Whalley

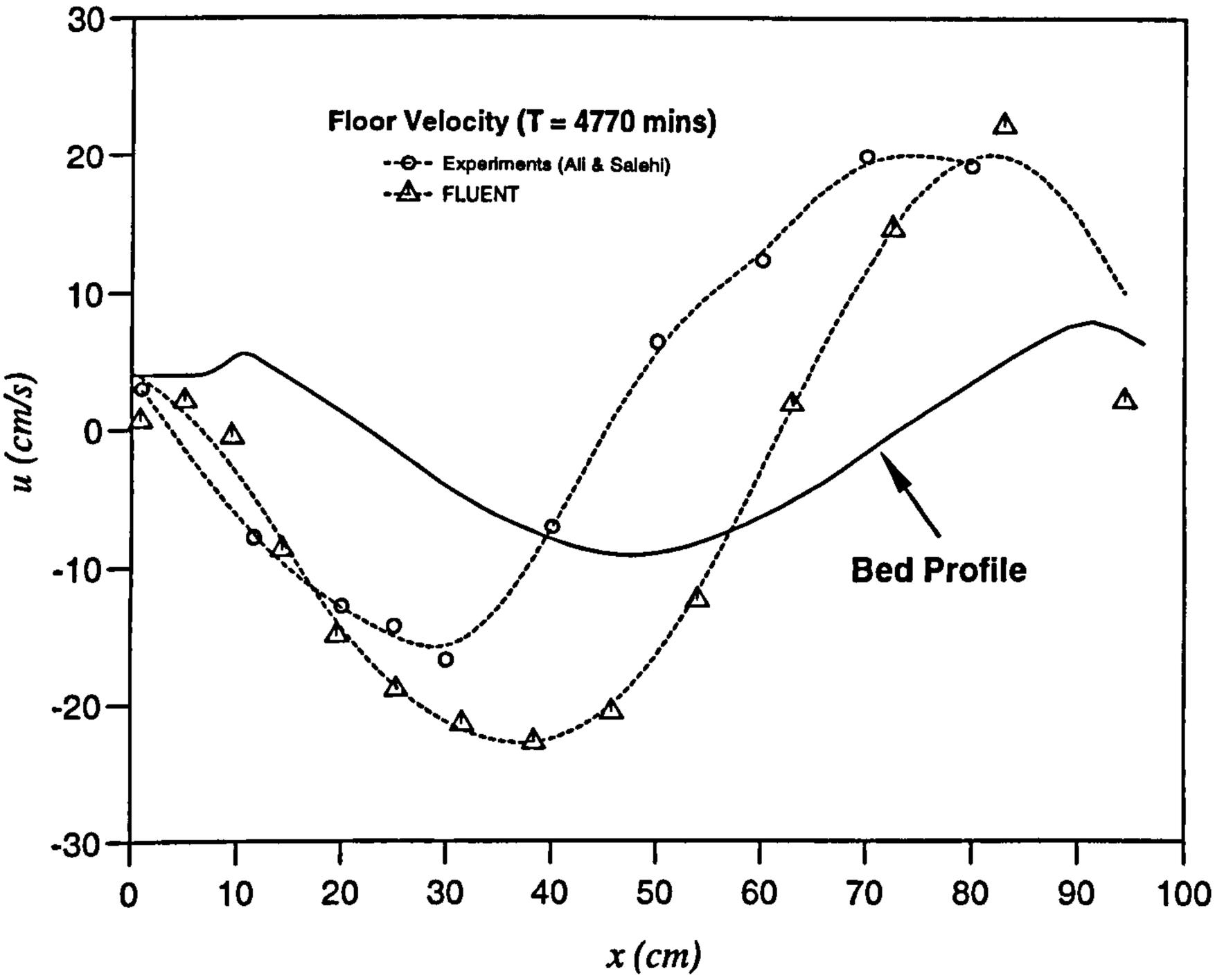

Figure 4.25 : Floor Velocity Plot (Test S205 of Ali and Salehi)

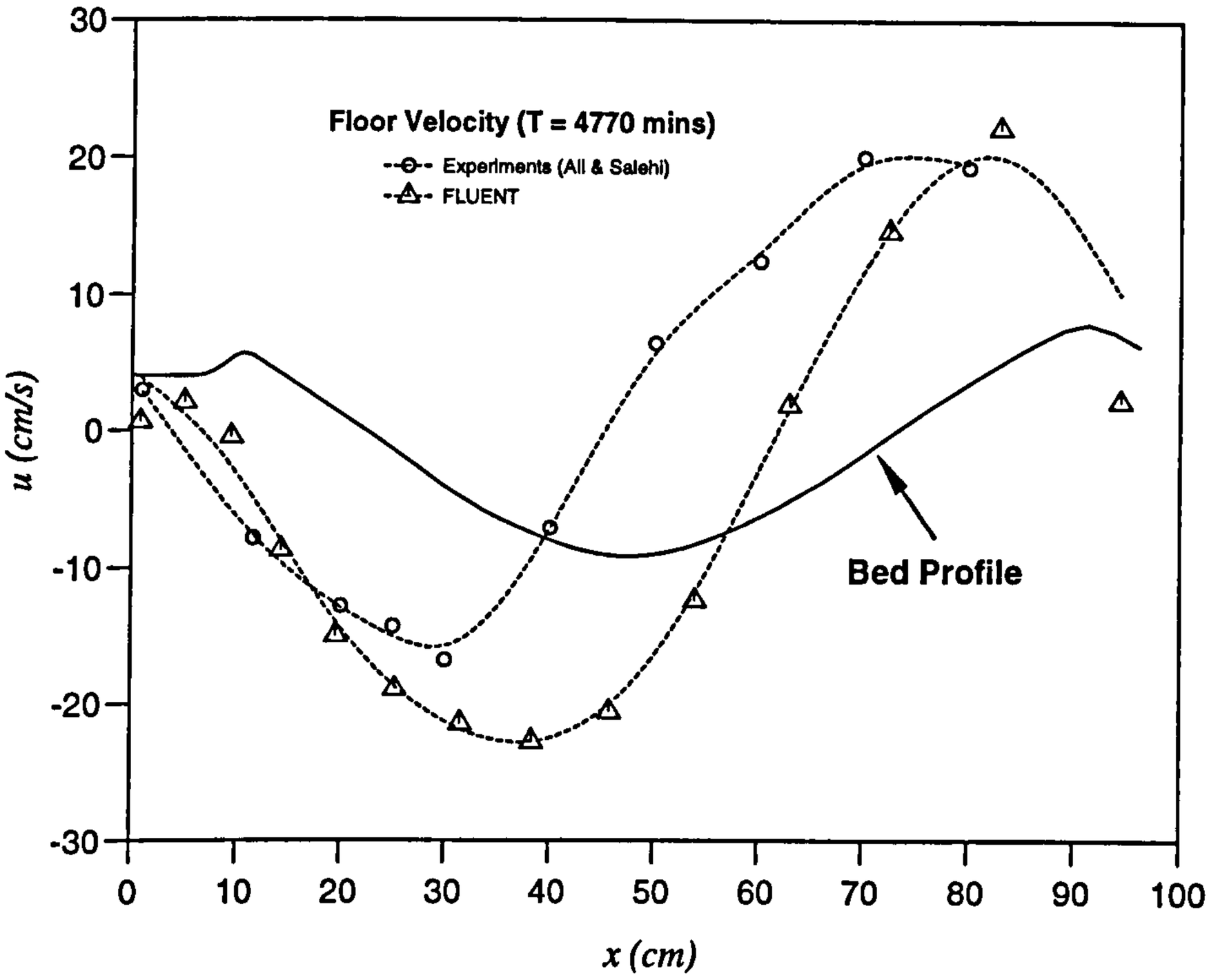

Figure 4.25 : Floor Velocity Plot (Test S205 of Ali and Salehi)

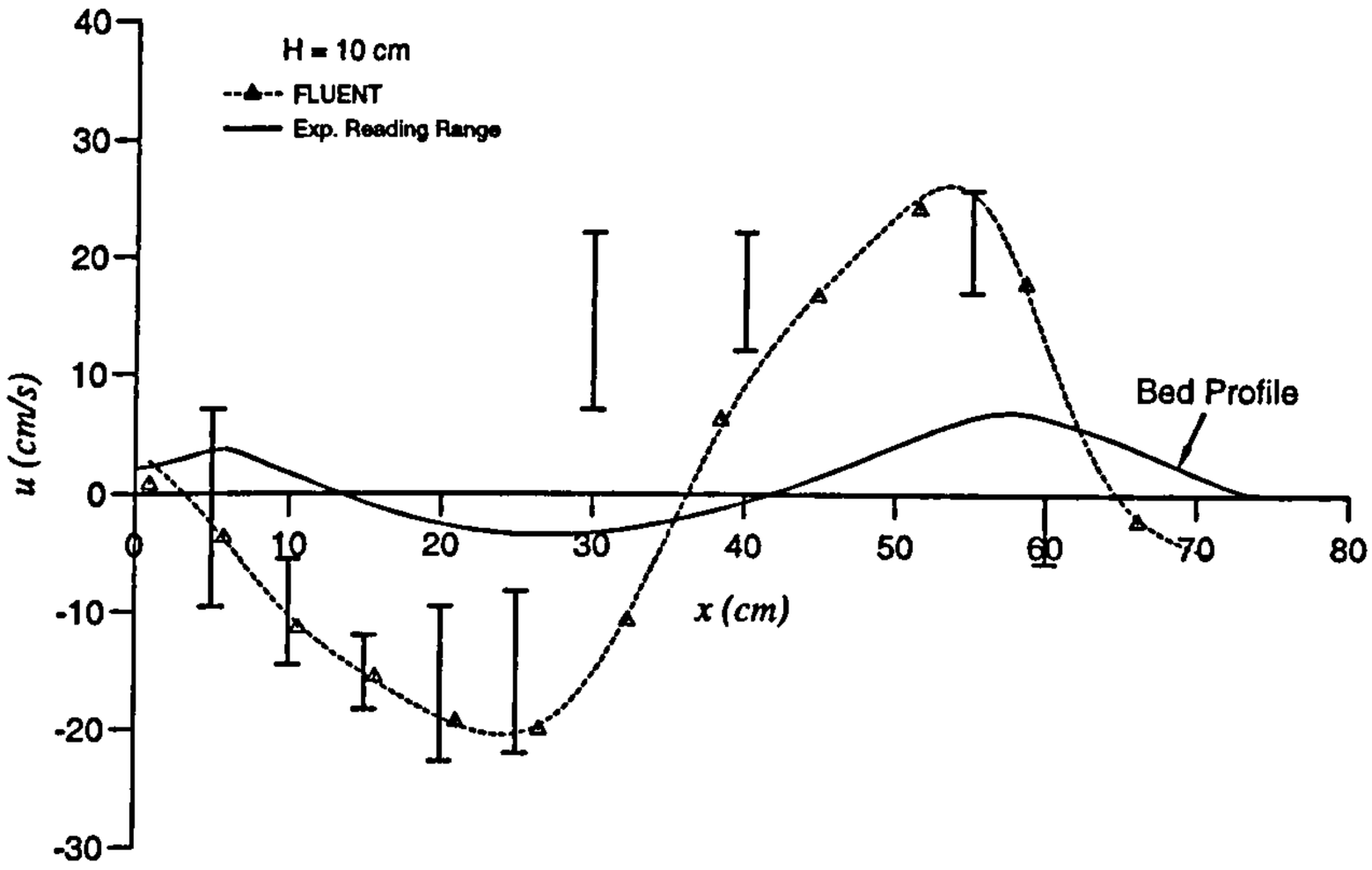

Figure 4.26 : Floor Velocity Plot (RUN 1 ; h= 10cm of Ali and Whalley)

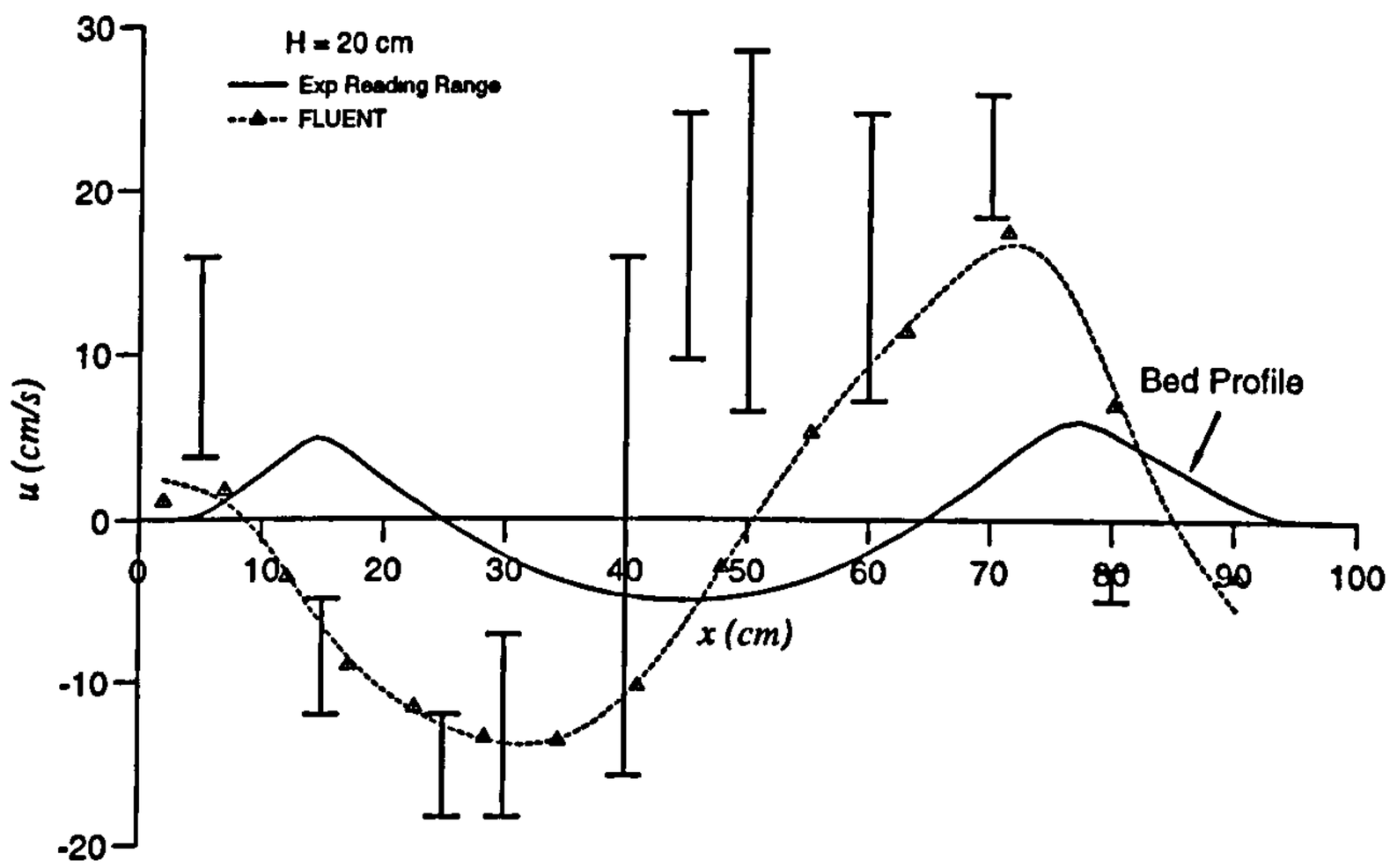

Figure 4.27 : Floor Velocity Plot (RUN 2 ; h= 20cm of Ali and Whalley)

NOTATIONS

b_o	Jet opening
f	Friction factor
F_o	Froude number
h	Jet height
H	Tailwater depth
k_s	Height of rough sand
u_m	Maximum velocity of the velocity profile at any x distance from the nozzle
U_o	Average jet velocity
X_A	Reattachment length
y	Vertical distance from the axis of jet at any x direction
y_o	Jet thickness
Y_m	Vertical distance between the point of maximum velocity and the bed
τ_b	Bed shear stress
ν	Kinematic viscosity
σ	Jet spread parameter

REFERENCES

Ali, K.H.M., and Salehi-Neyshabouri, A.A.,(1991). "Localized scour downstream of a deeply submerged horizontal jet", *Proc. Instn. Civ. Engrs*, Part 2, Mar. 1991, pp. 1-18.

Ali, K.H.M., and Whalley, P., Internal Report, Dept. of Civil Engineering, The University of Liverpool, 1992.

Ayukawa, K., and Shakouchi, T.,(1976). "Analysis of a Jet Attaching Offset parallel Plate", *Bull. of JSME*, V19, 1976, pp. 395-401

Bourque, C., and Newman, B. G.,(1960). "Reattachment of a Two-Dimensional Incompressible Jet to an Adjacent Flat Plate", *Aeronautical Quarterly*, Vol 11, Aug., 1960.

Bourque, C.,(1967). "Reattachment of a Two-Dimensional Jet to an Adjacent Flat Plate", *Advances in Fluidics*, ed. by F.T. Brown, ASME, New York, 1967, pp. 192-204.

Boucher, R.F.,(1968). "Incompressible Jet Reattachment Analysis Using A Good Free Jet Model", Third Cranfield Fluidics Conference, 8-10 May, 1968, F1-I

Brown, F.T., and Simpson, A.K., M.I.T. Department of Mechanical Engineering Report, 1964.

Hoch, J., and Jiji, L. M.,(1981). "Two-Dimensional Turbulent Offset Jet-Boundary Interaction", *ASME J. of Fluids Engr.*, V103, Mar 1981, pp. 154-161.

Kumada, M., Mabuchi, I., and Oykawa, K.,(1973). "Studies in Heat Transfer to Turbulent Jets with Adjacent Boundaries", *Bull. of JSME,* V16, 1973, pp. 1712-1722

Nozaki, T.,Hatta K., Sato, N., and Matsumura, H.,(1981). "Reattachment Flow Issuing from a Finite Width Nozzle", *Bull. of JSME*, V24, n188, Feb. 1981, pp. 363-369.

Parameswaran, V., and Alpay, S.A,(1975). "Studies on Re-attaching Wall Jets", *Trans. of Canadian Society of Mech. Engr.*, V3, 1975, pp 83-89.

Perry, C. C.,(1967)."Two Dimensional Jet Attachment", *Advances in Fluidics*, ed. by F.T. Brown, ASME, New York, 1967, pp 205-217.

Pelfrey, J.R.R.,(1984). "Characteristics of a Turbulent Plane Offset-Jet", PhD Diss., Clemson Univ., 1984

Prandtl, L.,(1929). "Influence of Stabilising Forces on Turbulence", Vortrage vas dem Gebeite der Aerodynamik und verwandte Gebite, Achen, 1929.

Rajaratnam, N., and Subramanya, N.,(1968). "Plane Turbulent Reattached Wall Jets", *ASCE J. of Hydraulics Div.*, V94, HY1, 1968, pp. 95-112.

Salehi-Neyshabouri, A. A., "Impingement of Offset Jets on Rigid and Movable Beds", PhD Thesis, University of Liverpool, 1988

Sawyer, R.A.,(1960). "The Flow Due To A Two-dimensional Jet Issuing Parallel to A Flat Plate" *J. of Fluid Mech.*, V9, 1960, pp. 543-560.

Sawyer, R.A.,(1963). "Two-Dimensional Reattaching Jet Flows Including the Effects of Curvature on Entrainment", *J. of Fluid Mech.*, V17, 1963, pp. 481-498.

Stoy, R. L., Stenhouse, M.H., and Hsia, A.,(1973). "Vortex Containment of Submerged Jet Discharge", *Jour. of the Hydr. Div.*, ASCE, Vol. 99, No. HY9, Proc. Paper 9999, Sept., 1973, pp. 1585-1597

CHAPTER

CHAPTER 5

SIMULATION OF FLOW AROUND PIERS

5.1 INTRODUCTION

The drowning of four rail passengers during the collapse of Glanrhyd Bridge on the swollen River Towy, October 1987, awakened engineers to the dangers of scour. Lack of practical knowledge about scour has left some hydraulic experts claiming that the collapse of a large bridge caused by foundation erosion is a disaster waiting to happen. With over 150,000 road bridges and 6000 rail bridges in the U.K., the problem could pose a serious safety problem as well as significant financial burden (Penson, 1996).

Continuous scour at a structure can lead to its failure, thus an understanding of the scouring process and the ability to predict the scour behaviour, is very important if steps in the design process are to be taken to protect against it.

Although the general flow field around a circular pier has been documented, the theoretical modelling of it has received little attention because the distribution patterns of the velocity components are not so clear. The present chapter reports the application of FLUENT to simulate the complex flow field around piers. Several experimental setup used by previous researchers were chosen for model comparison. In addition to that, experiments were also conducted at the Hydraulic Laboratory, University of Liverpool, to assess the scour around grouped-piers arrangement under clear water regime.

5.2 DESCRIPTION OF THE FLOW PATTERNS AND MECHANISM OF SCOUR AROUND PIERS

Piers for hydraulic structures such as bridges, barrages and regulators are often built in open channels. Generally, the structural engineer is concerned with the appearance of the piers in relation to the surrounding features, and the hydraulic engineer is concerned with the extent to which the piers cause obstruction to the flow, thereby affecting the flow pattern and dissipated energy. The scientific basis of structural design of bridges is highly advanced, but a unifying theory for estimating scour depth at piers is still in an embryonic stage, mainly due to the complex nature of the problem.

In recent years several papers have appeared dealing with aspects of scour at bridge piers. Most papers which are based on laboratory data, describe the behavioural pattern of bridge scour around cylindrical piers, avoiding the shape and alignment effects. This section reviews the general flow patterns and mechanism of scour around a cylindrical bridge pier as observed by previous researchers.

Piers, when introduced to a flow channel, result in significant changes to the flow pattern. A detailed description of the modified flow is essential to the understanding and analysis of the local scour which develops. The flow field around a pier is complex in detail, and the complexity is aggravated with the development of the scour hole. Detailed investigation on the flow pattern for such a case was reported by among others, Melville (1988), and Dargahi (1990). The important work on local scouring at piers was summarised by Breusers *et al.* (1977) and Dargahi (1982).

Melville (1977) conducted a detailed study of the changing flow patterns at a cylindrical pier throughout the development of a local scour hole. The principal

features of the flow pattern are shown in Figure 5.1. The flow decelerates as it approaches the cylinder coming to rest at the face of the pier. The associated stagnation pressures are highest near the surface, where the deceleration is greatest, and decrease downwards. In response to the downwards pressure gradient at the pier face, the flow reaches a maximum just below the bed level.

It is the downflow impinging on the bed which is the main scouring agent. The development of the scour hole around the pier also gives rise to a lee eddy, known as the horseshoe vortex. The horseshoe vortex is effective in transporting dislodged particles away past the pier and the two provide the dominant scour mechanism. Raudkivi (1986) noted that the horseshoe vortex is a consequence of scour, not the cause of it. The horseshoe vortex extends downstream, past sides of the pier, for a short distance before losing it identity and becoming part of the general turbulence.

The flow separates at the sides of the pier leading to the development of concentrated 'cast-off' vortices in the interface between the flow and the wake. These vortices are translated downstream by the mean flow and act like vacuum cleaners sucking up sediment from the bed.

Local scour occurs at a bridge site when the local flow field near the bridge piers is strong enough to remove bed materials. Local scour is a direct consequence of the flow obstruction caused by the bridge, the depth of scour being strongly dependent on the size of obstruction. Local scour is a time dependent process in which an equilibrium between the erosive capability of the flow and the resistance of motion of the bed material is progressively attained through erosion of the flow boundary. Scour hole development commences at the sides of the pier with the two holes rapidly propagating upstream around the perimeter of the cylinder to meet on the centreline. In this way, a shallow hole, concentric with the cylinder, is formed around most of the perimeter of the cylinder, but not in the wake

region. The downflow acts like a vertical jet eroding a trench in front of the pier, the eroded material being transported downstream by the flow. During early stages of development of the scour hole the lip of the trench is often very sharp and the face is almost vertical. The trench becomes shallow or disappears completely when scour approaches the equilibrium depth. Excavation of the trench undermines the scour hole slope above, which collapses in local avalanches of bed material such that the slope angle is maintained. The collapsed material is ejected from the trench by the downflow and carried downstream by the flow where a bar develops. The upstream part of the scour hole has the shape of a frustrum of an inverted cone with slope equal to the repose angle of the bed material under erosion conditions.

Dargahi (1989) carried out an experiment to investigate by means of flow visualisation and measurements, the coupling between the flow field and local scouring. The general development of the scour pattern observed upstream of the pier along plane of symmetry with respect to time are illustrated in Figure 5.2.

Generally the equilibrium of final depth of local scour is rapidly attained in live-bed conditions, but rather more slowly in clear-water conditions, Figure 5.3. Observations of the equilibrium scour depth in live-bed conditions will show fluctuations in depth(the dotted line in Figure 5.3) due to the effects of feature migration.

5.3 PREDICTION OF SCOUR DEPTH AROUND BRIDGE PIERS

Over the past 25 years numerous studies have been conducted and equations developed to predict bridge-pier scour. Most of these equations were developed using laboratory data and sometimes tested using limited field data. Due to the

number of parameters influencing scour and the difficulty in quantifying them a number of different models have been developed each with different limitations. Raudkivi (1986) in discussing the functional trends of scour at bridge piers summarised the controlling factors for scour depth at bridge as: (a) Pier width or diameter; (b) type and gradation of sediment; (c) flow depth relative to pier width or diameter; (d) size of sediment relative to pier width; and (e) alignments of piers. The shape of piers according to him, has only a small effect and this can be easily overshadowed by random effects, such as rafts of floating debris or ice caught on the pier. He also concluded that the trends established in the laboratory may help researchers understand results from the field where interactions are frequently very complex and parameter values cannot be established.

An extensive comparison of seven of the more commonly used and cited pier-scour equations has been carried out by Johnson (1995). He compared the equations using a large set of field data, both live-bed and clear-water scour. Despite so many equations available to predict the scour depth, he concluded that there is still a need for additional research on the scour process, especially for the cases in which flow velocities are near the critical velocity and for wide piers in relatively shallow water.

5.4 SIMULATION USING FLUENT

In this section, FLUENT applications to simulate flow pattern around piers are described. In order to examine the secondary flow in the present study, it is necessary to apply a fully three-dimensional circulation. The disadvantage with the three-dimensional approach is that it necessitates a more complex computer code and that the cost of calculations becomes greater. For a typical situation, a three dimensional calculation takes over an order of magnitude more computer resources than a two-dimensional approach. However, as mentioned above, if

effects of secondary flow are important for a particular case, a three-dimensional approach is therefore necessary. The prediction of flow around piers is compared with experimental and numerical results wherever possible. It should be noted here that due to the unavailability of detailed results, in most cases, comparisons are limited to being qualitative rather than quantitative. The experimental arrangements are briefly described along with the equivalent FLUENT simulations of the problems.

5.4.1 Olsen and Melaaen (1993)

Olsen (1991) and Olsen and Melaaen (1993) have carried out a numerical study on flow around a single cylindrical pier. Their problem definition was based on the physical model tests carried out at the Norwegian Hydrotechnical Laboratory. In the experiments, a cylinder of diameter 0.75 meter was placed vertically in the middle of a 3.65 m wide flume where the bed was covered with plastic particles. The particles had a relative density of 1.04 and a diameter of 3 mm. The water depth was fixed at 0.33 m with an average upstream velocity of 0.067 m/s.

A finite-volume method was adopted in their model to solve the nontransient Navier-Stokes equations for three dimensional setup. The flow field obtained from the numerical simulation was used to calculate the shear stress on the boundaries. Sediment concentration for the bed elements was then calculated using an expression developed by van Rijn's(1984).

FLUENT simulations

Figure 5.4(b) shows the grid size employed by Olsen (1991). For the present analysis, a three-dimensional grid system, similar to that of Olsen, except for the exit location which was moved further downstream, was generated for the FLUENT

simulations. The reason for the extended domain is to ensure that the exit boundary is located properly such that a fully developed flow is obtained. This is important in numerical calculations as an ill-posed outlet boundary may lead to an unconverged solution and results obtained may have no validity. After several trial runs, the present grid arrangement was found satisfactory. A 45 x 28 non-uniform grid was mapped in the domain cross section (x-y plane). Figure 5.4 illustrates the grid that is generated by PreBFC. The grid was smoothed using the differential equation grid solver in PreBFC prior to being read into FLUENT. In FLUENT the grid was extruded into the z-direction with 20 grid lines in the vertical (z) direction. Such procedure may not be applicable in generating grid involving scoured bed, as will be discussed later, and require the three-dimensional grid to be generated fully within PreBFC. The grid system consisted of half the flume and the cylinder, and a symmetry condition was applied on part of the wall. The inlet boundary and the exit boundary in the far wake were placed $3.0R$ and $6.0R$ (R being the radius of the pier) from the centre of the pier, respectively. A uniform velocity of 0.067 m/s was applied on the inlet boundary. The bed roughness factor, ELOG, was calculated using procedure explained in Chapter 2. Two different turbulence models were used; namely the k-ε model, and the RNG k-ε model. RSM closure model was not used here as it was shown earlier that it requires longer time to converge with no significant improvement to the results obtained by the RNG model.

The following solution-parameters were used for the runs:

Underrelaxation:	*0.2 (velocity, turbulence k.e. and eddy dissipation)*
	1.0 (pressure)
Sweeps :	*Alternating Direction with 2 (u,v)*
Convergence Criteria :	*1 x 10^{-3} residual sum*
Algorithm :	*SIMPLEC*

Solver :	*Multigrid for pressure correction*
Block Correction	*I:1, J:3, K:3*

Results and Discussions

Figures 5.5 (a) - (c) shows the velocity vectors near the bed predicted by FLUENT turbulence models and Olsen and Melaaen (1993). Figures 5.6 (a) - (c) shows the velocity vectors near the surface. Note that the qualitative comparisons are excellent. The plots clearly show the existence of a separation zone behind the cylinder. The location of the separation point extend further downstream at the surface than close to the bed. Dey *et al.* (1995) observed in their study that the main characteristics feature of the flow around a pier on a flat surface are a relatively large secondary vortex flow field. The wake region in the numerical model results was defined as the region in which the longitudinal velocities are in opposite direction to the main flow direction. This can be seen in Figure 5.5. The vorticity is an important quantity in a turbulence flow, since it is a measure for the intensity of the eddying motions, and the dynamics of turbulence are believed to be closely connected to vortex dynamics.

Comparison of the results from the two closure models adopted here show that the velocity fields are nearly identical.

A velocity map for the longitudinal profile along the symmetrical plane of the simulated domain is shown in Figure 5.7. The plot shows the existence of the horseshoe vortex downstream of the cylinder. This is in accordance with the flow description mentioned in Section 5.2.

Figure 5.8 (a) - (c) show the calculated bed shear stress distribution around the pier for the two models and those obtained by Olsen and Melaaen (1993). The plots have been made non-dimensional by dividing the shear stress by the bed

shear stress for the flume without the cylinder. In their study, they used the bed shear stress obtained from the model to calculate sediment concentrations for the bed elements, which gave changes in bed elevation. Using the modified bed, they calculated the new flow field and the new bed concentration. This sequence was repeated until the depth of the calculated scourhole was identical to the depth of the scour hole from the experimental study. Ten iterations were required before the resulting scour hole compared well with the measured scour hole and is shown in Figure 5.9. Such analysis was not performed here due to time and computer storage limitation. It is interesting to note, however, that as indicated by Olsen *et al.*, the shear stress is still above critical in the scour hole after the 10 macro time steps. Practically, this means that the scouring process will continue, hence deeper after more iterations. One justification for this, as explained by Olsen *et al.*, is that the measured bed contour used in Figure 5.9 was obtained after 12 hours, while the experimental study stated that equilibrium conditions had not been reached at this time.

Predictions of the flow field and the shear stress distribution were also made using FLUENT for square shaped pier, to see the effect of the shape on flow pattern around the pier. The predicted velocity vectors are shown in Figure 5.10. The figure obviously indicates that the eddy field occur at larger extend around the pier and downstream of the pier as may be expected. Figures 5.11 show the predicted 2-D flow patterns around various shapes of piers. However, the results cannot be verified quantitatively as no direct experimental results are available.

5.4.2 Yanmaz and Altinbilek (1990)

Yanmaz and Altinbilek (1990) conducted a series of experiments to study the development of scour around bridge pier models. The tests were carried out at the Hydromechanics Laboratory of Middle-East Technical University, Ankara, Turkey,

using a L-shaped horizontal rectangular open-channel 90 cm deep, 67 cm wide with a concrete bottom. Side wall (except the test section for visual observations) are made of steel. Single bridge pier models made of plexiglass were set at the middle of the flume. Only clear water conditions with a flat bed were studied. No sediment inflow was allowed into the scour hole from upstream. Three different sizes of pier were used in the experiments, but for the present simulation purposes results for the pier with a diameter of 6.7 cm were selected.

The materials used for the bed are quartz-sand with specific weights of 26.4 kN/m^3, mean particle sizes of 1.07mm with $\sigma_g = 1.13$. Bed materials were placed as a 15 cm thick layer in the flume bed.

Experiments were stopped at the end of different time durations to determine the contours of the scour hole around the bridge pier. The bed topography for T= 5, 60, 100 and 150 mins are shown in Figures 5.12. Yanmaz and Altinbilek (1990) observed that the average side angle of the scour holes around the pier was approximately equal to 33°, which is close to the natural angle of repose of quartz sand.

FLUENT Simulations

Based on the bed contours provided by Yanmaz (1994), three-dimensional orthogonal grid systems of 60 x 15 x 12 were generated using PreBFC, for T= 0, 5, 60 and 150 mins. Typical grid distribution is shown in Figure 5.13. The grid lines are packed together at an area surrounding the pier. As the bed contours are almost symmetrical along the axis of the cylinder parallel to the flow direction, only half of the cylinder were modelled, and a symmetry condition was applied on part of the wall. A uniform velocity of 0.33 m/s was applied at inlet boundary, located $12R$ (R being the diameter of the pier) upstream of the centre of the pier. Similarly the outlet was located $12R$ downstream. It is important to note here

that FLUENT V4.3 cannot simulate a free surface directly. The water surface was modelled by means of a "rigid-lid" boundary. The surface is approximated as a frictionless wall or slip wall, that is links to all scalar components were cut. Such assumption, therefore, will not allow FLUENT to simulate any changes in water level.

The following solution-parameters were used for all runs:

Underrelaxation:	*0.2 (velocity, turbulence k.e. and eddy dissipation)*
	(later 0.5), 1.0 (pressure)
Sweeps :	*Alternating Direction with 2 (u,v)*
Convergence Criteria :	*1 x 10^{-3} residual sum*
Algorithm :	*SIMPLEC*
Solver :	*Multigrid*
Model :	RNG k-ε

After 100 iterations (for T= 60 min) it was observed that the normalised residuals were converging stably but at a slower rate. The underrelaxation factor was therefore increased to 0.5 for the velocity, turbulence kinetic energy and eddy dissipation, to speed up the convergence. This value (number of iterations) vary from run to run and has to be evaluated carefully before an increase in the underrelaxation factors is applied, or otherwise the solution may lead to sudden divergence.

Results and Discussions

Figures 5.14 - 5.17 show the predicted velocity vectors and bed shear stresses for T=0, 5, 60, and 150 mins, respectively. FLUENT reported the bed shear stress in term of *X*, *Y*, and *Z* components. As the flow reaches the pier, separation occurs

and the *Y*-velocity component becomes significant. This can be seen from the figures where the *Y*-component bed shear stresses are relatively higher compared to the *X*-component bed shear stresses. The negative sign indicates the direction of the flow with respect to the sign convention used. Using modified Shields Diagram (Vanoni, 1975, p.99), the flat-bed critical shear stress, τ_c, for the material used in the experiment was calculated to be 0.48 N/m^2. It can be seen from Figure 5.14 that at some locations, especially at the neighbouring area of the pier, the predicted bed shear stress values exceeded the critical shear stress for the particles and therefore transport may be expected. It is interesting to note that Raudkivi (1986) in his paper stated that local scour in such case is due to the interference with the flow by the piers. He further stated that local scour at a pier commences when the shear velocity, u_*, or velocity U exceeds about half the critical or threshold value for movement of the sediment.

While the scour depressions at the sides of the cylinder deepen, the side slopes develop into the scour hole and sediment becomes very unstable (Dargahi, 1990). The instability causes sliding of sediment on the upper slope and this further increase the rate of transport. Since both drag (or shear) and self weight components are combining to dislodge the sediment, the shear required to move the grain downslope must essentially be less than the critical bed shear stress for the flat-bed. Lim (1985) in his study employed a formula derived by Brooks (1962) to determine the critical shear stress correction for bed slope. The formula is given as:

$$\frac{\tau_{sc}}{\tau_c} = -A \pm \sqrt{A^2 + B}$$

where τ_c = critical shear stress on a flat bed

τ_{sc} = corrected critical shear stress using Brook's formula

$A = (\sin\phi \sin\alpha) / \tan\theta$

$B = 1 - (\sin^2\phi / \sin^2\theta)$

ϕ = slope angle of bed profile (+ve downward slope)

α = angle between flow direction and slope direction measured in the plane of the slope

θ = static angle of repose of sediment (=33°)

To illustrate, consider downward slope along the symmetrical plane upstream of the pier for T=60. From Figure 5.12 the downward slope is calculated to be 29.7°. Taking $\alpha = 0$, as the direction of the velocity vector is parallel to the bed profile, the modification factor for critical bed slope using the above equations is equal to 0.42. This indicates that the critical bed shear stress for sloping bed reduces to almost half of the critical shear stress for the flat bed. For T=5 and 150 mins, the upstream downward slope is equal to 35.6° and 33°, respectively. The slope at T=5 mins exceeded the natural repose angle of the sediment. At this stage, the slope is caused mainly by the vortices and the reverse flow reflected by the pier, analogous to the processes shown in Figures 5.2. As the hole becomes deeper, the sediment on the upper slope continue sliding until all the forces acting on the bed reach equilibrium. At this stage the slope of the bed is equal to the repose angle of the sediment (*i.e.* 33° at T=150mins).

Figure 5.17(b) shows the longitudinal velocity vectors along the symmetrical plane. The plot indicated the presence of a downward flow at the face of the pier. In addition to the shear forces acting on the bed, it can be inferred that the downflow may also exert forces on the bed that initiate the eddy which causes the increase of local scour around the pier. Figure 5.18 shows the downflow velocity plot in front of the pier for T=0, 5, 60 and 150 mins. It can be concluded from this plot that the vertical downward flow in front of the pier increases with the increase in scour hole depth, until an almost equilibrium stage is reached.

From Table 5.1 it can be seen that the the maximum bed shear stress decreases as the hole becomes deeper. The shear stress value at the brim of the scour hole

(flat bed) along the symmetrical plane for each case is essentially less than the critical flat-bed shear stress, marking the boundary of the scour hole.

TABLE 5.1 : Maximum Shear Stress Around Pier

Time (mins)	Calculated Max. Shear Stress (Pa)		Shear Stress at the brim of scour hole (upstream of pier) along symmetrical plane (Pa)
	X-Direction	Y-Direction	
0	0.55	0.30	-
5	0.50	0.22	0.288
60	0.41	0.22	0.265
150	0.34	0.20	0.236

In the downstream region of the hole (Figure 5.17(b)), the decrease in depth between the bed and the 'fixed' water surface causes the flow to converge. According to principle of continuity, the velocity at this section will increase, so does the bed shear stress. In practise this might not be so, as this upward flow may be translated as an increase in water level. Thus, the velocity will not be as high as predicted by the numerical model. As mentioned before, FLUENT is not able to simulate the increase in the water surface. A simplification is used by assuming the free surface to be represented by a smooth 'closed-lid'. On that note, the results reported by FLUENT in such cases must be judged with great care.

5.5 EXPERIMENTAL INVESTIGATIONS

Experimental Setup and Procedure

Experiments were conducted in a glass-walled wave-current flume (Figure 5.19) at the Hydraulics Laboratory, University of Liverpool, to study the development of scour hole around offshore platform models. Two different piers arrangements (offshore platform models) were tested. The arrangements are shown in Figure 5.20 (Case A), and Figure 5.21 (Case B). The diameter of each pier in Case A and B is 50 mm and 5 mm, respectively. The experiments were carried out by the author together with Butterworth G. (1996) as part of the latter's final year undergraduate project. The glass flume is a straight horizontal rectangular open channel 72 cm deep, 6 cm wide and 15 m long, with a concrete bottom.

The experimental conditions that were maintained in the laboratory can be summarised as follows:

1. Only clear water conditions with a flat-bed were studied. No sediment inflow was allowed into the scour hole from upstream.
2. Only one type of uniform bed materials (crushed-olives stones) was used with the mean particle size of 0.2mm, specific gravity and settling velocity of 1.35 and 0.63 cm/s, respectively. The ratio of terminal velocity to shear velocity is in the range of 0.02 to 0.70.
3. Bed materials were placed as a 30 cm thick layer in the test section with a zero bed slope.
4. The piers were positioned at the centre of the flume such that angle of attack approach flow with the axis of pier arrangements was kept to zero. The piers were secured in it position to reduce vibration or movement of the piers cause by the flow forces imposed onto it.

The uniform flow was generated by two pumps located 6.0 m upstream of the test-section. At the start of each run, the two pumps were slowly adjusted until the desired uniform velocity was obtained. Extra caution was taken to ensure that the bed material were not disturbed during the initialisation process. Velocities were measured using a stream flow miniature current meter manufactured by Nixon Instrumentation Ltd. The measuring head of the current meter was 16 mm in diameter and consisted of five bladed P.V.C. rotor mounted on a hard stainless steel spindle. The quoted accuracy of the probe as provided by the manufacturer was:

5% from 2.5 - 7.5 cm/s

2% from 7.5 - 15.0 cm/s

1% from 15.0 - 150.0 cm/s

Since the probe only recorded positive velocities, negative velocities were noted when the rotor reversed its direction of turn.

At the end of the experiments the water was carefully drained out of the flume and the bed contours around the piers were measured relative to the initial bed level.

Results and Discussions

Figures 5.22 and 5.23 show the bed forms at the end of the experiments for Case A and B, respectively. It can be observed that the maximum scour depth occurred at the midpoints and the flanks of the upstream cylindrical piers. During the experiments, the grains at the upstream side of the piers were observed to be displaced by the horseshoe vortices as described. Scouring first appears on the edges and upstream faces of the front piers. This observation is analogous to

Dargahi (1986) and other researchers, as discussed in Section 5.2. The scour hole grows with time under the action of the vortex system. During the course of the experiments, sediment or turbulence bursts were also observed at the bed. This phenomena was also observed by Lim (1985) and was believed to be one of the factors that contributed to the increase in the rate of transport. As the scour hole enlarged with respect to time, the strength of the horseshoe vortices weakened, causing a decrease in rate of scour development. In laboratory experiments reported by Raudkivi and Ettema (1985), typically about 50 hrs of continuous running produced near threshold conditions, a scour depth which did not change measurably thereafter. For the present experiment the tests were terminated shortly after reaching a stage where further scour development was no longer noticeable, which was approximately 3 hours. Due to this there was no information on how close the final scour depth measurement is to the equilibrium value, that may be reached under the same test conditions.

The bed contours around the piers for both cases at the end of the experiments are shown in Figure 5.24 - 5.25. It can be seen that the scour patterns were not perfectly symmetric due to a slightly non-symmetric upstream velocity field. In addition to that the bed features assume a degree of three-dimensionality and the flow tends to meander. This leads to variation in bed level in cross sections.

The scour depth at the back piers is approximately 10mm less than the scour depth that took place at the front piers. This is true for both cases. The scour depth depends on the relative spacing a/b (a is the distance between the centreline of the piers and b is the common pile diameter). For two piers touching ($a/b = 1$), the scour depth at the front pier is the same as that for a single pier but with increasing separation, the front pier experiences a reinforcing effect which reaches a maximum at $a/b = 2.5$ and is evident until $a/b = 11$ (Raudkivi, 1991). For large spacing, the scour depth is the same as that of a single pier. Another reason for the reduced scouring at the rear piers is due to the sheltering

provided by the front piers. The upstream pile reduces the effective approach velocity for the downstream piles. The effect of the horseshoe vortex is decreased. Material deposited from the scouring of the upstream pile deflects the flow up and around the downstream pile producing a second form of scouring.

The plots of velocities at quasi-equilibrium stage from the experiments are shown in Figure 5.26 and 5.27.

FLUENT Simulations

Flow around the two piers arrangement mentioned above was also simulated using FLUENT. It should be stressed here that the simulation was carried out before the above-mentioned experiments, therefore the inlet velocity may not necessary be exactly the same. Only rigid-bed cases were considered. The grid systems for the two cases considered are shown in Figure 5.28 and 5.29. Only half of the hydrodynamic domain of the problems was simulated.

Uniform velocity of 0.87 m/s was used for both cases. Figure 5.28 and 5.29 show the simulated flow fields. FLUENT calculation shows the existence of small negative velocity component in the streamwise direction. This indicates the presence of a horseshoe vortex as would be expected. However, the experimental results did not show this negative component. The plot from the physical model study is based on too few points. This is partly due to the shape of the current meter and the arrangement of the piles, which does not allow measurement closed to the piers to be carried out. As a result a very detailed resolution of the experimental velocity field is not possible. The grids used in the numerical calculation, however, used more than 1500 points, for both cases, for the two dimensional projection of the bed in the horizontal plane. The piles arranged laterally to the flow direction introduced constriction. This effect may be seen in

Figure 5.28 and 5.29, where the velocity fields are greater between the passage of the piers.

The presence of the scour hole in the experiments influenced the velocity field. Therefore comparisons between the results from the experiments and the numerical calculation(rigid bed) cannot be expected to coincide completely. Furthermore, as mentioned earlier, the inlet velocity used may not be necessary the same. However, the general flow pattern obtained from the numerical study may be used to assist in understanding the processes that took place in the experiments.

5.6 CONCLUSIONS

The collated three-dimensional turbulence formulation in FLUENT has been validated against selected benchmark solution of flow around piers. The flow field predicted by FLUENT seems to correspond quantitatively well with limited available experimental results. The theoretical aspects of the flow dynamics, such as the horseshoe vortex, can also be interpreted from the output. The results obtained using the RNG k-ε model are virtually identical to those produced by the k-ε model.

After the scouring action had started, the bed shear stress fell and as the scour hole developed further the reduction became less apparent. The overall bed shear stress decreased with the increase in scouring time and with the increase in size of local scour. In general, the FLUENT results show that regions with the highest values of bed shear stress correspond to the region of highest floor velocity. The shear stress, predicted by FLUENT, is lowest in the region of maximum erosion and is highest near the crest region. At maximum erosion the cross sections of flow increased and from the continuity equation the mean velocity of the flow is

expected to reduce. Similarly at the crest the area decreases and causes an increase of flow velocity. In practise the change in the bed level may result in fluctuation of the water level. FLUENT, however, is not capable of taking this in effect as it modelled the water surface as 'close-lid'.

It can be concluded that the boundary shear stress alone did not account for the entrainment and transport of the sediment particles. The degree of the turbulence intensity, especially in an obstructed flow field also contributed significantly in the scouring process. In a physical model, not all relevant quantities could be furnished. Some physical quantities in a turbulence flow are difficult to measure. One of these quantities is the vorticity, which was known to be the major factor responsible for base scouring. With recent advances in flow visualisation technique, the measurement of this quantity is coming into reach of the experimentalist. In the present experiments, however, a very crude technique was employed. This did not provide adequate information for direct comparison with the results obtained from the numerical study.

On the other hand, it should also be expected that "perfect" results are difficult to obtain in view of the many factors involved which cannot be modelled directly using a numerical simulation. For instance, the presence of "turbulent bursts" which are widely observed and are capable of removing sediment from the bed. This results in enlargement of the scour hole. Unfortunately, FLUENT is not capable of predicting these bursts.

Despite of all the limitation, in general, FLUENT exhibits good qualitative predicted flow patterns around the piers. Further detailed and rigorous study need to be carried out to validate the results quantitatively. The ability of rapidly growing CFD package to model a complex flow such as described in this

chapter would provide a powerful tool in manipulating tests and analytical approaches complimentarily in order to predict the scour depth under various conditions and furthermore to devise effective disaster prevention work against local scouring.

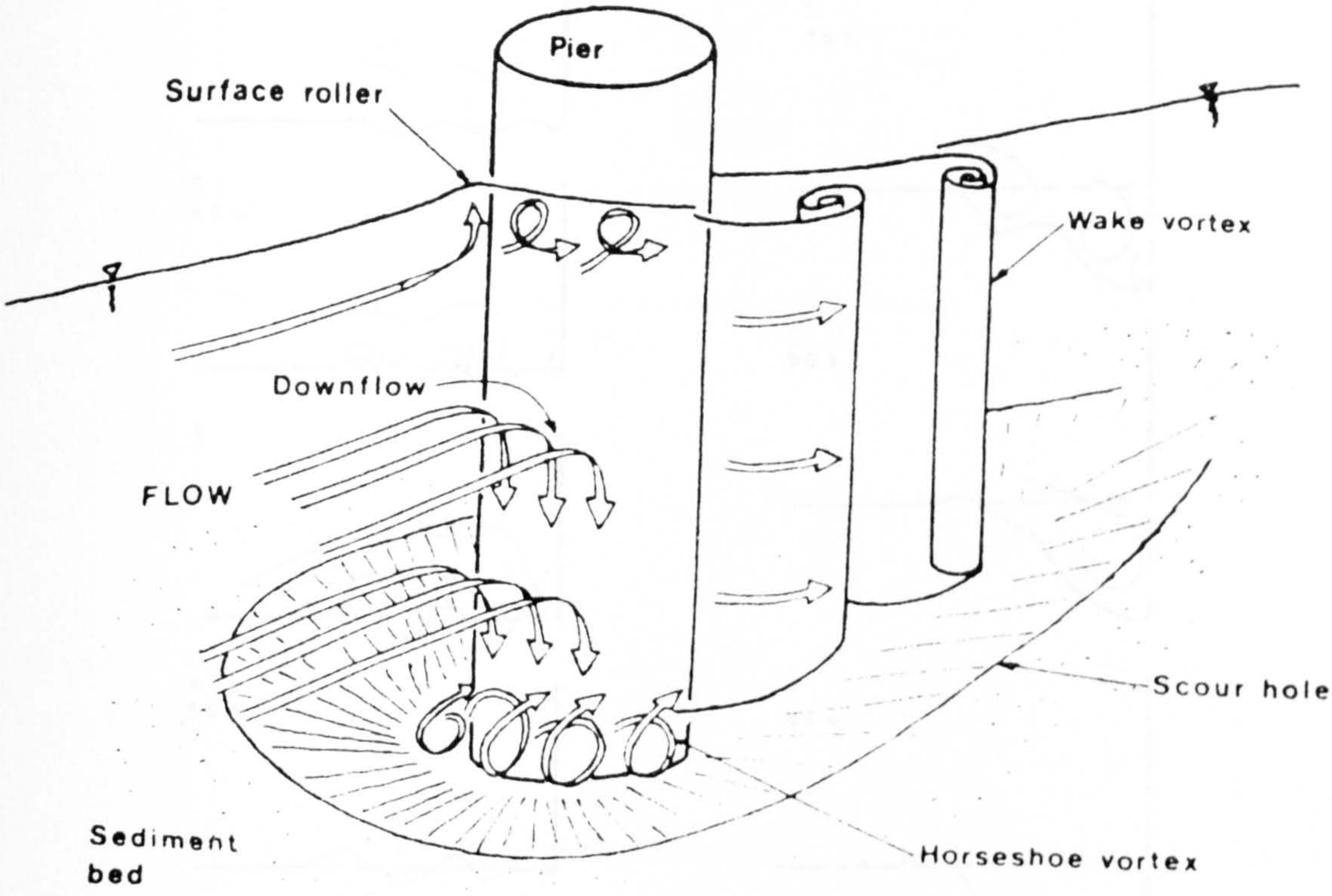

Figure 5.1 : Diagrammatic principal features of flow pattern around Cylindrical Pier (After Melville, 1988)

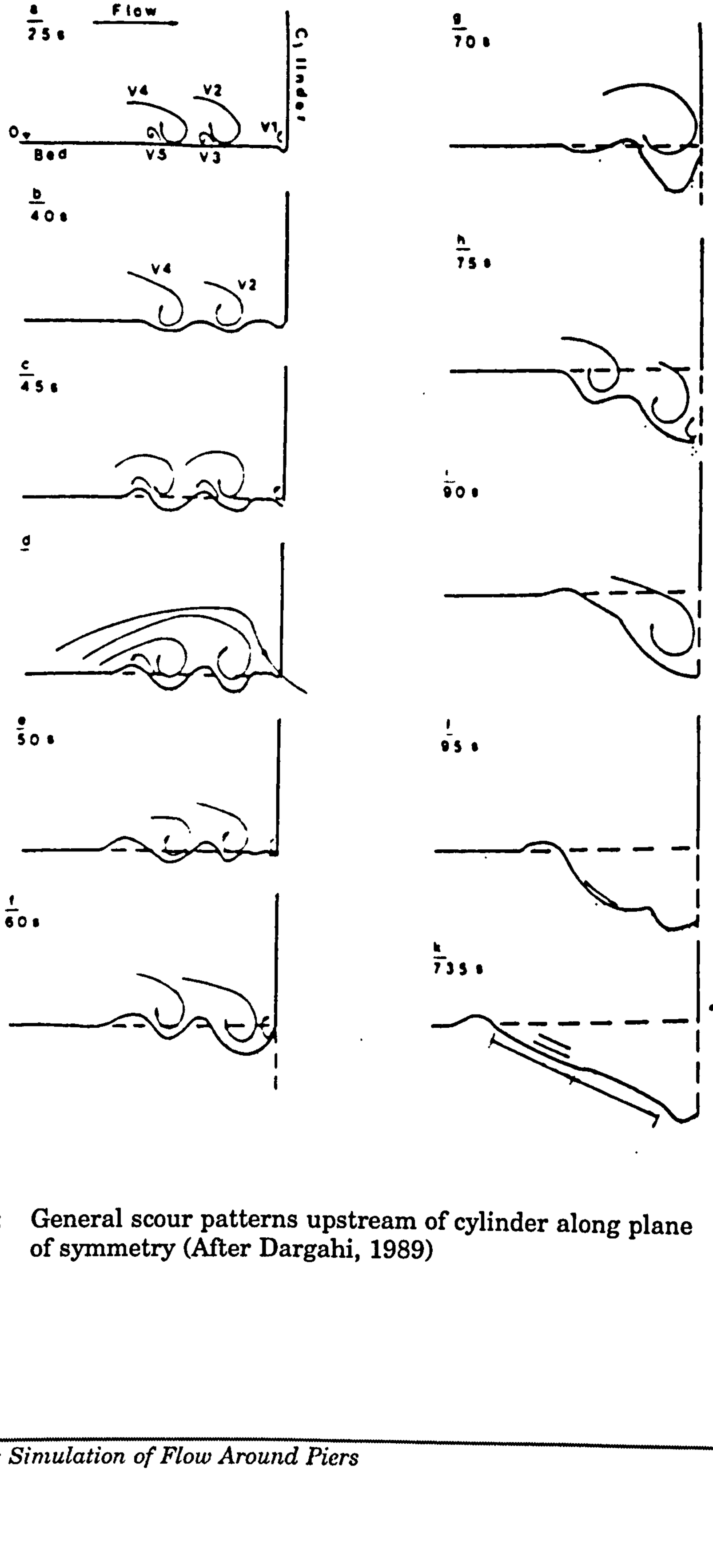

Figure 5.2 : General scour patterns upstream of cylinder along plane of symmetry (After Dargahi, 1989)

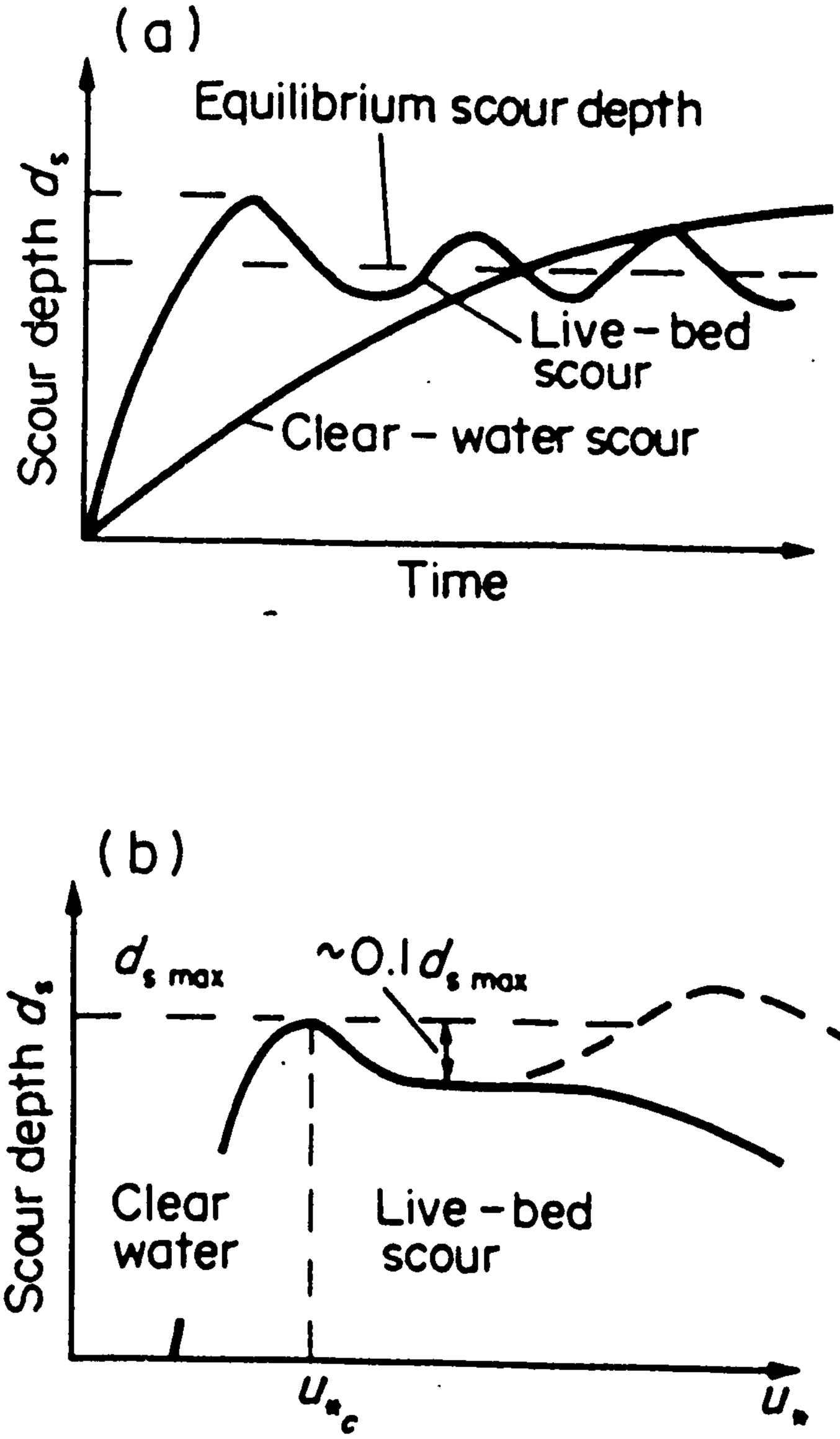

Figure 5.3 : Scour depth for a given pier and sediment size (a) as a function of time (b) as a function of shear velocity or approach velocity

(a) Olsen (1991)

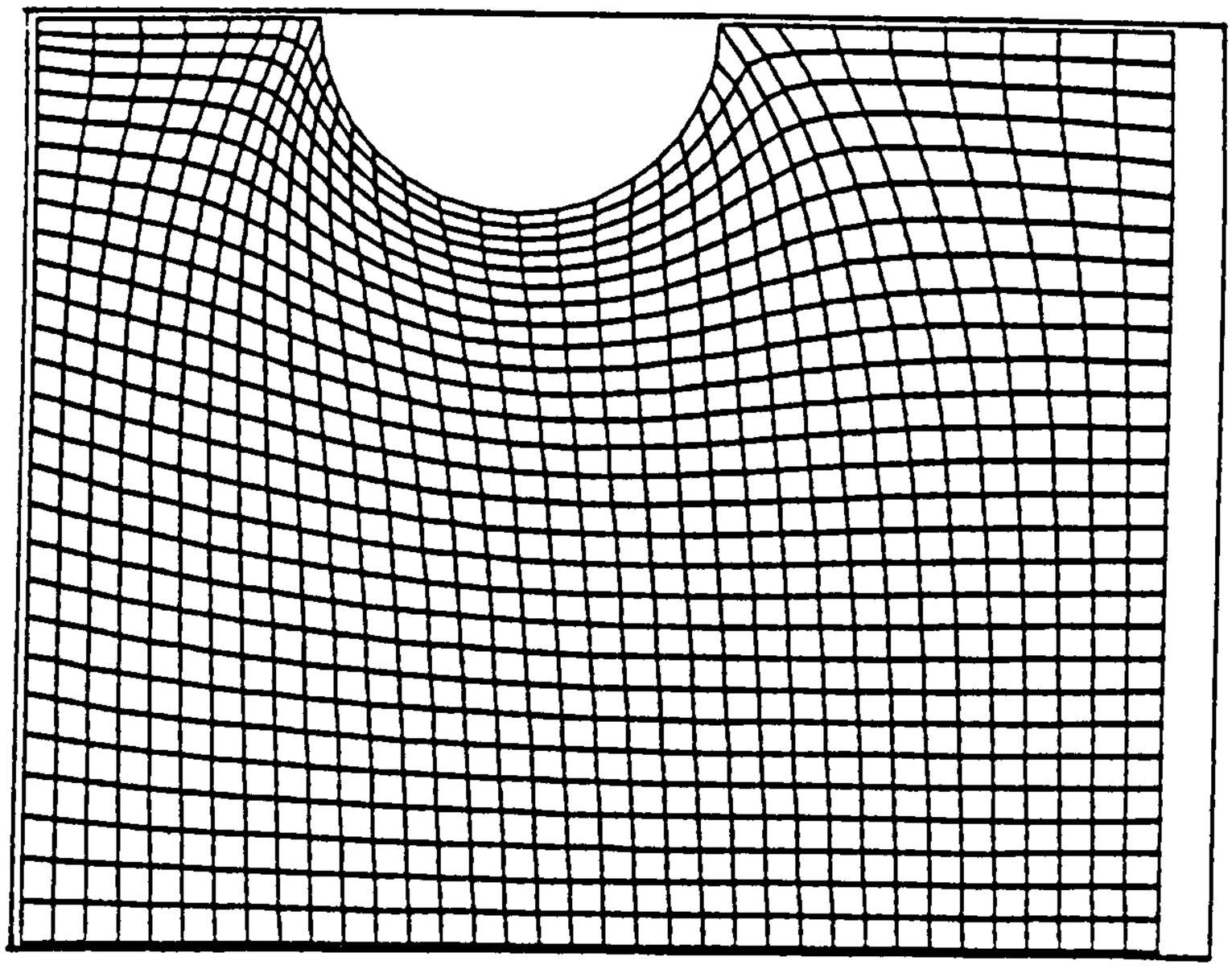

(b) FLUENT

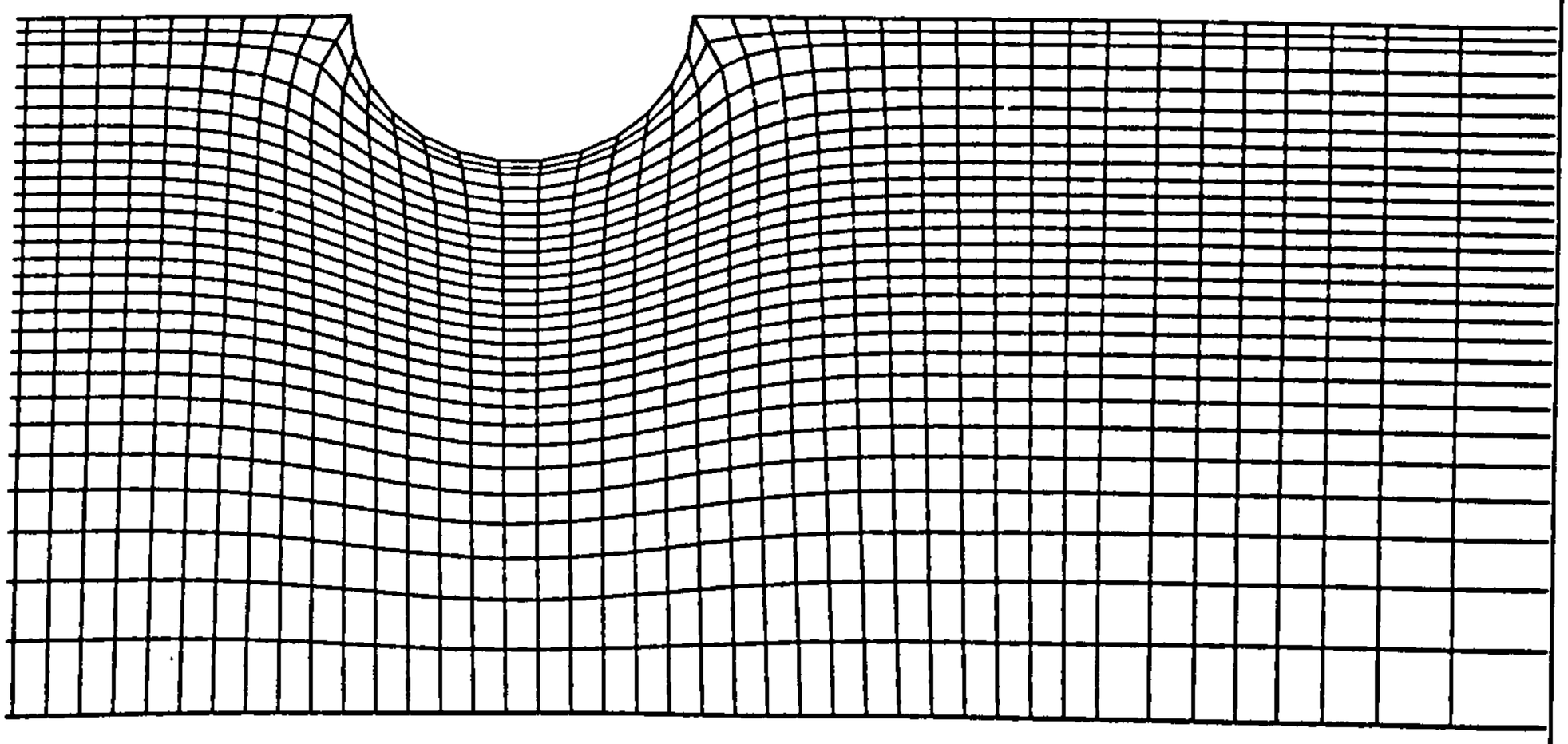

Y Z x	FLOW AROUND CYLINDRICAL PIER Grid (43 X 29 X 20) Slice: K=2	PIER Fluent 4.31 Fluent Inc.

Figure 5.4 : Grid setup for Flow around Pier

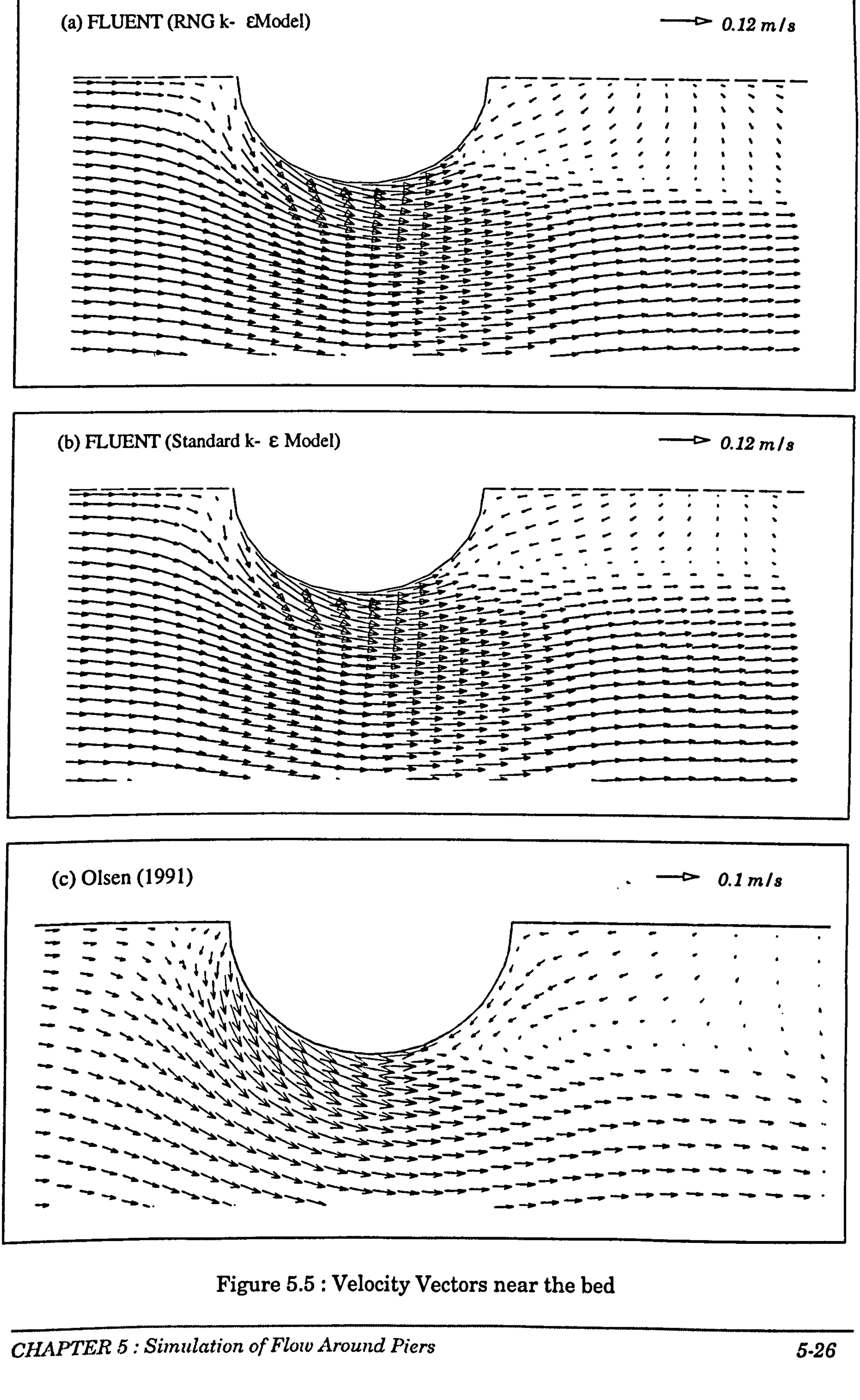

Figure 5.5 : Velocity Vectors near the bed

(a) FLUENT (RNG k- εModel)

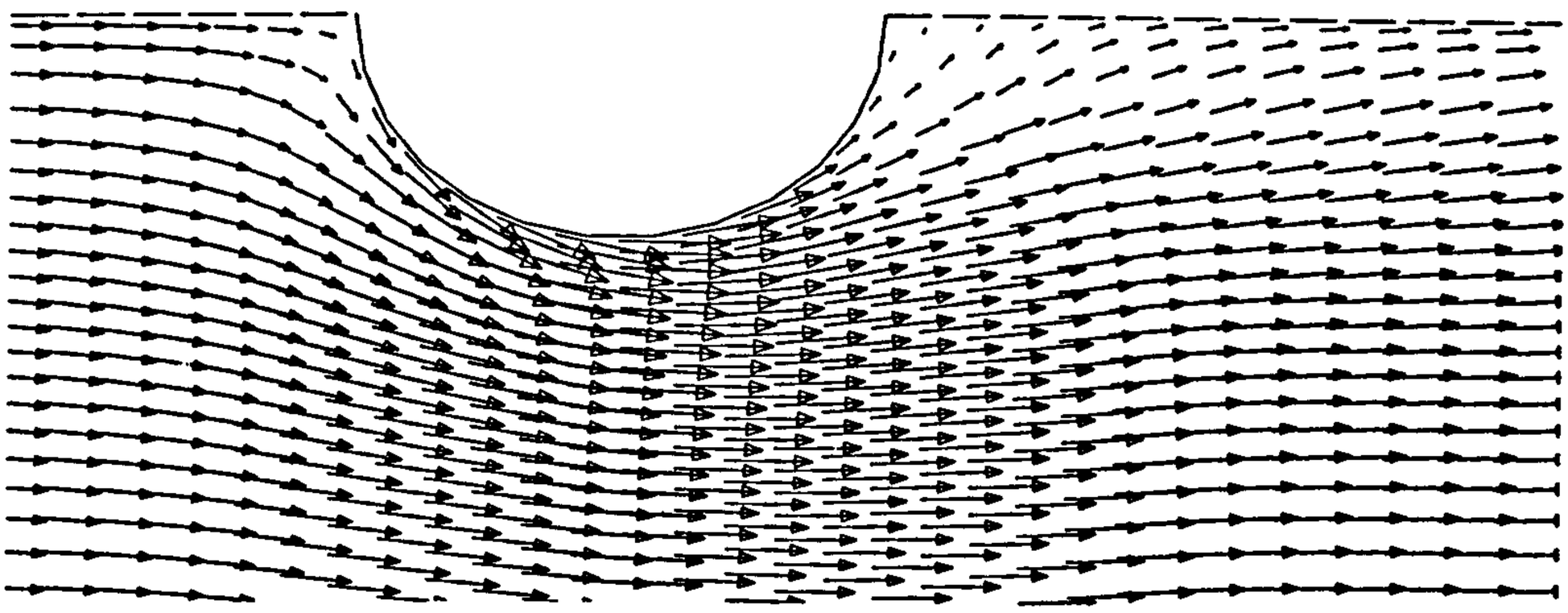

(b) FLUENT (Standard k- ε Model)

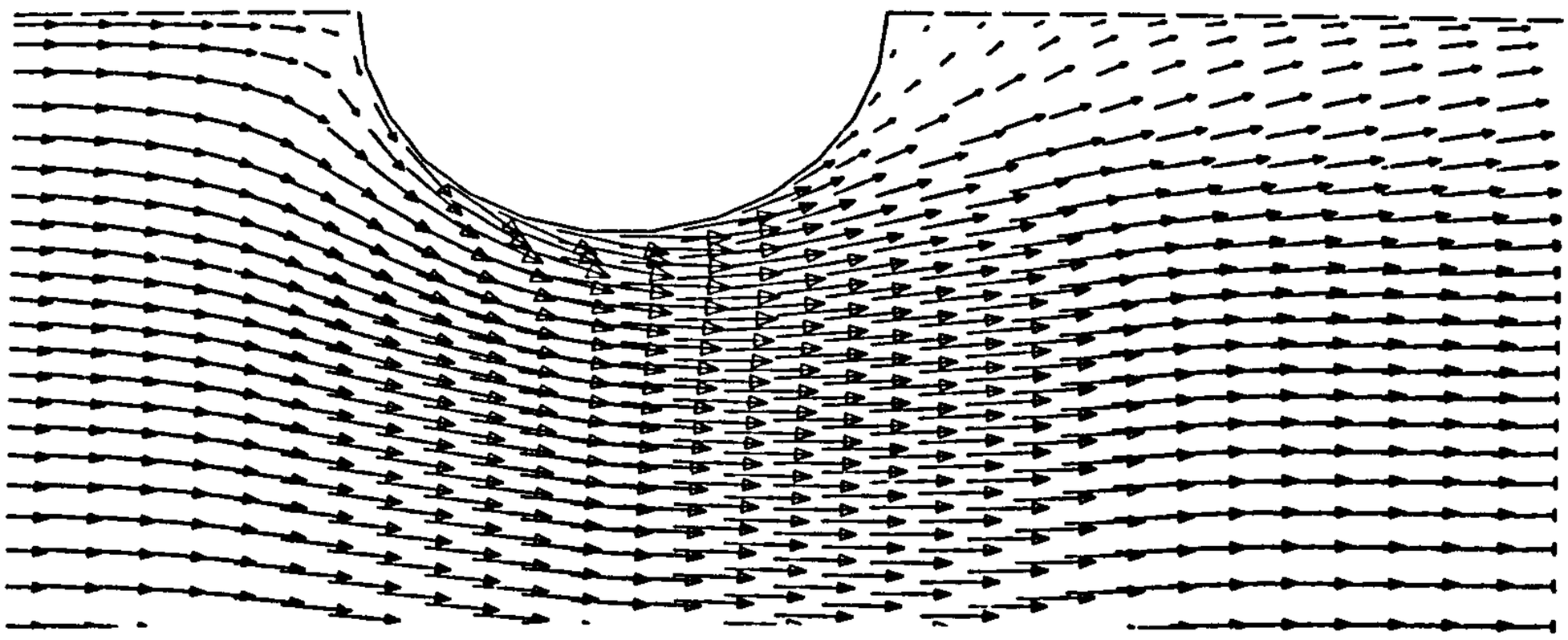

(c) Olsen (1991)

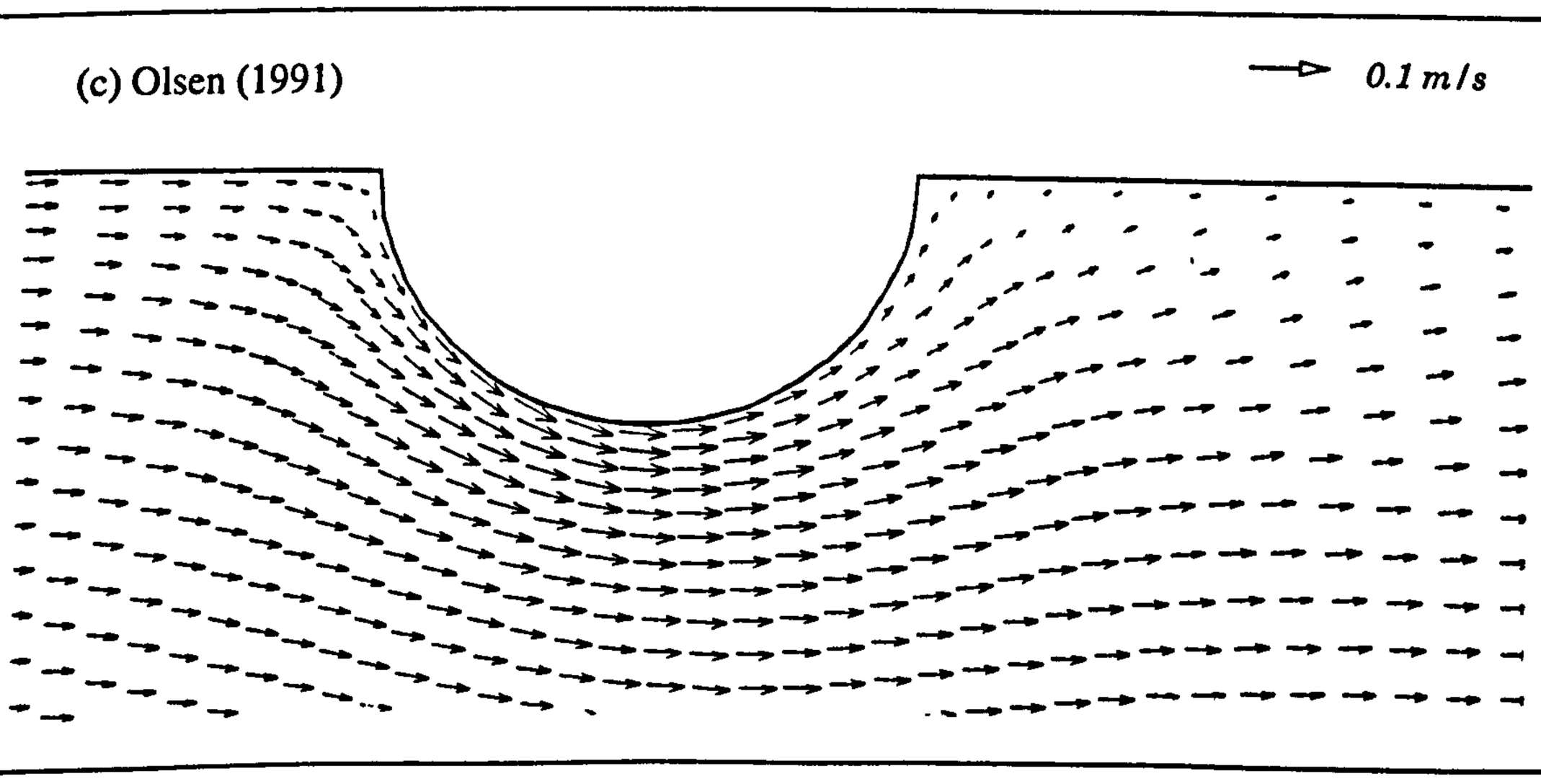

Figure 5.6 : Velocity Vectors near the surface

(a) FLUENT (RNG k- ε Model)

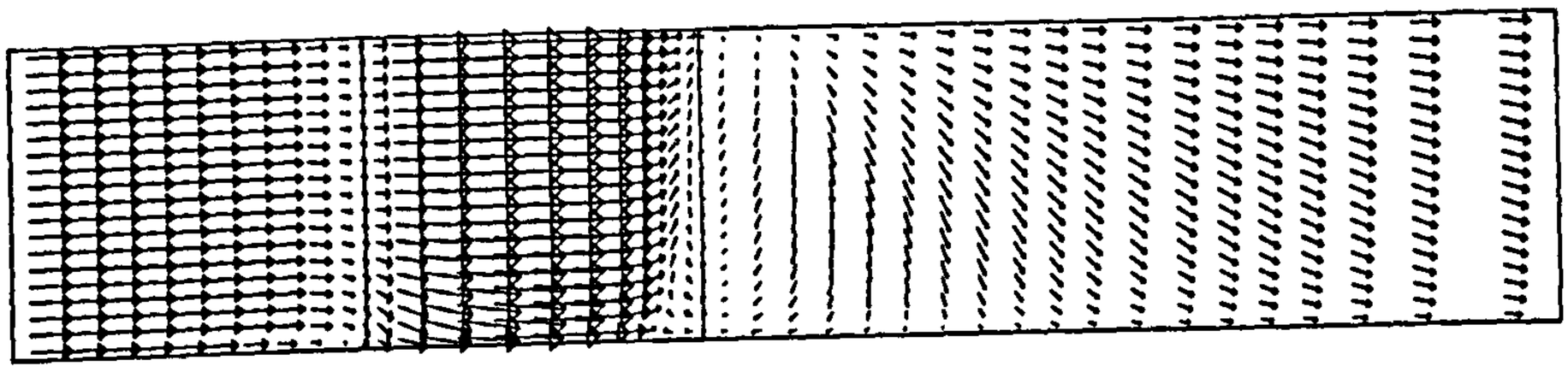

(b) FLUENT (Standard k- ε Model)

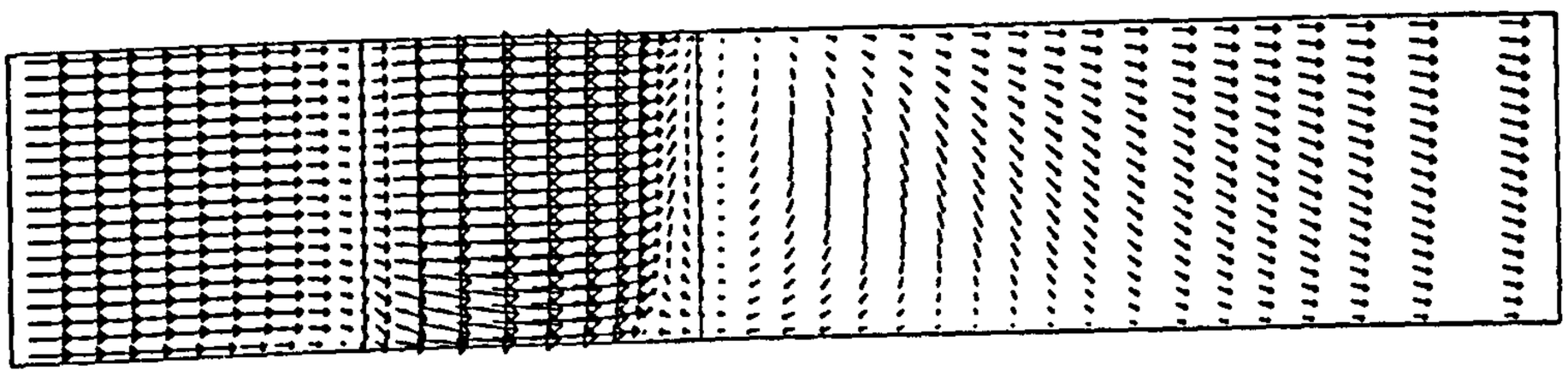

(c) Olsen (1991)

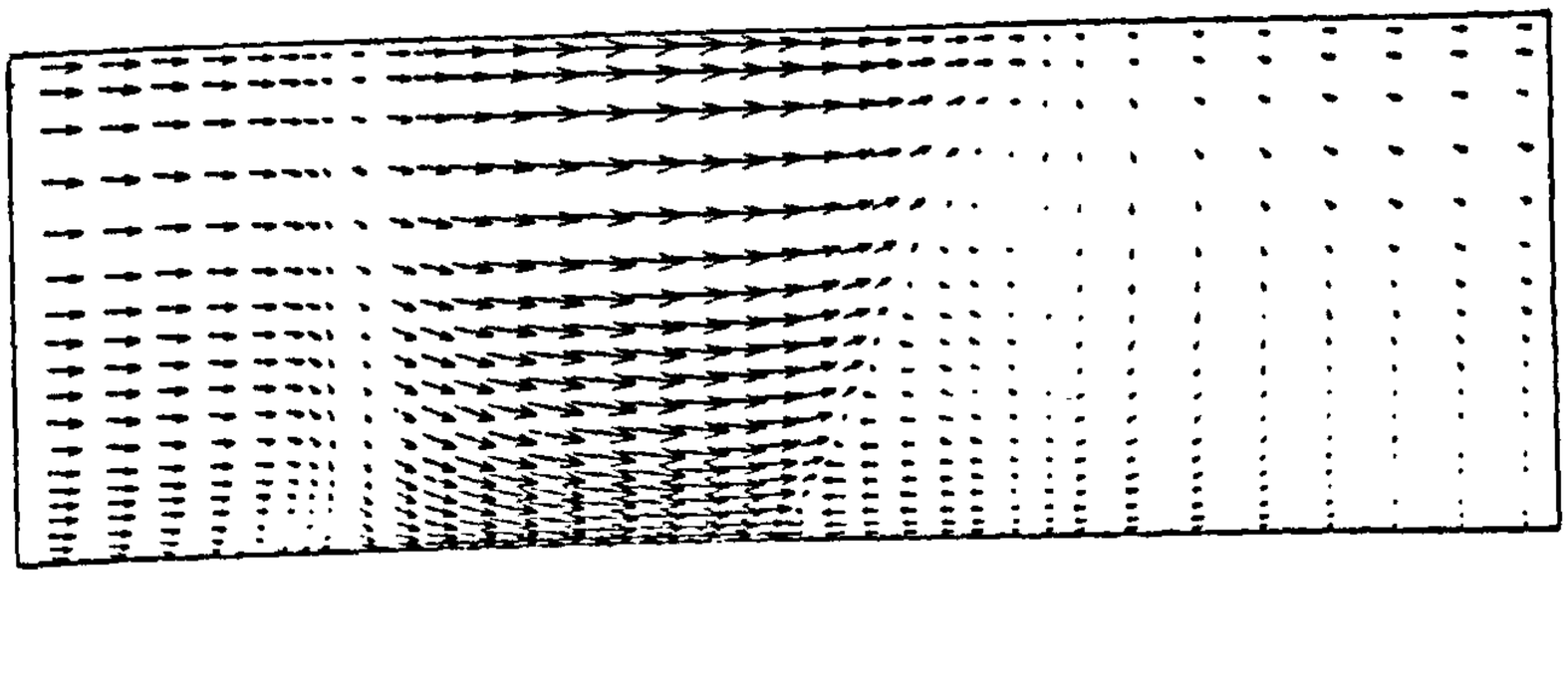

Figure 5.7 : Velocity Vector for longitudinal profile along centerline

(a) FLUENT (RNG k- ε Model)

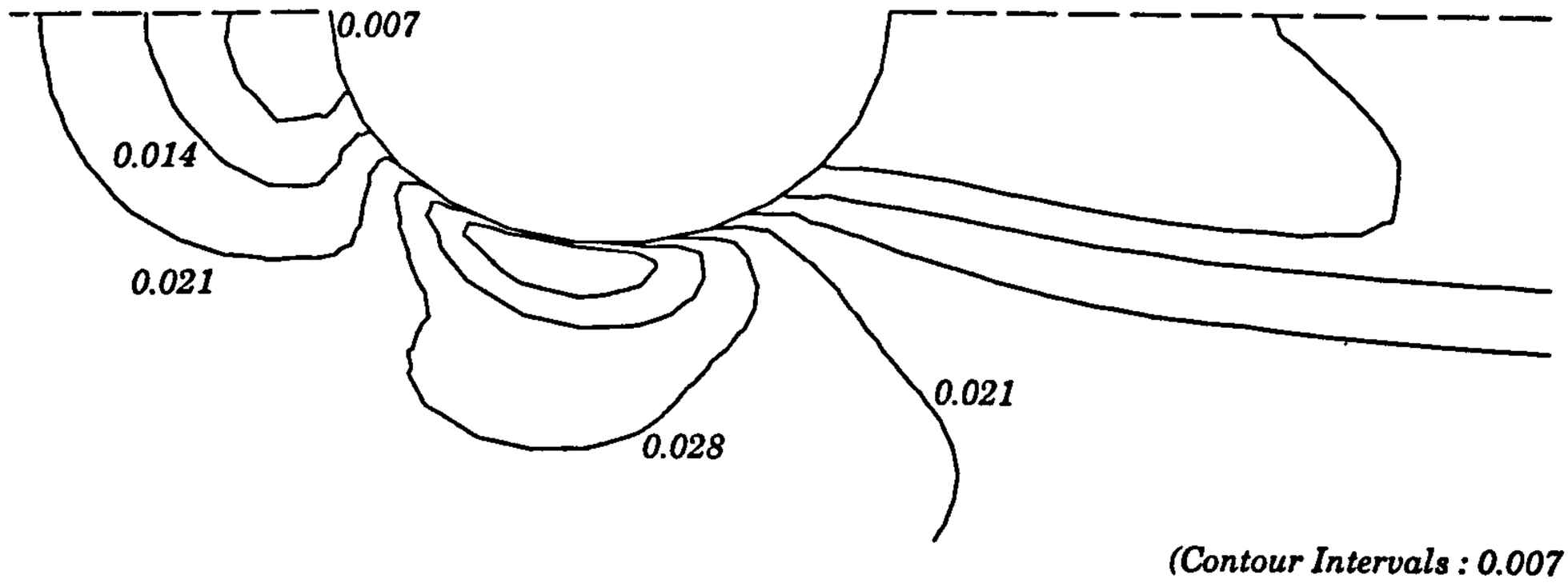

(Contour Intervals : 0.007 Pa)

(b) FLUENT (Standard k- ε Model)

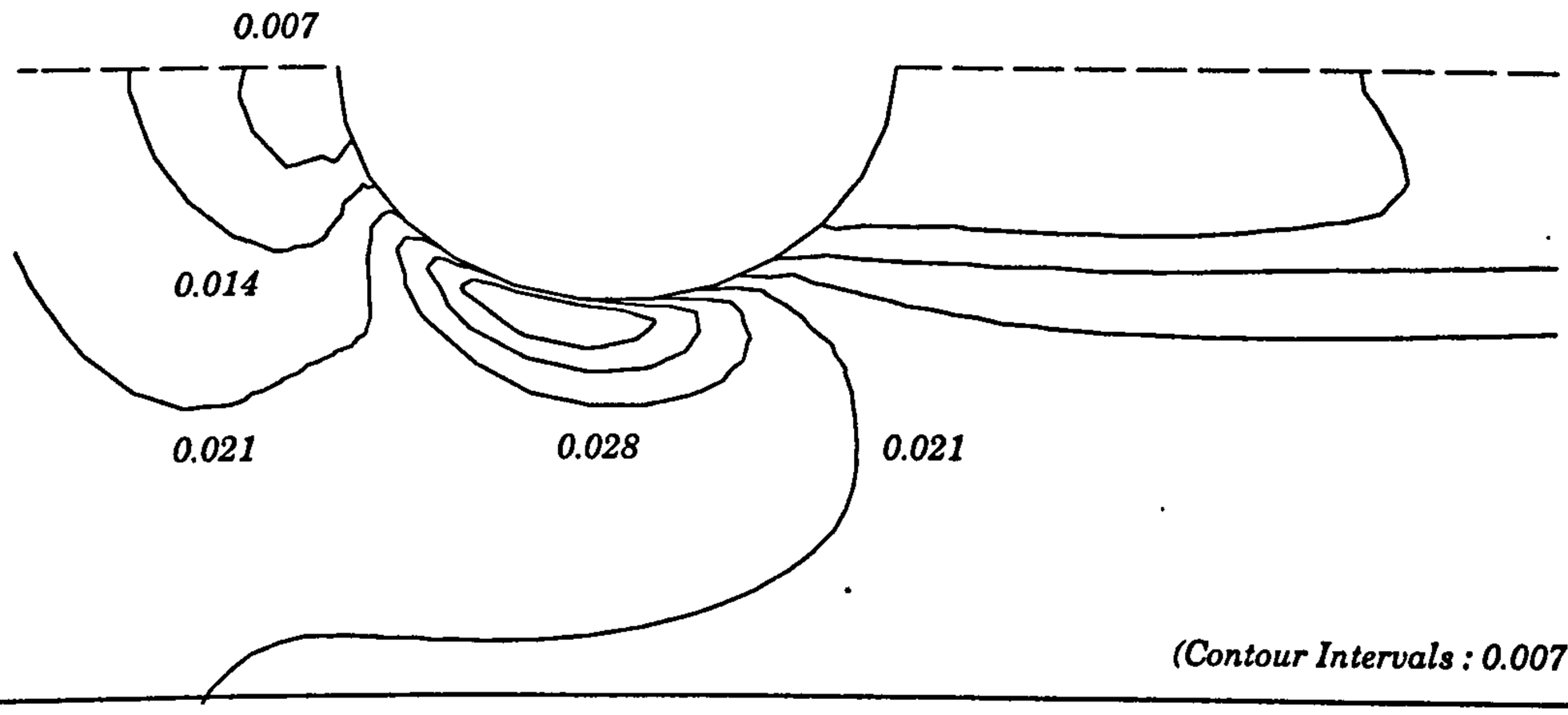

(Contour Intervals : 0.007 Pa)

(c) Olsen (1991)

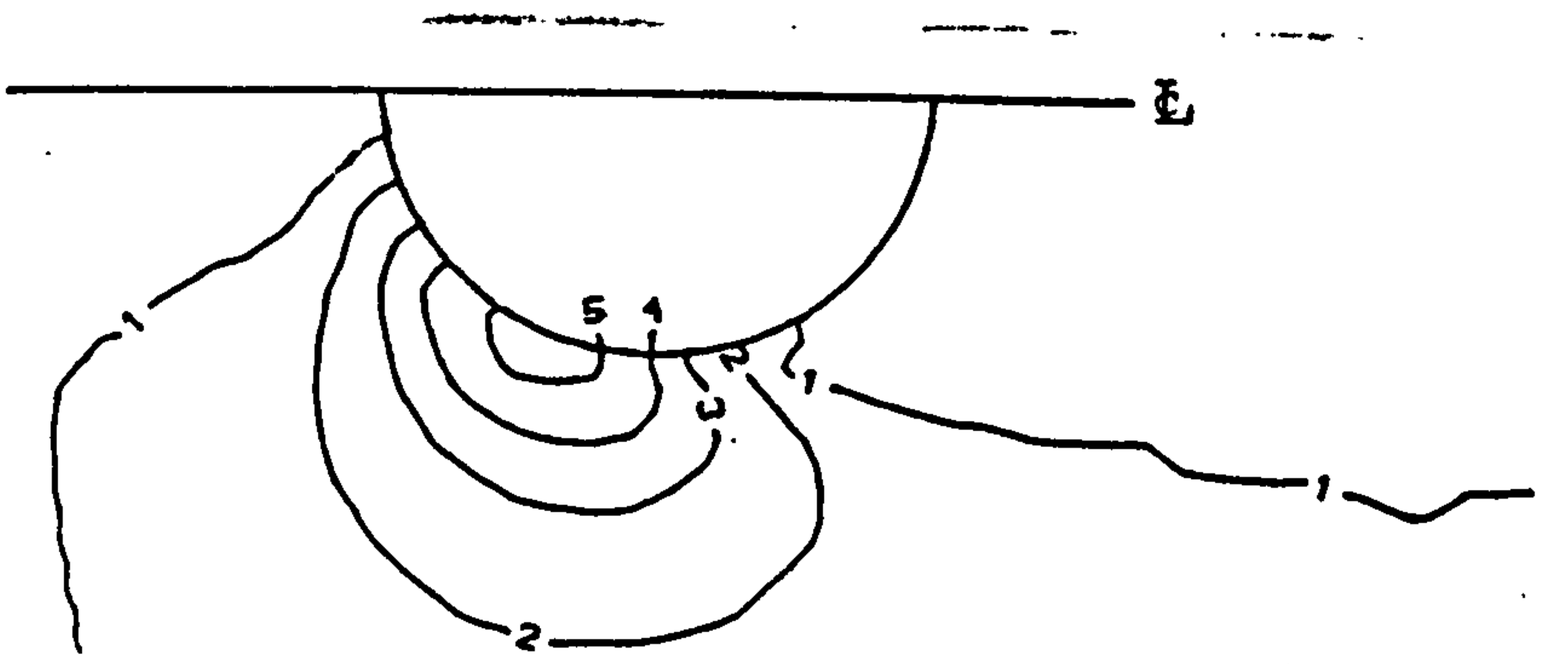

$$\text{Value} = \frac{\text{Shear stress with Pier}}{\text{Shear stress without Pier}}$$

Figure 5.8 : Computed Bed Shear Stress Distributions

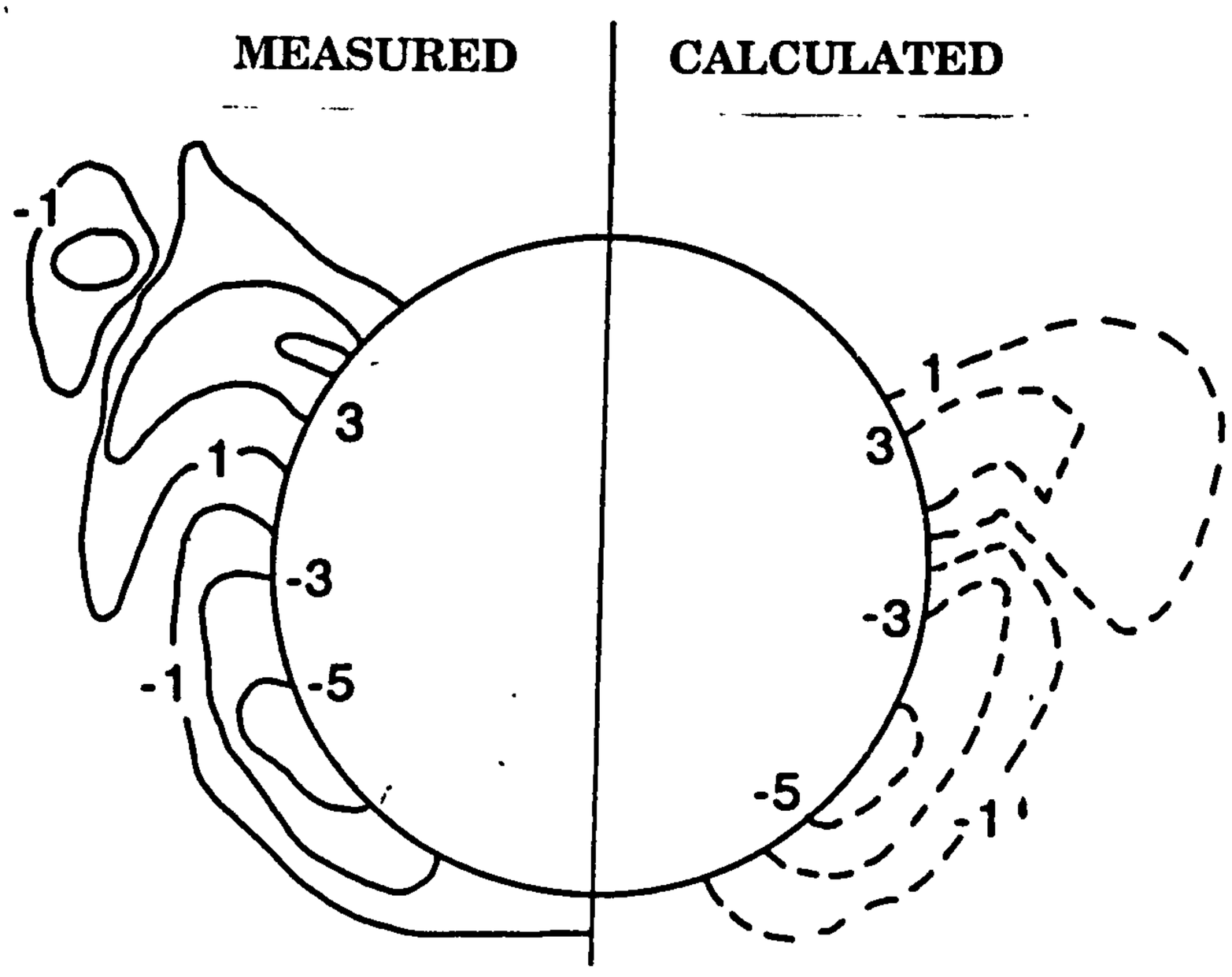

Figure 5.9 : Map of measured calculated scour hole after 10 iterations
- Contour line intervals ; 2cm (After Olsen and Melaaen, 1993)

(a) Near bed

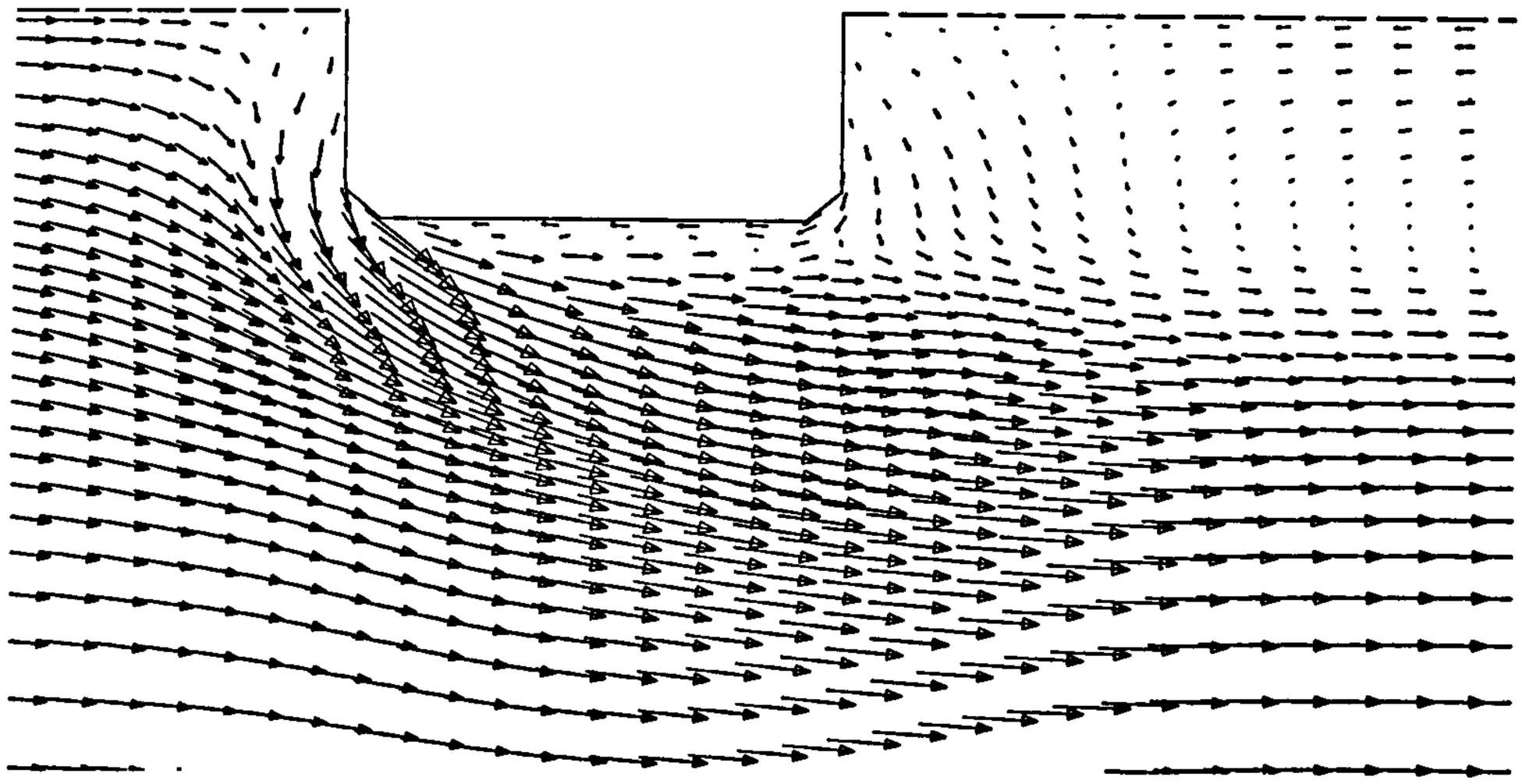

(b) Near surface

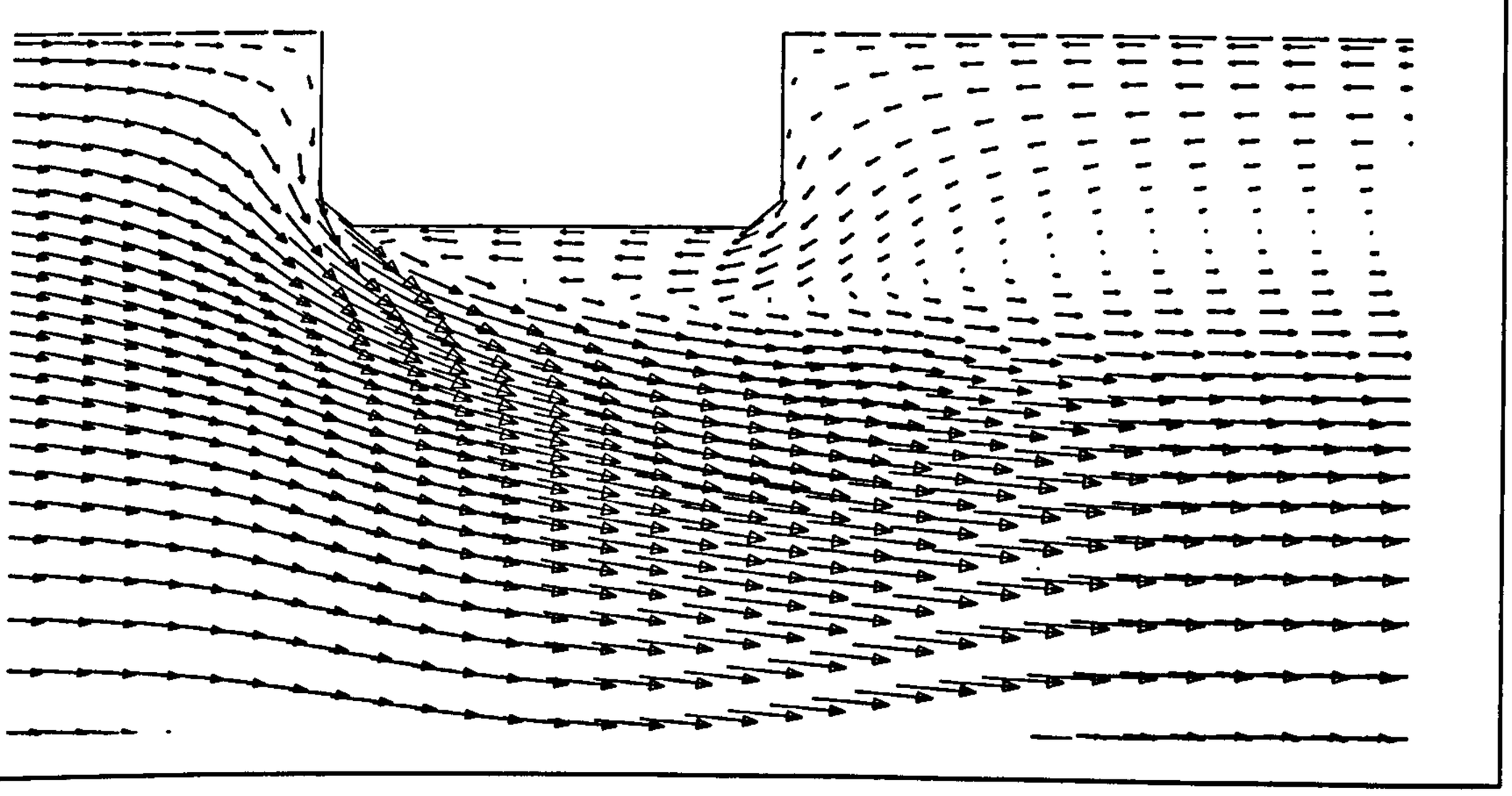

Figure 5.10 : Predicted Velocity Vectors Around Square-shaped Pier

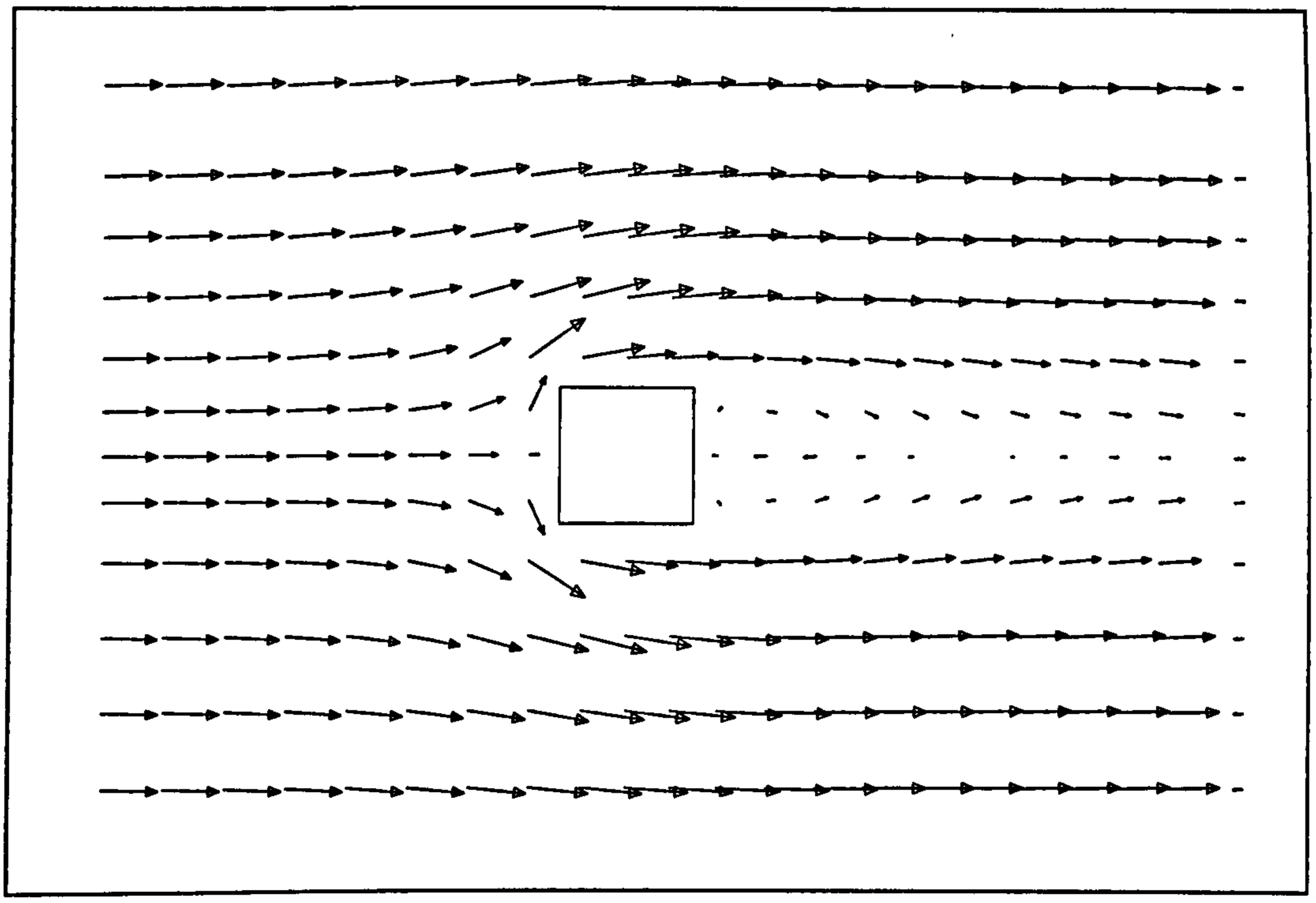

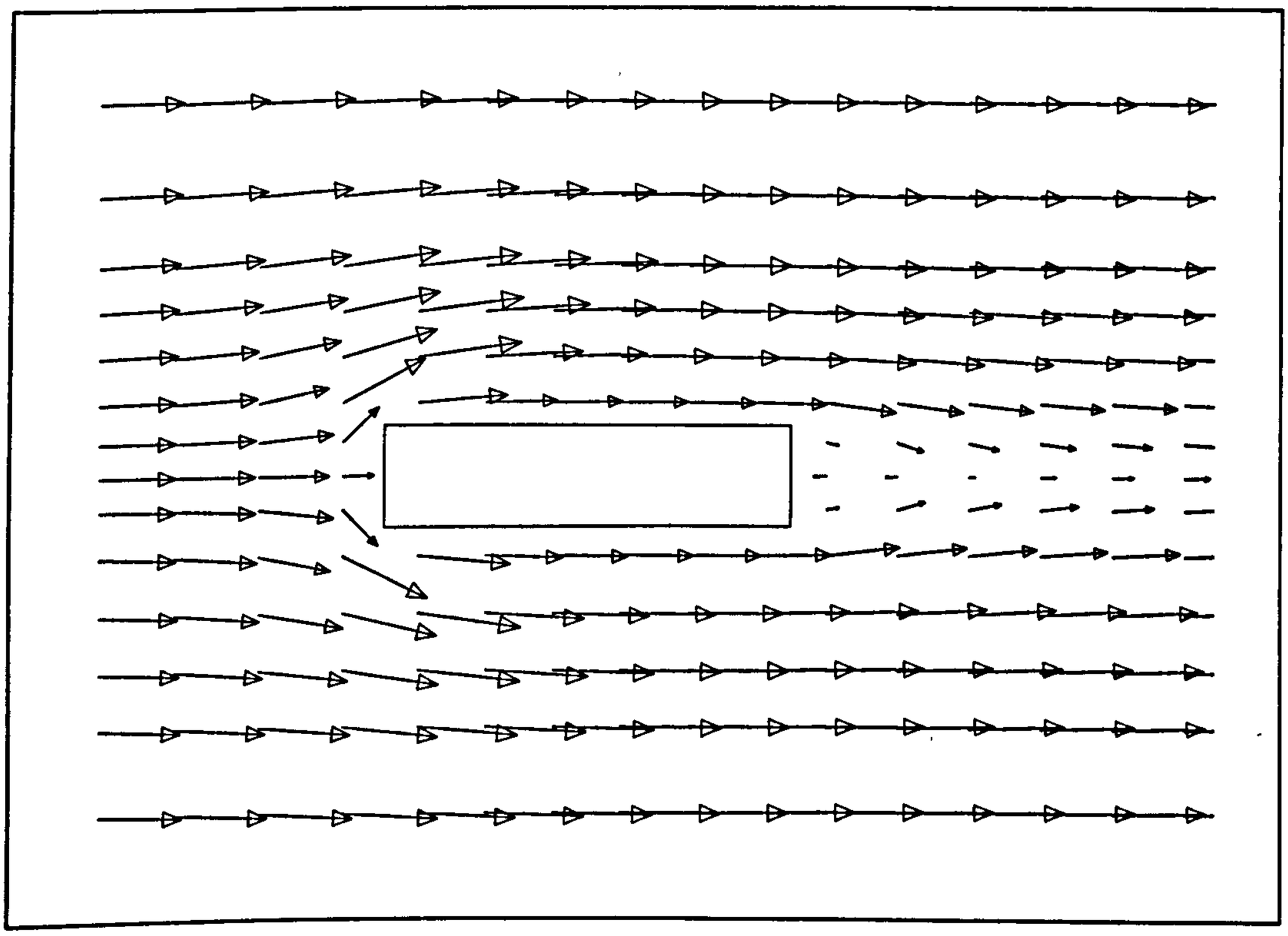

Figure 5.11 : Simulated 2-D flow pattern around various shape of piers.

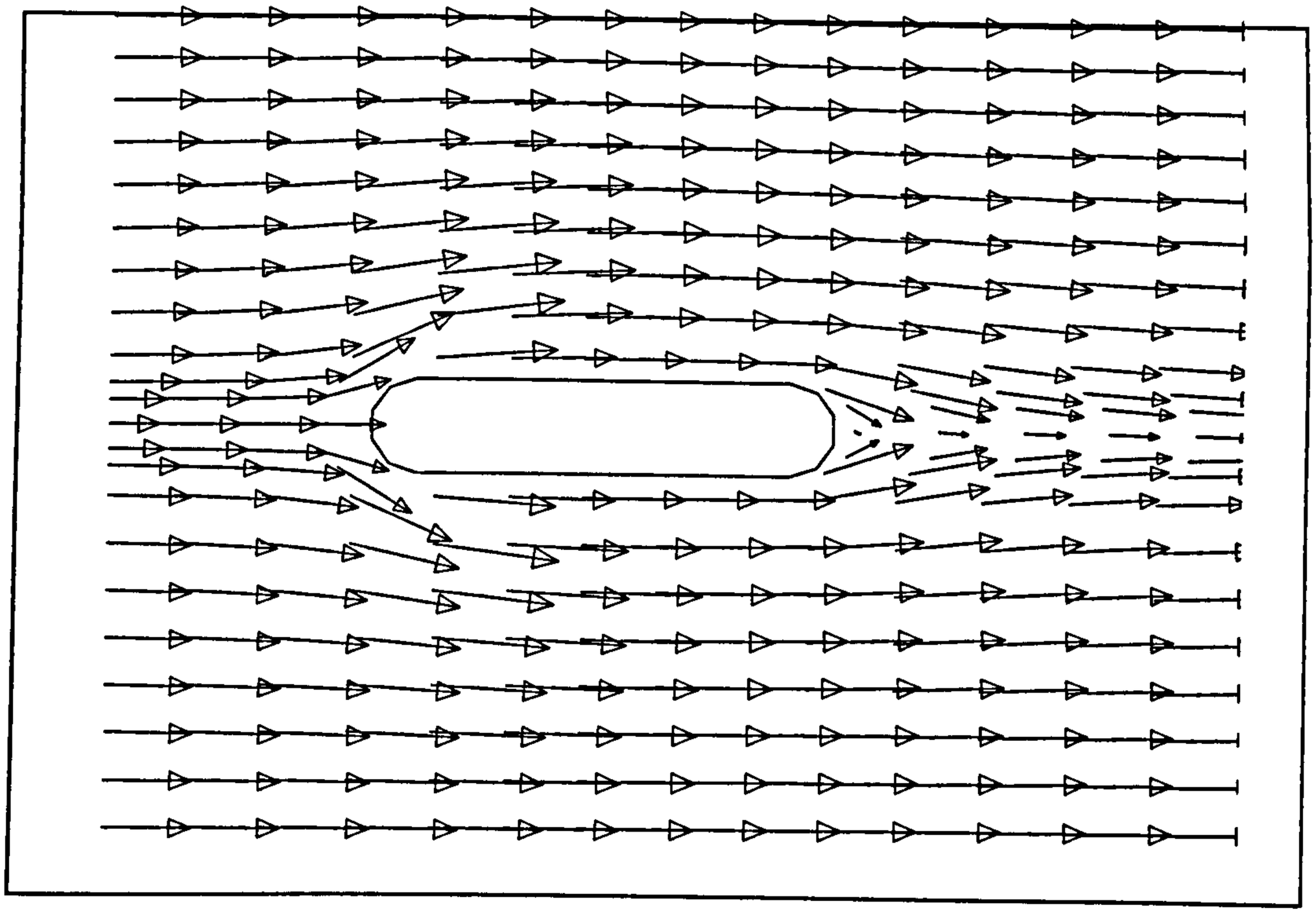

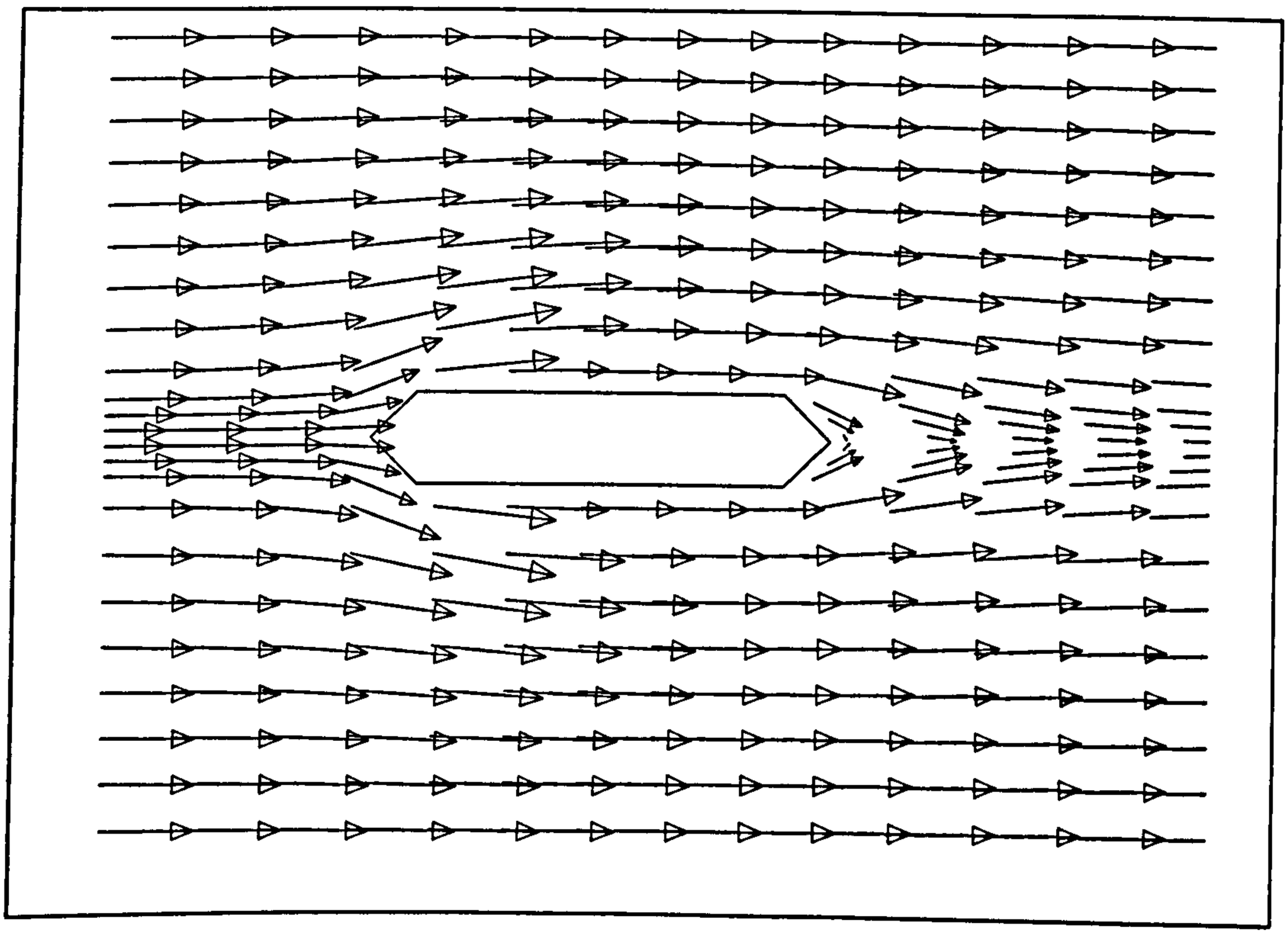

Figure 5.11 (ctn'd) : Simulated 2-D flow pattern around various shape of piers.

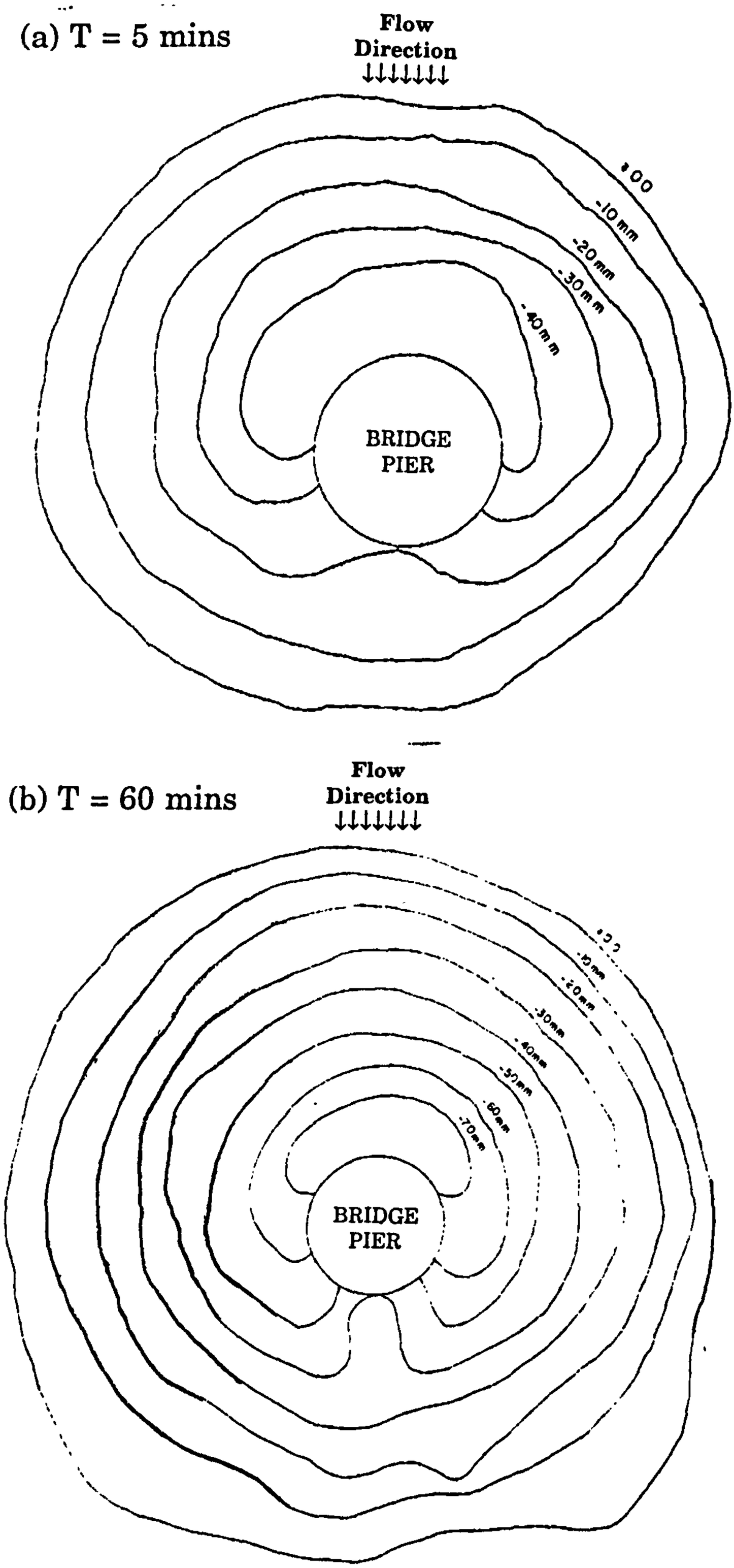

Figure 5.12 : Topographic map around Pier (a) T= 5 mins
(b) T= 60 mins (after Yanmaz, 1994)

(c) T = 100 mins

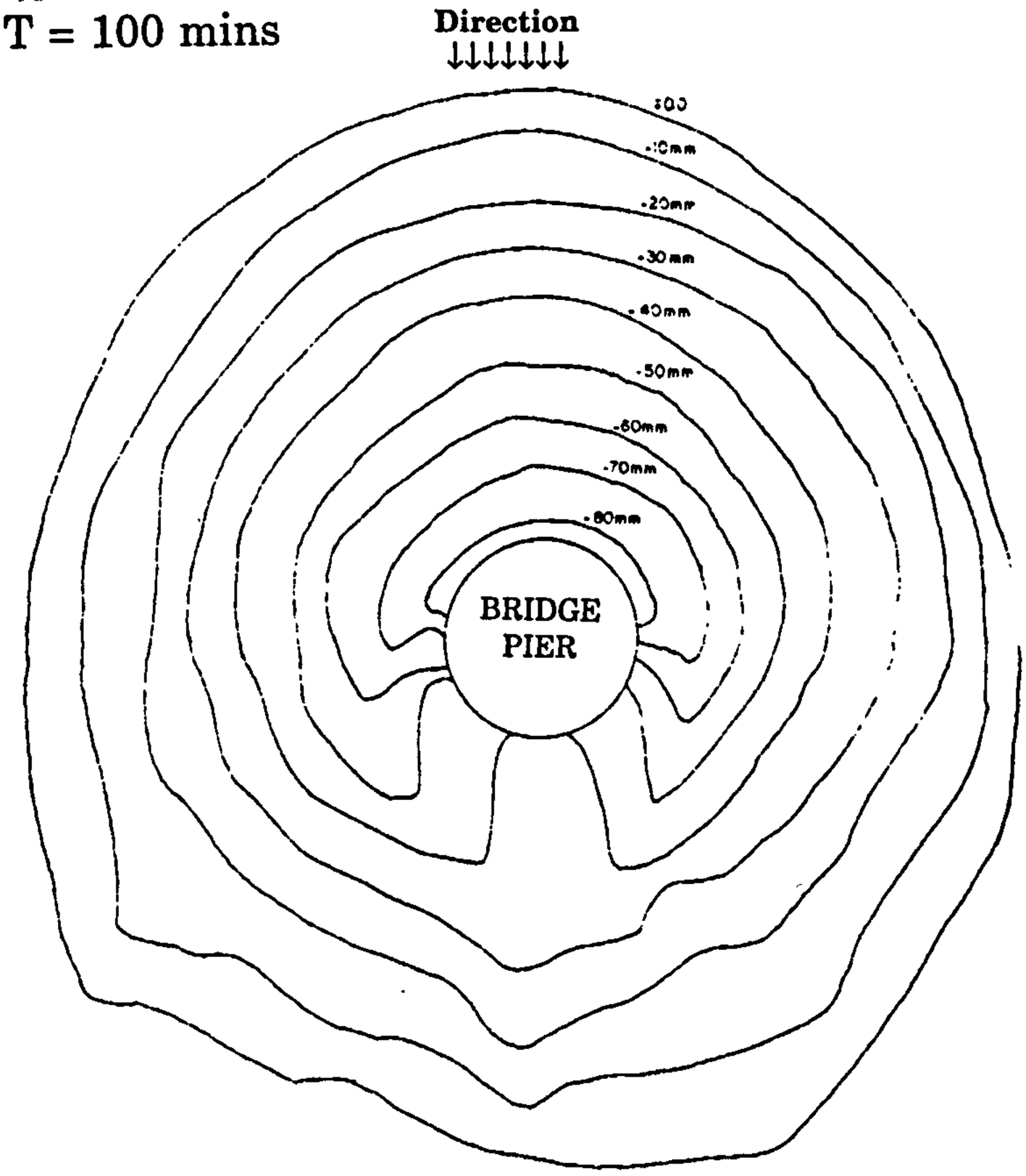

(d) T = 150 mins

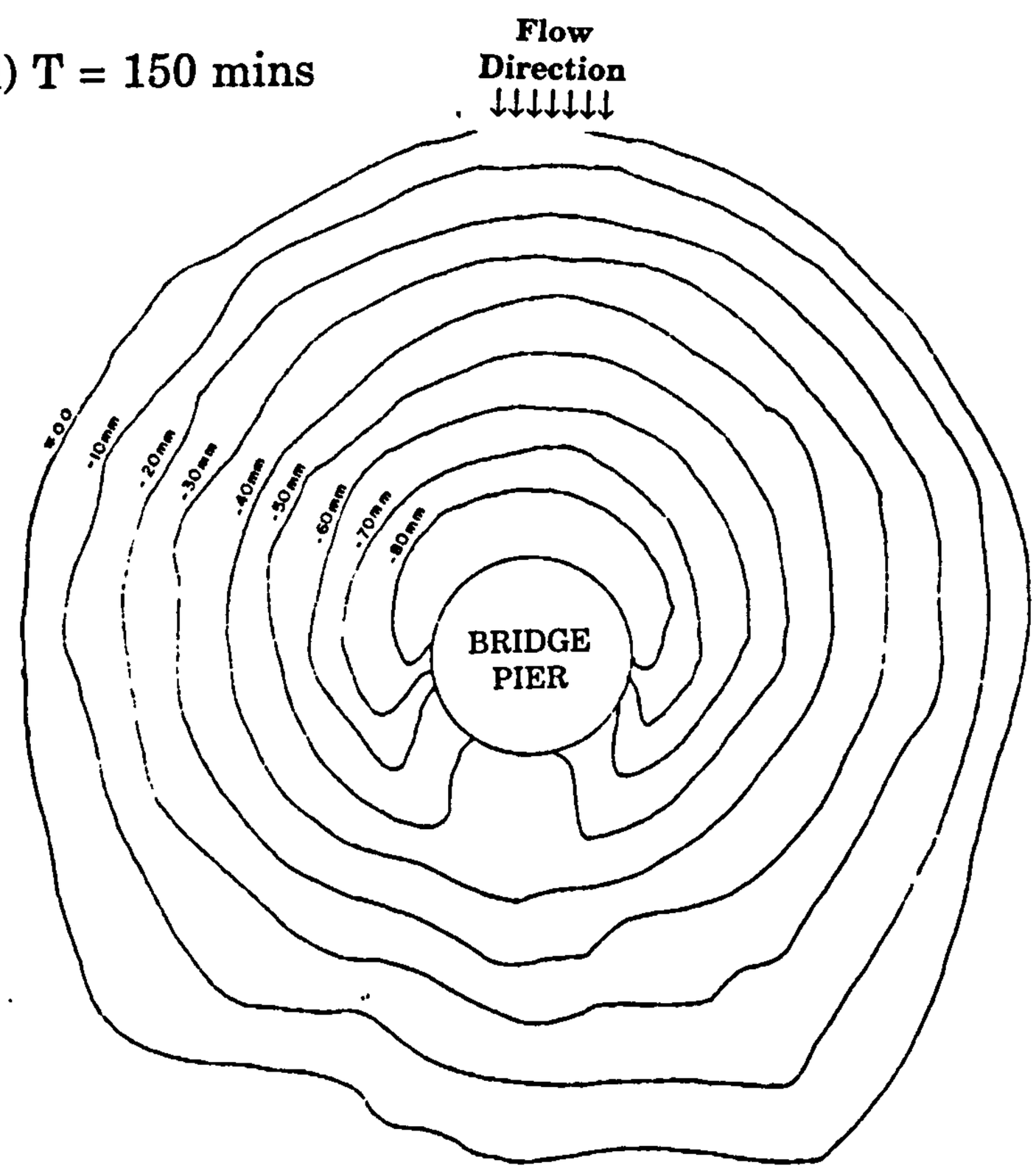

Figure 5.12 (cont'd) : Topographic map around Pier (c) T= 100 mins
(d) T = 150 mins (after Yanmaz ,1994)

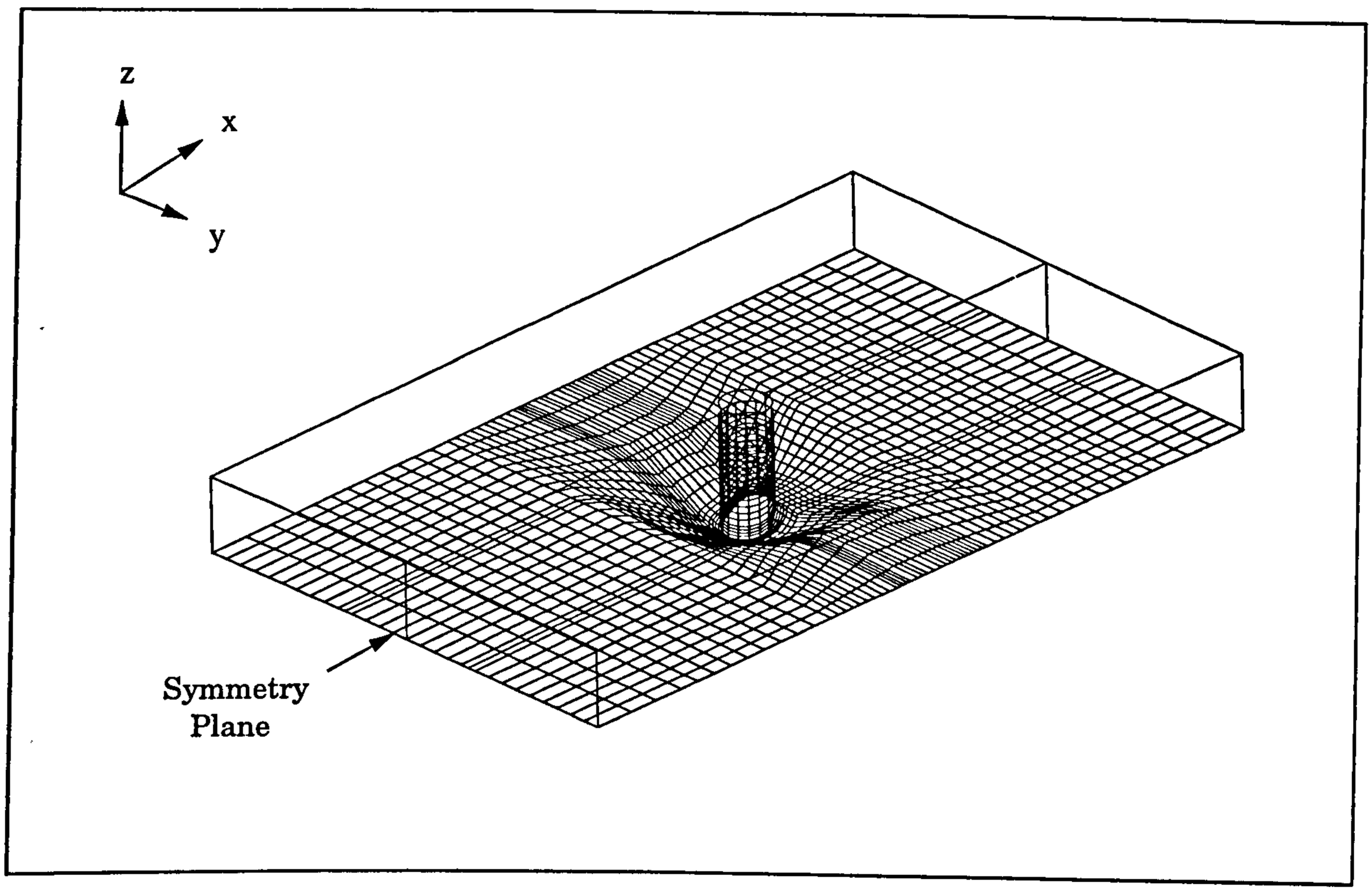

Figure 5.13 : Typical Grid setup (k=1) for FLUENT simulation (T = 150 mins)

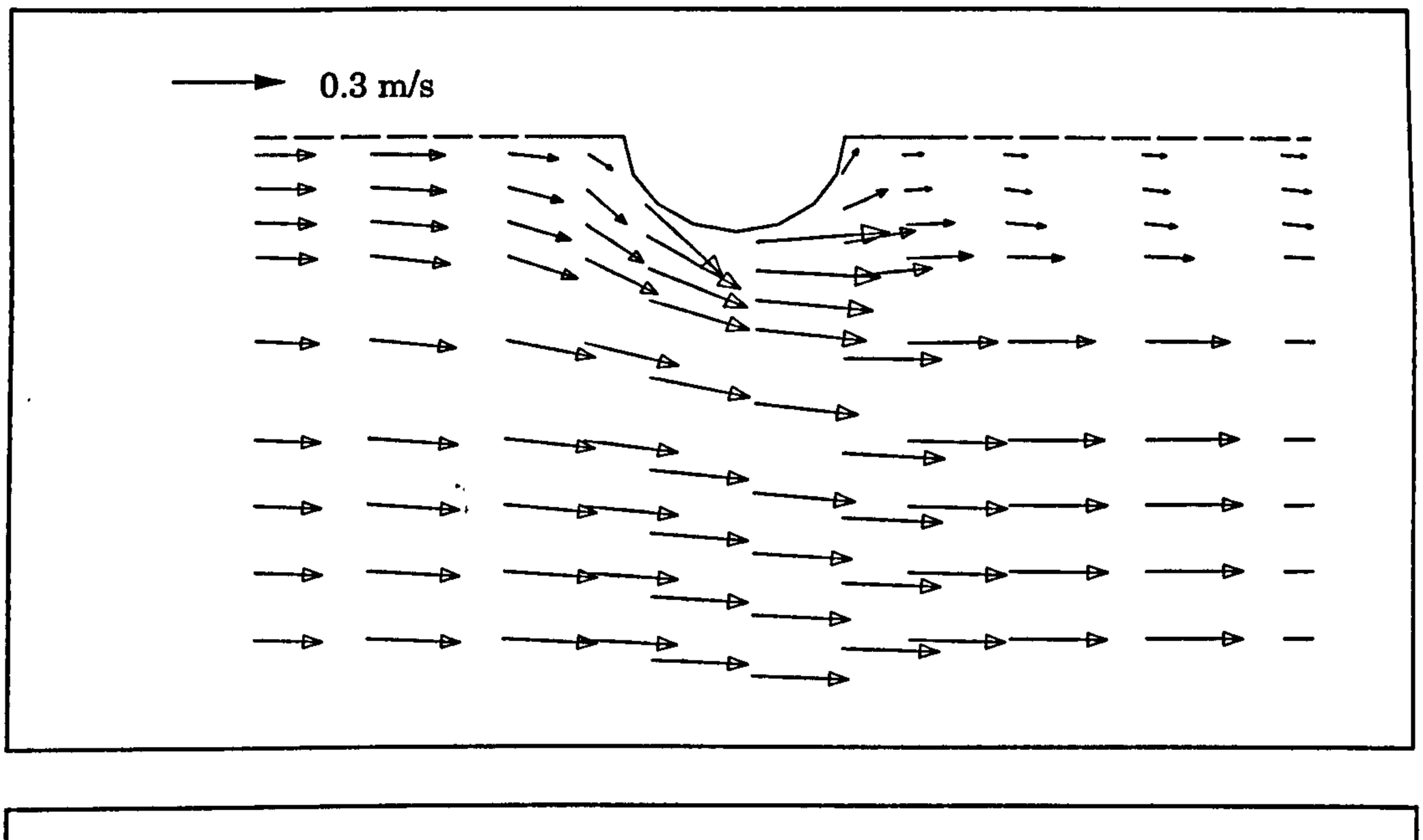

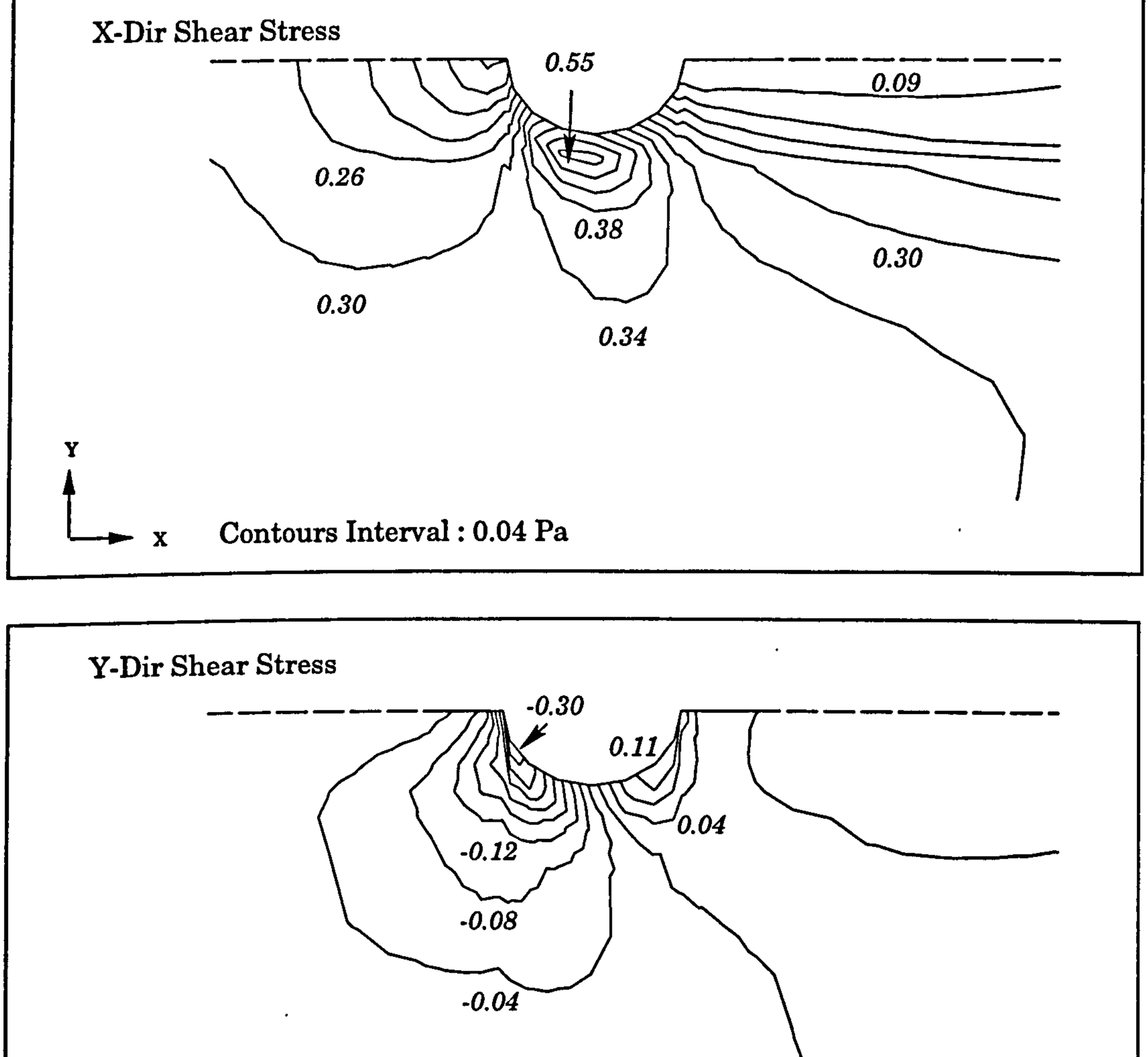

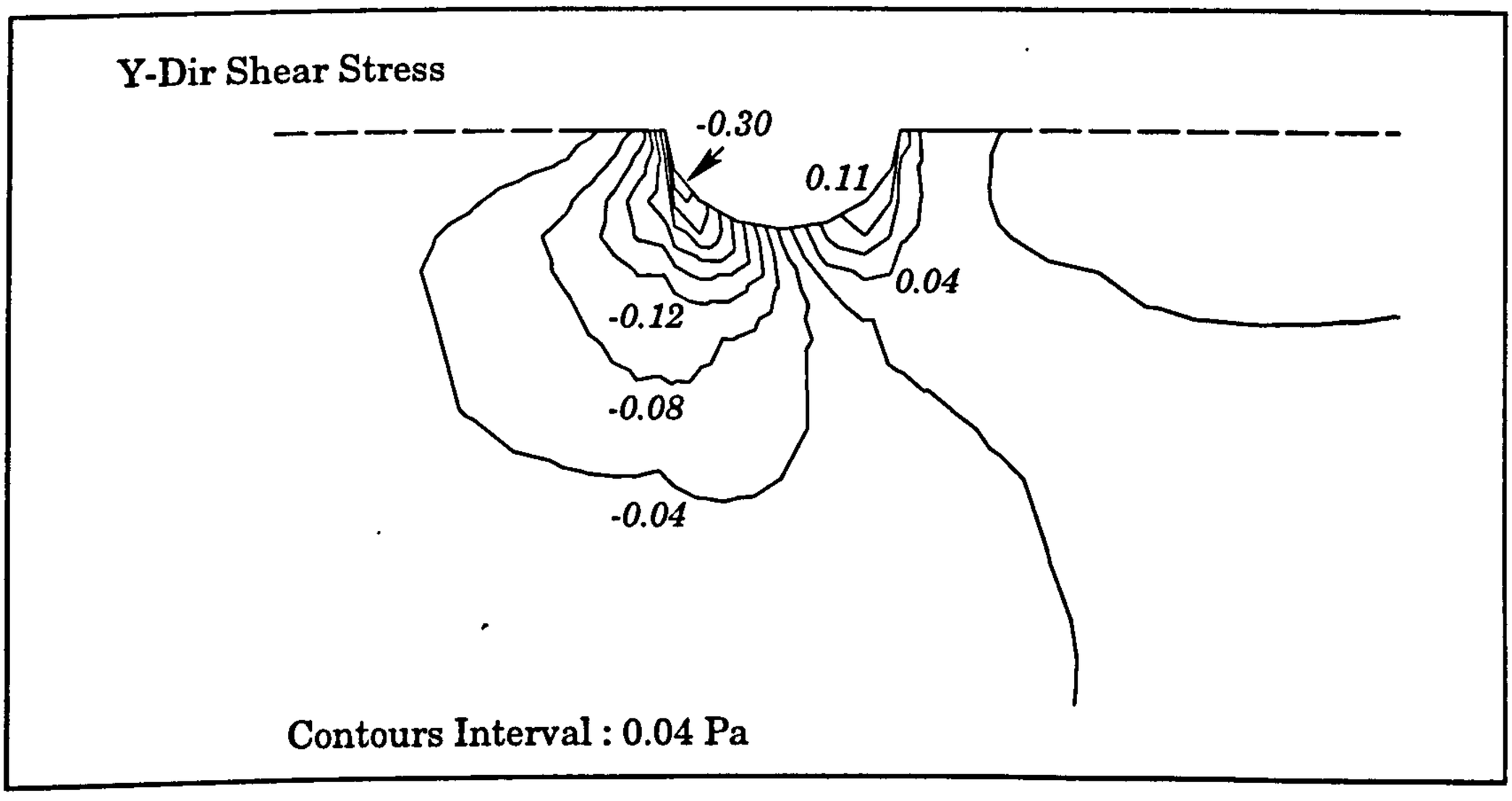

Figure 5.14 : Bed velocity vectors and shear-stress contours (Initial flat-bed)

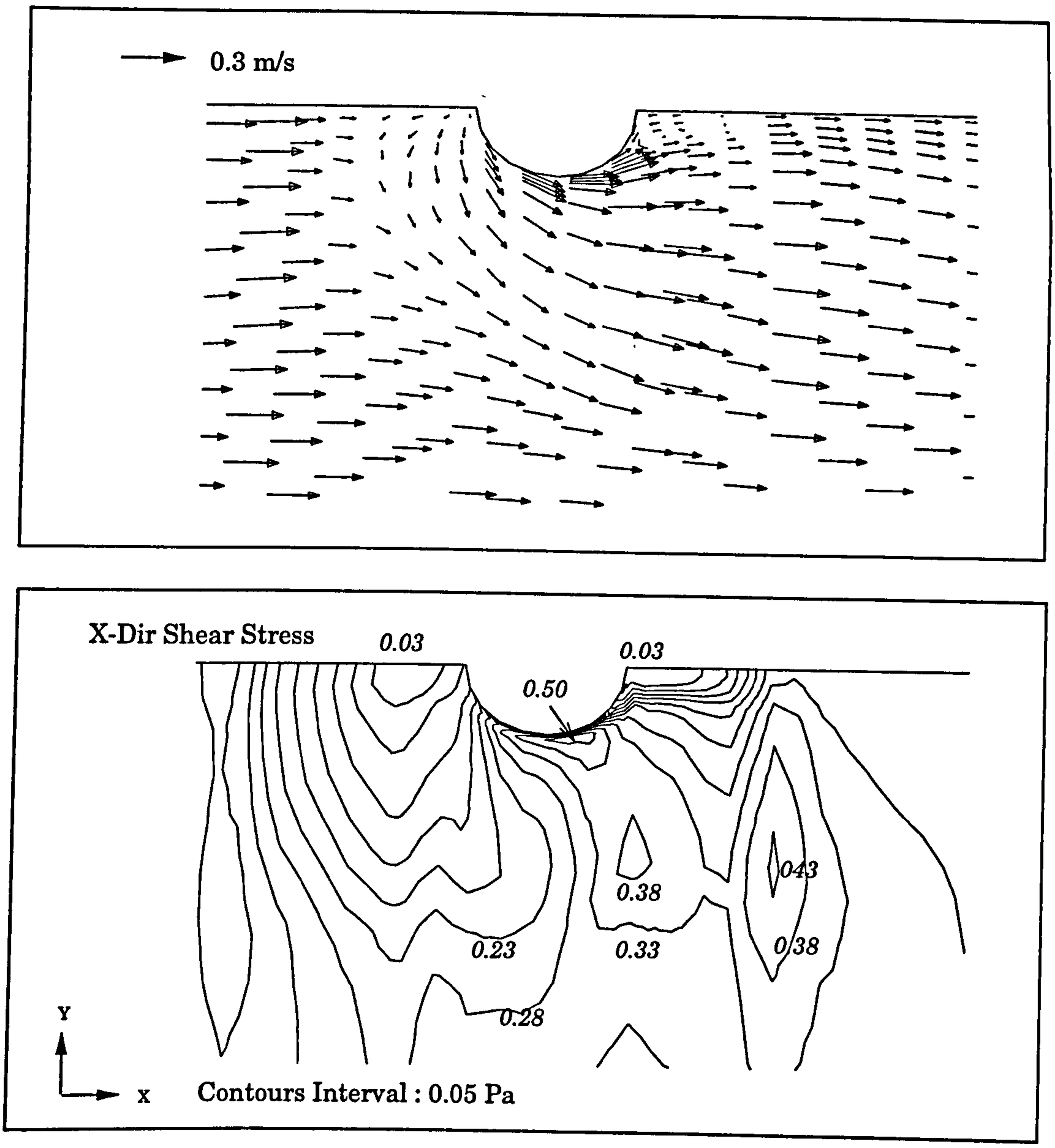

Figure 5.15 : Bed velocity vectors and shear-stress contours (T = 5 mins)

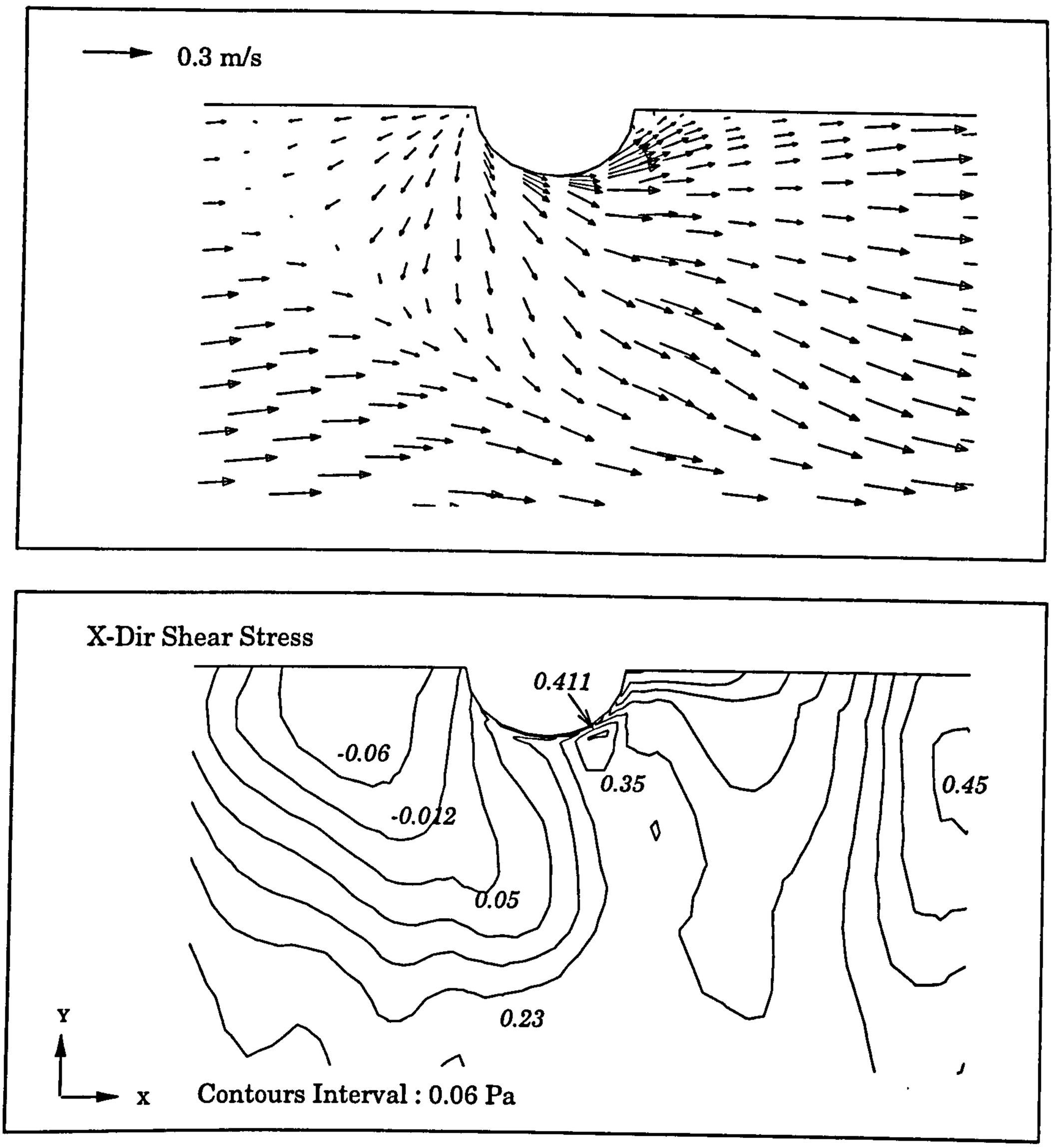

Figure 5.16 : Bed velocity vectors and shear-stress contours (T = 60 mins)

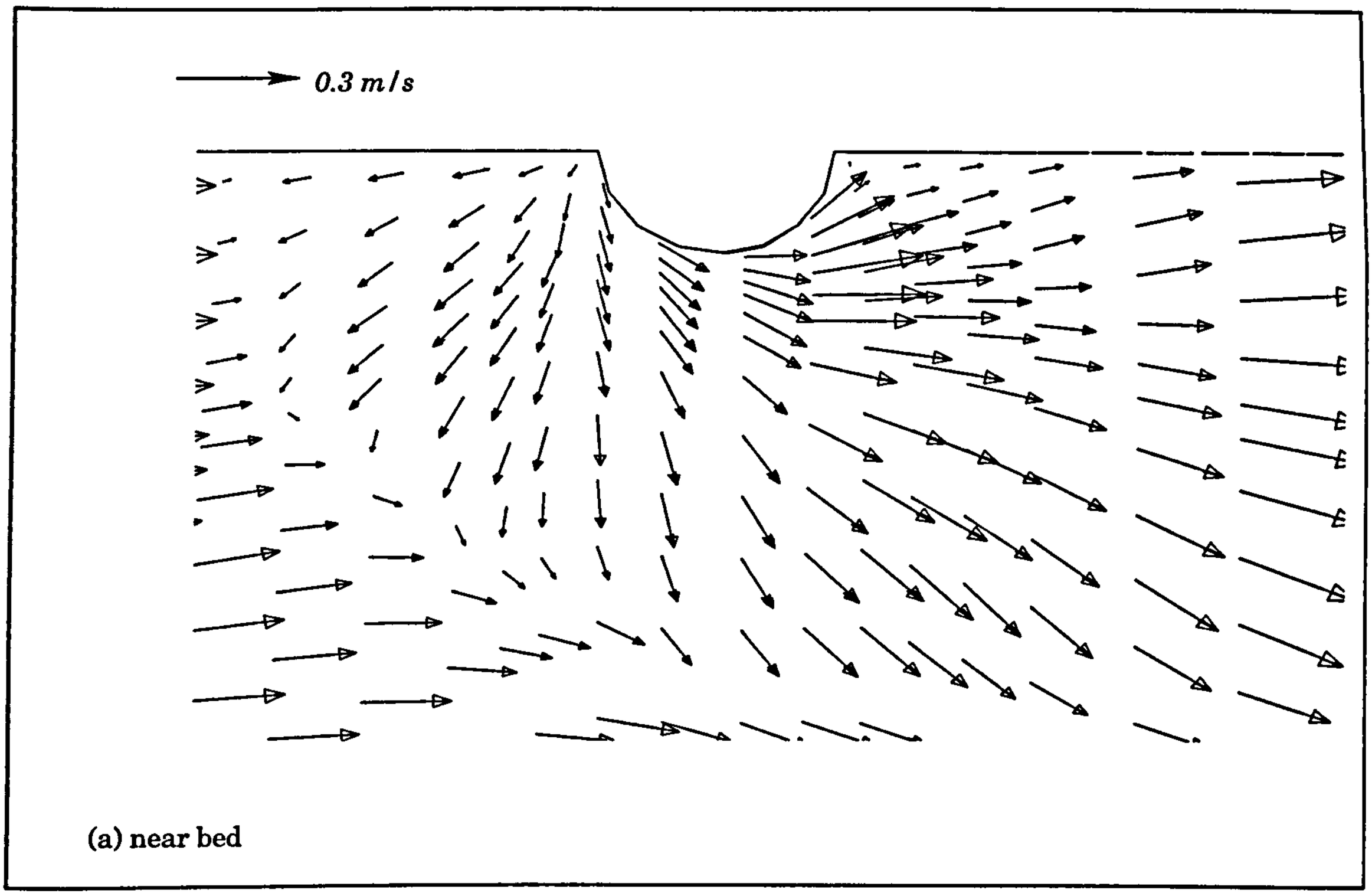

(a) near bed

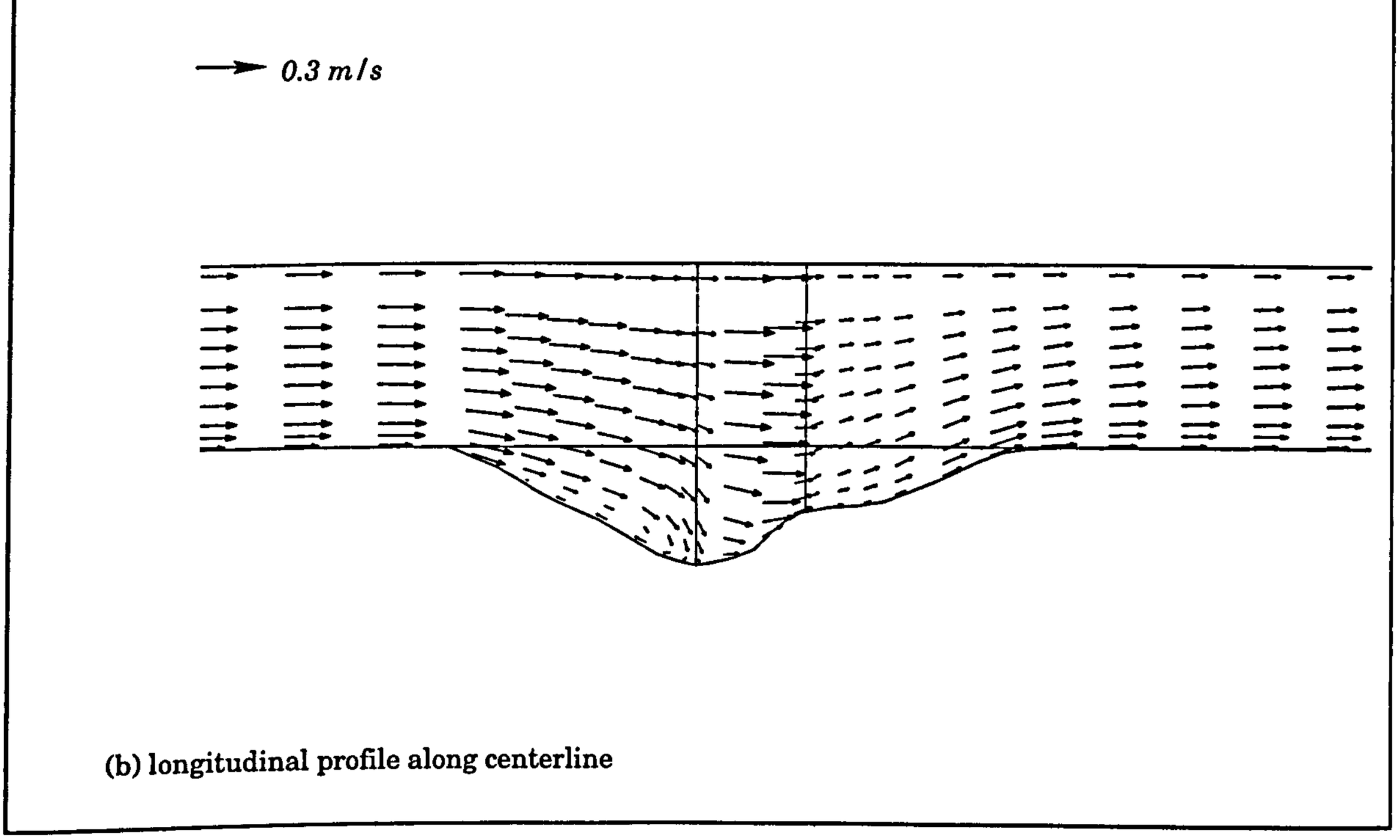

(b) longitudinal profile along centerline

Figure 5.17 : Velocity Vectors (T = 150 mins)

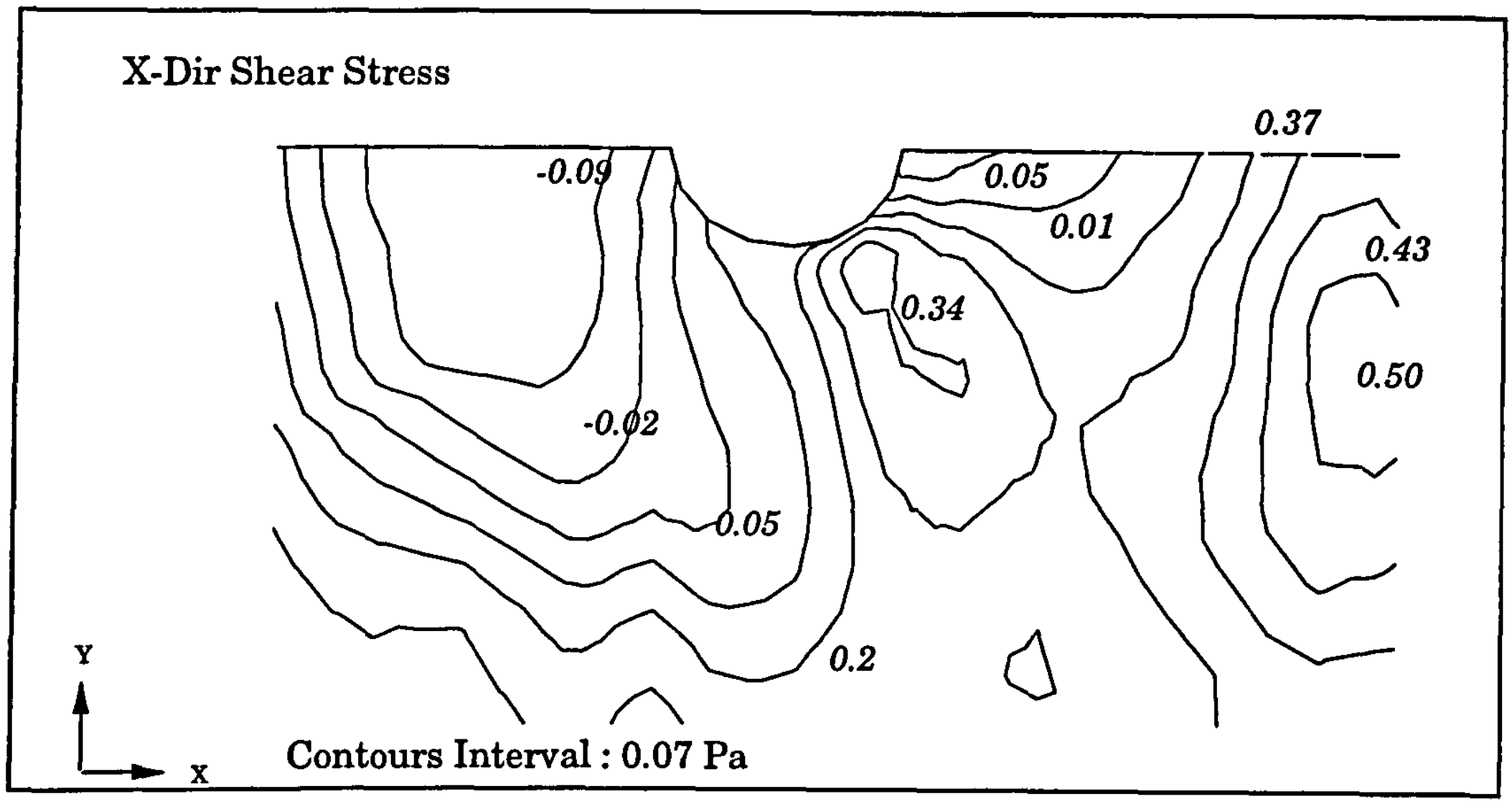

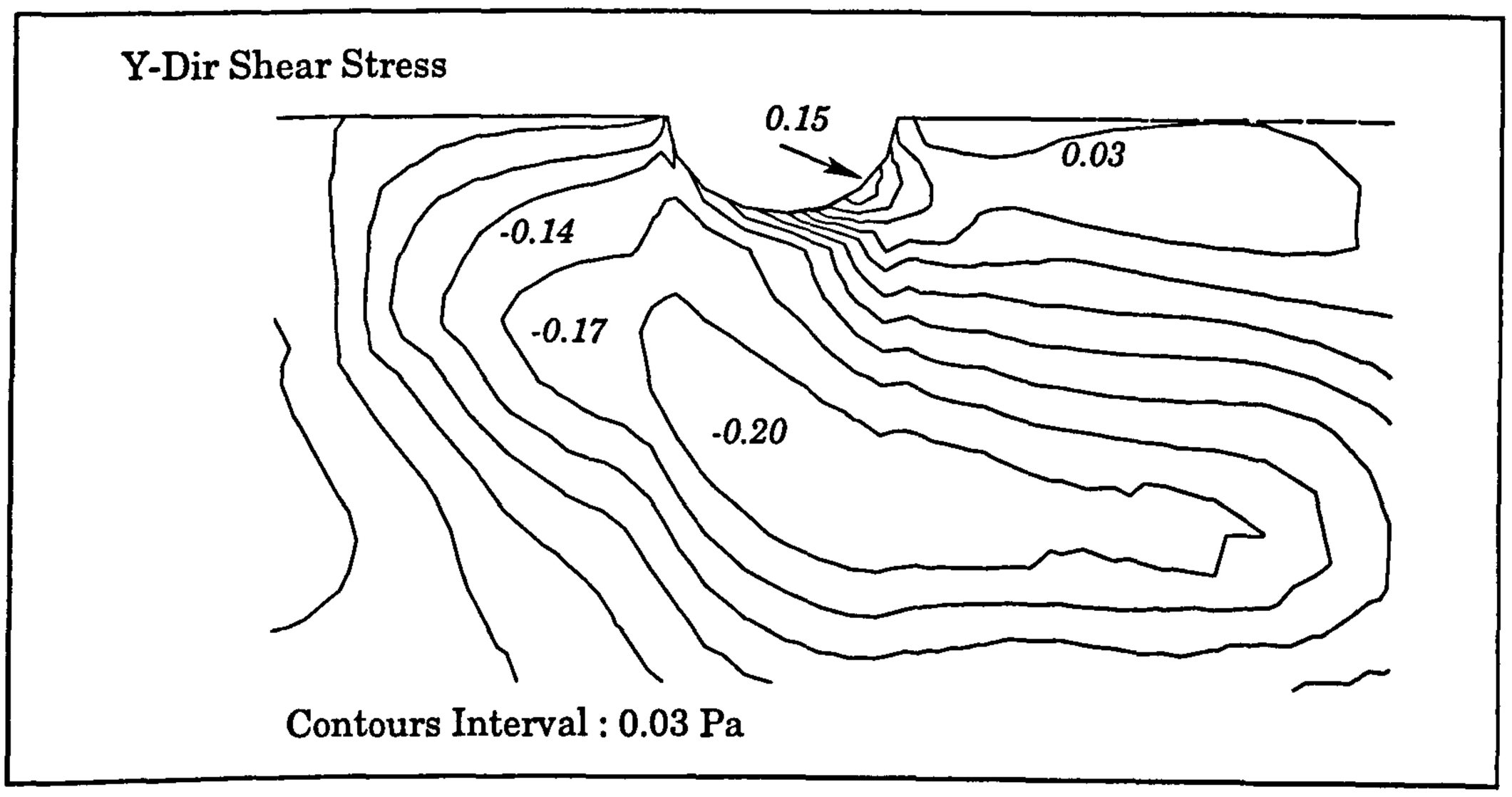

Figure 5.17 (ctn'd) : Bed shear-stress contours (T = 150 mins)

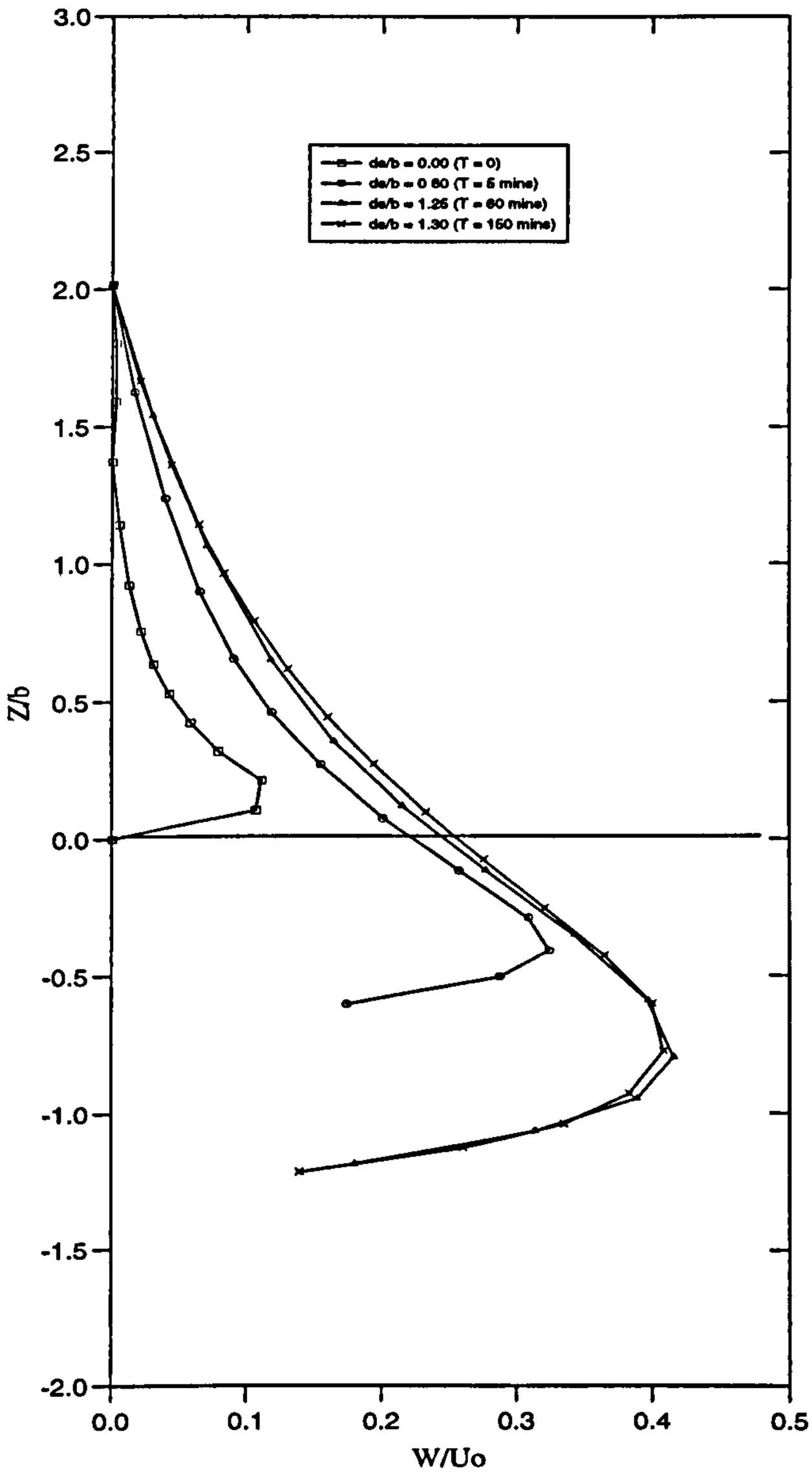

Figure 5.18 : Downflow velocity W in front of pier (Uo = uniform inlet velocity, Z = height above initial bed level, b = diameter of pier)

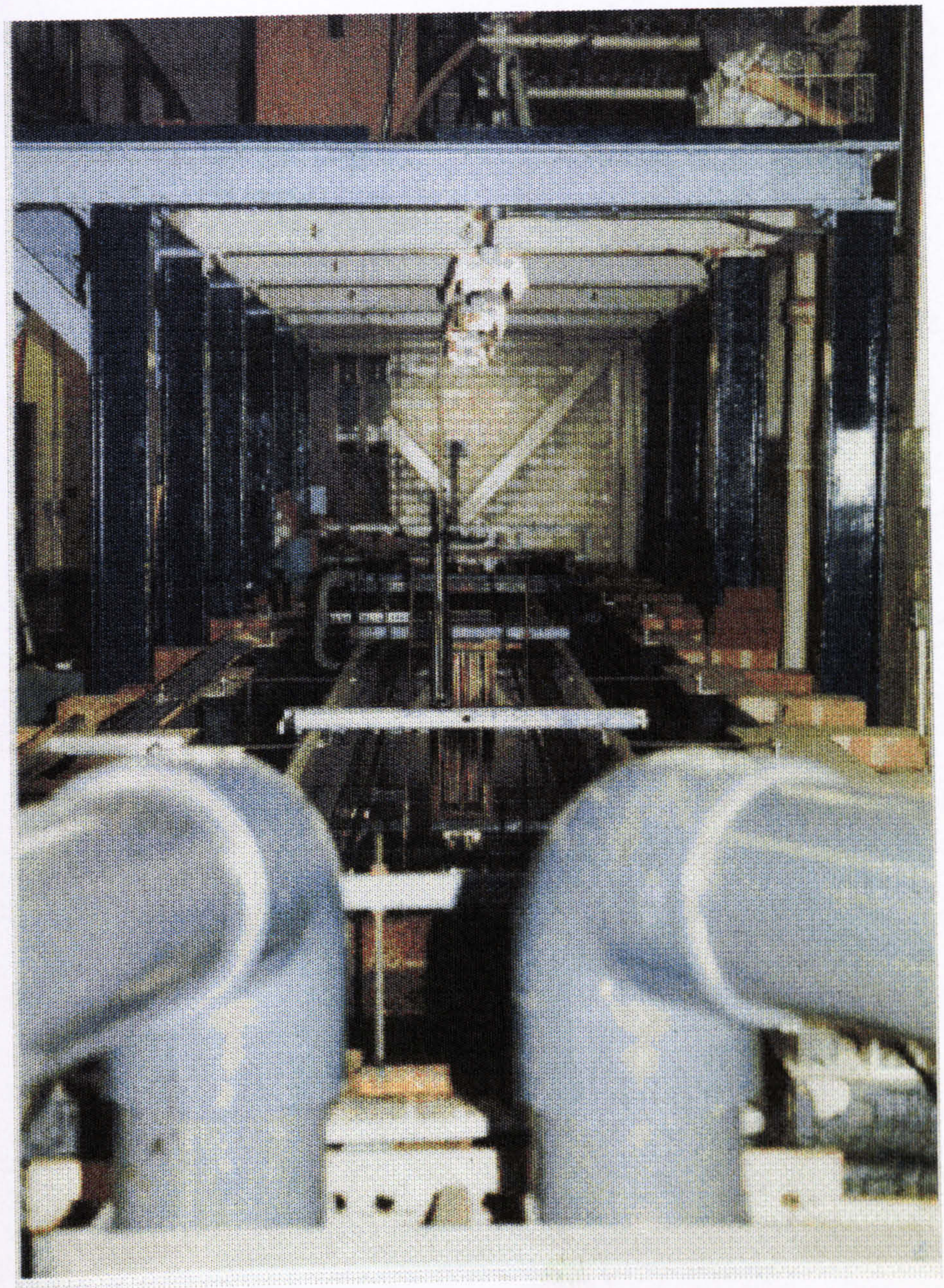

Figure 5.19 : Wave-current flume used in the Experiment

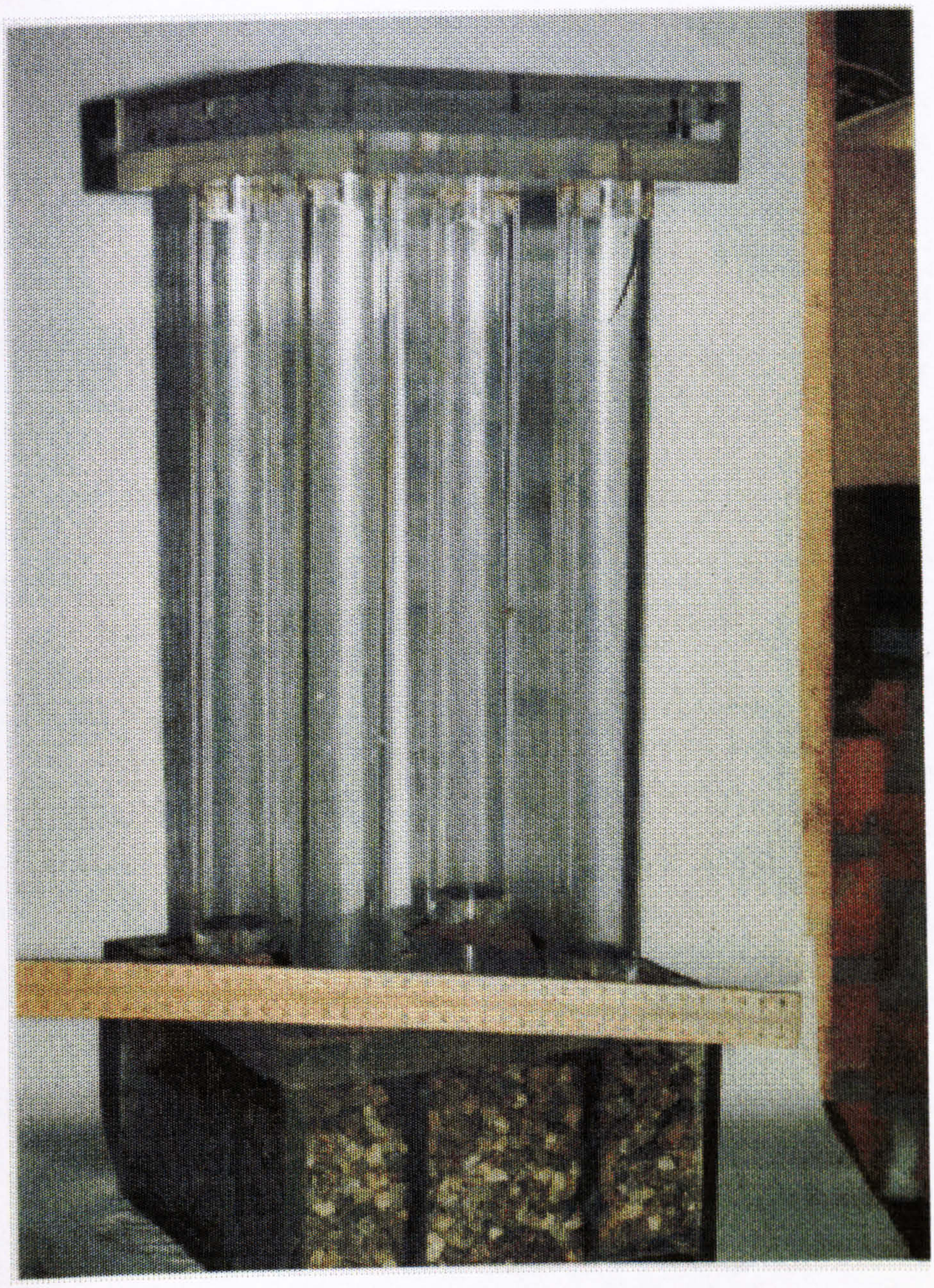

Figure 5.20 : Pier Arrangement (Case A)

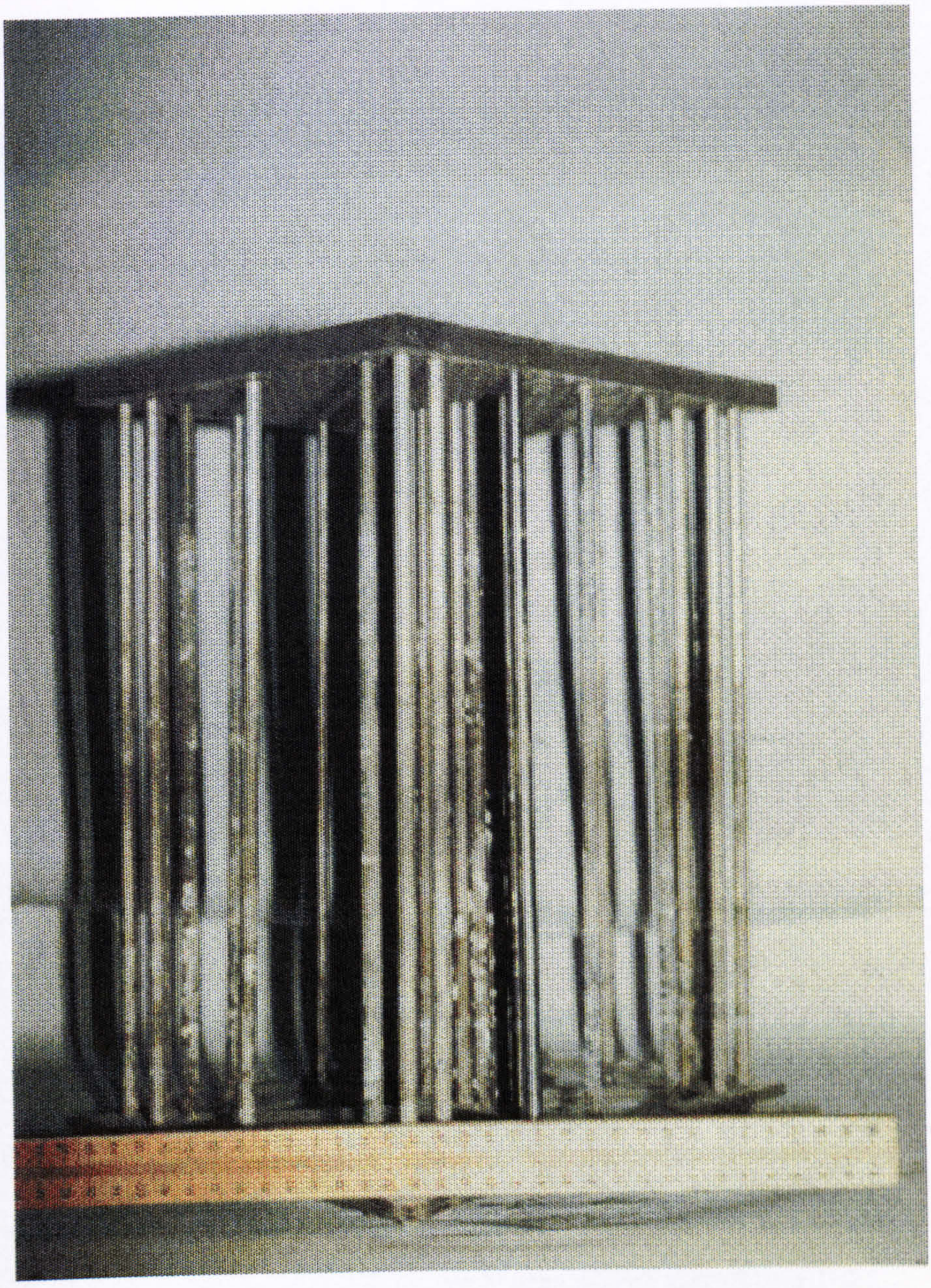

Figure 5.21 : Piers Arrangement (Case B)

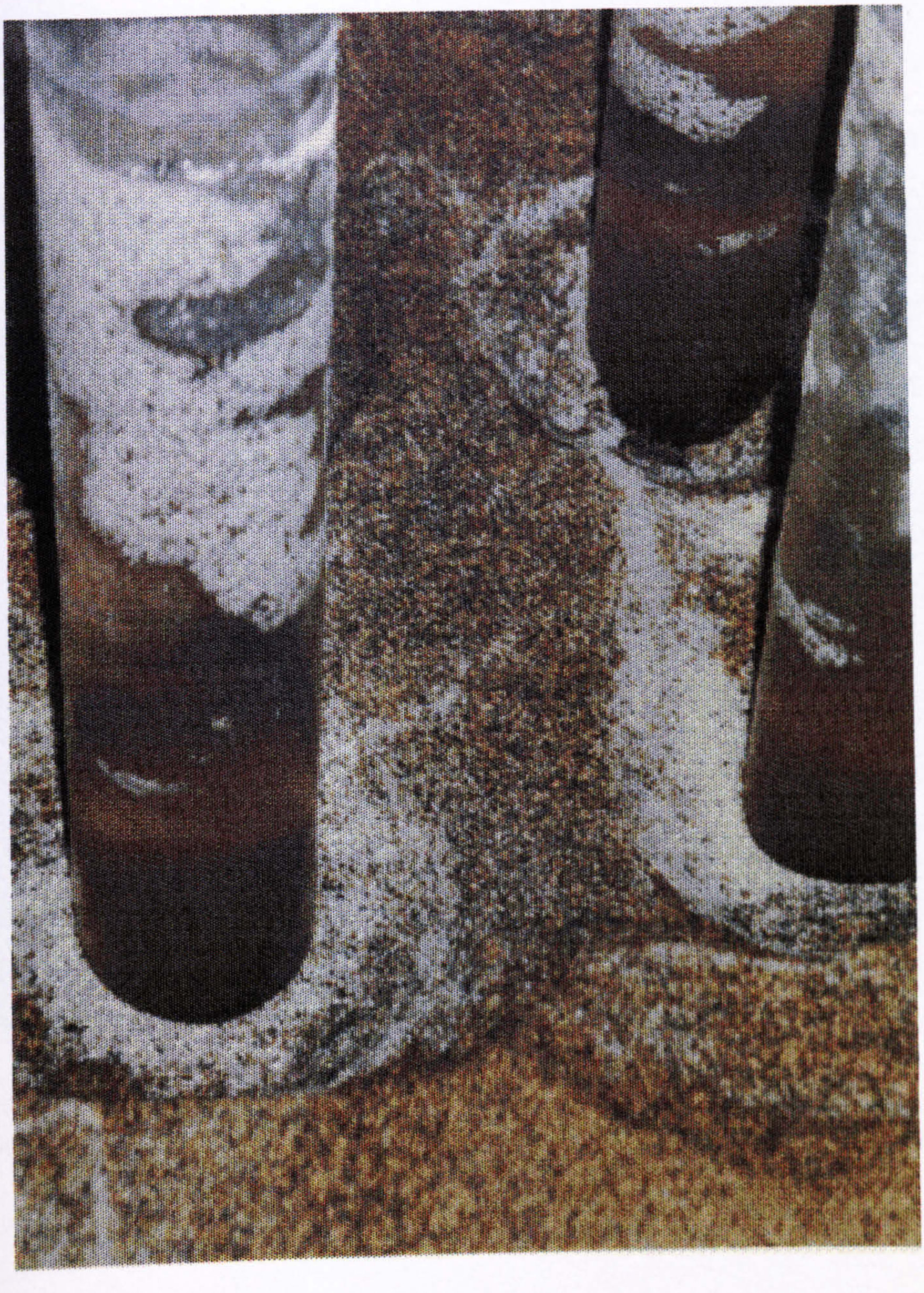

Figure 5.22 : Bed Profile at end of Experiments (Case A)

Figure 5.23 : Bed Profile at end of Experiments (Case B)

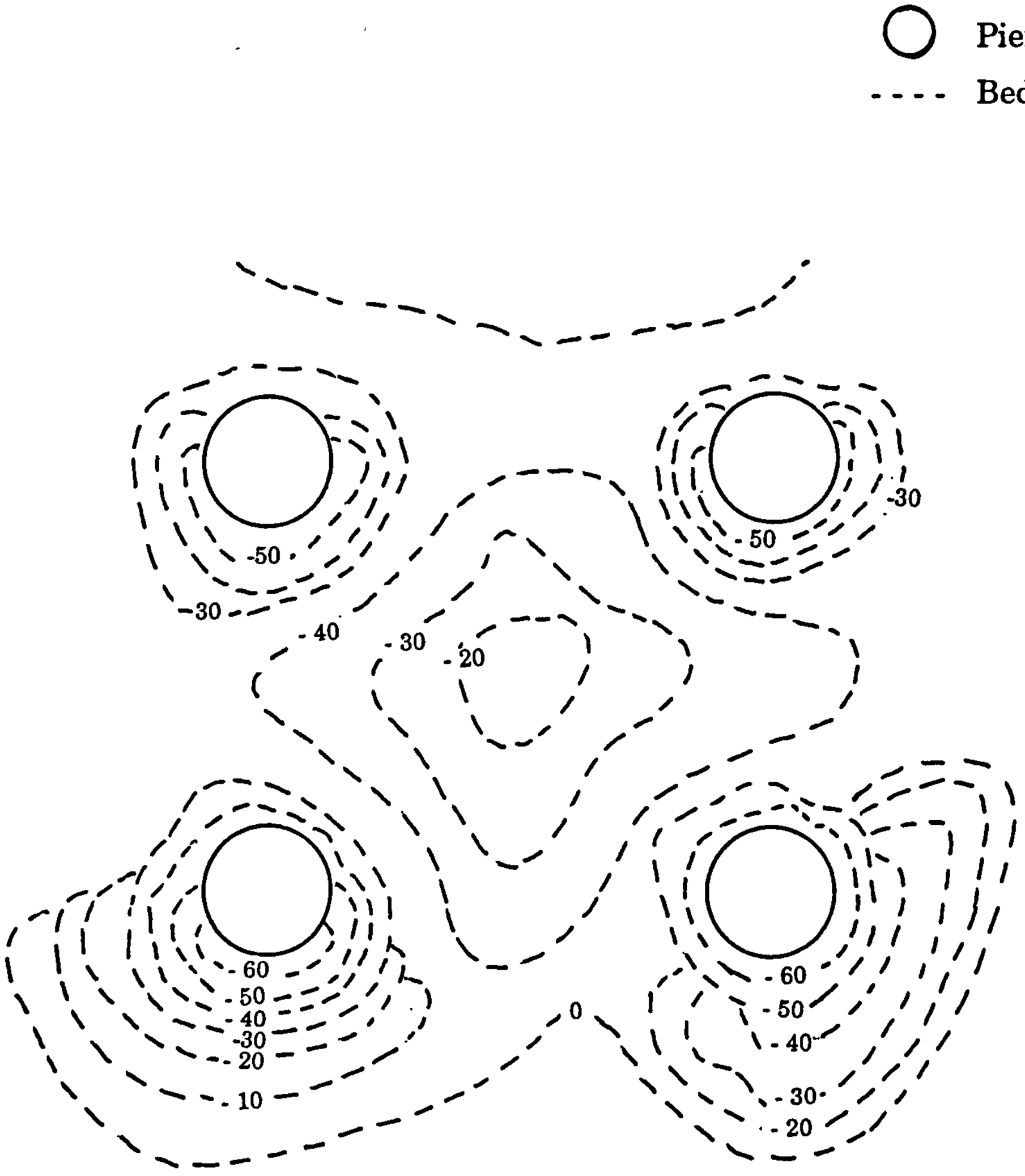

Figure 5.24 : Final Bed Contour (Case A)

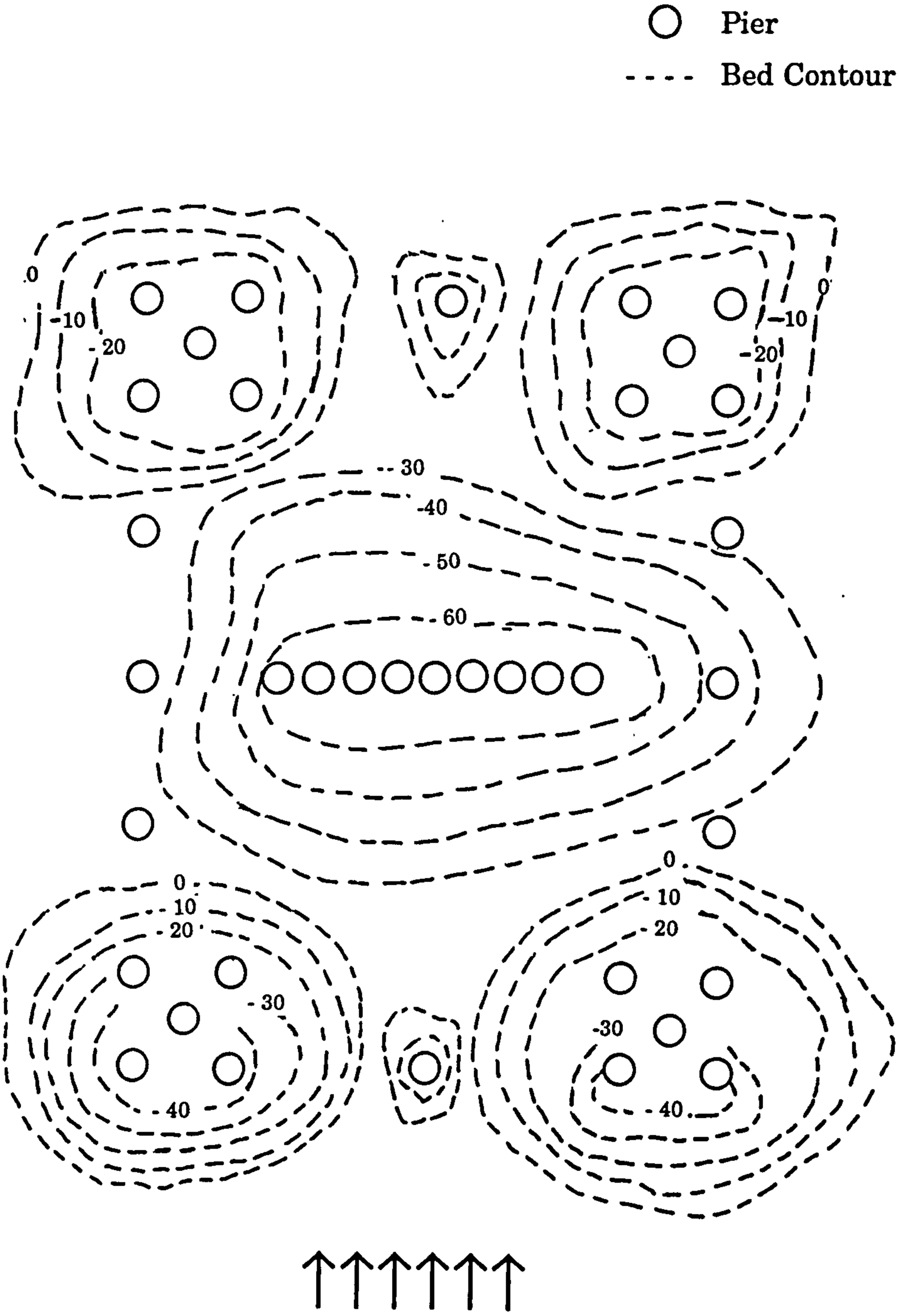

Figure 5.25 : Final Bed Contour (Case B)

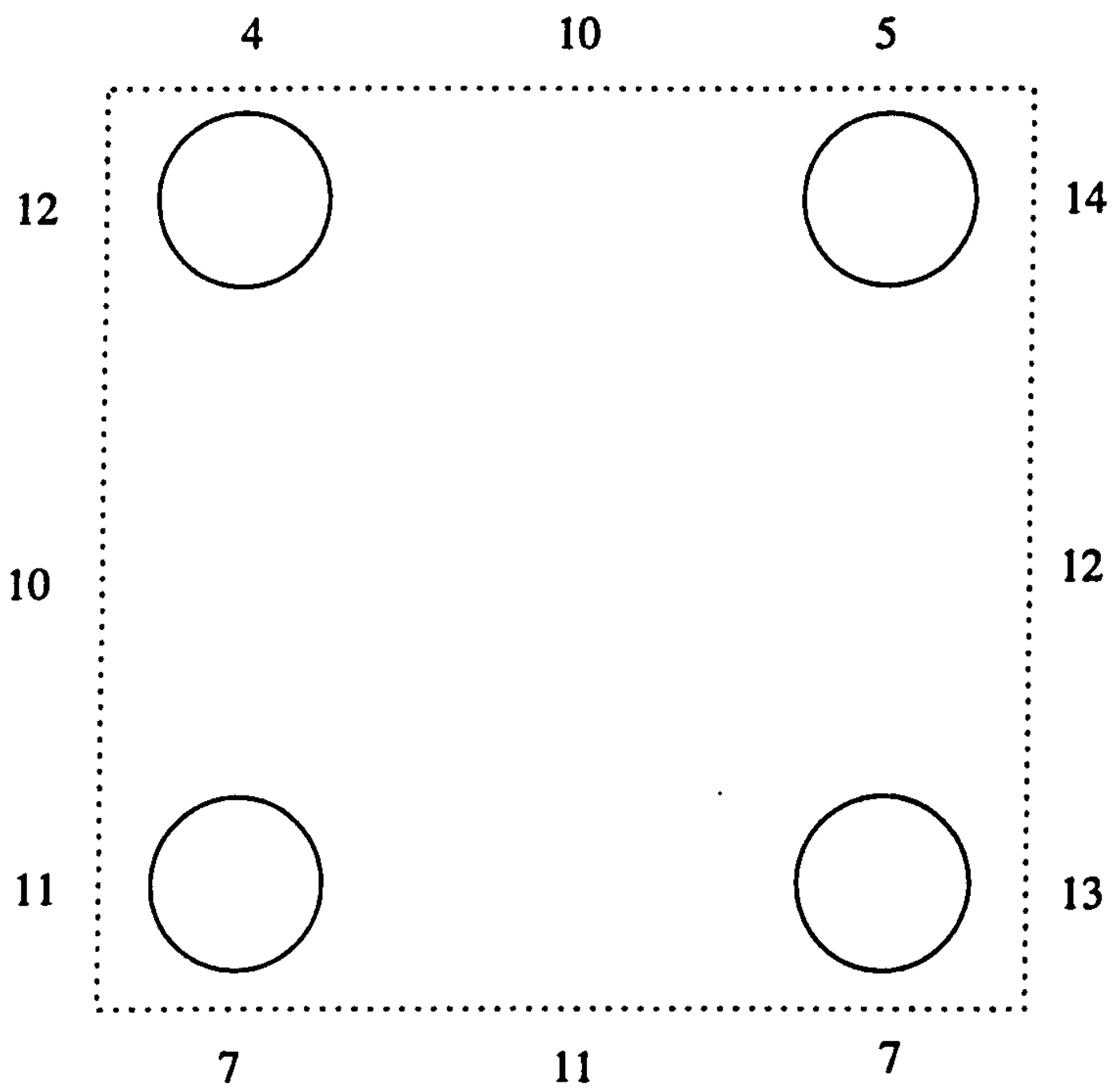

FLOW DIRECTION

Figure 5-26 : Velocity measurements at quasi-equilibrium state (Case A) (Value in cm/s)

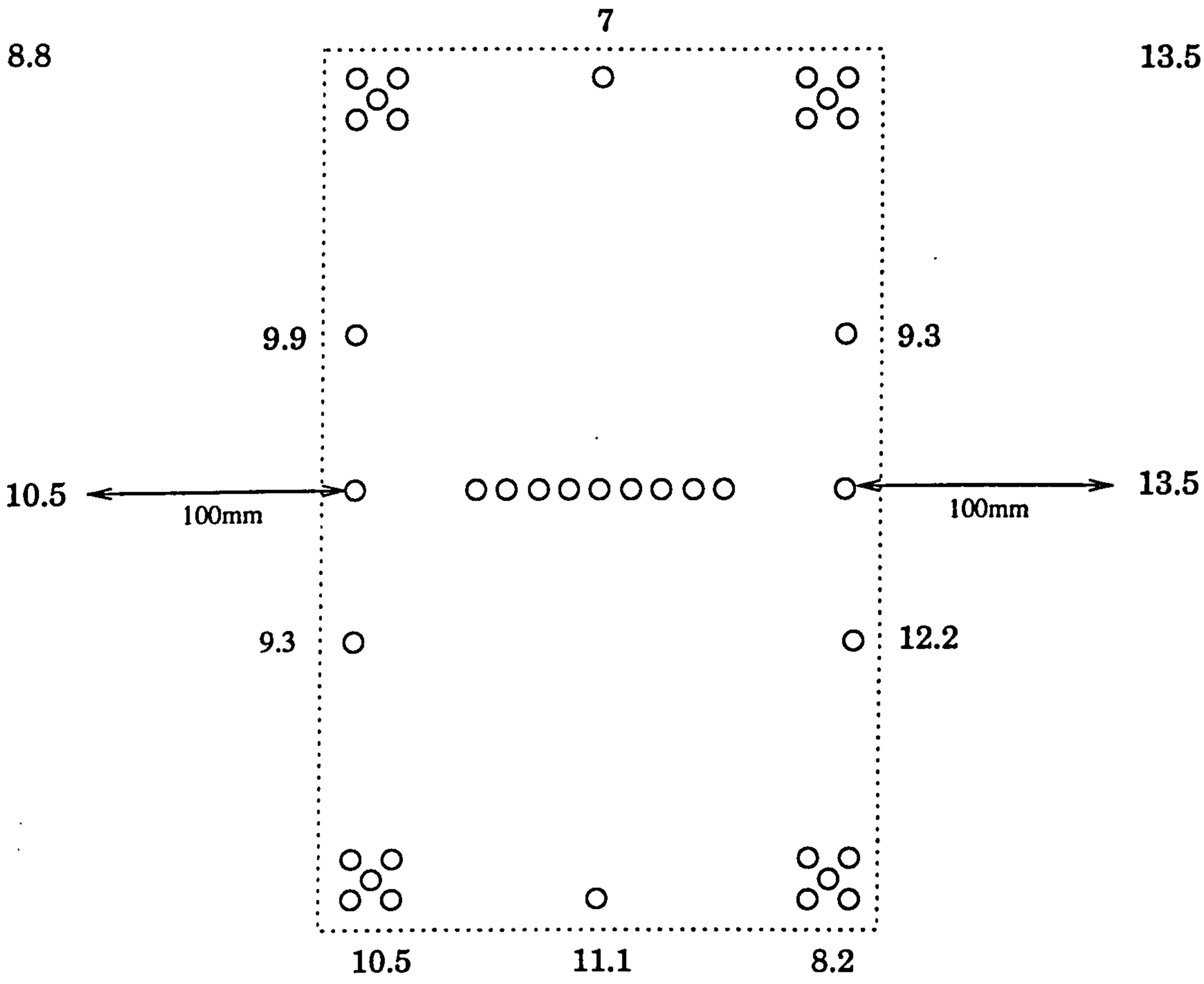

Figure 5-27 : Velocity measurements at quasi-equilibrium state (Case B)
(Value in cm/s)

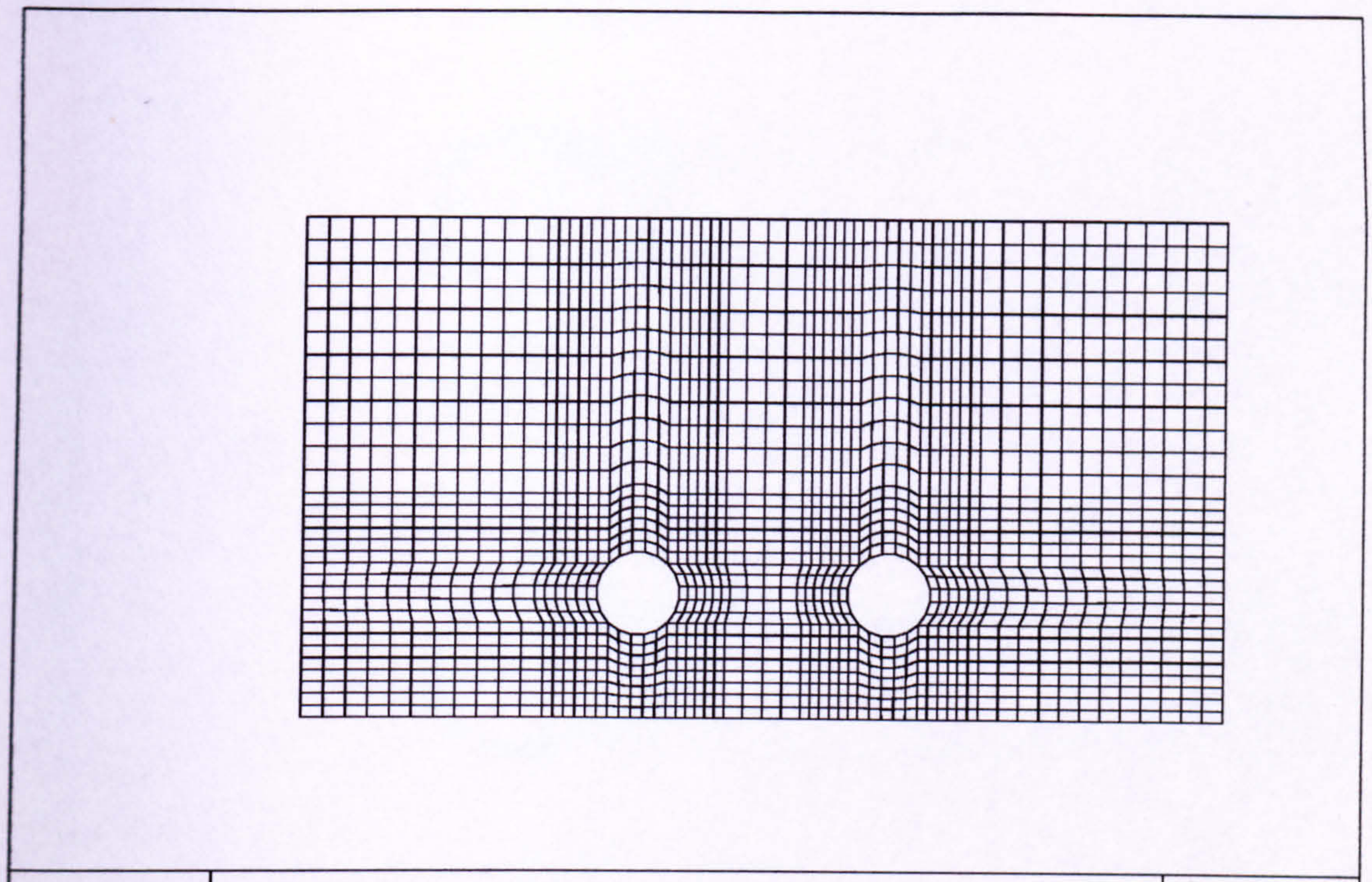

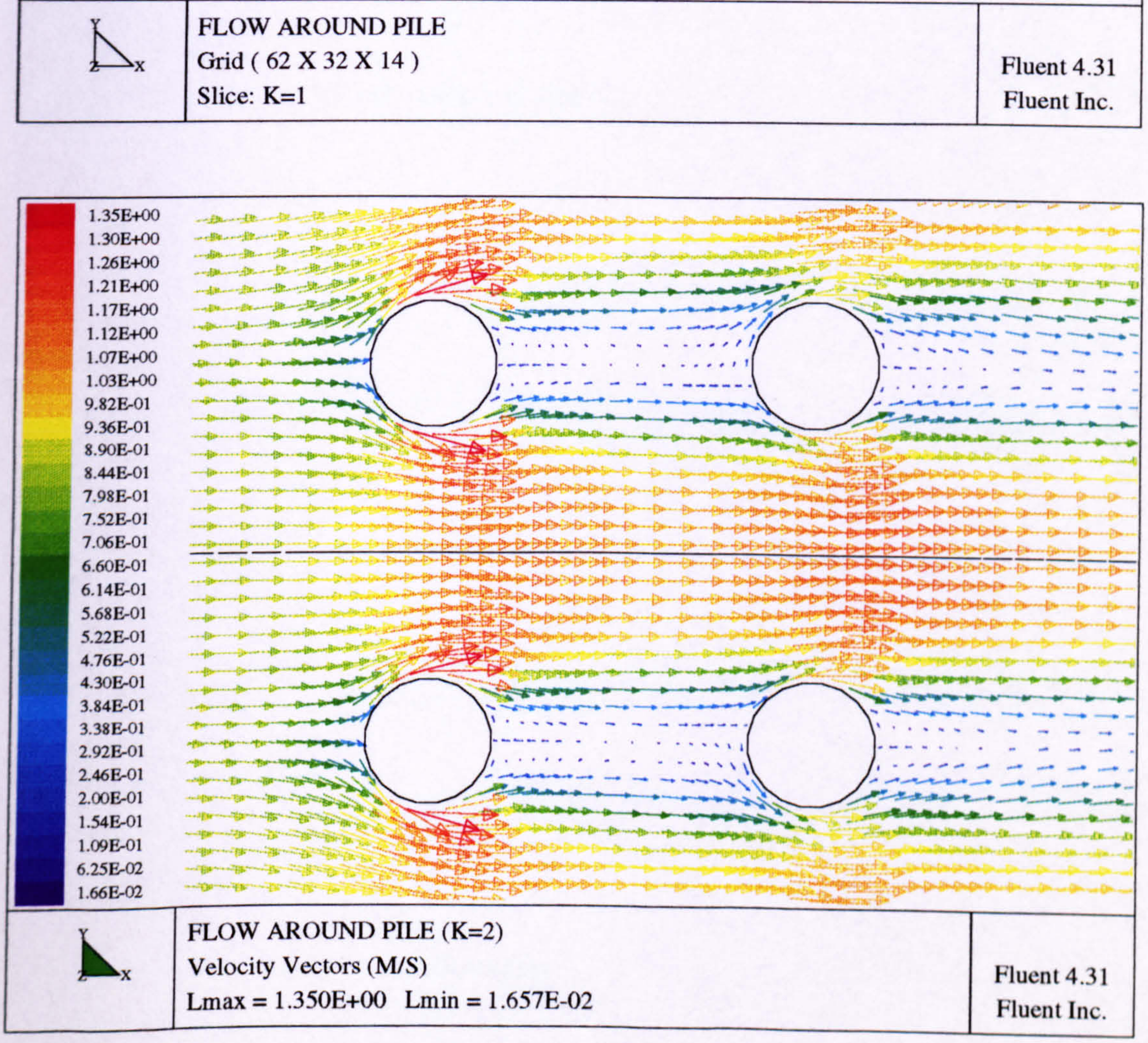

Figure 5.28 : Simulated Flow Around Piers (CASE A)

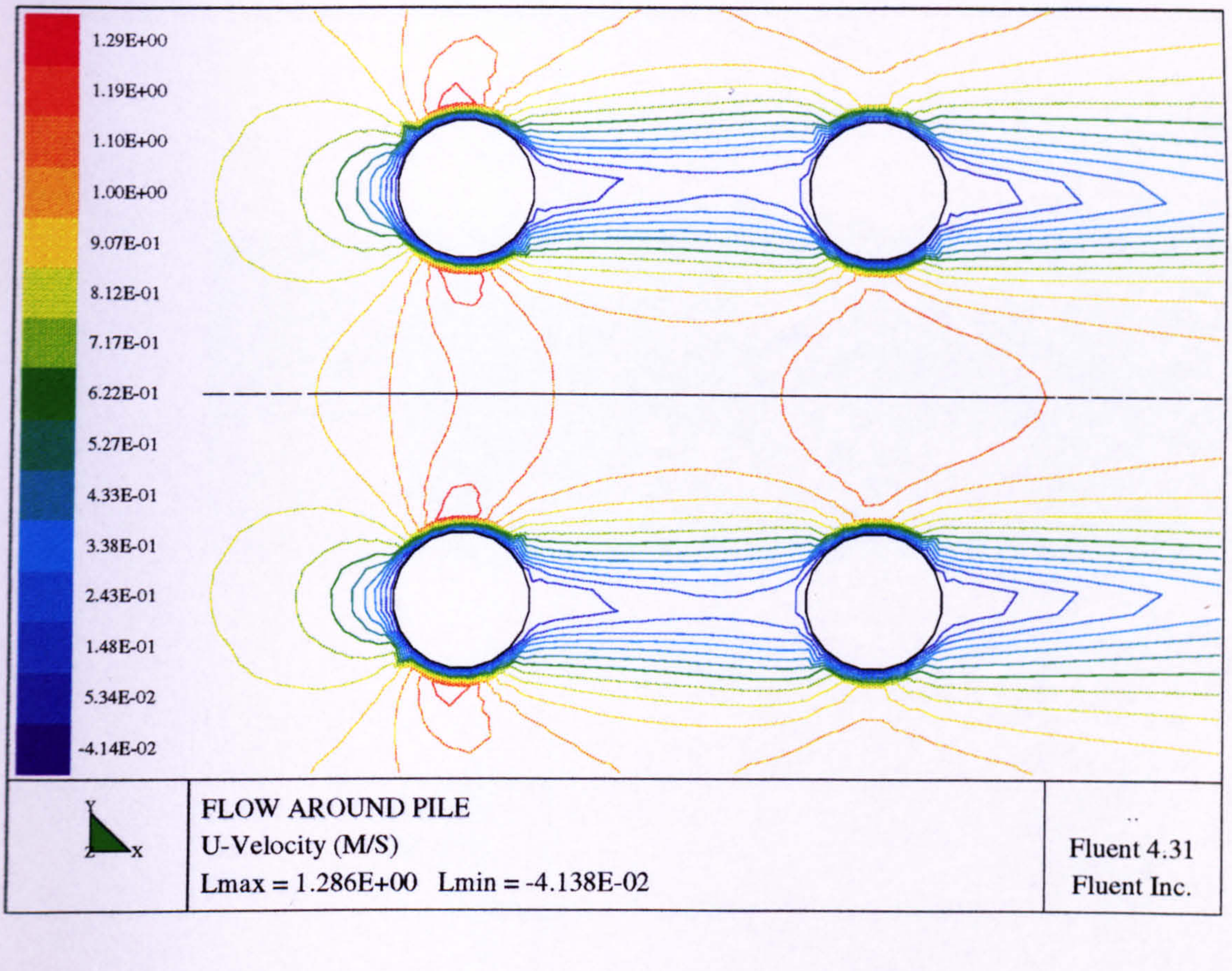

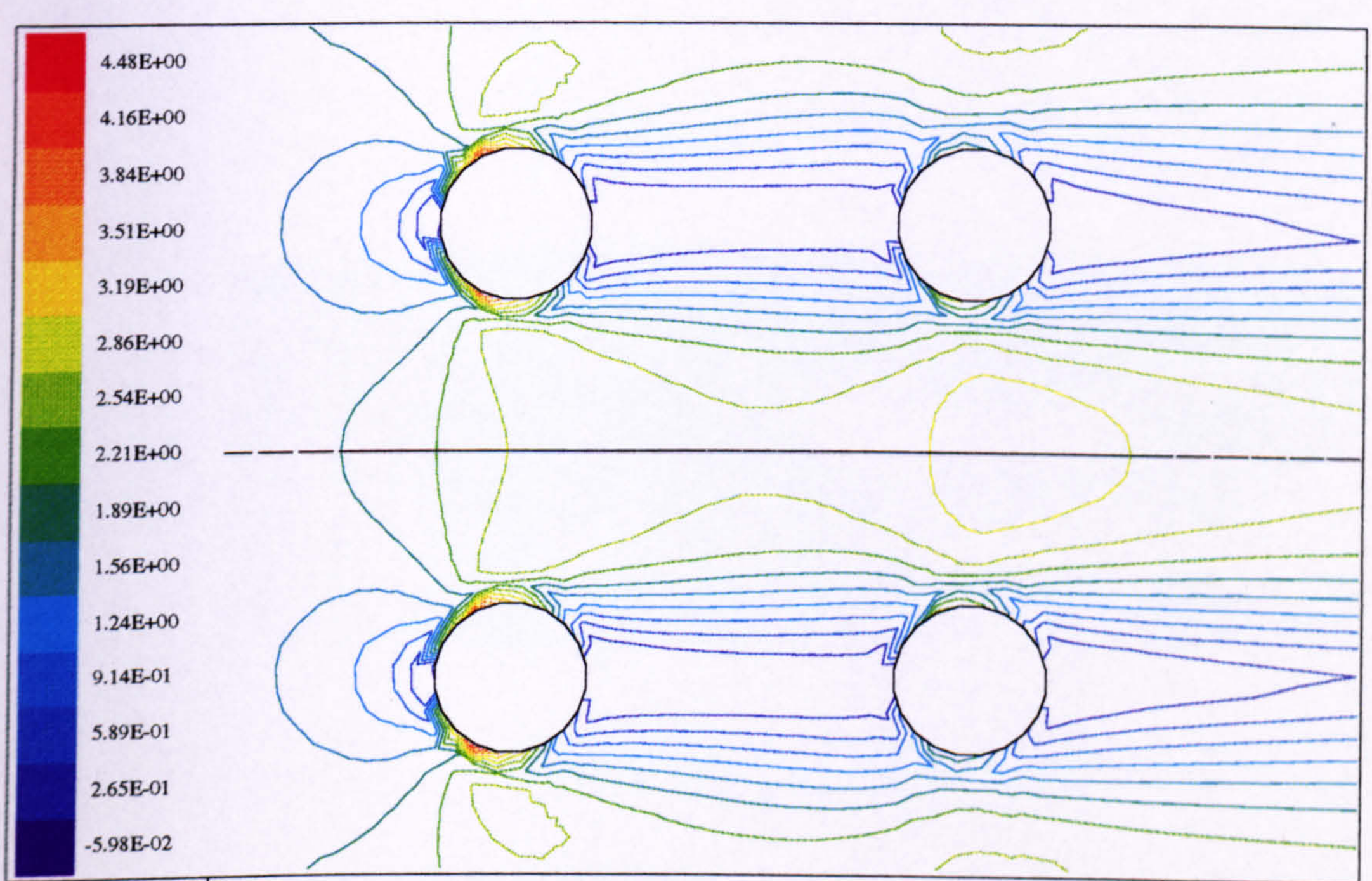

Figure 5.28(ctnd): Simulated Flow Around Piers (CASE A)

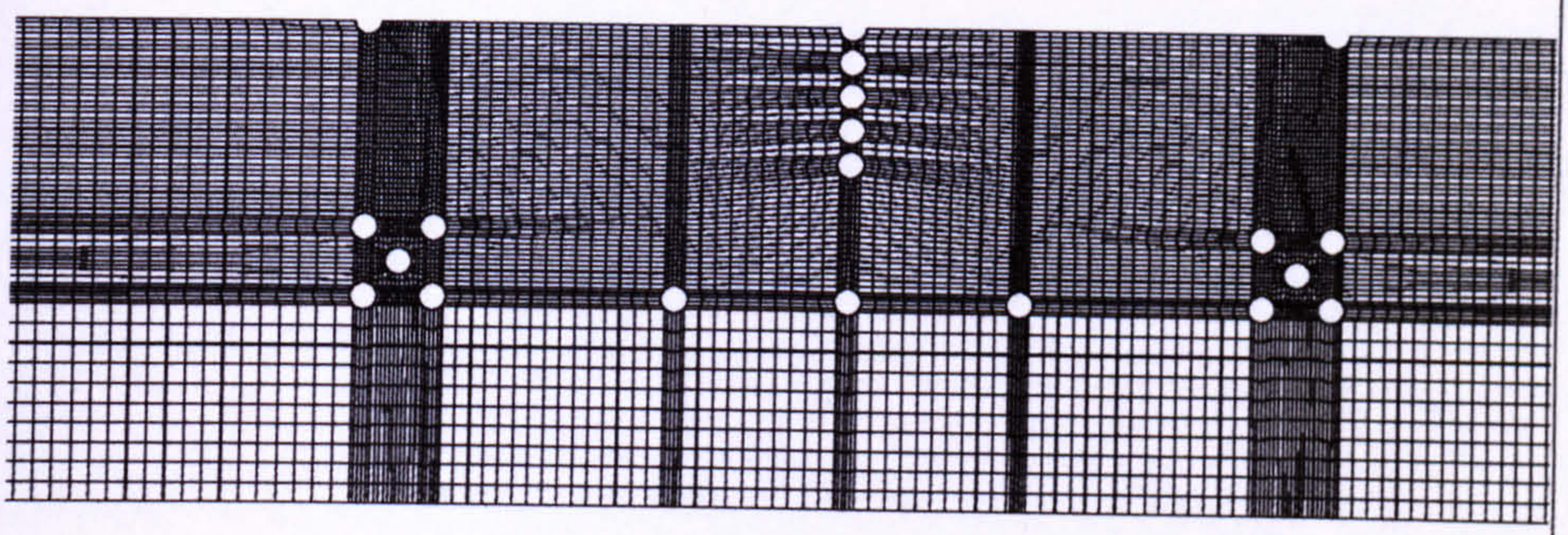

Y—X Z	FLOW AROUND PILE Grid (142 X 9 X 65) Slice: J=1	Fluent 4.31 Fluent Inc.

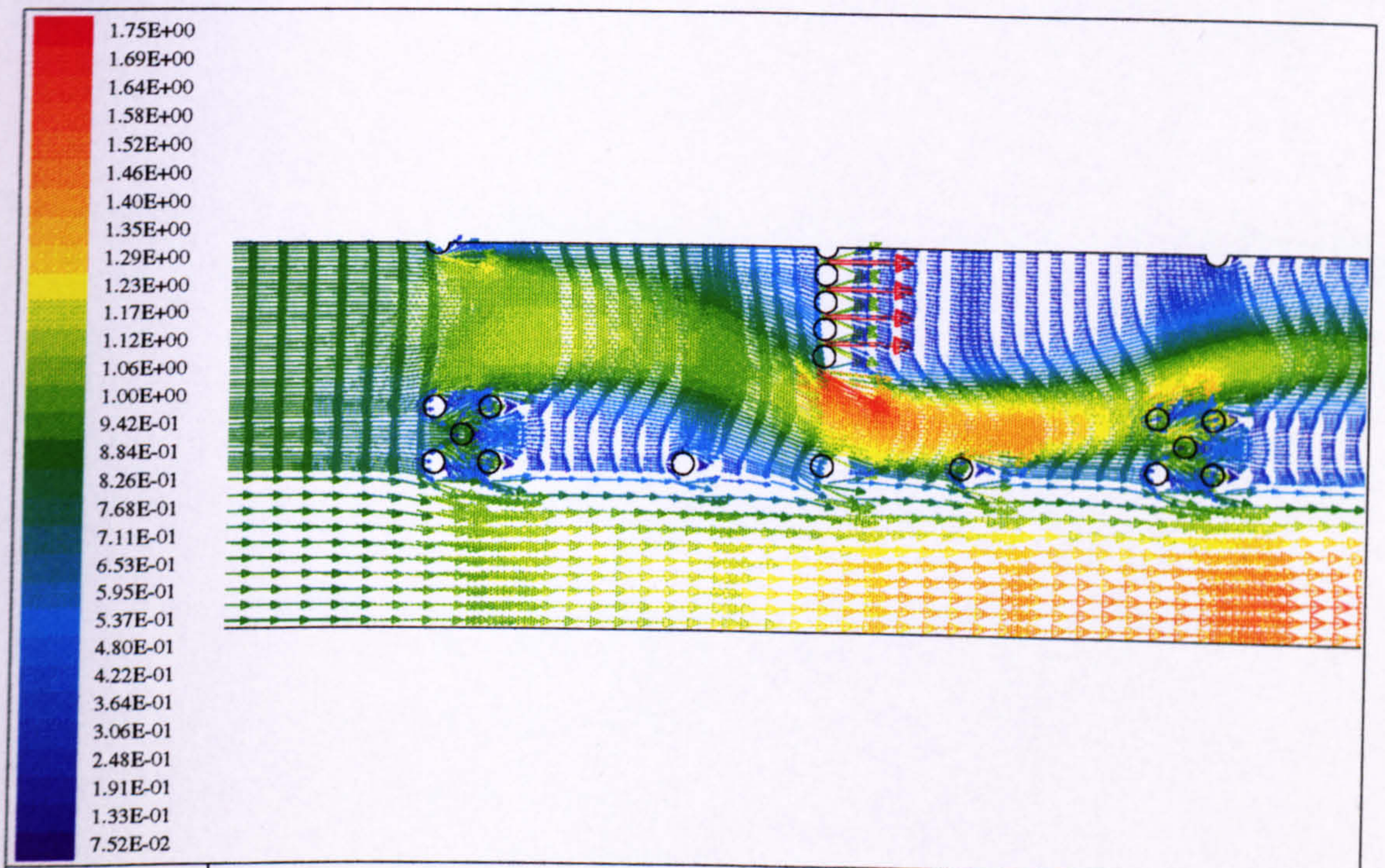

Y—X Z	FLOW AROUND PIER Velocity Vectors (M/S) Lmax = 1.751E+00 Lmin = 7.515E-02	Fluent 4.31 Fluent Inc.

Figure 5.29 : Simulated Flow Around Piers (CASE B)

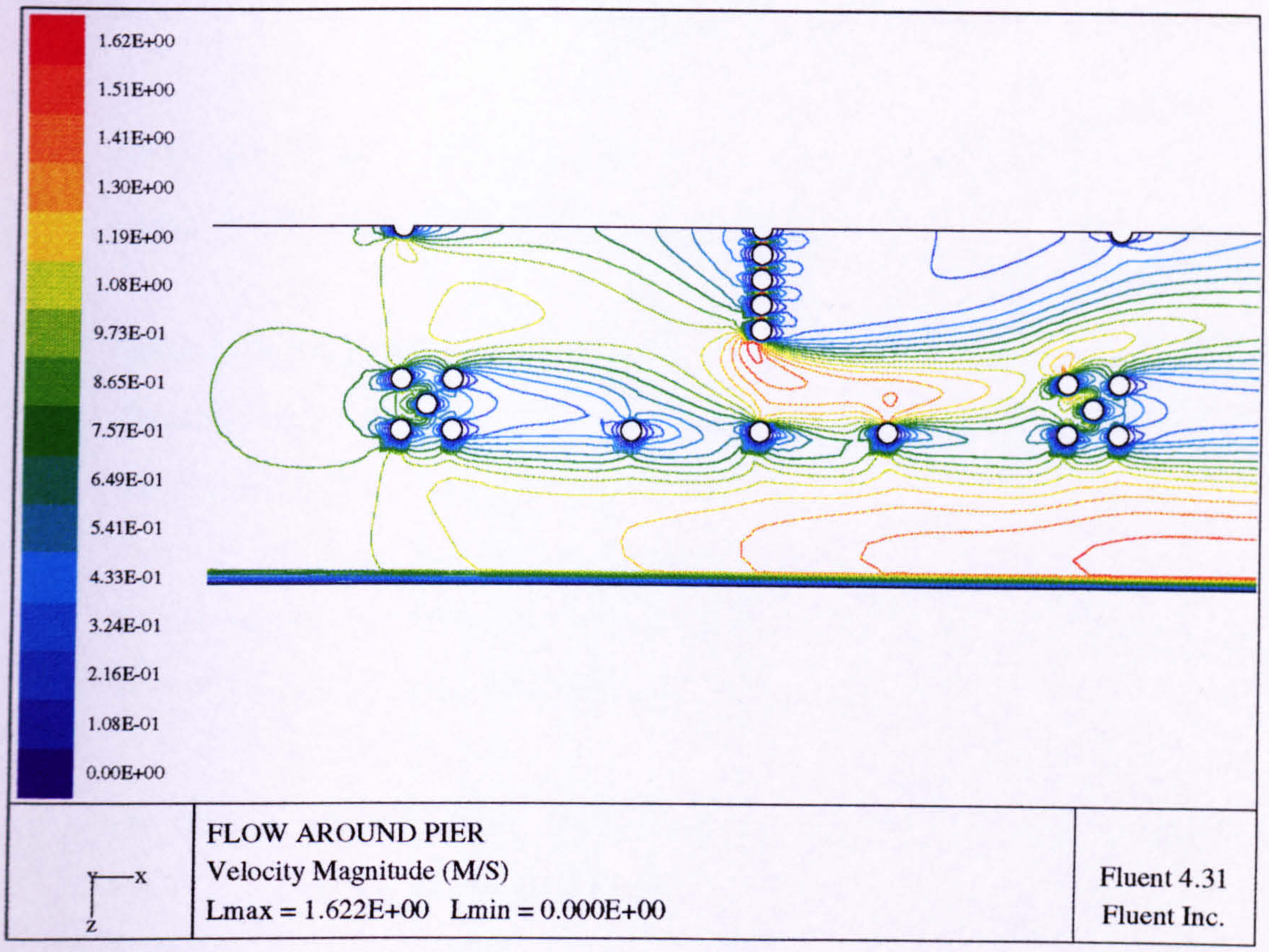

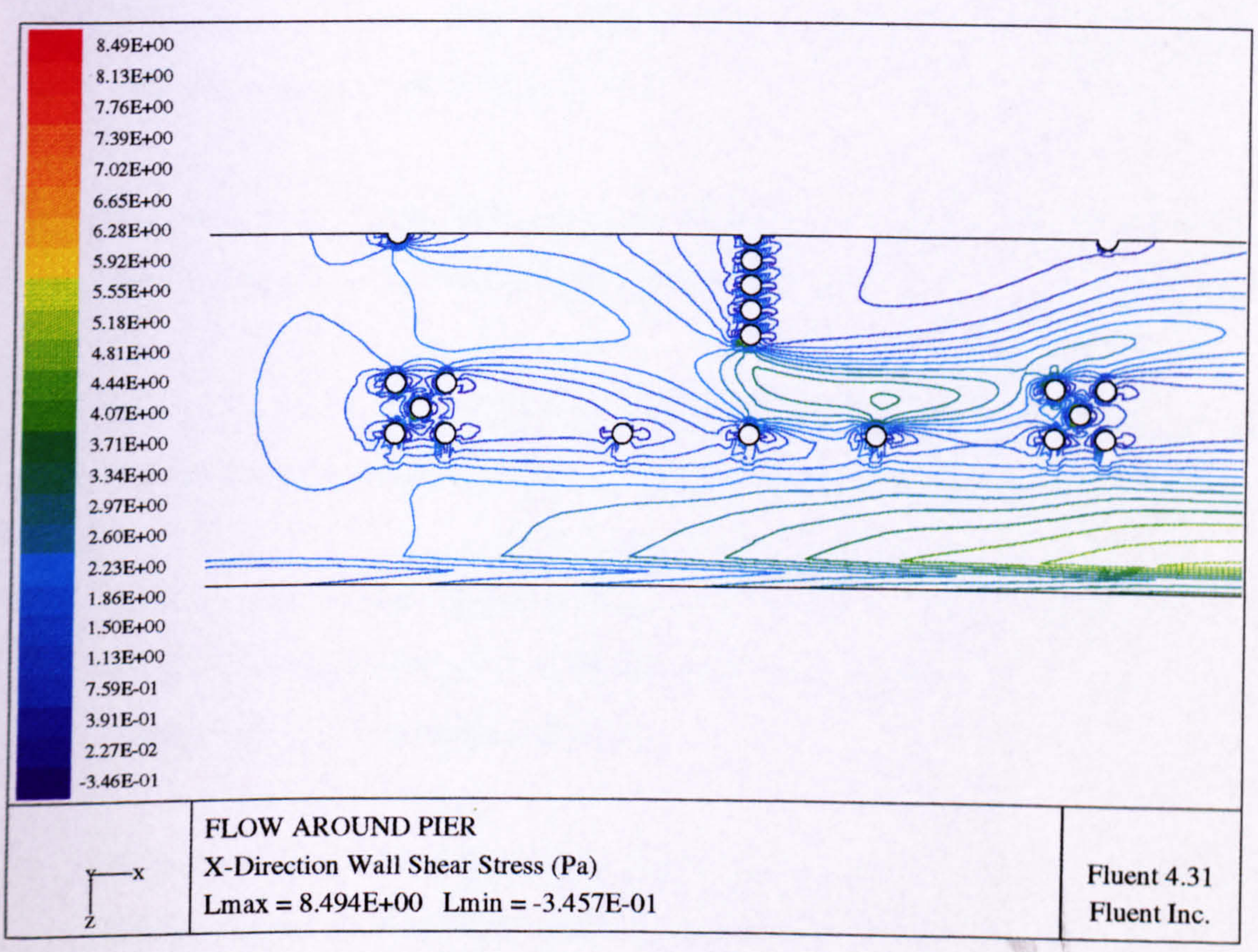

Figure 5.29(ctnd): Simulated Flow Around Piers (CASE B)

REFERENCES

Breusers, H.N.C., Nicollet, G., Shien, H.W. (1977). "Local Scour Around Cylindrical Piers", *J. Hydr Res.*, ASCE, 15(3), 1977, pp. 211 - 252.

Brooks, N.H. (1962), discussion of "Boundary Shear Stress in Curved Trapezoidal Channel" by A.T. Ippen and P.A. Drinker. (Proc. Paper 3273) *J. Hydr. Div*, ASCE, Vol 88. HY3, May 1963, pp. 327 - 333.

Butterworth, G. (1996), "Investigation of Local Scour Caused by Currents and Waves", *B.Eng. Thesis*, University of Liverpool.

Dargahi, B. (1990). "Controlling Mechanism of Local Scouring" , *J. Hydr. Engrg*, ASCE, Vol 116, No. 10, pp. 1197 - 1214.

Dargahi, B. (1982). "The Turbulent Flow Field Around a Circular Cylinder" , *Experiments in Fluids*, 8, pp. 1-12

Johnson, P.A. (1995). "Comparison of Pier-Scour Equations Using Field Data", *J. Hydr. Engrg.*, ASCE, Vol 121, No. 8, pp. 626 - 629.

Lim, S.Y., (1985) "Scour and particle diffusion caused by water jets" PhD Thesis, University of Liverpool.U.K.

Melville B.W. (1988), "Scour at Bridges", Chapter 15 of Civil Engineering Practise 2 (*Ed.* Cheremisinoff, P. N., Cheremisinoff, N.P., and Cheng, S.L.) ,Technomic Publishing Co., Pennsylvania U.S.A.

Melville, B.W. and Raudkivi, A.J., (1977). "Flow characteristics in Local Scour at Bridge Piers," *J. Hydr. Research*, ASCE, Vol 15, pp. 373-380.

Olsen, N.R.B. (1991). "A Three-Dimensional Numerical Model for Simulation of Sediment Movement in Water Intake", *Dr. Ing. Dissertation*, The Norwegian Institute of Technology, Trondheim, Norway.

Olsen, N.R.B., Melaaen, C.M. (1993). "Three-Dimensional Calculation of Scour Around Cylinders", *J. Hydr. Engrg*, ASCE, Vol 119, No. 9, pp. 1048 - 1054.

Penson, S. (1996), "Investigation Of the Flow Around a Bridge pier Using the FLUENT package". *M.Sc.(Eng) Thesis*, University of Liverpool.

Raudkivi, A.J. (1986). "Funtional Trends of Scour at Bridge Piers", *J. Hydr. Engrg*, ASCE, Vol 112, No. 1, pp. 1 - 12.

Raudkivi, A.J. and Ettema, R. (1977). "Effect of Sediment Gradation on Clear Water Scour", Proceedings ASCE, Vol 103, No HY10, pp. 1209 - 1213.

Rijn L. van, (1984). "Sediment Transport" (in three part). *J. Hydr. Engrg*, ASCE, Vol 110(10,11,12).

Vanoni, V.A., (ed), (1975). "Sedimentation Engineering", ASCE Manual No. 54, New York: ASCE.

Yanmaz, A. M., Altinbilek, H.D. (1991), "Study of Time-Dependent Local Scour Around Bridge Piers", *J. Hydr. Engrg*, Vol 117, No. 10, pp. 1247 - 1268.

Yanmaz, A. M. (1994). - Personal Correspondence (1994)

CHAPTER

CHAPTER 6

INVESTIGATION OF THE FLOW PATTERN AROUND SPUR DYKES

6.1 INTRODUCTION

The problem of scour around any obstruction placed in alluvial channel is of great importance to hydraulic engineers. In practise, a channel is often obstructed by one means or other. Such structures, when introduced to a flow channel, result in significant changes to the flow pattern. Detailed description of the modified flow, due to the obstruction, is essential to understanding and analysis of the local scour which develops. In the previous chapter, the flow around piers has been discussed. This chapter will examine another type of such structure, known as a spur-dyke, or also referred to as a groyne. Schematic layout of typical channel and spur-dyke arrangement is shown in Figure 6.1.

Spur-dykes are hydraulic structures with one end adjacent to the bank and the other end projecting into the main flow, constructed mainly to: (1) protect river banks against erosion; (2) train the river along a desired course by attracting, deflecting or repelling the flow in the channel; (3) create a slack flow with the objective of silting up the area in the vicinity; and (4) create local scour holes and provide stable, submerged stony substrate for habitat improvement (Meyerle *et al.* 1995). The most important aspects to be considered in their design are the layout, plan view, shape, length, spacing, crest longitudinal shape, crest elevation, orientation, permeability, construction materials, bed material and local scour. The majority of these aspects can nowadays be examined with numerical models. Numerical model simulations are usually more cost-effective and faster than

physical model studies, and have no inherent limitation on spatial extent. This chapter is therefore aimed at investigating the capability of the FLUENT package in simulating the flow in the vicinity of spur dykes.

6.2 LITERATURE REVIEW

It is not intended here to give any detailed review of literature on the spur-dykes problem. However, a brief reference to several works relevant to the present analysis is made. Numerical models capable of simulating the flow near a spur dyke are rare. Zaghloul and McCorquodale (1973, 1975) developed such a model solving the Helmoltz vorticity equation and Poisson-type equation. Tingsanchali and Maheswaran (1990) simulated the flow around a spur dyke by solving the 2D, depth averaged equations with a k-ε turbulence model. Their results agreed with the experimental data only after a streamline curvature factor was applied to the k-ε model. More recently Mayerle *et al.* (1995) simulated the flow near spur dykes using a 3D numerical model developed at the Center for Computational Hydroscience and Engineering in Oxford, USA. Comparisons were made between six eddy viscosity approaches. The results were also compared with measurements carried out at the Franzius Institute in Hannover, Germany.

One of the major difficulties in numerically simulating flows in the vicinity of spur dykes or bridge piers, is the adequate reproduction of the wake or secondary flow formed downstream. The proper reproduction of the wake length is of fundamental importance to the design of dykes since it defines the length of the protected bank and thus the spacing between sequent dykes. Some work, although not as much as piers related problems, has been done about various aspects of the hydraulic characteristics of spur-dykes. Laboratory measurements (Garde *et al.*, 1962) show that the wake length is affected by the ratio of the dyke length to the channel width, the angle between the dyke centre line and the current, and the

flow depth. It is also influenced by the bottom roughness which generates smaller wake length in the field. Contrary to expectations, Barbarutsi *et al.* (1989) concluded from their investigations that the Froude number has little influence on the wake length.

In numerical model simulations, the wake length is strongly influenced by the eddy viscosity field (Mayerle, *et al.*, 1995). The full development of mathematical models as reliable engineering tools is, at present, hindered by the lack of an acceptable theory for the mixing coefficients especially on the horizontal plane. Even though algebraic models have been successfully applied to predict certain types of near parallel flows and different geometric configurations, usually a different model needs to be formulated and modified for each individual type of flow. The use of more sophisticated turbulence models is not always the answer to the problem, since in addition to more equations to be solved and inherent difficulties in using these models, some of them are based on local velocity gradients. Furthermore, other uncertainties in the simulation in rivers and coastal areas regarding the exact bathymetry and bottom boundary conditions whenever sediment transport is included hardly justifies the use of more advanced models. The main purpose of this chapter is to investigate the suitability of the existing FLUENT code to compute and analyse the flow velocity patterns in the vicinity of a spur dyke.

6.3 FLUENT VALIDATION

Velocity results obtained from a numerical model and experimental work reported by Mayerle *et al.* (1995) are used as benchmarks to validate the effectiveness of the FLUENT numerical model to simulate flows in the vicinity of the dykes. Subsequently, the FLUENT package is used to predict the flow field and

bed shear stress over a scoured bed caused by a spur dyke, as obtained by Zaghloul and McCorquodale (1973) .

6.3.1 Mayerle *et al.* (1995)

Mayerle *et al.* (1995) simulated the flow near spur dykes using a 3D numerical model developed at the Center for Computational Hydroscience and Engineering in Oxford, USA. The model was based on the solution of time-dependent nonlinear Navier Stokes equations, the kinematic condition of the free surface, and the continuity equations respectively for the velocities in the horizontal plane, the surface elevation, and the vertical velocity. A numerical methodology named "*Efficient Element Technique*" which combines the advantages of both finite element and finite difference method was employed. In their study, Mayerle *et al.* compared results from six different eddy viscosity turbulence approaches with measurements carried out at the Franzius Institute in Hannover, Germany. The measurements were carried out in a 32.4 m long by 2.5 m wide concrete flume with a horizontal bottom and a Manning's coefficient of 0.02. The rectangularly shaped spur dyke normal to the main flow direction was 0.25 m long and 0.05 m thick. Velocity profiles along the longitudinal and transversal directions at eleven positions near the dyke, and cross-sectional velocity measurements in the circulation region were carried out using an ultrasonic current meter. The measurements were carried out for a flow with a discharge of 200 l/s and a depth of 0.23 m over a period of 102.4 seconds. A reattachment length equal to 2.88 m (11.5d, d being the dyke length), was observed.

FLUENT Simulation

The hydrodynamic system of the physical model described above, was represented by a 3-dimensional finite volume grid system of 40x 20 x 10. Time dependence model was activated with time increment, Δt set to 0.01 secs. In general, it is

desirable to increase grid resolution in regions where the flow variables exhibit large gradients. For the spur dykes problem, the area around the spur and the recirculation zone qualify as high-gradient regions; consequently, the grid was packed near the spur, near the sidewall to which the spur was attached and near the bottom. The simulated domain and the grid system is shown in Figure 6.2. The inlet and outlet boundaries were placed, respectively 1.5m upstream and 3.0m downstream of the spur-dyke. These distances were considered appropriate to avoid disturbances due to the presence of the dyke. Uniform velocity of 0.08 m^2/s was assigned to the inlet boundary. At the bottom, the roughness coefficient (ELOG) was calculated based on an equivalent roughness height of 0.0023 m. The free surface was modelled as slip boundary.

The following solution-parameters were used for the runs:

Underrelaxation:	*0.2 (velocity, turbulence k.e. and eddy dissipation)*
	1.0 (pressure)
Sweeps :	*Alternating Direction with 2 (u,v)*
Convergence Criteria :	*1 x 10^{-3} residual sum*
Algorithm :	*SIMPLEC*
Solver :	*Multigrid for pressure correction*
Block Correction	*I:1, J:3, K:3*
Model :	RNG k-ε (time-dependence model)

Results and Discussions

The quasi steady state three dimensional conditions were obtained after 120 secs (12,000 iterations) whereby the normalised residuals reported by FLUENT are almost constant. This is consistent with number of iteration reported by Mayerle *et al.* Figures 6.3 - 6.5 show the velocity vectors and corresponding bed shear stresses for t=40, 80 and 120 secs , respectively, for model RNG. The recirculation

zone downstream of the dyke in the numerical model results was defined as the region in which the longitudinal velocities are in opposite direction to the main flow direction. This region is represented by the contours of negative velocity behind the dyke as depicted in Figures 6.3-6.5.

Figures 6.6 compare longitudinal velocity profiles at six positions (cross section A,B, and C - Figure 6.2), between the FLUENT results, Mayerle *et al.* model results and the physical model measurements. It can be seen from the figures that none of the simulated results (FLUENT and Mayerle's models) agrees systematically with the measurements. Mayerle *et al.* argued that at the dike tip (position A3) the results vary significantly from the measurements probably due to the locally non-hydrostatic pressure. Downstream of the dike and outside the recirculating region (position B1 and C1), both FLUENT and Mayerle's model are not able to capture the decrease in the longitudinal velocities towards the free surface shown by measurements. However, FLUENT predicts the velocity better in this region compared to Mayerle's approaches. Figures 6.7 shows comparisons of the longitudinal velocities near the bed along two cross sections of the channel. The cross sections are taken as 0.338 m (section D) and 1.55 m (section E) downstream of the dyke axis. FLUENT's result fit reasonably well within the range of results obtained by Mayerle *et. al.*

The reattachment point was taken as a point where separation of flow occur at the wall boundary. It can be seen from Figure 6.3 - 6.5 that the recirculation zone, hence the attachment point, increases with time. For the present analysis, reattachment length at quasi-equilibrium stage (T=120secs) was found to be 2.74 m ($\approx 11d$), downstream from the dyke axis. This compared very well with the value obtained from the physical model (2.88 m or $11.5d$). Mayerle, *et al.* (1995) reported reattachment lengths ranging from $8.4d$ to $15.2d$, the nearest being $10.8d$. Independent studies by Francis *et al.* (1968) and Ishii *et al.* (1983) reported reattachment lengths approximately equal to $11.5d$ for dykes placed

perpendicularly to the main flow direction having a ratio of dyke length to channel width equal to 0.1. Francis *et al.* carried out their measurements in a 0.46 m wide rectangular cross section channel using groyne lengths of 0.023 m, 0.0509 m and 0.080 m whereas Ishii *et al.* used two laboratory flumes (0.8 m and 0.396 m wide) to investigate the effect of some dimensionless properties on the shape of separation formed behind dykes.

6.3.2 Zaghloul and McCorquodale (1973, 1975)

Zaghloul and McCorquodale (1973) developed a numerical model for local scour prediction around a single spur dyke. They also conducted experiments to verify their mathematical model. The clear-water scour experiments were carried out in a rectangular channel of width 45.75 cm, containing a sand bed with a mean particle diameter of 4.5 mm. The specific gravity and the angle of repose for the bed material are respectively 2.65 and 30°. The critical shear stress on a level bed for the sediments were found experimentally to be approximately 3.6 Pa. Several flow conditions were investigated and scour patterns were monitored, to determine the effect of the following parameters on the maximum depth of scour; (i) flow rate, (ii) upstream water depth, (iii) Opening ratio, *i.e.* ratio of width of channel at spur dyke to width of channel upstream, (iv) Froude number upstream of spur dyke, (v) Angle of inclination of spur dyke to the flow, and (vi) running time. Typically, duration of 3 hours is observed before limiting scour condition was reached. They suggested an empirical shear stress equation which was generated from the computed local velocity, turbulence and vorticity, and has the form:

$$\tau_b = \frac{\gamma}{C^2} v_R^2 \left(1 + K_1 \frac{\omega}{\omega_o} + K_2 \right)^2 \qquad (6.1)$$

in which τ_b is the shear stress acting on the bed, γ is the specific weight of water

C is Chezy coefficient, v_R is the resultant velocity, K_1 *and* K_2 are constants and ω_o is a reference vorticity e.g. the vorticity at the nose of the dyke. Adjustments were made to the calculated eroded depth so that the final computed scour profile conformed to the condition that the local shear equalled the bed resistance. An expression controlling the development of the scour hole was formulated as:

$$\Delta z = K_3 (\tau - \tau_{sc}) \qquad (6.2)$$

where Δz is the increment in the eroded bed, K_3 is the constant, and τ_{sc} is the critical shear stress for the bed material taking into account the local bed slope. It was however not clear how they calculated the value of the τ_{sc}. They obtained an excellent agreement between theoretical and experimental scour patterns. The calculated and experimental scour pattern for the flow condition with an average upstream velocity and water depth of 40.87 cm/s and 20.32 cm, respectively, are shown in Figure 6.8.

FLUENT Simulation

The time development of scour represents a very complicated flow phenomenon involving the movement of sediment-water mixture along the bed of the scour hole. The existence of structure such as spur-dyke that obstruct the flow adds to the complexity of the problem. The accelerated flow at the tip of the structure combined with the vortices and the shear stress at the bed are among major factors that lead to extensive erosion in the vicinity of the spur-dyke. Because of the continuously changing flow boundary as scour progresses with time, the velocity distribution pattern in the scour hole would likewise be different at different stages of the erosion process. In the present study, no attempt was made to simulate these transient non-uniform flow patterns. Instead a steady-state

flow model was simulated based on the initial flat bed condition, and final scoured pattern as observed by Zaghloul and McCorquodale (1975).

The opening ratio, α, defined as $(B-d)/B$ (B being the width of the channel and d being the length of the spur dyke) is equal to 0.67. A uniform velocity of 0.4087 m/s was applied at inlet boundary. The outlet boundary was first located at $40d$, a distance greater than the expected attachment point. Initial trial runs for rigid-bed case indicated that this distance was not appropriate, as the flow at the exit does not reach steady-state. This distance was then increased to $80d$, and was found to be appropriate for practical computational purposes. In addition, several grid arrangements were tried to ensure that the results were independent of grid size distribution. A three-dimensional grid size of 70 x 25 x 12 was used in the simulation.

Results and Discussions

Figures 6.9 show the computed steady-state velocity vectors plots and resulting bed shear stress for flat-bed. It can be seen from these figures that with an opening ratio, α, of 0.67, the attachment length, L, is equal to $37.3d$, almost four times greater than the distance obtained in the previous study (i.e $11d$ for opening ratio of 0.9). Another run with shorter spur-dyke length (Figure 6.10) with the opening ratio of 0.78 resulted in shorter attachment length (= $15.3d$). Francis *et al.* (1968) and Tingsanchali and Maheswaran (1990) observed the same trend in which the distance L increases with the decreases in the opening ratio. Tingsanchali and Maheswaran (1987) further reported from their numerical analysis that beyond a certain length of the spur-dyke, the presence of the opposite wall limits the growth of the recirculation width, H_{max} (see Figure 6.1), and thus the length of recirculating zone.

A run with a thinner spur-dyke (W = 1.5 cm , Figure 6.10) shows that the attachment distance is smaller than a wider spur-dyke with the same opening ratio (=0.67). The attachment length, L, in this case was calculated to be $30.3d$ from the dyke axis. This preliminary results indicate the importance of the spur shape, for instance in determining the spacing of spurs. Unfortunately no experimental data are available for comparison in this case.

As the water flows around the spur-dyke, the flow pattern is changed due to the reduction of the width of channel, and as a result of this the shear distribution around the spur-dyke is modified. This leads to scouring action until equilibrium is established between various forces influencing the scouring action. In almost all cases, the maximum scour depth occurred at the nose of the spur-dyke. The scour hole upstream of the spur-dyke was conical in shape, whereas downstream, it was elongated and had a shallower shape (Garde *et al.*, 1962). Experimental work carried out by Rajaratnam and Nwachukwu (1983), using 75 mm and 150 mm groynes, observed that the shear stress near the groyne was higher for the smaller opening ratio. They also indicate that the results for the 75 mm groyne for which the opening ratio is 0.92, might represent the asymptotic case, *i.e.*, the opening ratio for which the effect of constriction on the channel flow farther away is negligible. The result exhibited by FLUENT (Figure 6.10) is consistent with this finding. Similarly, Garde *et al.* (1962) and Zaghloul and McCorquodale (1975) showed that the scour hole increases as the opening ratio decreases. Zaghloul formulated an empirical equation, based on the experimental findings, to illustrate the degree of dependence of the scour depth on various influencing factors. This equation is given by:

$$\frac{D_s}{H} = 2.62(F)^{2/3}\left(\frac{1}{\alpha}\right)\left(\frac{1}{\theta}\right)^{0.043} \qquad (6.3)$$

where D_s = maximum depth of scour, F = Froude number, α = opening ratio and θ = angle of inclination of the spur-dyke with respect to the main flow.

Garde *et al.*(1961) proposed an equation given as:

$$\frac{H + D_s}{H} = \left(\frac{K}{\alpha}\right) F^{2/3} \qquad (6.4)$$

where H = average depth of water flow. The above equation was derived for angle of inclination $\theta = 90^{o}$.

Zaghloul and McCorquodale (1973, 1975) suggested that allowances in the numerical models need to be made to account for the shedding mechanisms of vortices and the increased shear resulting from the horseshoe vortex in the vicinity of the dyke. They proposed an empirical equation (Eq. 6.1) which took into account the effect of the vortices. Roger (1994), on the other hand, used the bed shear stress formulated by Melville and Raudkivi:

$$\tau_b = \rho f u^2{}_b / 8 \qquad (6.5)$$

where ρ is the density of water, f is Darcy Weisbach friction factor and u_b is the velocity measured at bed. This equation may not be applicable in a strongly curved flow, such as spur-dyke and piers, since its simplicity does not take into account the swirling effect.

Similarly, FLUENT may not have taken into account such factors in the determination of the bed shear stress. Consequently, the magnitude of the shear stress calculated by FLUENT, as shown in the figure 6.9, were considerably less than critical shear stress for the material for flat bed (τ_c = 3.6 Pa). The results obtained for scoured bed are essentially lower than the results obtained for rigid bed (Figure 6.11). This is because as scour hole developed, the length of eddy zone

and intensity of eddy currents in it decreased. Also, velocities near the bed decreased because of the increase in total water depth. In the downstream region of the hole, however, the decrease in depth between the bed and the 'fixed' water surface causes the flow to converge and causes the velocity to increase thus higher bed shear stress.

6.4 CONCLUSIONS

The RNG k-ε formulation in FLUENT has been validated against selected benchmark solutions of flow in the vicinity of spur dykes. Extensive testing procedures have been implemented to ensure that the equations and solution algorithms used by FLUENT would provide an accurate simulation of flow, in particular the grid-independent and the location of the outlet/exit boundary.

Overall, the FLUENT results are good in balance. FLUENT successfully verifies that when a dyke is placed in a channel, it causes a significant disturbance downstream to the flow for a short distance upstream and for a longer distance downstream. FLUENT predicted reasonably well the attachment point downstream of the dyke in the flat-bed case.

It can be concluded that the shape of the spur-dyke effects to some extent, the location of the attachment point as well as the distribution of the shear stress in the vicinity of the spur-dykes. It is therefore important for numerical simulation purposes that the geometrical shape of the spur-dyke to be input as accurately as possible.

In general it was shown, experimentally and numerically, that the maximum bed shear stress occurred near the dyke nose and the immediate neighbourhood of the dyke. Comparison between calculated bed shear stress and the experimental

critical bed shear stress for the flat bed, however, indicated that FLUENT results are considerably lower. This may be due to the failure of FLUENT to include the effect of the vorticity in the determination of the bed shear stress.

Another shortcoming of the FLUENT is that the present code is not capable of simulating the changes in the water level. Observation by Rajaratnam & Awachukwu (1983) and Mayerle *et al.* (1995) describe the lowering of the free surface at the nose of the spur dyke and behind it which FLUENT would not be able to simulate.

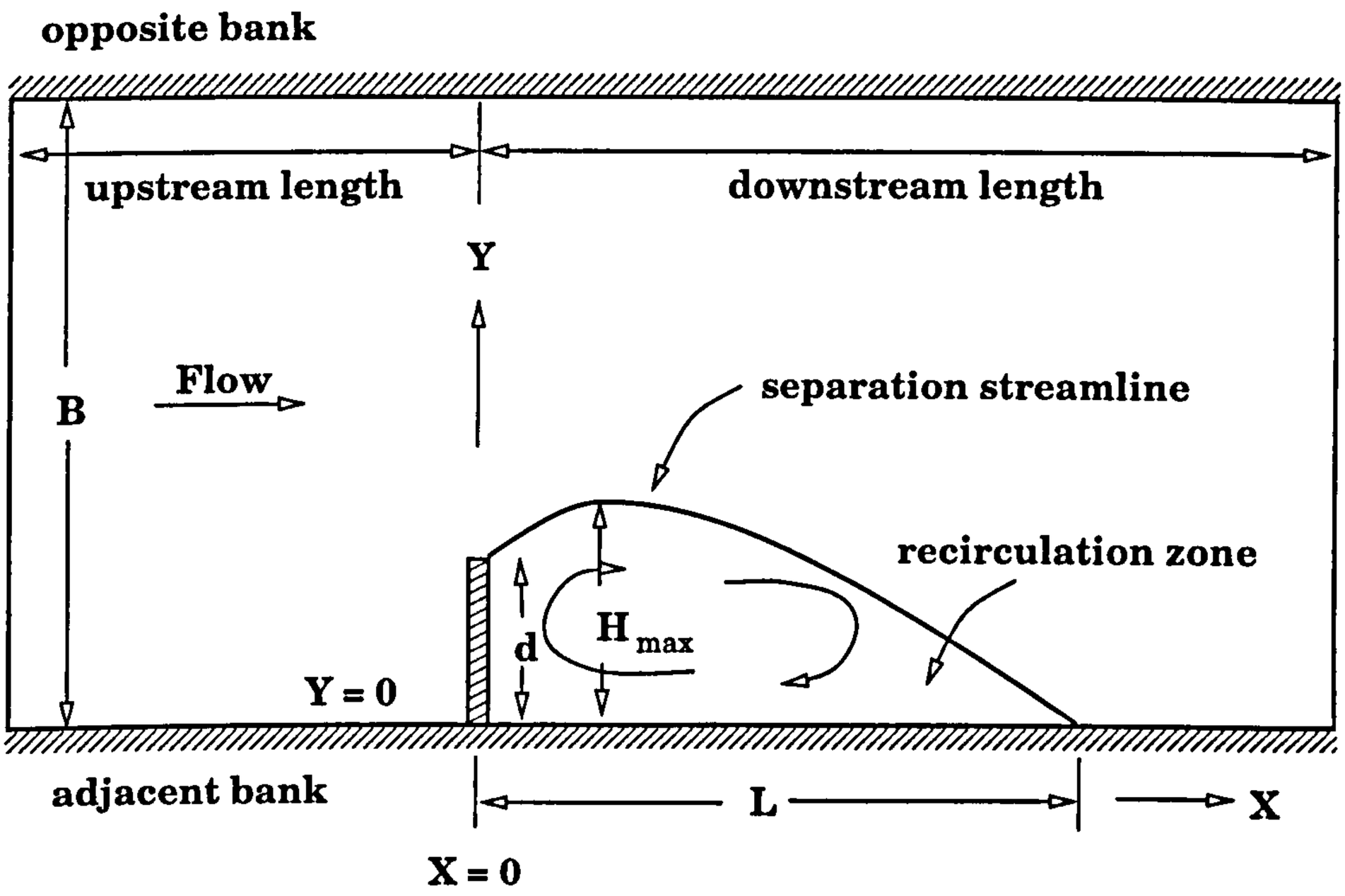

Figure 6.1 : Schematic Layout of Channel and Spur-Dyke

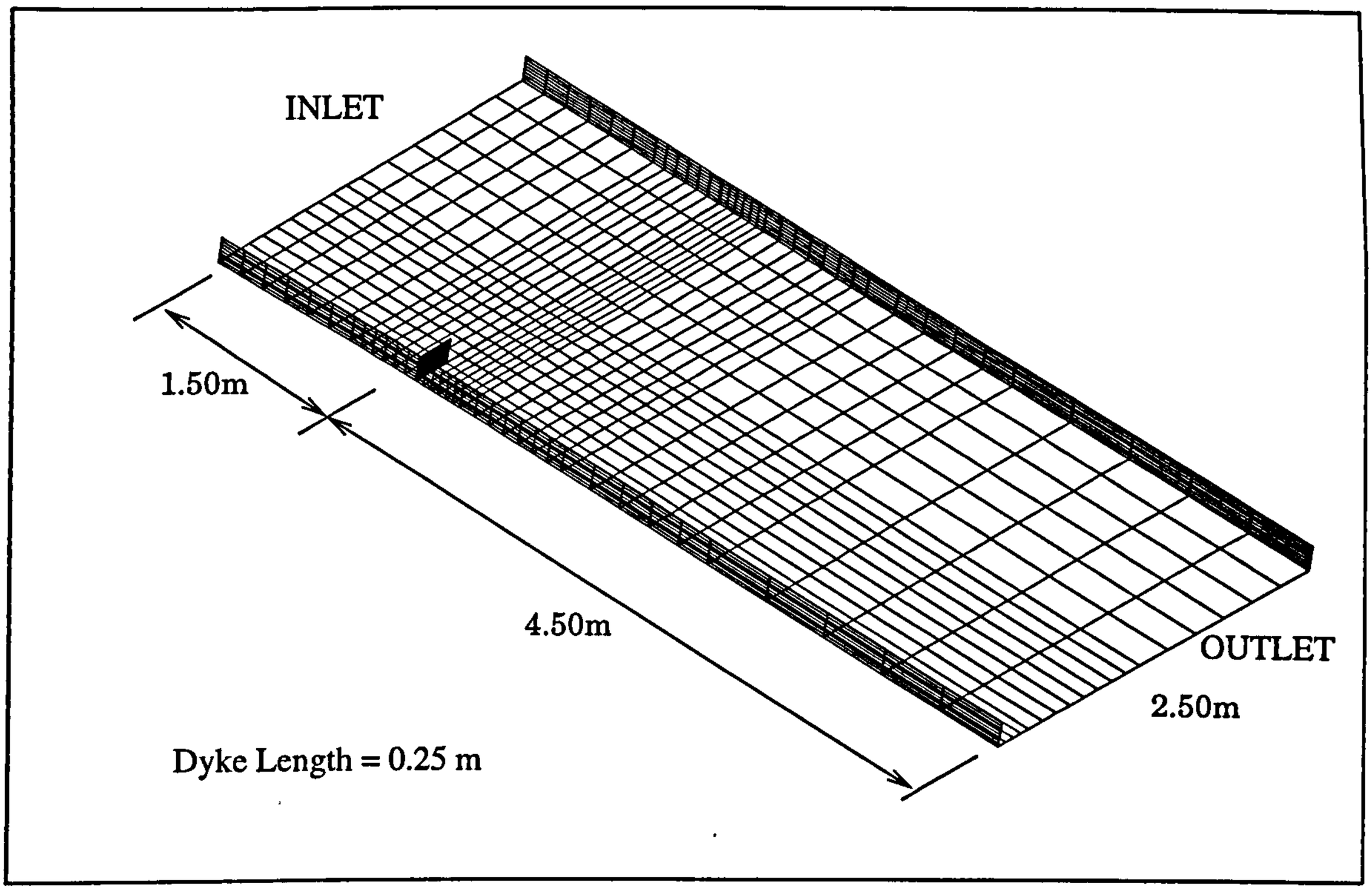

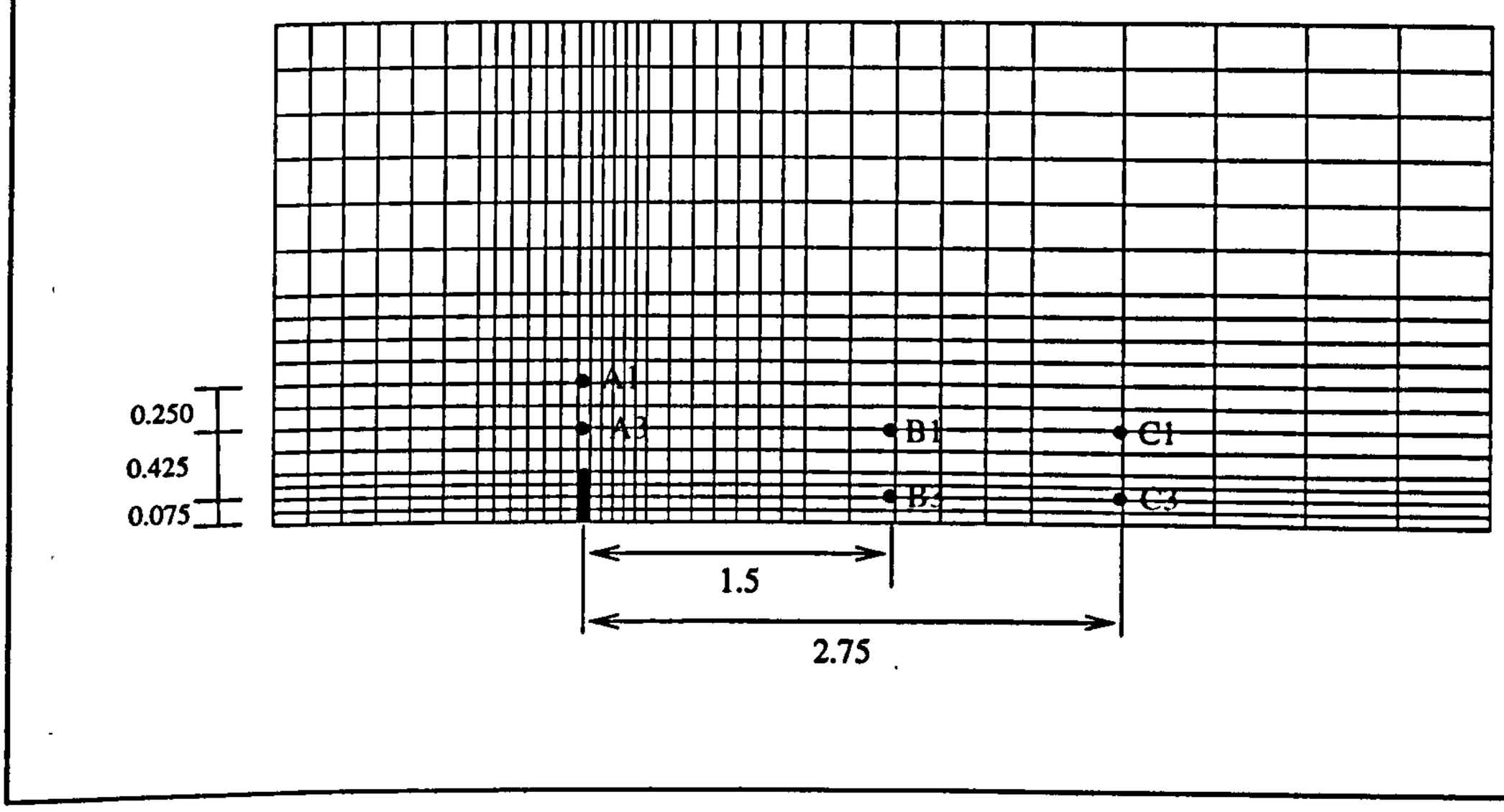

Figure 6.2 : Simulated Domain and Grid-System in FLUENT

(a) Velocity Vectors

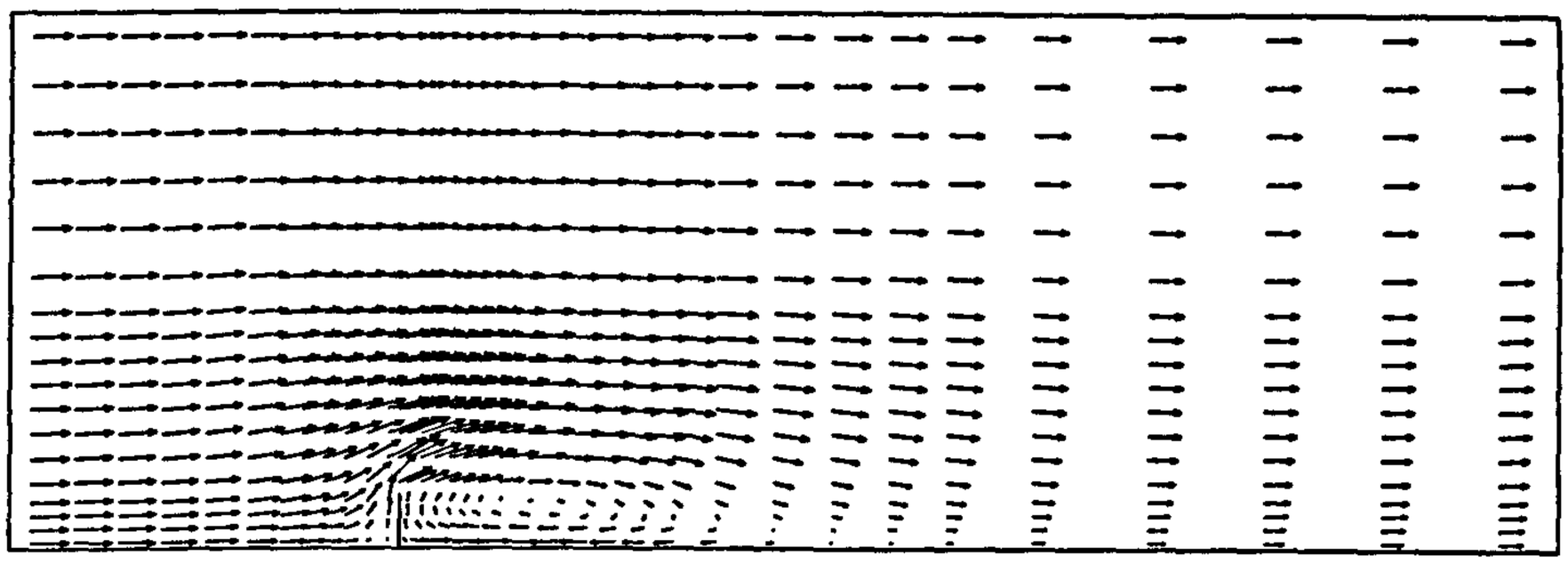

0.40 m/s

(b) U-Velocity Contours

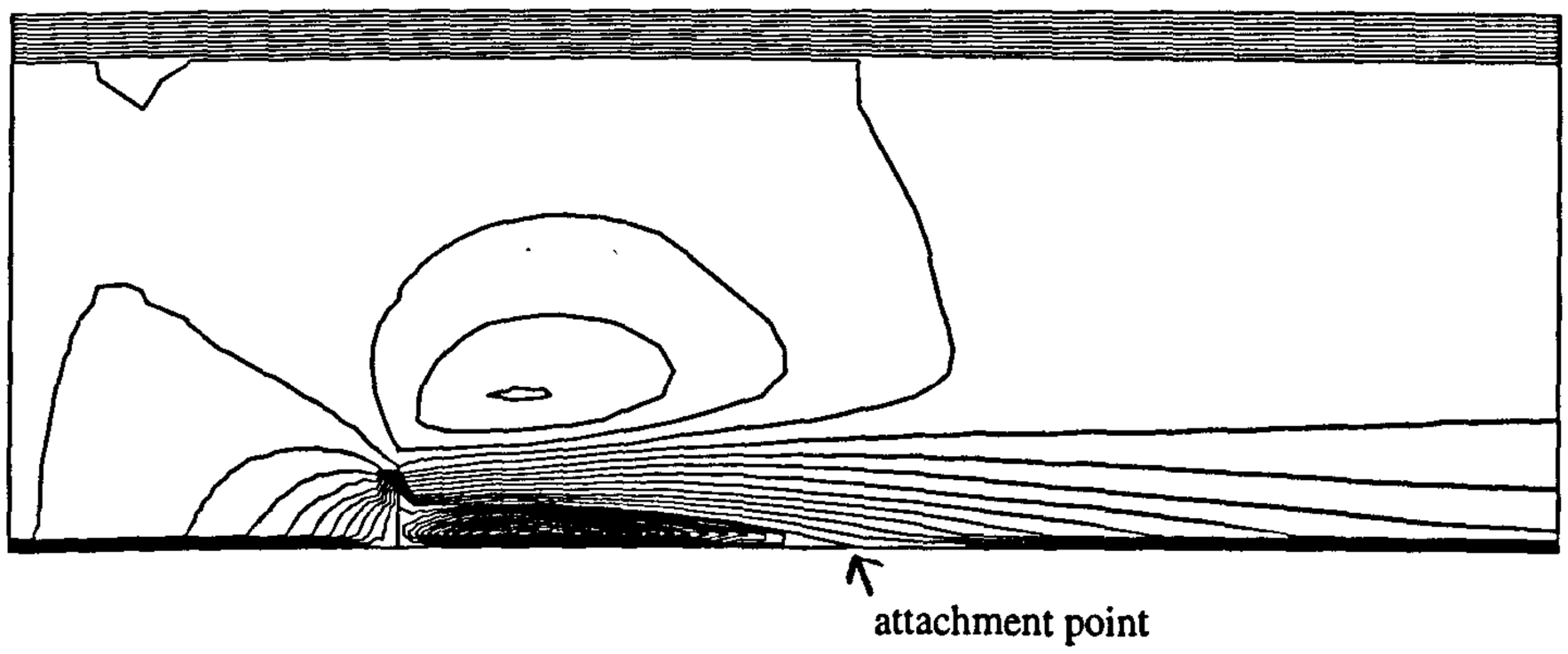

(c) X-Dir Bed Shear Stresses

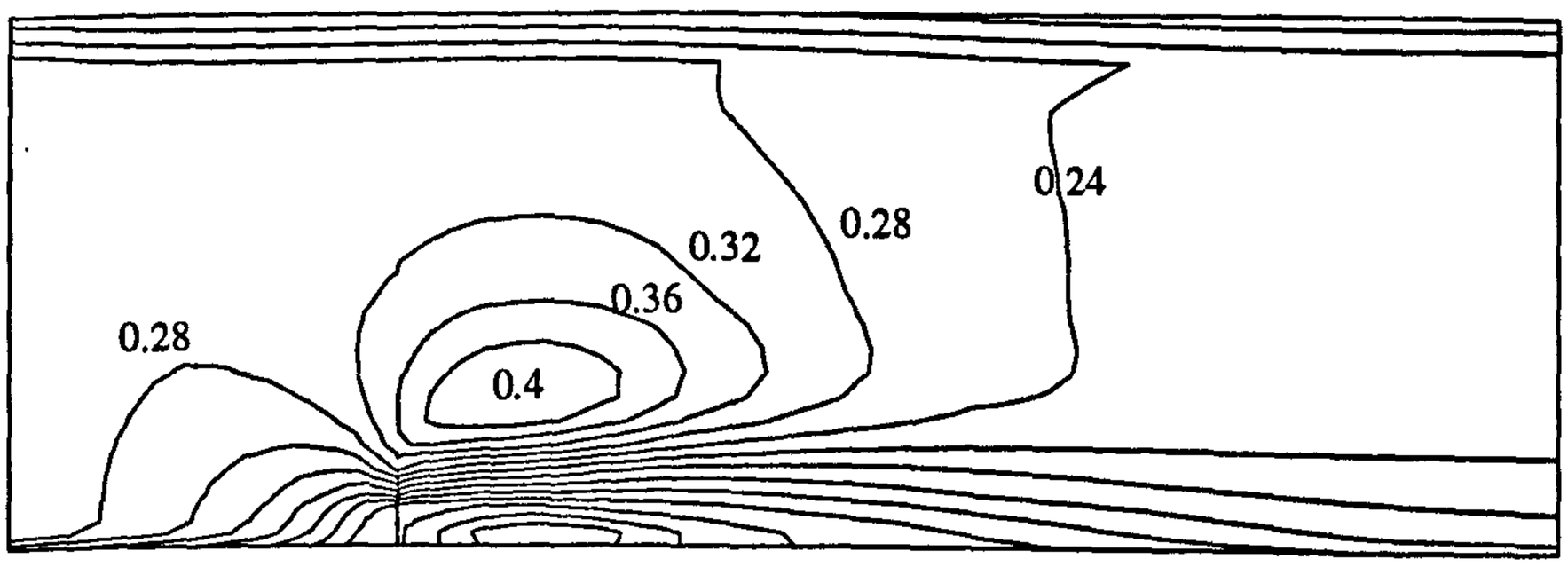

Contours Interval : 0.04 Pa

Figure 6.3 : FLUENT Output (t = 40 secs)

(a) Velocity Vectors

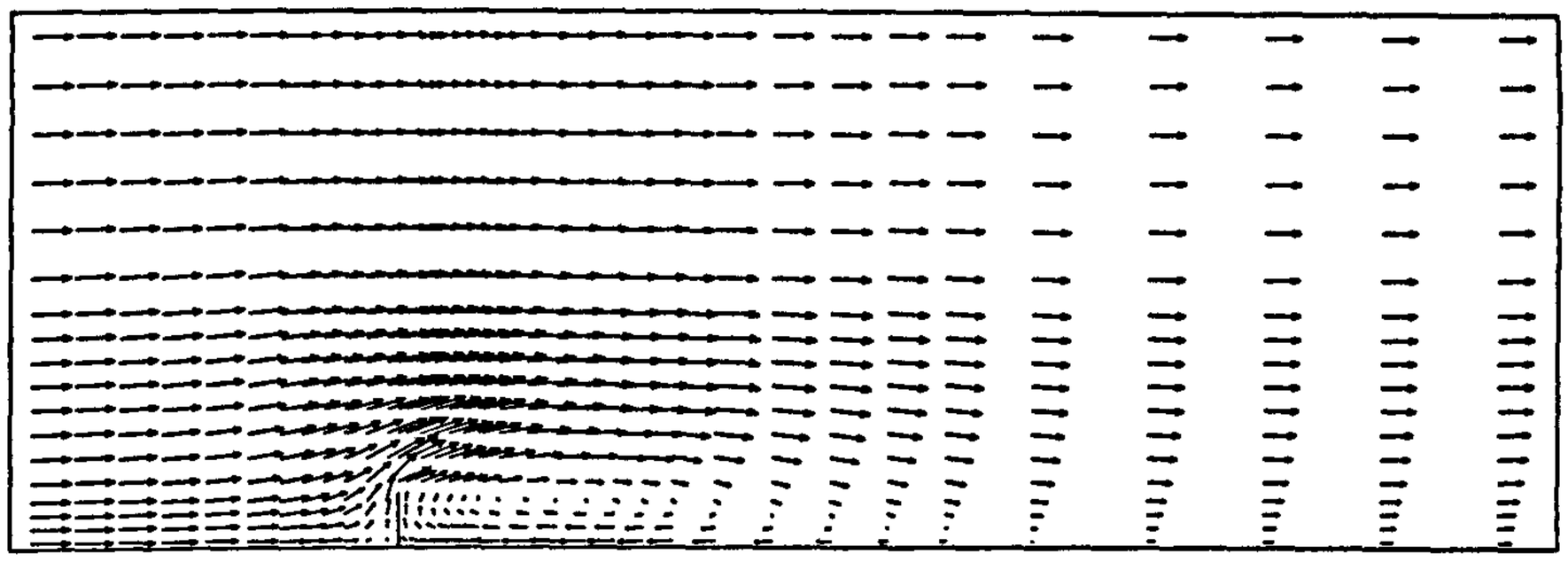

0.40 m/s

(b) U-Velocity Contours

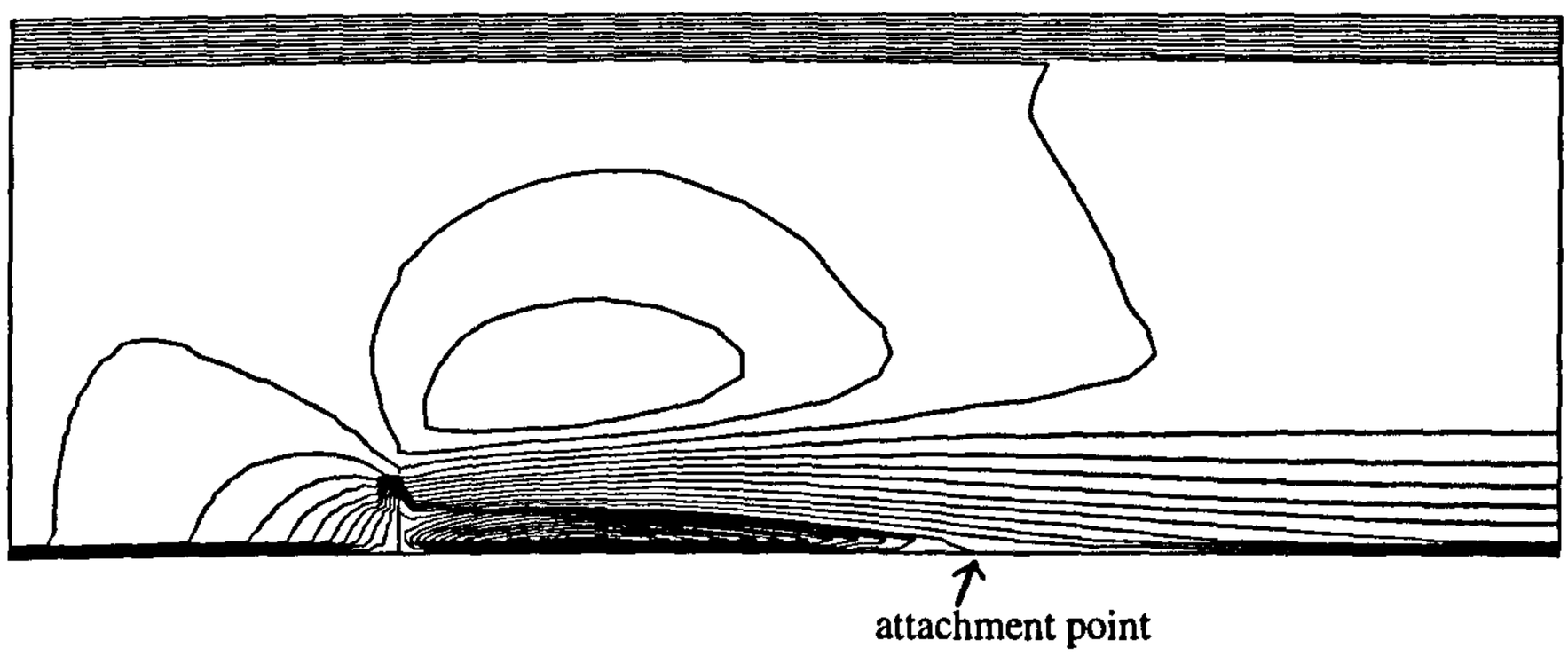

(c) X-Dir Bed Shear Stresses

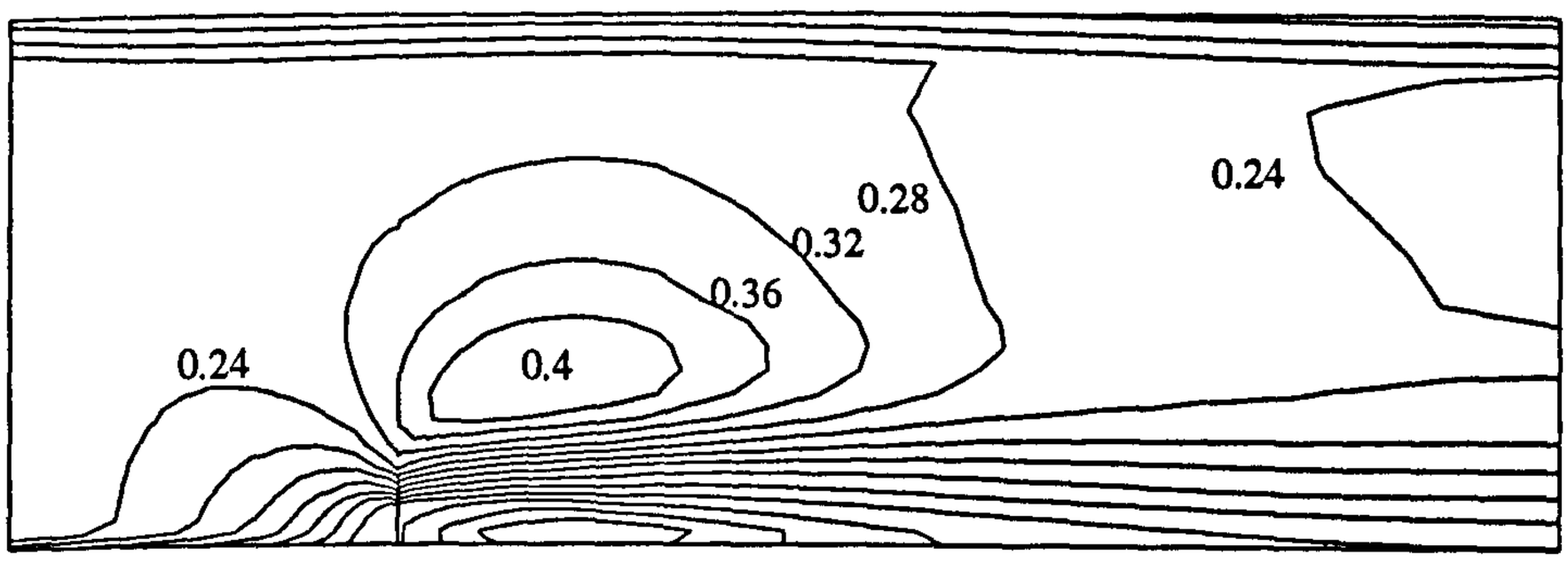

Contours Interval : 0.04 Pa

Figure 6.4 : FLUENT Output (t = 80 secs)

(a) Velocity Vectors

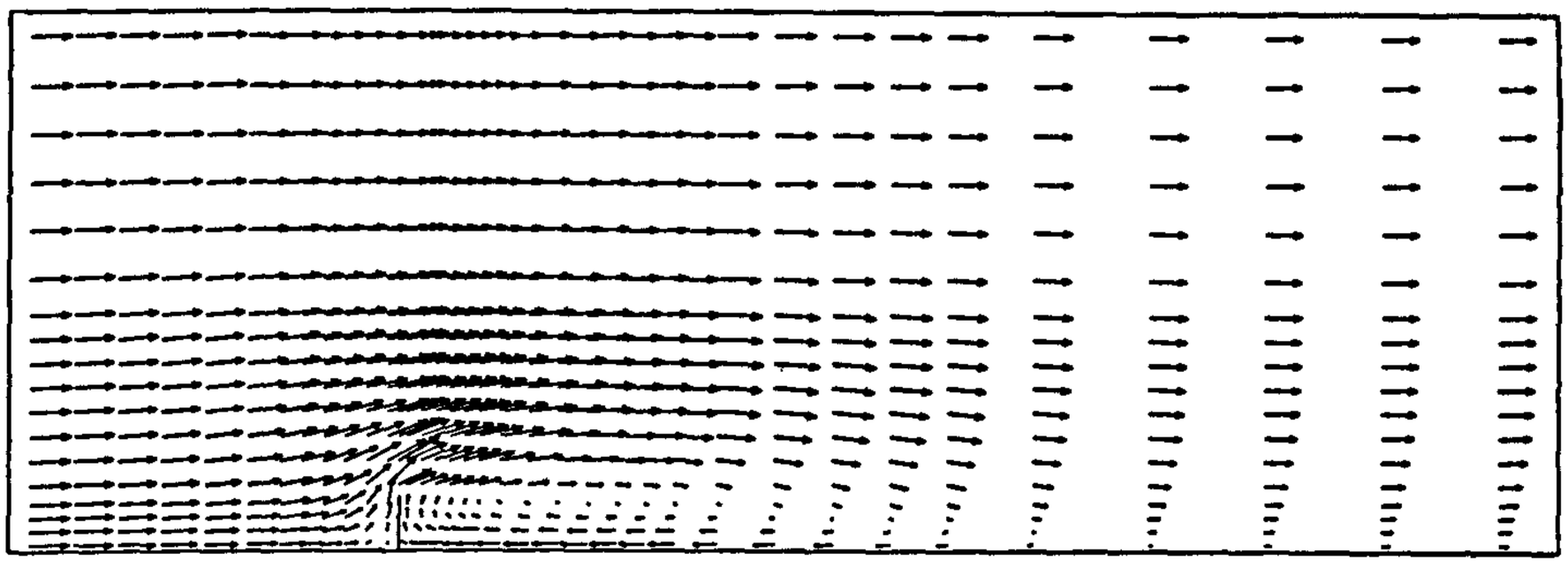

0.40 m/s

(b) U-Velocity Contours

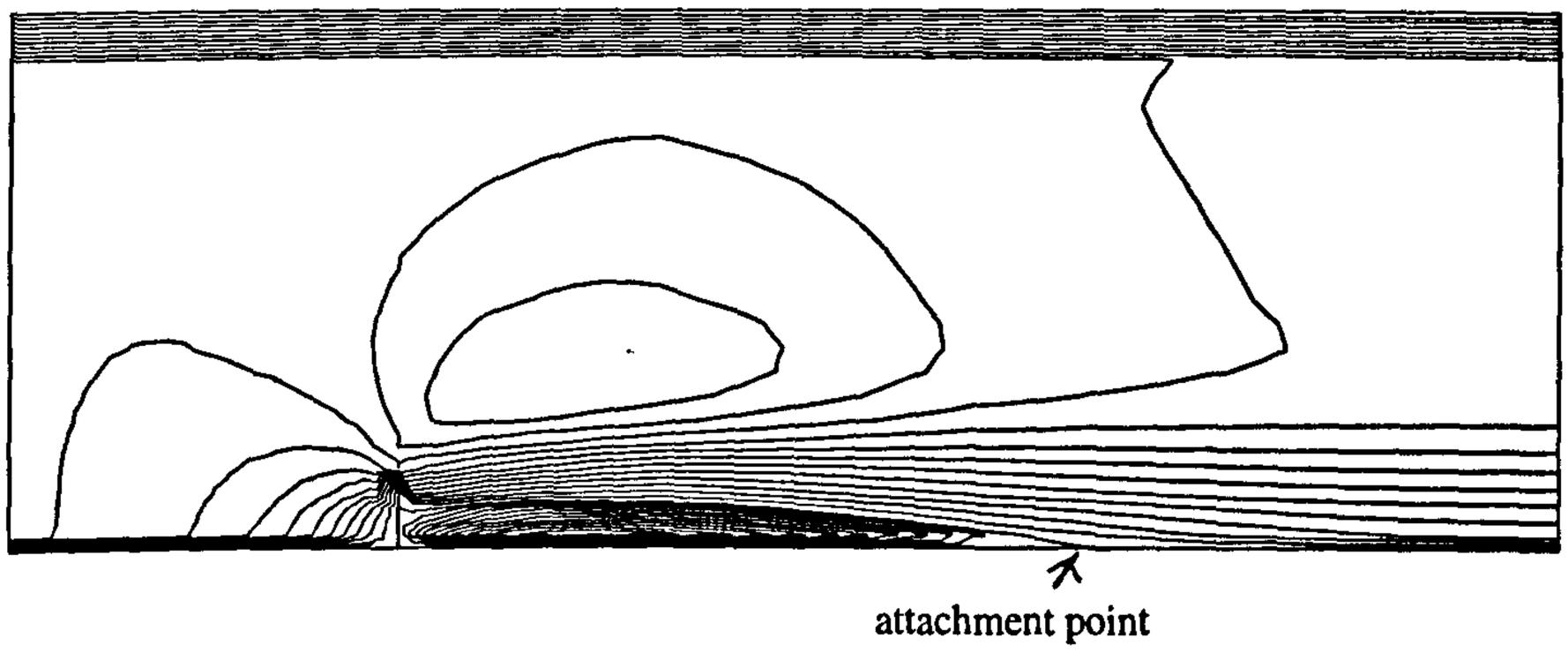

(c) X-Dir Bed Shear Stresses

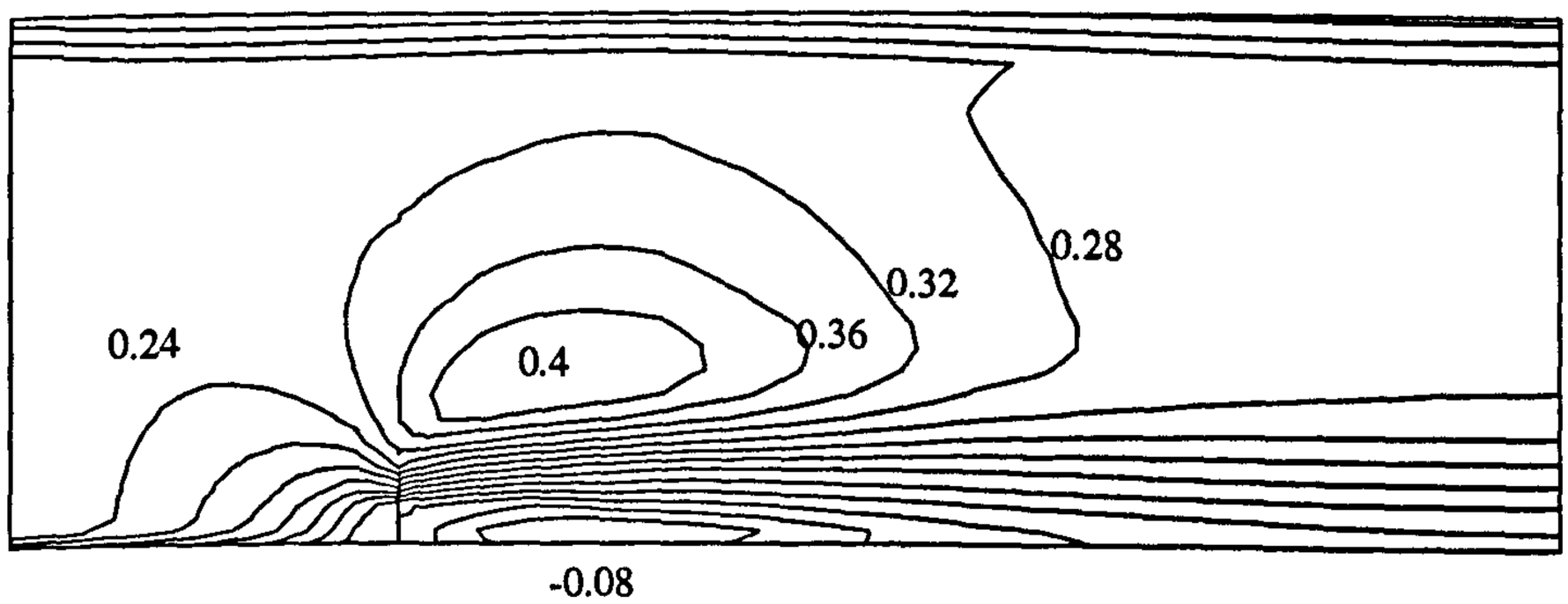

Contours Interval : 0.04 Pa

Figure 6.5 : FLUENT Output (t = 120 secs)

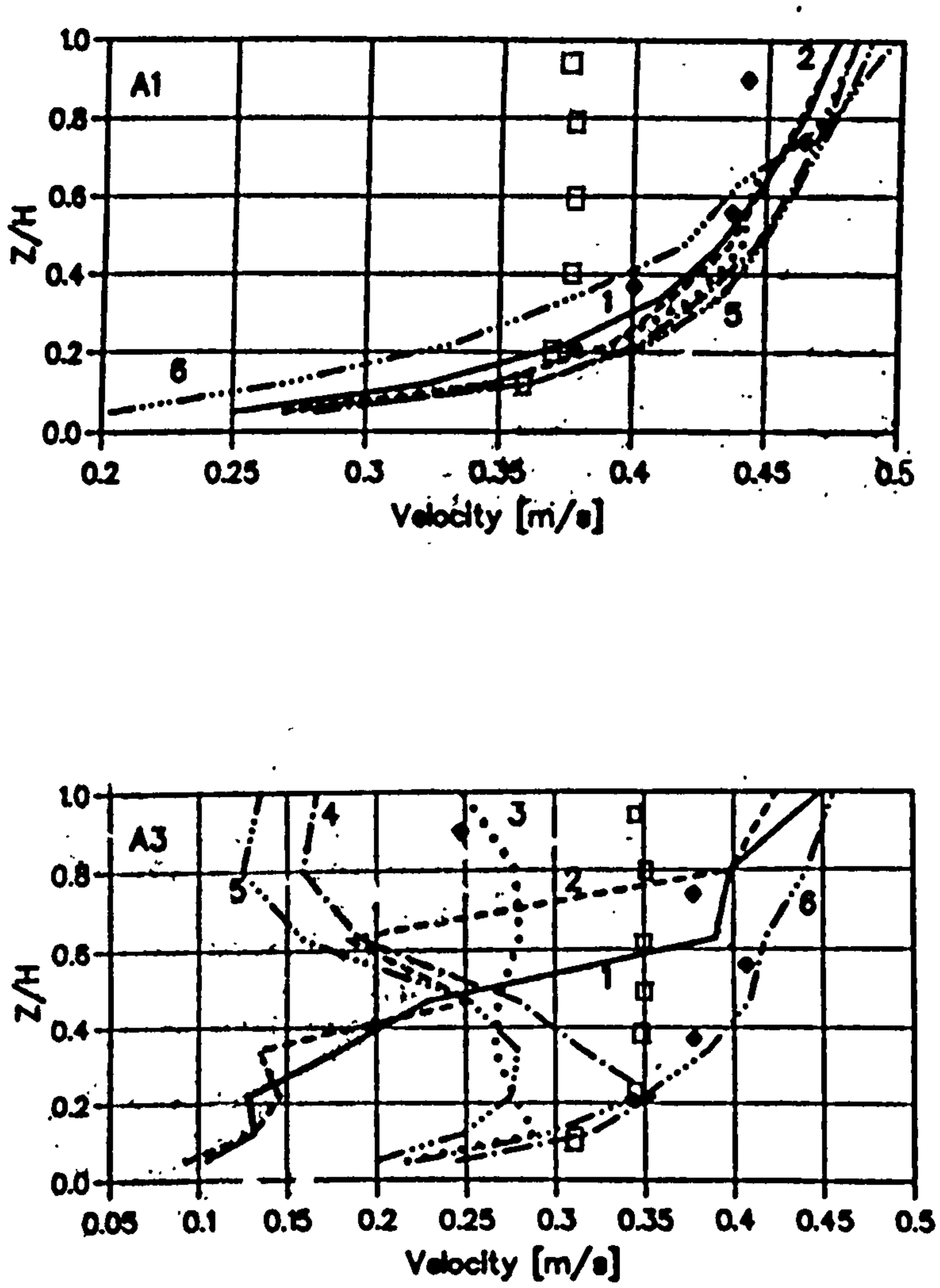

Figure 6.6 : Comparisons of longitudinal vertical velocity profile
(□ - FLUENT, ♦ Experimental, 1-6 : Mayerle et al's models)

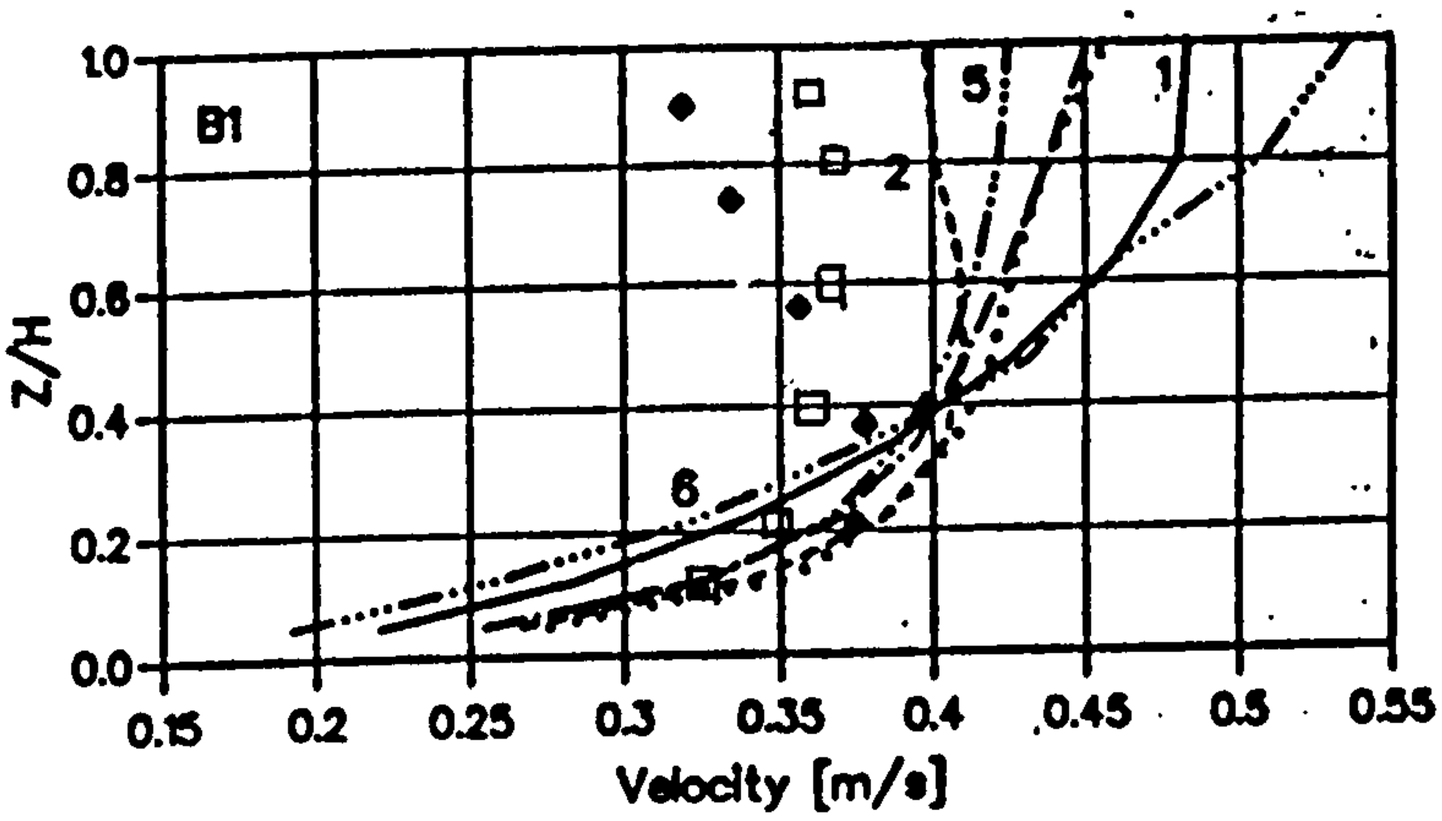

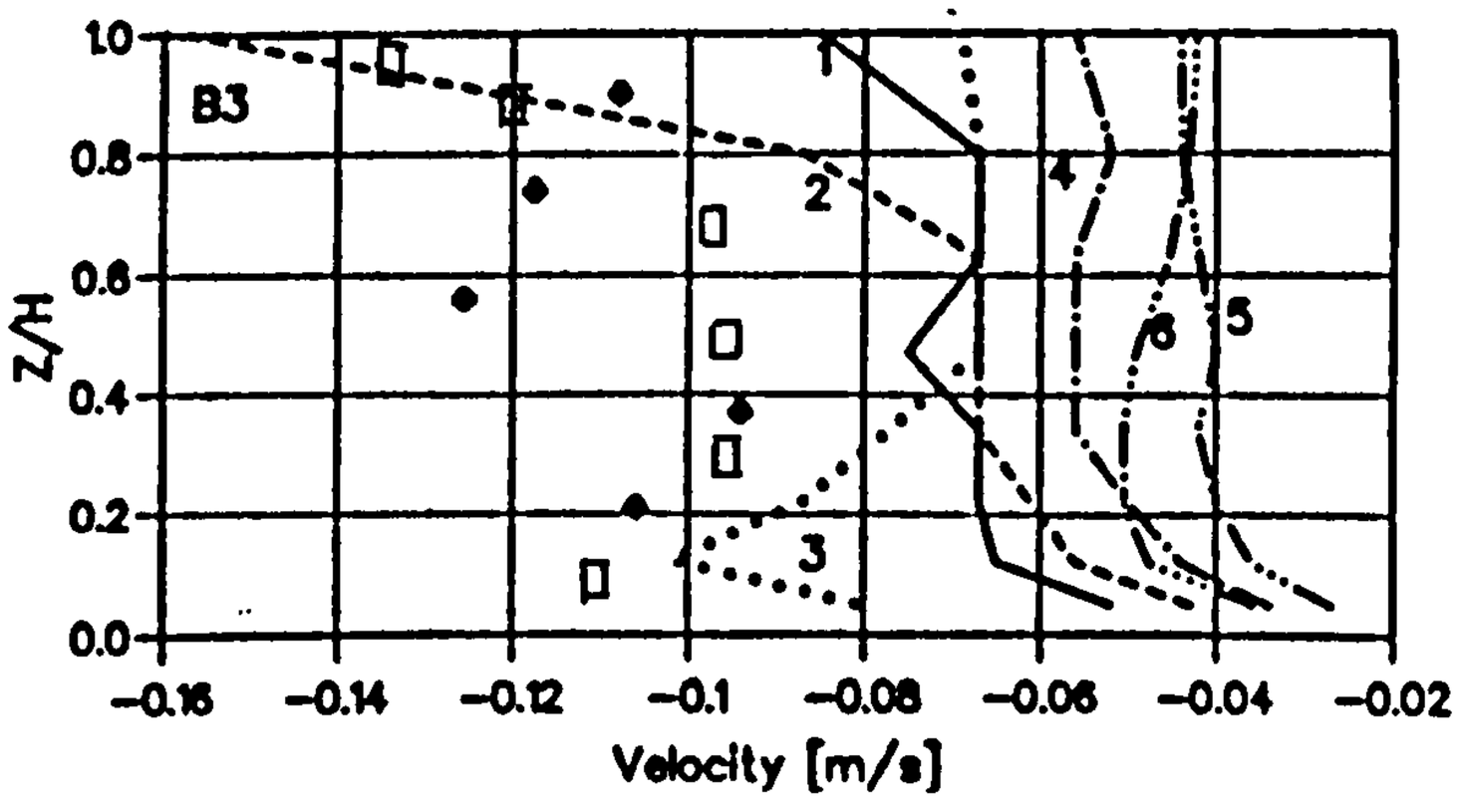

Figure 6.6 (ctn'd) : Comparisons of longitudinal vertical velocity profile
(□ - FLUENT, ♦ Experimental, 1-6 : Mayerle et al's models)

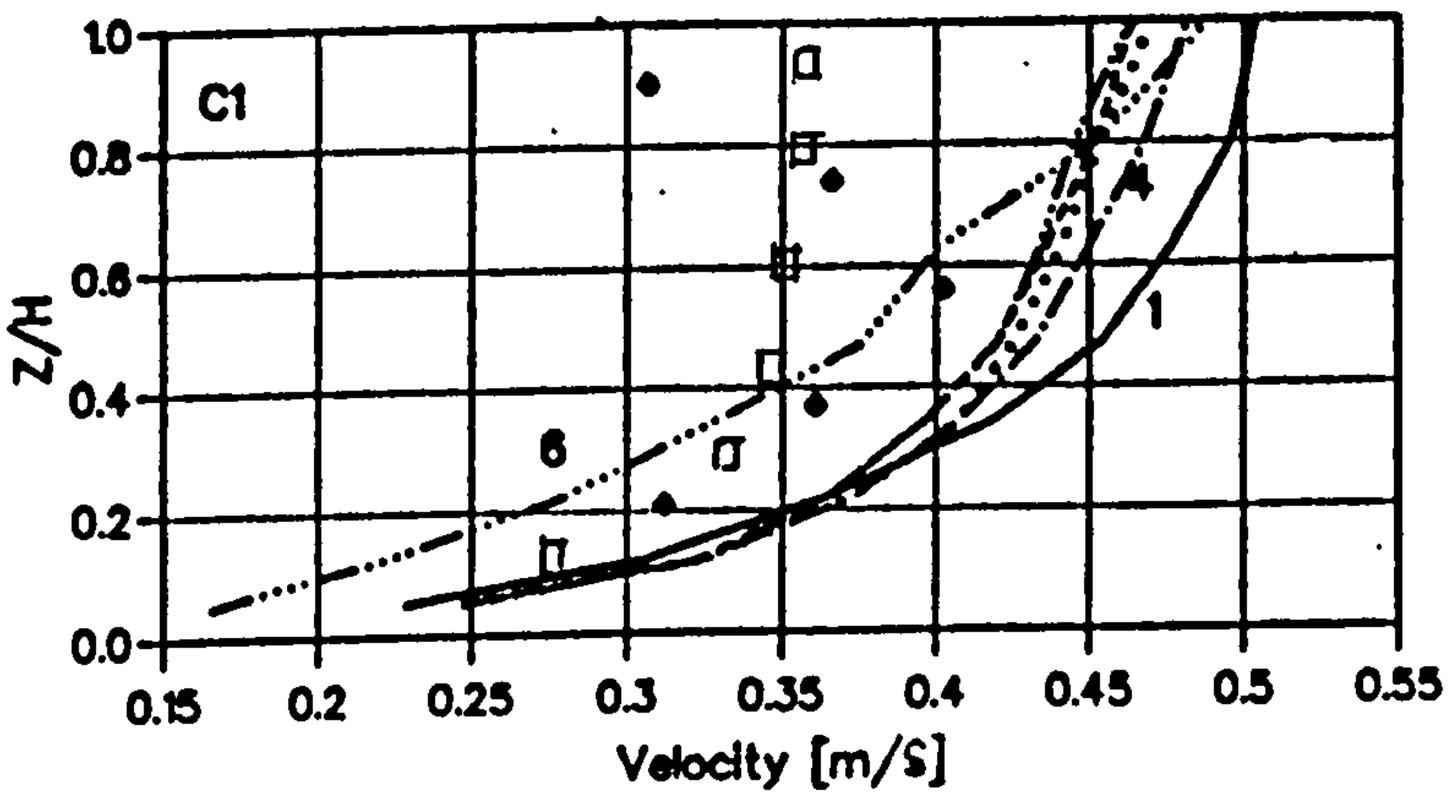

Figure 6.6(ctn'd) : Comparisons of longitudinal vertical velocity profile
(□ - FLUENT, ♦ Experimental, 1-6 : Mayerle et al's models)

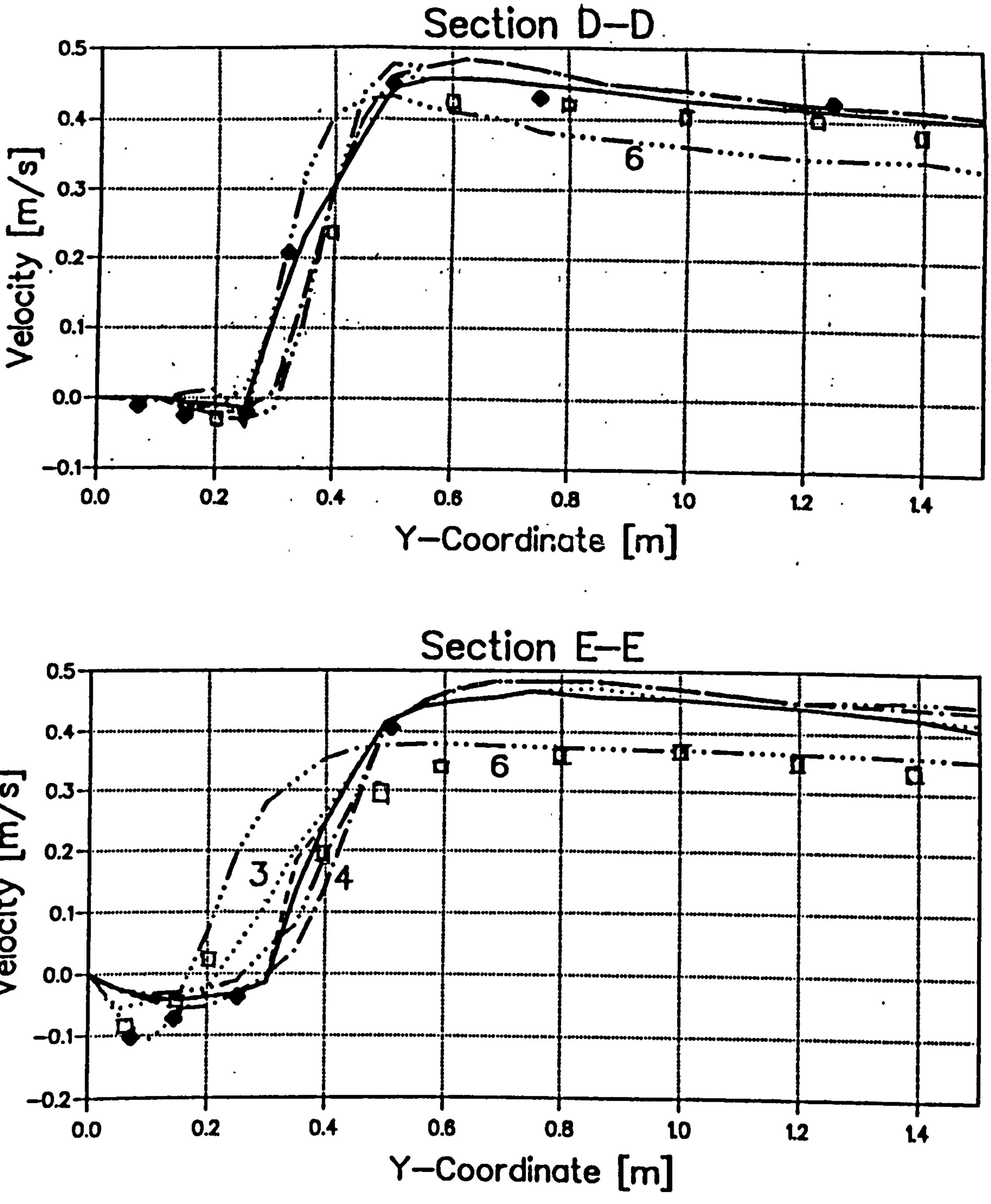

Figure 6.7 : Cross sectional plots of the longitudinal velocities downstream of spur-dyke (Section D-D : 0.338m ; Section E-E : 1.55m downstream) (□ - FLUENT, ♦ Experimental, 1-6 : Mayerle et al's models)

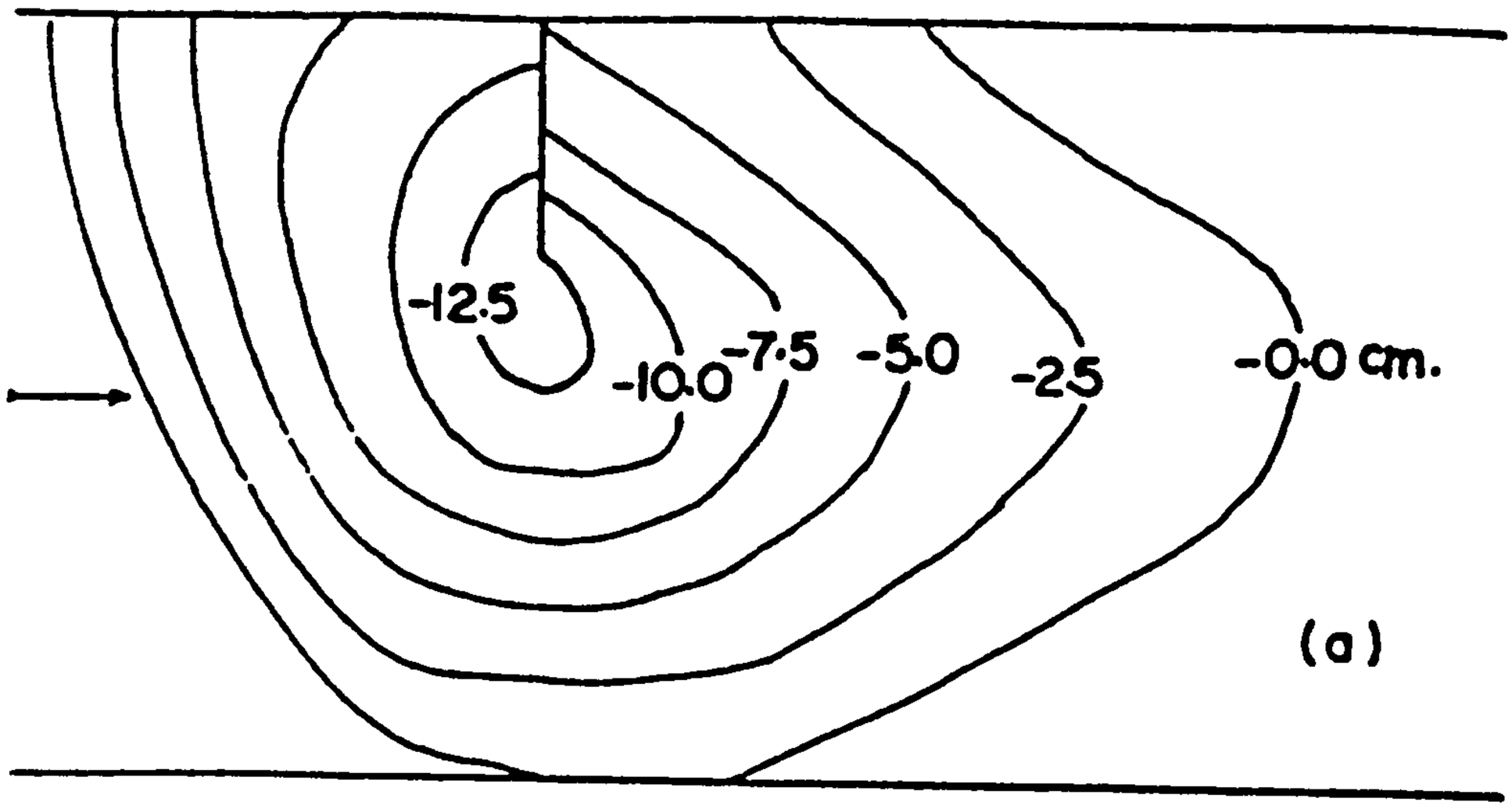

Figure 6.8 : (a) Experimental and (b) Computed Scour Pattern
(after Zaghloul and McCorquodale, 1975)

(a) Velocity Vectors

Width of Channel : 0.46 m
Spur length, d = 15 cm
Spur Width, w = 3.5 cm

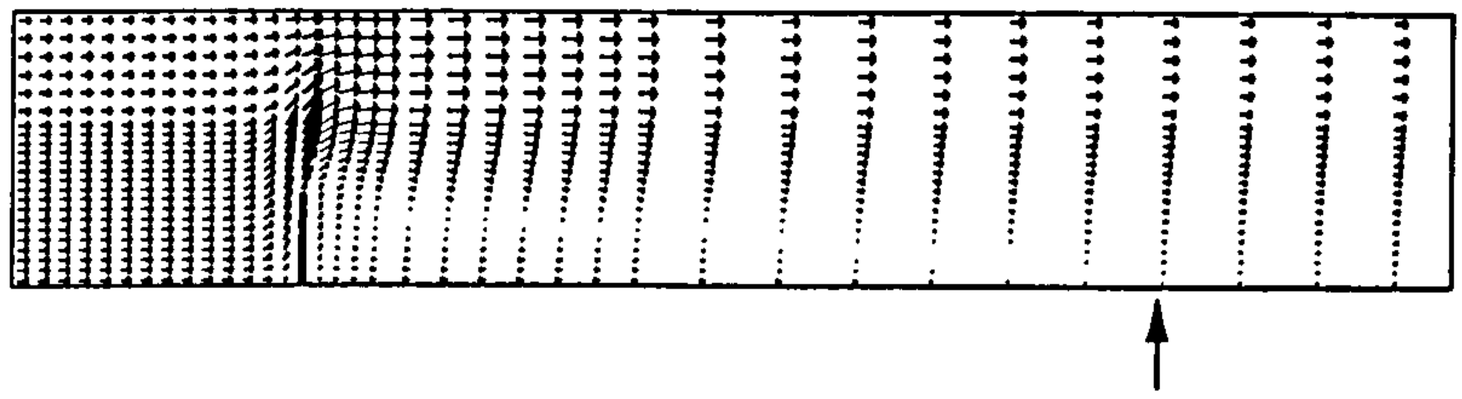

0.8 m/s

Note : Scale is distorted in Y direction (5x)

(b) X-Dir Bed Shear Stresses

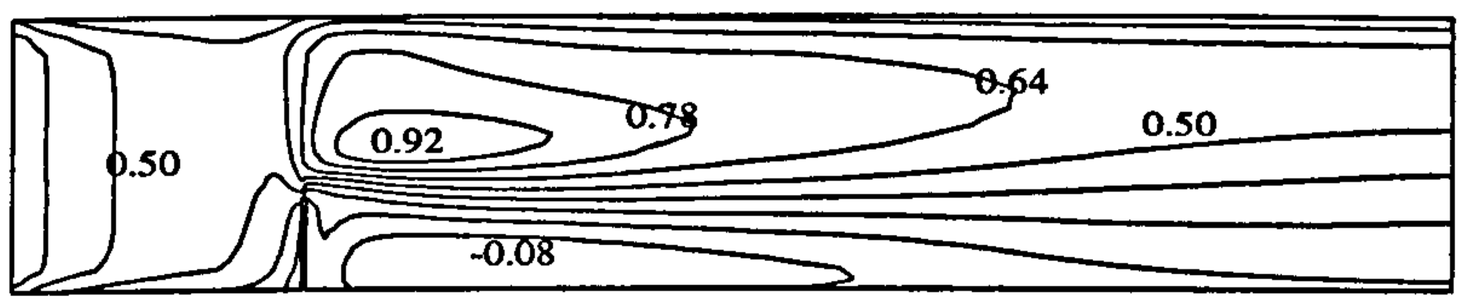

Contours Interval : 0.14 Pa

(c) Y-Dir Bed Shear Stresses

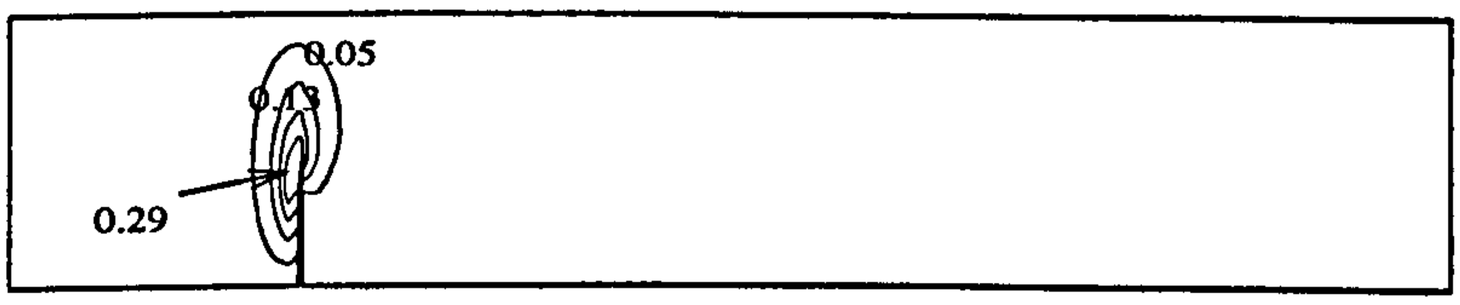

Contours Interval : 0.08 Pa

Figure 6.9 : FLUENT Output (Flatbed)

Width of Channel : 0.46m
Spur Length, d = 10 cm
Spur Width, W = 3.5 cm

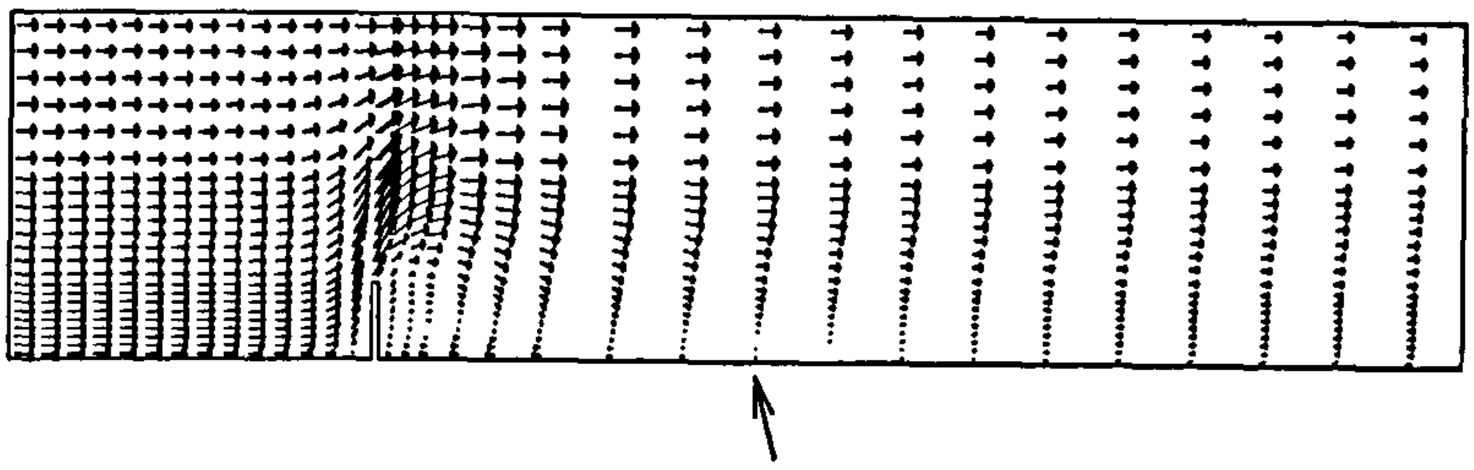

Attachment point

Bed Shear Stress

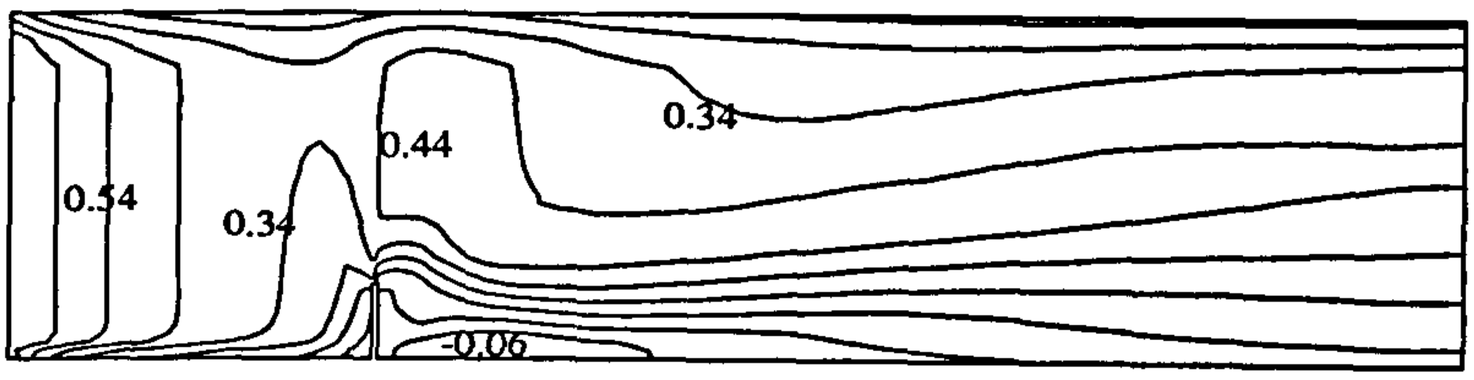

Width of Channel : 0.46m
Spur Length, d = 15 cm
Spur Width, W = 1.5 cm

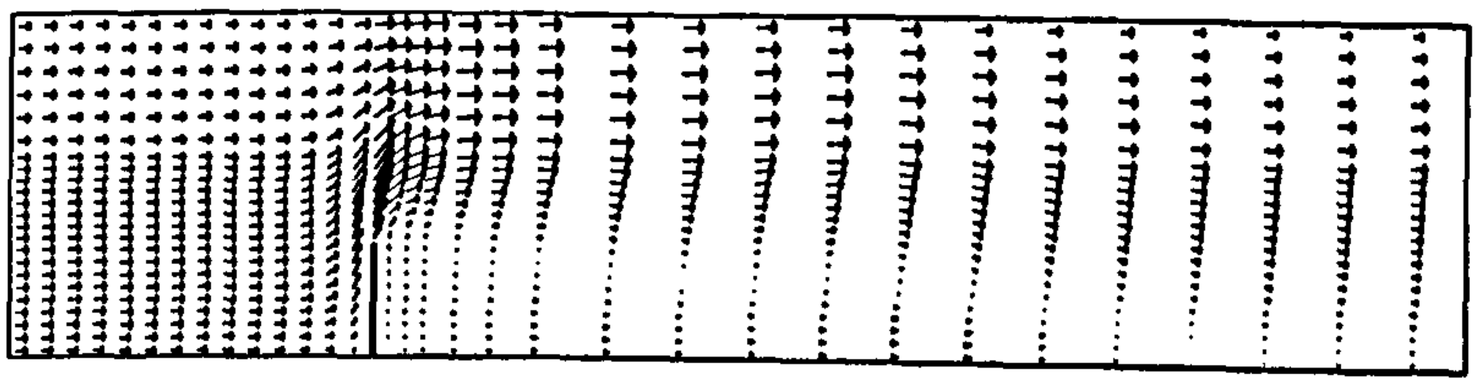

Attachment point

Figure 6.10 : Effect of Changing Spur-dyke Geometry
(scale distorted in y direction (5x))

(a) Velocity Vectors (at bed)

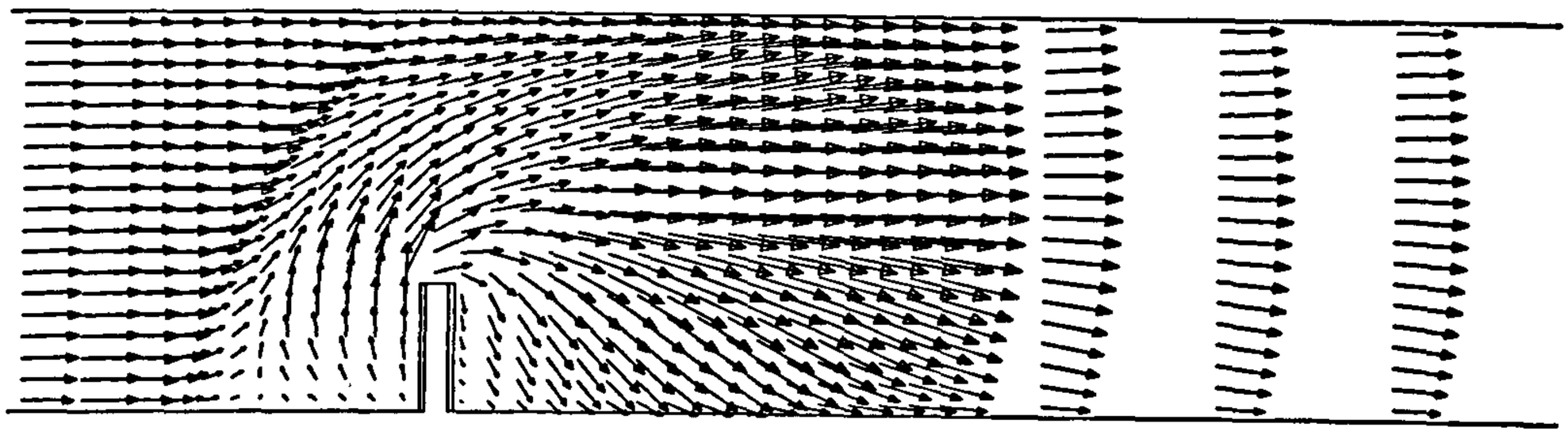

0.48 m/s

(b) X-Dir Bed Shear Stresses

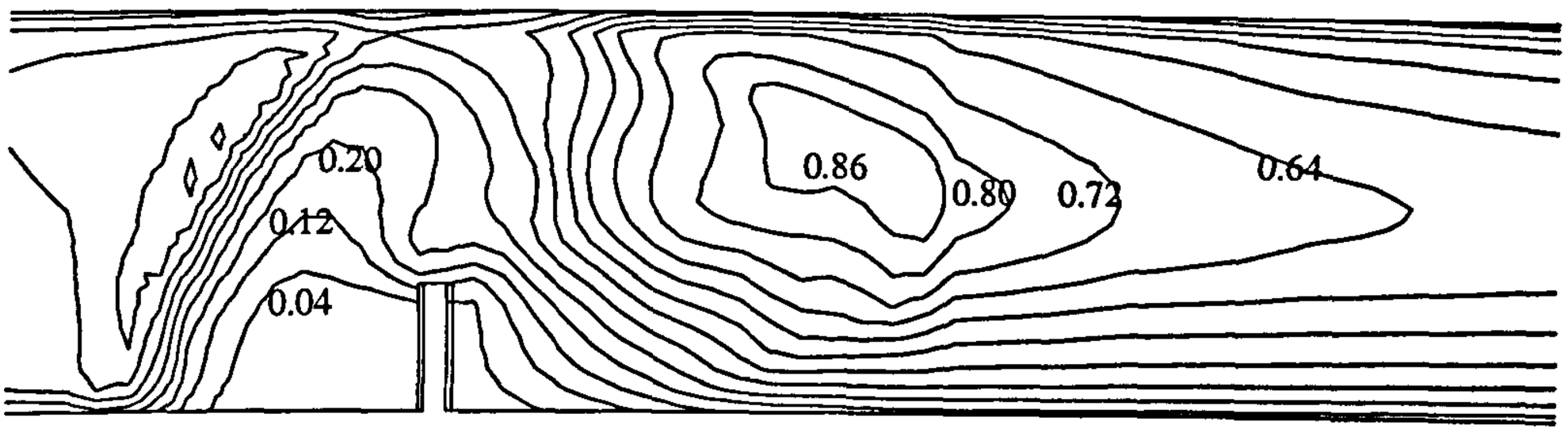

Contours Interval : 0.08 Pa

(c) Y-Dir Bed Shear Stresses

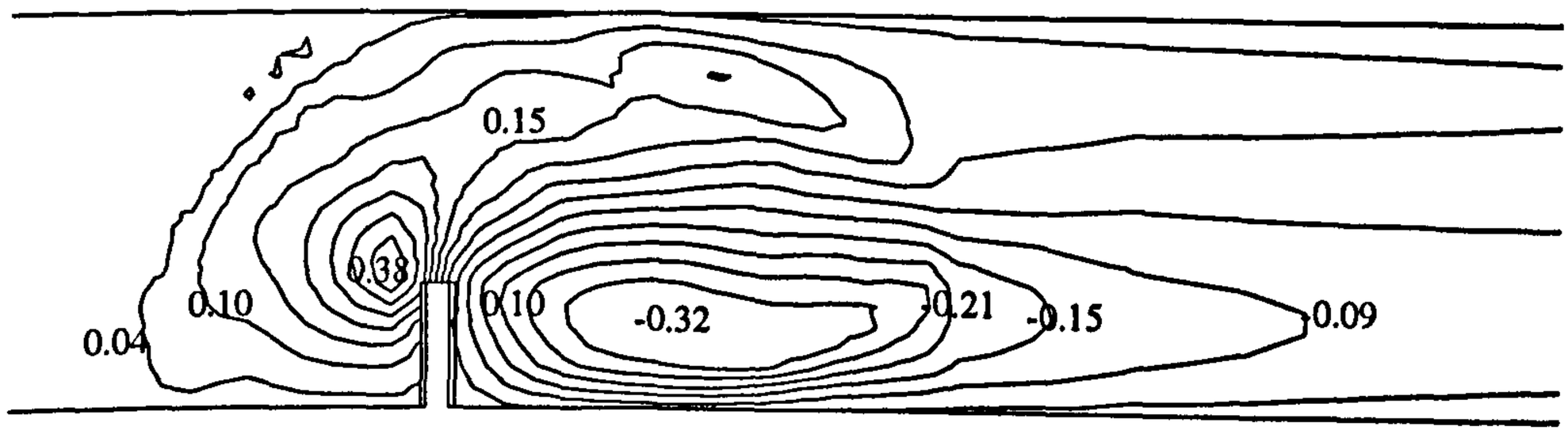

Contours Interval : 0.06 Pa

Figure 6.11 : FLUENT Output (Scoured bed)

NOTATIONS

B	Width of channel
C	Chezy coefficient
d	Dyke length
D_s	maximum depth of scour
f	Darcy Weisbach friction factor
F	Froude number
H	Upstream water depth
H_{max}	Recirculation width
K_1, K_2, K_3	Constants
u_b	Velocity measured at bed
v_R	Resultant velocity
W	Width of spur-dyke
α	Opening ratio = $(B-d)/B$
γ	Specific weight of water
Δt	Time increment (FLUENT calculations)
Δz	increment in erdoded bed
θ	angle of inclination of the spur-dyke with respect to main flow
ρ	Density of water
τ_b	Shear stress acting on the bed
τ_c	Critical bed shear stress
ω_o	Reference vorticity e.g vorticity at the nose of the dyke

REFERENCES

Barbarutsi, S. Ganoulis, J. and Chu, V. H., "Experimental Investigation of Shallow Recirculation Flows", *J. of Hydraulic Engineering*, ASCE, Vol 115(No. 7). pp 906-924, 1989

Francis, J.R., Pattanick, A. and Wearne, S., "Observations of Flow Patterns Around Some Simplified Structures in Channels", Technical Note No. 8, Proc., pp. 829-846, Inst. of Civil Engineers, London, 1968.

Garde, R.J., Subramanya, D.K., and Nambudripad, K.D., (1961). "Study of Scour Around Spur-Dikes", *J. of Hydraulic Division,*ASCE, Vol 87, HY 6, November 1961, pp. 23 - 37.

Holly Jr., F.M. Dispersion in Rivers and Coastal Waters -1. Physical Principles and Dispersion Equations. In P.Novak (Editor) Developments in Hydraulical Engineering - 3. Elsevier Applied Scienc Publishers, London and New York, 1985.

Ishii, C., Asada, H. and Kishi, T. "Shape of Separation Region Behind a Groyne of Non-Overflow Type in Rivers", *Proceedings of the XX IAHR Congress*, Vol II, pp 405-412, Moscow 1983.

Mayerle, R. Toro, F.M, and Wang, S.S.Y., (1995), "Verification of a three-dimensional numerical model simulation of the flow in the vicinity of spur dikes", *J. of Hydr Res.*, ASCE, Vol 33, 1995, No. 2, pp.243-256.

Rajaratnam, N., and Nwachukwu, B.A., (1983). "Flow near Groin-Like Structures", *J. of Hydraulic Engineering*, ASCE, Vol 109(No. 3), March 1983, pp 463-480.

Roger, J.W. (1994), "Investigation of The Flow Pattern Around a Spur Dyke Using the FLUENT Package", MSc Thesis, University of Liverpool, September 1994

Tingsanchali, T. and Maheswaran, S. (1987), "2D Depth Averaged Flow Computation Near Groyne", *J. of Hydraulic Engineering*, ASCE, Vol 116(No. 1), January 1990. pp 71-86

Zaghloul, N. and McCorquodale, J.A. (1973), "A Numerical Model for Flow Past a Spur Dyke", *Proceedings of the First Canadian Hydraulics Conference,* University of Alberta, Edmonton, May 1973. pp. 355 - 368

Zaghloul, N. and McCorquodale, J.A. (1975), "A Stable Numerical Model for Local Scour ", *J. of Hydr Res.*, ASCE, Vol 13, No. 4, pp. 425-444

CHAPTER

CHAPTER 7

INVESTIGATION OF JET-FORCED WATER CIRCULATION IN WATER SUPPLY RESERVOIRS

7.1 INTRODUCTION

The growth of population and the industrialisation of societies increases the demand for water resource. Streams are known as abundant and natural sources of water which can supply irrigation and hydro-electric projects as well as city waterworks. However due to the seasonal variation of the streams flows it may not always be possible to fulfill the needs for consumption. Moreover, the quality of the river water may decline due to pollution discharged into the river upstream by industry, residential areas and agriculture. Storage of water on the other hand, permits the stabilisation of the supply demand.

In the planning of the water supply reservoirs, a growing concern with the quality of their output has been evident in recent years. This is particularly true of service reservoirs where purified water is stored before passing to the consumer, especially where these are shallow. Here the quality of the product depends - apart from the purity input - on the general flow patterns, the mixing processes and the retention times in the basin.

Open reservoirs are usually subject to wind-induced circulations which efffectively dilute any objectionable regions, but such circulations are relatively irregular and uncontrolled. In deep basins thermal stratification may be set up and at times this may nullify the wind-driven circulation.

Controlled circulation-patterns can, however, be established by means of suitable water-jet inlets, or by forced air bubble flows (Goosen, 1979). Arrangements of multiple jets can exert profound effects on the resultant circulations, mixing processes and retention times. The total effect of these arrangements, on the quality of the output, may be great.

Experimental investigation of jet-forced circulation, both in tanks and reservoirs, has been studied by many researchers, mostly using scale model tests. Among others include Falconer (1976), Fosset and Prosser (1949), Robinson (1979), and Sobey and Savage (1974).

Analytical work concerning the effects of wind and the earth's rotation has been carried out and well documented. However, the analysis of jet forced circulation has attracted relatively few researchers. Sobey and Savage (1974) developed a two-dimensional theoretical solution for a tangential jet discharging into a circular reservoir. Mills (1977) developed a solution for steady two-dimensional viscous motion within a circular cylinder generated by either the rotation of part of the cylinder wall or fluid entering and leaving through slots in the wall. Mills' solution is however, applicable for very small Reynolds numbers.

Falconer (1976) produced a two-dimensional mathematical model describing the jet forced circulation in reservoirs having very large inlets and outlets. Ali *et al* (1978) applied the well-known behaviour of two-dimensional turbulent jets to the problem of the circulation in reservoirs. Later, Ali and Pateman (1981) developed an analysis which took account of inflows as well as geostrophic and wind effects. The analysis for the jet forced circulation was based on the assumption of a constant friction factor for the reservoir.

Extensive experiments were conducted at the Department of Civil Engineering of the University of Liverpool over the last twenty years to study the effects, on the

circulation, of jet momentum, position and size of inlets, and the geometry and aspects ratio of the reservoir.

7.2 THEORETICAL CONSIDERATION

7.2.1 Dimensional Analysis of Reservoir Circulation

Because of the large number of parameters involved in this type of problem, dimensional analysis is often used to show the relative importance of the various dimensionless groupings.

Using the Buckingham π theorem, Sobey(1972) obtained the following functional relationship:

$$\frac{\overline{Q}_c}{\sqrt{K_j}\,L} = \Psi\left[\frac{1}{L}\left(\frac{K_j}{f^2}\right)^{\frac{1}{4}}, \frac{\sqrt{K_j}\,L}{Q_j}, \frac{L}{H}, \frac{\sqrt{K_j}}{\nu}, \frac{K_j}{Q_j\sqrt{gh}}, \frac{k_s}{h}\right] \qquad (7.1)$$

where $\overline{Q}_c$ is the mean circulating discharge and is defined as follows:

The circulating discharge Q_c is given by:

$$Q_c = h\int_0^R v\,dr \qquad (7.2)$$

where h is the water depth in the reservoir, and v is the peripheral velocity. The mean circulating discharge, $\overline{Q}_c$ is given by:

$$\overline{Q}_c = \frac{1}{2\pi}\int_0^{2\pi} Q_c\,d\theta \qquad (7.3)$$

where θ is the angle from the jet, K_j = kinematic jet momentum flux (= Q_jV_j), V_j is the jet velocity, f is the Coriolis parameter (=2Ω sinϕ), Ω = the Earth's angular velocity of rotation, ϕ = latitude angle of the reservoir, k_s = bed roughness height, ν = kinematic viscosity of water, $\sqrt{K_j}/\nu$ is a form of the jet Reynolds number, $K_j/[Q_j\sqrt{(gh)}]$ is the reservoir's Froude number, and k_s/h is the relative roughness of the reservoir.

Sobey (1972) also investigated theoretically the relative importance of the various parameters in the Equation (7.1) and obtained, for a stationary reservoir, the following relationship:

$$\frac{\overline{Q}_c}{\sqrt{K_j}\ L} = \Psi\left[\frac{L}{h}, \frac{k_s}{h}\right] \qquad (7.4)$$

Using Sobey's theoretical curves, for the variation of $\overline{Q}_c/\sqrt{(K_j)}L$ versus L/h for different values of k_s/h, Ali and Pateman (1981) fitted the following relationship:

$$\frac{\overline{Q}_c}{\sqrt{K_j}\ L} = \left[5.527 - 9.226\left(\frac{k_s}{h}\right)^{0.238}\right]\left[\frac{L}{H}\right]^{-1} \qquad (7.5)$$

7.3 EXPERIMENTAL ARRANGEMENTS AND MODELS

7.3.1 Experimental Setup

Extensive experiments were conducted by Ali and his collaborators at Liverpool to study reservoir circulation. Some of the models used are described below (see also Table 7.1):

Table 7.1 : Experimental Models and Inlet-Outlet Arrangements

Model	Arran-gement	L=2R (m)	h (mm)	bo (mm)	do (mm)	Scale Ratio (α)	Bed Material
1	1	7.36	70,120, 170, 220, 280	50	2	-	painted concrete
1	2	7.36	70, 120, 170, 220, 280	50	2	-	painted concrete
2	1	3.00	20, 50, 100, 200	20	2	-	glass
2	2	3.00	20, 50, 100, 200	20	2	-	glass
2	3	3.00	20, 50, 100, 200	20	2	-	glass
3	4	2.44	46	20, 8	2, 30, 60, 130	-	painted wood
Prescot No. 4	1	1.6	16	12.2	2.4	250	painted wood
Prescot No. 4	2	1.6	16	1.6 (dia)	1.6 (dia)	250	painted wood
Prescot No. 3	1	1.7	16	1.6 (dia)	1.6 (dia)	250	painted concrete

(i) A large circular reservoir of 3.68m radius was used. It had a painted concrete bed. An inlet jet 50 mm high and 2 mm wide was used. In some of the experiments, this jet was located in a tangential position, together with a central outlet. In other experiments, this jet was used in a radial position. Two outlets, one on either side of the radial jet were also used (Figure 7.1, Model 1, Arrangement 2).

(ii) A smooth circular reservoir having a radius of 1.5 m was also used. A jet having a height (b_o) of 20 mm and a width (d_o) of 2 mm was used in a tangential position together with a central outlet, one on either side of the jet were used.

(iii) Another circular reservoir of 1.22 m radius was used to investigate the effect of the jet momentum and area on the reservoir circulation (Figure 7.1, Table 7.1). The jet discharge was kept constant and the momentum was changed by altering the jet area. The values of b_o x d_o used were 20 x 2, 8 x 30, 8 x 60, 8 x 90 and 8 mm, 130 mm.

(iv) Scale models of two water-supply reservoirs were built to the horizontal scales of 1/500 and 1/250. These were the Prescot No. 3 and No. 4 service reservoirs (City of Liverpool, U.K) and are shown in Figure 7.2. The 1/250 models had a moulded concrete bed and sides, with a fixed vertical exaggeration of 5:1 (α/β = 5, α = horizontal scale and β = vertical scale). For certain tests, a false flat aluminum bed and dummy vertical scales were fitted, in order to investigate the effect of vertical exaggeration on reservoir circulation and mixing. The 1/500 model had a flat plywood base and vertical Lucite sides. Its vertical scale could be varied from 1/500 to

1/100 or less. Another model of reservoir No. 4 was built to the scale 1/83.3. It had a flat concrete bed and vertical brick sides so that, as with the 1/500 and 1/250 models, the vertical scale could be varied.

7.3.2 Measuring Techniques

The various methods used to study reservoir circulation and mixing are listed below:

1. Large velocities were measured with a miniature current-meter, but surface floats were used to measure small velocities. Some of the experiments depended on illuminated floats, with time-lapse photography.

2. Dye photography was used on all models to permit rapid study of circulation-patterns and degrees of mixing.

3. The conductivity and fluorometric methods were used to study reservoir mixing directly. Continuous and instantaneous injections, through the inlet, were used. Details of the mixing experiments are given by Ali and Pateman (1983).

7.3.3 Experimental Results

Tangential Jet Inlet

Figure 7.3 shows velocity-distributions obtained by Ali and Whittington (1979), for various discharges and water-depths using the 3m diameter smooth reservoir. This figure shows a general increase in the maximum velocities with increase in discharge, for a constant water-depth. A more symmetrical velocity-distribution is noticed for the bigger water-depths.

Ali and Whittington (1979) obtained the following relationship:

$$\frac{Q_c}{\sqrt{K_j}\ L} = 1.36\left(\frac{h}{L}\right)\left[1.70 + \frac{123.89}{(\sqrt{K_j}/\nu)^{2.5}\ (h/L)^{2.5}}\right] \qquad (7.6)$$

Ali and Pateman (1981) obtained relationships for the velocity distributions, in circular reservoirs, produced by radial and tangential jets. These relationship can be used very easily to obtain velocity fields similar to those given in Figure 7.4.

Effect of Jet Momentum on Reservoir Circulation (Radial Jet)

Ali(1983) conducted series of experiments in the 2.44 m diameter reservoir to study the effect of jet momentum on circulation (Figure 7.1 Model 3, Arrangement 4, Table 7.1). Jet discharge and water-depth were kept at 0.192 x 10^{-3} m^3 and 46 mm respectively. The inflow momentum was altered by changing the area of the jet. Areas of 0.4 cm^2, 2.4 cm^2, 4.8 cm^2, 7.2 cm^2 and 10.4 cm^2 were used. The outlet was 0.38 m wide and located opposite to the inlet.

Figure 7.5 - 7.8 shows measured velocity-distribution for the above radial jets. These figures are given for different times from the start of injection of the dye. Clearly, the increase in jet area for a given jet discharge results in a reduction in circulation.

Figure 7.9 shows measured velocity-distribution for the various jet areas. This figure demonstrates clearly the increase in reservoir velocities resulting from the increase in jet momentum.

For the reservoir with a jet area of 0.4 cm^2 (b_o = 2cm, d_o =0.2 cm) the ratio $\overline{Q}_c/Q_j$ was 8.86. Observations indicated that altering the position of the outlet had little effect on the circulation pattern in the reservoir. This is expected since for steady flow, the flow throughout the outlet is Q_j.

For the reservoir with a jet area of 10.4 cm^2, $\overline{Q}_c$ / Q_j was found to be 1.65. Changing the position of the outlet in this case had a profound effect on the circulation pattern. The following relationship was fitted to the experimental results:

$$\frac{\overline{Q}_c}{Q_j} = 0.0292\sqrt{R} + 1 \qquad (7.7)$$

where;

$$R = hV_j / \nu \qquad (7.8)$$

Equation (7.5) can also be written in the following form:

$$\frac{\overline{Q}_c}{Q_j} = \frac{A_s}{d_o^{1/2}} + 1 \qquad (7.9)$$

where;

$$A_s = 0.0292 \left(\frac{Q_j h b_o}{\nu} \right)^{1/2} \qquad (7.10)$$

The value of b_o for four for our inlet jets was 8 mm. Using this value of b_o and substituting for the other constants gives A_s = 7.67 m$^{1/2}$.

For a two-dimensional plane jet (Daily and Harleman, 1973) we have:

$$\frac{Q_c}{Q_j} = 0.62\left(\frac{x}{d_o}\right)^{1/2} \qquad (7.11)$$

Putting $x = R$ in Equation (7.11) gives $A_s = 6.85$ m$^{1/2}$ compared with 7.67 m$^{1/2}$ given in Equation (7.10).

Use of Twin Radial Jets Positioned at the Perimeter Wall

The 3 m diameter circular reservoir was used to observe the effect of two identical radial jets set 90° apart in the reservoir wall (b_o = 20 mm, d_o =2 mm) (Figure 7.1, Model 2, Arrangement 3). Water depths of 20, 50, 100 and 200 mm were used in different runs (for the same jet discharges). Figure 7.10 shows dye photographs (h=50 mm) demonstrating the spread of the two "identical" jet with time. Deflection of the jets to form a very asymmetrical circulation is very evident.

Figure 7.11 and 7.12 show similar experiments conducted with reservoir water depths of 100 and 200 mm. Clearly, the circulation patterns are very symmetrical in these experiments (Ali, 1983). Velocities measured at mid-depth for the h=100 mm are shown in Figure 7.13. The velocity distribution from the jet to the centre of the reservoir is restricted in width by gyres A and B (for each jet). The two gyres meet at the centre of the reservoir wall. At the wall, the jet divides into two wall jets which move round the reservoir circumference.

Verification of Sobey's Theoretical Predictions

Sobey (1972) derived a two-dimensional solution for the reservoir circulation generated by a single tangential jet whose height was the same as the water-

depth in the reservoir. Sobey assumed the velocity-distribution, in the reservoir, to be made up of a rectangular wall portion and a triangular reservoir portion. He also assumed that peripheral velocities were zero everywhere for distances less than $0.5R$ from the centre.

Figure 7.14 shows plots of $\overline{Q}_c/(\sqrt{K_j}L)$ against L/h for the various model reservoirs. This figure shows that:

a. the aspect ratio (L/h) is very important;

b. the values of $\overline{Q}/(\sqrt{K_j}L)$, for the same L/h are very close for the different sizes of the Prescot No. 4 models confirming that the effect of jet Reynolds number is small for these experiments.

c. the values of $\overline{Q}/(\sqrt{K_j}L)$ for the Prescot No. 4 are very different from the other results, indicating a different type of flow.

7.4 PREDICTION OF RESERVOIR CIRCULATION USING FLUENT

The FLUENT package was used to predict reservoir circulation for simple and complicated examples. These examples were chosen in order to compare with existing experimental results. It must be stressed that all of the FLUENT solutions presented in this paper are for two-dimensional (depth-averaged) flows.

(a) Radial Jet Discharging into a Circular Reservoir

(i) A circular reservoir 2.44 m in diameter was used (Figure 7.1, Model 3, Arrangement 4). The jet discharge was 244 cm^3/s. An outlet 38 cm wide was located opposite to the inlet (see Figure 7.8). Radial

jets 3, 6, and 13 cm wide were used. The experimental results are given in Figure 7.8. The circulations predicted by FLUENT are shown in Figure 7.15. Clearly, there is excellent agreement with the experimental results.

(ii) A radial jet was used together with two outlets inside the reservoir (Figure 7.1, Model 1, Arrangement 2). The experimental velocity distributions are given in Figure 7.16 and the FLUENT circulation is given in Figure 7.17. Again, the predicted circulation is very similar to that obtained experimentally. It is interesting to note that for this example, the entrained discharge is much bigger than the inflow and, therefore, the effect of the outlets is very small and localized.

(b) Complicated Reservoir Geometries and Inlet/Outlet Arrangements

Extensive experiments were conducted on scale models of the Liverpool No. 3 and 4 reservoirs at Prescot (Ali *et.al*, 1978).

(i) Figure 7.18 shows surface circulation patterns generated by a floor pipe in reservoir No. 4 using the 1/250 model with $\alpha/\beta = 1$. Figure 7.19 and Figure 7.20 give the FLUENT depth-averaged circulation patterns generated using one inlet and one outlet. Figure 7.19 gives the results using the actual inflow velocity whilst Figure 7.20 gives the results obtained using a depth-averaged inflow momentum. The two predicted solutions are quite similar to the experimental circulation. In all cases two gyres are observed in the reservoir. Clearly, the effect of the outlet is very small.

(ii) Figure 7.21 shows the experimental surface velocity diagram for two nozzles positioned at mid-depth. The two nozzles direct water jets towards the centre of the reservoir, and on each side of the jet, gyres are set up. Those near the inlet jets lead to the production of further gyres.

Figures 7.22 and 7.23 show predicted results obtained for the original nozzle velocities and for depth-averaged values. The effect of the change in velocity, on the circulation patterns, is small. The FLUENT results show two main gyres quite similar to those obtained experimentally. The two small gyres, near the outlet, obtained in this experiment are not reproduced in the numerical solution. Also the predicted circulation at the north-eastern part of the reservoir is very different from the measured one.

The main reason for the different circulation patterns produced by the physical model and by FLUENT is that the relatively small physical models had a vertical exaggeration of 5:1. The numerical solutions were, however, run for the prototype reservoirs (undistorted, full scale).

It is well known (Ali *et al.* 1978) that the change in reservoir's aspect ratio, as a result of vertical exaggeration, has a profound effect on the tendency of radial jets to deflect from their straight path. Figure 7.24 shows dye photographs for twin jets in the 1/250 and 1/83.3 models for various value of α/β. These results show that with vertical exaggerations of less than 3 to 1, deflection of the jets takes place. As the aspect ratio increases, the effective hydraulic depth is reduced relative to the horizontal distance travelled. The consequent diminution in jet momentum presumably causes a

diminution in the separate identity of each jet. Each jet forces its way through the other's field with increasing difficulty (Ali *et al.* 1978).

(iii) Figure 7.25 shows surface circulation patterns generated by two nozzles positioned at mid-depth in the scale-model of Prescot No. 3 reservoir. The results were obtained for a 5:1 vertical exaggeration. There is good surface movement almost everywhere.

Figure 7.26 and 7.27 show the predicted circulations using two actual and the depth-averaged velocities. The predicted circulations are very similar. There is, however, a general reduction in velocities on depth-averaging of velocity.

Clearly, the predicted circulations are very different from the measured ones.

7.5 CONCLUSIONS

1. When mixing is produced in a circular reservoir, by a tangential or a radial jet, the circulation patterns depend on the Reynolds number of the jet, the aspect-ratio and relative-roughness of the reservoir.

2. Experiments with $(L/d_o) > 50$ show that the outlets have little influence on the circulation in reservoirs. Due to considerable entrainment; the circulating discharge is usually much bigger than the discharge of the inlet.

3. An implication of conclusion 1, that the aspect-ratio is of great importance, was verified in detailed experiments on scale-models of water-supply reservoirs. It follows that the common practice of exaggerating the vertical scale is not automatically valid.

4. The use of multiple jets improves the circulation and mixing and reduces the stagnation zones in reservoirs. Here, jet momentum and location are of primary importance.

5. Sobey's theoretical predictions are in reasonable agreement with the results obtained from experiments carried out at The University of Liverpool.

6. In most cases, the FLUENT package gives excellent prediction of jet-forced reservoir circulation. Solutions of very complicated reservoir geometries and multiple inlet/outlet arrangements require further verification using undistorted physical models.

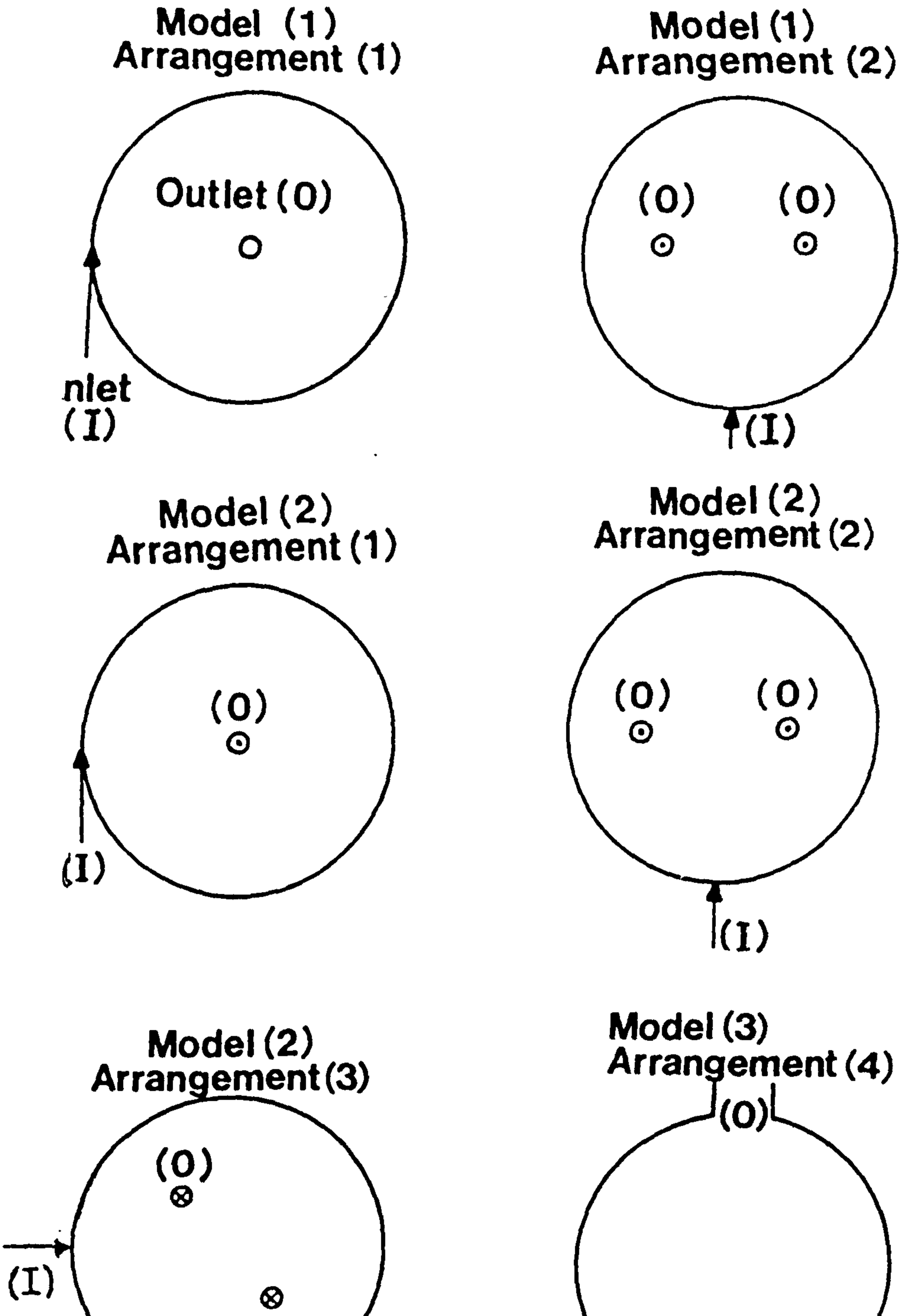

Figure 7.1 : Details of Circular Reservoir Models Used in Experiments

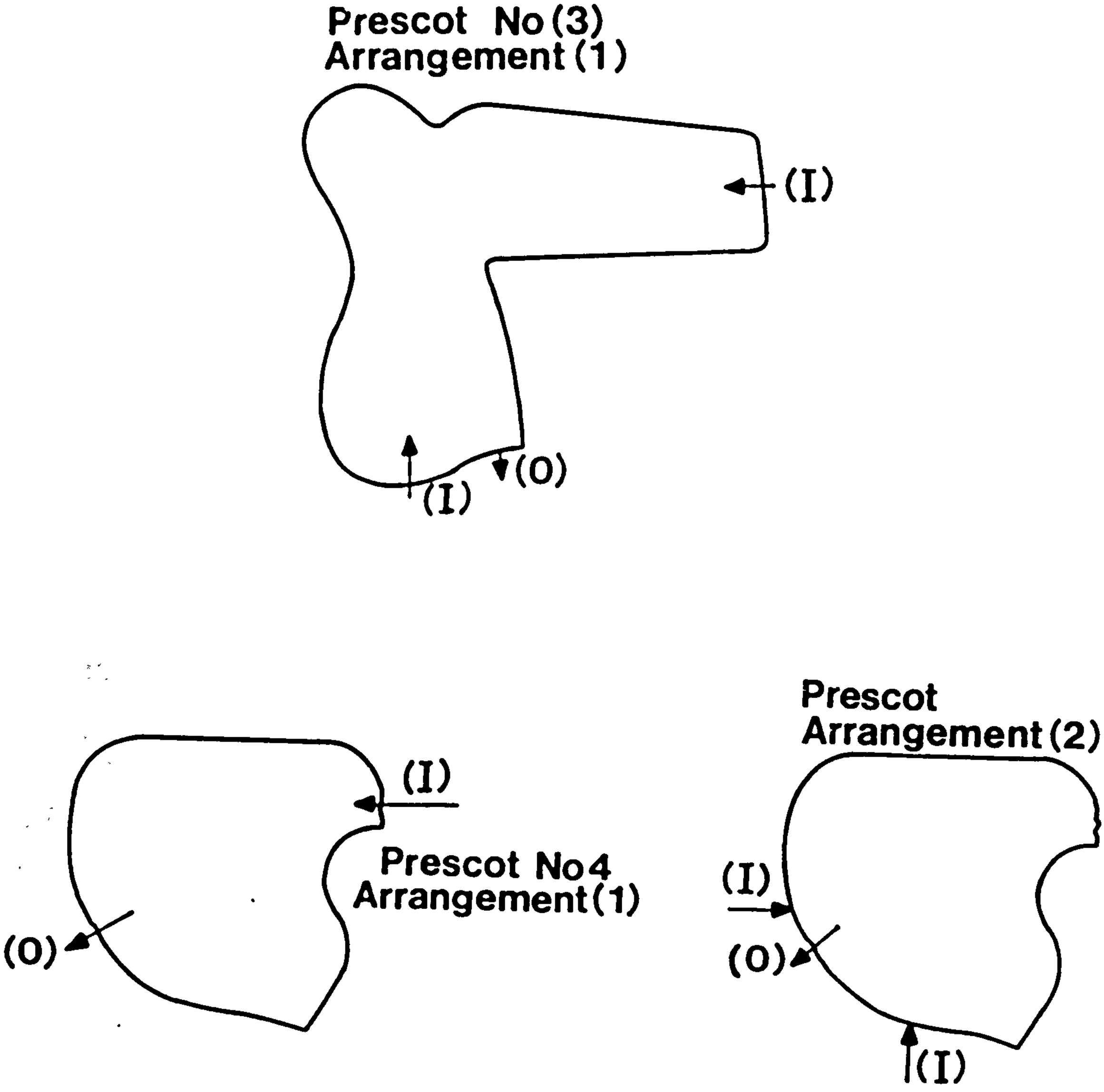

Figure 7.2 : Details of Prescot No.3 and No. 4 Reservoir Models

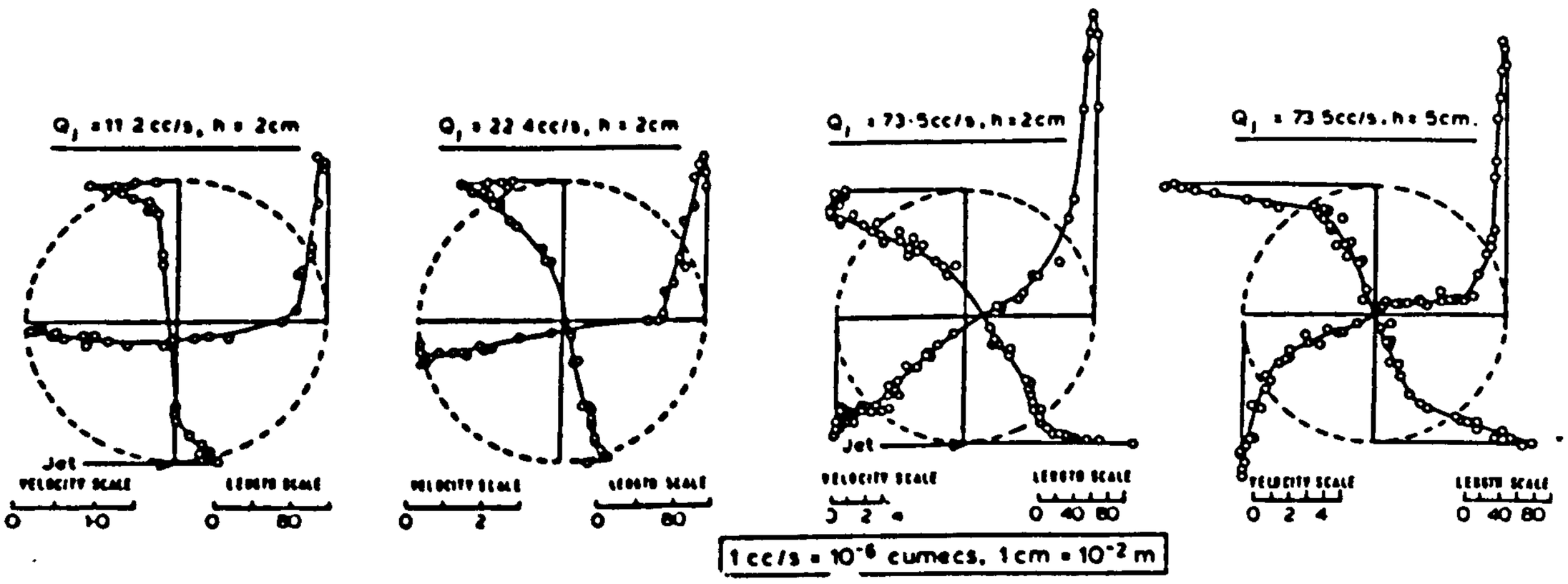

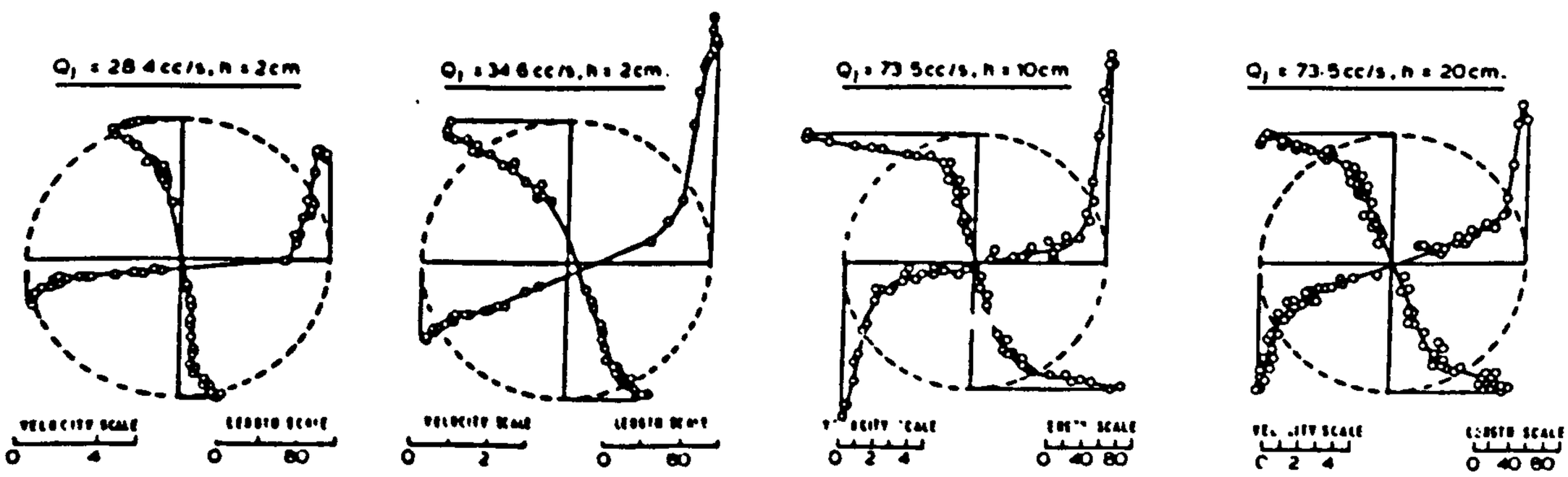

Figure 7.3 : Measured Velocity Distributions
(After Ali and Whittington, 1979)

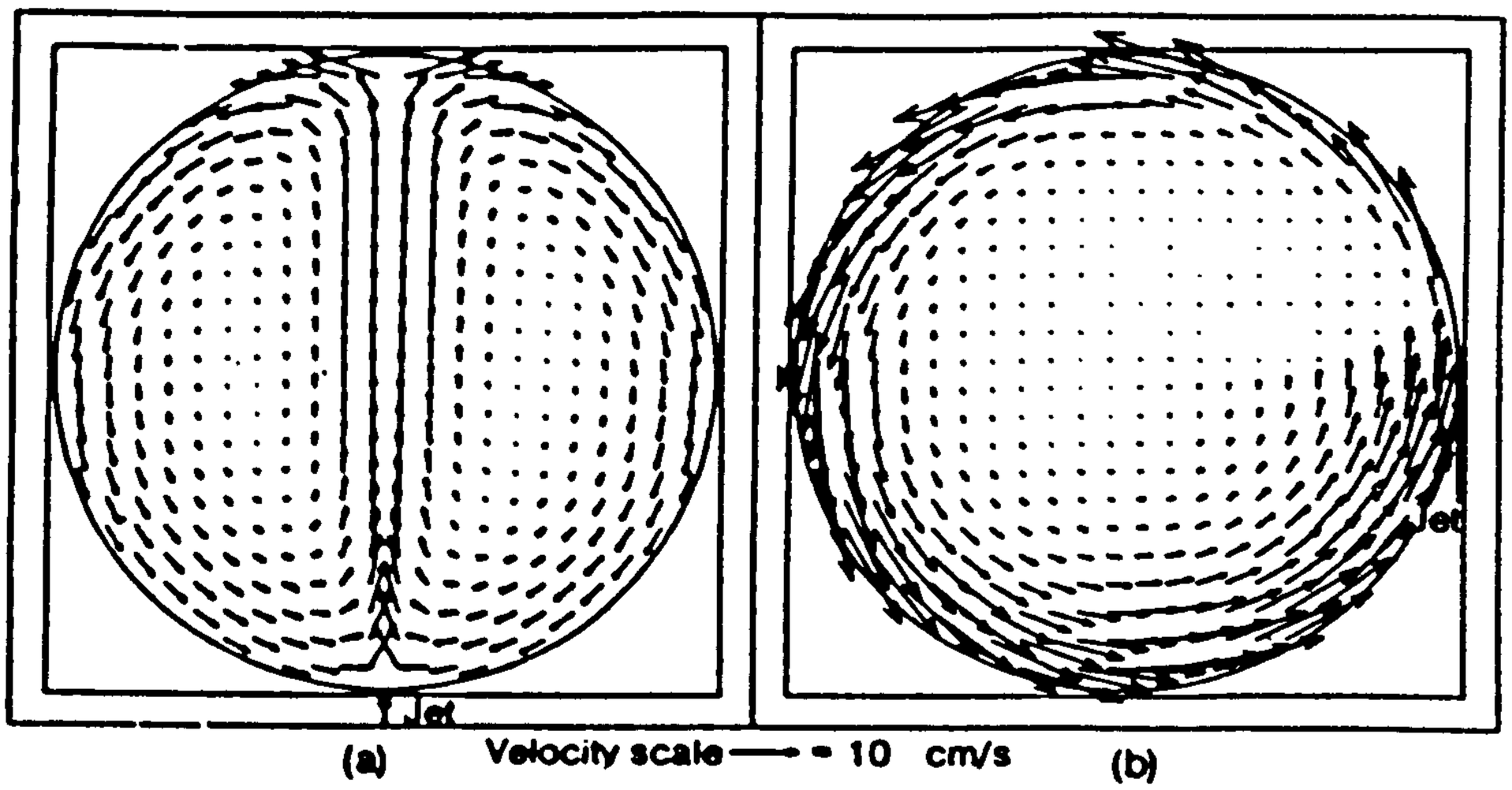

Figure 7.4 : Typical Circulation Produced by Two-dimensional (a) Radial and (b) Tangential Jet Inlets (after Ali and Pateman, 1981)

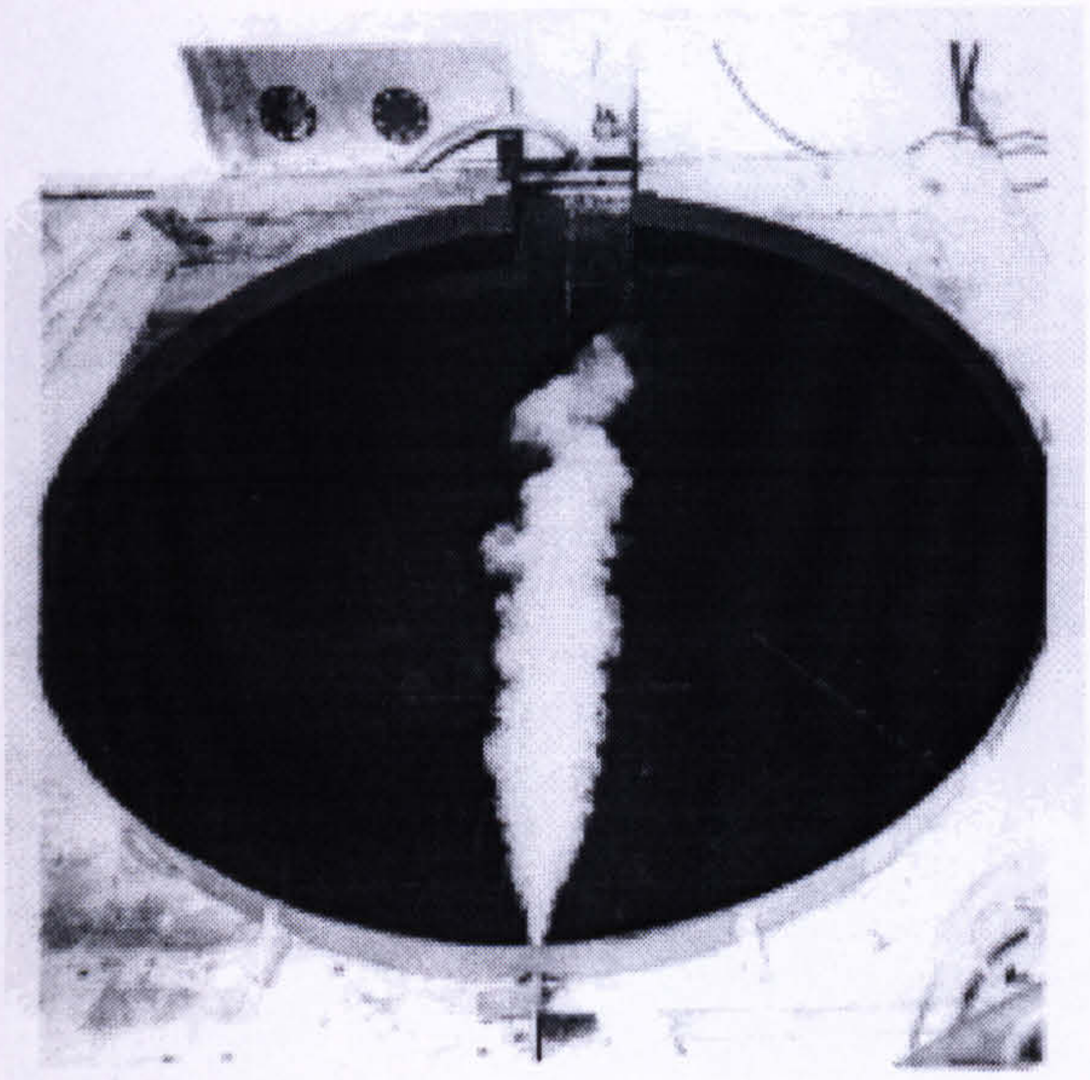

2 secs

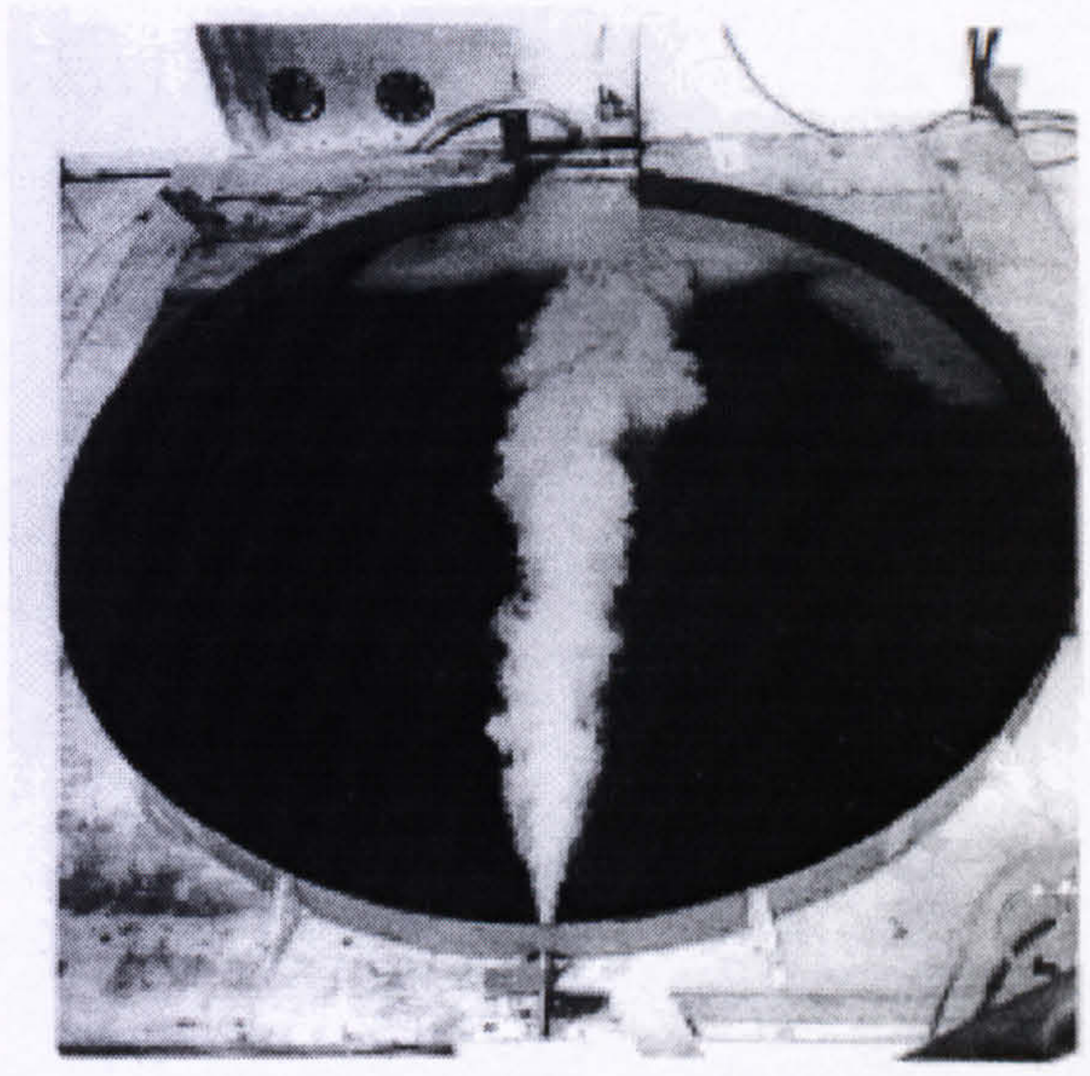

10 secs

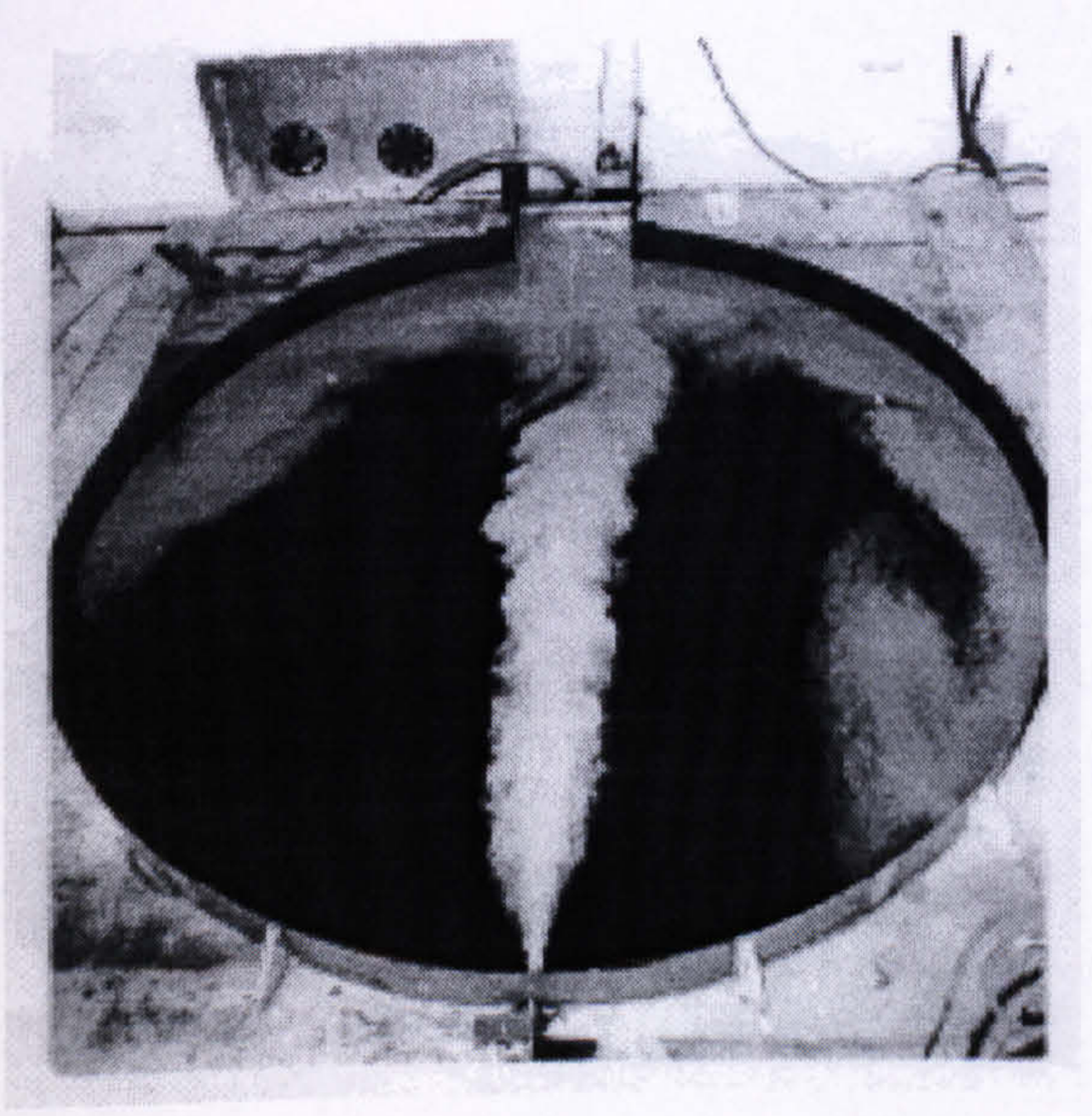

20 secs

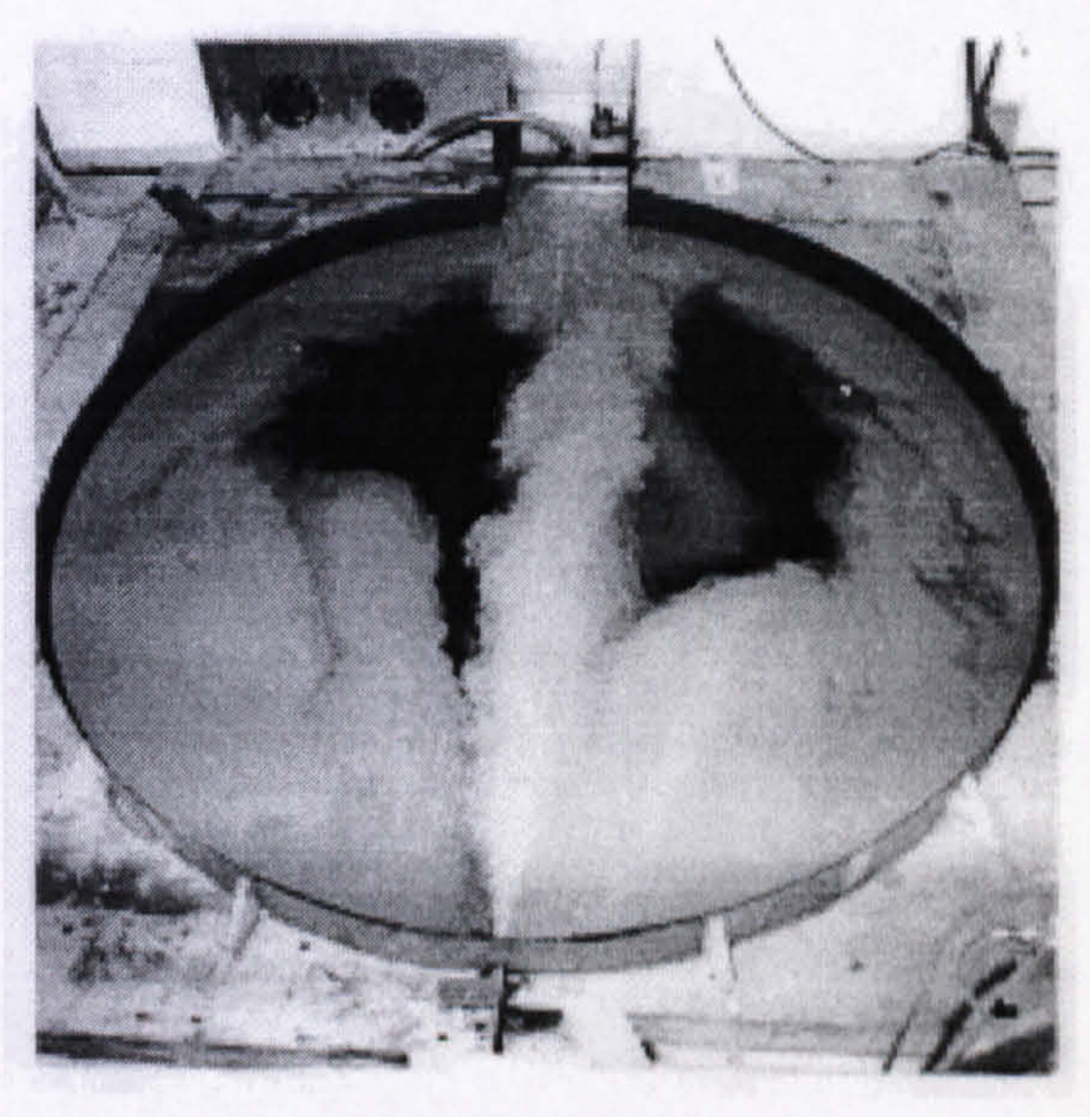

40 secs

Figure 7.5 : Dye Mixing (Radial Jet Q_j = 192 cm ^{3}/s; A_j = 0.4cm ^{2} ; L = 243.8 cm)
(After Ali, 1983)

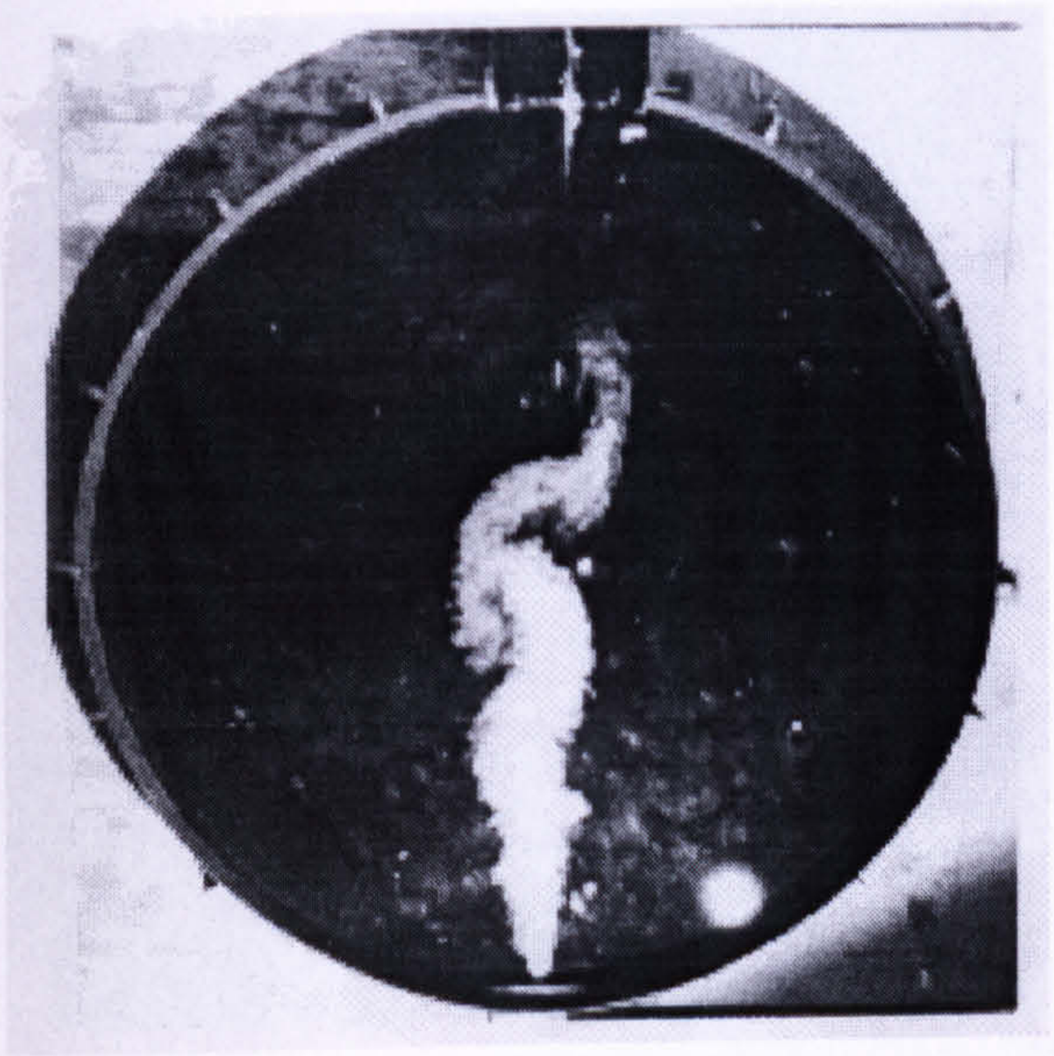

20 secs

65 secs

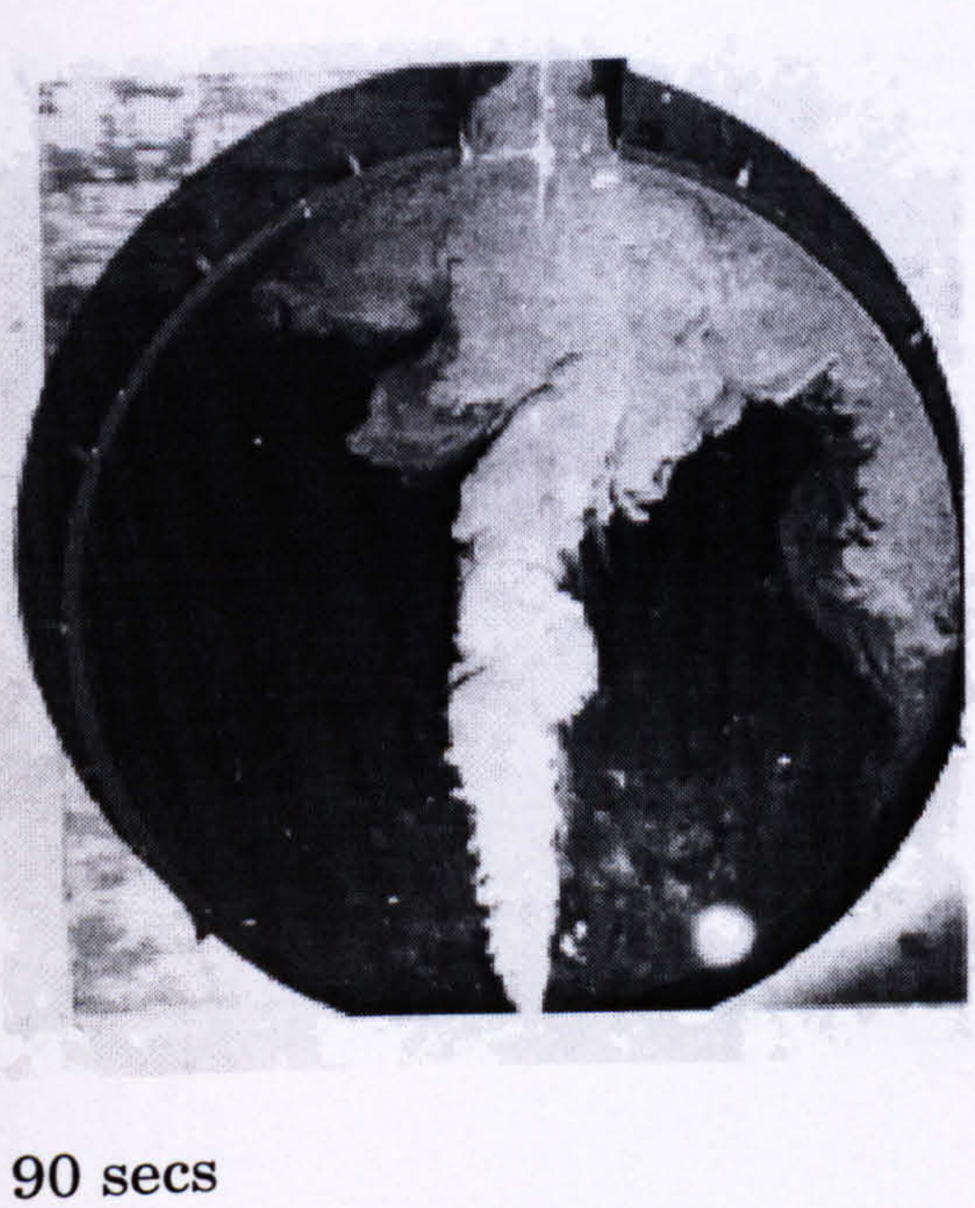

90 secs

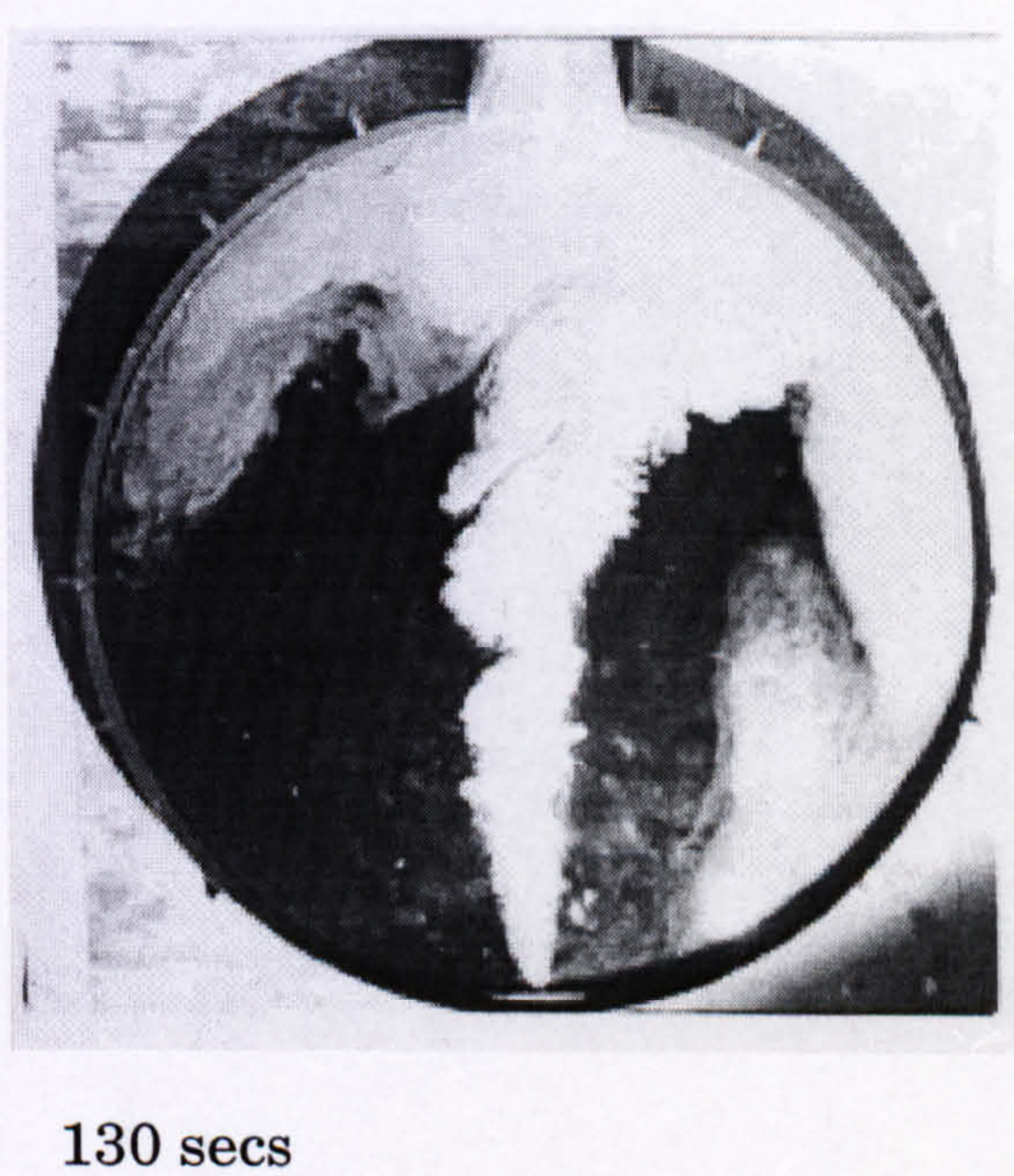

130 secs

Figure 7.6 : Dye Mixing (Radial Jet Q_j = 192 cm ^{3}/s; A_j = 2.4cm ^{2} ; L = 243.8 cm)
(After Ali, 1983)

25 secs

60 secs

80 secs

140 secs

Figure 7.7 : Dye Mixing (Radial Jet Q_j = 192 cm ^{3}/s; A_j = 4.8cm ^{2} ; L = 243.8 cm)
(After Ali, 1983)

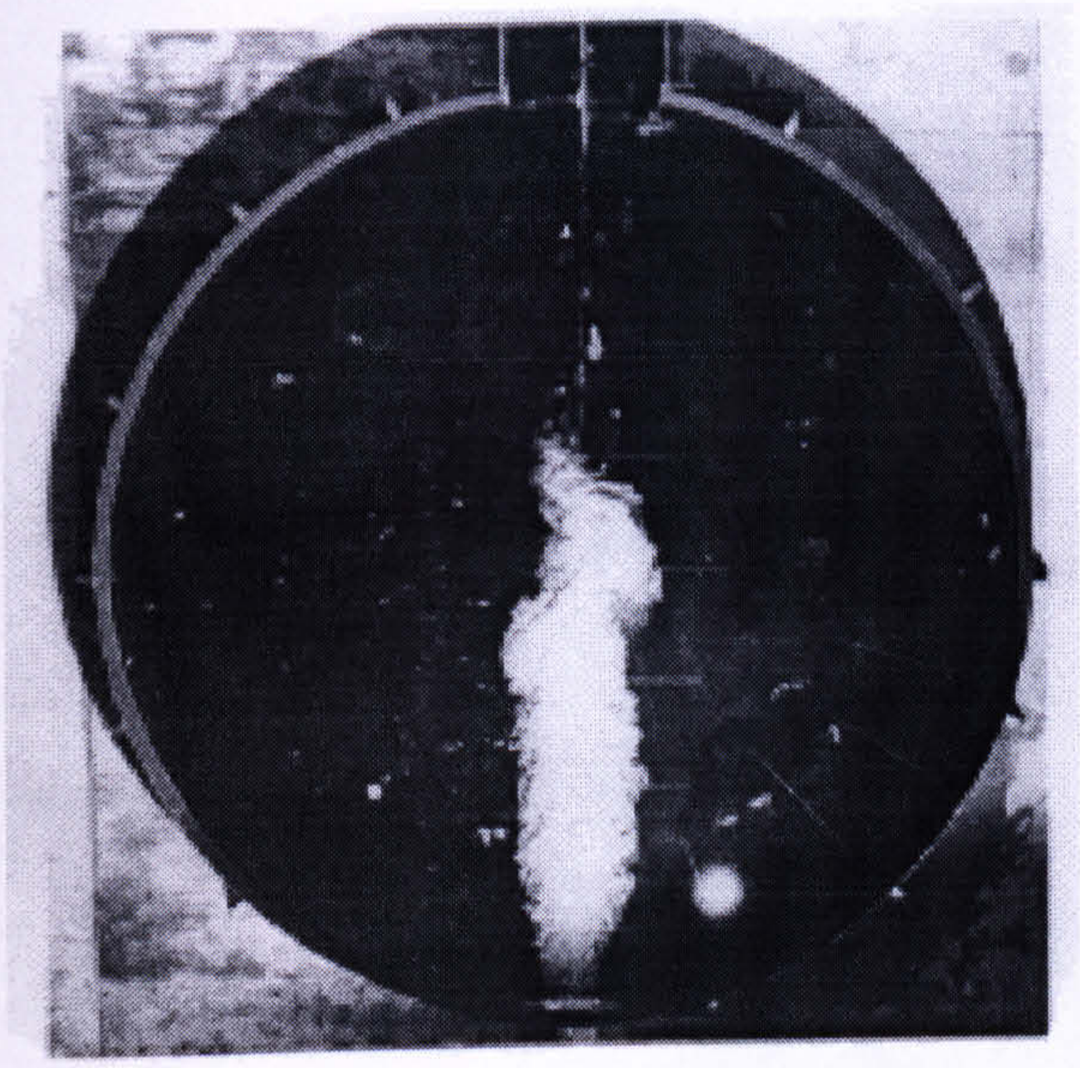

30 secs

85 secs

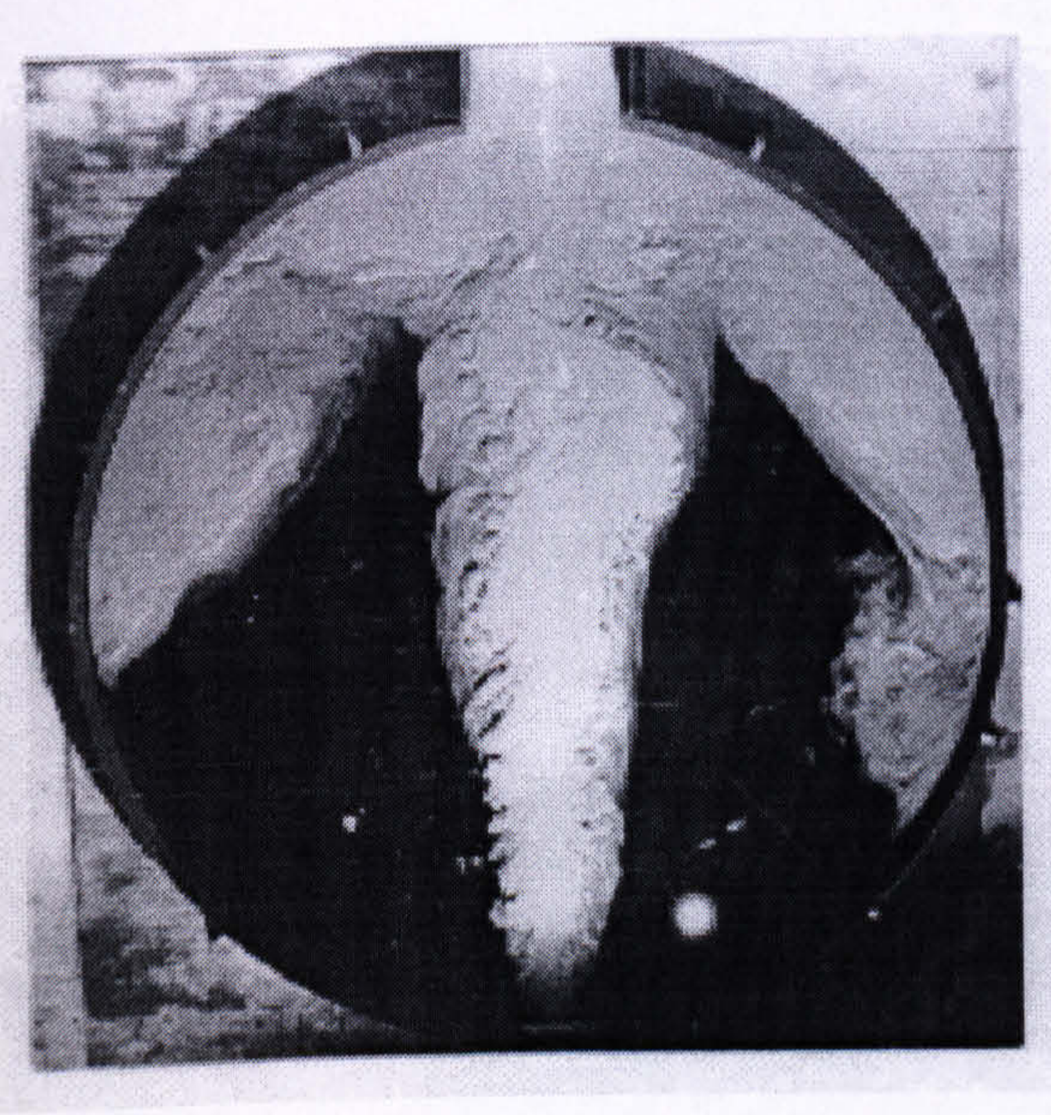

125 secs

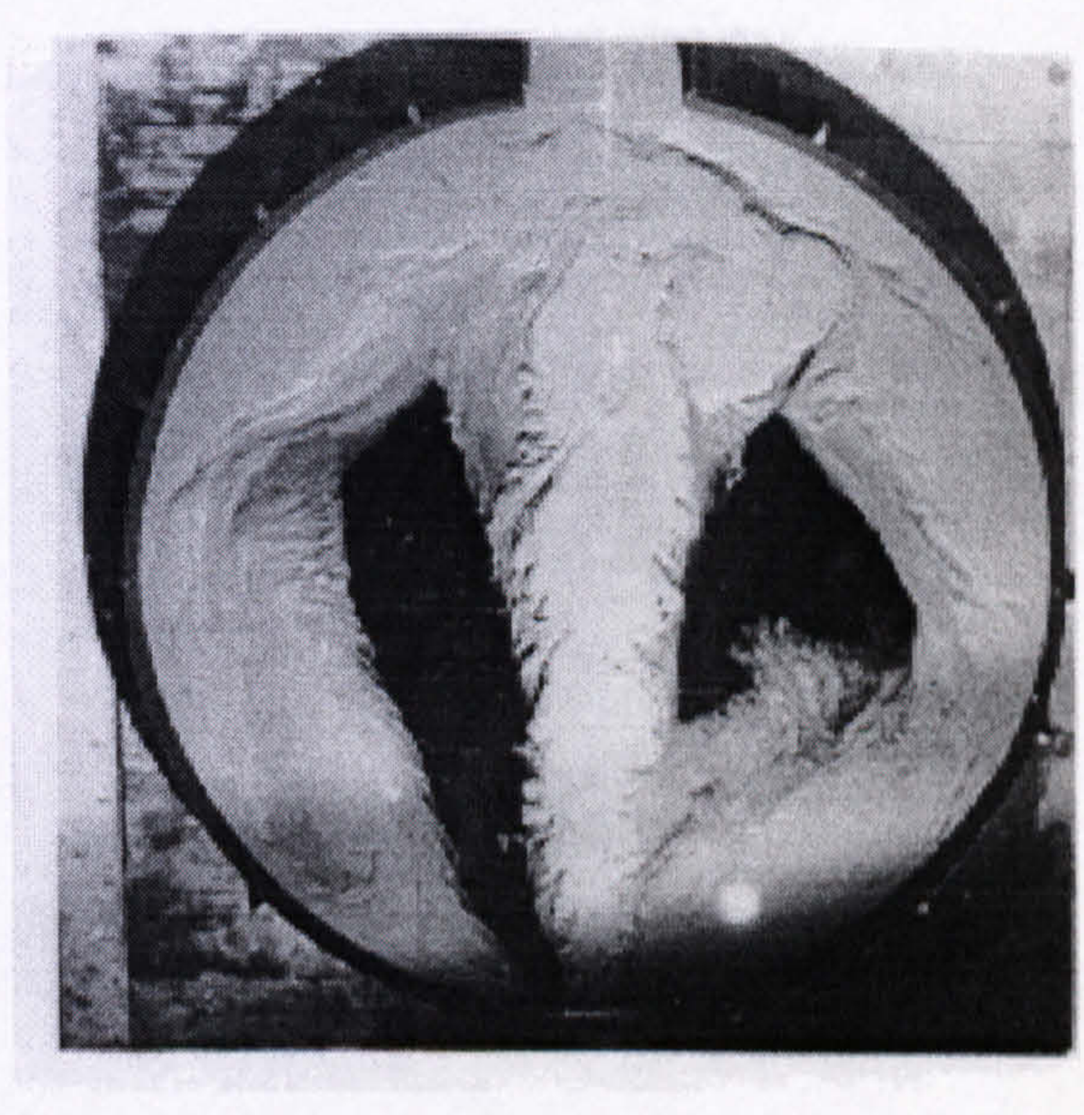

200 secs

Figure 7.8 : Dye Mixing (Radial Jet Q_j = 192 cm ^{3}/s; A_j = 10.4cm ^{2} ; L = 243.8 cm)
(After Ali, 1983)

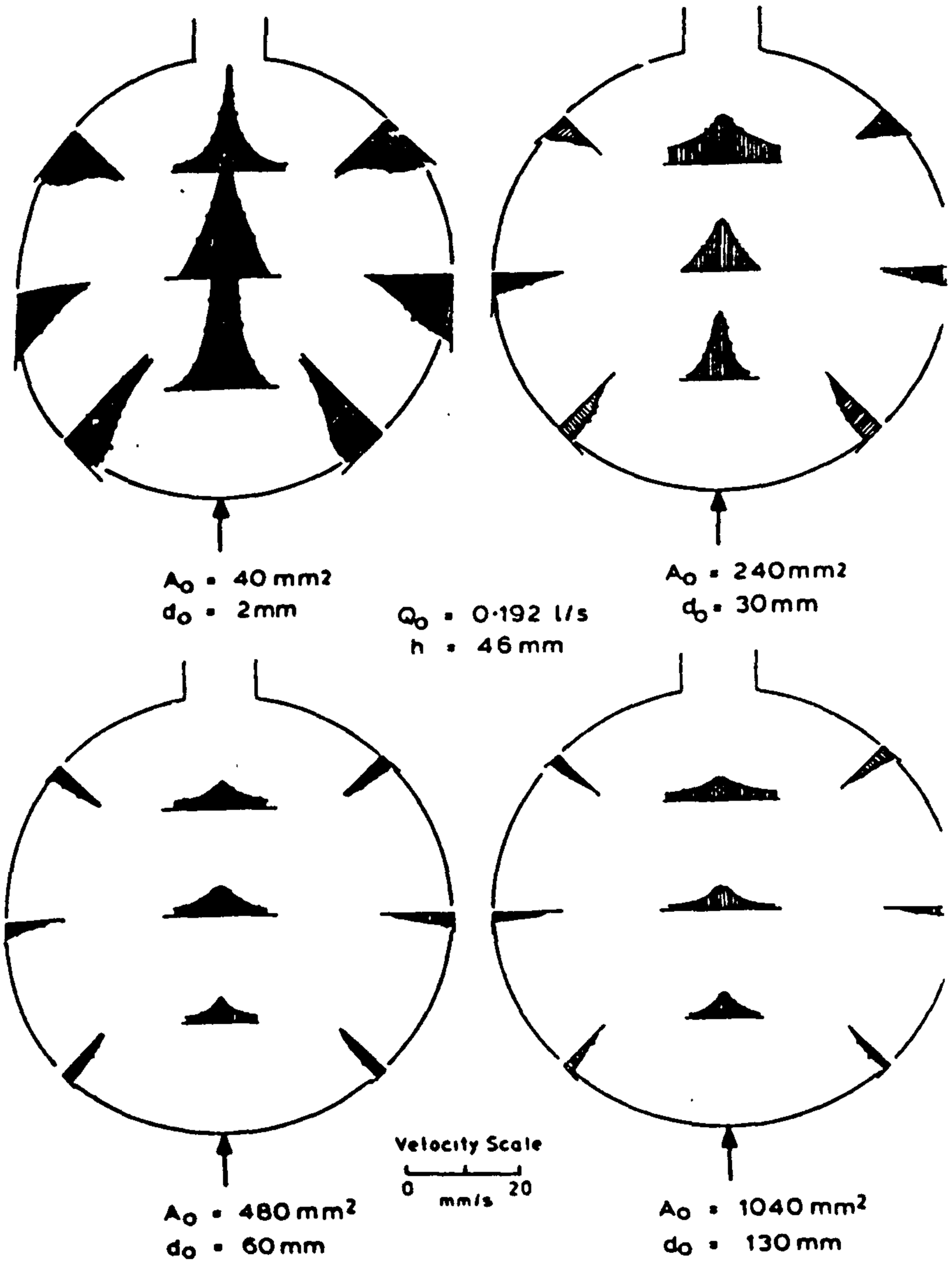

Figure 7.9 : Velocity Distributions for Radial Jets of Various Areas
(a) A_j = 480 mm² (b) A_j = 240 mm² (c) A_j = 480 mm² (d) A_j = 1040mm²
(After Ali, 1983)

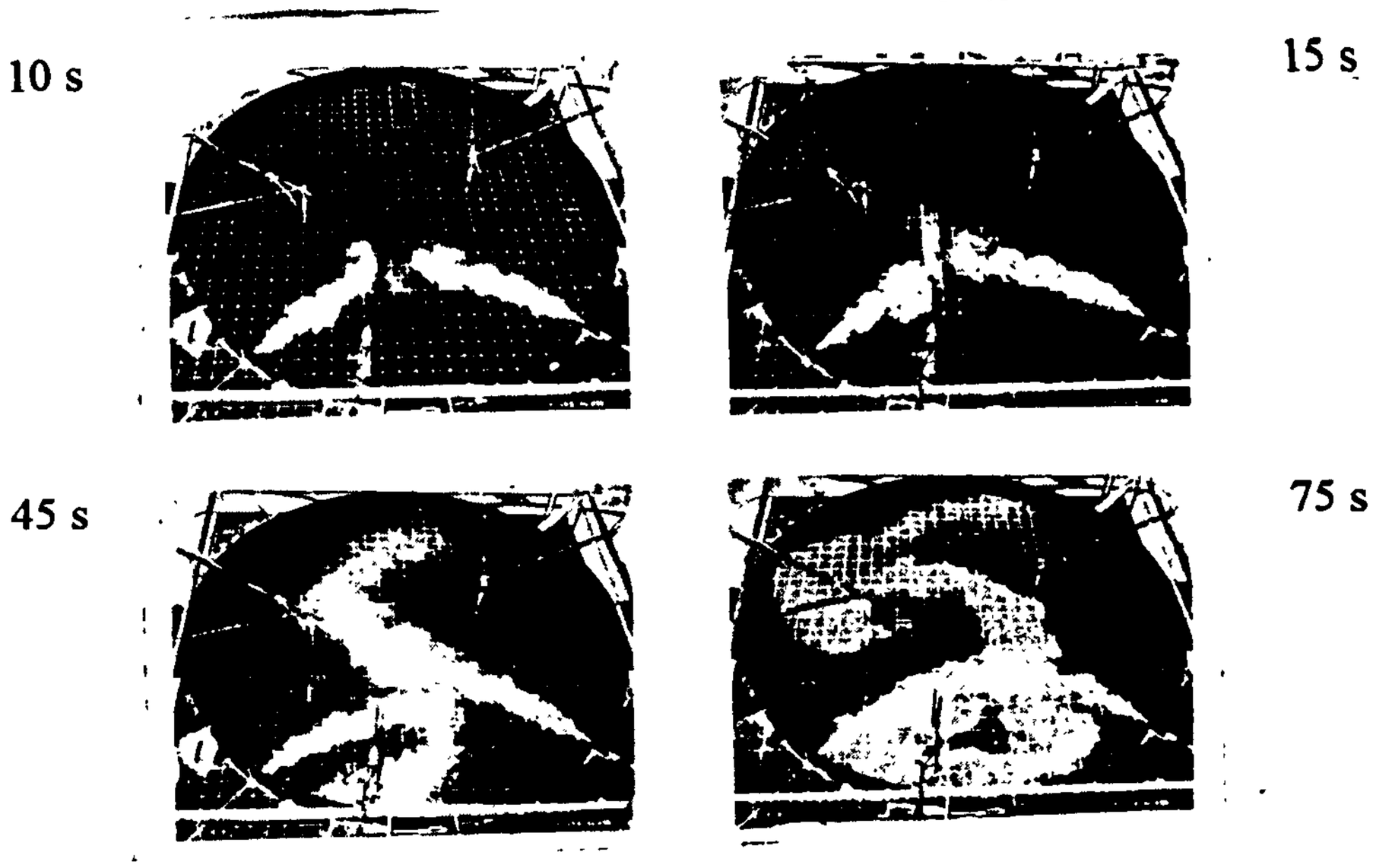

$L = 3m,\ h = 5cm,\ Q_j = 89$ cc/secs, $L/h = 60$

Figure 7.10 : Dye Mixing Produced by Twin Radial Jets (L/h = 60)
(After Ali, 1983)

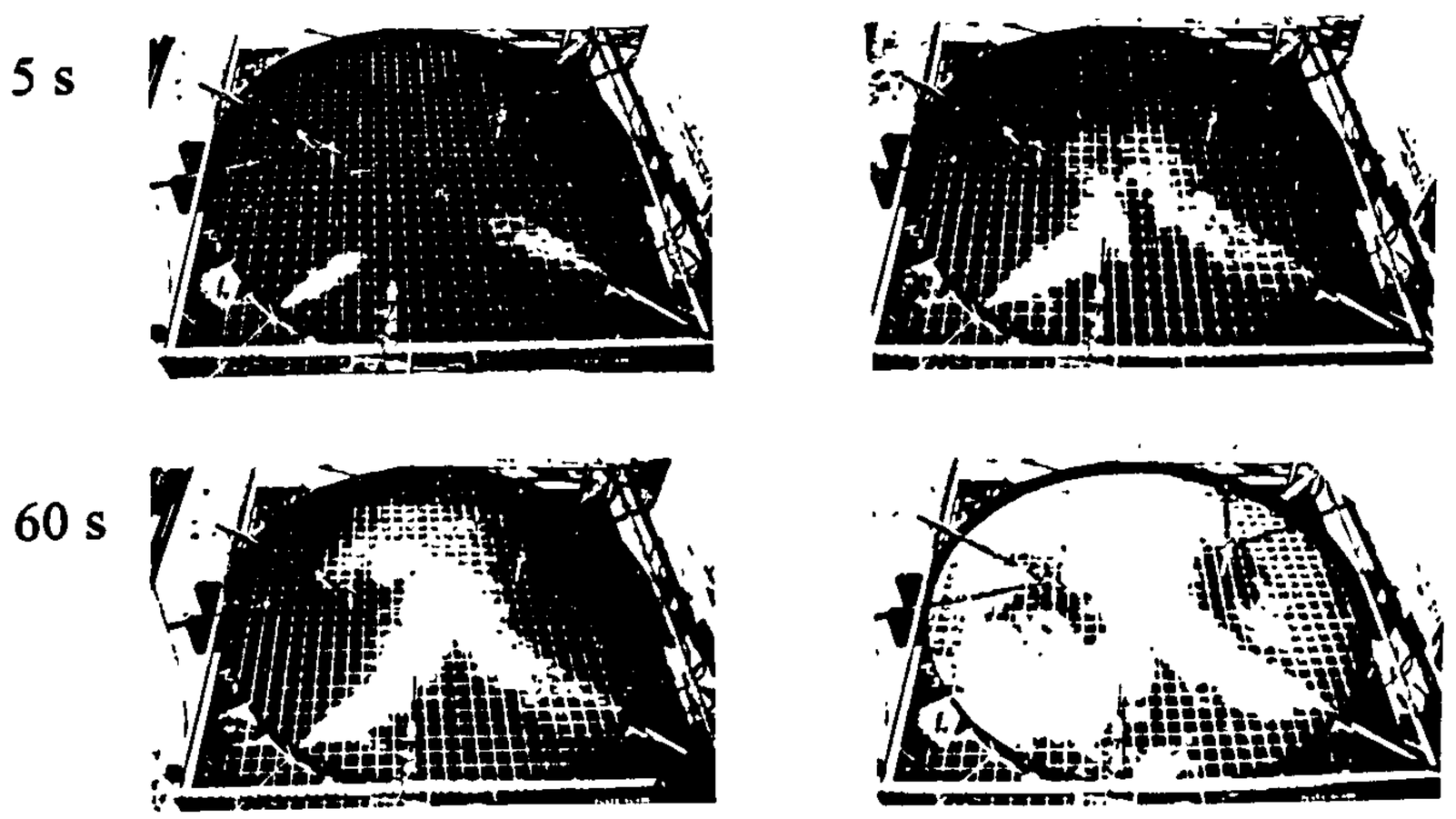

$L = 3.0m,\ Q_j = 89ml/s,\ h = 100mm$

Figure 7.11 : Dye Mixing Produced by Twin Radial Jets (L/h = 30)
(After Ali, 1983)

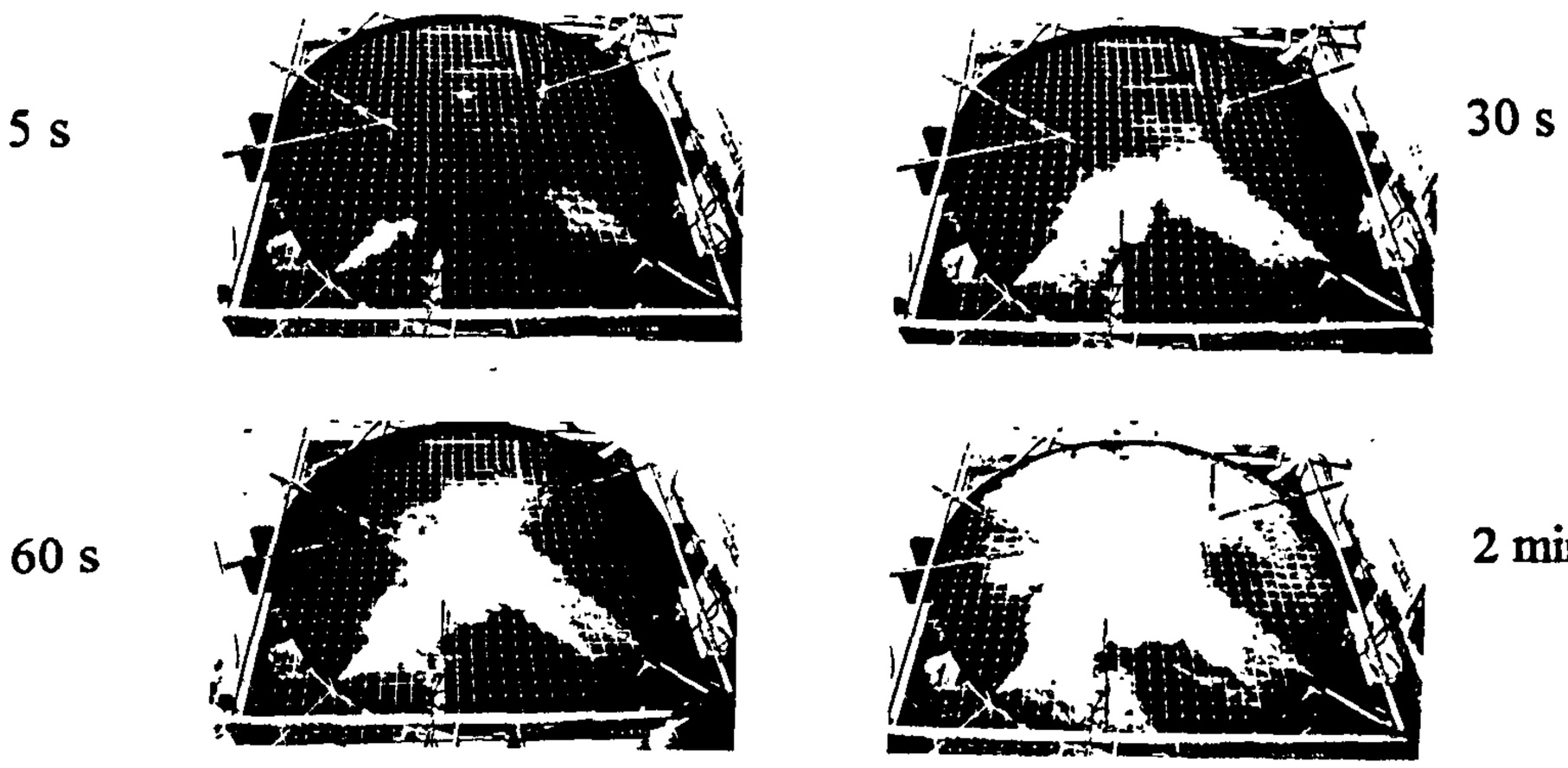

$L = 3.0m,\ Q_j = 89ml/s,\ h = 200mm$

Figure 7.12 : Dye Mixing Produced by Twin Radial Jets (L/h = 15)
(After Ali, 1983)

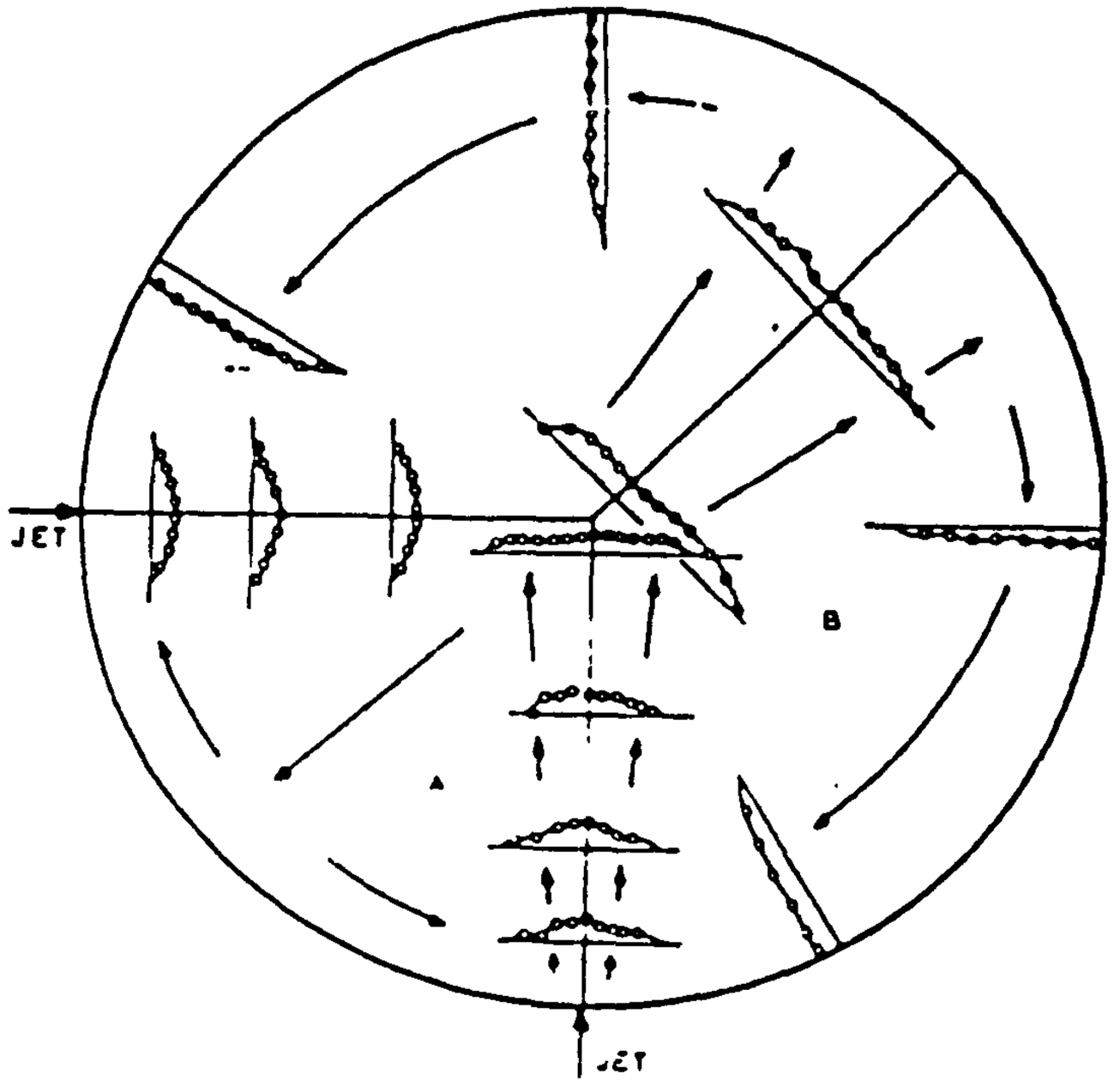

Figure 7.13 : Experimental Velocity Distributions For Twin Radial Jets
(After Ali, 1983)

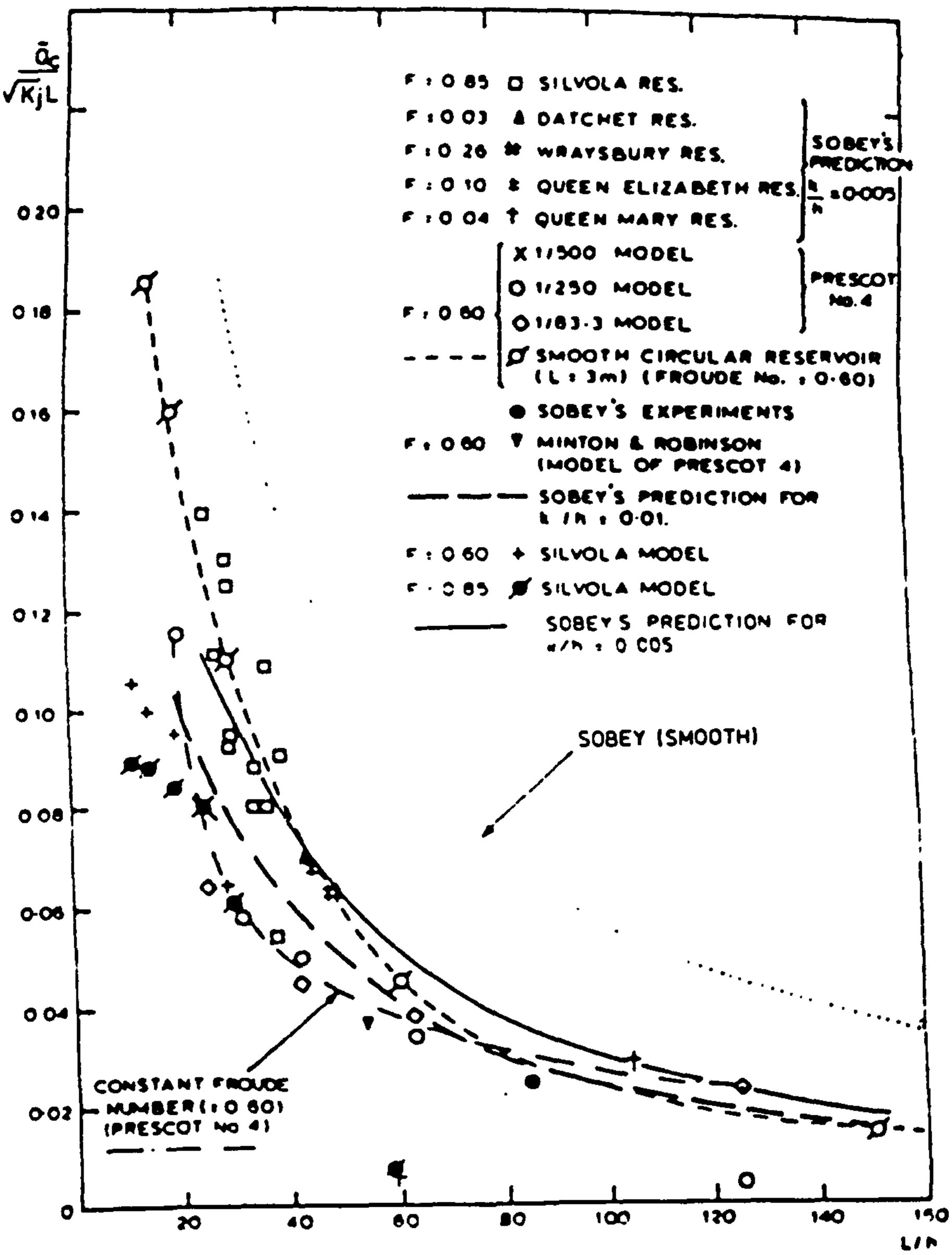

Figure 7.14 : Variation of $\overline{Q}_c$ / $\sqrt{(K_j)L}$ with L/h for a Tangential Jet

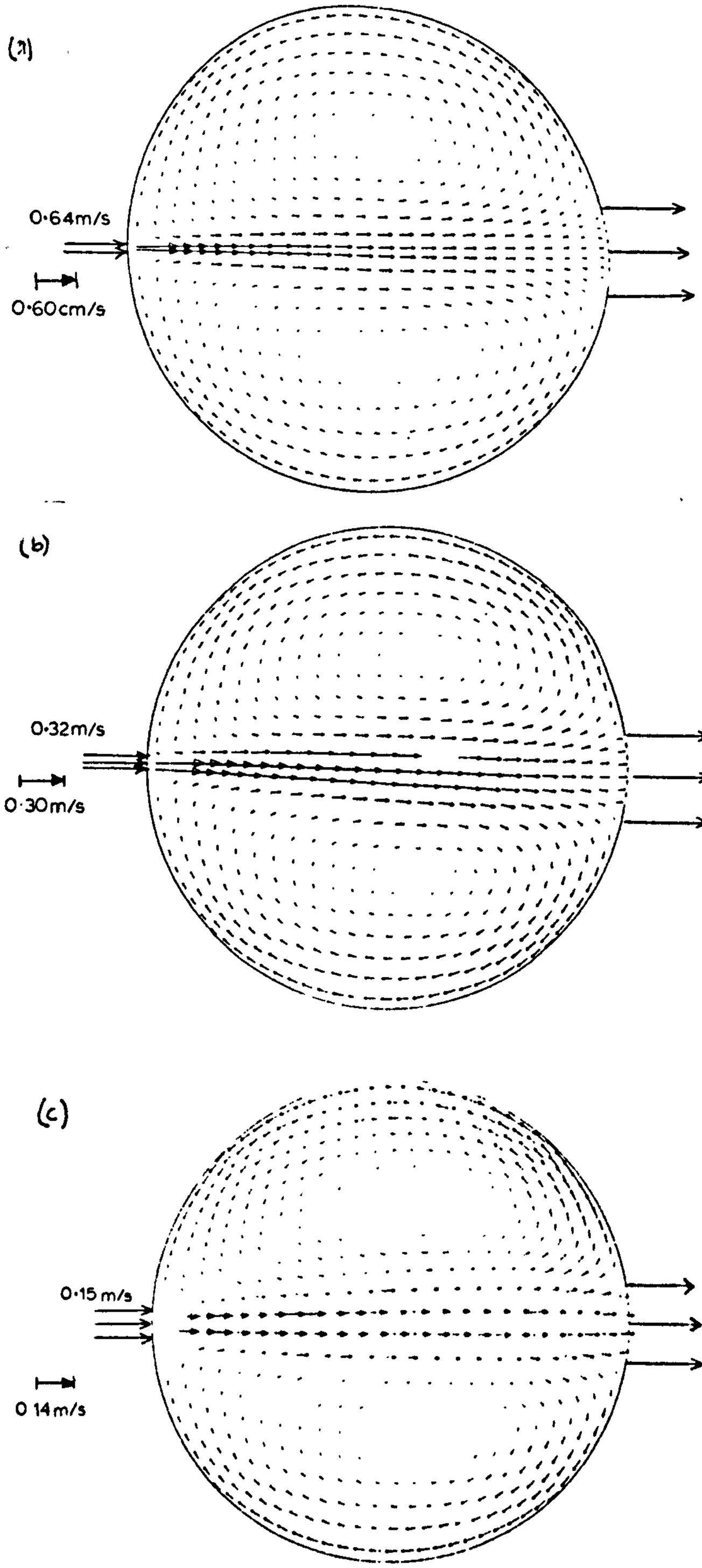

Figure 7.15 : Predicted Circulation Produced by a Radial Jet
(a) d_o = 3cm (b) d_o = 6cm (c) d_o = 13cm

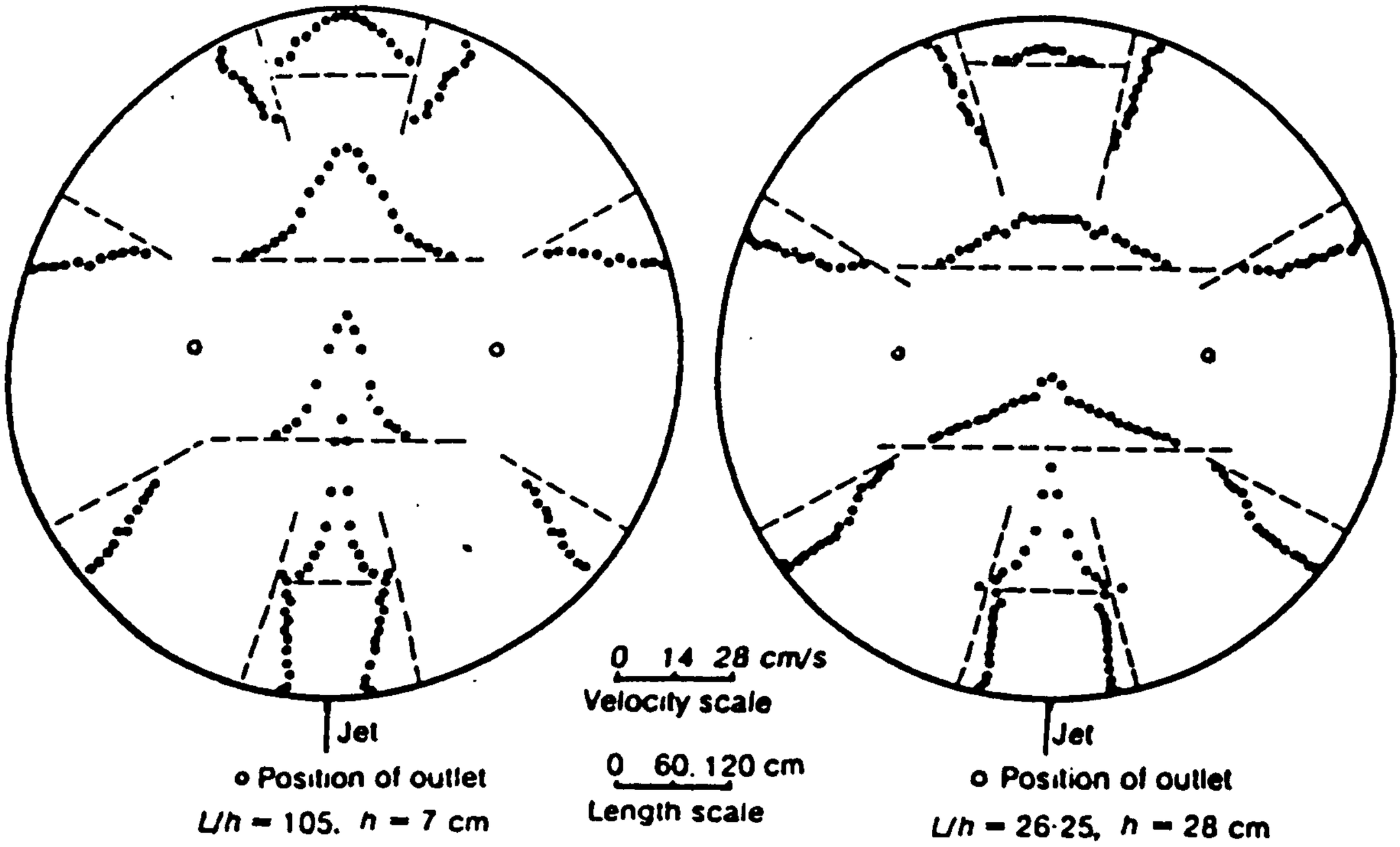

Figure 7.16 : Experimental Velocity Distributions For a Radial Jet With Two Outlets Inside the Reservoir (L = 735cm, Q_j = 615 cm^3/s)

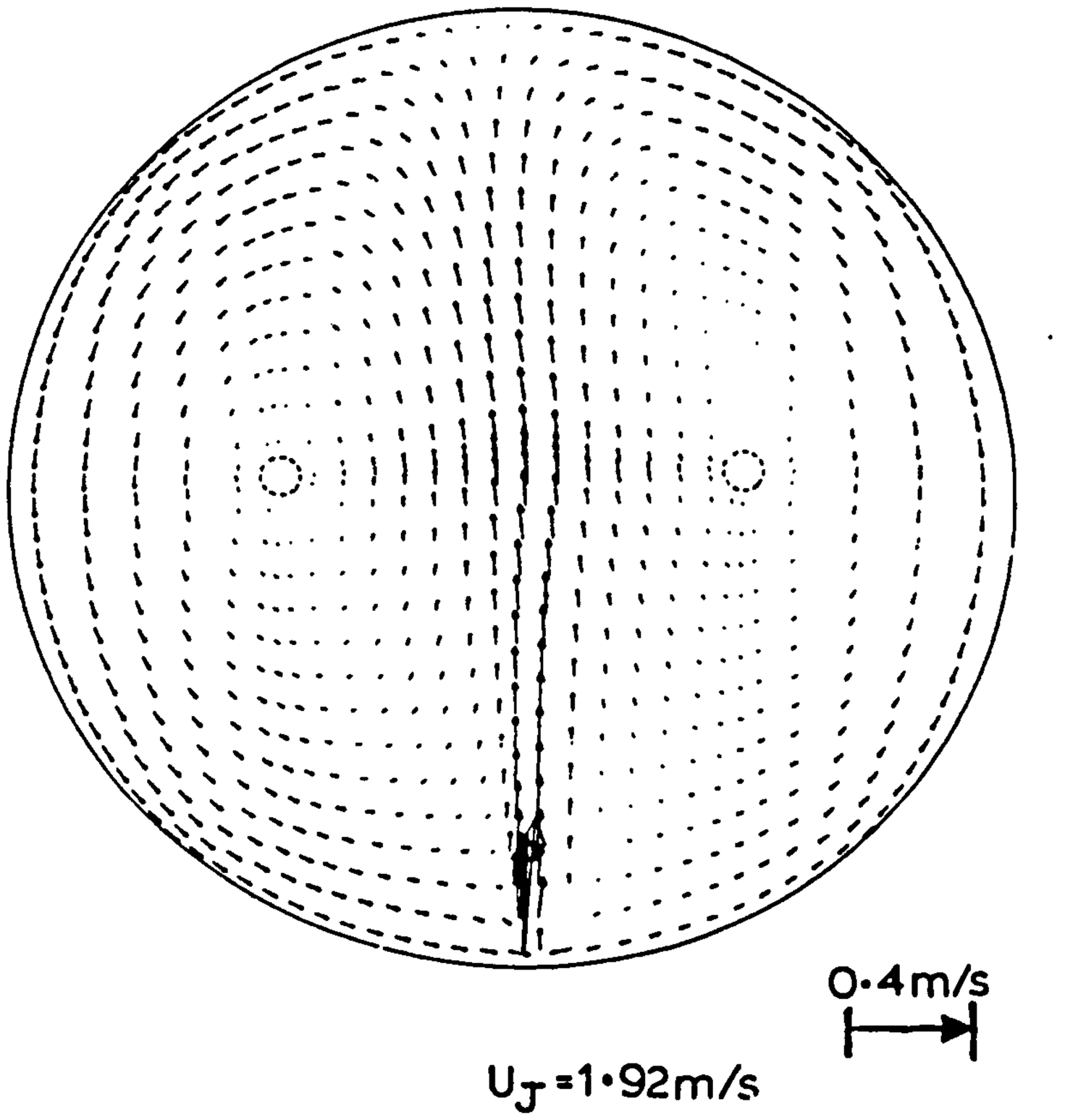

Figure 7.17 : Predicted Circulation Prodeuced by A Radial Jet with Rwo Outlets Inside The Reservoir

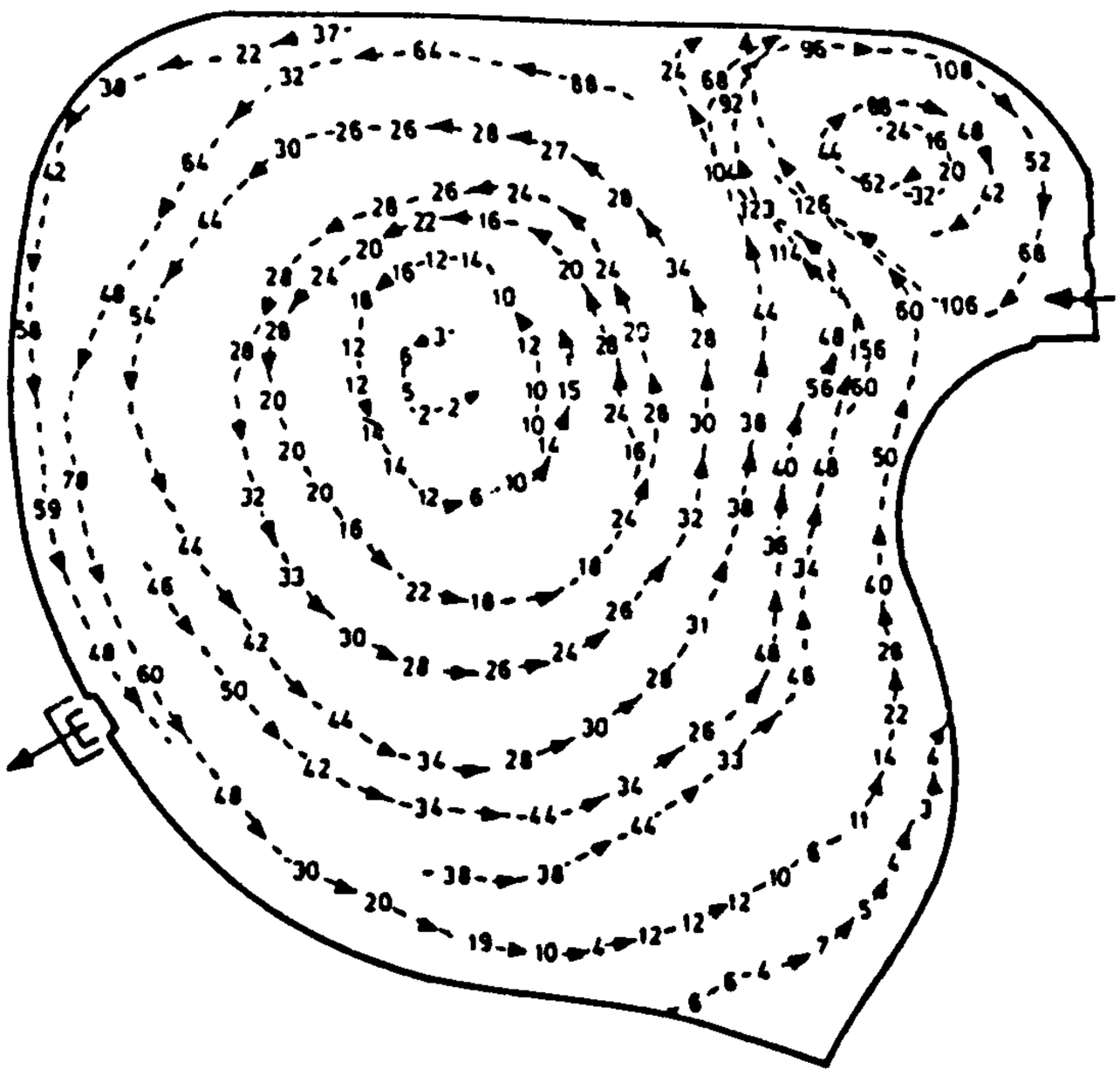

Figure 7.18 : Velocity Distributions From the 1:250 Scale Model of Prescot No. 4 Reservoir (5:1 Exageration)

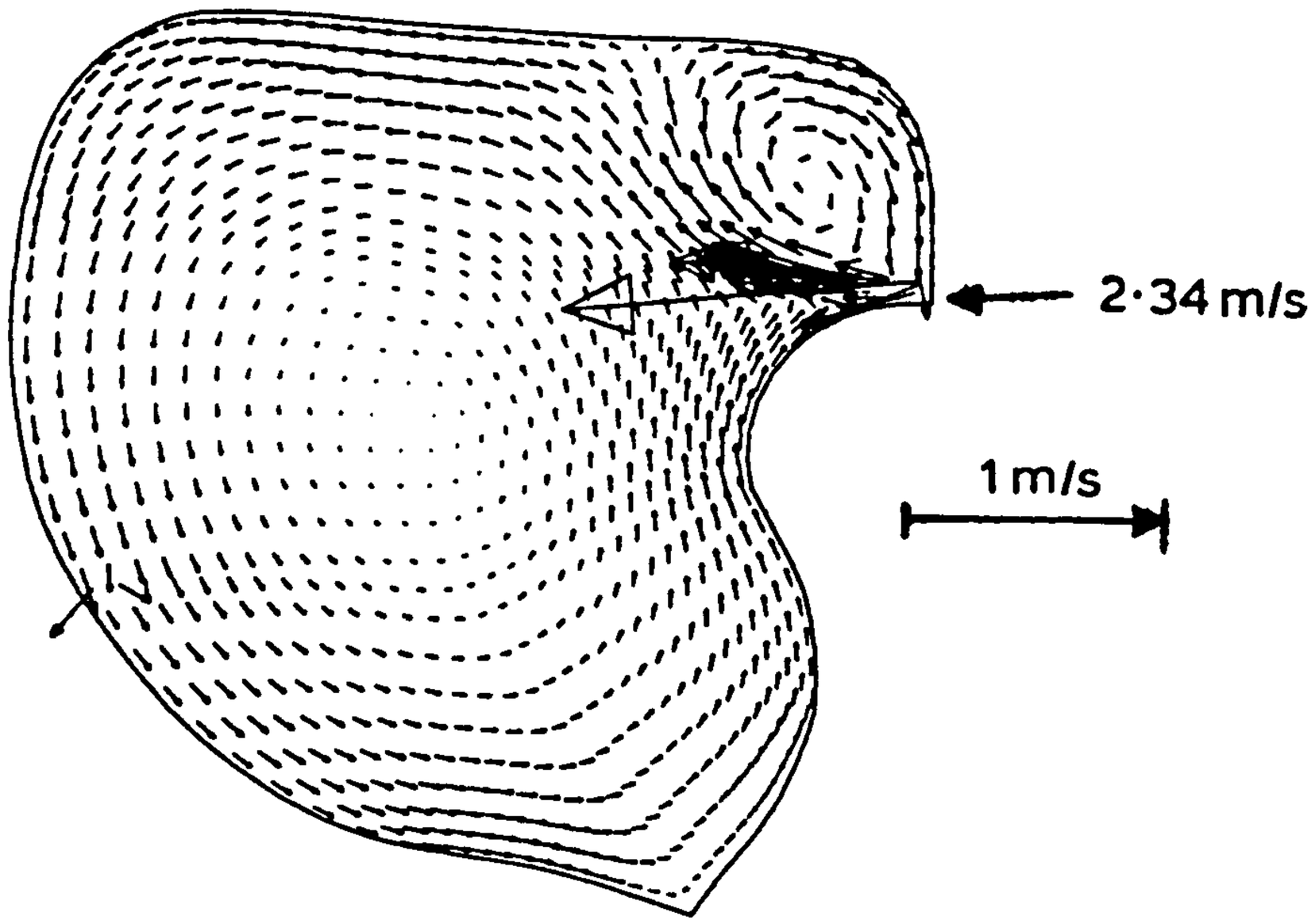

Figure 7.19 : Predicted Reservoir Circulation Produced by One Inlet For Prescot No. 4 Reservoir (Original Jet Velocity)

FIG 21 PREDICTED RESERVOIR CIRCULATION PRODUCED BY ONE INLET FOR PRESCOT NO 4 RESERVOIR (ORIGINAL JET VELOCITY)

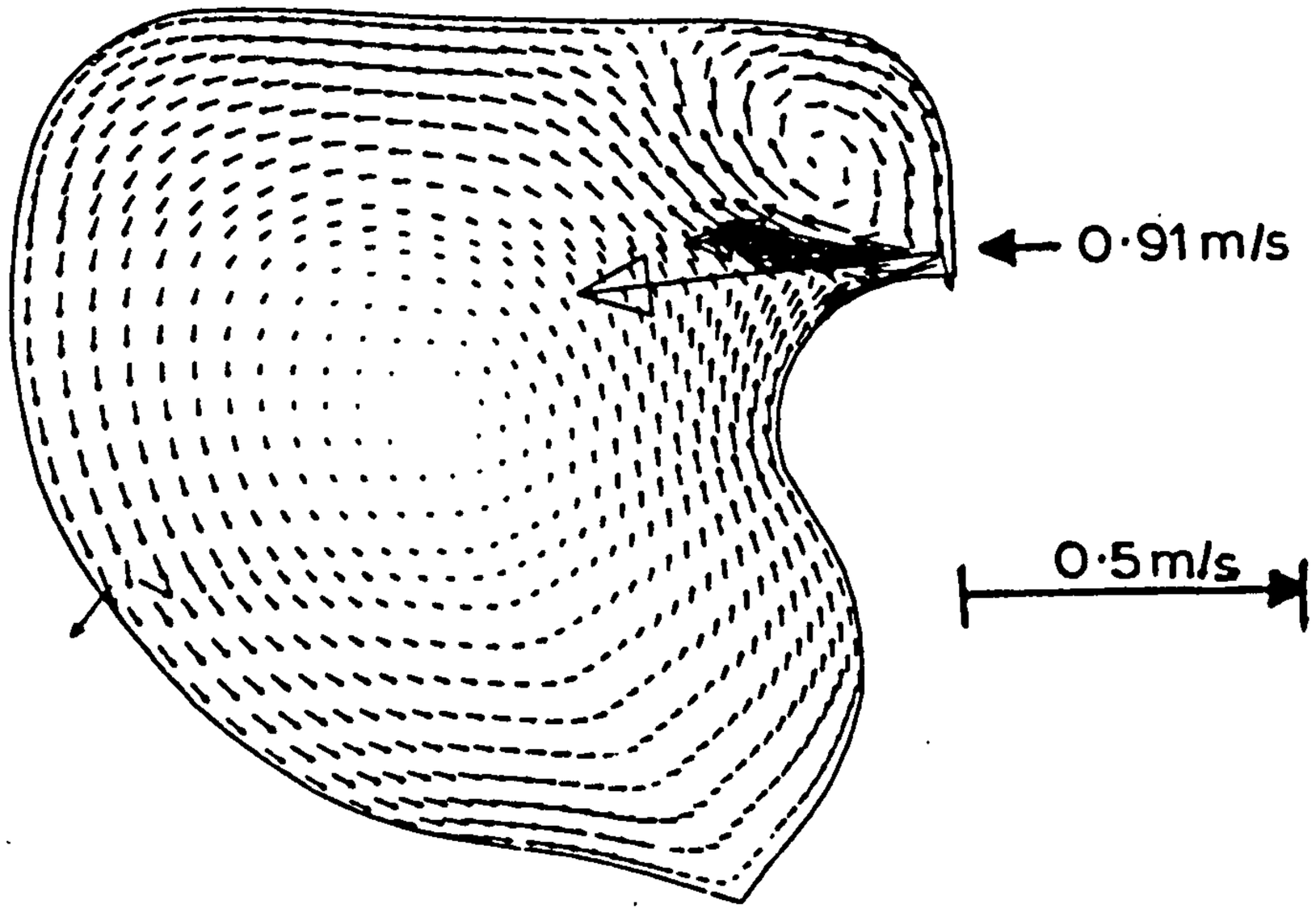

Figure 7.20 : Predicted Reservoir Circulation (Using Depth-Averaged Inflow Momentum)

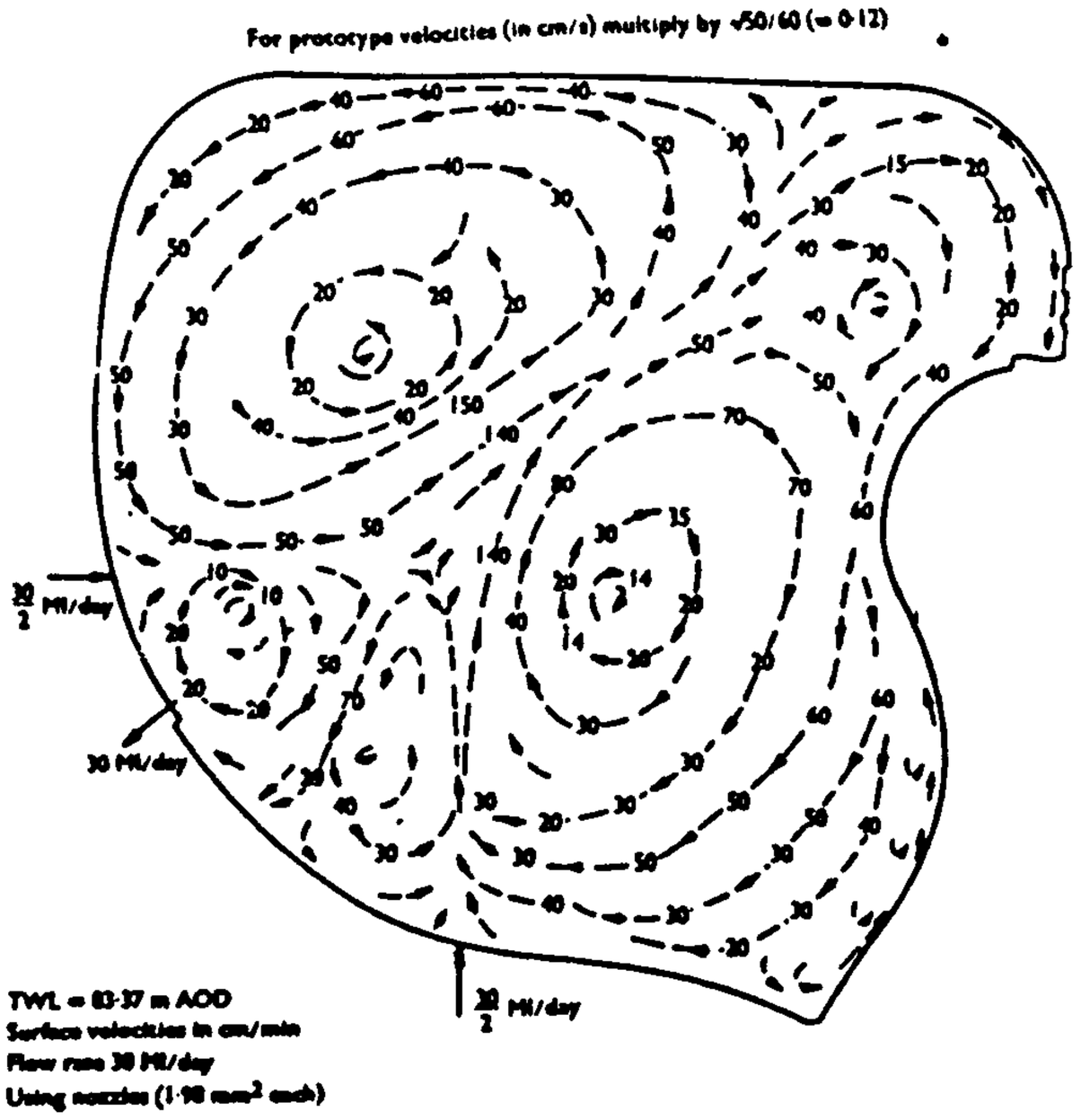

Figure 7.21 : Experimental Surface Flows Produce by Two Nozzles at Mid-Depth (1:250 Model with 5:1 Vertical Exaggeration)

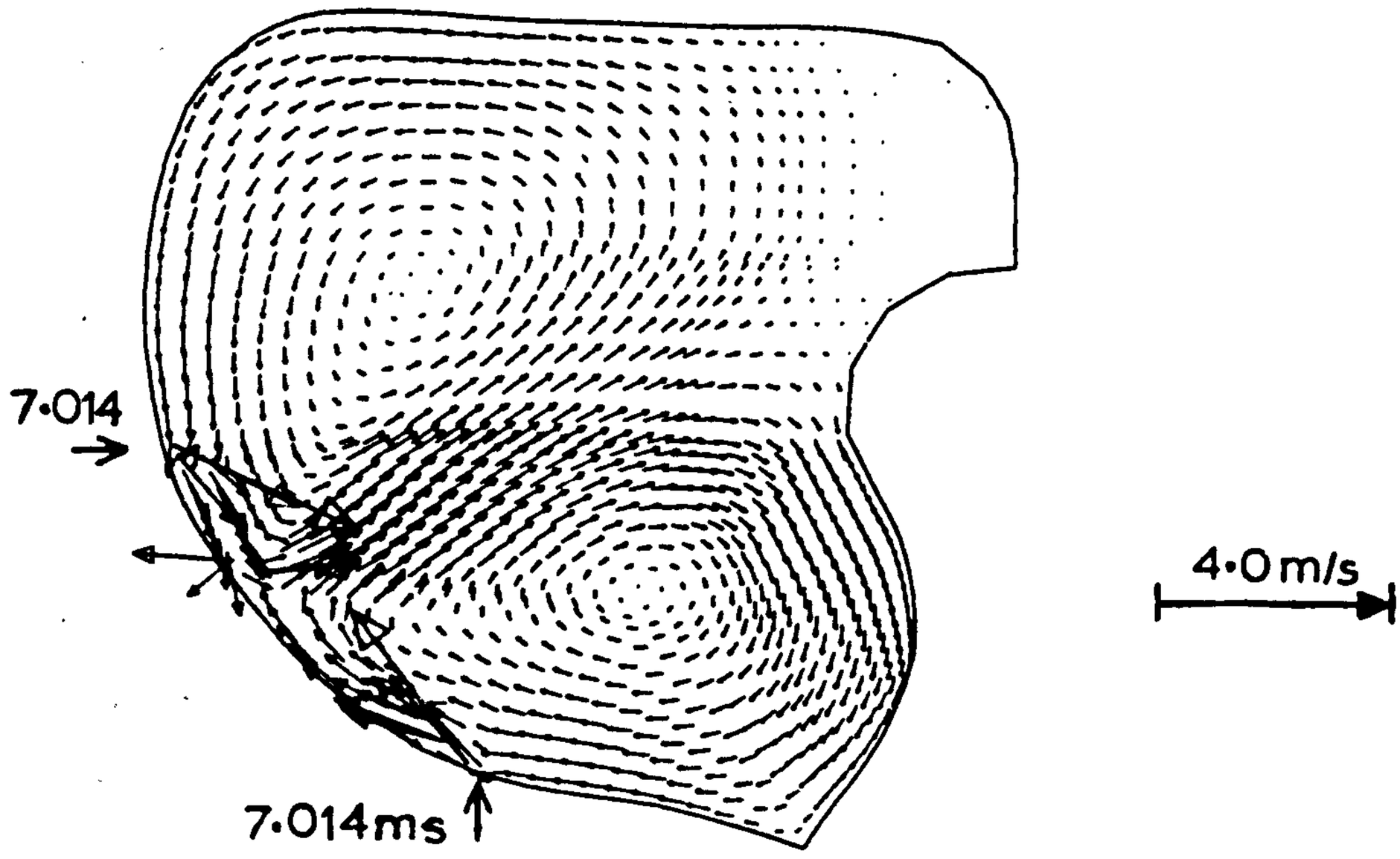

Figure 7.22 : Predicted Circulation Using Two Nozzles
(Using Original Nozzle Velocities)

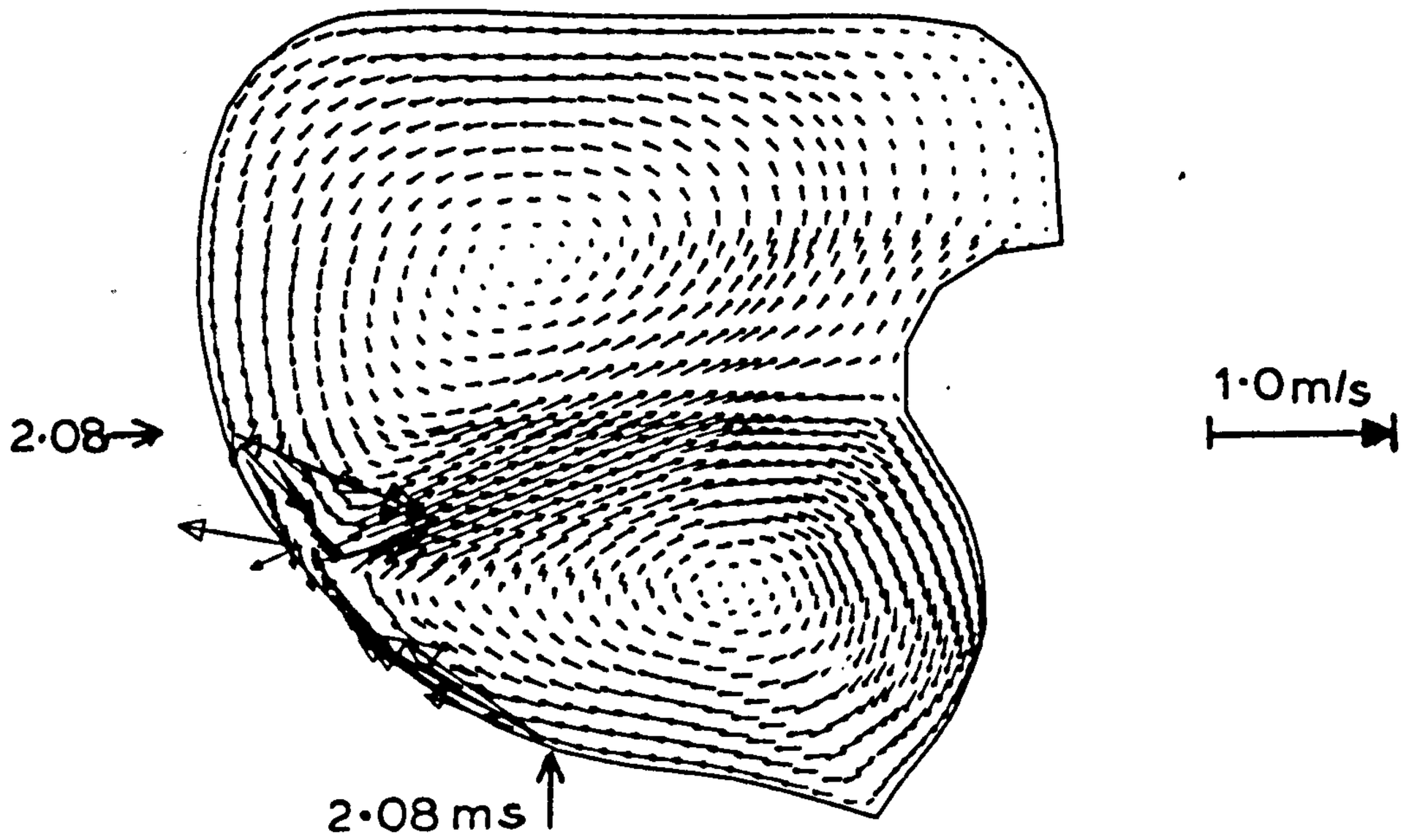

Figure 7.23 : Predicted Circulation Using Two Nozzles
(Using Depth-Averaged Nozzle Momentum)

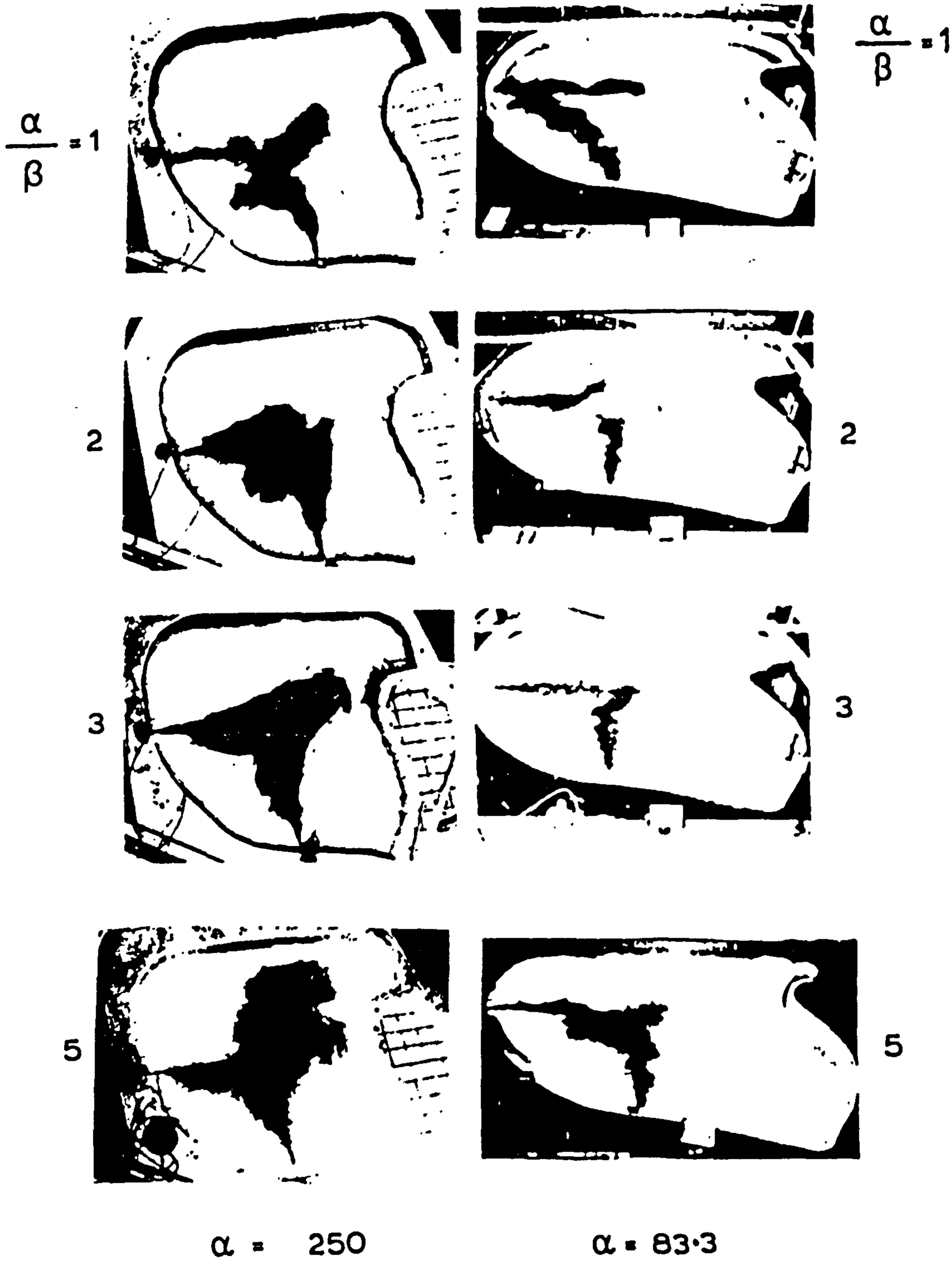

Figure 7.24 : Dye Photographs for Twin Jets in The 1/250 and 1/83.3 Scale Models

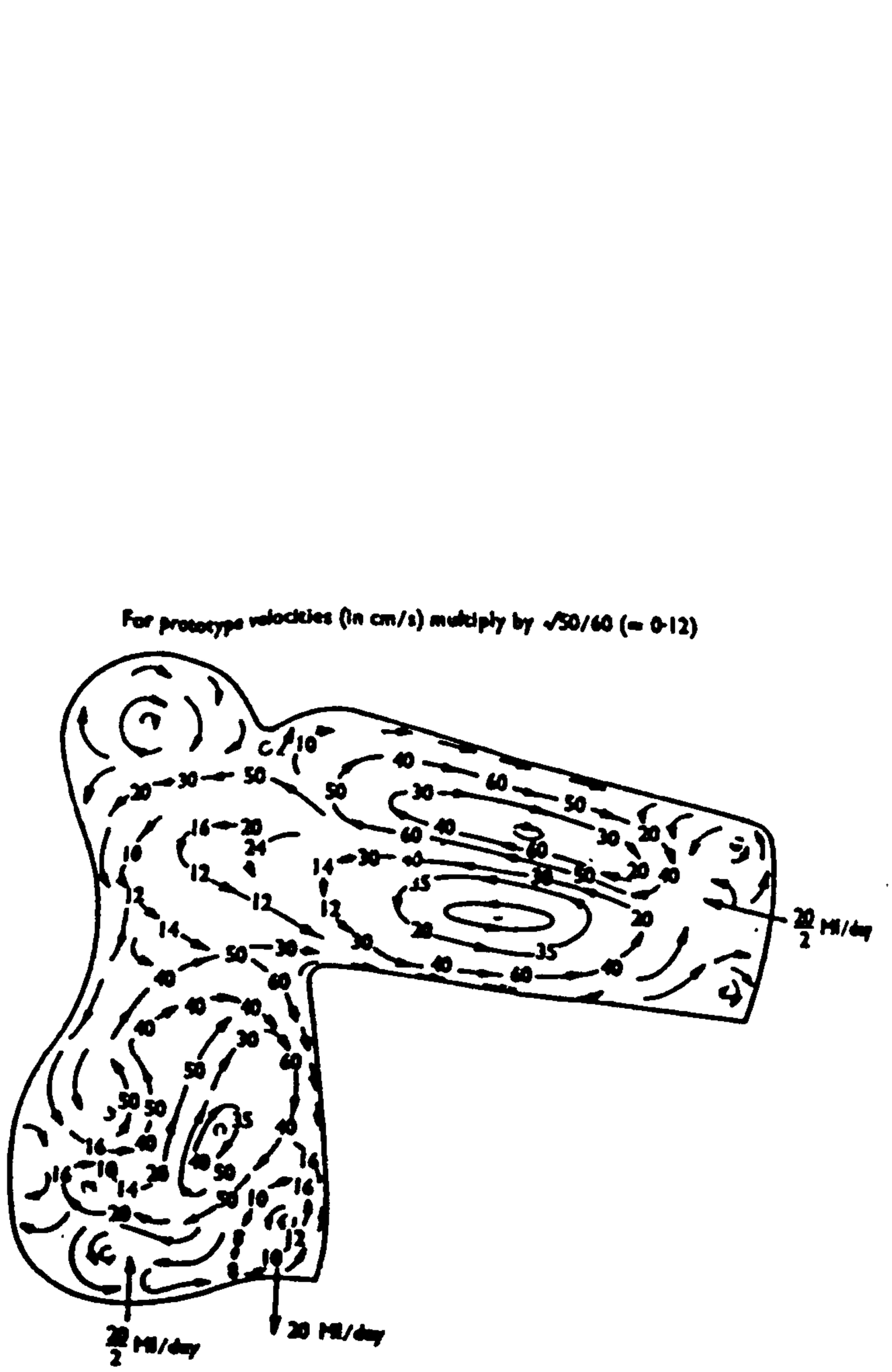

Figure 7.25 : Experimental Surface Flows Produced by Two Nozzles at Mid-Depth in Prescot Reservoir No. 3 Reservoir (1: 250 Model with 5:1 Vertical Exaggeration)

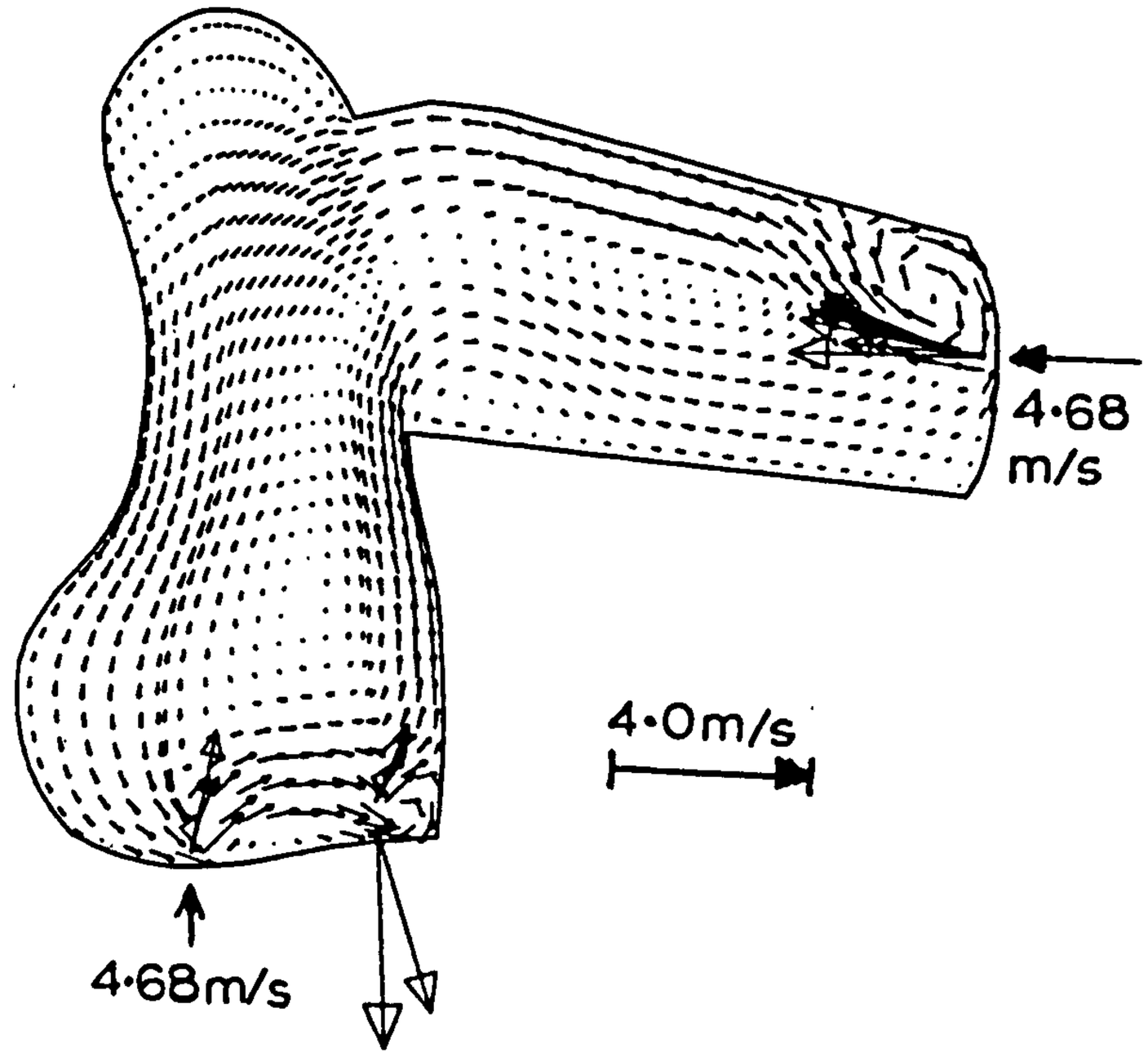

Figure 7.26 : Predicted Circulation Using Original Nozzle Velocities

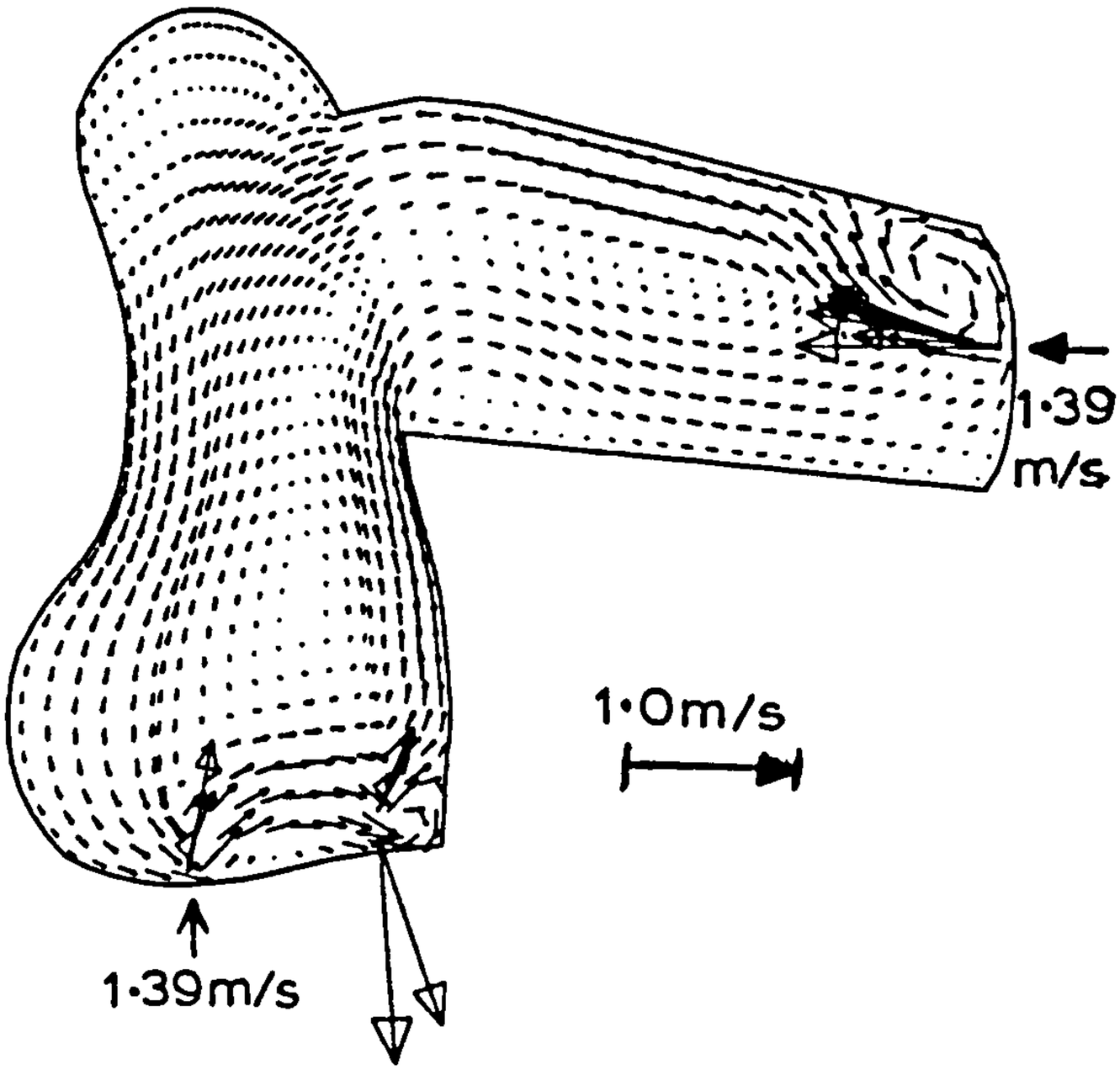

Figure 7.27 : Predicted Circulation using Depth-Averaged Nozzle Momentums

NOTATIONS

b_o	Height of inlet jet
d_o	width of two-dimensional jet
f	Coriolis parameter
F	Reservoir Froude number (= $V_j / \sqrt{gh}$)
g	Acceleration due to gravity
h	Water-depth of reservoir
k_s	Roughness height of reservoir
K_j	Kinematic jet momentum flux
L	Diameter of reservoir
Q_c	Circulating discharge at given θ
$\overline{Q_c}$	Overall average circulating discharge
Q_j	Discharge of inlet jet
v	Local tangential velocity
V_j	Average velocity of inlet jet
x	Distance from virtual origin of jet
α	Horizontal scale ratio
β	Vertical scale ratio
ϕ	Latitude of reservoir
θ	Angle form the jet
ν	Kinematic viscosity of water
ψ	Dimensionless function
Ω	Angular speed of rotation of the earth

REFERENCES

Ali, K.H.M. and Hedges, T.S., "Discussion on Jet-Forced circulation in water supply reservoirs", by R.J. Sobey and S.B. savage. *J. Hydraul. Div.* Am. Soc. Civ. Engrs., 1975, 101, HY12, Dec., 1543-1546.

Ali, K.H.M. et al, "A scale model investigationof circulation in reservoirs", *Proc. Instn. Civ. Engrs.*, Part 2, 1978, 65, Mar., 129-161.

Ali, K.H.M. and Pateman, D., "Prediction of the circulation in reservoirs", *Proc. Instn. Civ. Engrs., Part 2,* 1981, 71, June, 472-461.

Ali, K.H.M. and Whittington, R.B., "Liquid-liquid mixing in tanks and reservoirs", *Proc. Brit. Hydromech. Res. Assn.* 3rd Eur. Conf. Mixing, York, 1979, 37-60.

Ali, K.H.M., "The investigation of reservoir circulation", Modelling of Env. Flow Systems, Winter Annual Meeting of the ASME, Boston, Massachusetts, Nov. 1983, pp 25-34.

Ali, K.H.M. and Pateman, D.R., "Dispersion of marked fluid in reservoirs", *Advances in Water Resources*, 1983, Vol. 6, Dec., pp 190-199.

Ali, K.H.M., "Reservoir Circulation caused by jets, wind and by the earth's rotation", Int. Symposium on Modelling Environmental Flows, Albuquerque, New Mexico, June 1985, pp 71-80.

Cooley, P. and Harris, S.L., "The preventive of stratification in reservoirs", *J. Instn. Wat. Engrs.*, 1954, 8, 517-531.

Daily, F.W. and Harleman, D.R.F., "Fluid Dynamics", Addison-wesley, Massachusetts, 1973, 419-423.

Falconer, R.A., "Mathematical modelling of jet-forced circulation in reservoirs and harbours", Ph.D thesis, Imperial College, 1976.

Fluent Incorporated, Fluent Version 4.2.2 User's Guide, Fluent Incorporated, Lebanon, New Hampshire, U.S.A., 1993.

Fosset, H. and Prosser, L.E., "The application of free jets to the mixing of fluids in bulk", Proc. Instn. Mech. Engrs., 1949, 160, 224-232.

Goossens, L.J., "Reservoir destratification with bubble columns", Delft University Press, 1979.

Metropolitan Water Board, "Model tests for flow patterns in Wraysbury and Datchet reservoirs", Metropolitan Water Board, 1962, 1972, Internal Reports.

Mills, R.D., "Computing internal viscous flow problems for a circle by integral methods", *J. Fluid Mech.*, 1977, 79, Part 3, pp 609-624.

Robinson, S.J., "Hydraulic modelling of circulation in reservoirs", M. Phil. thesis, Imperial College, 1979.

Sobey, R.J., "Flow patterns in lakes and reservoirs", Ph.D thesis, Imperial College, 1972.

Sobey, R.J. and Savage, S.B., "Jet-forced circulation in water-supply reservoirs", *J. Hydraul. Div.* Am. Soc. Civ. Engrs., 1974, 100, HY12, Dec., 1809-1828.

CHAPTER

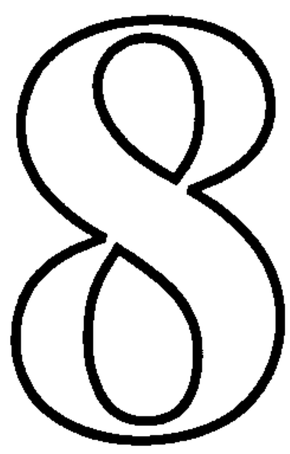

CHAPTER 8

GENERAL CONCLUSIONS AND RECOMMENDATIONS

FLUENT V4 is a multi-purpose computer software for modelling fluid flow, heat transfer and chemical reaction which enable a rapid analysis of complex flows. It can model a wide range of physical phenomena including:

- 2D/3D geometries in Cartesian, Cylindrical or General Curvilinear Coordinates,
- Steady State or Transient Flow,
- Incompressible or Compressible Flow,
- Laminar or Turbulent Flow,
- Coupled Conduction/Convection Heat Transfer,
- Radiation Heat Transfer, Mixing of Chemical Species,
- Temperature and Composition Dependent Fluid/Material Properties,
- Flow Porous Media, and
- Dispersed Second Phase Particles/Bubbles/Droplets.

The size and scope of the problem to be solved (in terms of the number of computational nodes) is limited only by the available computer memory and the site-specific installation of FLUENT on user's system.

The physical models listed above enable the use of FLUENT to a wide range of applications such as aerodynamic design, combustion design and engineering including gaseous combustion, liquid fuel, and coal combustion, heat transfer

operations, fire research, manifold design and turbomachinery component design.

In the present study, the collated turbulence formulation in FLUENT V4 and associated closure models have been applied to various type of flows, namely; turbulence wall jet, submerged offset jet, flow around piers and spur-dykes and finally jet-forced water circulation in water supply reservoirs. The results are compared with experimental results of previous researches mainly of Department of Civil Engineering, University of Liverpool, as well as other research establishment. Discussions and conclusions for each cases have been presented in each chapter accordingly. This chapter aims at presenting overall conclusions with regards to the application of the CFD package in simulating flows in the field of hydraulic engineering. Occasionally, a few recommendations for further research are included.

1. The FLUENT CFD model was, in most cases, capable of producing results giving a good fit to the experimental results. When an accurate fit was not attained, the main features of the measured flow were still reproduced qualitatively; and the lack of correspondence was attributed to either inaccurate input data, numerical and/or experimental errors.

2. Extensive testing procedures have been implemented to ensure that the equations and solution algorithms used by FLUENT would provide an accurate simulation of flow. However, inaccuracies may arise on specific engineering problems regarding the spacing of the computational grid, suitability of the physical model utilised, or the choice of boundary condition. It was shown that grid spacing would be of great importance to the modelling accuracy. It should also be emphasised that errors in input data (i.e. bed profiles, inlet velocity, etc.) could introduce errors as serious as those caused by the numerical approximations.

3. One of the major drawbacks of the package is the inappropriate modelling of the free surface. In FLUENT, the free surface is approximated by a fictitious plane boundary. This boundary can be thought as an inviscid "rigid lid" or alternatively as a plane of symmetry. Such treatment involves certain error, mainly in continuity, because superelevated regions are implicitly considered hydrodynamically passive. Most cases studied here involved a free surface, and the errors are obvious where flows are disrupted by an obstruction such as pier or spur dyke, or when flow converged at the peak of scour holes. In practise when such events occur, a decrease and/or an increase of water level was reported. Consequently, the velocities reported by FLUENT are slightly higher than the measured data. Modification of the code to include the fluctuation of the water level would therefore be necessary. One possible way is to employ the Bernoulli Equation to calculate the surface slope based on the non-zero pressure gradients at the surface boundary (as a result of the constraint imposed on the flow by the fictitious lid).

4. In general it can be concluded that the turbulence models are flow geometry dependent. This means, that a turbulence model which works well in one case may not be applicable in another flow geometry. As a result, a single turbulence model is generally restricted to apply to certain classes of flows. Turbulent flows may be classified according to the source of turbulence, i.e. shear produced flows such as jet flows or channel flows. However, as shown in the present study that turbulence modelling may also differ for cases which have the same source of turbulence but vary in flow geometry, for example plane wall jet *vs*. offset-jet, and rigid bed *vs* scoured-bed.

5. One of the difficulties in comparing different measurements for turbulence jet flows is that the experimental setup can differ in various experiments in several respects. This means that we are in fact comparing different jets. Differences are for instance found in the ambient conditions for the jet, such as temperature and size of confinement. If there is a temperature difference between the jet and the surroundings this may influence the results by buoyancy. Moreover, regardless of a temperature difference between jet and surroundings, the temperature can influence viscosity and therefore the Reynolds number; therefore, the temperature should be constant during a run, but this is not always checked.

6. Many other factors can influence the experimental results too; some are: the smoothness of the sluice, the exact form of the velocity profile at the sluice gate, the outflow conditions and the Reynolds number. Experiments by Ali and Salehi(1991) and Ali and Whalley (1992) are a good example for this, in which different results were obtained for tests under similar conditions. Differences between the various experiments were also found because of the use of different measuring techniques. A problem here is the fluctuation level, especially near the edges of the standard jet. It is known, that even flow reversals do occur in free jets. This means, that the (often used) static hot wire measurements become unreliable in this region. Alternatives, such as Laser-Doppler or modern measurements technique can cope with this problem.

7. It can be concluded that the boundary shear stress alone did not account for the development of scour holes (entrainment and transport of the sediment particles). The degree of the turbulence intensity, especially in an obstructed flow field also contributed significantly to the scouring process. In a physical model, not all relevant quantities could be

furnished. Some physical quantities in a turbulence flow are difficult to measure. One of these quantities is the vorticity, which was known to be the major factor responsible for base scouring. Another example is the presence of "turbulent bursts" which are widely observed and are capable of removing sediment from the bed. Unfortunately, FLUENT is not capable of predicting these bursts.

8. On the other hand, it should also be expected that "perfect" results are difficult to obtain in view of the many factors involved which cannot be modelled directly using a numerical simulation. In some cases, therefore, it is difficult to compare simulation results which do not predict the experimental data within accepted level of accuracy, especially after making every effort to provide the best solution possible and still falling short. But the author believes that such an exercise provides credibility to this growing CFD industry and will ultimately serve the interests of the engineering and scientific community.

9. Clearly demonstrated in this exercise, is that further detailed and rigorous study needs to be carried out to validate the results quantitatively. With recent advances in flow visualisation techniques, the measurement of most of the turbulence quantity such as vorticity, is coming into reach of the experimentalist, thus providing better representation of the real situation to be compared with the numerical results.

APPENDIX

Sixth International Symposium on River Sedimentation 1995, New Delhi, India

SCOUR AND DEPOSITION DOWNSTREAM OF HYDRAULIC STRUCTURES

K.H.M. Ali and O.A. Karim

The University of Liverpool, Department of Civil Engineering
Brownlow Street, Liverpool, L69 3BX, United Kingdom

ABSTRACT

The paper describes various theoretical and experimental methods for the investigation of local scour and general changes in bed levels for different hydraulic structures. Experimental results of an extensive research programme are presented herein. Effects of jet shape, size, orientation and submergence were considered. Sediments of various sizes and densities were used Several analytical and semi-empirical methods were compared with the experimental results.

INTRODUCTION

The prediction and control of erosion and deposition problems is an important subject in hydraulic engineering Rational methods have been developed by many workers for computing the development of local scour and the changes in local morphology. There is still a considerable need for reliable sediment transport models that can predict such changes.

This paper deals with the following examples:

(a) Two-dimensional wall jet discharging into a deep pool of water;

(b) Two-dimensional offset jets;

(c) Two-dimensional offset jets;

(d) Three-dimensional flow downstream of flap-gates;

(e) Changes in bed form in a long sea outfall.

Complexity of the flowfields resulted in different approaches to these problems. Dimensional analysis was used to combined the results into more useful form. Numerical analysis was also used to obtain flowfields in scour holes. Resulting boundary shear stresses will enable an accurate use of sediment discharge relationships.

THEORETICAL CONSIDERATIONS

A depth-averaged sediment transport model for non-cohesive sediments was developed by O'Connor and Nicholson 1990. Their model computes the bed level changes in two stages. Firstly, the depth-averaged version of the unsteady-state diffusion-advection equation is solved for the suspended sediment concentrations. The expression can be written in the following form:

$$\frac{\partial}{\partial t}(hC) - \frac{\partial}{\partial x}\left(hD_x\frac{\partial C}{\partial x}\right) - \frac{\partial}{\partial y}\left(hD_y\frac{\partial C}{\partial y}\right) + \frac{\partial}{\partial x}(hUC) + \frac{\partial}{\partial y}(hVC) - R_D - R_E = \upsilon \qquad (1)$$

where:

C	=	depth-averaged suspended sediment concentrati ,
D_x	=	longitudinal dispersion coefficient;
D_y	=	lateral dispersion coefficient;
h	=	flow depth;
R_D	=	sediment deposition rate;
R_E	=	sediment entrainment rate;
t	=	time;
U	=	depth-averaged longitudinal velocity;
V	=	depth-averaged literal velocity;
x	=	longitudinal co-ordinate;
y	=	lateral co-ordinate.

The second stage of the calculations of bed level changes involves solving the bed continuity equation. This equation can be written in this form[ ]:

$$(1 - \bar{p})\,\rho_s\,\frac{\partial z}{\partial t} - R_D + R_E = 0 \qquad (2)$$

where:

$\bar{p}$	=	porosity of the bed material;
z	=	elevation of the bed relative to an arbitrary datum;
ρ_s	=	density of the bed material.

Equations (1) and (2) can be solved for various initial and boundary conditions.

Dimensional Analysis

Many sediment transport problems are too difficult to analyse. Dimensional analysis forms a very useful means of showing the relative importance of the various parameters. An example of a complicated problem is that of two-dimensional wall jet scour downstream of a sluice gate.

Assume that the maximum depth of the scour hole Y_D is given by (Fig. 1):

$$Y_D = \phi(V_o, a, \theta, p, h, \rho, \mu, W, d, g, t) \quad (3)$$

where

V_o	=	mean sluice gate velocity;
a	=	sluice gate opening;
ρ	=	density of the fluid,
mu	=	viscosity of the fluid;
W	=	fall velocity of the particles,
d	=	mean diameter of the sand,
g	=	acceleration due to gravity, and
t	=	time.

Using dimensional analysis and combining the dimensionless groups in a more useful form, ali 1994 obtained:

$$\frac{Y_D}{a} = f'\left(\frac{V_o t}{a}, \frac{D}{a}, \frac{V_o}{W} \right) \quad (4)$$

Equation (4) was applied to he experimental results of Laursen 1952.

The Method of Altinbilek and Basmaci

Several similar empirical methods for predicting local scour have been developed by Laursen 1952, and Altinbilek and Basmaci 1980. These methods attempt to find a solution to the following sediment continuity equation:

$$\frac{dV_s}{dt} = Q_s - Q_i \quad (5)$$

where dV_s/dt is the rate of change of the volume of sediment removed from the scour hole, Q_s is the volume rate of sediment transported out of the scour hole and Q_i is the volume rate of sediment being transported into the scour hole.

Altinbilek and Basmaci's method proposed an expression for Q_s and assumed that the volume of the scour hole can be closely approximated by a triangular scour hole profile function (Altinbilek and Basmaci 1980). They next used an empirical equation for the scour depth at the asymptotic state to obtain a relationship for the variation of the maximum scour depth with time.

The Fluent Package

Fluent is a general purpose computer program for modelling complicated flow fields. It incorporates techniqus based on fundamental principles for simulating a wide range of fluid flow problems. FLUENT/BFC is the primary set-up package for modelling complex geometries. FLUENT uses a finite difference numerical procedure to solve the fundamental equation governing fluid flow (the Reynolds Equations). Additional equations are solved for the conservation of the parameters of the k - epsilon turbulence model, chemical species and entropy.

The numerical technique involves the subdivision of the domain of interest into a finite number of cells, the partial differential equations being discretised over these cells to obtain sets of simultaneous algebraic relations. Because of the non-linearity and interdependence of the differential equations, an itterative solution procedure is adopted (Fluent Inc. 1993)

Experimental Equipment and Arrangements

Several experimental arrangements were used for conducting the experiments described in this paper. These arrangements are described in Ali and Lim 1986, Ali 1988 and Waldeck 1988. Experiments were conducted using various grades of sand material as well as different types of polymer particles (see Ali et al 1994)

RESULTS

Three main experimental studies were undertaken to investigate the extent and nature of localized scour produced by turbulent water jets. Results of outfall sedimentation are also described herein:

(i) **Flap-gate experiments**

Experiments were conducted for fixed flap-gate angles of 0°, 45° and 60° to the horizontal for a fixed discharge and for tailwater depths of 3.7 and 9.6cm. In these experiments all relevant dimensions of the three dimensional scour holes were measured for various t. Additional experiments were conducted for fixed downstream depths and varying discharges. Theoretical expressions were developed for the volumes of the scour holes. These agreed closely with measured values (Waldeck 1988). Figures 2 and 3 show the variation of maximum depth of scour with time for θ = 0, 45 and 60° and for downstream water depths of 3.7 and 9.6cm. The curves are all of a similar shape, i.e. sharp increase in maximum depth for smaller times, and then not much increase for further times. The results for the downstream depth of 9.6cm resulted in much smaller depth and volume of scour hole. Figure 4 shows scour hole contours for various gate angles.

(ii) **Flow downstream of vertical sluice-gate**

(a) **Deep downstream submergence**

The experimental results of Laursen (1952) for the distance to the position of the maximum scour hole were used to verify Eq. (4). Laursen's experiments were for local scour using particles with medium sizes of 0.23, 0.68 and 1.50mm. Tests were conducted using 17 jet velocities. Figure 5 shows a comparison between Larsen's experimental values of X_D/a and the following expression (based on Eq. (5)):

$$\frac{X_D}{a} = 13.8 \left(0.35 + 30.8 \frac{D}{a} \right) \left(\frac{V_o}{W} - 2.5 \right) \left[\log_{10} \left(\frac{Wt}{a} \right) - \left(1.87 + 3.6 \frac{D}{a} \right) \right] \quad (6)$$

(b) **Two-Dimensional Scour Downstream of a Sluice Gate under Shallow Submergence**

Detailed experimental results are given by Ali and Lim 1986. Herein, the Fluent package is used to compare the theoretical and experimental boundary shear stress distributions.

As the diffused jet of water starts to flow over an erodible bed, and if the shear stress acting over it is high, then scouring action will begin. As the size of the scour hole gradually increases, the shear stress reduces to the critical value with the attainment of the equilibrium state. A method was used to convert the loose sand scour hole into a fixed bed model (Ali and Lim (1986). The velocities near the floor were measured using a stream flow miniature current

meter. The boundary shear stress was calculated from $\tau_b = \rho f u_b^2/8$ where f is the friction factor. The theoretical boundary shear stress along the scour hole was otained using numerical modelling. One of the packages avilable is FLUENT which incorporates finite difference technicues to solve the flow problem. Figure 6 shows the computed values of the wall shear stress, τ_b using the FLUENT package corresponding to bed profiles for the 4.1 x 60.7cm JET (Sluice Gate) obtained by Ali and Lim in their experiment. The values represent the x-components of the shear force at each wall-fluid interface divided by the area of that interface which was projected on to the x-axis. Ali and Lim estimated the mean bed shear stress using the mean velocity measured very near to the bed.

Figures 7(a) - (c) show the comparison of results obtained from the FLUENT package and Ali and Lim's values for t = 15min., 90min. and 400min. respectively. It can be seen that, in general, the value of τ_b obtained from FLUENT was higher at sections between the jet and the maximum scour. This was probably due to the fact that FLUENT reports only the x-direction wall shear stress and not the total shear stress as in the case of Ali and Lim. The difference is greater where the slope of the bed is steeper because the area projected on to the x-axis is smaller. Beyond the section of maximum erosion, it can be seen that τ_b increases and reaches a maximum value of $0.4N/m^2$ and $0.5N/m^2$ for t = 15 and 90min. scour holes respectively, as the bed profiles approach the original flat bed, compared to $0.72N/m^2$ and $0.54N/m^2$ obtained by Ali and Lim. However, the agreement was particularly good in the region of maximum erosion.

Turbulence Model

The default closure model used in FLUENT is the k-ε (k-ε) model or termed as Simplec model based on Renormalization Group Theory, the RNG k-ε model. This powerful RNG-based k-ε model provides both accuracy and efficiency in modelling of highly-strained turbulent flows, flows with high streamline curvature and low Reynolds numbers. The comparison of the results obtained from the three different models are presented in Figure 8. There is no significant variation in the computed values of all the models. However, the RNG model converges twice as fast as the other two models, thereby increasing the computational efficiency.

Computational Grid

Ali and Lim used the floor velocity, u_b for computation of τ_b which was measured using the propeller meter at 0.8cm above the bed. In order to simulate this in FLUENT a computational grid size of 1.6cm was used horizontally along the bed, so that the wall stress is computed 0.8cm above the bed (at the mid-point of the grid). An attempt was made to calculate the value of wall stress even closer to the boundary by doubling the grid. By doing so, the size of the grid is reduced to half and therefore the velocity calculated at 0.4cm above the bed will be used. The results are shown in Figure 9. It can be seen that the values do not change significantly, except in the region between the jet and maximum scour.

Turbulence Intensity

The turbulence intensity is defined as the ratio of the turbulent fluctuations in velocity to the mean flow velocity (u'/u_{avg}) expressed as a percentage. The inlet values of k and ε are calculated by FLUENT from the specified inlet TURBULENCE INTENSITY, I, as follows:

$$k = 1.5(u')^2 \text{ or } k = 1.5(u_{avg}I)^2$$

The dissipation rate is then given by:

$$\varepsilon = C^{2/3}(k^{1.5}/l)$$

where C is an empirical constant (0.09) and l is a length scale characteristic of the turbulence in the inlet flow.

In the current problem three different values of turbulence intensity have been used They are 5%, 10% and 15% and are shown in Figure 10. It can be seen that changing the turbulence intensity does not alter the results significantly.

(iii) **Two-dimensional Local Scour Downstream of an Offset Jet Under Deep Submergence**

Only a very brief summary of some of the new results on offset jets are given in this paper. More details are given in Ali and Neyshaboury 1991.

Figured 11 shows centreline scour profiles for elevations of the centre of the jet of 0.581, (wall jet), 10 and 20cm. These results are given for deep submergence for jet height of 11.6mm and for a jet velocity of 64cm/s. Clearly, scour is extensive for the case of the wall jet. Figure 12 shows comprehensive experimental velocity distributions for the asymptotic conditions of the above runds. In all cases, considerable revers flow is clearly noticeable in the scour holes.

volumes of the scour holes at the asymptotic state were measured and the following relationship was obtained for the volume per unit width (V):

$$\frac{V}{b_o^2} = 2.93F^2 \qquad (7)$$

where F is the densimetric Froude number.

Figure 13 shows a comparison between theoretical and experimental velocity distributions for an offset jet with a rigid bed (see Ali 1988).

(iv) **Experiments on Outfall Sedimentation**

Experiments on ripple and dune formation were conducted using a 13.75cm diameter outfall pipe, 4.5m in length. Experiments were conducted using various grades of sand and crushed Olive Stones which had a much lower specific gravity and smaller diameter thus being more representative of the behaviour of actual outfall sediment. Figures show profiles for 0.321mm sand and crushed Olive Stones respectively.

A two-dimentional morphology model was obtained from a simplification of the emthod of O'Connor and Nicholson (see (Ali, Burrows and Wose 1994). The relevant equations were solved using finite difference. Figures 16 and 17 show a comparison between the theoretical and experimental bed profiles for various times.

CONCLUSIONS

Several experimental and analytical methods were used to investigate deposition and errosion problems. These methods resulted in the following conclusions:

(a) The size and shape of the scour hole downstream of a flap-gate is dependent on sediment size, gate angle, discharge and downstream water depth.

(b) The main characteristics of a scour hole, like its maximum depth, vary with log t.

(c) The Fluent package provides a powerful tool for the investigation of various local scour problems.

(d) Detailed measurements of scour hole profiles and velocity distributions produced by an offset jet show that the height of the jet has a major influence on the results.

(e) Predicted bed profiles, for an outfall pipe, are in reasonable agreement with the experimental results.

ACKNOWLEDGEMENTS

The authors would like to express their gratitude for the help given by the following students and colleagues in conducting some of the experiments described herein: S. Y. Lim, Waldeck, Neyshabouri, Walley.

REFERENCES

Ali, K.H.M. and Lim, S.Y., "Local scour caused by submerged wall jets", Proc. Instn. Civ. Engrs., Part 2, 1986, 81, Dec., 607-745.

Ali, K.H.M., "Characteristics of offset jets", University of Liverpool, Dept. of Civil Engineering Report, 1988.

Ali, K.H.M. and Salehi Neyshaboury, A.A., "Localized scour downstream of a deeply submerged horizontal jet", Proc. Instn. Civ. Engrs., Part 2, 1991, 91, March, 1-18.

Ali, K H.M., Burrows, R. and Wose, A.E., "Sedimentation in long sea outfalls", IAWQ, International Specialized Conference on Marine Disposal Systems, Istanbul, Turkey, 9-11 Nov., 1994, 149-156.

Altinbilek, H.D. and Basmaci, Y., "Localized scour below submerged vertical gates", Proc. Speciality Conf. Computer and Physical Modelling in Hydraulic Engineering, Chicago, Aug , 1980, 39-50.

Fluent Inc. (1993), Fluent user's guide version 4.2.

Laursen, E.M., "Observations on the naure of scour", Proc. 5th Hydraulics Conf. Bulletin 34, University of Iowa, 1952, 179-197.

Man, J.W.S., "Sediment ripple formation and sedimentation in long sea outfalls", M.Sc. Thesis in Env. civil Eng. University of Liverpool, 1993.

O'Connor, B.A. and Nicholson, J., "An estuarine and coastal sand transport model , Coastal and Estuarine Studies, Ed. D. Pandle, American Geophysical Union 1990, pp 507-526.

Waldeck, P.c., "Scouring by turbulent jets", B.Eng. Thesis, University of Liverpool, 1988.

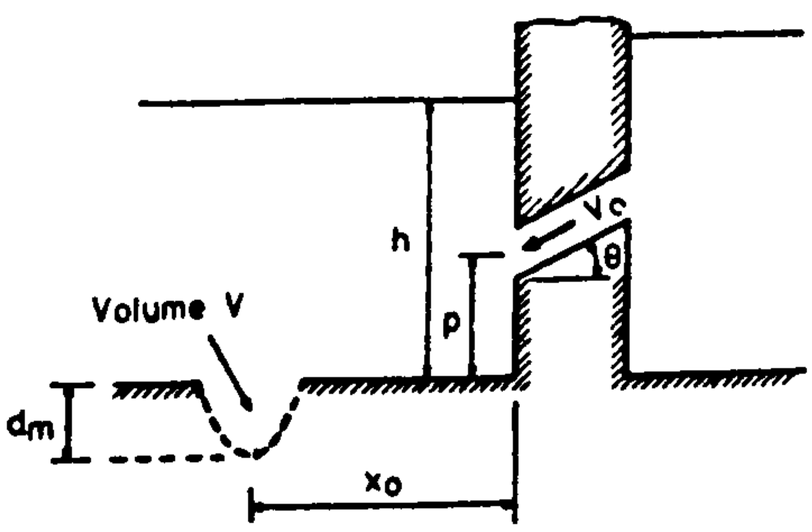

FIG. 1 DEFINITION SKETCH FOR LOCAL SCOUR PROBLEM

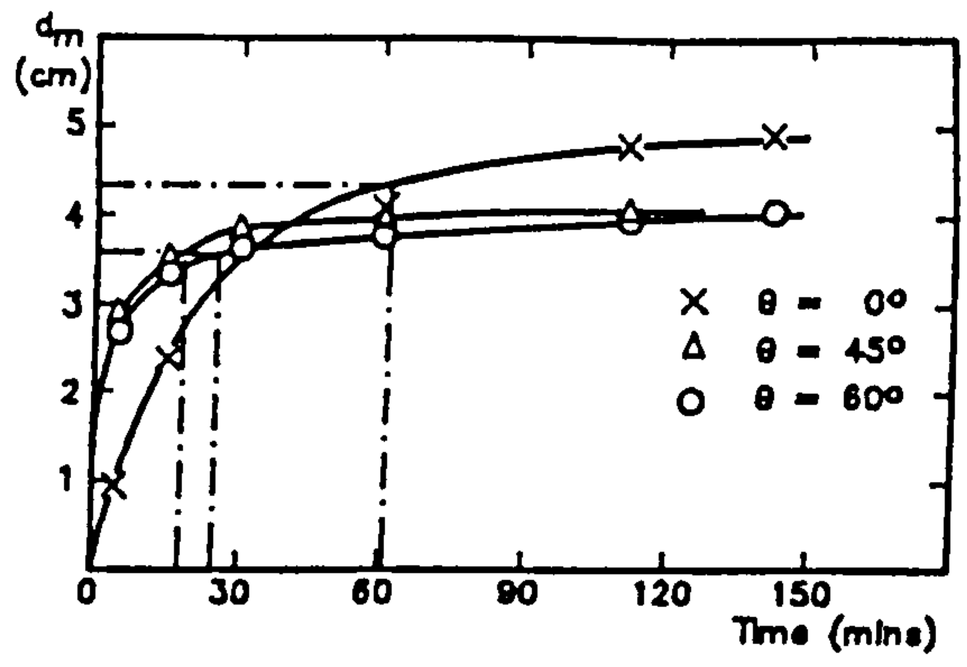

FIG. 2 VARIATION OF MAXIMUM DEPTH OF SCOUR HOLE WITH TIME FOR FLAP-GATES (H = 3.7cm)

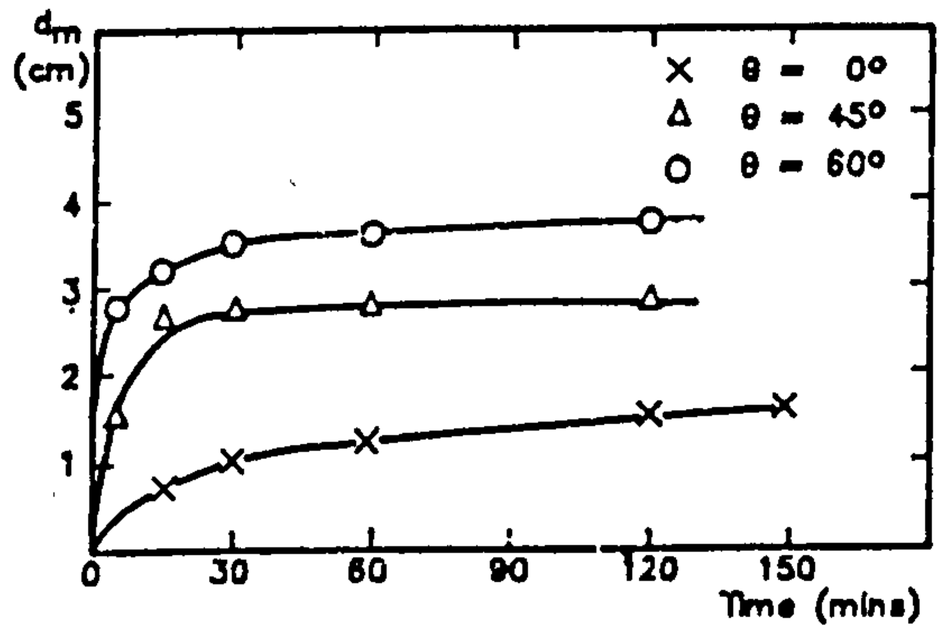

FIG. 3 VARIATION OF MAXIMUM DEPTH OF SCOUR HOLE WITH TIME FOR FLAP-GATES (H = 9.6cm)

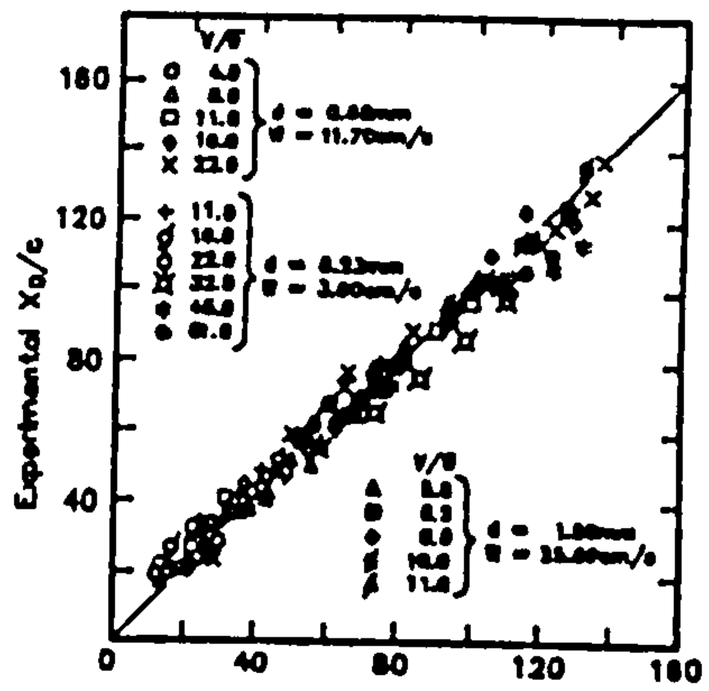

FIG. 5 COMPARISON BETWEEN FITTED AND EXPERIMENTAL X_o/e

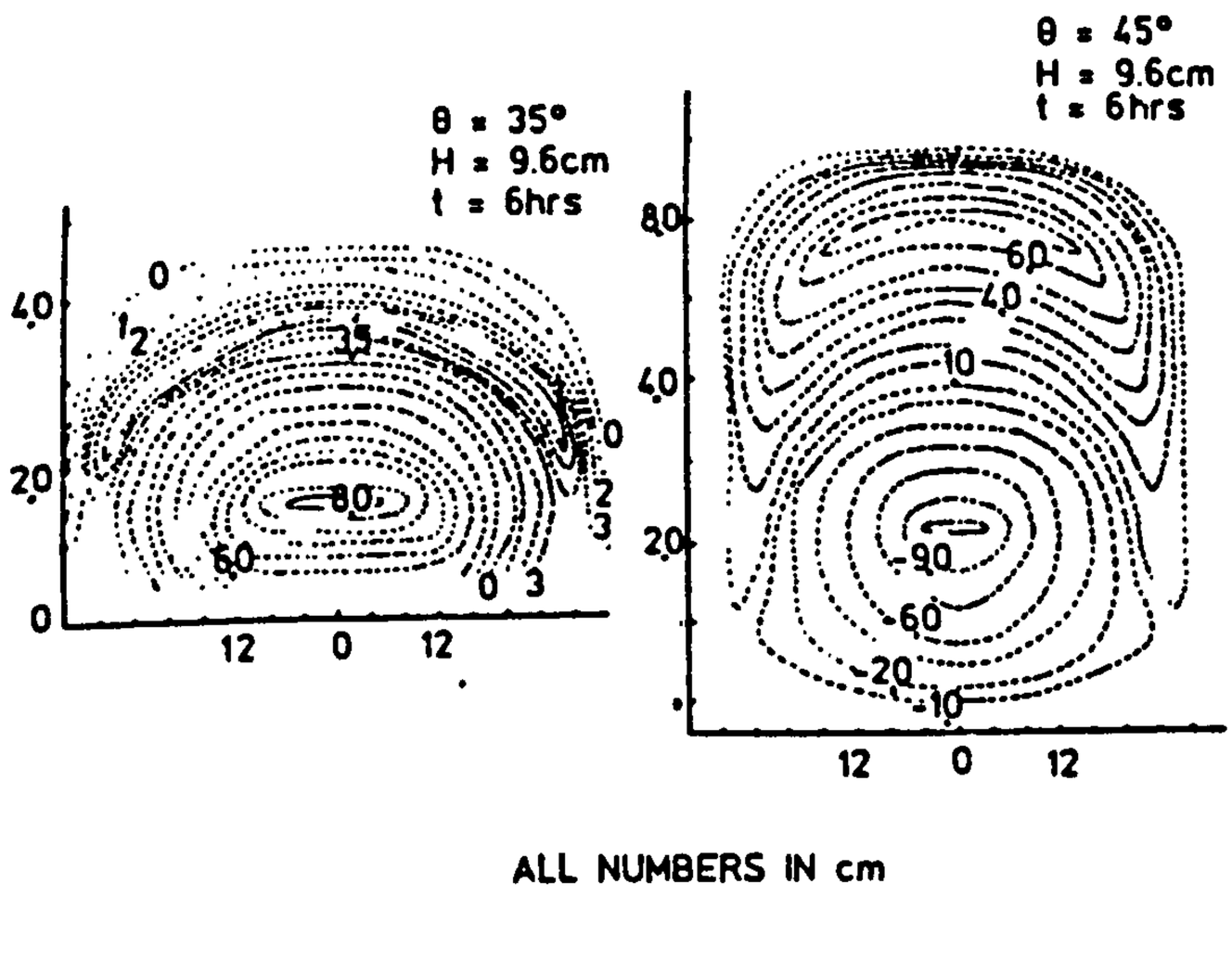

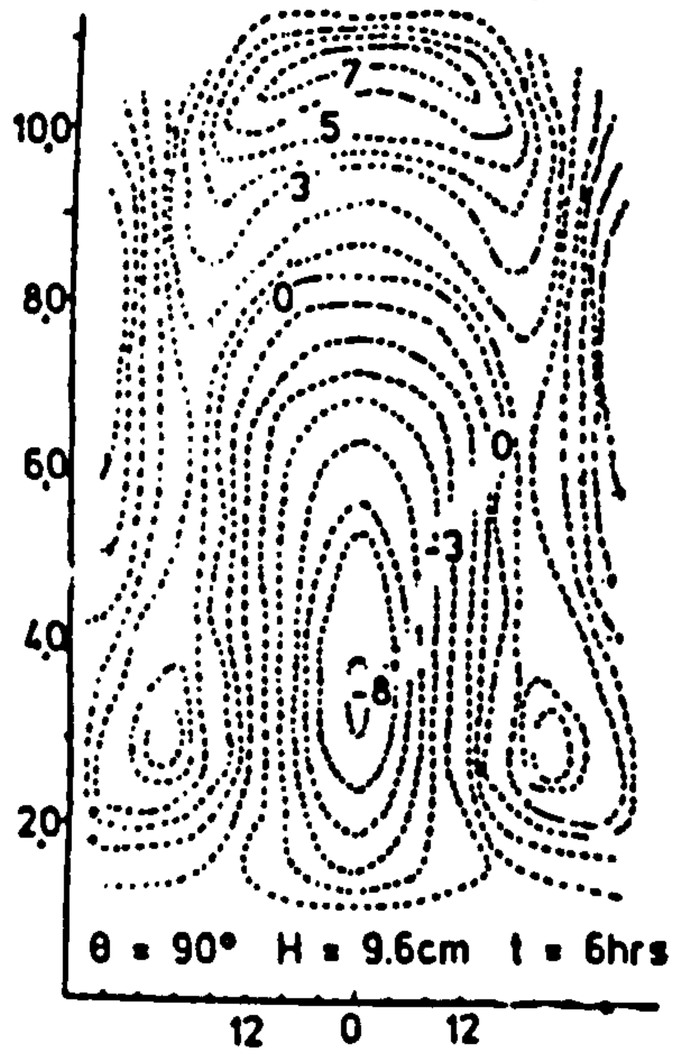

FIGURE 4 BED CONTOURS FOR DIFFERENT FLAP-GATE ANGLES AND DOWNSTREAM WATER DEPTHS.

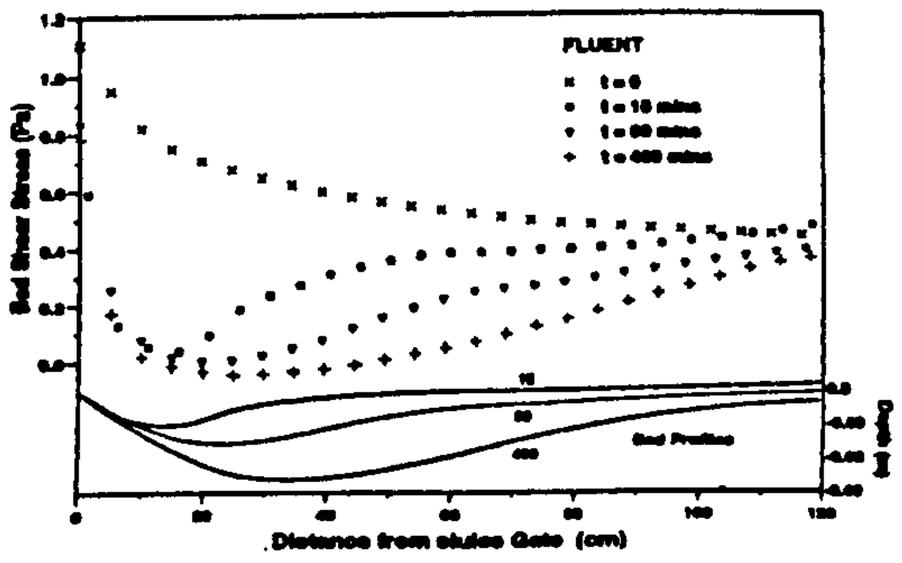

FIGURE 6 SHEAR STRESS DISTRIBUTIONS FOR VARIOUS TIMES

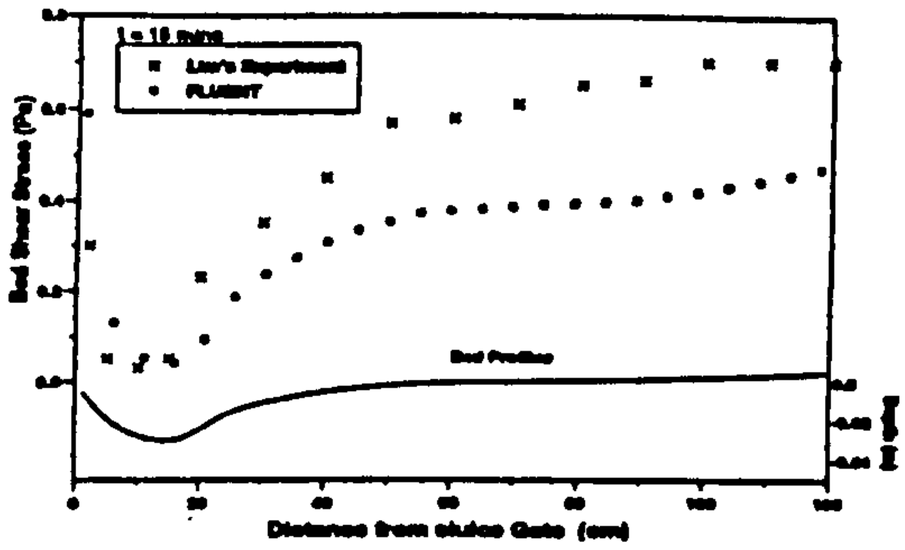

FIGURE 7a COMPARISON BETWEEN EXPERIMENTAL AND FLUENT SHEAR STRESSES (t = 15 mins)

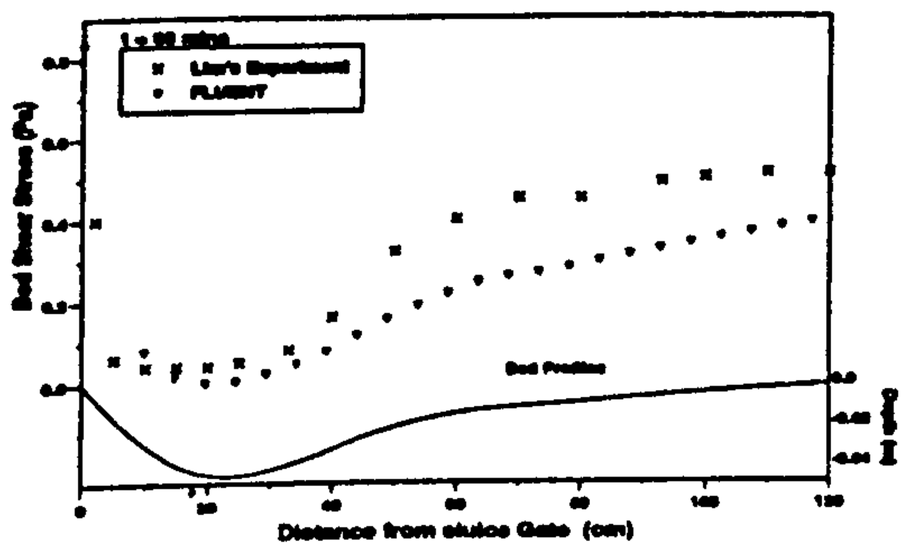

FIGURE 7b COMPARISON BETWEEN EXPERIMENTAL AND FLUENT SHEAR STRESSES (t = 90 mins)

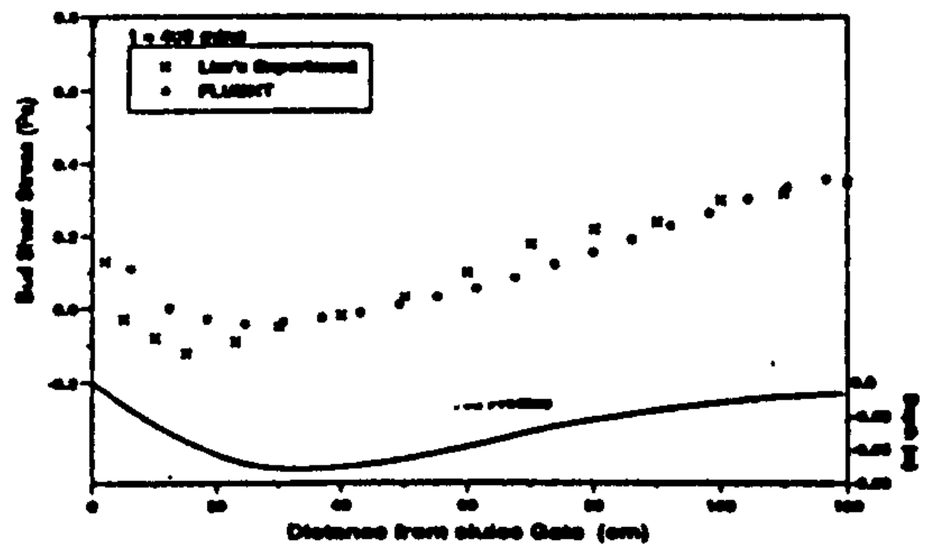

FIGURE 7c COMPARISON BETWEEN EXPERIMENTAL AND FLUENT SHEAR STRESSES (t = 400 mins)

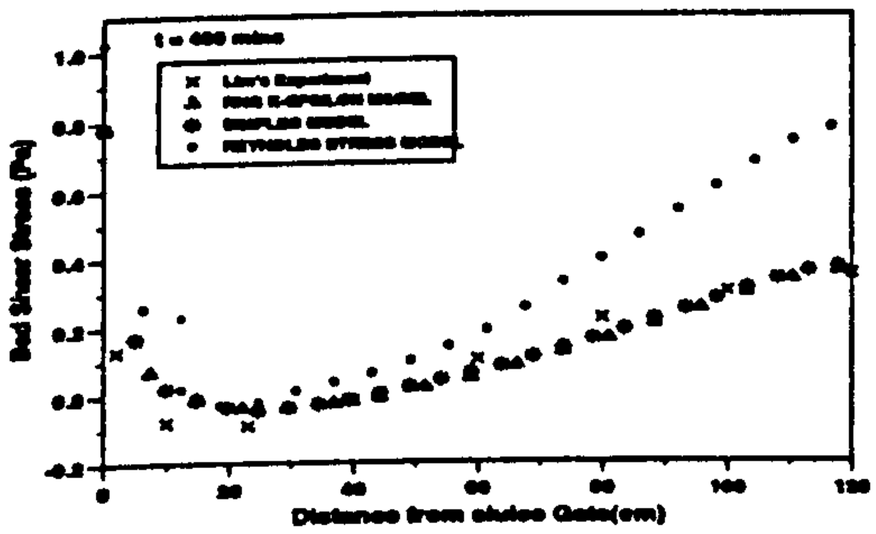

FIGURE 8 EFFECT OF VARIOUS TURBULENCE MODELS OF SHEAR STRESS DISTRIBUTION

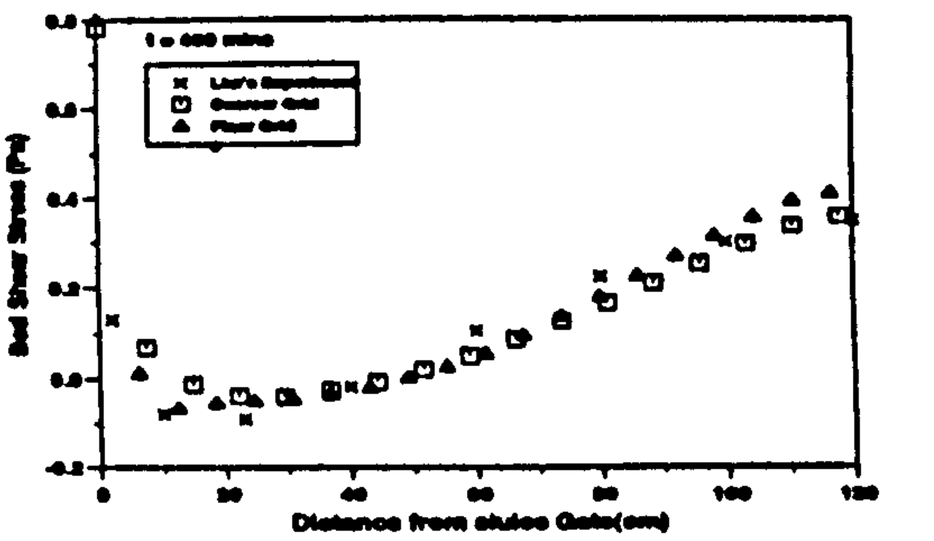

FIGURE 9 EFFECT OF GRID SIZE ON SHEAR STRESS DISTRIBUTION

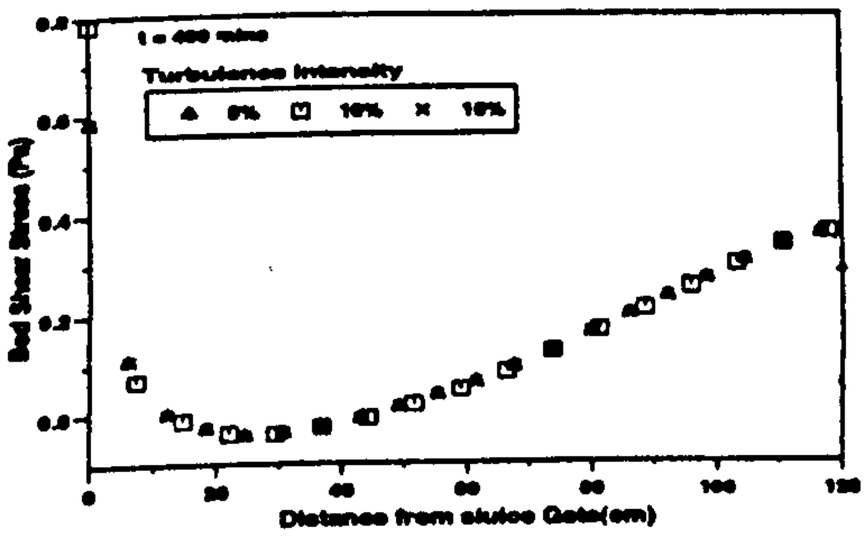

FIGURE 10 EFFECT OF TURBULENCE LEVEL ON SHEAR STRESS DISTRIBUTION

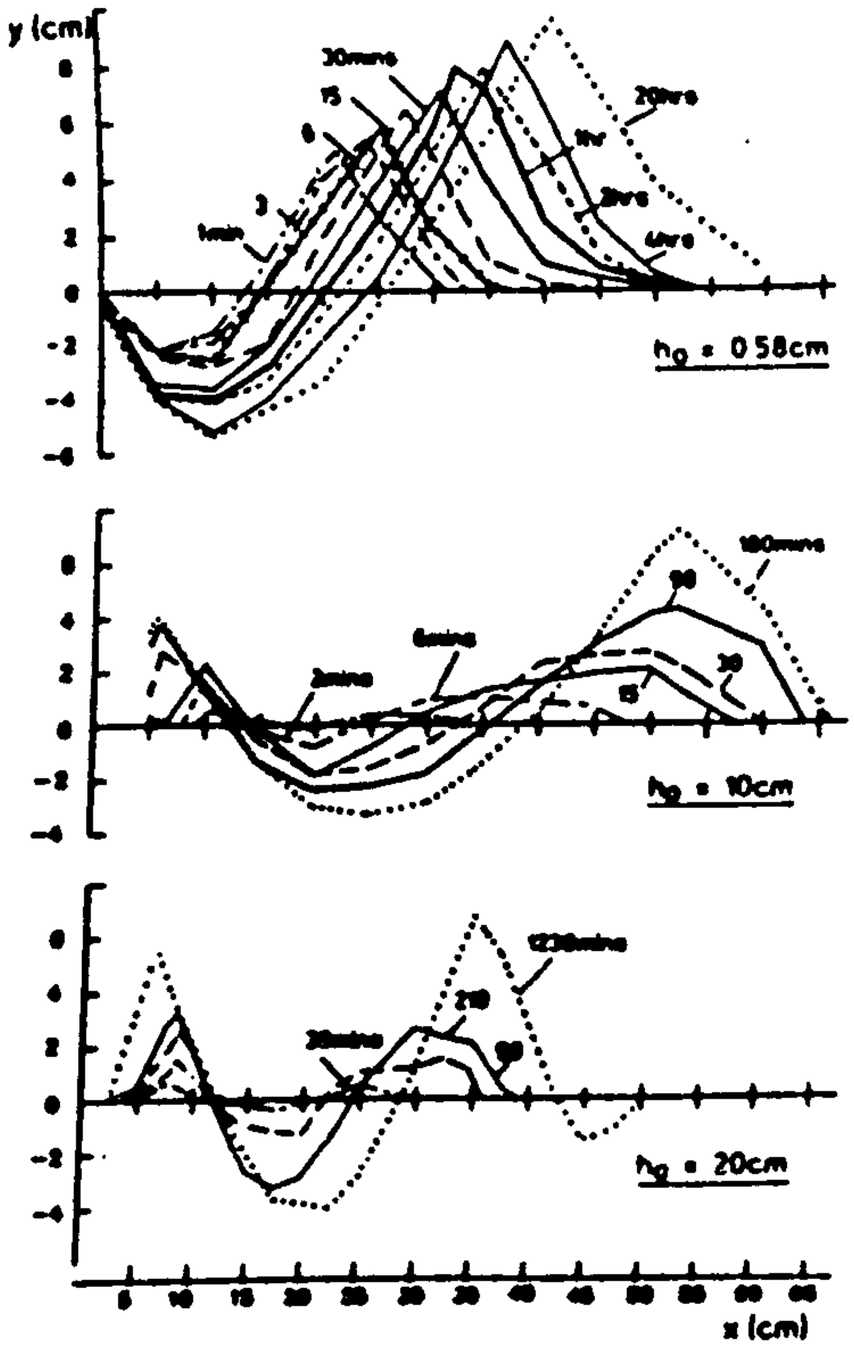

FIGURE 11 SCOUR HOLES FOR DIFFERENT OFFSET JETS

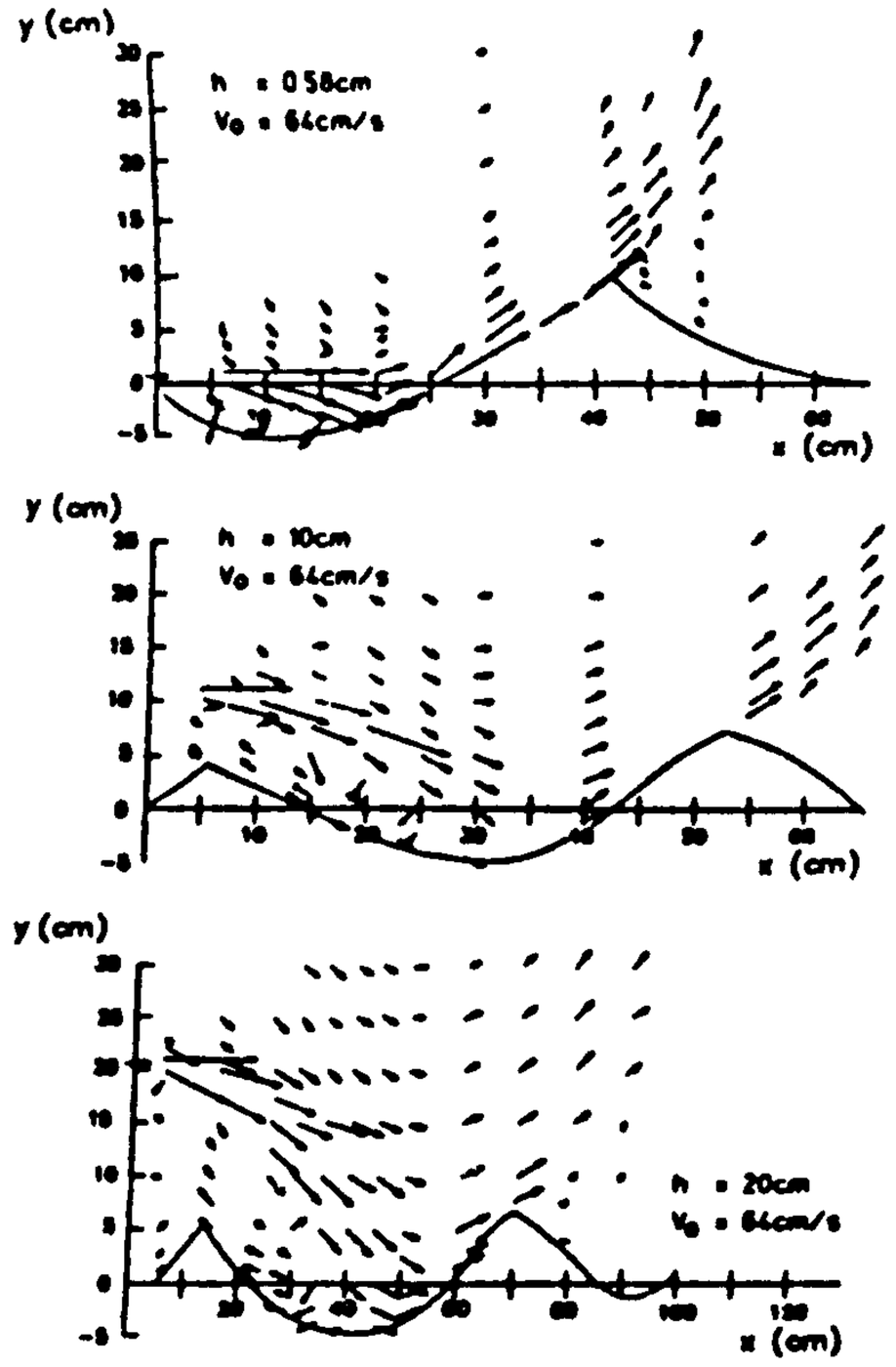

FIGURE 12 VELOCITY DISTRIBUTIONS AT THE ASYMPTOTIC STATE

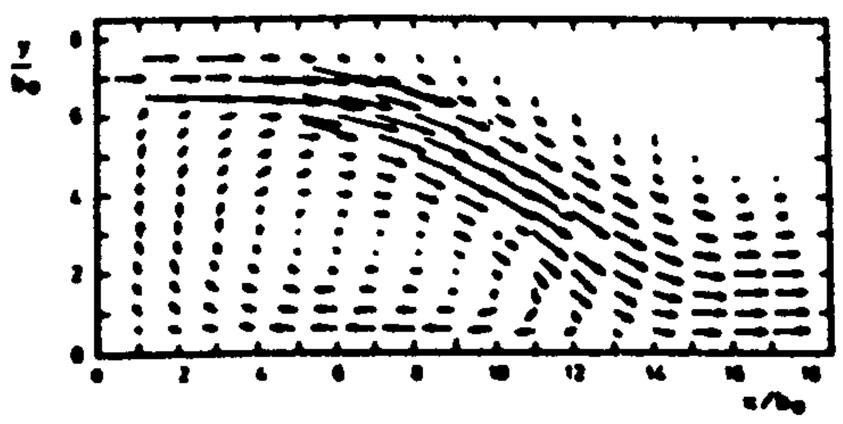

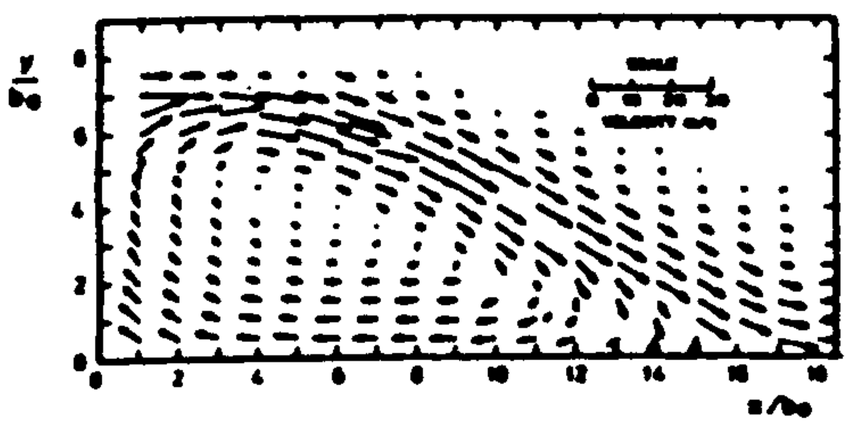

FIGURE 13 COMPARISON BETWEEN PELFREY'S AND ALI'S VELOCITY-DISTRIBUTIONS

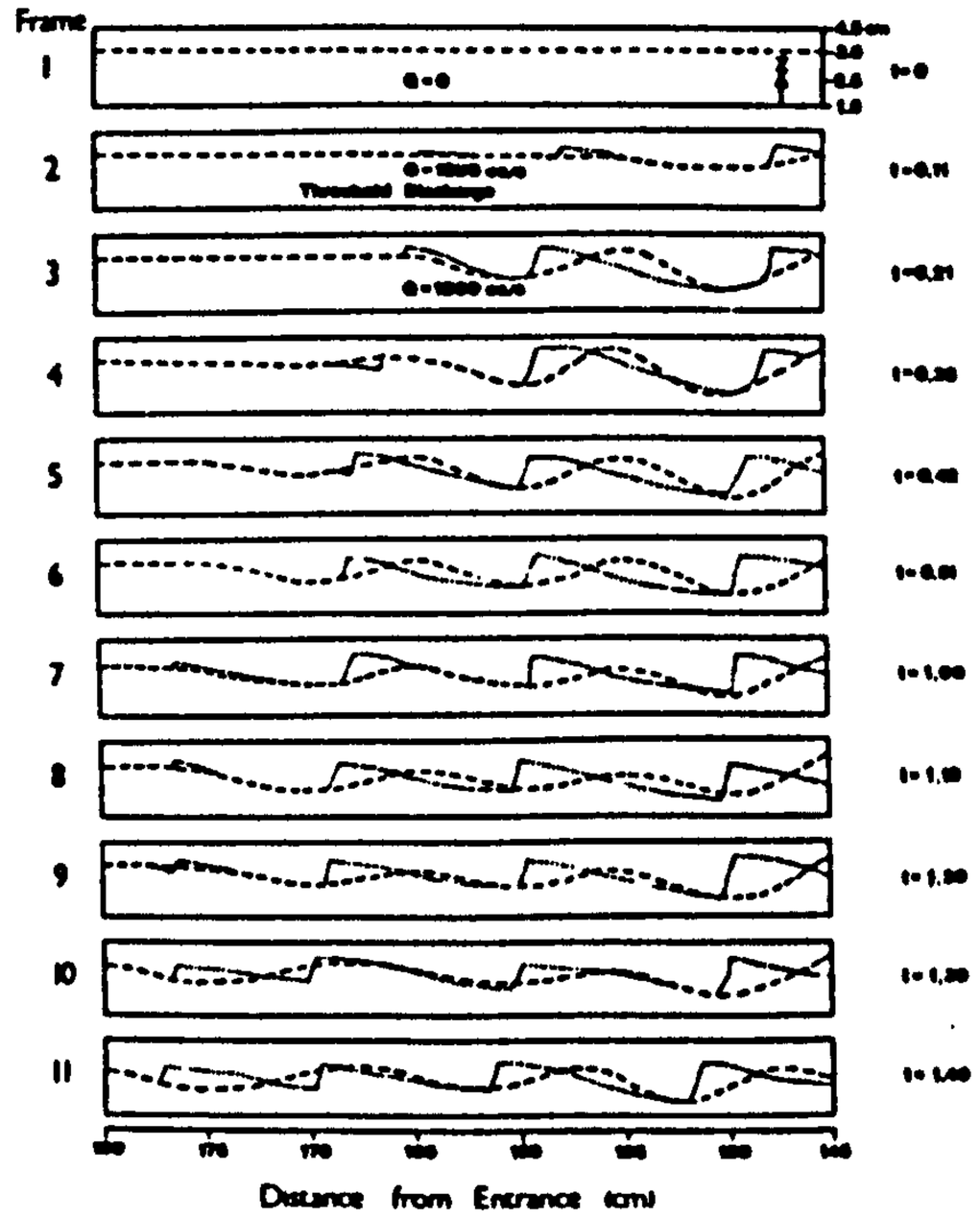

FIGURE 14 SEDIMENT DUNE PROFILES IN MODEL OUTFALL PIPE FOR SAND.

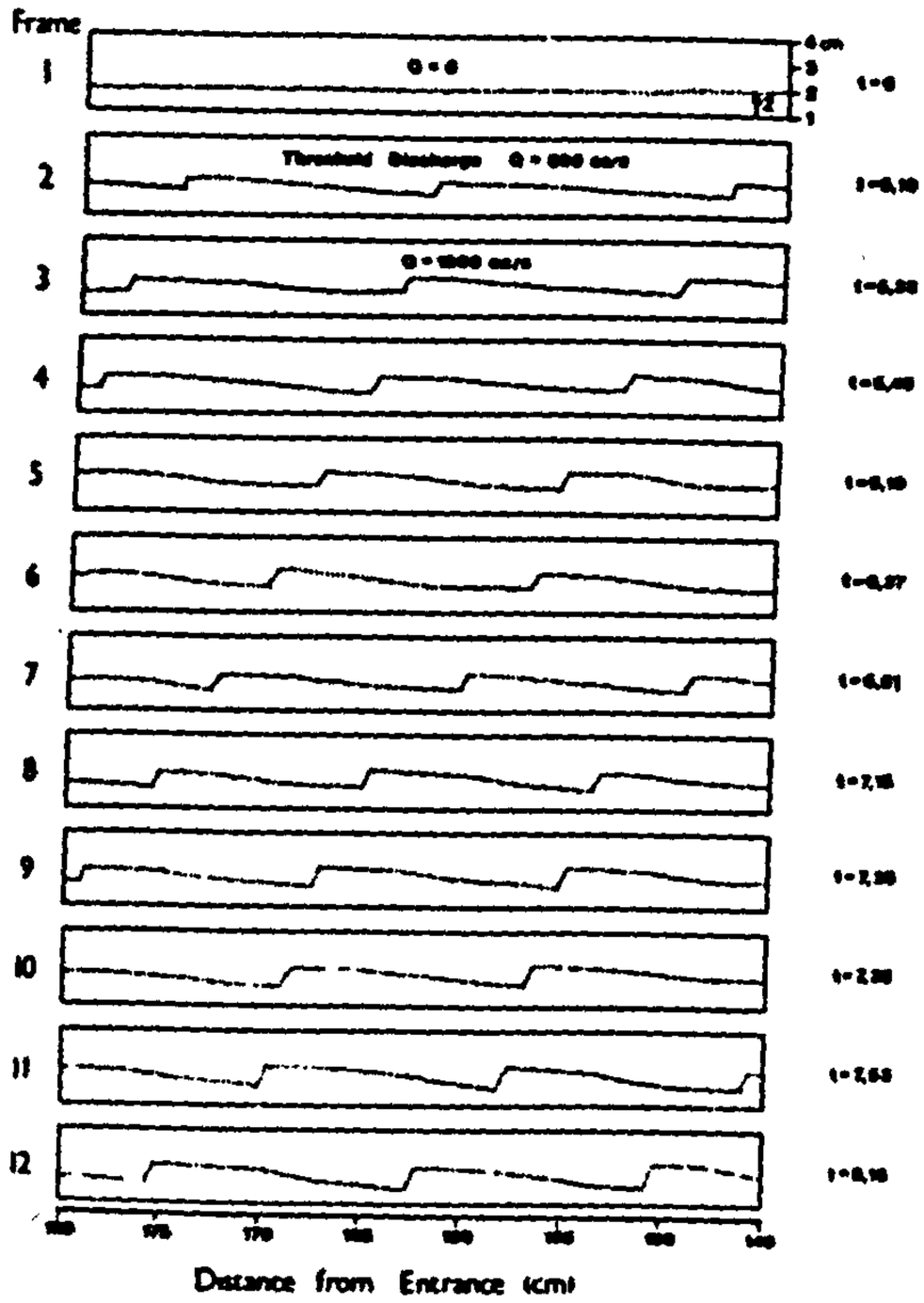

FIGURE 15 EXPERIMENTAL PROFILES (CRUSHED OLIVE STONES)

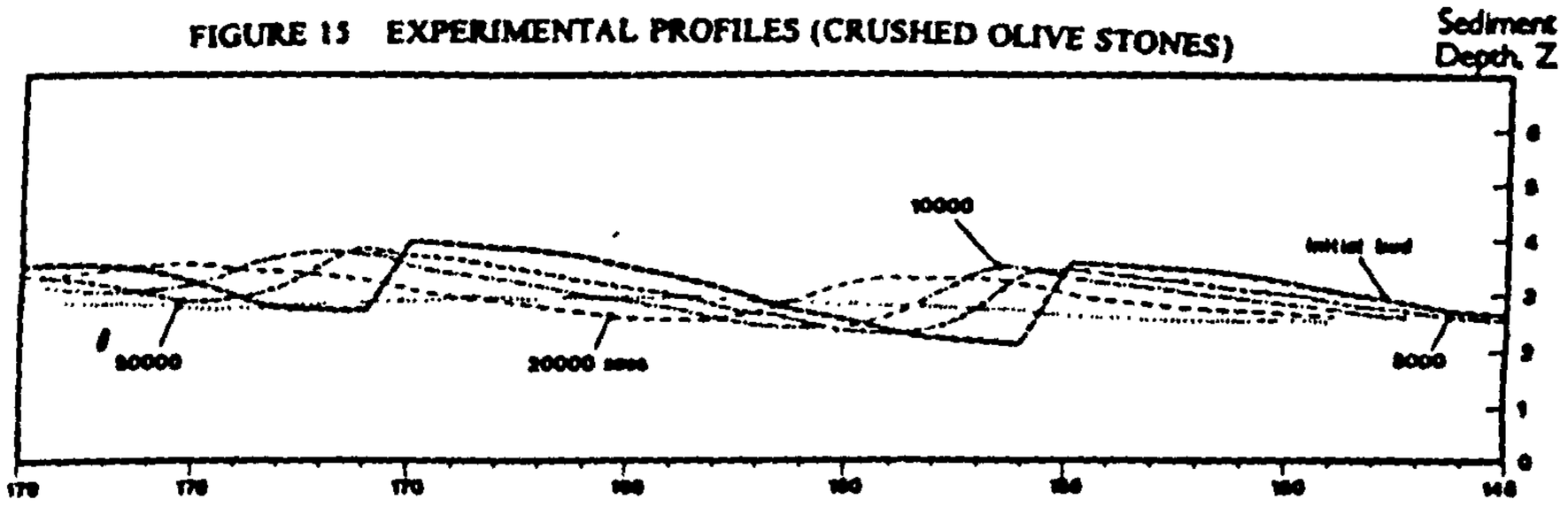

FIGURE 16 PREDICTED BED PROFILES (SAND)

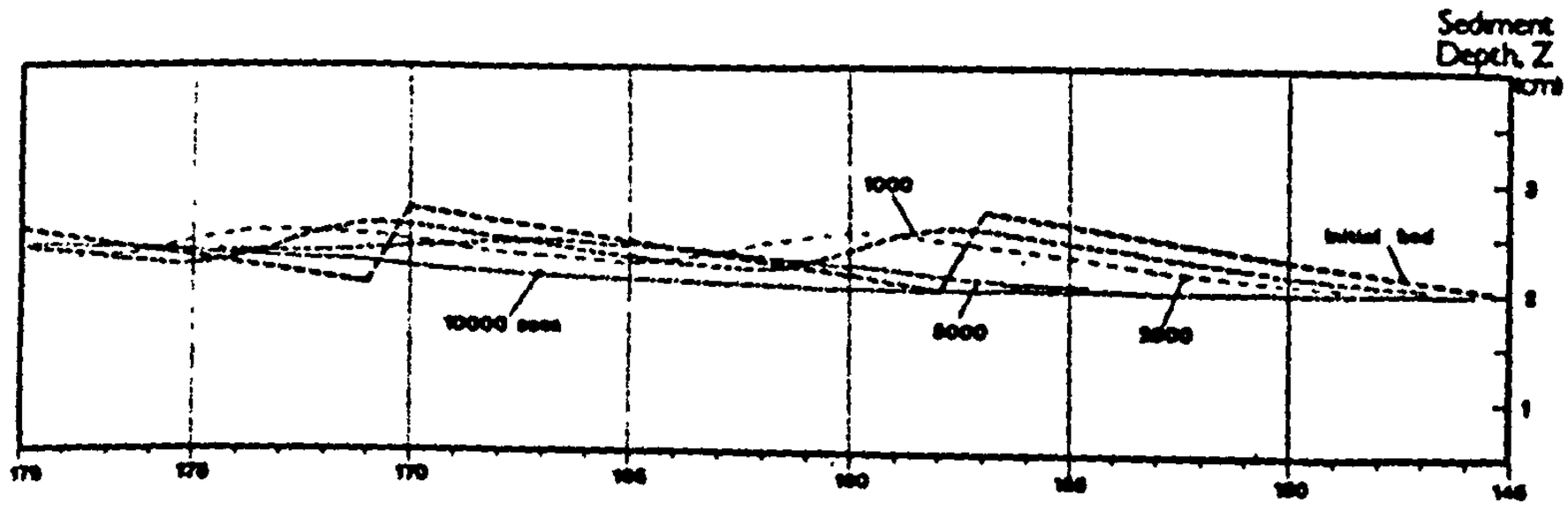

FIGURE 17 PREDICTED BED PROFILES (CRUSHED OLIVE STONES)

PREDICTION OF FLOW GENERATED BY TURBULENT JETS

Kamil H. M. Ali, Othman A Karim and Brian A O'Connor

Department of Civil Engineering, University of Liverpool, L693BX, UK.

ABSTRACT: The paper gives predicted flowfields downstream of two-dimensional wall and offset jets. results were obtained for different downstream water depths and for flat beds as well as for scour holes of various sizes. The FLUENT computer package was used for this purpose. The effects of various turbulence models were investigated. The numerical solutions were compared with various experimental results obtained by many researchers in this field.

INTRODUCTION

Prediction of local scour holes that develop downstream of hydraulic structures plays an important role in their design. Excessive local scour can progressively undermine the foundation of the structure. Because complete protection against scour is too expensive, generally, the maximum scour depth and the upstream slope of the scour hole have to be predicted to minimize the risk of failure.

The localized scour phenomenon has been the subject of extensive investigations by many researchers and numerous literature exists for scour caused by 2- and 3- dimensional turbulent jets. Most of the studies conducted on scour have been empirical because of the complexity of the physical processes (see Rouse (1939), Laursen (1952), Rajaratnam and Beltaos (1977), Ali and Lim (1986).

Far less research has been conducted on offset and re-attached jets (see Ali et al (1991, 1992); Rajaratnam, N. and Subramanya, N. (1986) and Kumada et al (1973).

The FLUENT Package

FLUENT is a general-purpose computer program for modelling complicated flow fields. It incorporates techniques based on fundamental principles for simulating a wide range of fluid flow problems (Fluent Inc. 1993). FLUENT/BFC is the primary set-up package for modelling complex geometries. FLUENT uses a finite difference numerical procedure to solve the fundamental equations governing fluid flow.

Three turbulence closure models are incorporated in FLUENT:

(a) The standard k - ϵ model;
(b) The Reynolds Stress Model (RSM);
(c) The Renormalization Group (RNG) model.

In the present study, an evaluation is made of these models.

The aim of this paper is to verify the effectiveness of the numerical procedure available in FLUENT in predicting the flow characteristics in turbulent wall and offset jets. For that purpose velocity measurements carried out by Wu and Rajaratnam (1995), Ali and Lim (1986) and Ali and Walley (1992) were used. The analysis was divided into three sections:

Wall Jets

(a) Flat rigid bed - deep submergence (Wu and Rajaratnam);
(b) Flat rigid bed - shallow submergence (Ali and Lim);
(c) Scour hole - shallow submergence (Ali and Lim, t = 15, 90 and 400 mins)

Offset Jets

(a) Flat rigid bed - deep submergence (Rajaratnam and Subramanya);

(b) Flat rigid bed - deep submergence (Salehi-Nayshaboury, 1988);
(c) Scour hole - deep submergence ((Ali and Walley (1992), t = 4770 mins.).

Comparison between FLUENT'S predictions and relevant experimental results

1. Wall Jets

Figure 3 is reproduced from Wu and Rajaratnam (1995), and gives their experimental velocity distributions in dimensionless form. The parameters u_m (Figure 1) were used as velocity and length scales respectively. They observed that except for the sections very close to the nozzle (within the potential core region) and far away from the nozzle, the velocity profiles at all sections, in the forward flow region, were similar. This is in agreement with the general description of the classical wall jet.

The FLUENT predictions are given in Figure 4 and show excellent agreement for the free jet zone. The boundary-layer region is, however, underestimated.

Ali and Lim (1986) conducted experiments to study scour produced by a two-dimensional wall-jet. Figure 5 shows the FLUENT results applied to these experiments and are given for times of 0, 15, 90 and 400 minutes from the start of the run. These predictions are in good agreement with the relative experiments.

Figure 6 shows computed bed shear stresses for t = 15, 90 and 400 mins. The values, represent the x-components of the shear force at each wall-fluid interface divided by the area of that interface. These values are compared with the values computed by Ali and Lim (based on velocity at y = 0.8cm from the bed). It can be seen that good agreement is obtained between the values calculated from the experimentally-measured "floor velocities" and those obtained from FLUENT.

Figure 7 shows a comparison between the FLUENT results using the three closure models. There is no significant difference in the computed values between the standard k - ϵ model and the RNG k - ϵ model. However, the RNG model converges twice as fast as the other models, thereby increasing the computational efficiency. The RSM model yields good agreement except at the section beyond the maximum scour.

2. Offset Jets

The choice of geometry setup and grid system used for the offset jet simulations is similar to that adopted for the wall jets.

Figure 9 is reproduced from Rajaratnam and Subramanya (1968). It shows experimental velocity distributions at various sections from the jet. Figures 10 and 11 show the corresponding predicted FLUENT profiles. It can be seen that although the general pattern of the flow is in good agreement, FLUENT, however, underpredicts the values of the maximum velocity u_m and underestimates the "pull" of the solid boundary. This results in a flatter curve of the maximum velocity profile near the impingement region (Figure 8).

Location of the intersection of the dividing streamline with the offset-jet's downstream channel, i.e. the re-attachment point, X_A, (Figure 8) is usually taken at the position where the wall static pressure is a maximum (Kumada et al (1973)). Comparison was made of the predicted and measured re-attachment length ratio for the offset jet. In most cases, FLUENT's results were smaller than the measured values by 2 - 25%. The RNG and k - ϵ models gave better estimation compared to the RSM and a Higher Order Discretization scheme.

To define a trajectory for the offset jet is very useful in theoretical work. The locus of the position of the maximum velocity was chosen as the reference streamline. Using the results of 6 different FLUENT runs, a least square fit was performed and the following coefficients were obtained.

C_o = 0.9970; C_1 = -0.1949; C_2 = 0.3269;
C_3 = -1.0096; C_4 = 0.4807

The equation of profile is given by:

$$y = C_o + C_1x + C_2x^2 + C_3x^3 + C_4x^4$$

where $y = Y_m/h$ and $x = X/X_A$.

Figure 12 shows a comparison between the profile predicted by FLUENT and the curve obtained by Salehi (1988). The later was based on the results of many researchers.

Figures 13 show experimental velocity distributions obtained by Ali and Walley (1992) in scour holes produced by horizontal jets positioned at elevations of 0, 10 and 20cm above the original horizontal bed. The scour holes were produced after 4770 minutes (asymptotic state). Figures 14 show the corresponding velocity vectors predicted by FLUENT. Clearly, there is reasonable agreement between the experimental and the FLUENT results.

CONCLUSIONS

1. The numerical prediction scheme provided by FLUENT was applied to two-dimensional wall and offset jets for horizontally-rigid and scoured beds. Overall, the FLUENT velocities and boundary shear stresses, for wall jets, are in close agreement with th experimental results.
2. The k - ϵ and the RNG k - ϵ turbulence models described the flow near the bed better than the RSM model.
3. FLUENT results for simulating offset jet flow fields were compared with relevant experimental results for rigid and scoured beds. In general, the FLUENT results exhibited good qualitative agreement throughout the flow fields. In the rigid bed cases, the predicted attachment lengths were reasonably accurate to within 10% when the RNG and k - ϵ models were used. However, large errors resulted on using the RSM model. Numerical instability occurred on using the Higher Order scheme.
4. For the scoured beds produced by offset jets, reasonable agreement was obtained between FLUENT and the relevant experimental results.

REFERENCES

1. Ali, K. H. M. and Lim, S.Y. (1986), "Local scour caused by submerged wall-jets". Proc. Instn. Civ. Engrs., London, England, 81(2), pp 607-645.
2. Ali, K. H. M. and Salehi-Neyshabouri, A. A. (1991), "Localized scour downstream of a deeply-submerged horizontal jet", Proc. Instn. Civ. Engrs., Part 2, pp 1 - 18.
3. Ali, K. H. M. and Walley, P. (1992), "Local scour caused by offset jets", Internal Report, Dept. of Civil Engineering, Univ. of Liverpool.
4. Fluent Incorporated (1993), "Fluent Users Guide", Version 4.2.
5. Kumada, M., Mabuchi, I. and Oykawa, K., "(1973), "Studies in heat transfer to turbulent jets with adjacent boundaries", Bull. of JSME., Vol. 16, pp 1712 - 1722.
6. Laursen, E. M. (1952), "Observations on the nature of scour", Proc. of 5th Hyd. Conf., Bull. 34, Univ. of Iowa, Iowa, pp 179 - 197.
7. Rajaratnam, N. and Subramanya, N. (1968), "Plane turbulent re-attached wall jets", ASCE, J. of the Hyd. Div. Vol. 94, HY1, pp 95 - 112.
8. Rajaratnam, N. and Beltaos, S. (1977), "Erosion by circular turbulent wall jets "J. Hydr. Res., 15(3), pp 277 - 289.
9. Rouse, H. (1939), "Criteria for similarity in the transportation of sediment", Proc. Hyd. Conf. Studies in Engineering Bull., Univ. of Iowa, pp 39-49.
10. Salehi-Neyshaboury, A. A. (1988), "Impingement of offset jets on rigid and movable beds", Ph.D Thesis, University of Liverpool.
11. Wu, S. and Rajaratnam, N. (1995), "Free jets, submerged jumps and wall jets", J. of Hydr. Res. Vol. 33, No. 3, pp 197 - 212.

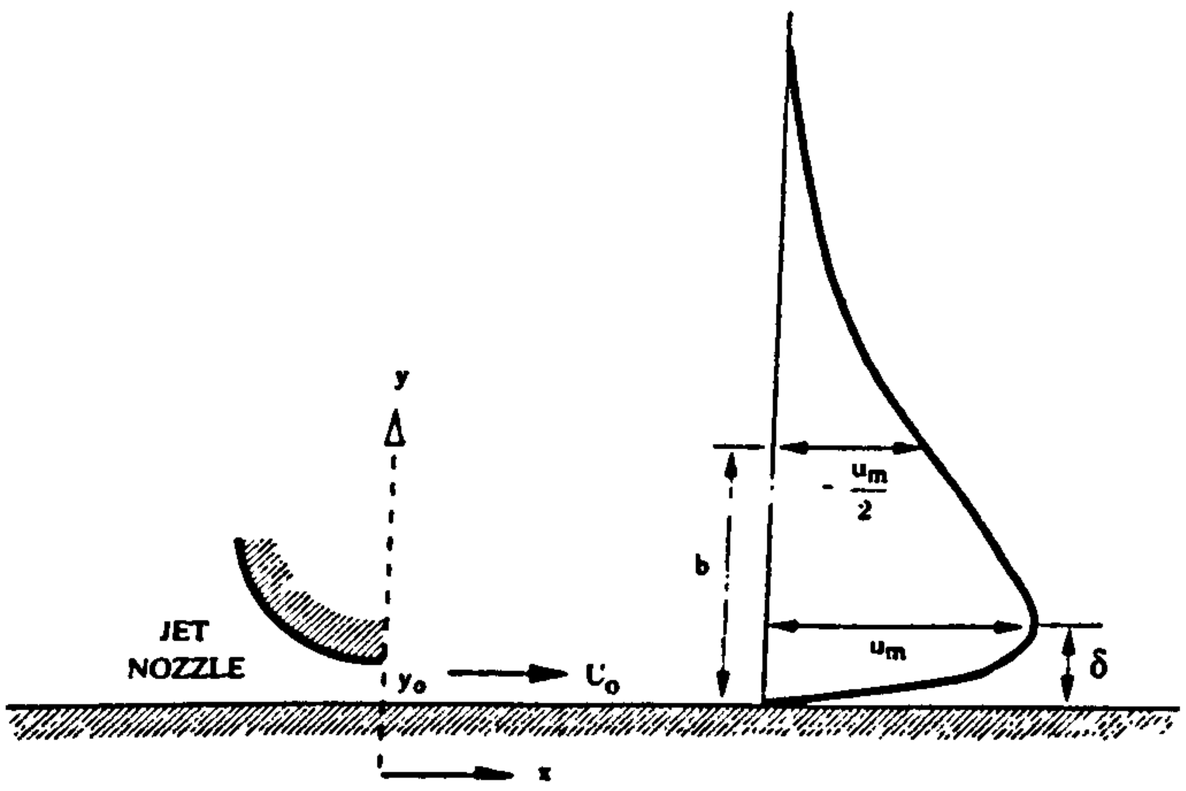

FIGURE 1 **Definition sketch for the classical wall jet**

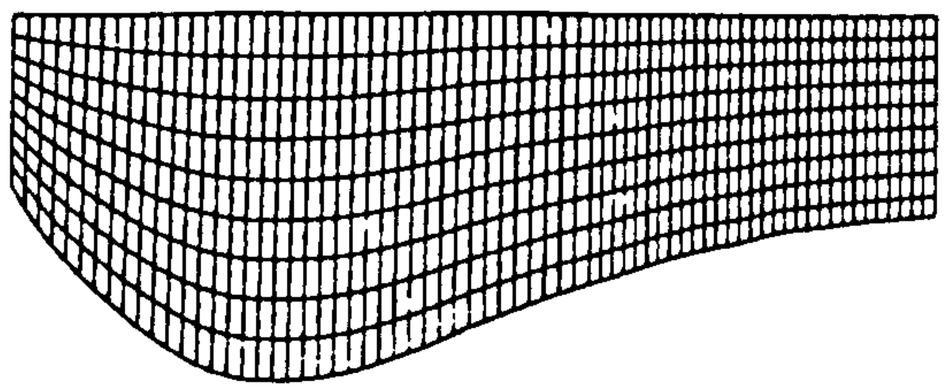

FIGURE 2

Body-fitted co-ordinates for a scour hole

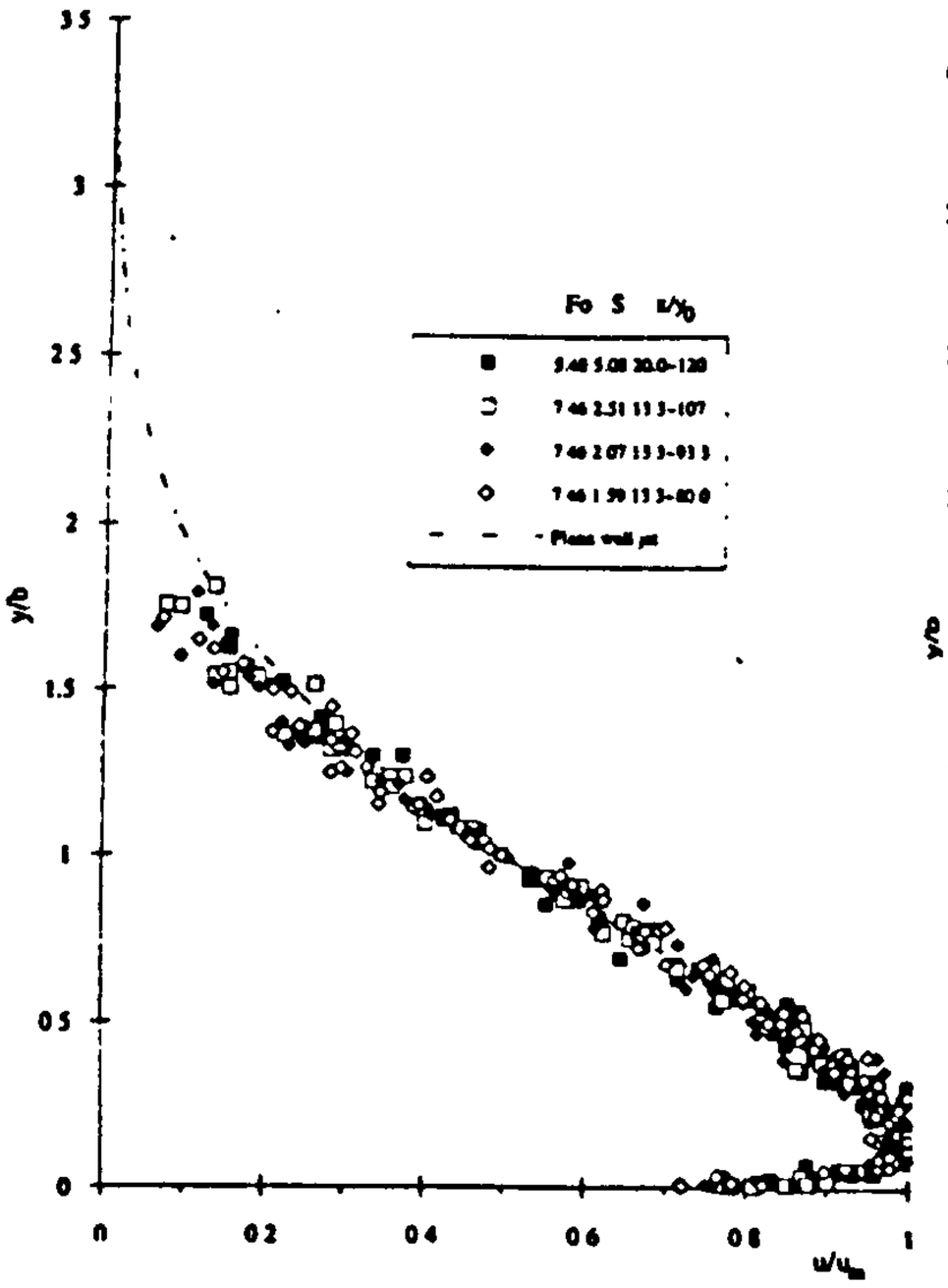

FIGURE 3

Dimensionless velocity distributions for a wall jet (Wu and Rajaratnam, 1995)

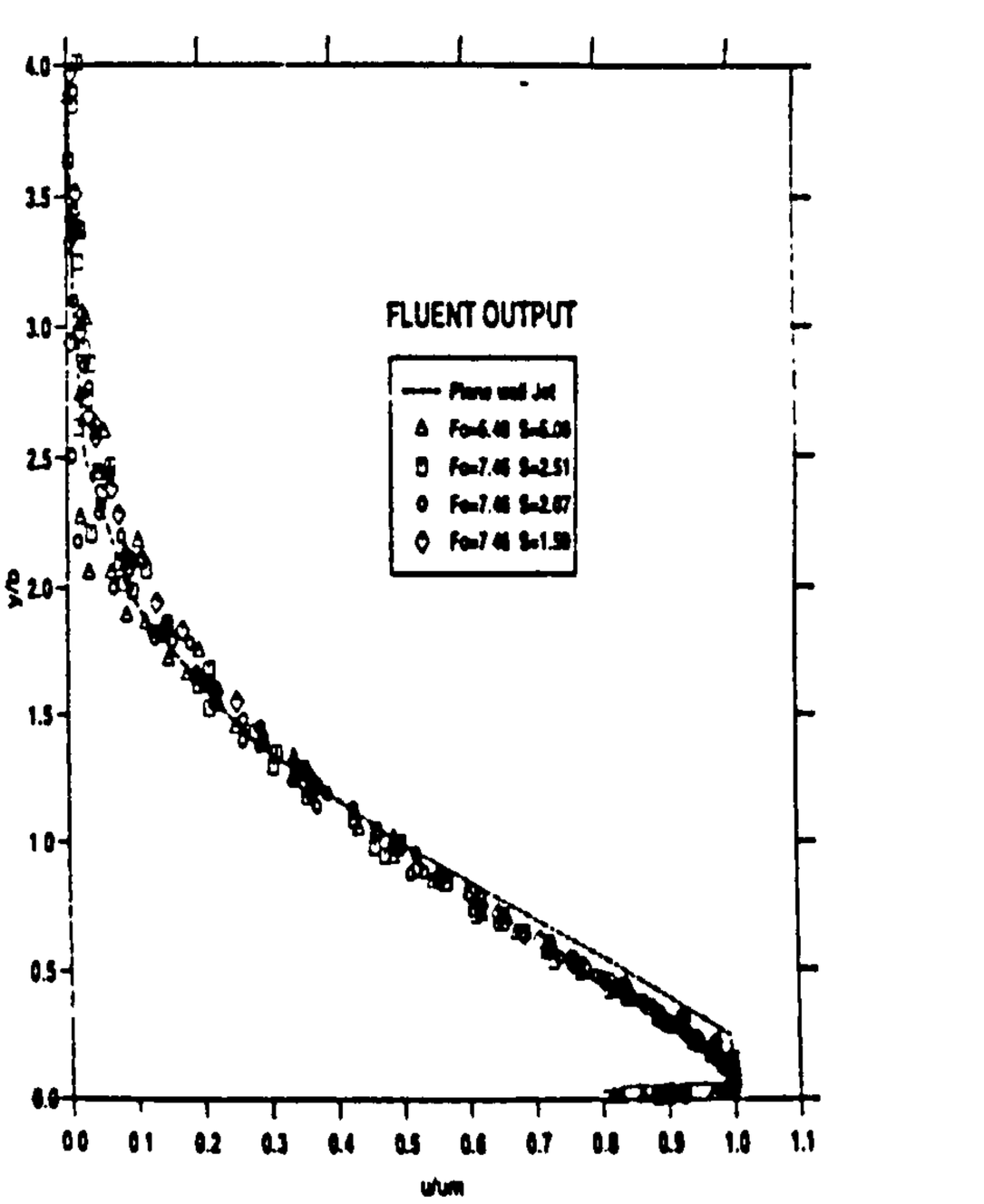

FIGURE 4 **Predicted dimensionless velocity**

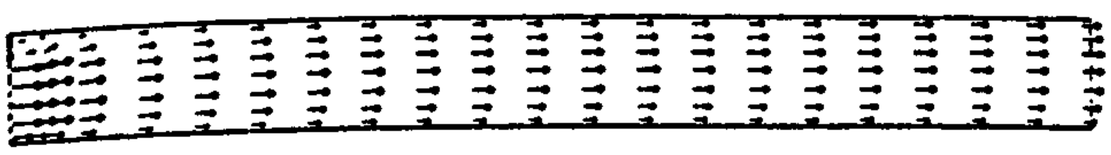

t = 0

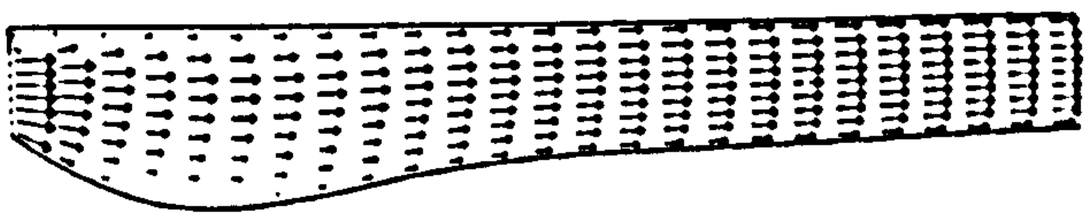

t = 90 mins

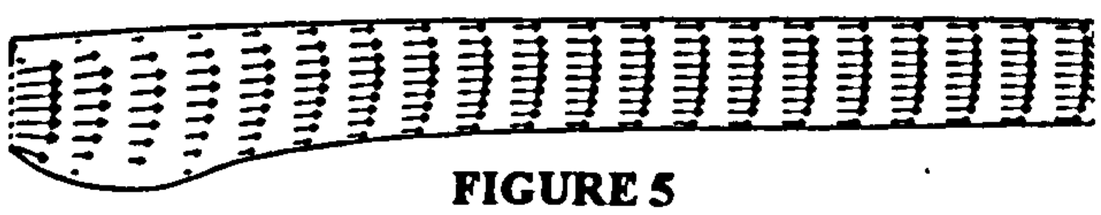

t = 15 mins

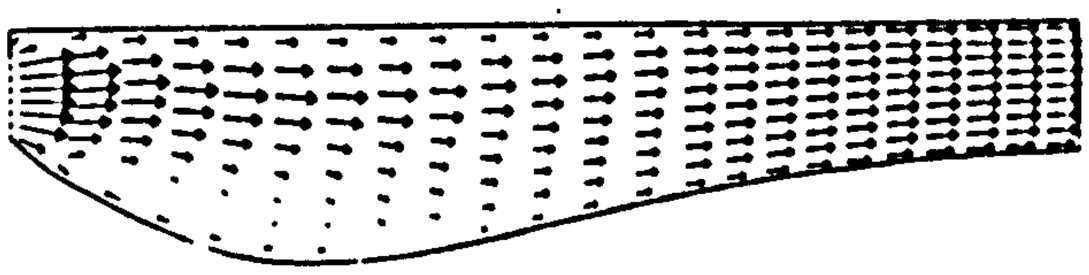

FIGURE 5

Predicted velocity contours downstream of wall jet for various sizes of scour hole

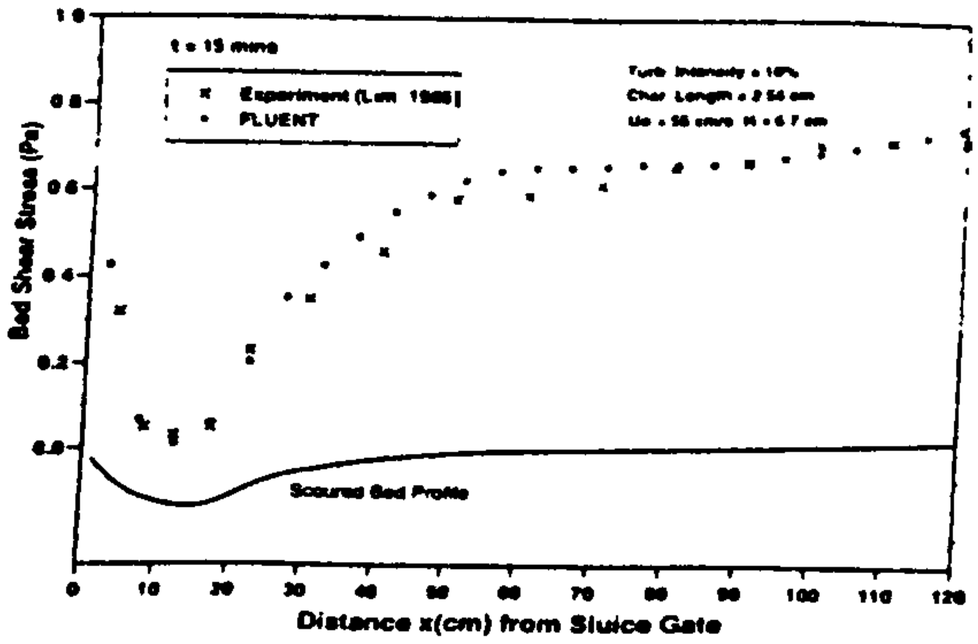

FIGURE 6

Bed shear stress distribution (t = 15 mins)

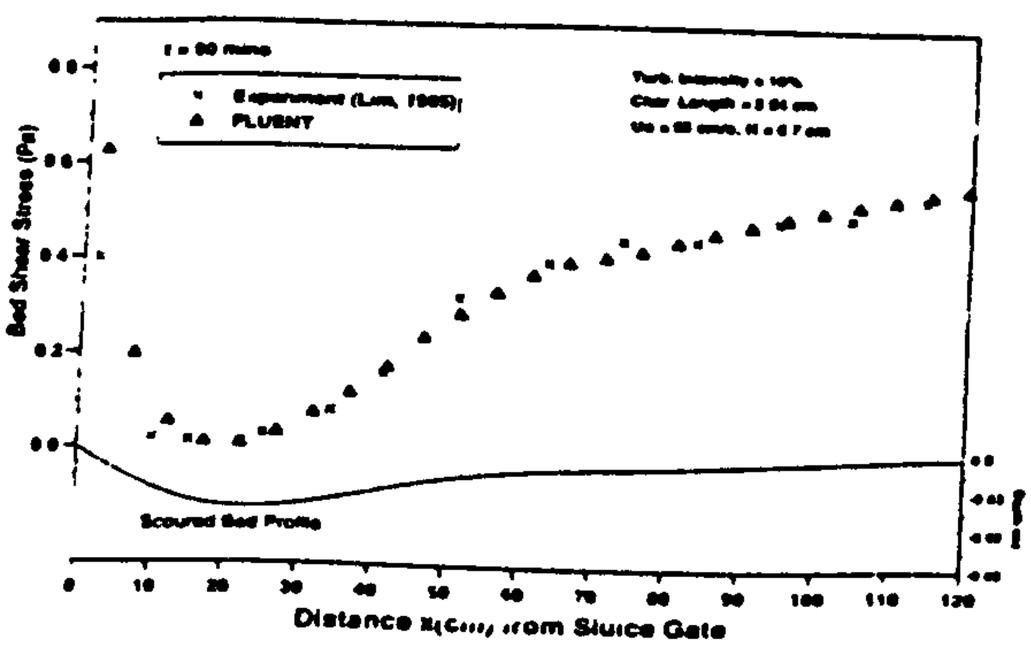

FIGURE 7

Bed shear stress distribution (t = 90 mins)

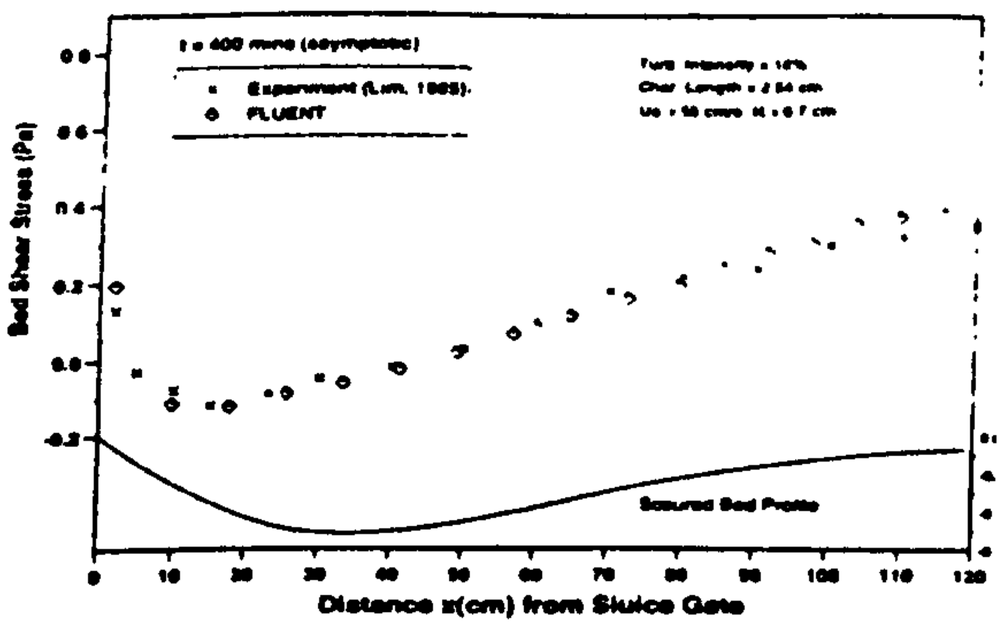

FIGURE 8

Bed shear stress distribution (t = 400 mins)

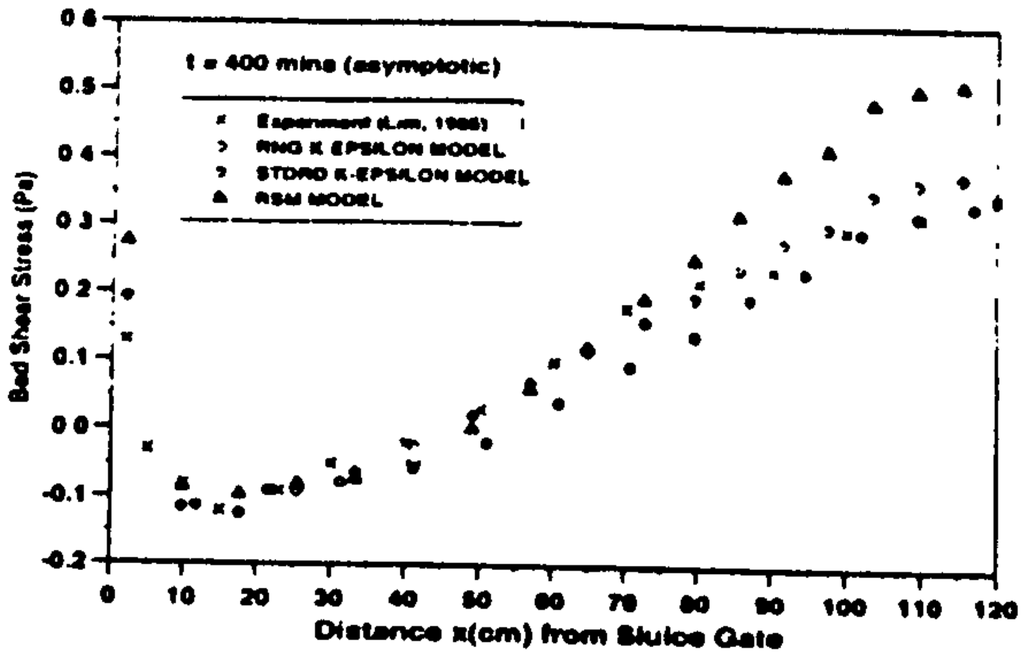

FIGURE 9

Comparison between three closure models available in FLUENT (t = 400 mins)

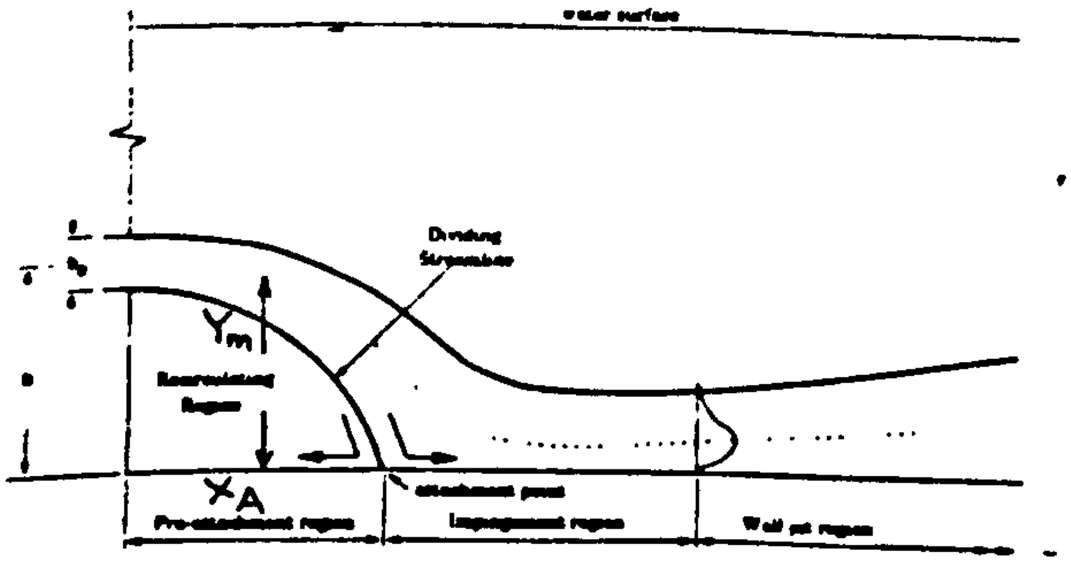

FIGURE 10

Typical flow geometry of an offset-jet

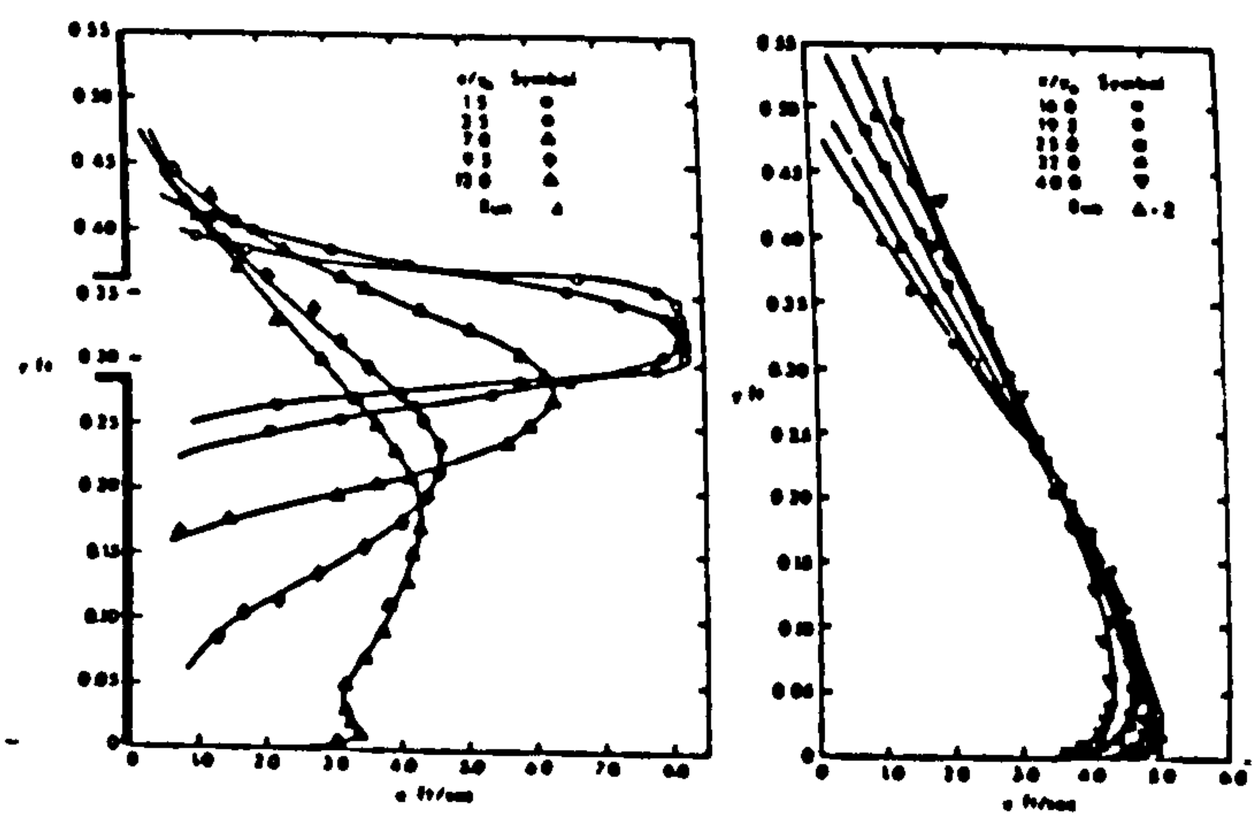

FIGURE 11 **Typical velocity distributions obtained by Rajaratnam and Subramanya (1968)**

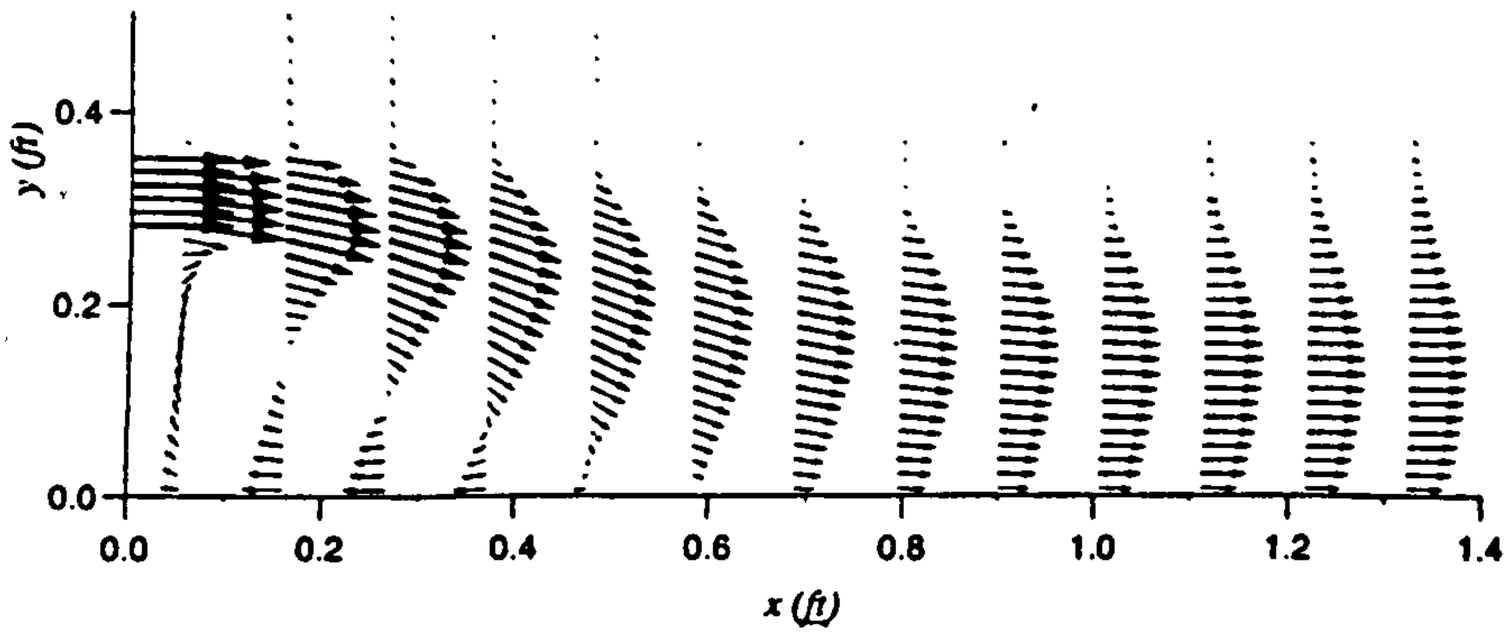

FIGURE 12

Velocity distributions predicted by FLUENT

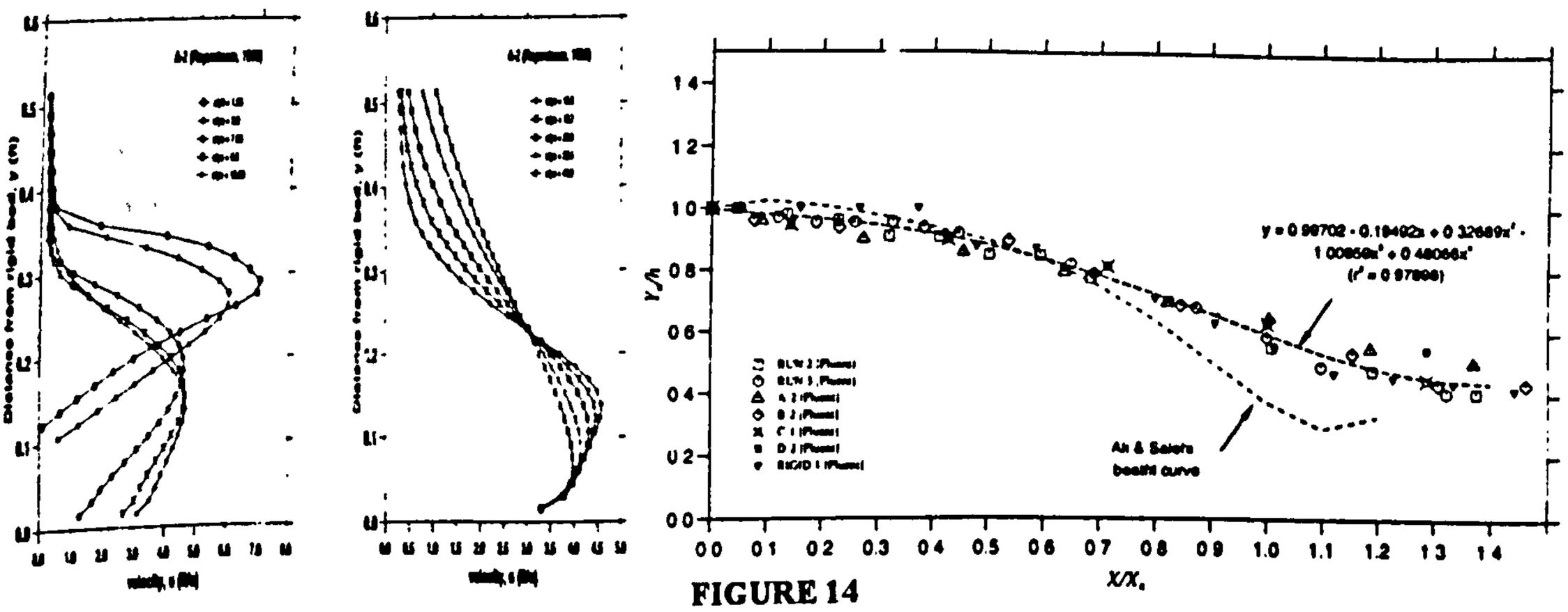

FIGURE 13 **Predicted longitudinal velocity profiles**

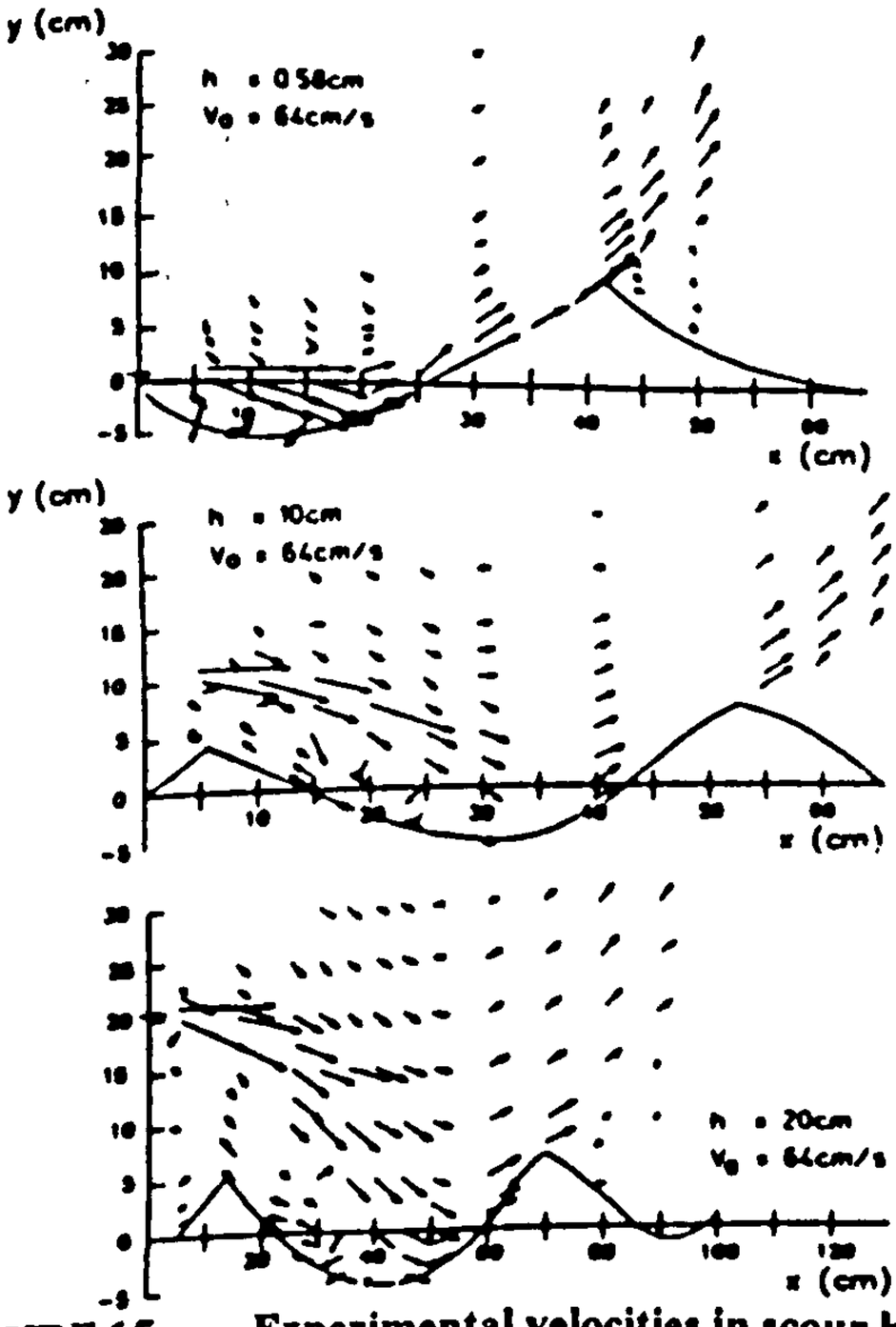

FIGURE 15 **Experimental velocities in scour holes for different jet heights (Ali and Walley, 1992)**

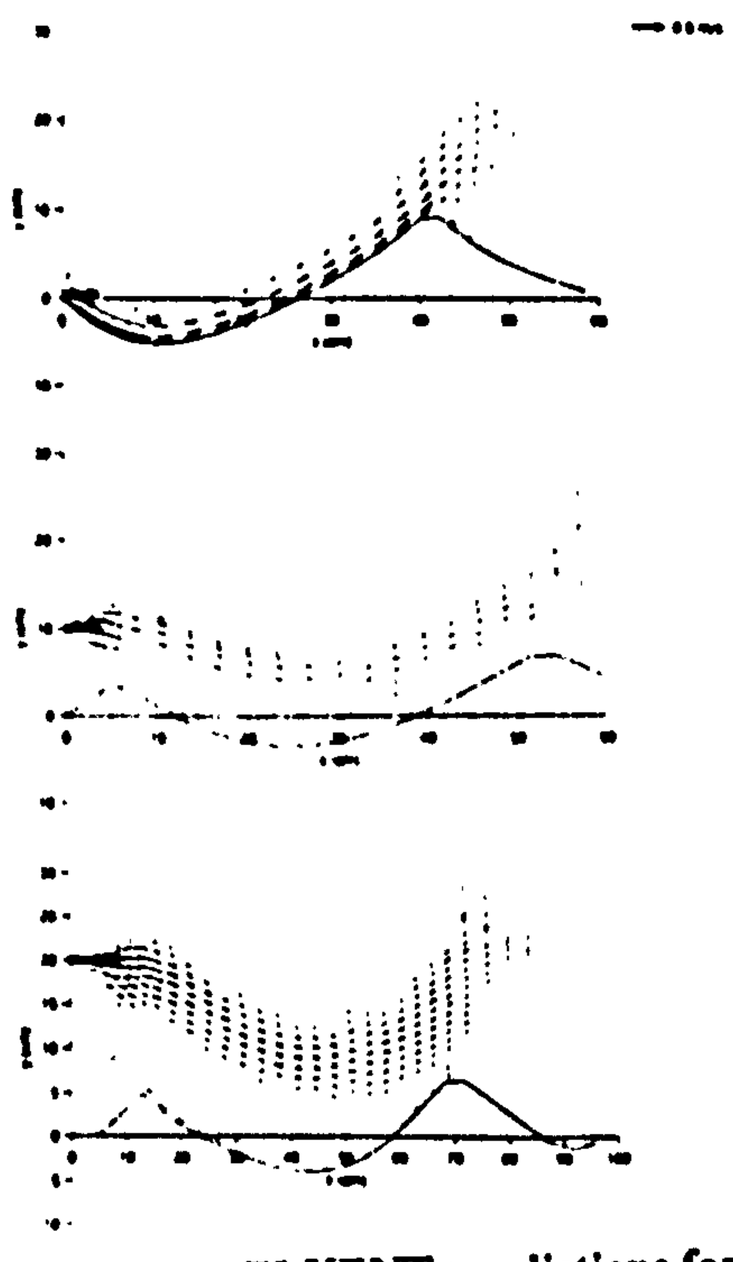

FIGURE 16 **FLUENT predictions for Ali and Walley's experiments**

FIGURE 14

Profile of the line of maximum velocity of an offset-jet

FLOW PATTERNS AROUND BRIDGE PIERS AND OFFSHORE STRUCTURES

Kamil H. M. Ali, Othman A. Karim and Brian A. O'Connor

Department of Civil Engineering, University of Liverpool, L69 3BX, UK.

ABSTRACT: The ultimate objective of this research is the prediction of scour hole geometries associated with single bridge piers of various shapes and offshore platforms of complicated geometries. Accurate calculations of velocity fields and bed shear stresses were obtained using the FLUENT package. Relevant experiments were conducted for verification purposes. Calculated bed shear stresses can be used in appropriate sediment continuity equations for the prediction of scour hole geometries.

1. INTRODUCTION

Sediment transport governs or influences many situations that are of importance to mankind. Erosion and scour may sometimes undermine hydraulic structures. Lack of reliable practical knowledge of scour has left some hydraulic experts to claim that the collapse of a large bridge as a consequence of foundation erosion is a disaster waiting to happen. For example, with over 150,000 road bridges and 6000 rail bridges in the U.K., this phenomenon could pose a serious safety problem as well as a significant financial burden, Penson, S. (1996).

Continuous scour at a structure can lead to its failure, thus an understanding of the scouring process is very important if steps in the design process are to be taken to protect against it.

Scour is a very complex process. No single analytically derived equation is available because of the difficulties associated with the problem, such as the combined effects of complex turbulent boundary layers, time-dependent flow patterns, and sediment transport mechanism in the scour hole.

An accurate prediction of the boundary shear stress is essential in the prediction of the time development of a scour hole. The authors used the FLUENT package to predict the boundary shear stress distributions for single cylinders of various shapes and for scour holes of various sizes. FLUENT was also used to predict the velocity field and boundary shear stress distributions for two different types of offshore structures under the influence of a steady current. Experiments were conducted to study the resulting scour patterns. Crushed olive stones were used as the movable bed.

The FLUENT package is a general purpose computer program for modelling complicated flow fields. It incorporates techniques based on fundamental principles for simulating a wide range of fluid flow problems. FLUENT/BFC is the primary set-up package for modelling complex geometries. FLUENT uses a finite volume numerical procedure to solve the fundamental equations governing fluid flow (the Reynolds Equations). Additional turbulence model equations are also used.

2. EXPERIMENTAL ARRANGEMENT

The experiments described herein were conducted in a glass-sided wave/current flume. The flume had a width of 0.6m, depth of 0.7m and length of 15m. The sediment used was crushed olive stones of median size of 0.2mm, specific gravity of 1.35 and terminal velocity of 0.63cm/s.

The water current was generated by two pumps located 6m from the working section. A streamflow propeller meter was used to measure the velocity field. Bed levels were measured using a depth gauge.

Two different offshore platforms (Figs. 6,7) were used. The appropriate platform was positioned at the centre of the flume and the olive stone bed was levelled. At the start of each run, the two pumps

were slowly adjusted to give the required flow rate. Great care was taken to ensure that the bed material was not disturbed. Bed levels and velocities were measured over a wide area and for a long period of time until the equilibrium state was reached.

3. RESULTS

Figure 1 shows the body-fitted co-ordinate grid used for modelling the flow round a vertical cylinder. The flow was assumed to be symmetrical and only one half of the cylinder and the flowfield was analysed. Dimensions of the cylinder and the flow parameters were based on the experiments of Yanmaz and Altinbilek (1991). The diameter of the cylinder was 67mm, water depth 0.135m. The sand particle size was 1.07mm and the specific gravity was 2.64. Bed contours were obtained at run times of 5, 20, 60, 100 and 150 minutes.

Figures 2 and 3 show velocity and bed shear stress distributions for four different shapes of piers and for a rigid bed. In all cases, the maximum bed shear stress corresponds to the maximum velocity. The maximum shear stress occurs at midpoint of the circular and square piers extending approximately two diameters across the channel showing a 25% increase compared with the average upstream value.

FLUENT solutions were obtained using the scour holes obtained by Yanmaz for t = 15, 20, 60, 100 and 150 mins. Figures 4 and 5 show the velocity vectors and bed shear stress distributions for t = 150mins. At the beginning of the experiment, t = 0mins, the bed was flat. The FLUENT results show that the initial boundary shear stress is at the side of the pier but at t = 5mins it moved to the pier symmetrical centreline at the start of the scour hole. The velocity distributions reveal that the deceleration of the velocity became more severe as the hole became deeper. In the downstream region of the hole the decrease in depth between the bed and the water surface causes the flow to converge and hence increase the mean velocity of the section, Penson, S., (1996). A steep fall in bed shear stress values occurs just after scouring action starts and as it developes further the rate of reduction becomes very slow. Negative shear stresses were obtained for those sections where reversed flow was observed. The negative sign indicates that the boundary shear stress is in the direction of the flow.

It was observed in all the experiments on the platforms shown in Figures 6 and 7 that the maximum scour depth occurred at the mid points and flanks of the upstream cylindrical piers, Butterworth, G., (1996). Bed particles at the upstream side of the piers were observed to be displaced due to the horseshoe vortices. The approach velocities decreased by approximately 20% from the free surface down to a depth 130mm below the free surface resulting in the stagnation pressure at the upstream faces of the piers being greater nearer the free surface than near the bed. This caused a vertical velocity component in the downward direction upstream of the cylinders. A so-called horseshoe vortex is produced which stretches around the piers. A horseshoe-vortex is a strong three-dimensional boundary layer phenomenon, which erodes a hole next to the pier. Scouring first appeared on the flanks and upstream faces of the front piers. As the scour hole enlarged with time, the strength of the horseshoe vortices weakened, causing a smaller and smaller rate of scour development. The scoured bed contours for the two platforms are shown in Figures 9 and 12. The scour patterns were not perfectly symmetrical due to the slightly uneven upstream velocity field. The scour depth at the rear of the upstream piers was smaller than that produced at the front. These observations are consistant with those of Melville, B.W. (1975).

The scour depth at the back piers was approximately 10mm less than that at the front piers (Figures 9,12). The scour depth depends on the relative spacing a/b, where a is the distance between the centrelines of the piers and b is the common pile diameter. For two piers touching (a/b = 1), the scour depth at the front pier is the same as that for a single pier but with increasing separation, the front pile experiences a reinforcing effect which reaches a maximum at a/b = 2.5 and is evident until a/b = 11 (Raudviki, A.J. (1991). For large spacing, the scour depth is the same as that for a single pile. Another reason for reduced scouring at the rear piers is the protection provided by the front piers. The placing of the piers upstream lessens the impact of the incident current thus weakening the vortex that generates the erosion.

Measured velocities near the bed were compared with those obtained using FLUENT for a flat bed. The FLUENT velocities and shear stresses for the platform in Fig. 6 (rigid, flat bed), are shown in Figs. 10 and 11. These results show that the velocities at the bed at the front piers had a small negative component in the streamwise direction. This indicates the presence of a horseshoe vortex as would be expected. However, the experimental results did not show this negative component. This could be because the velocity was measured too far from the pier. However, the presence of the scour hole undoubtedly affects the velocity field. Comparison between the measured floor velocities and that obtained from FLUENT showed reasonable agreement. The highest shear stress was on the upstream flanks of the front piers. The depth of the scour hole was greatest at that point. This compared well with the location of the maximum shear stress from the FLUENT solution. The numerical velocity vectors for the pile platform are given in Fig. 8.

4. CONCLUSIONS

1. Dynamics of flow around the various single piers is rather similar. It can be seen, however, that the square pier causes sharp changes in velocity and thus high shear stresses giving rise to a high possibility of scour, while in comparison the circular pier show smooth velocity changes.
2. The simulated flow in FLUENT seems to correspond well with available experimental results. The theoretical aspects of the flow dynamics, such as the horseshoe vortex, can also be interpreted from the output.
3. The FLUENT results show that the regions with the highest values of bed shear stress correspond to the region of highest floor velocity.
4. After the scouring action started, the bed shear stress falls and as the scour hole developed further the reduction became less apparent. The overall bed shear stresses decreased with the increase in scouring time and with the increase in size of scour hole.
5. The shear stresses, predicted by FLUENT, is lowest in the region of maximum erosion and is highest near the crest region.
6. The bed shear stress values, especially in the eroded part of the hole are all less than the critical value for the initiation of particle motion on a flat bed.
7. The shape of the scour hole, generated by a uniform current, around the piers of an offshore platform remains almost unchanged with time. The rate of change decelerates as time elapses. The produced scour hole can be approximated to an inverted cone with a base diameter several times that of the pier and with side slopes equal to the submerged angle of repose of the crushed olive stones.

5. ACKNOWLEDGEMENTS

The authors would like to express their sincere thanks to K. Owen, S. Penson and G. Butterworth, Graduate Engineers for their help in some of the numerical and experimental work described in this paper. We also thank A. M. Yanmaz for providing us with some of his experimental results.

REFERENCES

1. Yanmaz, A. M. and Altinbilek, H. D. (1991), "Study of time-dependant local scour around bridge piers, Journal of Hydraulic Engineering, Vol. 117 No. 10, ASCE.
2. Butterworth, G. (1996), "Investigation of local scour caused by currents and waves", B.Eng. Thesis, University of Liverpool.
3. Fluent Incorporated (1993), "Fluent User Guide", Version 4.2.
4. Melville, B. W. (1975), "Local scour at bridge sites", Report No. 117, University of Auckland, Auckland, New Zealand.
5. Penson, S. (1996), "Investigation of the flow around a bridge pier using the FLUENT package", M.Sc.(Eng.) Thesis, University of Liverpool.
6. Raudkivi, A. J. (1991), "Loose boundary hydraulics", Third Edition, Pergamon Press, Oxford, U.K.

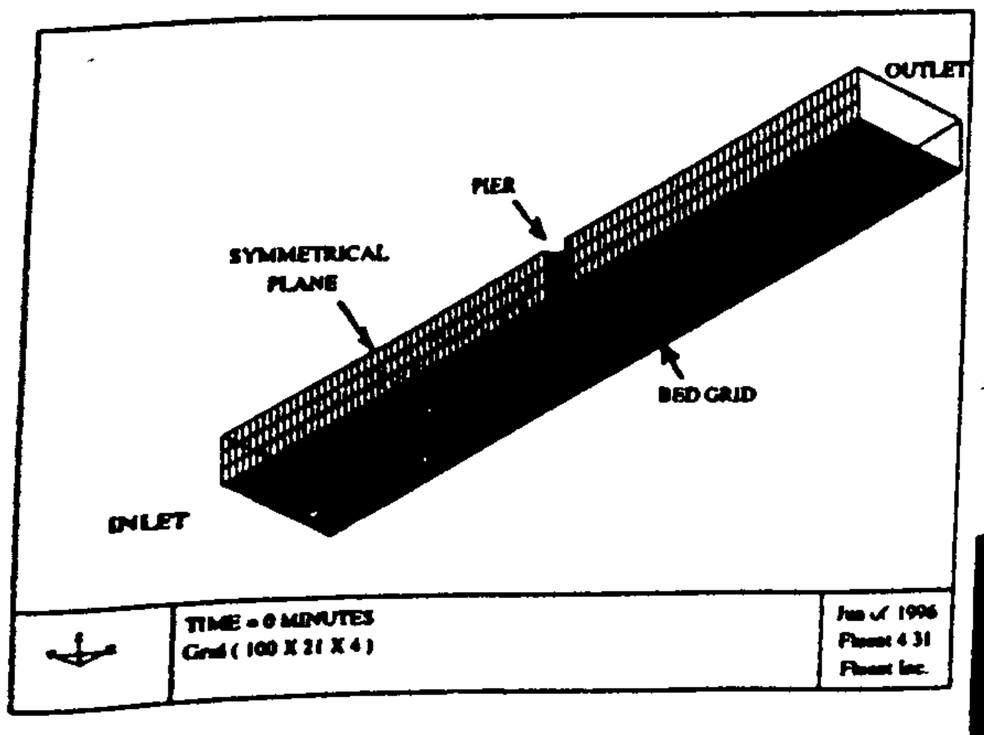

FIGURE 1

Grid arrangement for a circular cylinder

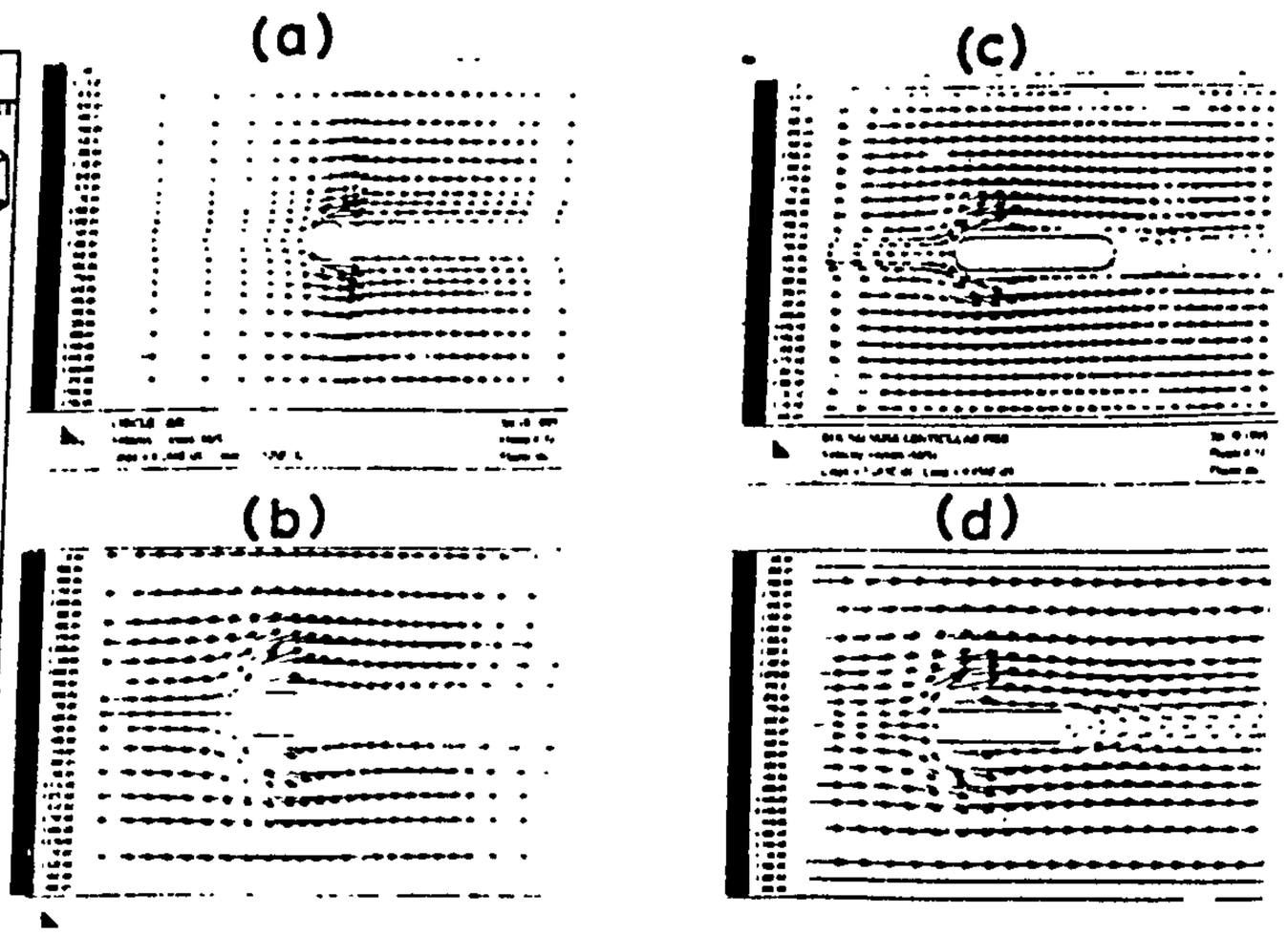

FIGURE 2 Predicted velocity distributions

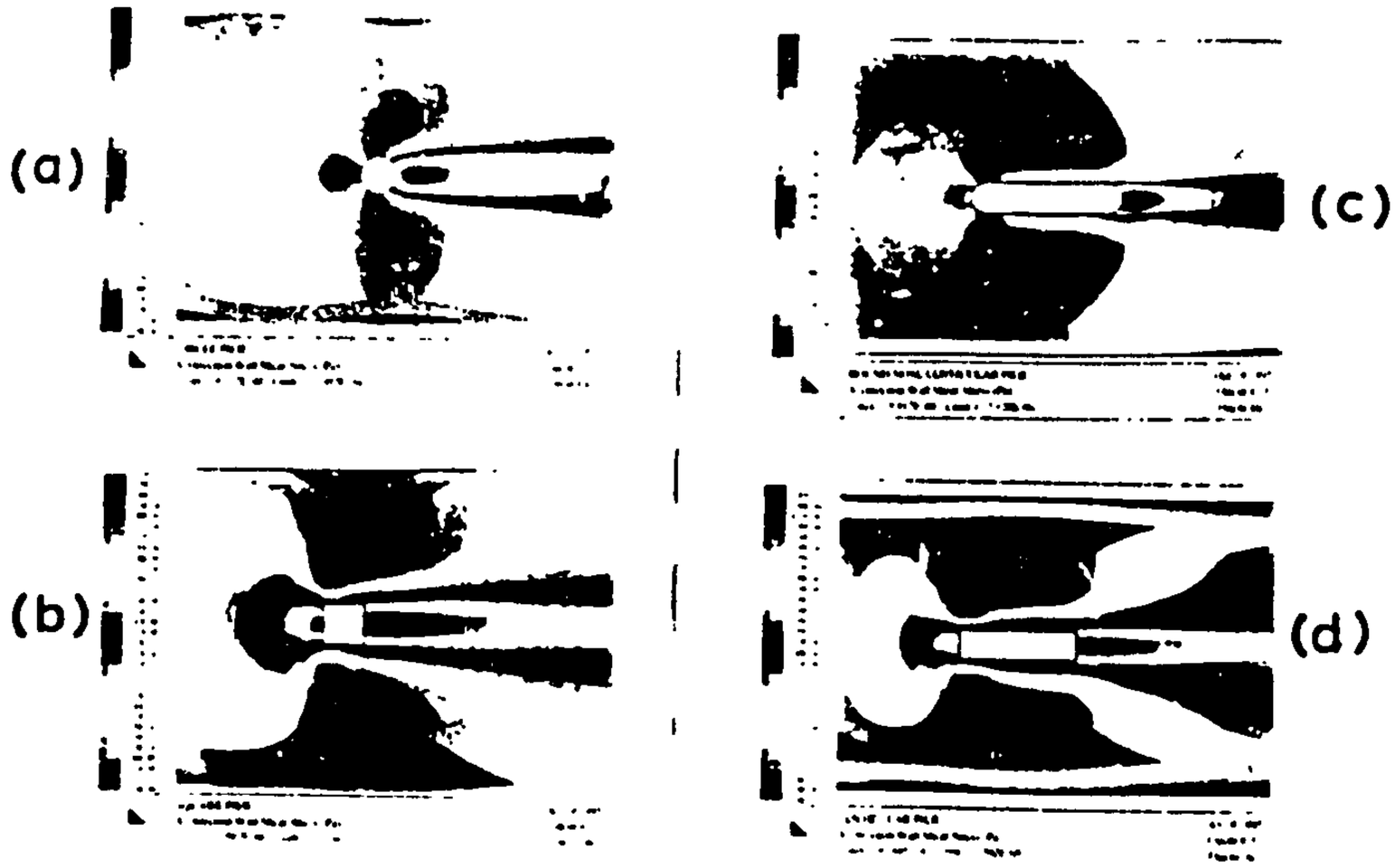

FIGURE 3 Predicted boundary shear stress distributions

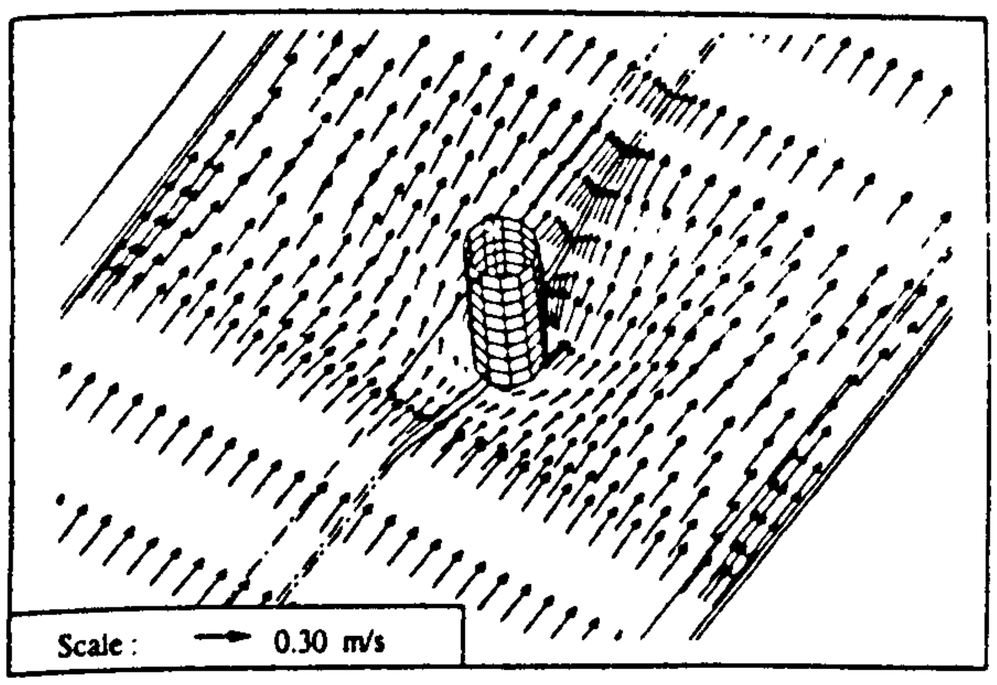

FIGURE 4

Floor velocity vectors in a scour hole (t = 150 mins)

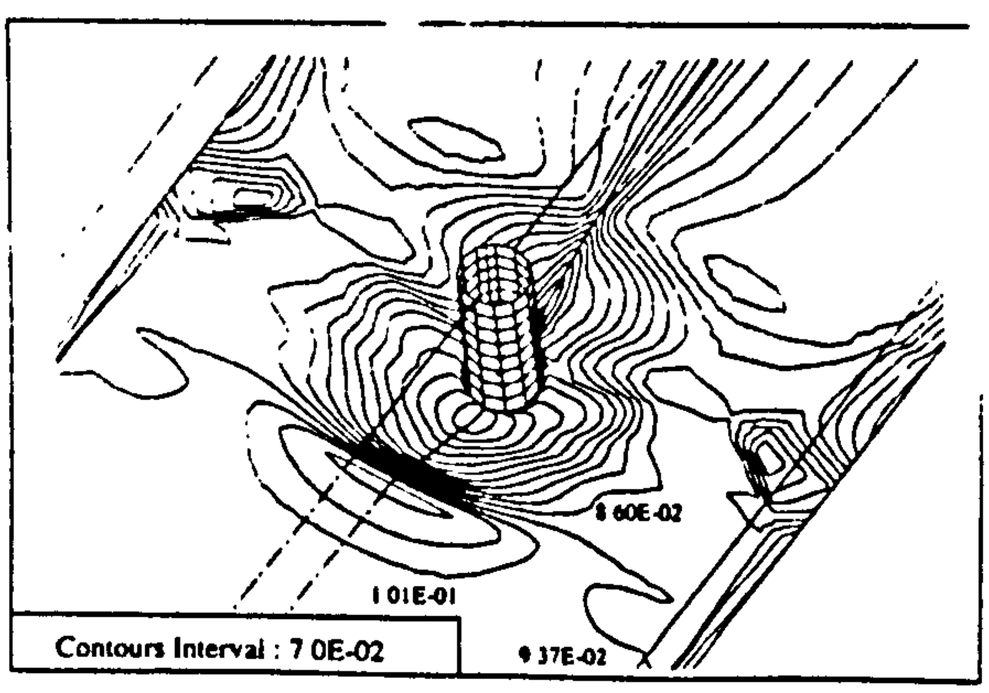

FIGURE 5

Bed shear stress contours i a scour hole (t = 150 mins)

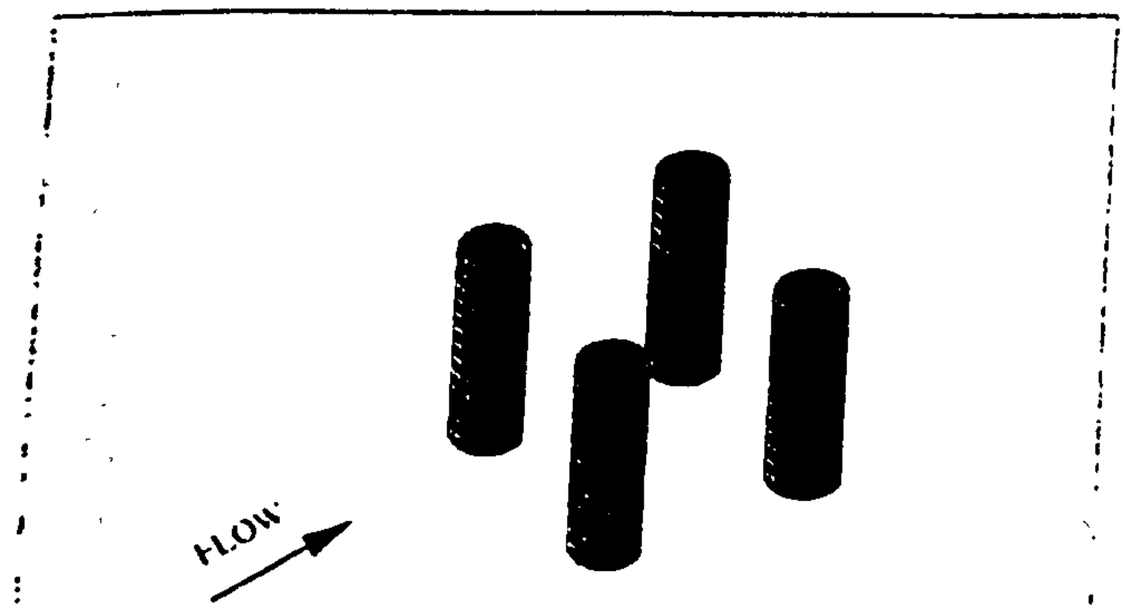

FIGURE 6 Offshore platform with 4 piers

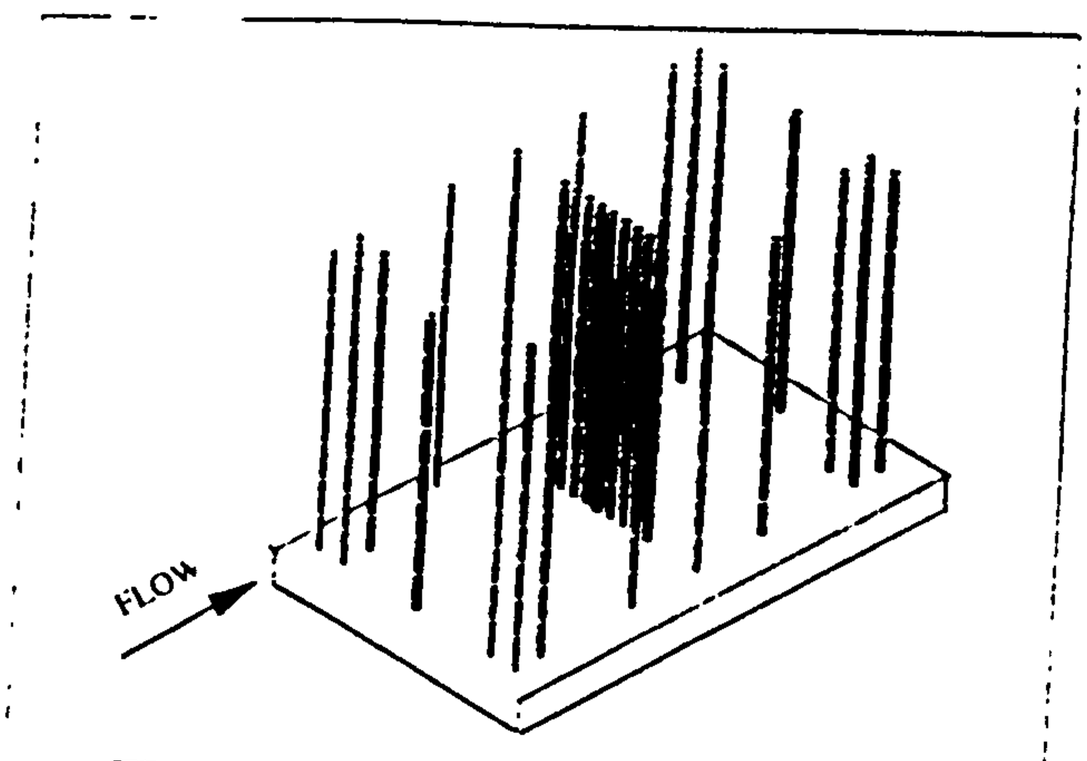

FIGURE 7 Multi-piled platform FLUENT

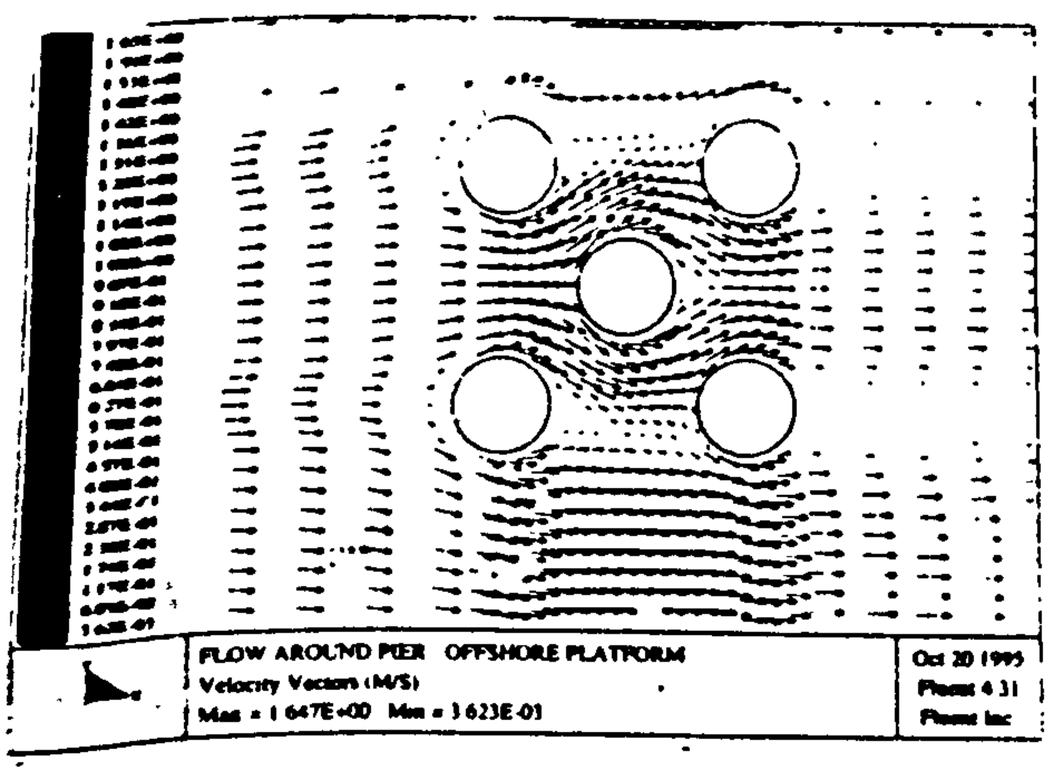

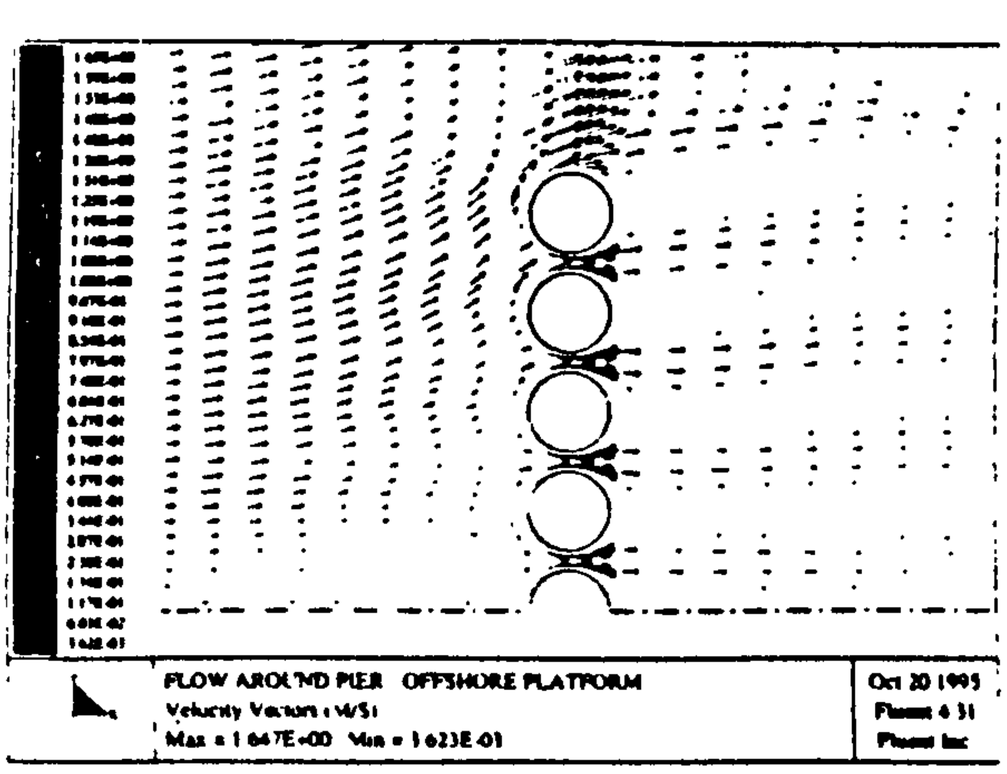

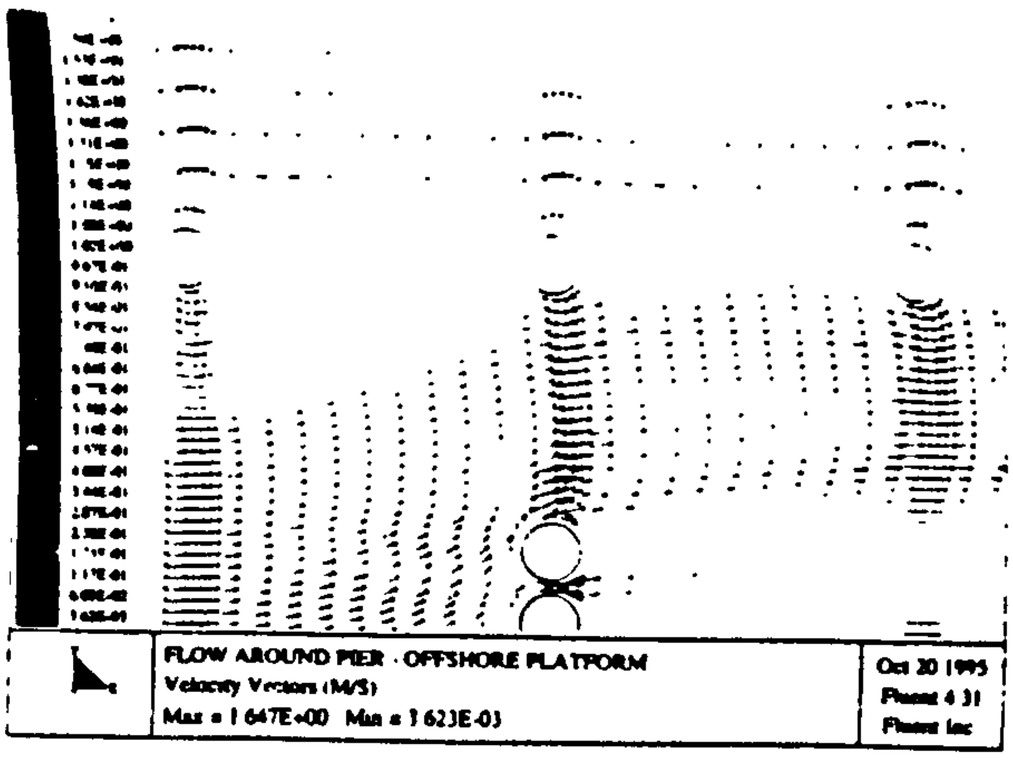

FIGURE 8 Velocity vectors near the bed for the platform in Fig. 7

FIGURE 9 Experimental bed contours

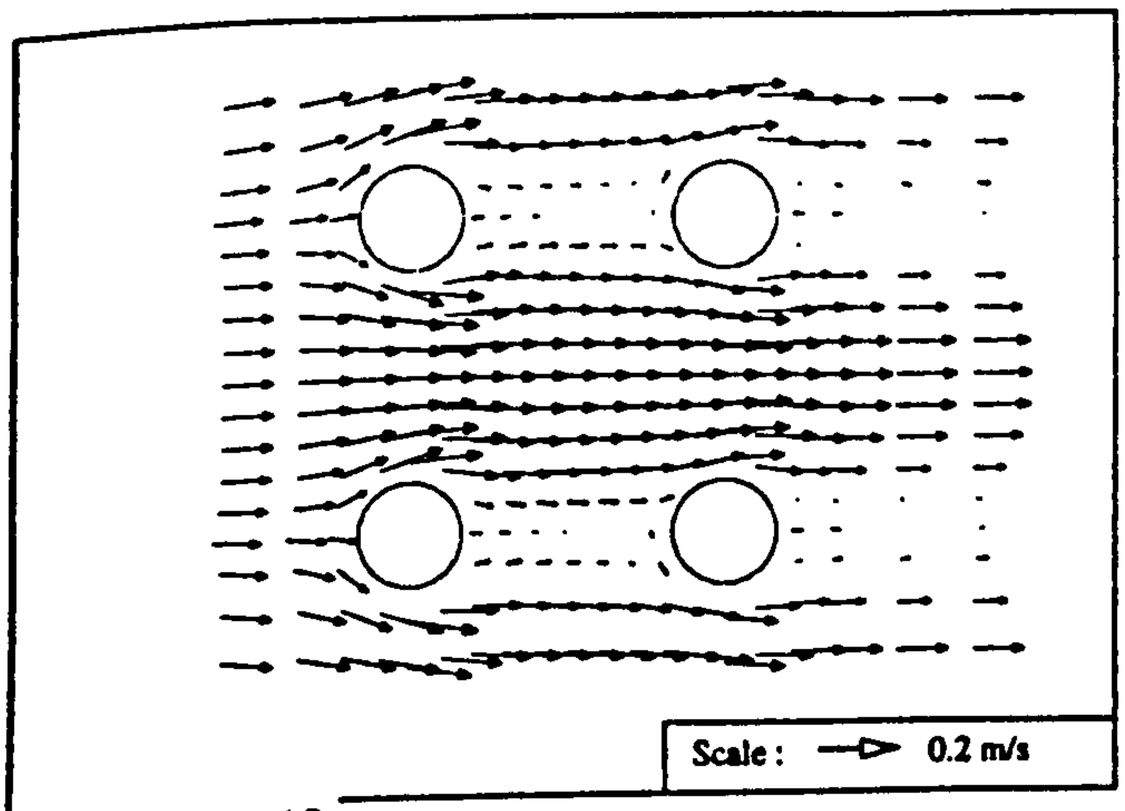

FIGURE 10

Predicted velocity contours near the bed (Platform in Fig. 6)

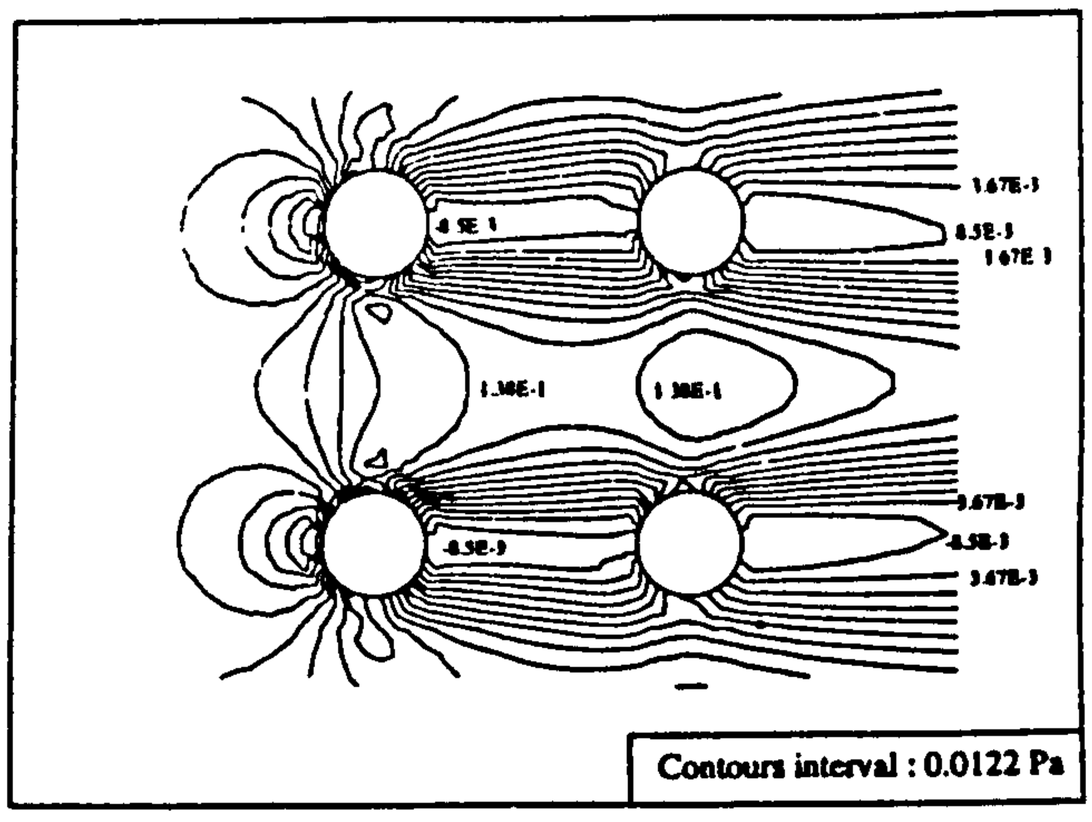

FIGURE 11 Predicted bed shear stresses

FIGURE 12 Experimental bed contours for platform in Fig. 6

INVESTIGATION OF JET-FORCED WATER CIRCULATION IN RESERVOIRS

ABSTRACT

The paper describes an experimental and theoretical investigation of the circulation in water-supply reservoirs. Different inlet and outlet arrangements were used in reservoirs of various shapes. Experimental results, using scale model reservoirs, are also given. The effects of model size, the reservoir's aspect-ratio and the Reynolds number were investigated. Numerical predictions using the Fluent package were compared with experimental results.

INVESTIGATION OF JET-FORCED WATER CIRCULATION IN RESERVOIRS

by

K. H. M. ALI, M.Eng.,Ph.D.[1] and K. OTHMAN, B.Sc.,M.Sc.(Eng.)[1]

INTRODUCTION

The factors affecting circulation in water-supply reservoirs include the shape and depth of the reservoir, wind action, water-density differences and inflow/outflow arrangements.

Local wind can be relied on to cause substantial mixing in exposed shallow reservoirs. Energy from the wind imparted to the water causes the water near the surface to move in the wind direction, with the water near the bottom moving in the opposite direction. The Coriolis force (caused by rotation of the earth) also causes water particles in motion to be deflected, thus influencing the degree of mixing[10].

Water density differences caused by the climate lead to a warm surface layer (the epilimnion) floating above a colder main body (the hypolimnion) during the Summer[8]. As the water at the surface cools in the Autumn it sinks, thereby promoting a general circulation. These differences in density are minute but may also prevent the wind forces from mixing the upper and lower layers. Experiments have shown that density differences as little as one part in ten thousand can cause the upper and lower layers to move quite independently.

It is also possible for density differences to exist between the inflow and the water stored in a reservoir, thus leading to stratification.

Wind density effects cannot be controlled and various remedial measures have been developed to minimize the water-quality problem posed by stratification and stagnation. These include the ability to withdraw water from selected depths and forcing the interfacial mixing by vertical jets of air or water[14].

Improvement of the inlet and outlet arrangements offer considerable potential as a preventive technique aimed at including conditions less favourable to the formation of stratification and stagnation.

Experimental investigation of jet-forced circulation, both in tanks and reservoirs, has been studied by many researchers, mostly using scale model tests[11,13,19,21-24].

Analytical work concerning the effects of wind and the earth's rotation has been carried out and is well documented[11,16,17,18,25].

---

[1]Department of Civil Engineering, University of Liverpool, U.K.

However, the analysis of jet forced circulation has attracted relatively few researchers. Sobey[23,24] developed a two-dimensional theoretical solution for a tangential jet discharging into a circular reservoir. Mills[20] developed a solution for steady two-dimensional viscous motion within a circular cylinder generated by either the rotation of part of the cylinder wall or fluid entering and leaving through slots in the wall. Mills' solution is, however, applicable for very small Reynolds numbers.

Falconer[11] produced a two-dimensional mathematical model describing the jet forced circulation in reservoirs having very large inlets and outlets. Ali and Whittington[4] applied the well-known behaviour of two-dimensional turbulent jets to the problem of the circulation in reservoirs[15]. More recently, Ali and Pateman[3] developed an analysis which took account of inflows as well as geostrophic and wind effects. The analysis for the jet forced circulation was based on the assumption of a constant friction factor for the reservoir.

The powerful "Fluent" general purpose computer programme was used by the present authors to predict reservoir circulations for different inlets, outlets and reservoir geometries.

Extensive experiments were conducted at the Department of Civil Engineering of the University of Liverpool over the last twenty years to study the effects, on the circulation, of jet momentum, position and size of inlets, and the geometry and aspect ratio of the reservoir.

THEORETICAL CONSIDERATIONS

a. Dimensional Analysis of Reservoir Circulation

Because of the large number of parameters involved in this type of problem, dimensional analysis is often used to show the relative importance of the various dimensionless groupings.

Using the Buckingham π theorem, Sobey[23] obtained the following functional relationship:

$$\frac{\bar{Q}_c}{\sqrt{K_j}\,L} = \psi\left[\frac{1}{L}\left(\frac{K_j}{f^2}\right)^{1/4}, \frac{\sqrt{K_j}\,L}{Q_j}, \frac{L}{h}, \frac{\sqrt{K_j}}{\nu}, \frac{K_j}{Q_j\sqrt{gh}}, \frac{k_s}{h}\right] \qquad (1)$$

where $\bar{Q}_c$ = mean circulating discharge and is defined as follows:

The circulating discharge Q_c is given by

$$Q_c = h\int_0^R v\,dr \qquad (2)$$

where h = water depth in the reservoir, v = peripheral velocity.

The mean circulating discharge $\bar{Q}_c$ is given by

$$\overline{Q_c} = \frac{1}{2\pi} \int_0^{2\pi} Q_c \, d\theta \qquad (3)$$

where θ = angle from the jet, K_j = kinematic jet momentum flux (= $Q_j V_j$), V_j = jet velocity, $f = 2\Omega \sin\phi$ = Coriolis parameter, Ω = the Earth's angle of rotation, ϕ = latitude angle of the reservoir, k_s = bed roughness height, υ = kinematic viscosity of water $\sqrt{K_j}/\upsilon$ is a form of the jet Reynolds number, $K_j/(Q_j\sqrt{gh})$ is the reservoir's Froude number, and k_s/h is the relative roughness of the reservoir.

Soby[23] *also investigated* theoretically the relative importance of the various parameters in Eq. (1) and obtained, for a stationary reservoir, the *following relationship:*

$$\frac{\overline{Q_c}}{\sqrt{K_j}\, L} = \psi_1 \left[\frac{L}{h}, \frac{k_s}{h} \right] \qquad (4)$$

Using Sobey's theoretical curves, for the variation off of $\bar{Q}_c/(\sqrt{K_j}L)$ versus L/h for different values of k_s/h, the present authors fitted the following relationship:

$$\frac{\overline{Q_c}}{\sqrt{K_j}\, L} = \left[5.527 - 9.226 \left(\frac{k_s}{h} \right)^{0.238} \right] \left[\frac{L}{h} \right]^{-1} \qquad (5)$$

The Fluent Package

Fluent is a general purpose computer program for modelling complicated flow problems[12]. FLUENT/BFC is the primary set-up package for modelling complex geometries. FLUENT uses a finite difference numerical procedure to solve the fundamental equations governing fluid flow (The Reynolds Equations). Additional equations are solved for the conservation of the parameters of the k - ϵ turbulence model, chemical species and entropy.

The numerical technique involves the subdivision of the domain of interest into a finite number of cells, the partial differential equations being discretized over these cells to obtain sets of simultaneous algebraic relations. Because of the non-linearity and interdependence of the differential equations, an iterative solution procedure is adopted.

Fluent will be used to predict the circulation patterns in reservoirs of simple and complicated geometries.

EXPERIMENTAL ARRANGEMENTS AND MODELS

Extensive experiments were conducted at the Department of Civil Engineering of the University of Liverpool to study reservoir circulation. Some of the models used are given in Table 1 and Figure 1 and are described below:

(i) A large circular reservoir of 3.68m radius was used. It had a painted concrete bed. An inlet jet 50mm high and 2mm wide was used. In some of the experiments, this jet was located in a tangential position, together with a central outlet. In other experiments, this jet was used in a radial position. Two outlets, one on either side of the radial jet were also used (Figure 1, model 1, arrangement 2).

(ii) A smooth circular reservoir having a radius of 1.5m was also used. A jet having a height (b_o) of 20mm and a width (d_o) of 2mm was used in a tangential position together with a central outlet. In some cases this jet was used radially with two outlets in the same positions as in (i).

(iii) Another circular reservoir of 1.22m radius was used to investigate the effect of the jet momentum and area on the reservoir circulation (Figure 1 Table 1). The jet discharge was kept constant and the momentum was changed by altering the jet area. The values of b_o x d_o used were 20 x 2, 8 x 30, 8 x 60, 8 x 90 and 8mm, 130mm.

(iv) Scale models of two water-supply reservoirs were built to the horizontal scales of 1/500 and 1/250. These are the Prescot No. 3 and No. 4 reservoirs (City of Liverpool, U.K.). The 1/250 models had a moulded concrete bed and sides, with a fixed vertical exaggeration of 5:1 ($\alpha/\beta = 5$, α = horizontal scale and β = vertical scale). For certain tests, a false flat aluminium bed and dummy vertical sides were fitted, in order to investigate the effect of vertical exaggeration on reservoir circulation and mixing. The 1/500 model had a flat plywood base and vertical Lucite sides. Its vertical scale could be varied from 1/500 to 1/100 or less. Another model of reservoir No. 4 was built to the scale 1/83.3. It had a flat concrete bed and vertical brick sides so that, as with the 1/500 and 1/250 models, the vertical scale could be varied.

(v) A scale model of the Silvola reservoir (Helsinki, Finland) was built (Figure 1 Table 1). A horizontal scale ratio of 400 was used. The vertical scale ratio was varied and experiments were conducted with $\alpha/\beta = 5, 4, 3, 2$ and 1. This reservoir operated with 3 inlets and two central outlets (see Figure 1 and Ref. (7)). Alterations to the vertical scale required jets of different sizes to be used.

MEASURING TECHNIQUES

The various methods used to study reservoir circulation and mixing are listed below:

1. large velocities were measured with a miniature current-meter, but surface floats were used to measure small velocities. Some of the experiments depended on illuminated floats, with time-lapse photography.

2. Dye photography was used on all models to permit rapid study of circulation-patterns and degrees of mixing.

3. The conductivity and fluorimetric methods were used to study reservoir mixing directly. Continuous and instantaneous injections, through the inlet, were used. Details of the mixing experiments are given in Ref. 6.

EXPERIMENTAL RESULTS

Tangential Jet Inlet

Figure 2 shows velocity-distributions obtained by Ali and Whittington[4] for various discharges and water-depths using the 3m diameter smooth reservoir. This figure shows a general increase in the maximum velocities with increase in discharge, for a constant water-depth. A more symmetrical velocity-distribution is noticed for the bigger water-depths.

Ali and Whittington[4] obtained the following relationship:

$$\frac{\bar{Q}_c}{\sqrt{K_j}\,L} = 1.36\left(\frac{h}{L}\right)\left[1.70 + \frac{123.89}{\sqrt{K_j}/\nu)^{2.5}\ (h/L)^{2.5}}\right] \qquad (6)$$

Ali and Pateman[3] obtained relationships for the velocity-distributions, in circular reservoirs, produced by radial and tangential jets. These relationships can be used very easily to obtain velocity-fields similar to those given in Figure 3.

Effect of Jet Momentum on Reservoir Circulation (Radial Jet)

Ali[5] conducted a series of experiments in the 2.44m diameter reservoir to study the effect of jet momentum on circulation (model 3, arrangement 4, Figure 1, Table 1). Jet discharge and water-depth were kept at $0.192 \times 10^{-3} m^3/s$ and 46mm respectively. The inflow momentum was altered by changing the area of the jet. Areas of $0.4cm^2$, $2.4cm^2$, $4.8cm^2$, $7.2cm^2$ and $10.4cm^2$ were used. The outlet was 0.38m wide and located opposite to the inlet.

Figures 4-8 show dye photographs of reservoir circulation produced by the above radial jets. These figures are given for different times from the start of injection of the dye. Clearly, the increase in jet area for a given jet discharge results in a reduction in circulation.

Figure 9 shows measured velocity-distribution for the various jet areas. This figure demonstrates clearly the increase in reservoir velocities resulting from the increase in jet momentum.

For the reservoir jet area of $0.4cm^2$ (b_o = 2cm, d_o = 0.2 cm), the ratio $\bar{Q}_c/Q_j$ was 8.86. Observations indicated that altering the position of the outlet had little effect on the circulation pattern in this reservoir. This is expected since for steady flow, the flow through the outlet is Q_j.

For the reservoir with a jet area of $10.4\ cm^2$ $\bar{Q}_c/Q_j$ was found to be 1.65. Changing the position of the outlet in this case had a profound effect on the circulation pattern.

The following relationship was fitted to the experimental results:

$$\overline{Q}_c/Q_j = 0.0292\sqrt{R} + 1 \qquad (7)$$

where

$$R = hV_j/\nu$$

Equation (5) can also be written in the following form:

$$\overline{Q}_c/Q_j = A_s/d_o^{1/2} + 1 \qquad (8)$$

where

$$A_s = 0.0292\ (Q_j h b_c/\nu)^{1/2}$$

The value of b_o for four of our inlet jets was 8mm. Using this value of b_o and substituting for the other constants gives $A_s = 7.67m^{1/2}$.

For a two-dimensional plane jet (9) we have:

$$\overline{Q}_c/Q_j = 0.62\ (x/d_o)^{1/2} \qquad (9)$$

putting x = R in Eq. (9) gives $A_s = 6.85m^{1/2}$ compared with $7.67m^{1/2}$ given by Eq. (8).

Circulation Generated by Radial Jets at Centre of Reservoir

Figures 9a-9c show velocity-distribution obtained using four, two and a single radial jet at the centre of the reservoir (Figure 1, model 3 arrangements 5,6). These figures show that the number of gyres generated by the jets is twice the number of jets used. For example, the use of 4 jets resulted in eight gyres which in practice will help in reducing the zones of stagnation in the reservoir.

Using the velocity-distributions given in Fig. 9, average circulating discharges were calculated. For 1, 2 or 4 jets, the total jet-momentum flux per unit density was 3.534×10^{-4}, 0.845×10^{-4} and $0.656 \times 10^{-4} m^4/s^2$ respectively. The resulting average values of $\overline{Q}_c/Q_j$ were 7.57, 5.65 and 3.89. Clearly, circulation increases with the increase in jet momentum flux per density (K_j).

Use of Twin Radial Jets Positioned at the Perimeter Wall

The 3 metre diameter circular reservoir was used to observe the effect of two identical radial jets set 90° apart in the reservoir wall (b_o = 20mm, d_o = 2mm) (Figure 1, model 2 arrangement 3). Water depths of 20, 50, 100 and 200mm were used in different runs (for the same jet discharges). Figure 10 shows dye photographs (h = 50mm) demonstrating the spread of the two "identical" jets with time. Deflection of the jets to form a very asymmetrical circulation is very evident.

Figures 11 and 12 show similar experiments conducted with reservoir water depths of 100 and 200 mm. Clearly, the circulation patterns are very symmetrical in these experiments[5].

Velocities measured at mid-depth for the h = 100mm are shown in Fig. 13. The velocity distribution from the jet to the centre of the reservoir is restricted in width by gyres A and B (for each jet). The two gyres meet at the centre of the reservoir wall. At the wall, the jet divides into two wall jets which move round the reservoir circumference.

Verification of Sobey's Theoretical Predictions

Sobey[23] derived a two-dimensional solution for reservoir circulation generated by a single tangential jet whose height was the same as the water-depth in the reservoir. Sobey assumed that velocity-distribution, in the reservoir, to be made up of a rectangular wall portion and a triangular reservoir portion. He also assumed that peripheral velocities were zero everywhere for distances < 0.5R from the centre.

Figure (14) shows plots of $\bar{Q}_c/(\sqrt{K_j}L)$ against *L/h* for the various model reservoirs. This Figure shows that:

a. the aspect ratio (L/h) is very important;

b. the values of $\bar{Q}_c/(\sqrt{K_j}L)$, for the same L/h are very close for the different sizes of the Prescot No. 4 models confirming that the effect of jet Reynolds number is small for these experiments.

c. the values of $\bar{Q}_c/(\sqrt{K_j}L)$ for the Prescot No. 4 and the small Silvola models ($\alpha/\beta = 1$) are very different from the other results, indicating a different type of flow.

d. the prototype values of $\bar{Q}_c/(\sqrt{K_j}L)$ for the Silvola reservoir are much higher than those of its small model. It was not possible to eliminate the circulation caused by wind action from the prototype values.

Prediction of Reservoir Circulation Using FLUENT[12]

The analytical treatment described earlier is usually adequate for predicting water circulation, in reservoirs of uncomplicated geometries, caused by simple inlet and outlet arrangements.

More real, and therefore difficult cases, can be solved using the FLUENT package[12]. It must be stressed, however, that it usually takes considerable time and effort to master this complicated package.

(a) Radial Jet Discharging into a Circular Reservoir

(i) A circular reservoir 2.44m in diameter was used (Figure 1, model 3, arrangement 4). The jet discharge was 244cm³/s. An outlet 38cm wide was located opposite to the inlet (see Figures 4-8). Radial jets 3, 6 and 13cm wide were used. The experimental velocity results are given in Fig. 8. The body fitted grids chosen are shown in Fig. 15 and the circulations predicted by FLUENT are shown in Fig. 16. Clearly, there is excellent agreement with the experimental results.

(ii) A radial jet was used together with two outlets inside the reservoir (Figure 1, model 1, arrangement 2). The experimental velocity distributions are given in Fig. 17 and the FLUENT circulation is given in Fig. 18. Again, the predicted

circulation is very similar to that obtained experimentally. It is interesting to note that for this example, the entrained discharge is much bigger than the inflow and, therefore, the effect of the outlets is very small and localized.

It must be stressed that all of the FLUENT solutions presented in this paper are for two-dimensional (depth-averaged) flows.

(b) <u>Complicated Reservoir Geometries and Inlet/Outlet Arrangements</u>

Extensive experiments were conducted at the Department of Civil Engineering of the University of Liverpool on scale models of the Liverpool No. 3 and 4 reservoirs at Prescot[2].

Figure 19 shows examples of two grid options available with FLUENT for reservoir No. 4. It is clear that the simple cartesian grid system will not give an accurate description of the flow at the solid boundaries. It was therefore decided to use the body fitted coordinate system throughout this paper.

(i) Fig. 20 shows surface circulation patterns generated by a floor pipe in reservoir No. 4 using the 1/250 model with $\alpha/\beta = 5$. Figs. 21 and 22 give the FLUENT depth-averaged circulation patterns generated using one inlet and one outlet. Figure 21 gives the results using the actual inflow velocity whilst Fig. 22 gives the results obtained using a depth-averaged inflow momentum. The two predicted solutions are quite similar to the experimental circulation. In all cases, two gyres are observed in the reservoir. Clearly, the effect of the outlet is very small.

(ii) Figure 23 shows the experimental surface velocity diagram for two nozzles positioned at mid-depth. The two nozzles direct water jets towards the centre of the reservoir, and on each side of the jet, gyres are set up. Those near the inlet jets lead to the production of further gyres.

Figures 24 and 25 show *predicted results* obtained for the original nozzle velocities and for depth-averaged values. The effect of the change in velocity, on the circulation patterns, is small. The FLUENT results show two main gyres quite similar to those obtained experimentally. The two small gyres, near the outlet, obtained in this experiment are not reproduced in the numerical solution. Also, the predicted circulation at the north-eastern part of the reservoir is very different from the measured one.

The main reason for the different circulation patterns produced by the physical model and by FLUENT is that the relatively small physical models had a vertical exaggeration of 5:1. The numerical solutions were, however, run for the prototype reservoirs (undistorted, full size).

It is well known[1,2] that the change in the reservoir's aspect ratio, as a result of vertical exaggeration, has a profound effect on the tendency of radial jets to deflect from their straight path. Figure 26 shows dye photographs for twin jets in the 1/250 and 1/83.3 models for various values of α/β. These results show that with vertical exaggerations of less than 3 to 1, deflection of the jets takes place. As the aspect ratio increases, the effective hydraulic depth is reduced relative to the

horizontal distance travelled. The consequent diminution in jet momentum presumably causes a diminution in the separate identity of each jet. Each jet forces its way through the other's field with iιcreasing difficulty[2].

(iii) Figure 27 shows surface circulation patterns generated by two nozzles positioned at mid-depth in the scale model of Prescot No. 3 reservoir. The results were obtained for a 5:1 vertical exaggeration. There is good surface movement almost everywhere.

Figure 28 shows the grid chosen for this reservoir and Figures 29 and 30 show the predicted circulations using two nozzles using the actual and the depth-averaged velocities. The predicted circulations are very similar. There is, however, a general reduction in velocities on depth-averaging of velocity.

Clearly, the predicted circulations are very different from the measured ones.

CONCLUSIONS

1. When mixing is produced in a circular reservoir, by a tangential or a radial jet, the circulation patterns depend on the Reynolds number of the jet, the aspect-ratio and relative-roughness of the reservoir.

2. Experiments with $(L/d_o) > 50$ show that outlets have little influence on the circulation in reservoirs. Due to considerable entrainment; the circulating discharge is usually much bigger than the discharge of the inlet.

3. An implication of conclusion 1, that the aspect-ratio is of great importance, was verified in detailed experiments on scale-models of water-supply reservoirs. It follows that the common practice of exaggerating the vertical scale is not automatically valid.

4. The use of multiple jets improves the circulation and mixing and reduces the stagnation zones in reservoirs. Here, jet momentum and location are of primary importance.

5. Sobey's theoretical predictions are in reasonable agreement with the writers' experimental results.

6. In most cases, the FLUENT package gives excellent prediction of jet-forced reservoir circulation. Solutions of very complicated reservoir geometries and multiple,e inlet/outlet arrangements require further verification using large undistorted physical models.

ACKNOWLEDGEMENTS

The work described herein is part of an extensive study conducted at the Department of Civil Engineering of the University of Liverpool.

The writers are very pleased to acknowledge the help of the following graduate engineers in conducting some of the experiments described in this paper: N.H. Park, D. Chadwick, R.

Pollard, T.S. Hedges, M.H. Martin, S. Liaskos, K. Jones and D.R. Pateman.

APPENDIX I

REFERENCES

1. Ali, K.H.M. and Hedges, T.S., "Discussion on Jet-forced circulation in water supply reservoirs", by R.J. Sobey and S.B. Savage. J. Hydraul. Div. Am. Soc. Civ. Engrs., 1975, 101, HY12, Dec., 1543-1546.

2. Ali, K.H.M., Hedges, T.S. and Whittington, R.B., "A scale model investigation of the circulation in reservoirs", Proc. Instn. Civ. Engrs., part 2, 1978, 65, Mar., 129-161.

3. Ali, K.H.M. and Pateman, D., "Prediction of the circulation in reservoirs", Proc. Instn. Civ. Engrs., Part 2, 1981, 71, June, 427-461.

4. Ali, K.H.M. and Whittington, R.B., "Liquid-liquid mixing in tanks and reservoirs", Proc. Brit. Hydromech. Res. Assn. 3rd Eur. Conf. Mixing, York, 1979, 37-60.

5. Ali, K.H.M., "The investigation of reservoir circulation", Modelling of Env. Flow Systems, Winter Annual Meeting of the ASME, Boston, Massachusetts, Nov. 1983, pp 25-34.

6. Ali, K.H.M. and Pateman, D.R., "Dispersion of marked fluid in reservoirs", Advances in Water Resources, 1983, Vol. 6, Dec., pp 190-199.

7. Ali, K.H.M ., "Reservoir Circulation caused by jets, wind and by the earth's rotation", Int. Symposium on Modelling Environmental Flows, Albuquerque, New Mexico, June 1985, pp 71-80.

8. Cooley, P. and Harris, S.L., "The prevention of stratification in reservoirs", J. Instn. Wat. Engrs., 1954, 8, 517-531.

9. Daily, F.W. and Harleman, D.R.F., "Fluid Dynamics", Addison-wesley, Massachusetts, 1973, 419-423.

10. Ekman, V.W., "On the influence of the earth's rotation on ocean-currents", Ark. Mat. Astr. Fys., 1905, 2, No. 4.

11. Falconer, R.A., "Mathematical modelling of jet-forced circulation in reservoirs and hourbours", Ph.D thesis, Imperial College, 1976.

12. Fluent Incorporated, Fluent Version 4.2.2 User's Guide, Fluent Incorporated, Lebanon, New Hampshire, U.S.A., 1993.

13. Fosset, H. and Prosser, L.E., "The application of free jets to the mixing of fluids in bulk", Proc. Instn. Mech. Engrs., 1949, 160, 224-232.

14. Goossens, L.J., "Reservoir destratification with bubble columns", Delft University Press, 1979.

15. Guitton, D.E., "Two-dimensional turbulent wall jets over curved surfaces", Mechanical Engineering Research Laboratories, McGill University, Montreal, 1964, Report 64-7.

16. Liggett, J.A. and Hadjieheodorou, C., "Circulation in shallow homogeneous lakes", J. Hydraul. Div. Am. Soc. Civ. Engrs., 1969, 95, HY2, Mar., pp 609 -620.

17. Lindh, G. and Bengtsson, L., "Wind-induced circulation in a lake", Proc. 1st Int. Conf. Port Ocean Energy under Arctic Conditions, Technical University of Norway, 1971, 2, pp 893-908.

18. Liu, H. and Perez, H.J., "Wind-induced circulation in shallow water", J. Hydraul. Div. Am. Soc. Civ. Engrs., 1971, 97, HY7, July, pp 923-935.

19. Metropolitan Water Board, "Model tests for flow patterns in Wraysbury and Datchet reservoirs", Metropolitan Water Board, 1962, 1972, Internal Reports.

20. Mills, R.D., "Computing internal viscous flow problems for a circle by integral methods", J. Fluid Mech., 1977, 79, Part 3, pp 609-624.

21. Robinson, S.J., "Hydraulic modelling of circulation in reservoirs", M. Phil. thesis, Imperial College, 1979.

22. Schwarz, W.H. and Cosart, W.P., "The two-dimensional turbulent wall jet", J. Fluid Mech., 1961, 10, Part 4, June, 481-495.

23. Sobey, R.J., "Flow patterns in lakes and reservoirs", Ph.D thesis, Imperial College, 1972.

24. Sobey, R.J. and Savage, S.B., "Jet-forced circulation in water-supply reservoirs", J. Hydraul. Div. Am. Soc. Civ. Engrs., 1974, 100, HY12, Dec., 1809-1828.

25. Welander, P., "Wind action on a shallow sea, some generalizations of Ekman's theory", Tellus, 1957, 9, Feb., No. 1, pp 45-52.

APPENDIX II

NOTATION

b_o	Height of inlet jet
d_o	Width of two-dimensional jet
f	Coriolis parameter
F	Reservoir Froude number (= $V_j/\sqrt{gh}$)
g	Acceleration due to gravity
h	Water-depth of reservoir
k_s	Roughness height of reservoir
K_j	Kinematic jet momentum flux (= Q_jV_j)
L	Diameter of reservoir
Q_c	Circulating discharge at given θ
$\bar{Q}_c$	Overall average circulating discharge
Q_j	Discharge of inlet jet
v	Local tangential velocity
V_j	Average velocity of inlet jet
x	Distance from virtual origin of jet
α	Horizontal scale ratio
β	Vertical scale ratio
ϕ	Latitude of reservoir
θ	Angle from the jet
υ	Kinematic viscosity of water
ψ	Dimensionless function
Ω	Angular speed of rotation of the earth

TABLE 1 : Experimental Models and Inlet-Outlet Arrangements

Model	Arrange-ment	L = 2R (m)	h (mm)	b_o (mm)	d_o (mm)	Scale-ratio(∝)	Bed material
1	1	7.36	70, 120, 170, 220, 280	50	2	-	painted concrete
1	2	7.36	70, 120, 170, 220, 280	50	2	-	painted concrete
2	1	3.00	20, 50, 100, 200	20	2	-	glass
2	2	3.00	20, 50, 100, 200	20	2	-	glass
2	3	3.00	20, 50, 100, 200	20	2	-	glass
3	4	2.44	46	20, 8	2, 30, 60, 130	-	painted wood
3	5	3.00	70	50	2	-	pained wood
3	6	3.00	70	50	2	-	painted wood
Prescot No. 4	1	1.6	16	12.2	2.4	250	painted wood
Prescot No.4	2	1.6	16	1.6 (dia)	1.6 (dia)	250	painted wood
Prescot No.3	1	1.7	16	1.6 (dia)	1.6 (dia)	250	painted concrete
Silvola	1	2.5	27.5	7.5	1.5 (dia)	400	painted wood

Model (1)
Arrangement (1)

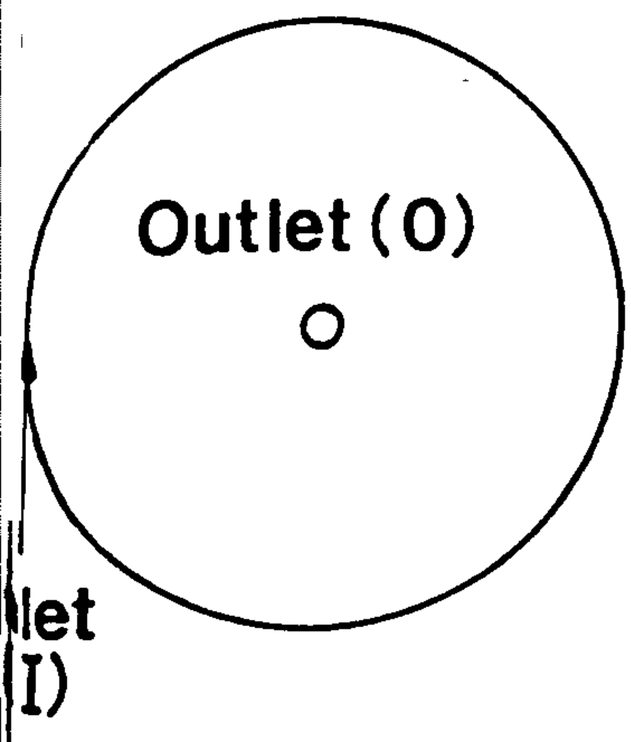

Model (1)
Arrangement (2)

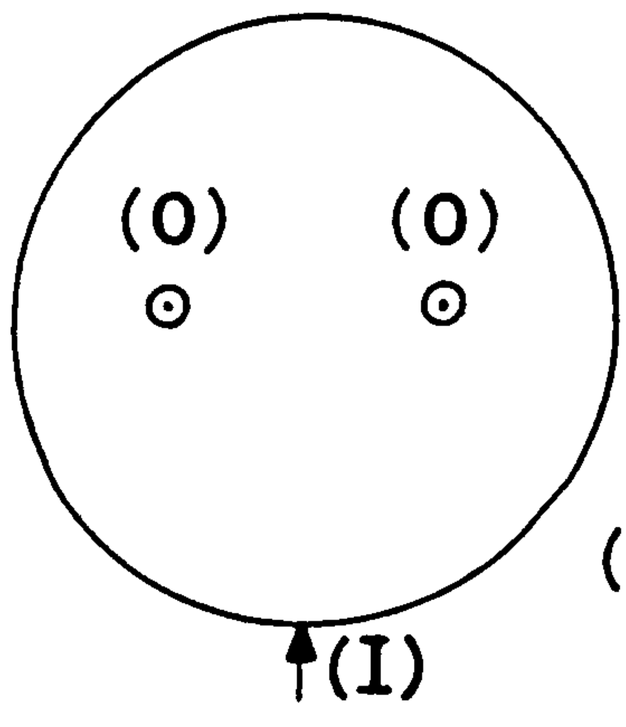

Model (2)
Arrangement (1)

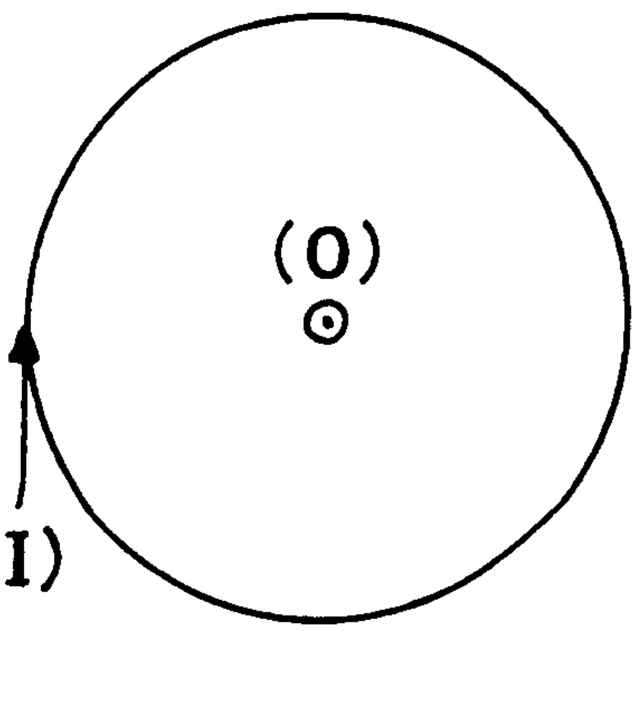

Model (2)
Arrangement (2)

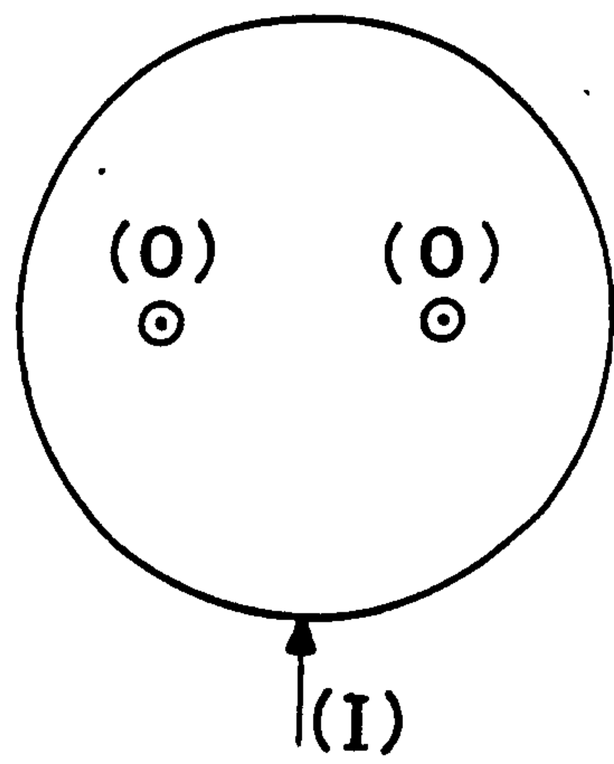

Model (2)
Arrangement (3)

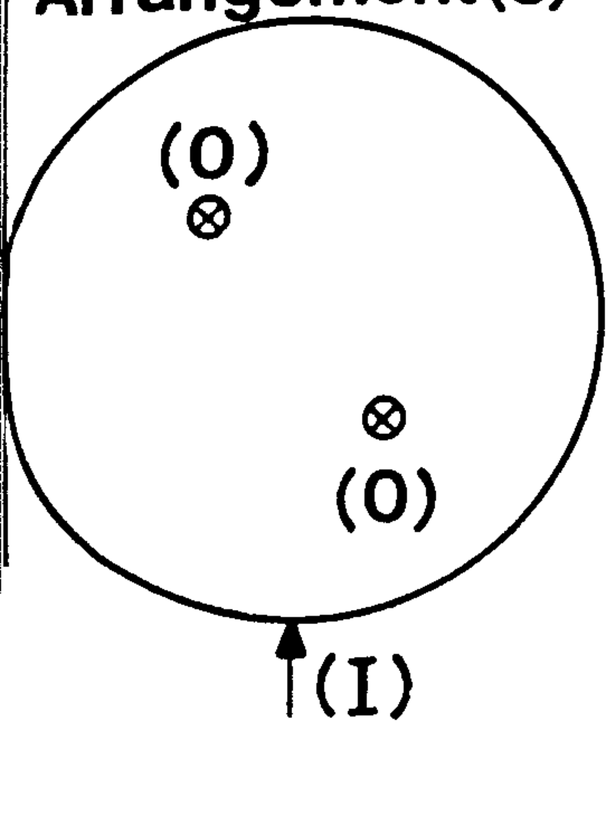

Model (3)
Arrangement (4)

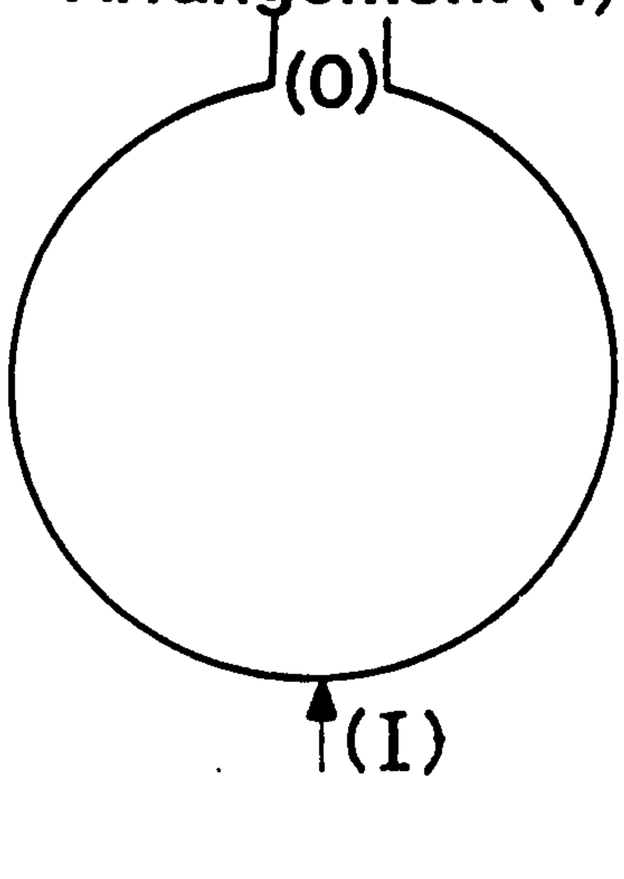

Model (3)
Arrangement (5)

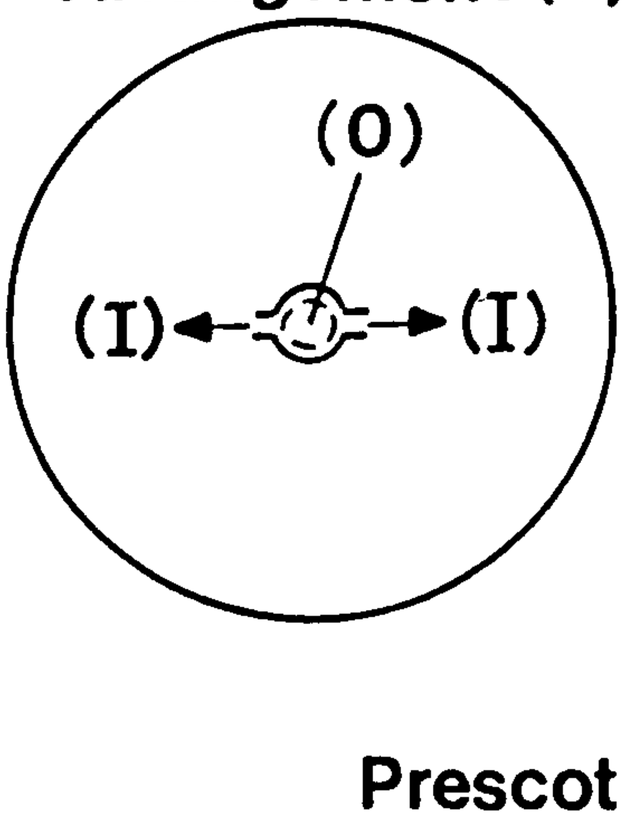

Model (3)
Arrangement (6)

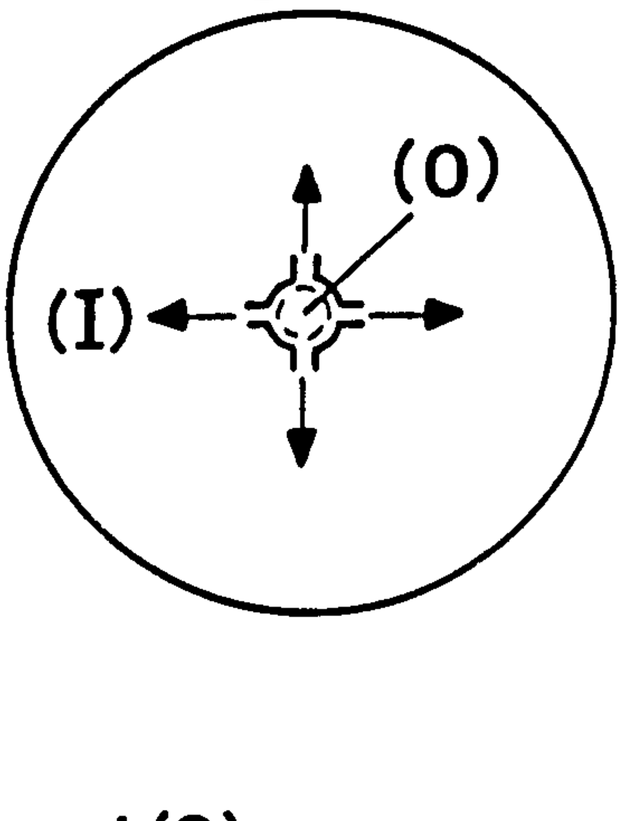

Prescot No4
Arrangement (1)

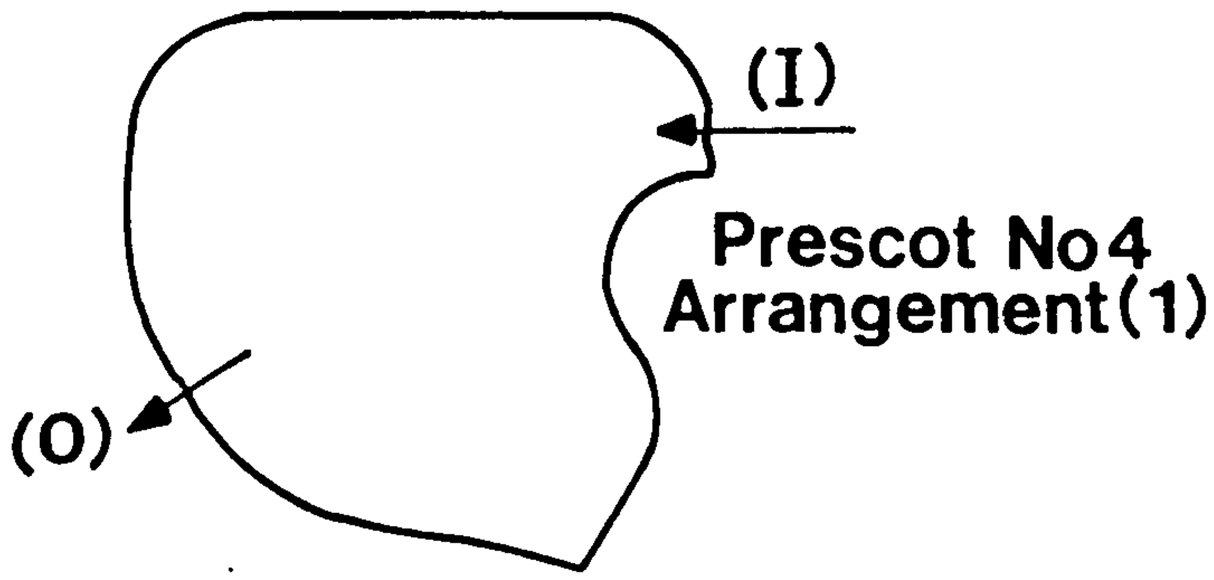

Prescot
Arrangement (2)

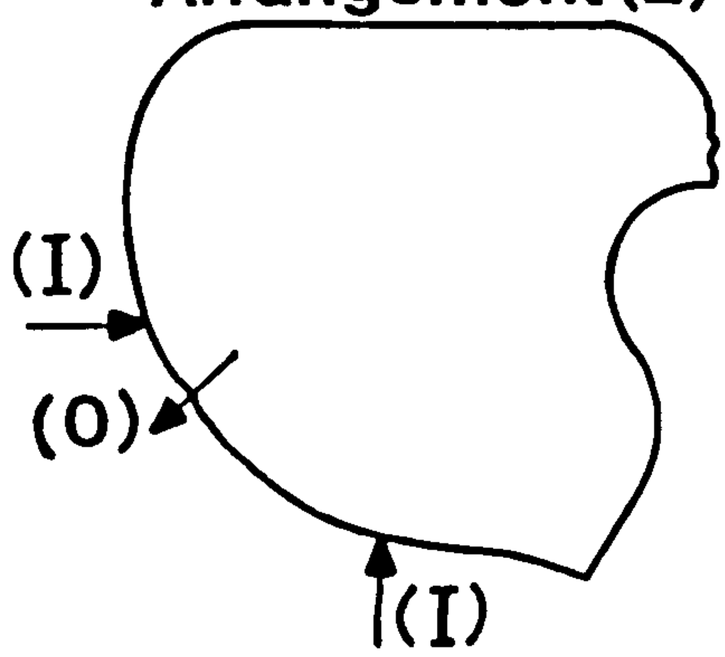

Prescot No (3)
Arrangement (1)

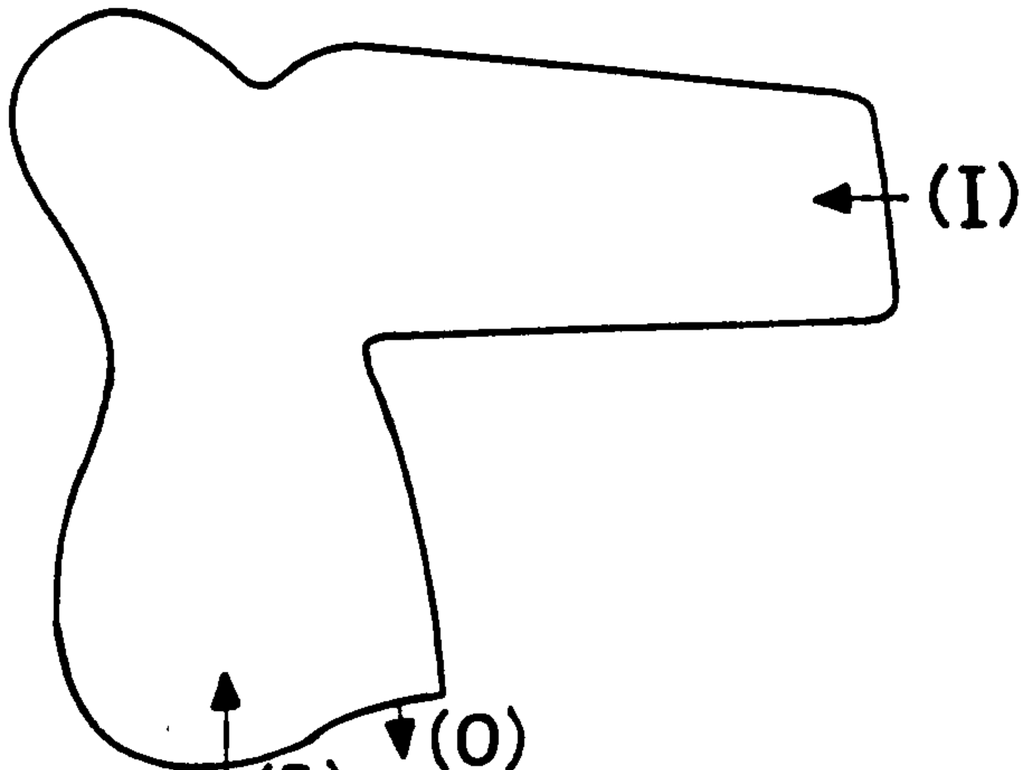

Silvola
Arrangement (1)

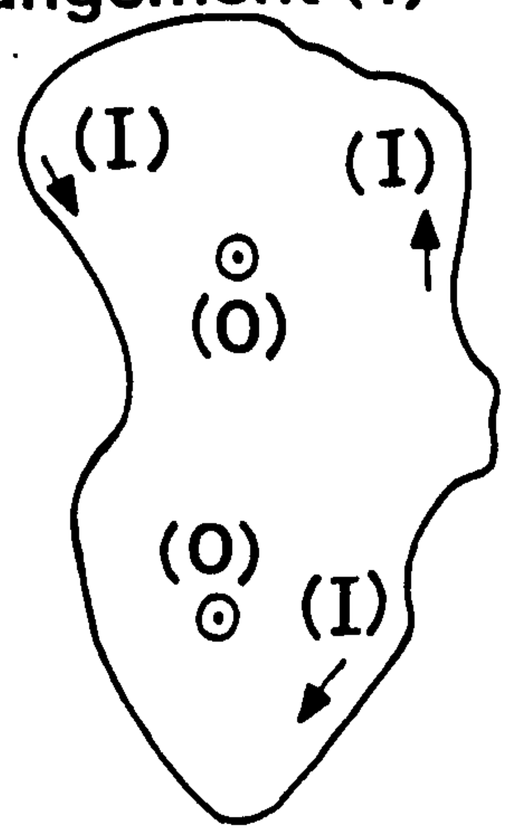

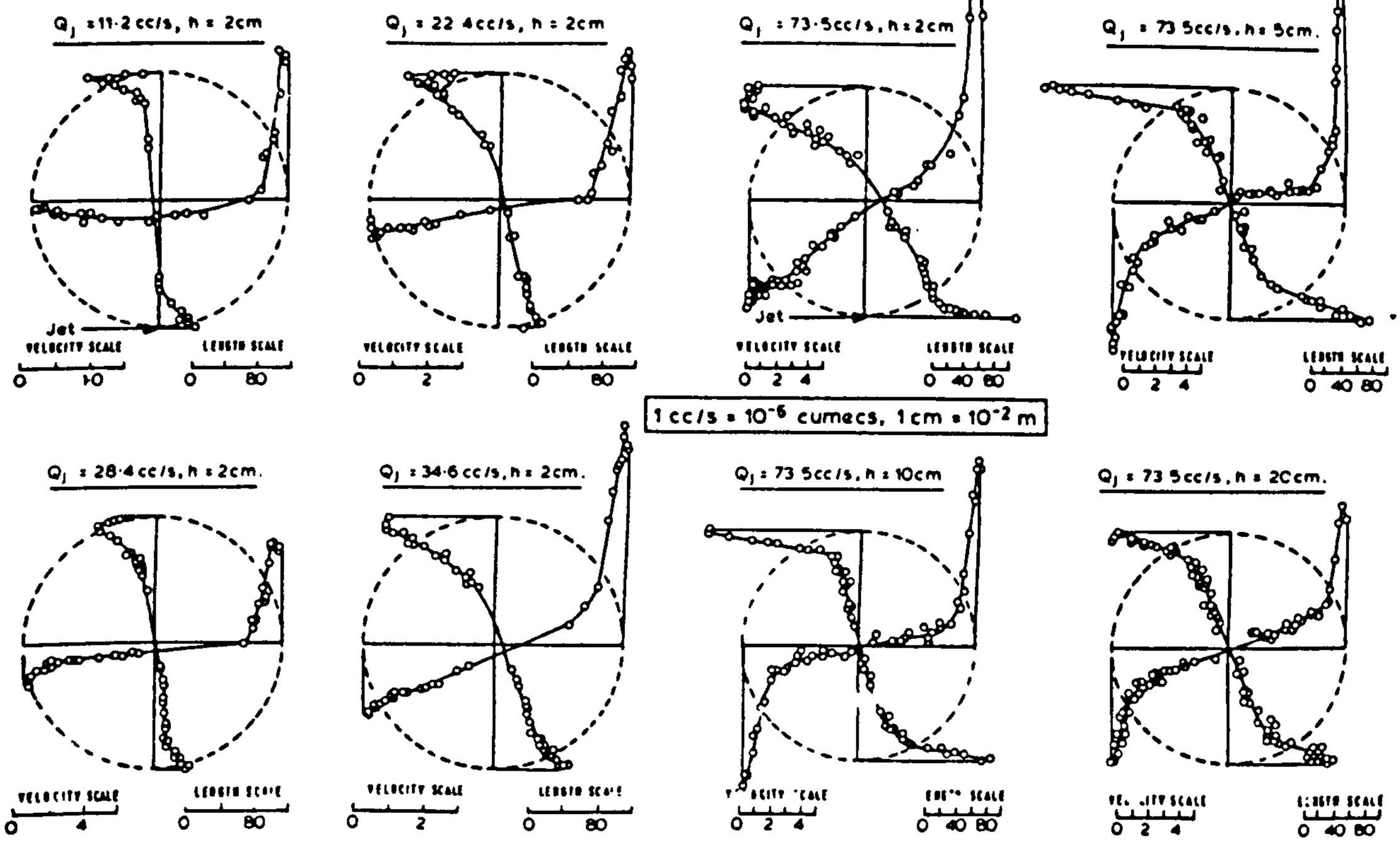

FIG 2. MEASURED VELOCITY - DISTRIBUTIONS.

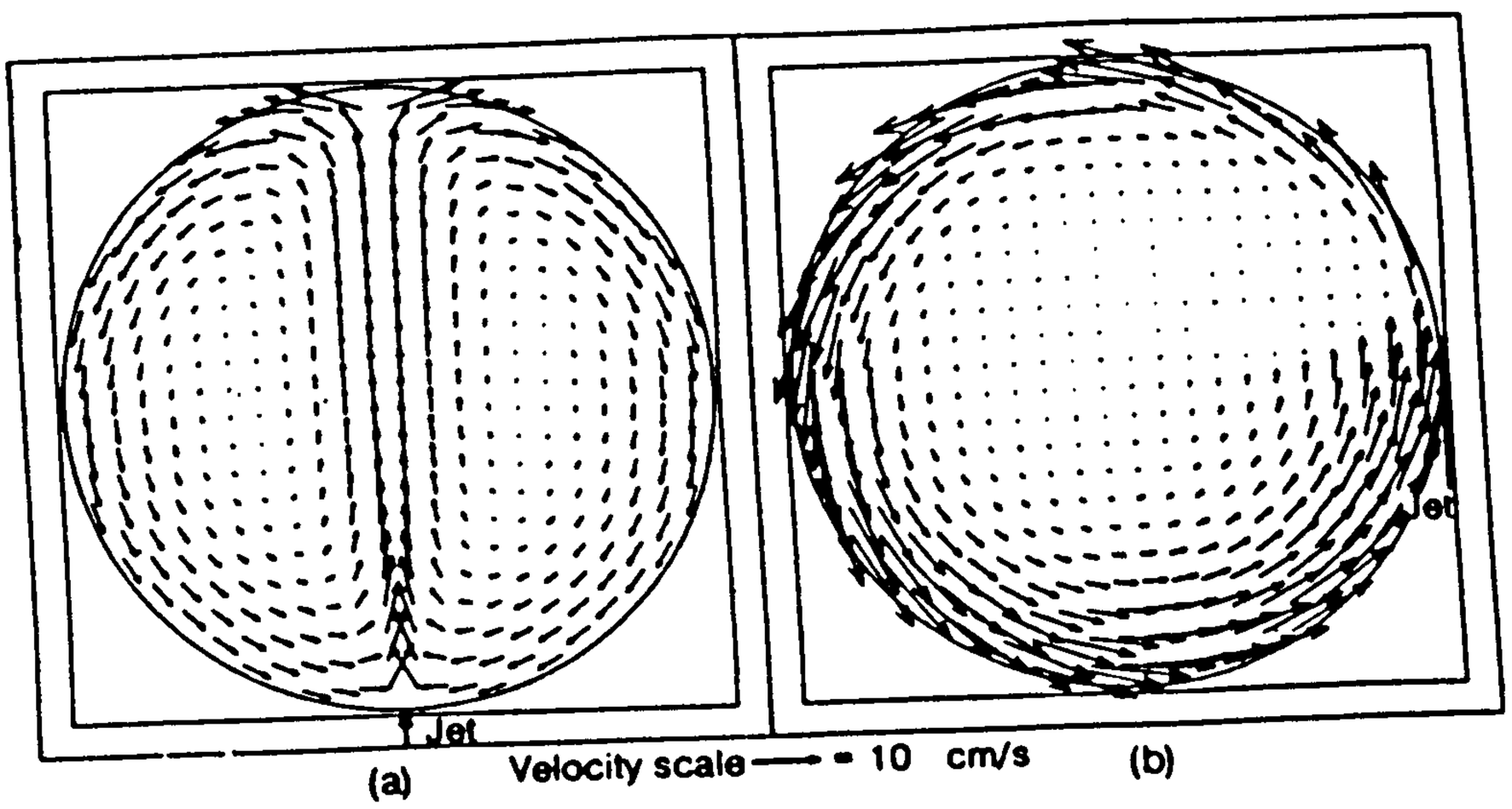

FIG. 3 TYPICAL CIRCULATION PRODUCED BY TWO-DIMENSIONAL (a) RADIAL AND (b) TANGENTIAL JET INLETS

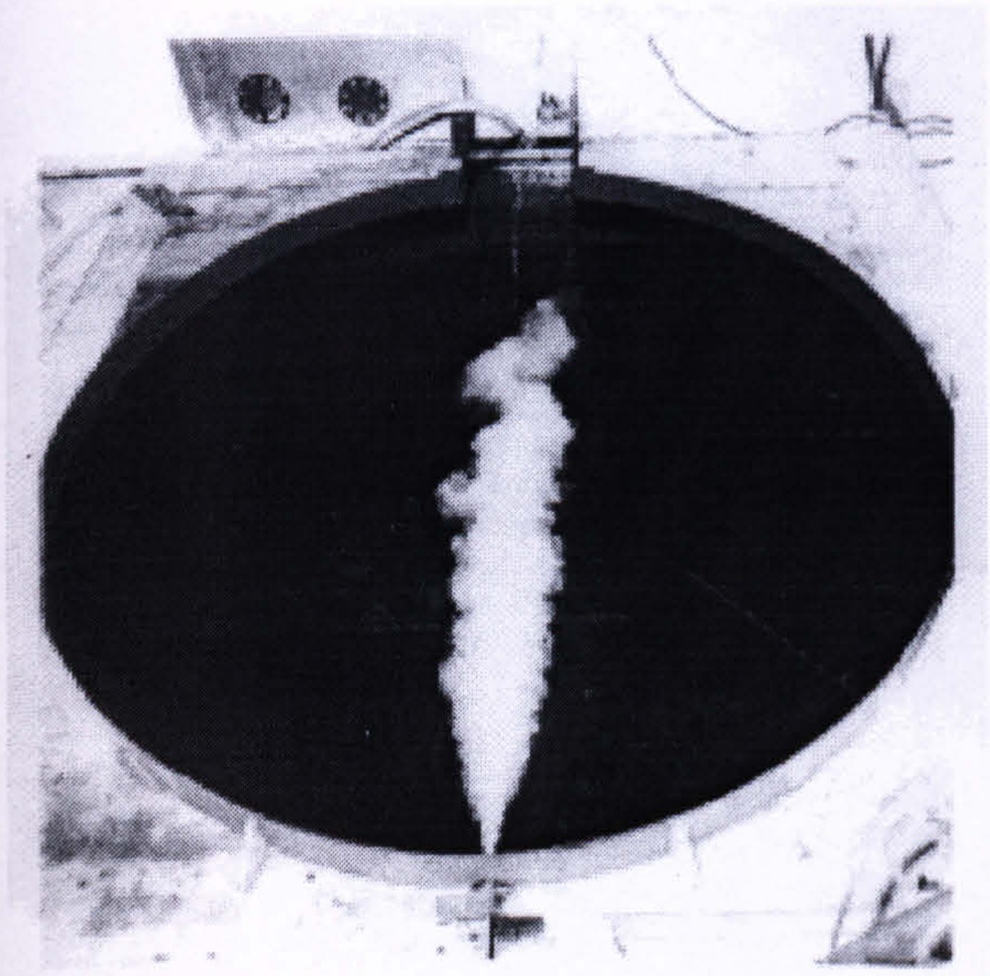

2 secs

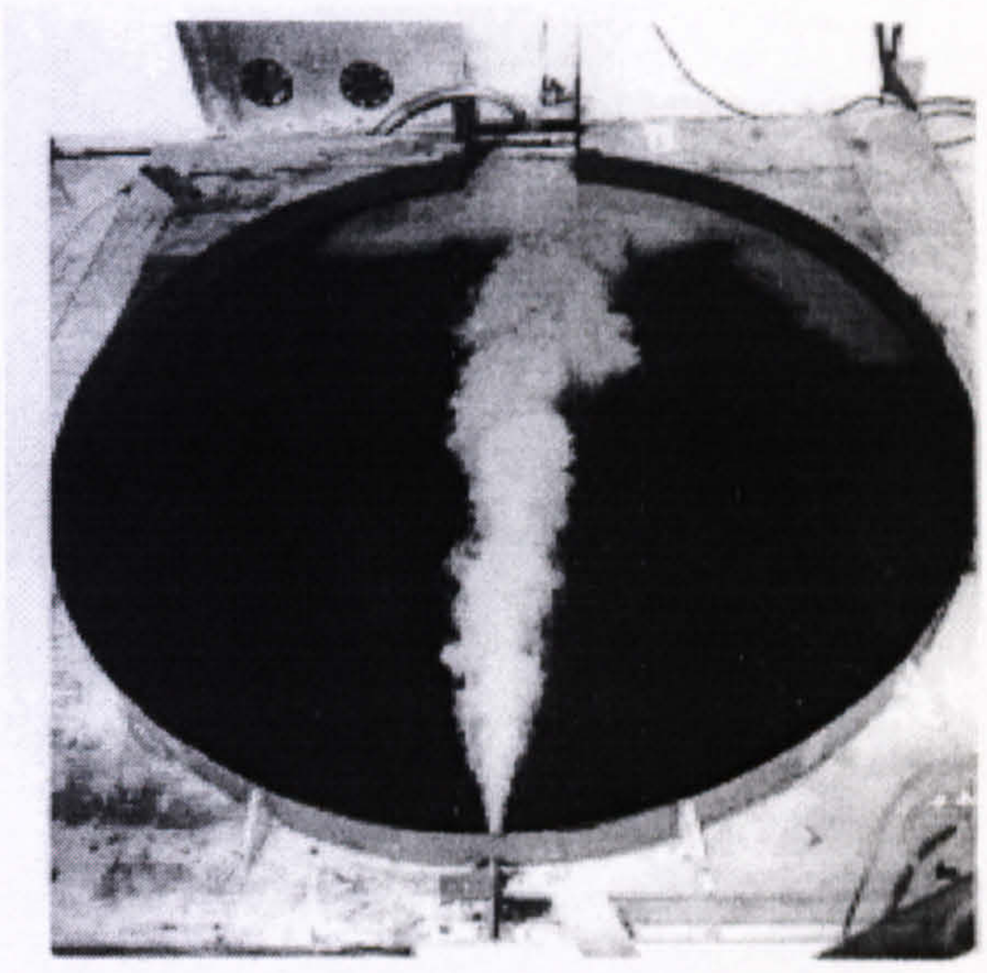

10 secs

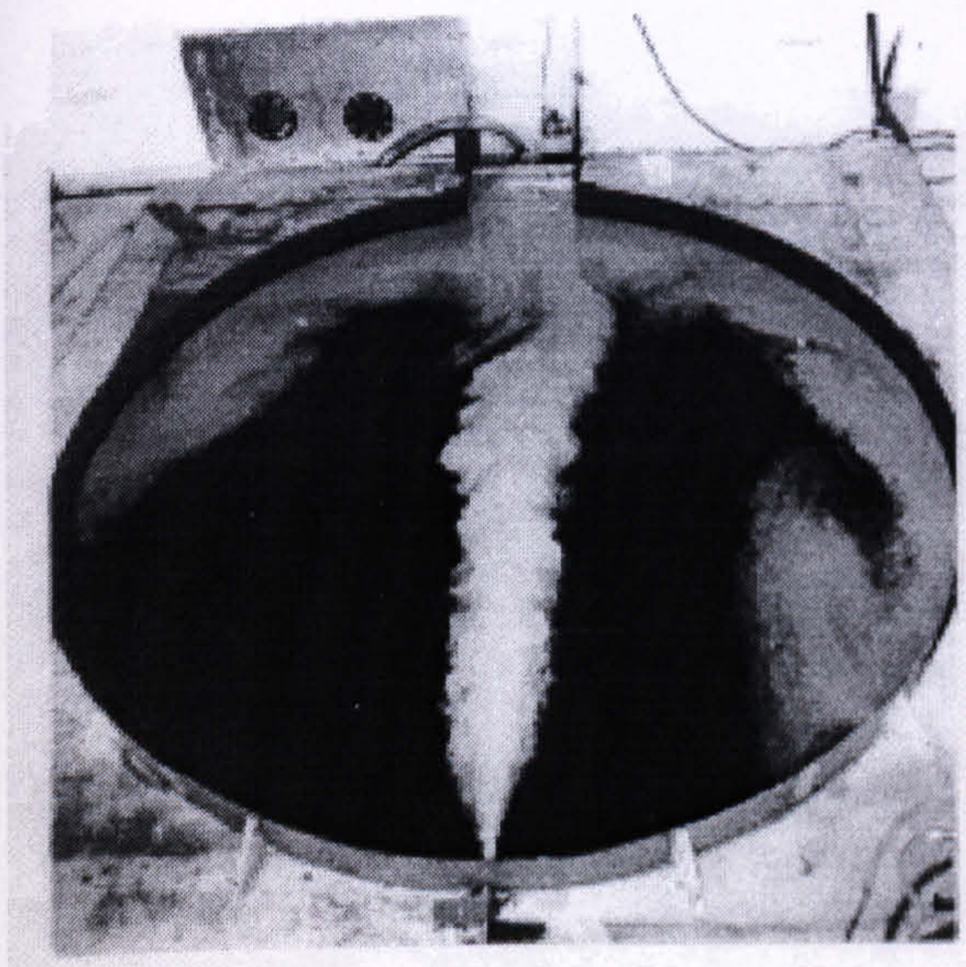

20 secs

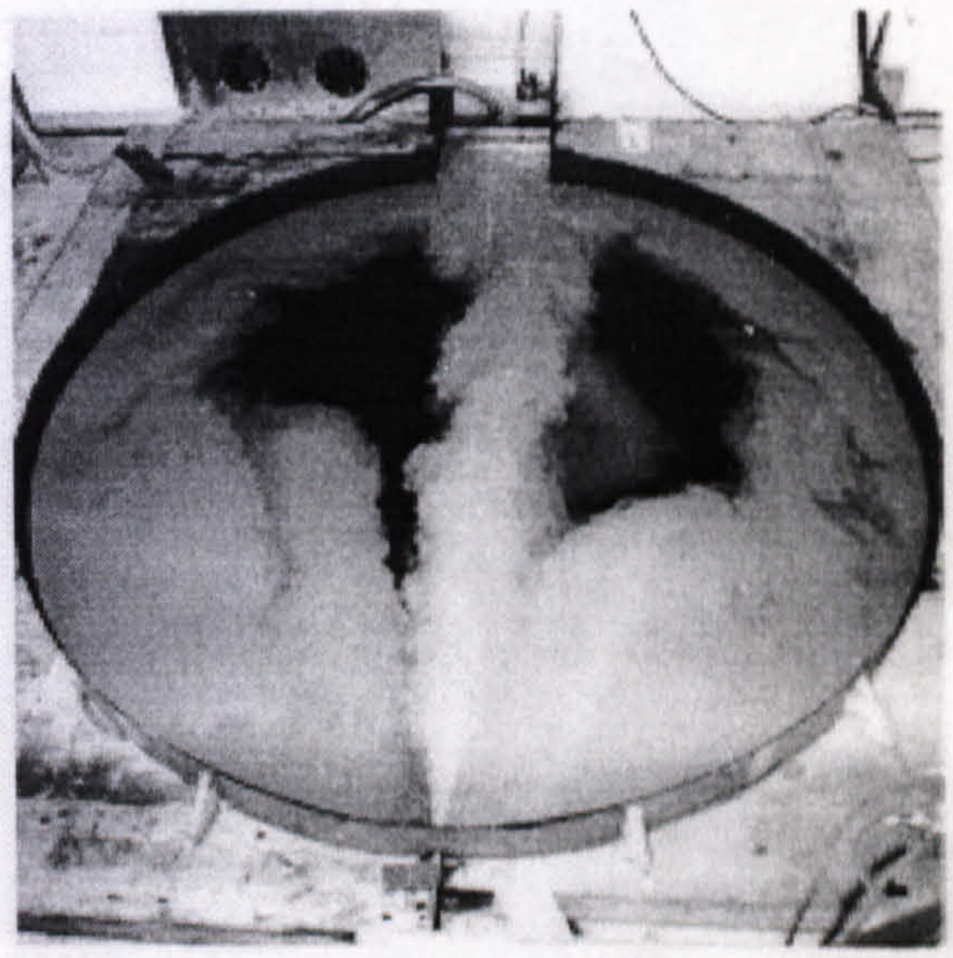

40 secs

Fig. 4 : Dye Mixing - radial jet

$Q_j = 192\ cm^3/s$

$A_j = 0.4\ cm^2$

$L = 243.8\ cm$

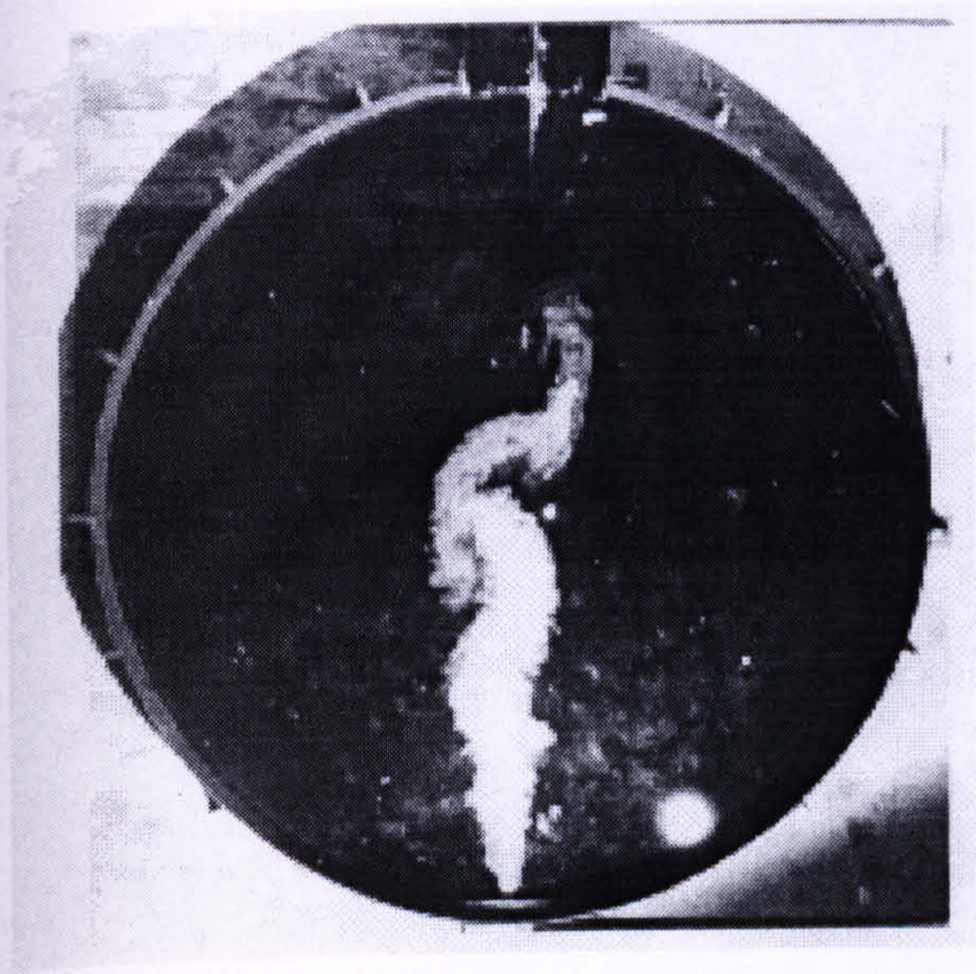

20 secs

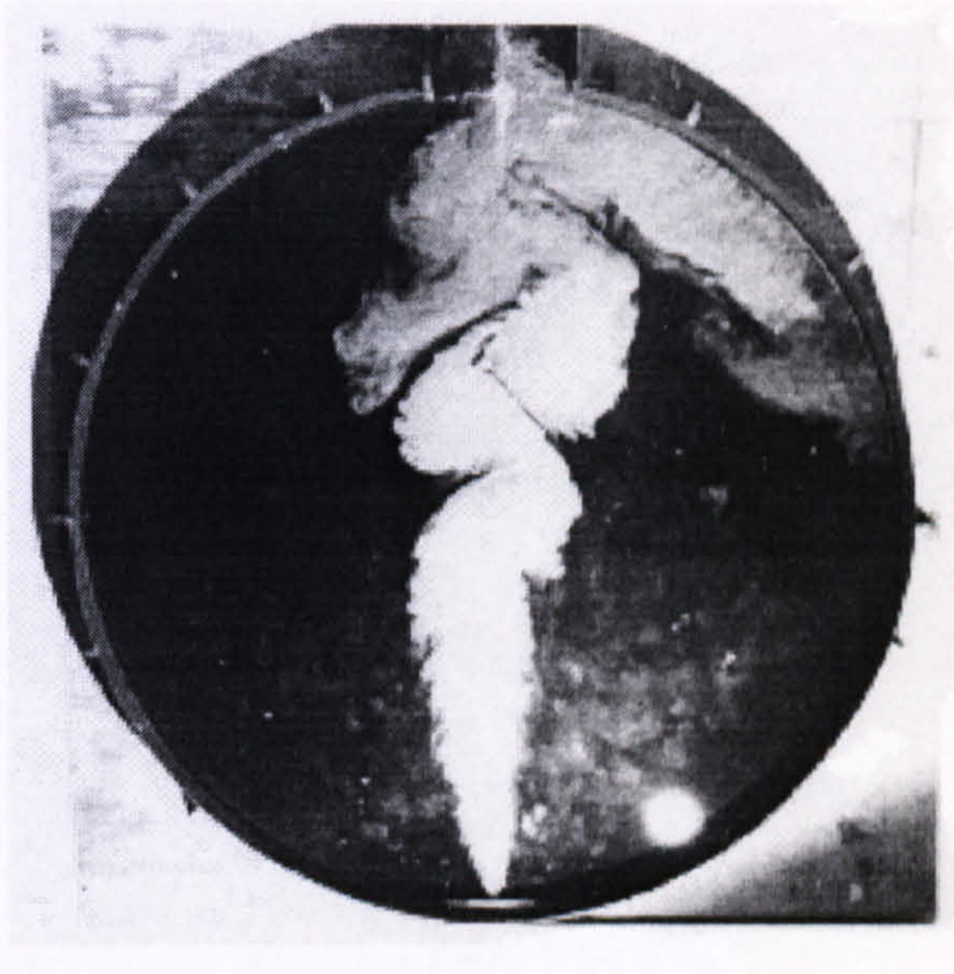

65 secs

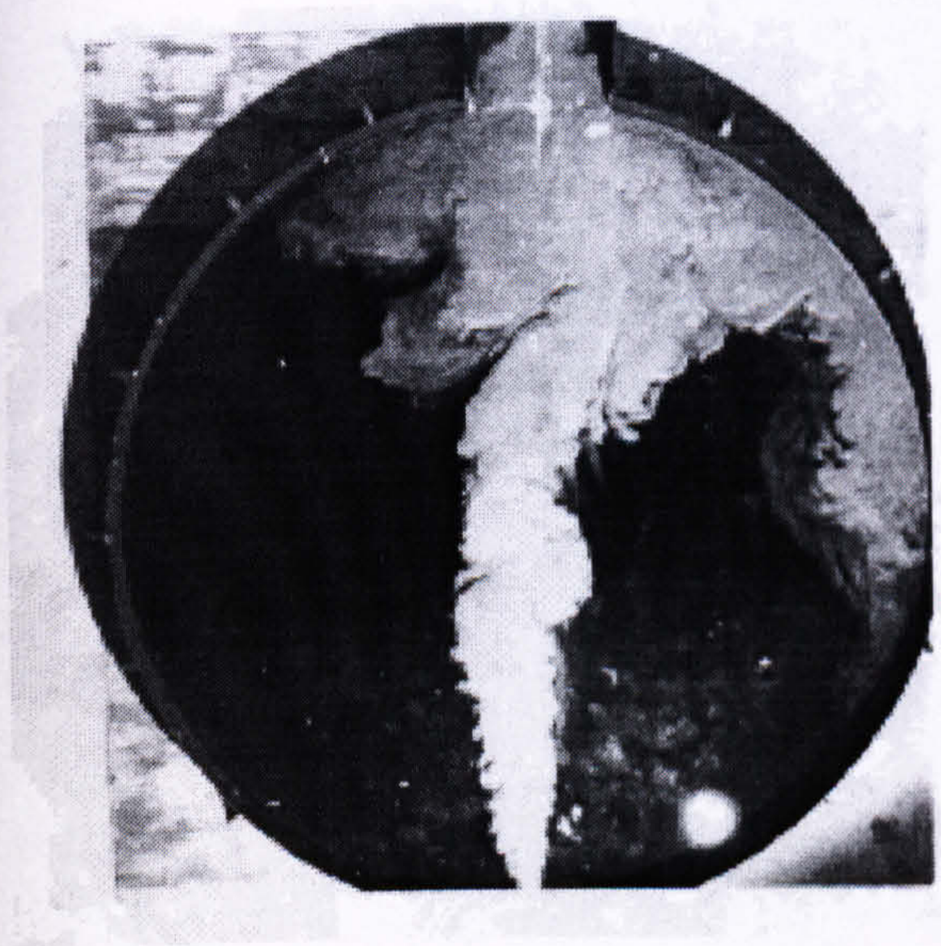

90 secs

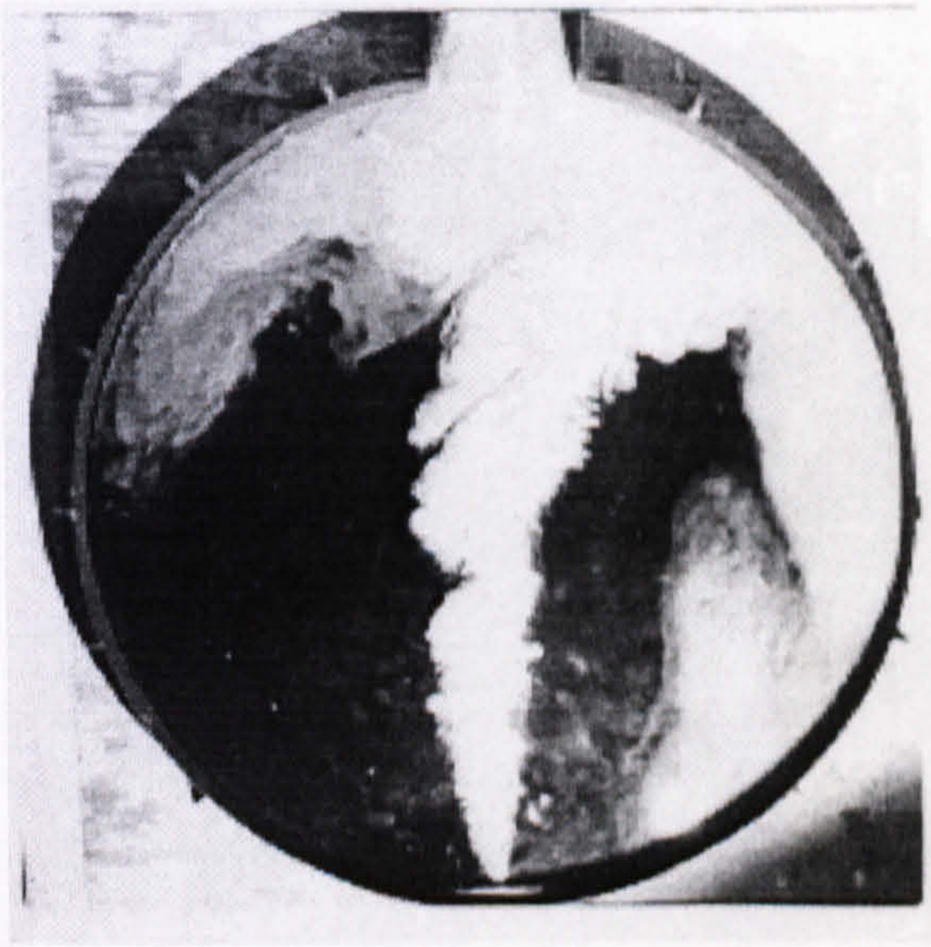

130 secs

Fig. 5 : Dye Mixing - radial jet

$Q_j = 192\ cm^3/s$

$A_j = 2.4\ cm^2$

$L = 243.8\ cm$

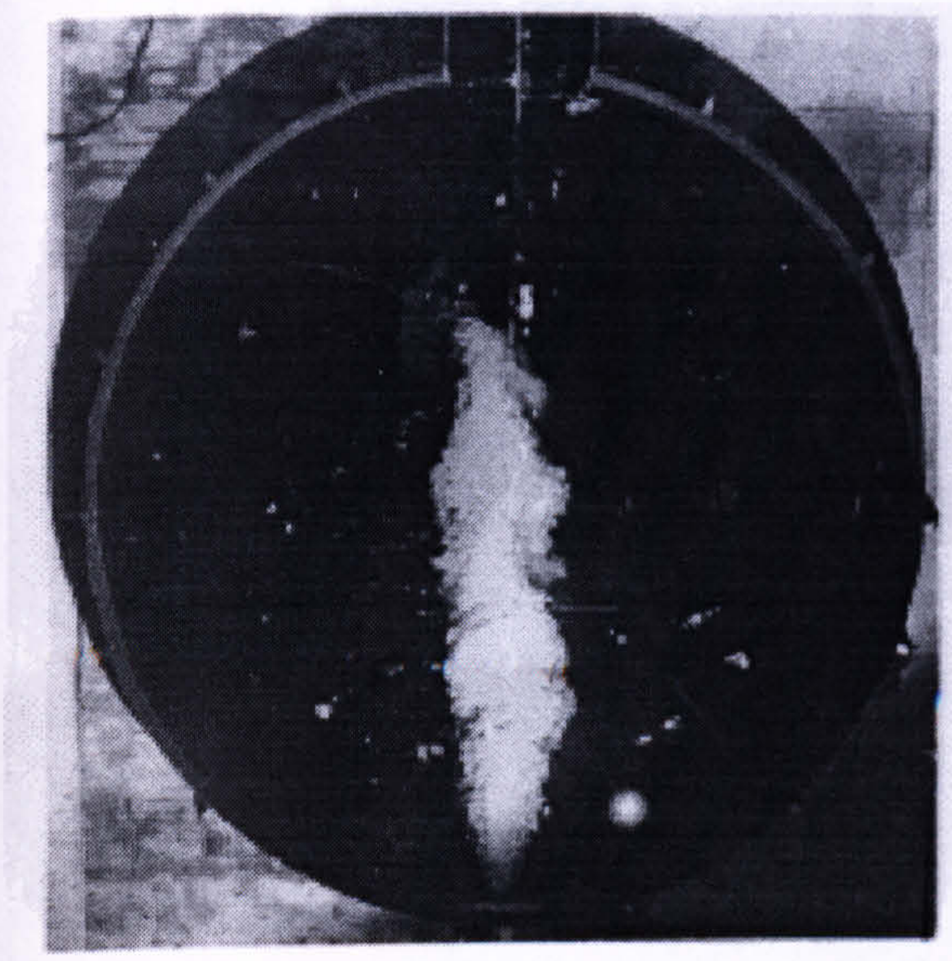

25 secs

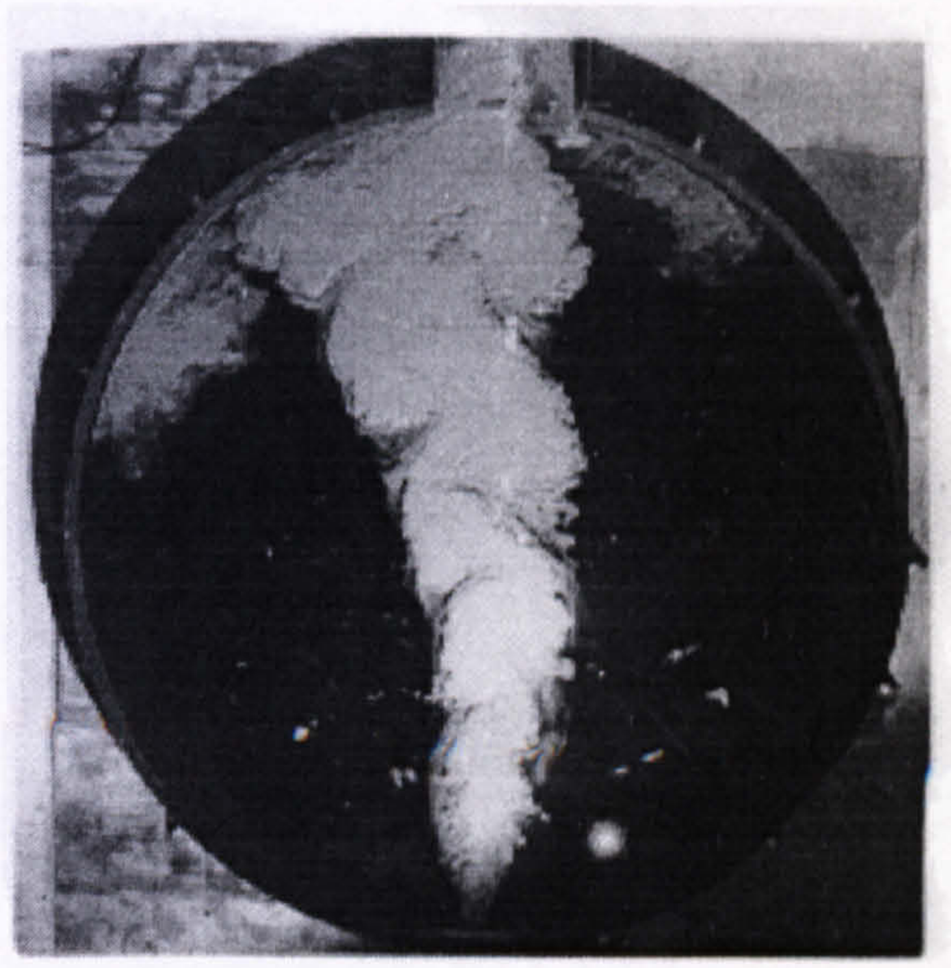

60 secs

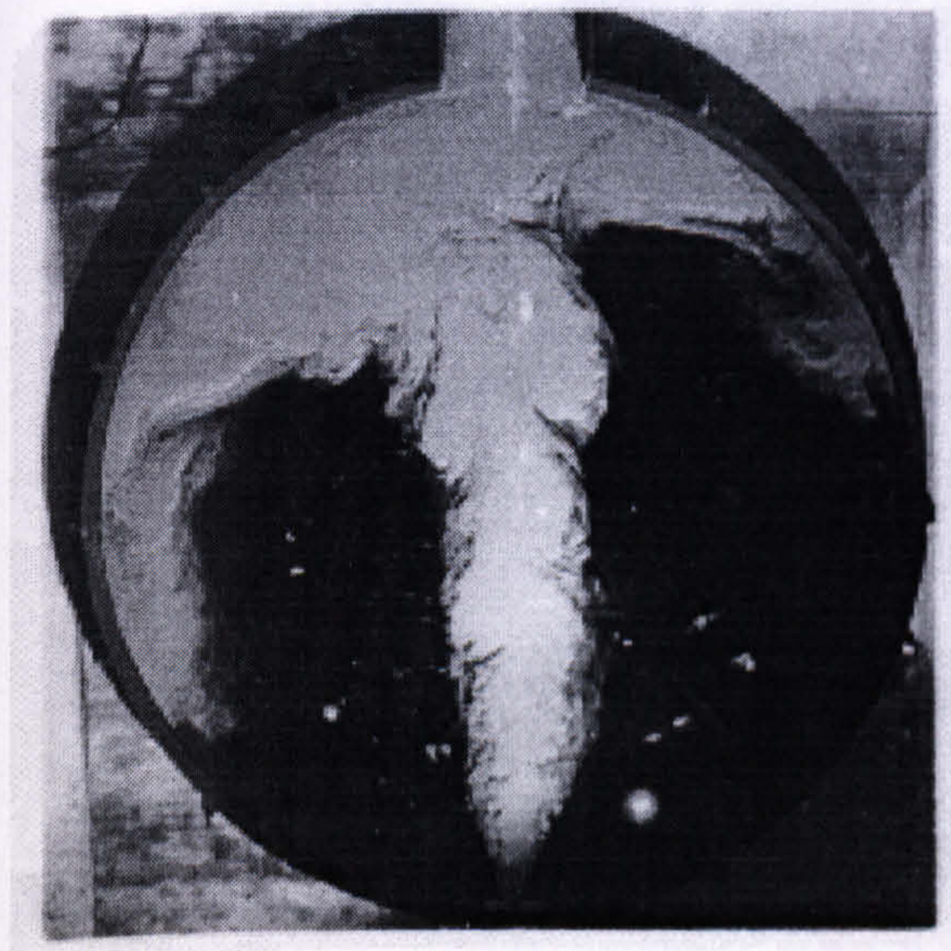

80 secs

145 secs

Fig. 6 : Dye Mixing - radial jet

$Q_j = 192 \text{ cm}^3/\text{s}$

$A_j = 4.8 \text{ cm}^2$

$L = 243.8 \text{ cm}$

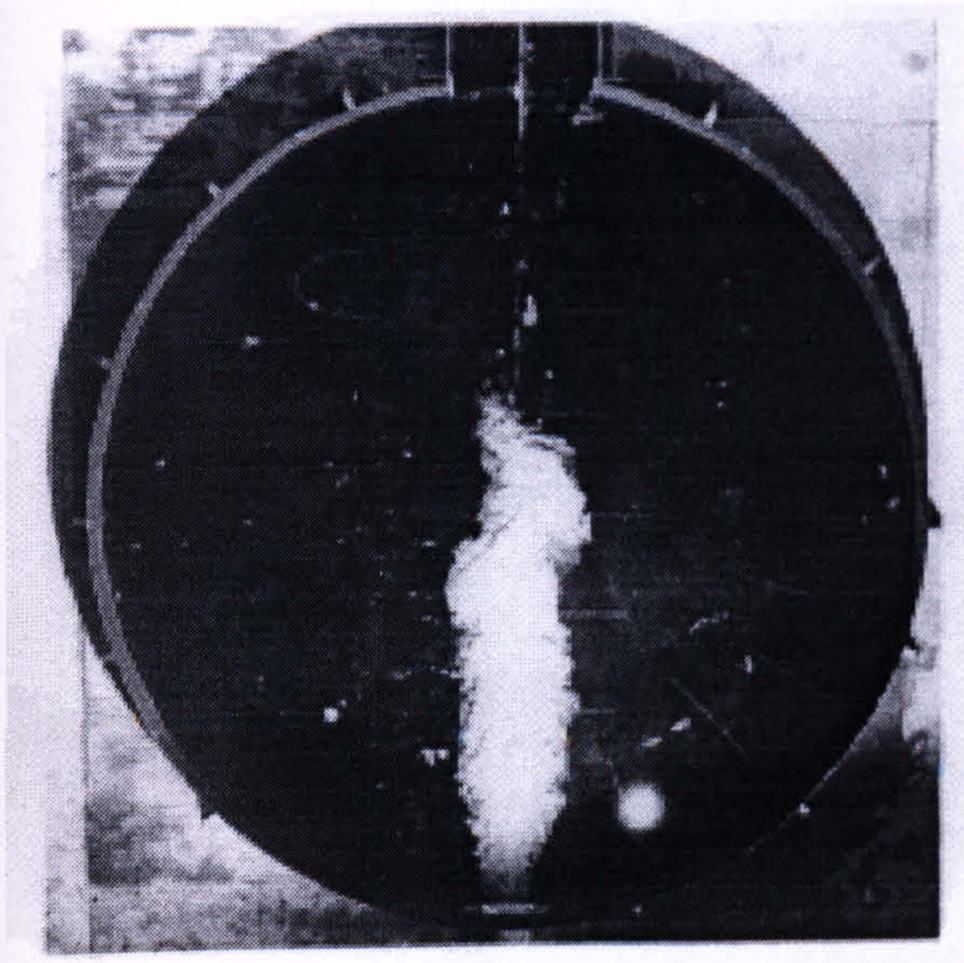

30 secs

85 secs

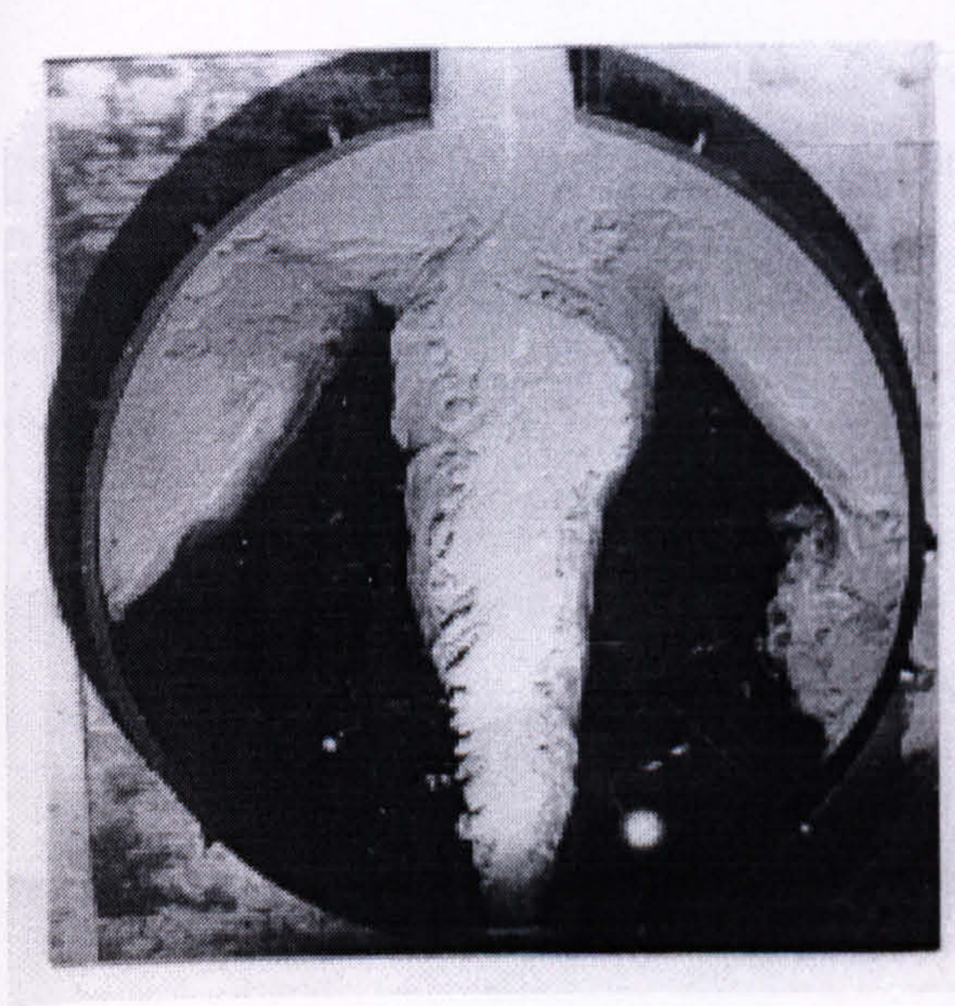

125 secs

200 secs

Fig. 7 : Dye Mixing - radial jet

$Q_j = 192\ cm^3/s$

$A_j = 10.4\ cm^2$

$L = 243.8\ cm$

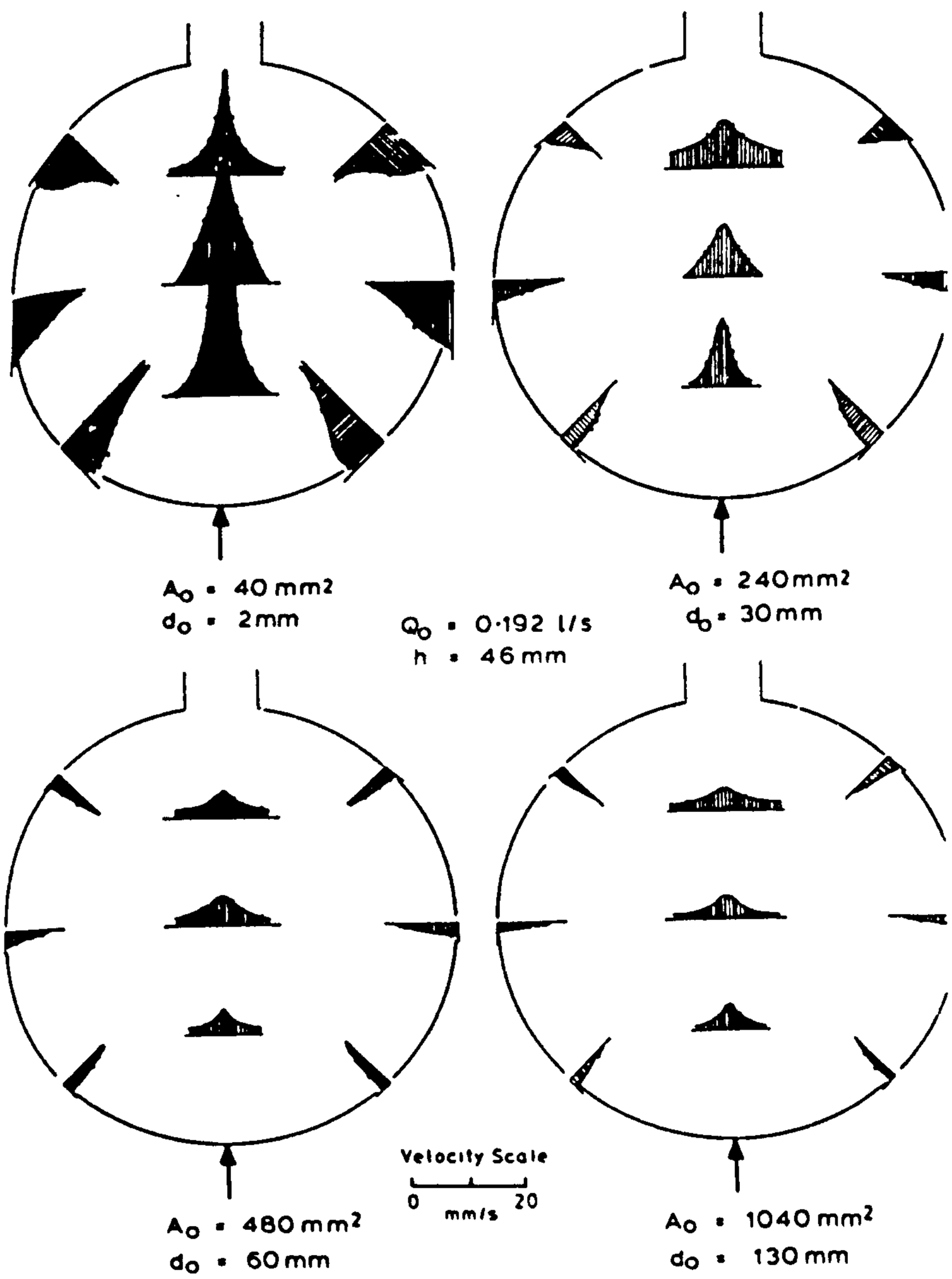

FIG. 8. VELOCITY-DISTRIBUTIONS FOR RADIAL JETS OF VARIOUS AREAS, (a) $A_j = 480mm^2$ (b) $A_j = 240mm^2$ (c) $A_j = 480mm^2$ (d) $1040mm^2$

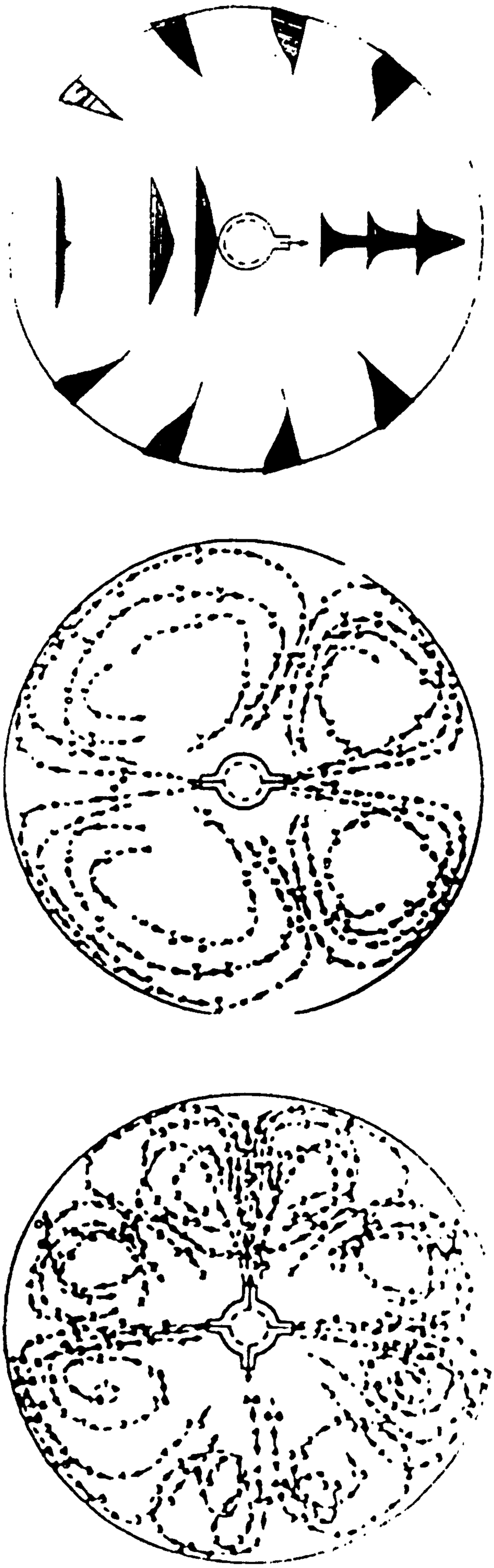

FIG 9 EXPERIMENTAL VELOCITIES FOR CENTRAL JETS

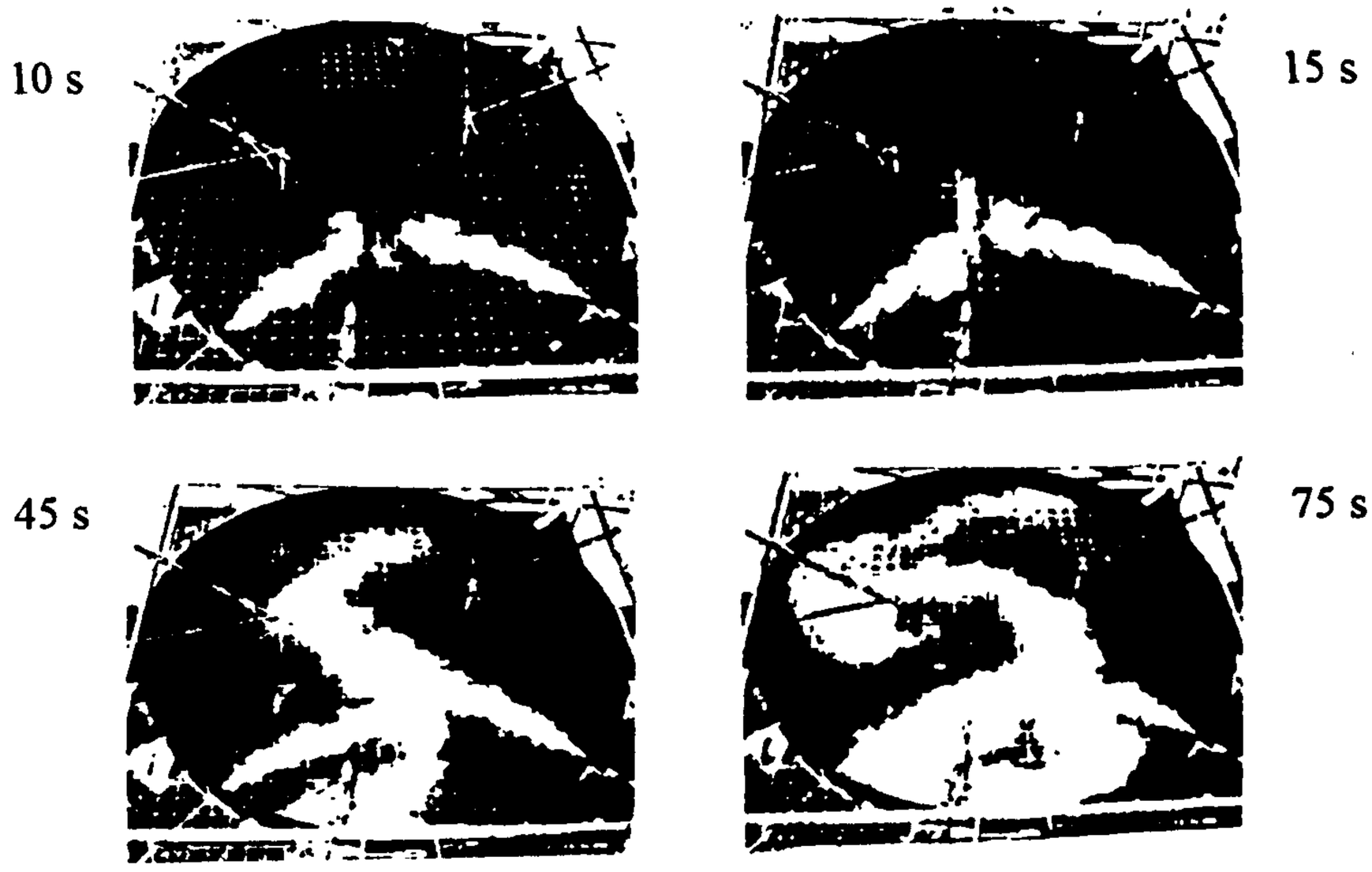

$L = 3m,\ h = 5cm,\ Q_j = 89$ cc/secs, $L/h = 60$

Fig 10 Dye mixing produced by twin radial jets (L/h = 60)

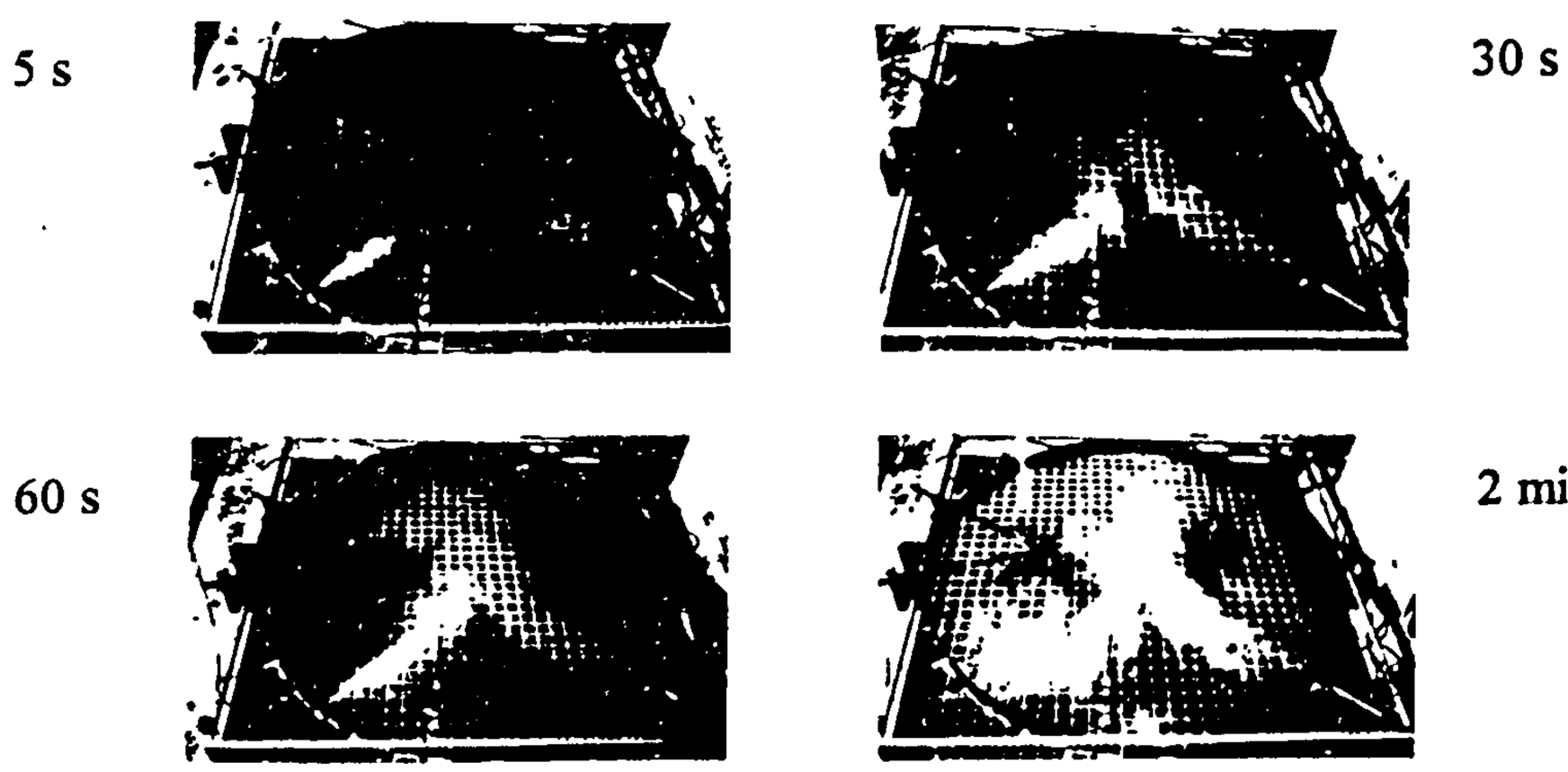

$L = 3.0m,\ Q_j = 89ml/s,\ h = 100mm$

Fig 11 Dye mixing produced by twin radial jets (L/h = 30)

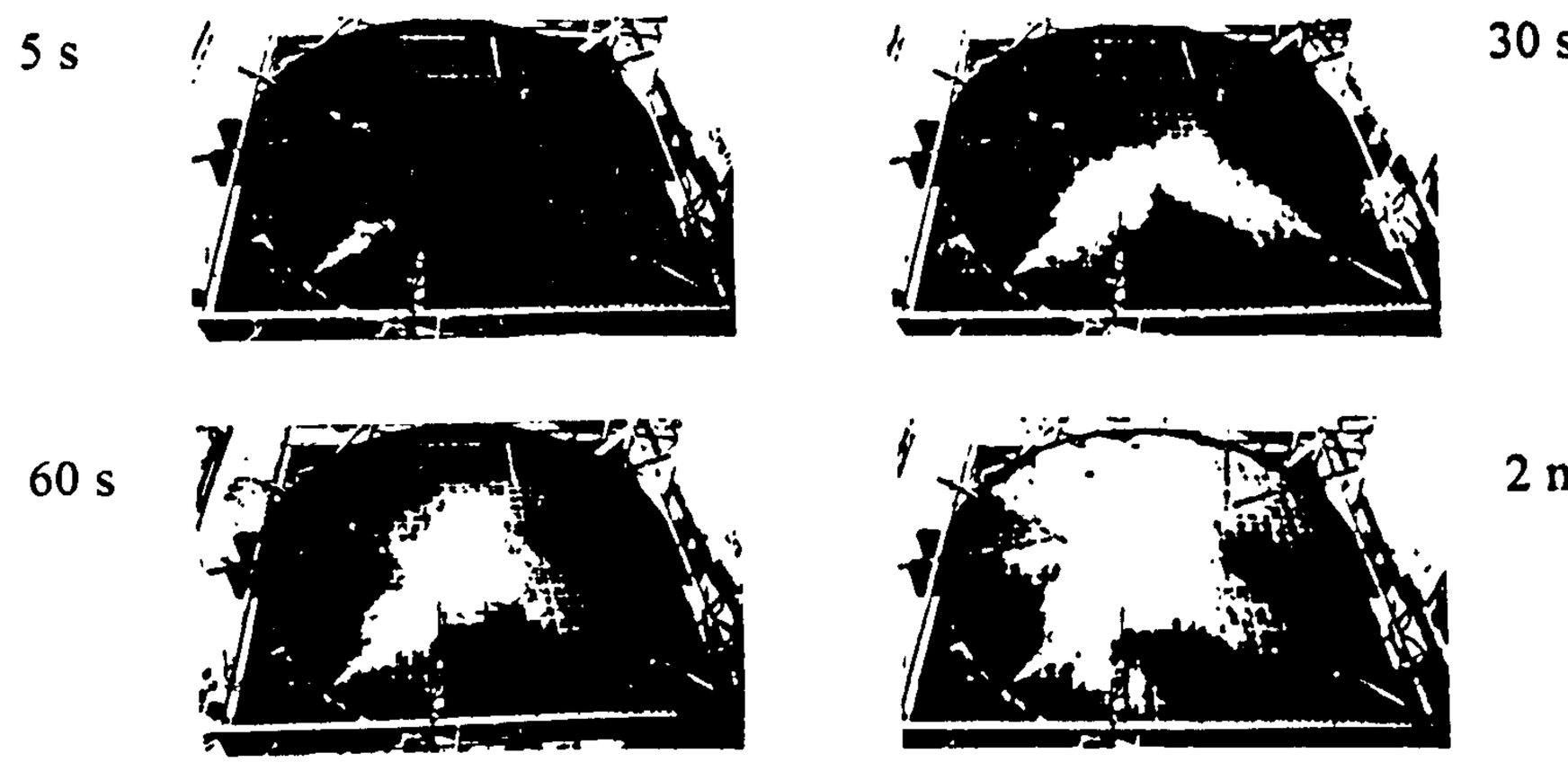

$L = 3.0m,\ Q_j = 89ml/s,\ h = 100mm$

Fig 12 Dye mixing produced by twin radial jets (L/h = 15)

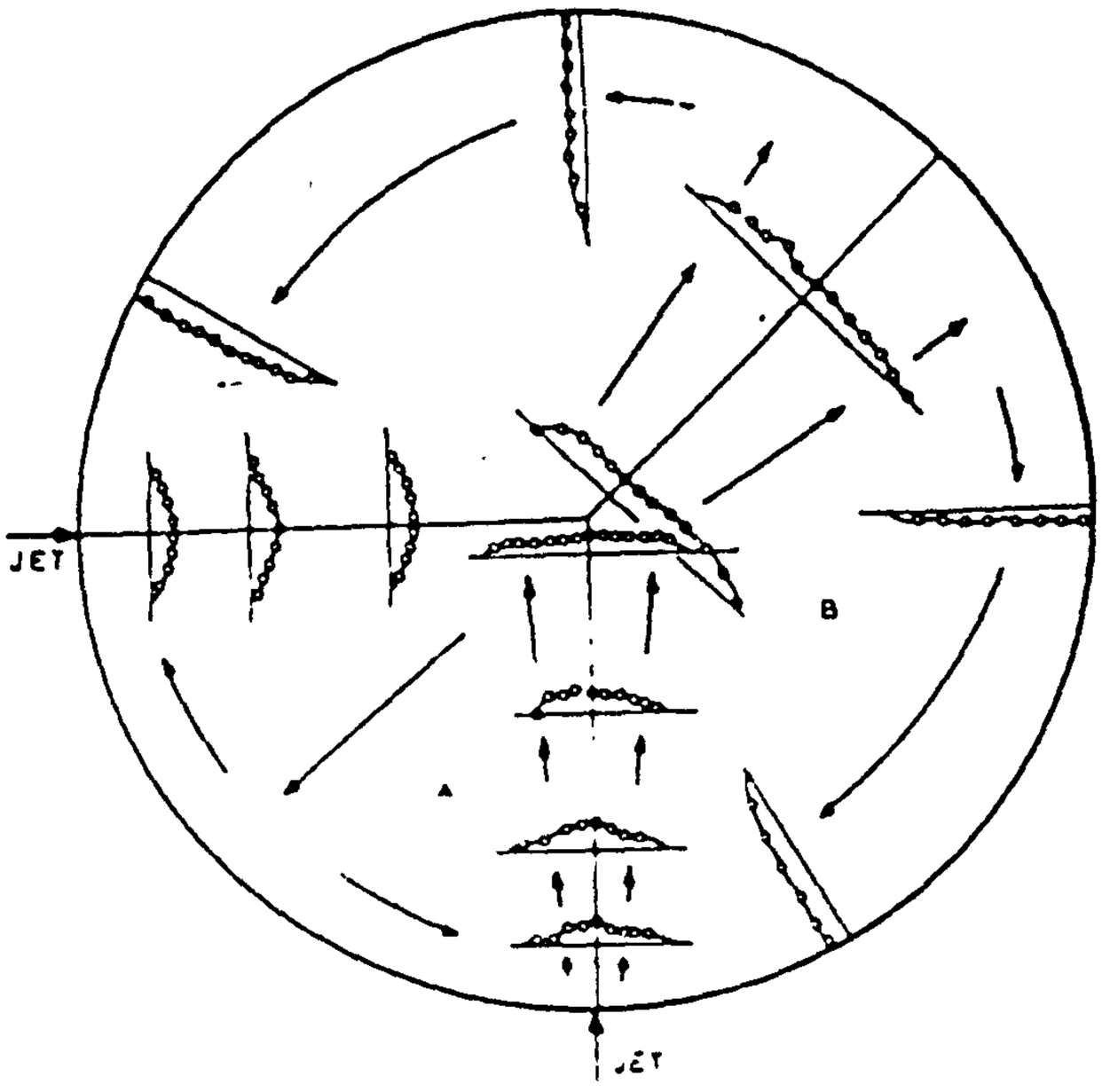

FIG. 13 EXPERIMENTAL VELOCITY DISTRIBUTIONS FOR TWIN RADIAL JETS

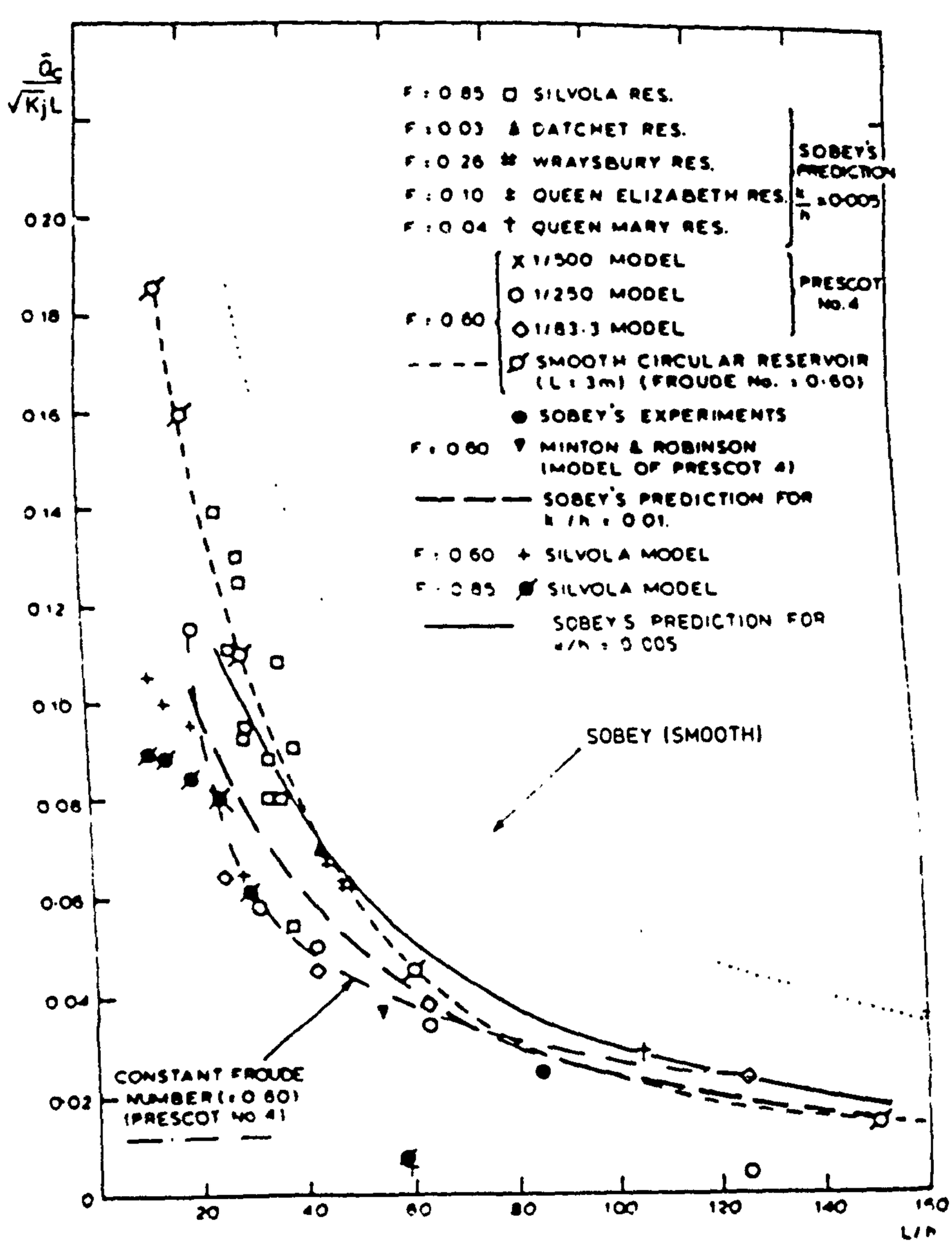

Fig. 14

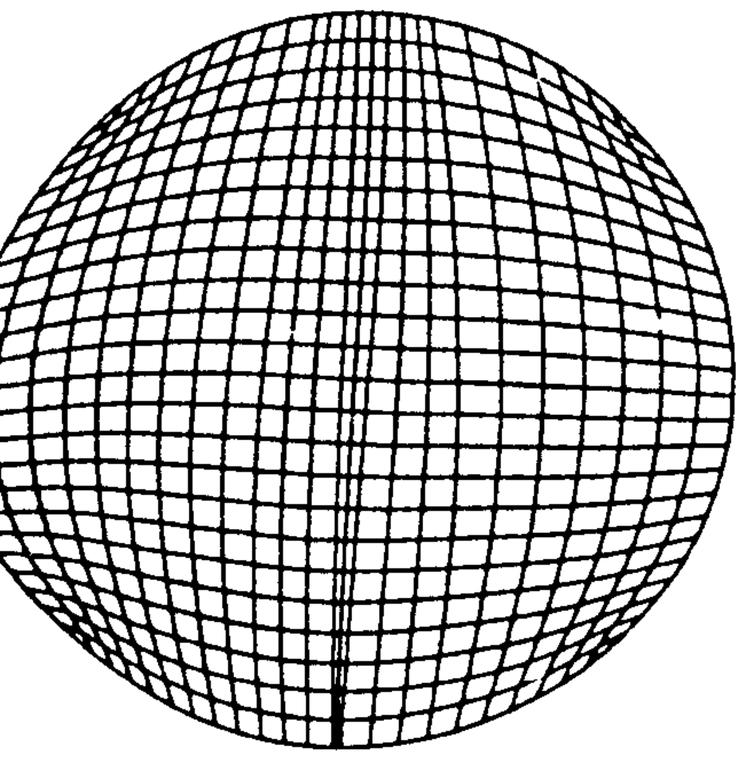

(a).

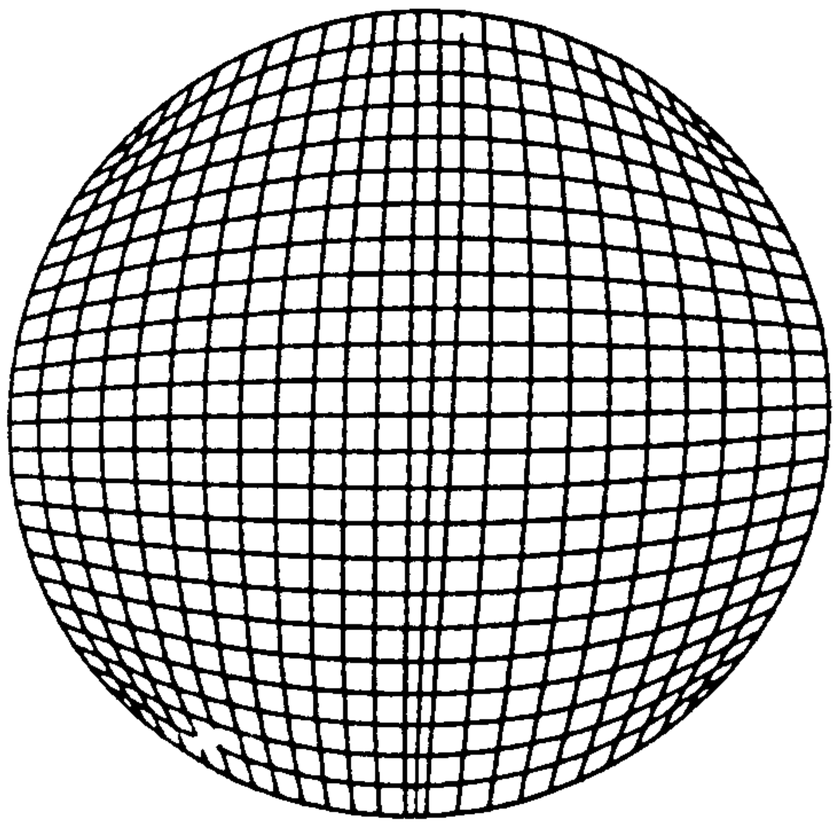

(b)

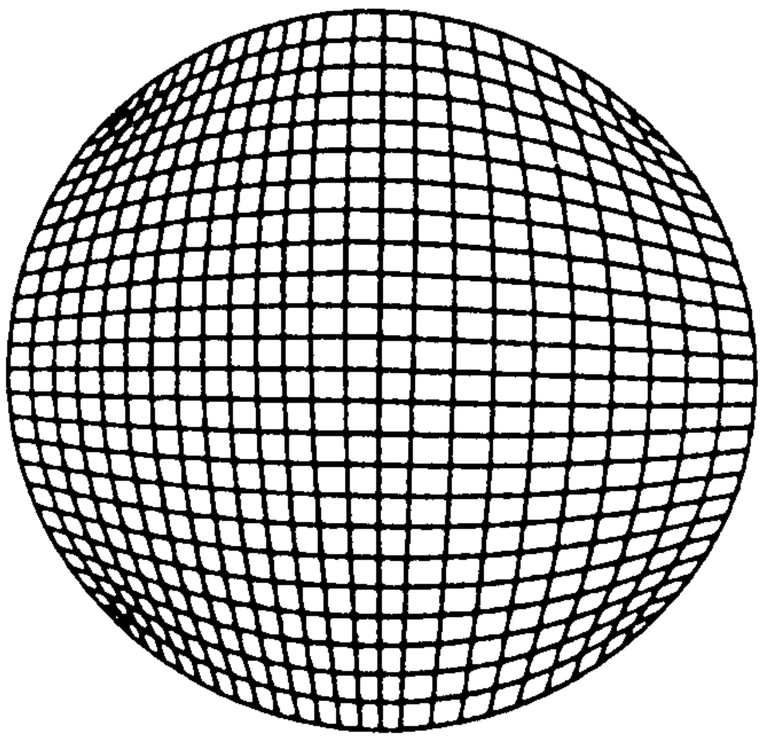

(c)

FIG. 15 CHOSEN GRIDS FOR RADIAL JET DISCHARGING NTO A CIRCULAR RESERVOIR (a) b_o = 3cm (b) b_o = 6cm (c) b_o = 13cm

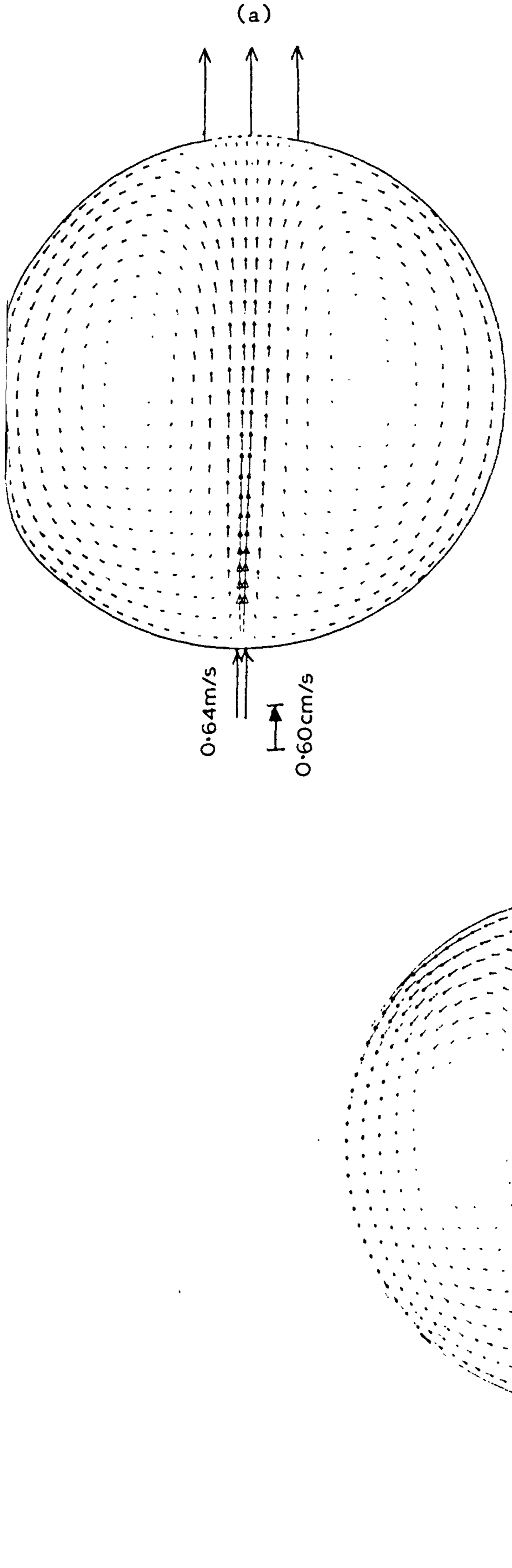

FIG. 16 PREDICTED CIRCULATION PRODUCED BY A RADIAL JET
(a) d_j = 3cm (b) d_j = 6cm (c) d_j = 13cm

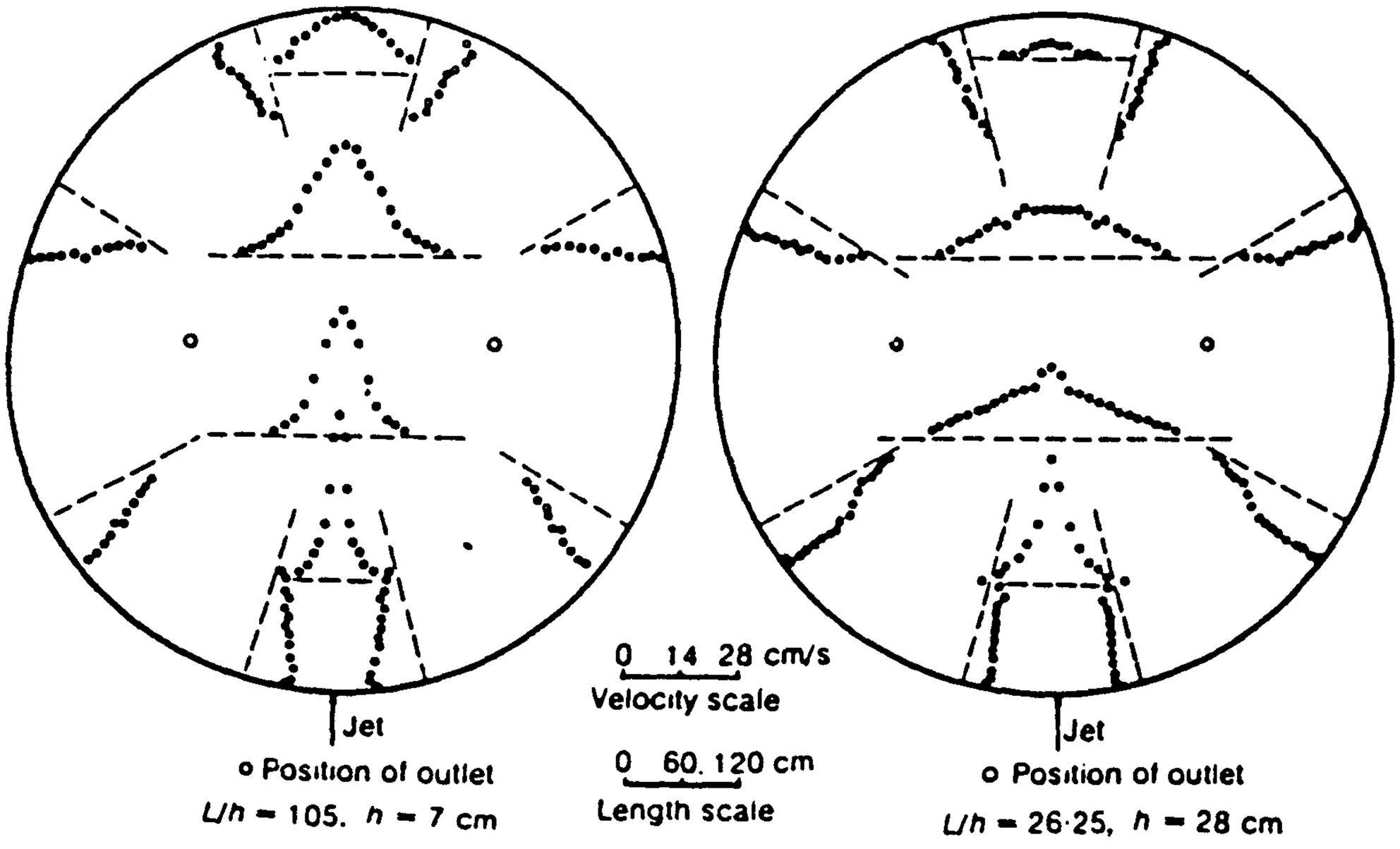

FIG. 17 EXPERIMENTAL VELOCITY DISTRIBUTIONS FOR A RADIAL JET WITH TWO OUTLETS INSIDE THE RESERVOIR (L = 735cm, Q_j = 615cm³/s)

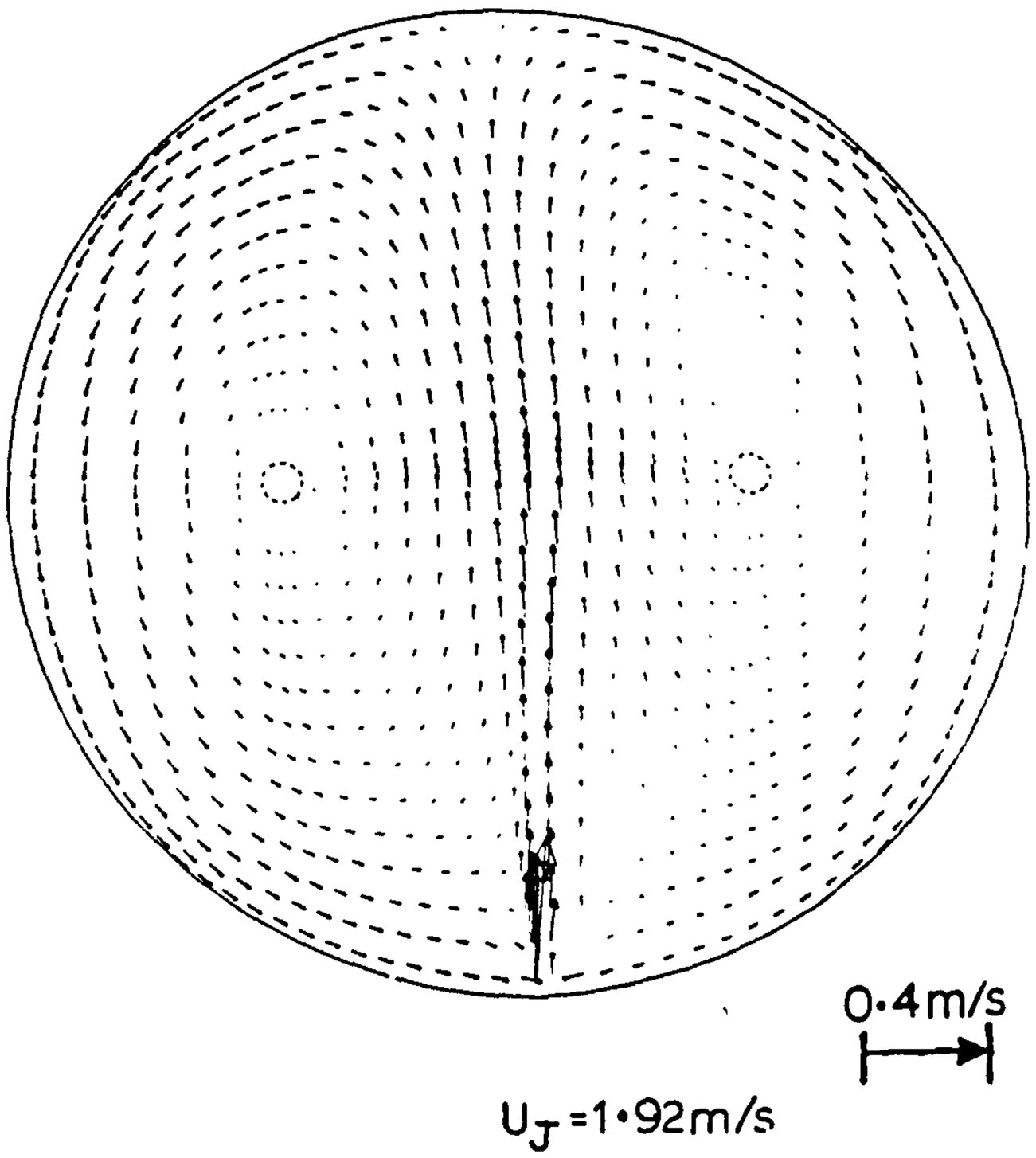

FIG.18 PREDICTED CIRCULATION PRODUCED BY A RADIAL JET WITH TWO OUTLETS INSIDE THE RESERVOIR

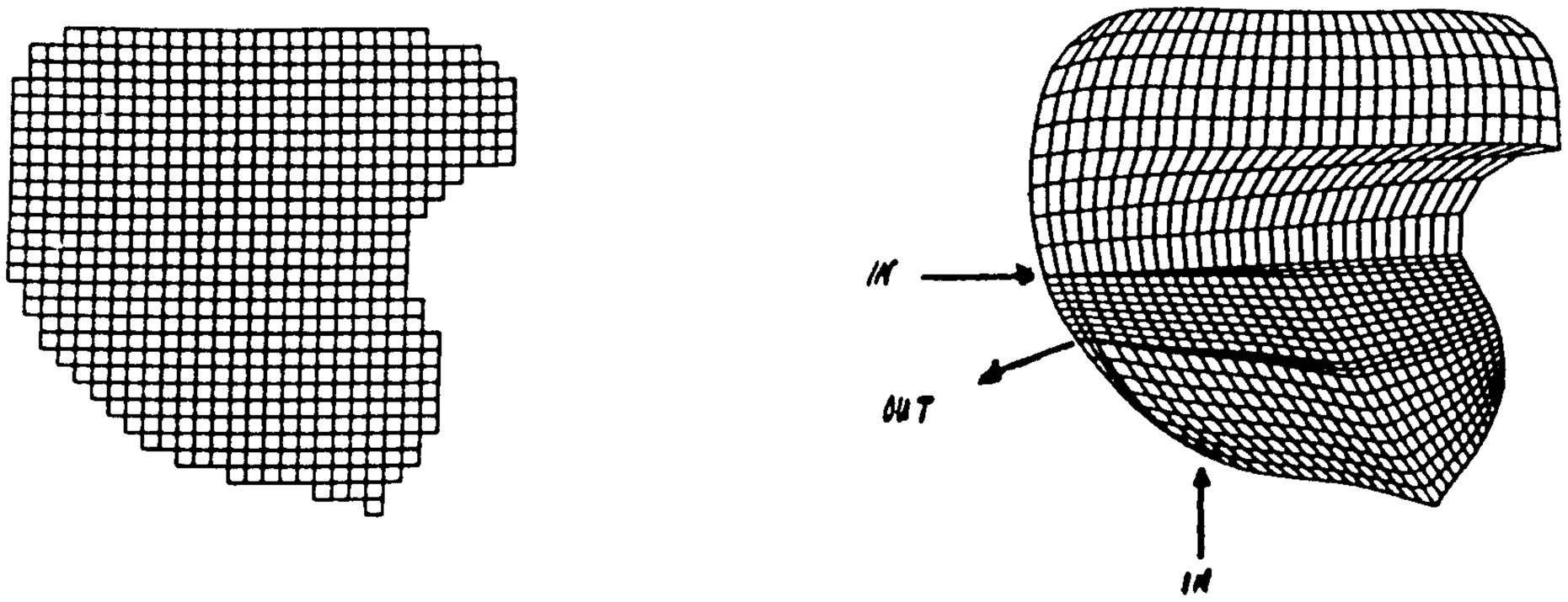

FIG. 19 TYPES OF NUMERICAL GRIDS FOR PRESCOT NO.4 RESERVOIR

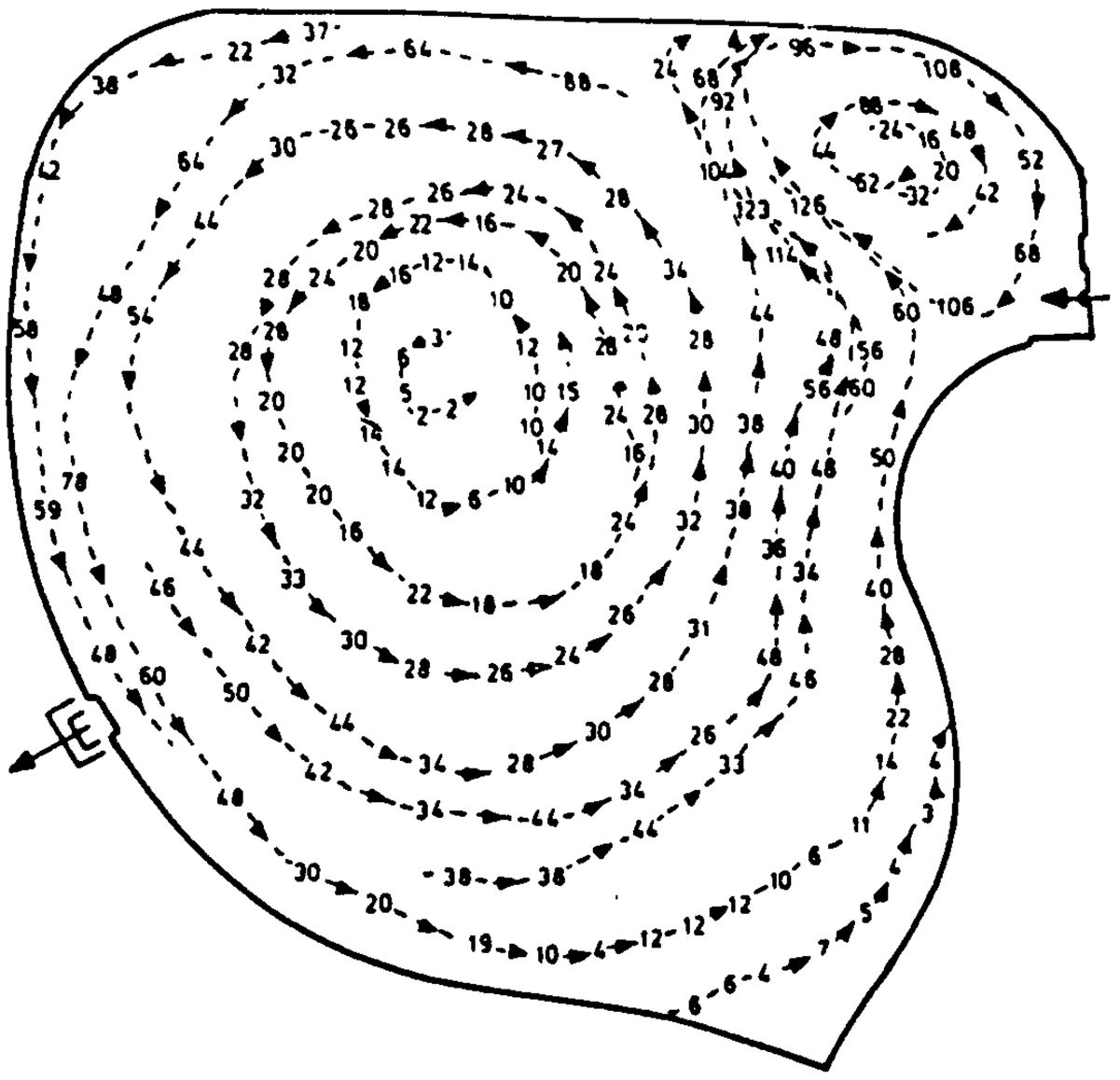

FIG 20 VELOCITY-DISTRIBUTIONS FROM THE 1 250 SCALE MODEL OF PRESCOT NO 4 RESERVOIR (5 1 VERTICAL EXAGERATION)

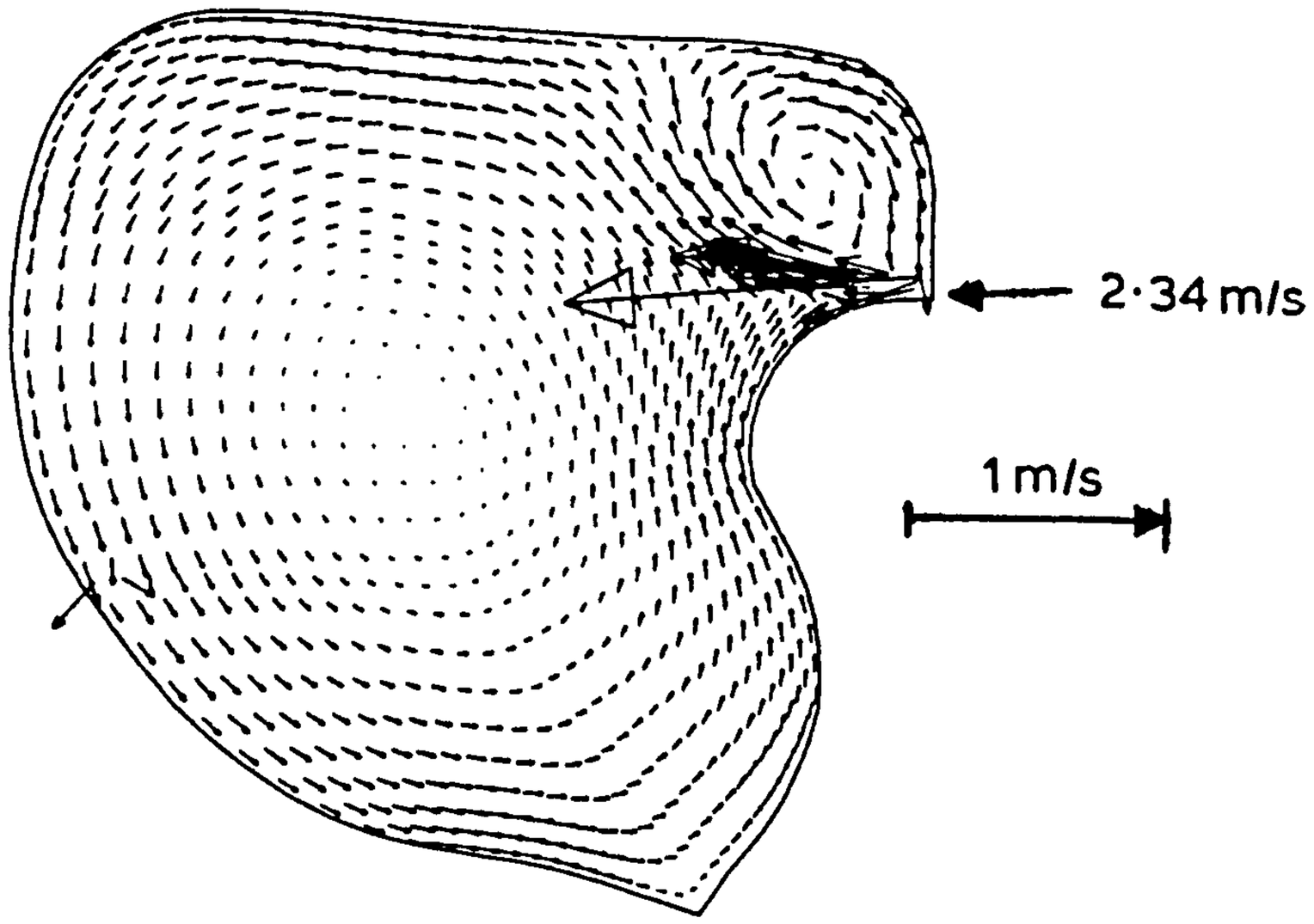

FIG 21 PREDICTED RESERVOIR CIRCULATION PRODUCED BY ONE INLET FOR PRESCOT NO 4 RESERVOIR (ORIGINAL JET VELOCITY)

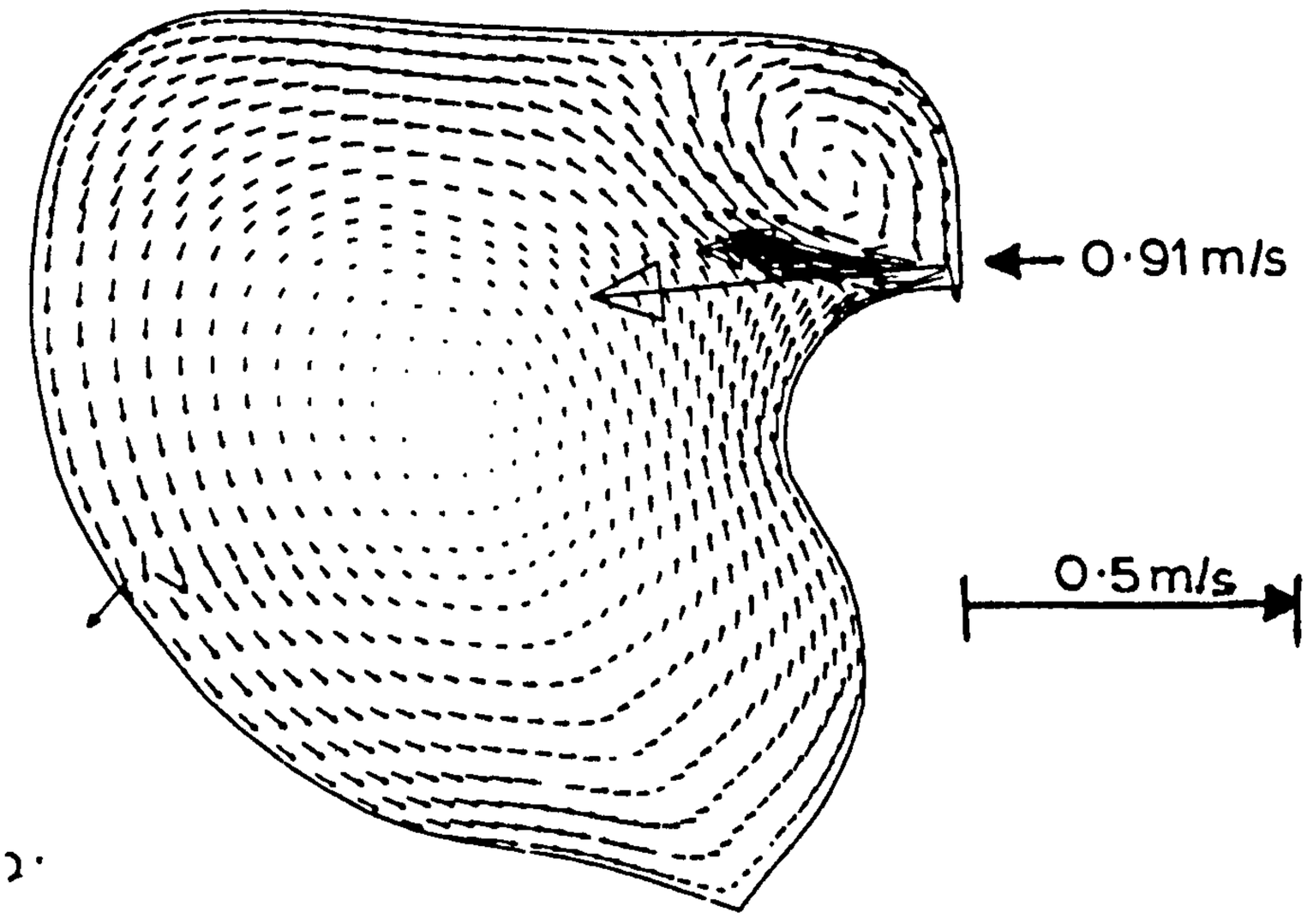

Fig. 22.

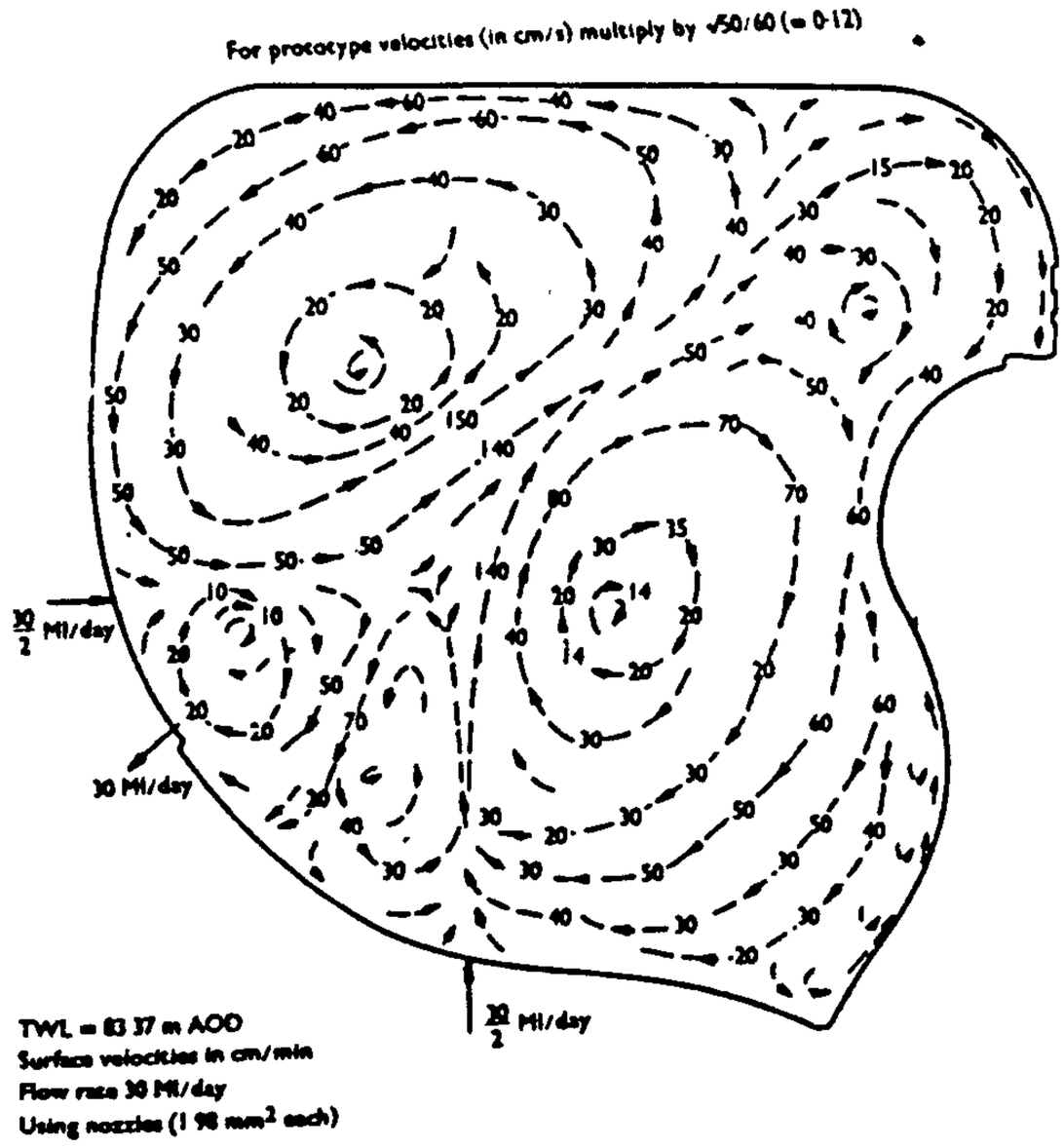

FIG 23 EXPERIMENTAL SURFACE FLOWS PRODUCED BY TWO NOZZLES AT MID-DEPTH (1·250 MODEL WITH 5 : 1 VERTICAL EXAGERATION)

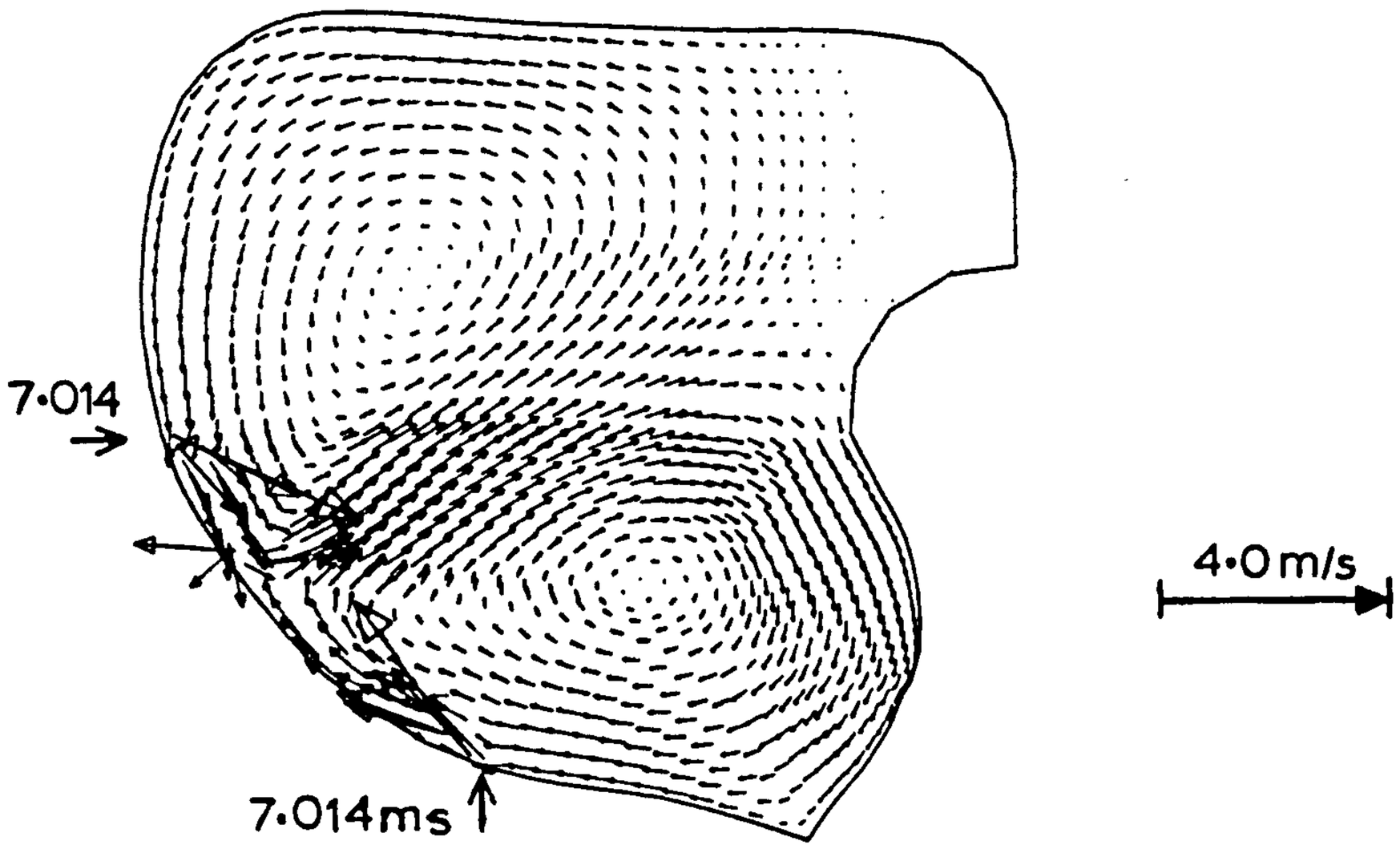

FIG 24 PREDICTED CIRCULATION USING TWO NOZZLES (USING ORIGINAL NOZZLE VELOCITIES)

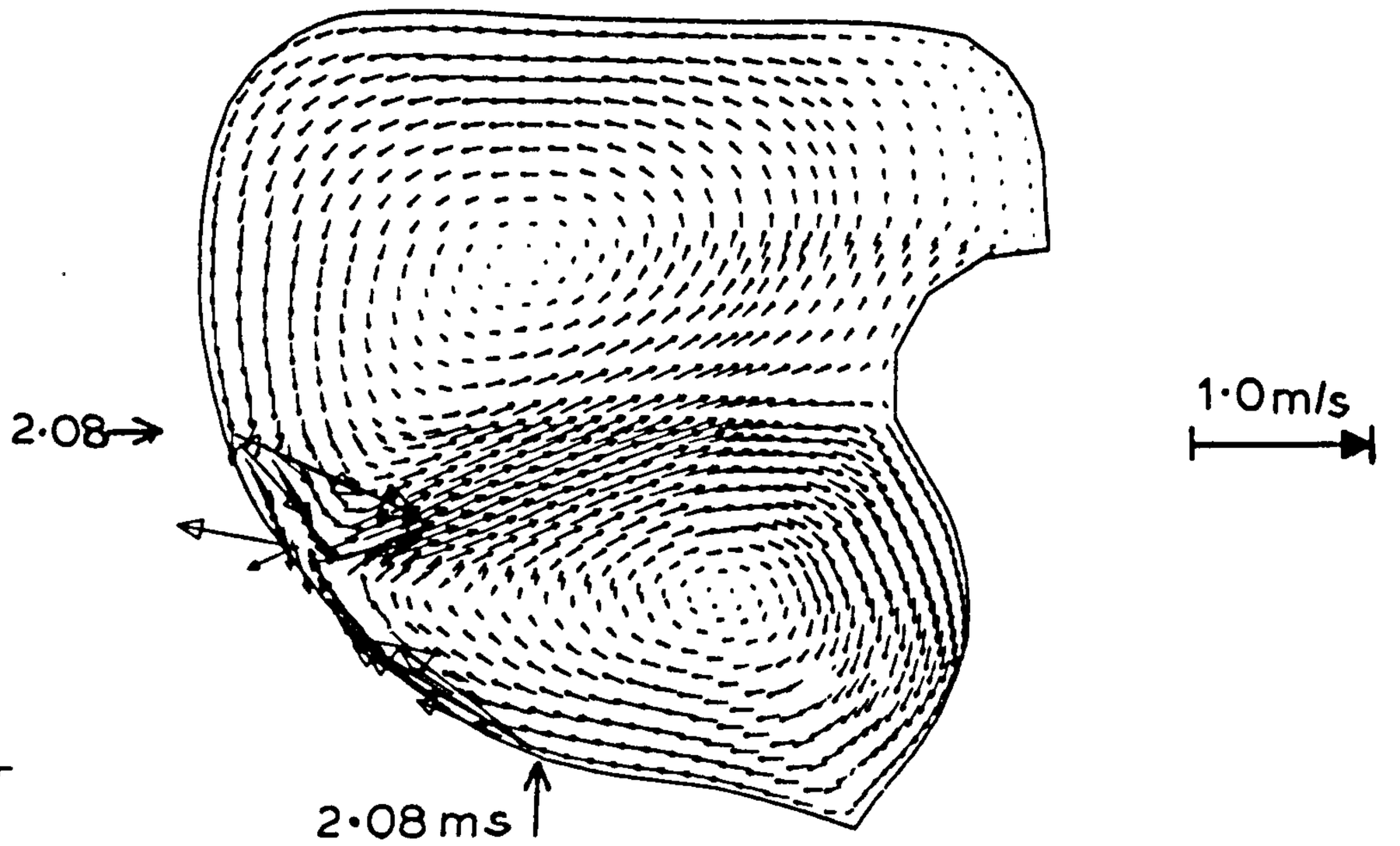

Fig. 25

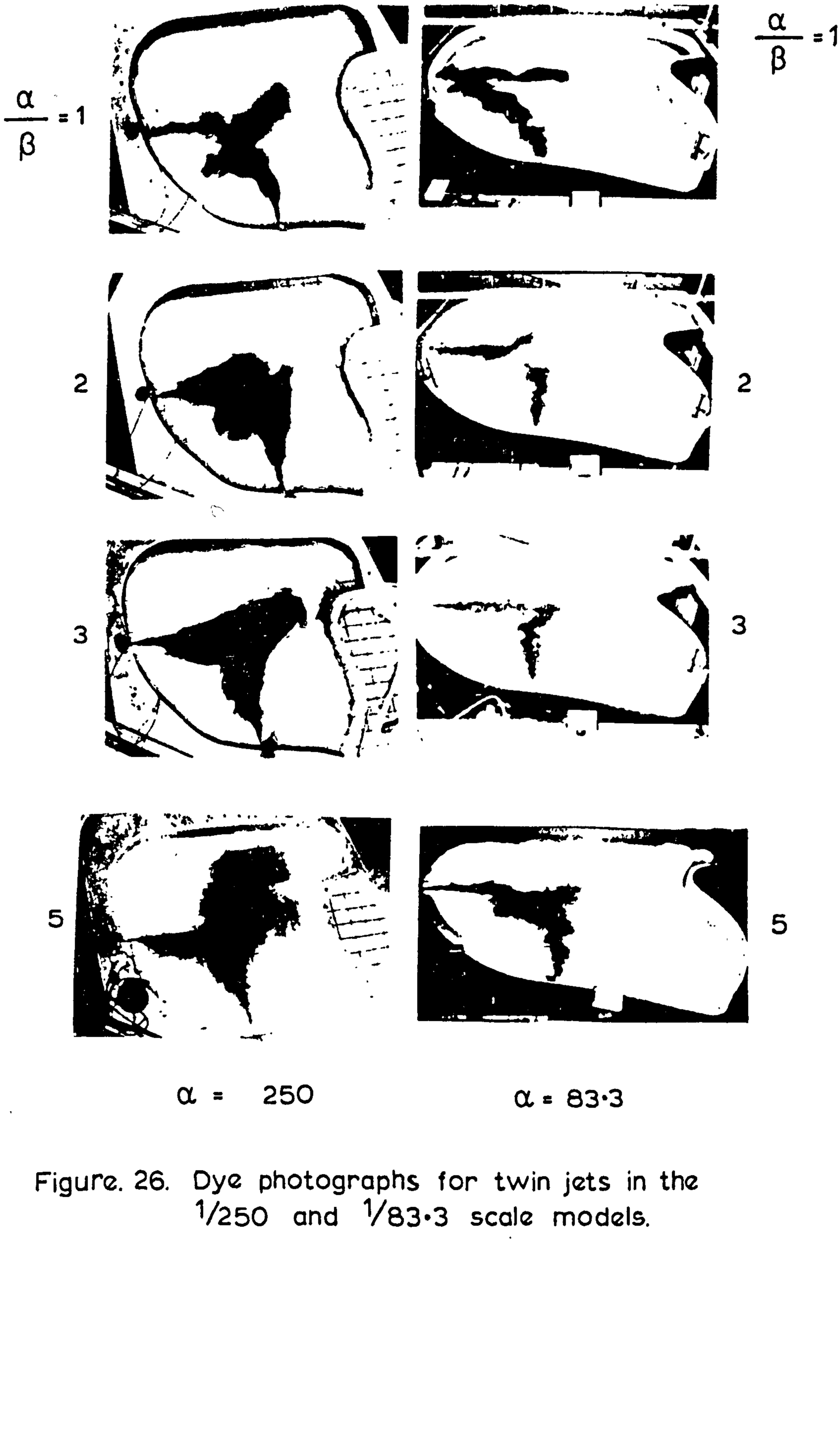

Figure. 26. Dye photographs for twin jets in the 1/250 and 1/83·3 scale models.

* For prototype velocities (in cm/s) multiply by √50/60 (= 0·12)

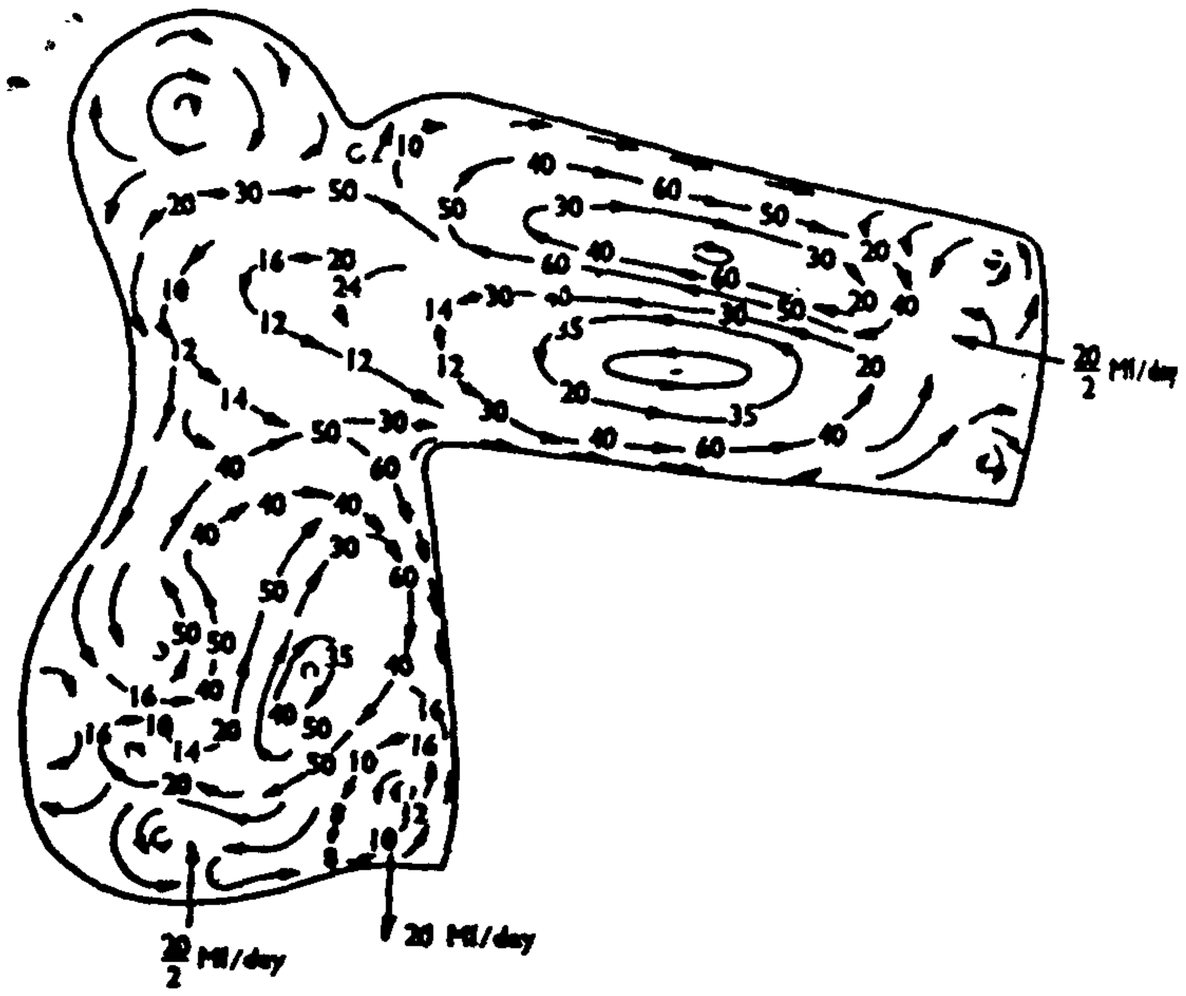

TWL = 83·37m AOD
Surface velocities in cm/min
Flow rate 20 Ml/day
Using tles (1·98mm² each)

FIG 27 EXPERIMENTAL SURFACE FLOWS PRODUCED BY TWO NOZZLES AT MID-DEPTH IN PRESCOT NO 3 RESERVOIR (1 250 MODEL WITH 5 1 VERTICAL EXAGERATION)

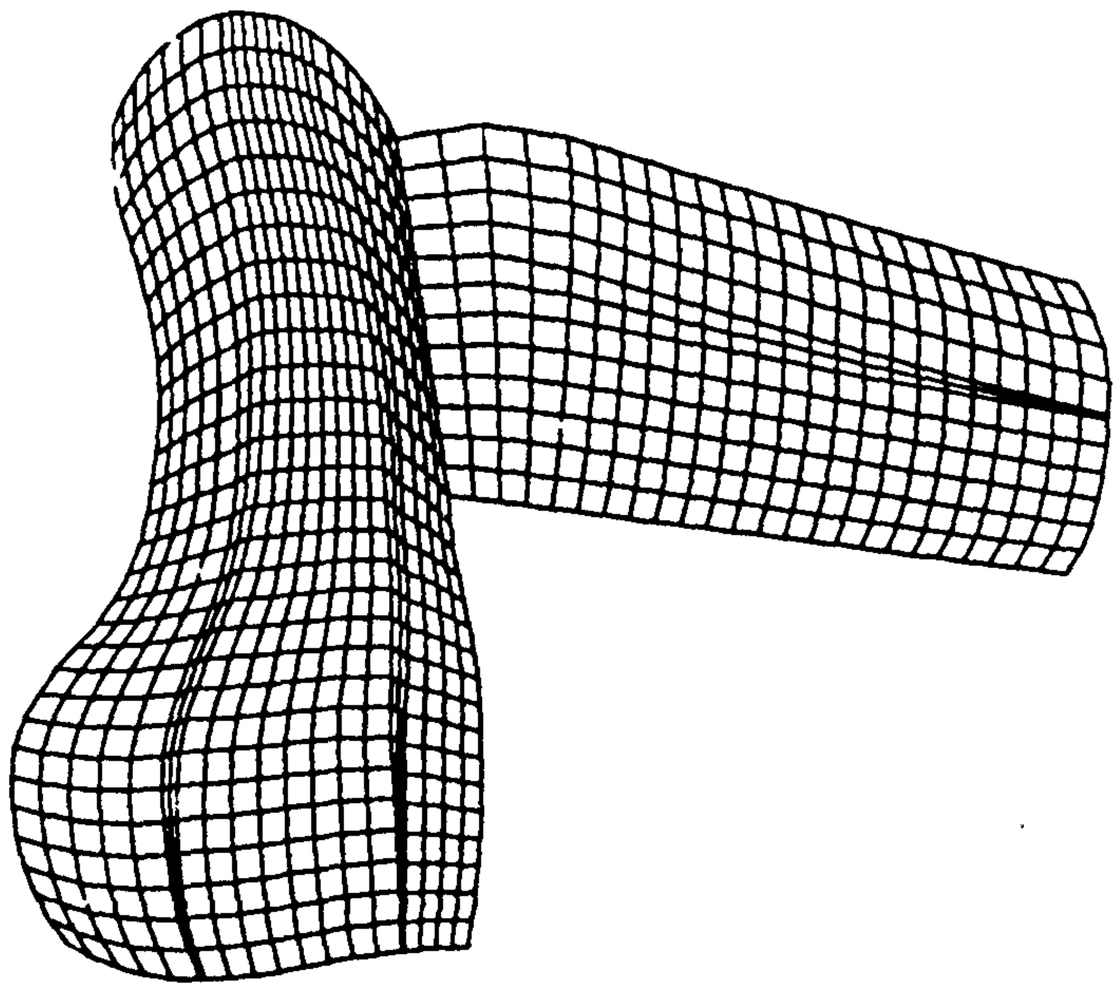

FIG 28 BODY-FITTED GRID FOR PRESCOT NO 3 RESERVOIR

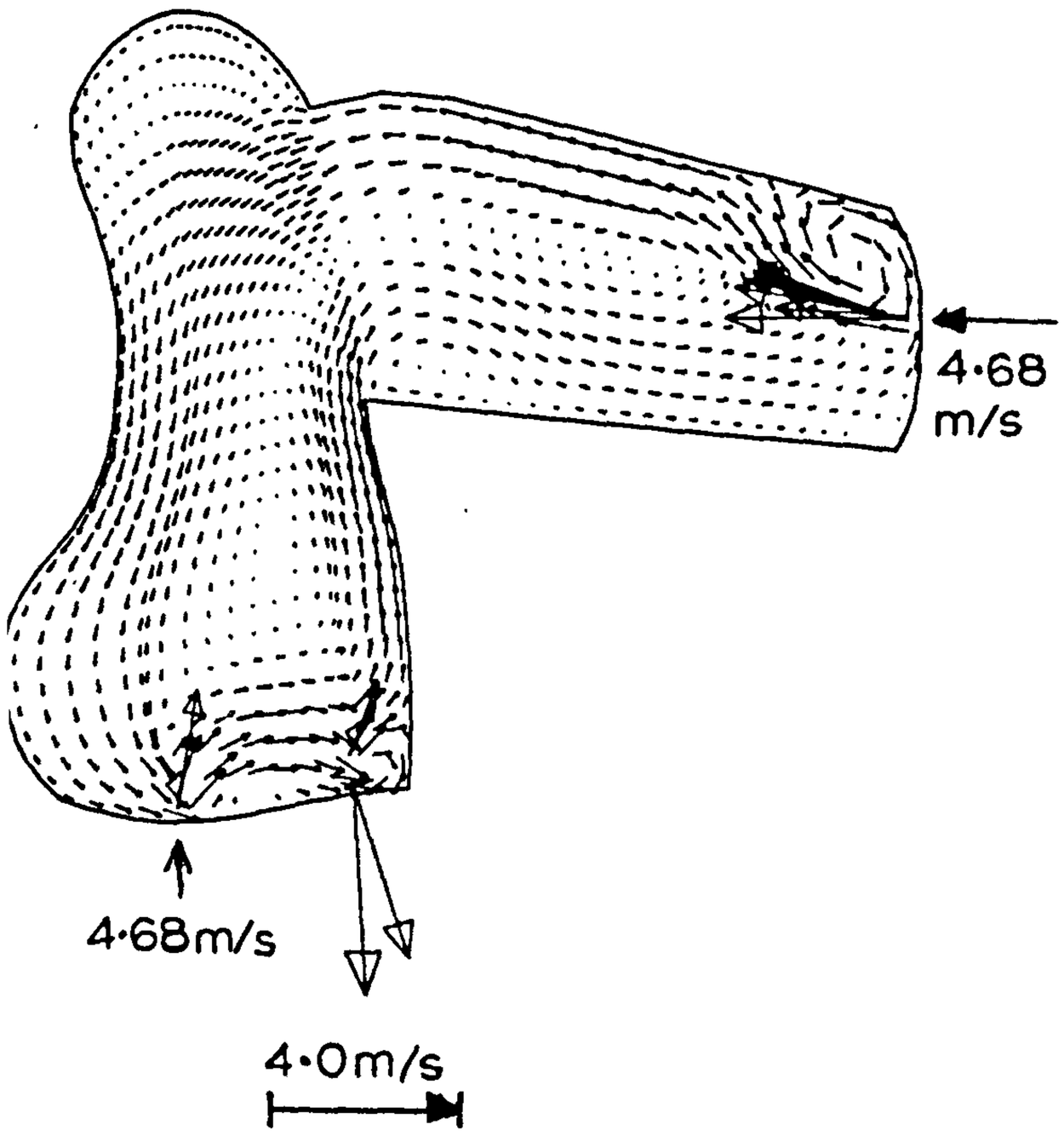

29 PREDICTED CIRCULATION USING ORIGINAL NOZZLE VELOCITIES

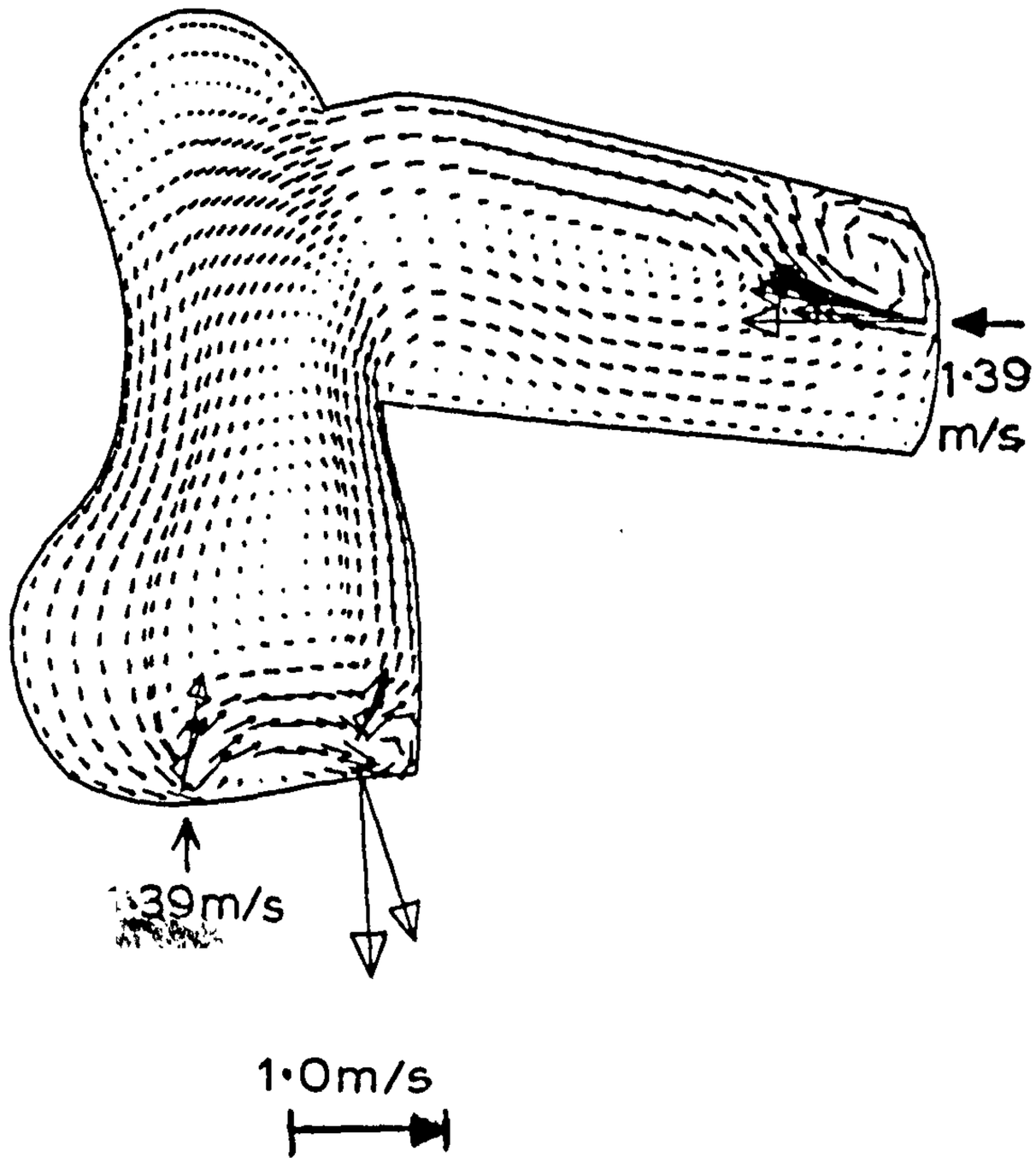

FIG 30 PREDICTED CIRCULATION USING DEPTH-AVERAGED NOZZLE MOMENTUMS